WONDERS OF THE ATMOSPHERE

STANLEY DAVID GEDZELMAN and JAN CURTIS

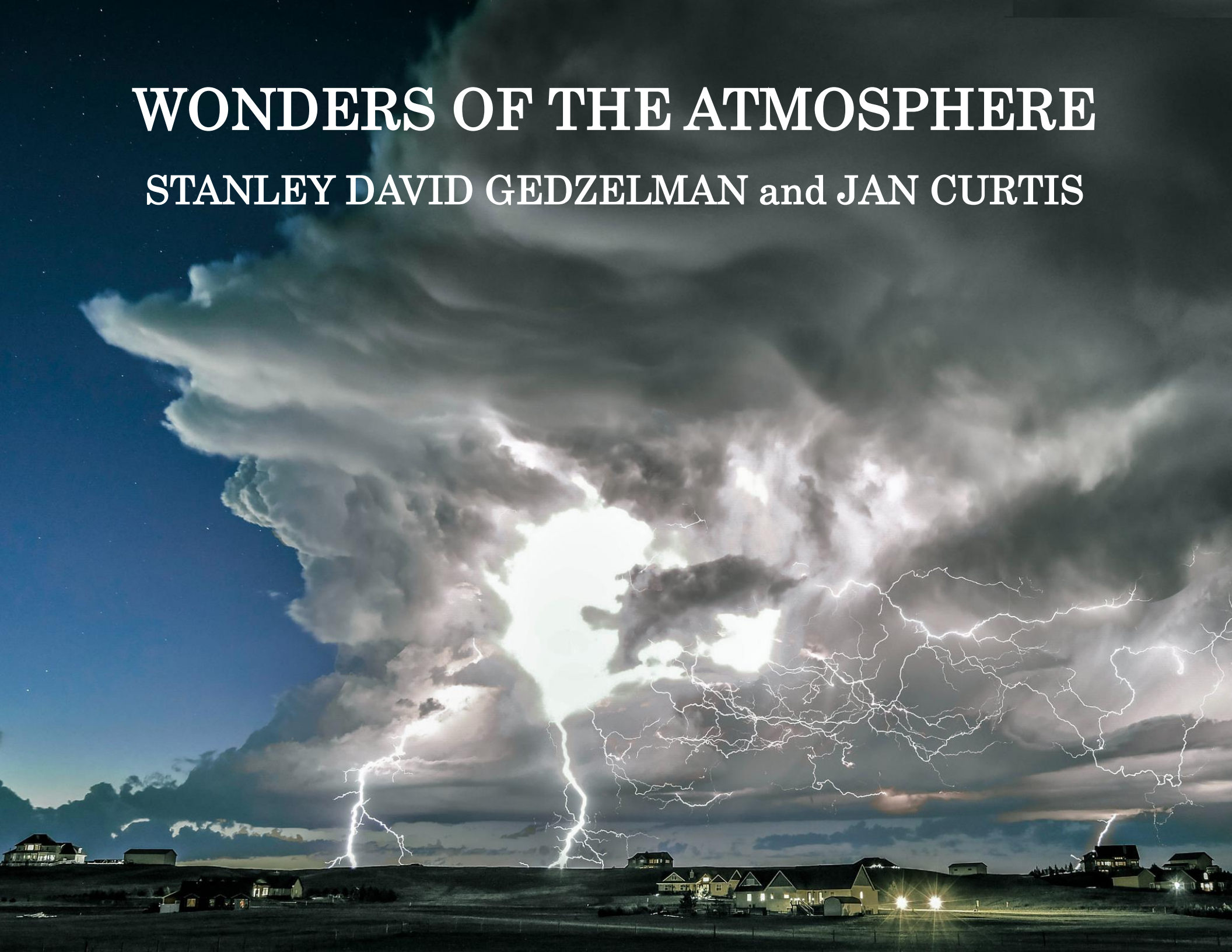

Wonders of the Atmosphere

Stanley David Gedzelman and Jan Curtis

Wonders of the Atmosphere

ISBN 978-0-9911976-4-4

This book can be found on the website www.stanrenaissanceman.com

Picture and Figure credits in the book are listed as,
JC = Jan Curtis
SDG = Stanley David Gedzelman

Front and Back Cover Photographs: Jan Curtis

Dedications

Jan: To all who look up and are inspired by the nature of nature.

Stan: To the adventurers, naturalists, and scientists who seek, ‘capture’, and explain nature at its most beautiful, awesome, and even terrifying.

Wonders of the Atmosphere
Table of Contents

Fig. P-1. Fire sky sunset, 24 Nov 2017, Cheyenne, WY. We describe and explain the source and cause of all these wondrous colors and fine rippled cloud structure.

Wonders of the Atmosphere
Table of Contents

Preface

1 The Sun and its Light
- 1.1 The Sun's Output
- 1.2 Reflection and Refraction
- 1.3 Light Waves: Interference and Diffraction
- 1.4 Light Waves: Scattering

2 The Clear Atmosphere: Sky Color and Mirages
- 2.1 The Colorful Canopy of Atmosphere
- 2.2 Molecular Atmosphere: Rayleigh Scattering
- 2.3 Earth's Thin Atmosphere and its Layers
- 2.4 Sky Color and Optical Thickness
- 2.5 Reddened Skies
- 2.6 Aerosols, Sky Light and Color: Mie Scattering
- 2.7 Polarization
- 2.8 Mirages: Refraction Gone Awry
- 2.9 The Green Flash and the Blue Flash
- 2.10 Light of the Eclipsed Moon and Ozone
- 2.11 Simulating Sky Color
- 2.12 Meteor Trails
- 2.13 Clear Sky Color Gallery

3 Auroras
- 3.1 Auroras and the Solar Wind
- 3.2 Auroras and Earth's Magnetic Field
- 3.3 Auroras and the Atmosphere
- 3.4 Colors of the Aurora
- 3.5 Auroral Morphology and Structure
- 3.6 Auroral (Magnetospheric) Substorms
- 3.7 Auroral Outliers
- 3.8 The Great Aurora Storm of 10-11 May 2024
- 3.9 Gallery

4 Clouds and Fog: Composition and Forms
- 4.1 The Composition of Clouds
- 4.2 Light and Colors of Clouds
- 4.3 Formation of Clouds and Precipitation
- 4.4 Cloud Forms
- 4.5 Fog
- 4.6 Cloud and Fog Gallery

5 Clouds and Storm Systems: The View from Above
- 5.1 The View from Above
- 5.2 Small-Scale Systems: Valley Fog
- 5.3 Satellite Pixel Size: Limits of Resolution
- 5.4 Small-Scale Systems: Sea Breeze
- 5.5 Large Scale Wind, Storm, and Cloud Systems
- 5.6 Tropical Cyclones
- 5.7 Extratropical Cyclones = Winter Lows
- 5.8 Gallery

6 Penetrative Clouds and Their Motions
- 6.1 Cumulus: The Nature of Penetrative Clouds
- 6.2 Changes of $\boldsymbol{T}$ and $\boldsymbol{T}_d$ in Rising and Sinking Air: Soundings and Stability
- 6.3 The Realm of Penetrative Clouds
- 6.4 Mountains: Orographic Cumulus
- 6,5 Motions: Mushrooms and More
- 6.6 The Time Lapse View of Cloud Motions
- 6.7 Pyrocumulus and Pyroanvils
- 6.8 Gallery

7 Cumulonimbus: Thunderstorms
- 7.1 Thunderstorm Facts and Statistics
- 7.2 Thunderstorm Structure and Features

7.3 Accessory Features of Thunderstorms
7.4 Green Thunderstorms and Rain/Hail Shafts
7.5 Tornadoes
7.6 Cumulonimbus Gallery

8 Lightning
8.1 Thunderbolts
8.2 Lightning and Thunder Characteristics
8.3 Discovering the Nature of Lightning
8.4 How Thunderstorms Generate Charge
8.5 The Life of a Lightning Bolt
8.6 Inventory of Lightning Types
8.7 Transient Luminous Events: Sprites, Etc.
8.8 Gallery

9 Rainbows, Fog Bows, and Rays
9.1 Observations and Properties of Rainbows
9.2 The Geometric Optics Rainbow
9.3 Rainbows to Reflect On
9.4 Twinned and Disjoint Rainbows
9.5 Supernumerary Bows and Fog Bows: Waves
9.6 Crepuscular and Anticrepuscular Rays
9.7 Hotspots and Heiligenscheins
9.8 Rainbow and Ray Gallery

10 Cirrus and the Layer Clouds
10.1 Contrails: The Usurpers
10.2 Cirrus: Angel Hair Clouds
10.3 Overcast Layer Clouds
10.4 Gallery

11 Ice Crystal Halos
11.1 Halos, Overlooked Cousins of Rainbows
11.2 The Incredible Variety of Halo Forms
11.3 Why Halos are so Varied
11.4 Forms of Ice Crystals
11.5 Crystal Orientation and Halo Forms
11.6 Geometric Optics of Halos
11.7 Complex Halo Displays
11.8 Halos and Optical Thickness
11.9 Simulating Halos: (Photorealism)
11.10 Gallery

12 Patterned Cloud Sheets
12.1 Properties of Patterned Cloud Sheets
12.2 Fire Skies
12.3 Honeycomb Cloud Cells
12.4 Shear Wave Clouds and Cloud Streets
12.5 Ranks and Rows
12.6 Cloud Wakes and Vortices
12.7 Patterned Cloud Sheet Gallery

13 Mountain Wave and Banner Clouds
13.1 Flying Saucers are Mountain Wave Clouds
13.2 Pileus Plus: Mountain Wave Cousins
13.3 Banner Clouds
13.4 Gallery

14 Coronas, Iridescence, and Glories
14.1 Coronas, Glories, Iridescence, and Icarus
14.2 Coronas vs Iridescence: Lee Diagram
14.3 Limiting Factors for Coronas
14.4 Pollen Coronas
14.5 Viewing Glories
14-6 Modeling Glories: Lee Diagram
14.7 Iridescent Contrails
14.8 Gallery

15 Diverse and Artistic Skies
15.1 Matching Painted and Photographed Skies
15.2 A Capsule Survey of Artistic Skies
15.3 Complex Clouded Skies: Animation
15.4 Complex Thunderstorm Clouds
15.5 Skies of Multi-level Clouds
15.6 Final Search: Multiple Optical Phenomena

Appendix 1: Sky Photography

Wonders of the Atmosphere
Preface:
Inspiration, Background, Sources, and People

Fig. P-1. Wonders abound from the ground to the upper atmosphere. The tornado (the severe thunderstorm's umbilical cord) with hints of green, east of Cheyenne, WY 12 Jun 2017, can put the lights out. The Aurora (Fairbanks, AK) turns the lights on in the darkness of polar nights. © JC.

Fig. P-2. Lenticular (Mountain Wave) Cloud with Cirrocumulus, 29 Nov 2020. © JC. See video at www.flickr.com/photos/79387036@N07/51715976668.

Wonders of the Atmosphere
Preface:
Inspiration, Background, Sources, and People

Writing for Book Started 02 Jun 2024, Completed Version on Web 12 Jan 2026

Why this Book?

The enveloping atmosphere enters us with every breath. Not only does it sustain us, it sways our moods even when it slumbers silently in the background. When it wakes it reveals a beauty and power that rivet attention and compel reverence. Displaying and explaining the faces of the roused atmosphere has been our aim in creating this book.

It is important to do this, not only for aesthetics but to wrench attention from news on the atmosphere, which focuses almost exclusively on the negative – the havoc and destruction its storms and extremes wreak and the fractious politics of how we either have or haven't altered and polluted it, all while the science remains unambiguous.

By showcasing the atmosphere's beautiful and awe inspiring phenomena, we hope to inspire in you some measure of the lifelong sense of wonder, awe, and reverence we have felt for the natural world and the care we must take as wardens when manipulating it.

Books cannot do full justice to the ever changing, dynamic atmosphere. Because of this we have put photos, videos, animations, and PowerPoint Presentations on our web sites,

https://www.flickr.com/photos/cloud_spirit/albums/

with thousands of photographs and videos with commentary, and,.

https://stanrenaissanceman.com/

with photos, PowerPoint Presentations, and the book, ***The Soul of All Scenery: A History of the Sky in Art***, summarized in Chapter 15.

Our Inspiration

What were the moments of inspiration that set us on our life paths? We are both children of New York City, where architecture masks Nature most of the time, so during those rare times when Nature asserts itself it is all the more impressive and stunning.

> **Jan**: "My first moment of inspiration occurred at the age of five when my mom took me to the roof of our apartment building in Brooklyn, NY after a thunderstorm to see a double rainbow. That technicolor image is as vivid in my mind as it was some 65 years ago."
>
> "A year later, on a trip with my dad at age six, I saw a nocturnal show of lightning that illuminated the Washington Monument and the Capitol, and wished I had a camera. Continuing the trip down the Blue Ridge Parkway I was astounded to see clouds from above for the first time. Later, while canoeing a thunderstorm overtook us, a wonderful drenching experience."
>
> For my 10th birthday my aunt bought me a mini-camera. Right away, I looked to the sky for inspiration, never having any desire to photograph people. About that time an uncle who had moved to Alaska showed up with tales of its natural wonders. I was fascinated by his descriptions of the aurora (Fig. P-1), which

included an account of hearing the aurora hiss and crackle. That was a factor in my later move to Fairbanks Alaska.

Stan: "The power and colors of the atmosphere, and big snowstorms have always excited me. At age three years and one month I remember happily walking chest deep in a snow drift in the back of my apartment building in Far Rockaway, NY from the record-breaking storm of 26 Dec 1947 that dumped 67 cm on New York City in 24 hours. The March 1956 double snowstorm that paralyzed New York City brought me unbounded joy. I waited impatiently for every big snowstorm."

"I did not wait for Hurricane Daisy in 1958, which struck by surprise on the return leg of a cruise to Nassau in the Bahamas with my grandfather. Waves that towered 10 m and shivered the ship, mixed with bubbles under the gray sky to produce a strange pea green color I had never imagined and have never seen since. That was two days after my first look at sparkling waters under the tropical Sun that graded from turquoise shallows to cobalt blue depths at Paradise Island Beach. That early fascination with light and color eventually congealed into my abiding interest in atmospheric optics."

Hurricane Donna, which struck New York City on 12 Sep 1960 sealed our conversions, transforming both of us to future meteorologists.

Jan: "Weather forecasts were not so accurate then, so school started that day but let out early as the weather rapidly deteriorated. Walking home in rising winds I grabbed a stop sign pole when a gust of wind lifted my legs and I was holding on for dear life like a wind-torn flag. I thought the occurrence was much more fun than dangerous."

Stan: "From the platform of the elevated Far Rockaway subway line I could see huge breaking waves crash near the boardwalk, flow under and even over it, cross the width of the Rockaway peninsula, and pour into Jamaica Bay. It was on that first day of my senior year in high school I decided to major in Meteorology."

Total solar eclipses inspired both of us.

Jan: "My first life altering event occurred on 7 March 1970, when I witnessed a total solar eclipse in Greenville, North Carolina with my dad. Before this event, few people travelled to see eclipses. Despite this phenomena occurring every 18 months somewhere on Earth, less than one percent of the Earth gets to see the perfect alignment of the Moon and Sun, so that an eclipse occurs on any specific point on Earth only every 360 years."

"The moment totality began, the PA speakers at the Eastern North Carolina University where I viewed this wonder of nature blared out the opening bars of Richard Strauss's ***Also Sprach Zarathustra*** (the theme of Author C Clark's ***2001: A Space Odyssey***). When I looked up after the blinding Sun was extinguished by the Moon, I felt the way the cave dwellers thousands of generations before me must have felt. My stomach had the feeling of falling in zero-G. Despite having seen countless images of totality, I was completely unprepared by my mind's inability to comprehend logically what I was witnessing. That feeling was both frightening and overwhelming."

Stan: "I very much wanted to see the 7 March 1970 total solar eclipse but was called away to my brother's engagement party. Five years later, in 1975, floundering around for a research topic that I would love, I chanced to see a photograph of the total solar eclipse of 15 Feb 1961 near Grenoble, France. All previous eclipse photos I had seen showed only the Sun; this photo showed the sky below the eclipsed Sun with the colors of twilight. I was stunned and thought 'This can't be. Those sky colors belong only to twilight.' Then, I thought, 'I am teaching Physical Meteorology and should be able to explain it.' It was the first natural phenomenon I 'mastered' through math. It gave me a great sense of joy and power."

"I finally experienced a total solar eclipse on 21 August 2017, some 12 km above sea level. Joe Rao, a former student and lifelong eclipse aficionado, arranged seats for me and my wife on Alaska Air's dedicated flight into the eclipse. As we entered the umbra and the Moon's shadow raced eastward, sweeping across the sea surface and the clouds below, everyone on the plane was cheering but I was sorely disappointed. I did not see the vivid twilight colors I had hoped for. Instead, just outside the umbra a dull, orange-brown salmon color tinted the low clouds, a color that, along with the darkness, must have scared the wits out of primitive people. I was utterly baffled, perplexed, and sad. The mystery consumed me; the pleasure was delayed until I was able to understand and explain it. The ability to be able to 'explain' in some way the ineffable has always given me great joy."

Both of us were beneficiaries of the post-Sputnik glow of Space Science in America. We met at the City College of New York, in 1970, completed our careers, and after retirement, resumed contact through Weatherwise Magazine's Annual Photography Contest.

Jan: "In the summer of 1969 when the Apollo 11 Astronauts landed on the Moon, I was selected to attend a National Science Foundation summer astronomy program for high school seniors at the Hayden Planetarium in New York City. That was one huge factor in my decision to major in meteorology. I suppose that opportunity set the stage for me to meet Professor Stan when I was a freshman at the City College of New York and eventually reunite us more than 50 years later to co-author this book."

"After retiring from the Navy, where as forecast officer I had seen much of the world, and inspired by my Uncle's tales, I headed up to Fairbanks, AK. There I served as research climatologist in the Geophysical Institute of the University of Alaska Fairbanks for six years and as a photographer for Syun-Ichi Akasofu's book, ***Exploring the Secrets of the Aurora***. I then did stints as the state climatologist of Wyoming, and as staff climatologist at the National Resources Conservation Service Oregon, always choosing to live in places that offered unbounded views of the sky."

"Cheyenne, WY, where I live now, is one of the sky's playgrounds. Located on the High Plains just east of the Front Range of the Rocky Mountains, spring and summer afternoon thunderstorms build over the mountains to the west, move overhead and race off to the east, flashing lightning into the night and sometimes producing tornadoes (Fig. P-1). In winter, strong west winds passing over the mountains frequently generate higher clouds including flying saucer-shaped, lenticular wave clouds that hover overhead (Fig. P-2). Around the peak of the Solar Cycle you can even see displays of the Aurora following solar storms. Of course, Alaska is a much better place to view the Northern Lights (Fig. P-1)."

"In 2000, during solar maximum, Alaska was the place to be to observe the Northern Lights. This is where I experienced my second epochal connection to nature. A major solar storm reached the magnetosphere and produced a display of the aurora that changed the snow cover from green to red with shadows from the surrounding trees dancing all over the ground. Then suddenly in the isolation and quietness of the moment, nearby wolves started to howl at the sky and my skin formed goosebumps that weren't caused by the subzero temperatures."

"At that moment, I felt that I was privileged to be a part of nature that most never experience. That was a spiritual experience that completed my journey connecting me to nature. I learned that nature has secrets and through patience and persistence, if one is very attentive, the answers will be revealed."

Patience and persistence, indeed! For decades we had only sporadic contact. Eventually, our paths crossed again.

Stan: "With photos of my views of the sky from my 9th floor office of the Science Building at City College (whose window I could open), from its roof, and from my 12th story apartment in

nearby Cliffside Park, NJ, I began writing illustrated articles about clouds and atmospheric optics for ***Weatherwise Magazine***. In 1993 Pat Hughes, recognizing my enthusiasm, asked me to be an Executive Editor. In that position, I became a judge in the Weatherwise Annual Photography Contest, a most rewarding experience. Jan, one of the contestants, submitted prize-winning photos year after year – in fact, too many to include in the contest. In 2021, Margaret Benner, Editor of Weatherwise, agreed that I should write an article dedicated to showcasing a few of the photographs that could not be included, and Jan and I worked together on it.

"In May 2024 it dawned on me that Jan would be the perfect collaborator for a book I had long wanted to write on all the wondrous things that can be seen in the atmosphere. His breathtaking photos and videos were the perfect complement for my more technical skills and, working with him on the article showed that we were of essentially the same mind set. I thank my lucky stars that Jan was also eager for the project, which we began promptly. Thus, our mutual love of the atmosphere and the natural world converged to form the basis of a collaboration, decades in the making."

Of course, no person or no two people can be everywhere at the same time or can witness, explore and delve into all things atmospheric. Both of us acknowledge, use, benefit, have learned from, been inspired by, and have collaborated with our kindred spirits. Our debts and gratitude to them are immeasurable. We must and gladly acknowledge them right up front. Their works, which have served as vital references for us, are praised and pointed out below.

The Pioneers

"Give me a place to stand and a lever long enough, and I will move the world." Archimedes.

Because none of the Ancients had such a place to stand their knowledge of the atmosphere was limited to local views. As a result, scientists focused on solving problems that could be 'bottled', such as rainbows. Understanding the rainbow was based on the growing knowledge of optics in the 13th century that convex lenses magnified letters by refracting (bending) light. (This interest, which led to the invention of spectacles by 1290 CE, doubled the productive years of technical and literary workers.)

In 1267 CE Roger Bacon, recognized that rainbows are produced by spherical raindrops, each raindrop acting like a combination of a prism lens and a mirror. He documented that the primary rainbow appears 42° from a viewer's shadow though he couldn't explain why. Around 1308 CE, the Persian scientist, Kamāl al-Dīn al-Fārisī and the German cleric, Theodoric of Freiburg independently (we think) aimed sunbeams at glass spheres filled with water to represent large raindrops. Both demonstrated that rainbows are caused when sunbeams suffer refractions upon entering and exiting the sphere plus either one reflection inside the sphere for the primary rainbow, or two for the secondary bow.

The next advance in understanding the rainbow took over 300 years. In 1637, Descartes, using the newly discovered law of refraction calculated numerous rays striking all over spherical raindrops and explained mathematically *why* the primary rainbow appears 42° and the secondary bow, 51º from the observer's shadow. Applying Descartes' approach to hexagonal ice crystals, Edmund Mariotte in 1676 explained the circular ice crystal halo that appears 22° from the Sun (or Moon).

Isaac Newton added color to these explanations of rainbows and halos. More than a century later, in 1801 Thomas Young showed that light consists of waves and used the properties of waves to explain (qualitatively) both supernumerary rainbows, which form as extra pastel-colored bands inside the primary rainbow, and coronas, which form in thin water-droplet clouds around the Sun and Moon.

About the same time, in 1802 and 1803, Jean Baptiste de Monet Lamarck in France and Luke Howard in England developed the first cloud classification and naming systems. A mere 20 years later, in 1823, Siméon Denis Poisson derived the law showing that most clouds form from the cooling due to the expansion of rising air.

Another century plus of discoveries and inventions from the telegraph to the radio, radar, computers, planes, and satellites, gave scientists the tools to see into clouds and out to large scale atmospheric phenomena including storms. The camera, movies, and videos not only recorded beautiful phenomena, but added the dimension of time by animating their motions and evolution.

With all the new tools available to study storms, research in atmospheric optics was sidelined for a generation. Knowledge at that time (1937) was summarized in Marcel Minnaert's classic, translated to English as ***The Nature of Light and Color in the Open Air*** (1954). Because of Minnaert's remarkable powers of observation and his profound insight, his book still serves as a fundamental reference to anyone interested in atmospheric optics.

The Modern Epoch

During the lull in research on atmospheric optics, knowledge advanced regarding every aspect of clouds – the air motions in and around them that give them their shapes, and the particles they are made of. In Vermont, Wilson Bentley, fascinated by snow crystals since childhood, learned to capture snow crystals, rush them under a microscope and photograph them before they changed too much. A generation later and a world away in Japan, Ukichiro Nakaya learned to grow and photograph snow crystals. Both of their books, laden with photographs, are classics.

Wilson Bentley, ***Snow Crystals*** (1931).
Ukichiro Nakaya, ***Snow Crystals: Natural and Artificial*** (1954).

Because Nakaya grew his snow crystals under controlled conditions, he was able to document how crystal shape (e. g., plate, pencil, or star, see §4.1 and §11.4) depends on temperature and humidity. Crystal shapes are important for understanding the various ice crystal halos and for their impact on weather and climate.

Charles Wilson invented the first cloud chamber by 1911, not to discover the value of the electric charge of an electron for which he won the Nobel Prize in Physics in 1927, but because of his fascination with the so-called Brocken Spectre (a glory) and other atmospheric optical phenomena produced by drops and crystals. Later cloud chambers or cloud wind tunnels were designed to investigate cloud particles, holding them still by suspending them in updrafts that exactly cancelled their fall speeds.

Meteorologists determined many features of clouds by flying through them. Alfred Wegener, famous for advancing the theory of continental drift, and adding to our understanding of how raindrops grow, explained a rare ice crystal halo arc (the Wegener arc) he observed during a balloon flight. In 1938, Joachim Kuettner, an enthusiast of the atmosphere and organizer of large scale atmospheric field projects throughout his life of 101 years, flew a sailplane through lenticular (mountain wave) clouds, which sometimes resemble and were the initial inspiration and model for flying saucers (Fig. P-2). In the process, he discovered the rotor (which can smash planes into the ground). Richard Scorer, trained in hydrodynamics, developed a theory of the conditions and airflow patterns that produce lenticular clouds. Scorer also revealed the normally invisible air motions in and around all the cloud genera, which he illustrated in his landmark book on almost every aspect of clouds (and optical phenomena), ***Clouds of the World: A Complete Color Encyclopedia*** (1972)

Cloud enthusiasts abound. Gavin Pretor-Pinney, founder of and Member 001 in the Cloud Appreciation Society, deserves special mention. Author of ***The Cloudspotter's Guide*** (2006), Gavin turned a fascination with Australia's famous Morning Glory cloud into an abiding, active passion. His website,

https://cloudappreciationsociety.org/

is a forum where sky lovers the world over view and submit photos of clouds and optical phenomena, and the collection has grown into something immense and eye watering. Even amateur sky observers can be in (or go to) the right place at the right time to photograph and record some extraordinary sight.

The standard reference for clouds, which contains all the cloud forms and photographs, often accompanied by descriptions of the weather conditions under which they occur is the ***International Cloud Atlas***,

https://cloudatlas.wmo.int/en/home.html

At last, Howard (Cb) Bluestein, who has been photographing clouds as an enthusiast and professional since 1967, and chasing tornadoes since his arrival at the University of Oklahoma in Norman, has assembled his best photos and insights into clouds in his long-awaited treasure book, ***The Architecture of Clouds*** (2024).

With the benefit of all the new cloud knowledge and the computer, the next major phase in research and understanding of atmospheric optics, got going shortly before 1970. Somewhat by coincidence, this was also about the time serious storm chasing began, which led to detailed understanding of the structure of severe and tornadic thunderstorms.

At the dawn of the 1970's, R. A. R. Tricker published his ***Introduction to Meteorological Optics*** (1970), which presents the mathematical side of the field. Tricker revealed the difficulty of finding solutions for the colors, brightness, and even shape of optical phenomena such as rainbows, and halos. These are formidable problems, some far too difficult and involved to solve analytically. This is where the computer enters the scene for atmospheric optics.

The computer's speed has made it possible to solve otherwise impossibly difficult problems in atmospheric optics by sheer brute force. Artificial Intelligence (AI) is a recent culmination of computer generated solutions to complex problems.

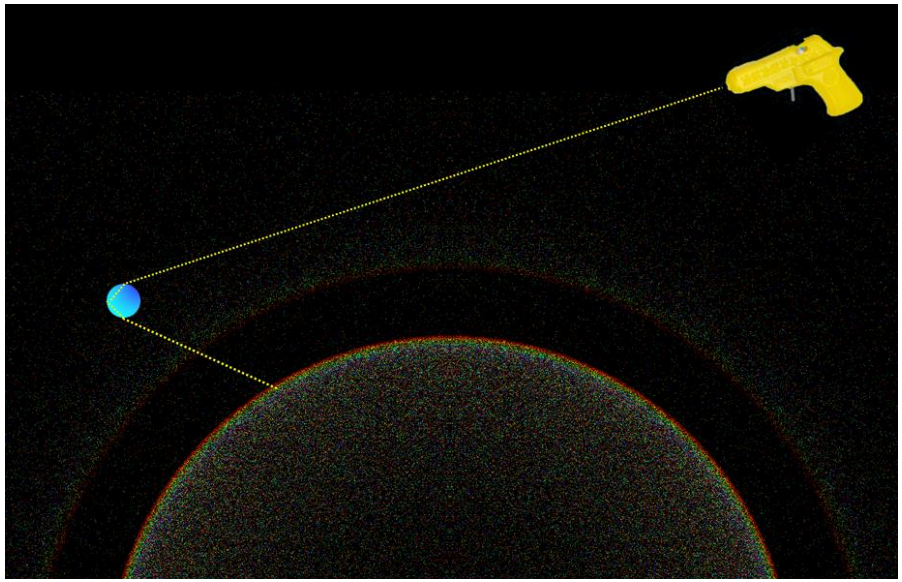

Fig. P-3. Monte Carlo dot map of a double rainbow showing one of 2 million random beams. The faint secondary bow appears outside the primary. SDG.

One classical approach, the Monte Carlo technique (and used as part of AI), shoots random computerized sunbeams at computerized raindrops, cloud droplets, ice crystals, air molecules, and aerosol particles, and records their path through the atmosphere to an observer. In a way, that is what Descartes did to explain the rainbow. To illustrate the Monte Carlo technique, imagine the Sun as a gun shooting sunbeams at a spherical raindrop, which deflects the beams onto a target (Fig. P-3). After enough beams are shot (2 million in this simulation, which took 10 seconds on a slow PC) a pattern matching a double rainbow emerges. The Monte Carlo and other numerical bludgeoning techniques have now advanced to the point where simulations of atmospheric optical phenomena appear photorealistic.

In 1966 Robert Greenler (with A. James Mallman) presented preliminary results of the first Monte Carlo simulations of an ice crystal halo phenomenon (a Sun pillar) at a scientific meeting in the Netherlands. This was long before the PC, and given the more

primitive computers at that time, black dots were plotted on a white background, but it was an impressive accomplishment for the time.

Marcel Minnaert was at that meeting, and he celebrated the presentation as a 'handing over the torch" event. Indeed, over the next decade, Greenler and colleagues produced Monte Carlo computer simulations of many different ice crystal halos, and there are many (see Chapter 11) which he presented for the first time in his now classic book, ***Rainbows, Halos and Glories*** (1980).

Greenler's book is a tour de force, and an eye opener at the time of its publication. It has color photographs and explanations of many of the atmosphere's optical phenomena. Greenler travelled far (from the Arctic Ocean to the South Pole) in search of unusual phenomena, and if others had better photos, he used them. These phenomena he described and explained using his keen observational skill graced by love and enthusiasm but nary an equation. Great progress has been made since the book's publication, in no small part due to the enthusiasm Greenler helped waken in many.

Greenler's lead and the success of the numerical techniques solved on the computer were important factors in reviving interest in atmospheric optics, but the time was also right. In 1968 Alistair Fraser, who had just finished his Ph. D. thesis under advisor Richard Scorer, began to proselytize on behalf of the beauty of the atmosphere. His photographs of clouds and of optical phenomena graced the walls at the University of Washington and at the National Center for Atmospheric Research (NCAR) in Boulder, CO where they served as an inspiration to many.

Beginning in 1978, International Meetings on ***Light and Color in Nature*** have been held to serve as a forum for all aficionados of atmospheric optics. Much like storm chasers, optics enthusiasts circle the globe to capture their optical prey. Several of them have written books on various aspects of Atmospheric Optics, most with beautiful photos. The list with brief descriptions includes,

Walter Tape, rigorous in his approach and meticulous in his photography, wrote the two definitive books on halos, ***Atmospheric Halos***, Antarctic Research Series, Volume 64 (1994) and, with Jarmo Moilanen, ***Atmospheric Halos and the Search for Angle X*** (2006).

David Lynch, a polymath with an eye for seeing things almost everyone misses, wrote ***Color and Light in Nature*** (2001) with astronomer William Livingston. Gunther Konnen performed wonders in revealing the subtle aspects of ***Polarized Light in Nature*** (1985).

Claudia Hinz and Wolfgang Hinz worked and lived (much of the time for more than a decade) on a mountaintop meteorological observatory, gathering the most stunning photos and assembling them with descriptions and explanations (in German) in ***Lichtphäniomene: Farbspiele am Himmel*** (2015) and at https://www.haloblog.net/

Michael Vollmer, a master experimentalist and physics educator, wrote ***Atmosphärische Optik für Einsteiger: Lichtspiele in der Luft*** (2019), which translates to Atmospheric Optics for Beginners (but not beginners in German). Michael's latest book, ***Optics and Its Phenomena*** will soon be published in English.

Raymond L. Lee, Jr, an art history major turned scientist, collaborated with his mentor and former Ph. D. advisor, Alistair B Fraser, to write ***The Rainbow Bridge: Rainbows in Art, Myth, and Science*** (2001). Both these fine scientists rivet attention with bombastic lecture styles.

Craig Bohren, their prolific colleague, wrote, in addition to several technical books, two popular books on simple experiments that bring optics to light, ***Clouds in a Glass of Beer*** (1987) and ***What Light Through Yonder Window Breaks*** (1990).

Joseph Shaw, another master experimentalist and charismatic lecturer turned his plane windows into aerial laboratories in ***Optics in the Air: Observing Optical Phenomena Through Airplane Windows*** (2017).

Other scientists have put their works on the Web. British Philip Laven seamlessly matched his photographic quality simulations with actual

photos of coronas, iridescence and glories on his website, http://philiplaven.com/. Fellow Brit, Les Cowley designed and for over two decades ran the superb website, now (for the time being at least) at

https://www.atoptics.org.uk/

Frigid Finland has its own network of dedicated observers, active since the 1970's, and a host of unusual optical phenomena (e. g., complex halo displays, superior mirages, noctilucent clouds) to keep them outdoors in the most discomforting weather. Among these dedicated observer-scientist-photographers are

Marko Riikonen https://www.haloblog.net/
https://www.avaruus.fi/uutiset.html

Pekka Parviainen http://www.polarimage.fi/
https://twanight.org/profile/pekka-parviainen/confirmed-photos/

> **Jan**: "I can testify to discomforts, for example, photographing auroras at -40°C. One time, in the rush to adjust my camera for optimal framing I placed the cable release in my mouth. It froze to everything in my mouth and I was only able to free myself by ripping my skin."

With storm chasing, real danger replaces freezing skin and bones. Storm chasing, pioneered by Roger Jensen in 1953 and David Hoadley in 1956, took time to catch on, beginning as a serious profession and avocation about the same time that optics enthusiasts began their global jaunts. Joe Golden began his landmark study of waterspouts in September 1967 as the result of a chance encounter with a line of waterspouts during a flight in a private plane to Key West, FL. That experience led him to chasing, or more often hunting tornadoes, which in the early years proved elusive because so little was known about them and because meteorological data was inadequate and not timely.

Finally, tornado hunting hit paydirt. The massive Union City, OK Tornado of 24 May 1973, was a seminal event because it came within range of the National Severe Storms Doppler Radar system so that the storm, with all its warning signs, could be seen into through its life cycle. That tornado proved the value of storm chasing and of doppler radar for identifying developing tornadoes.

Other professional meteorologists formed the club of early Storm Chasers including Al Moller and Chuck Doswell III, whose website is laden with photos of severe storms and more,

https://www.flame.org/~cdoswell/

A few years later, Howard Bluestein, who was 4 years old when the 09 June 1953 Worcester, MA tornado struck his home town to create a lifelong memory and inspiration, began his eminent career in meteorology. Howie's book, ***Tornado Alley: Monster Storms of the Great Plains*** (1999) and video,

https://www.youtube.com/watch?v=hyEqVrHfHUQ

cover much of tornado science and chasing.

Tom Grazulis, who has been sleuthing tornadoes for decades penned his book, ***The Tornado: Nature's Ultimate Windstorm*** (2001)

These pioneers are among the leaders in the effort to piece together a comprehensive picture of supercell thunderstorms and their attendant features such as hail, downbursts, and tornadoes, and who have an uncanny instinct for being in the right place at the right time to see exceptional events.

The film, ***Twister*** (1996), inspired by early storm chasers and by Howie Bluestein's TOTO device to measure conditions inside tornadoes, unleashed the floodgates of storm chasing. Now, there are countless videos of severe storms with sometimes uncomfortable near collisions with tornadoes (or other storm chasers). Among the videos about severe thunderstorms storms and more on YouTube, those by Pecos Hank stand out. And a fine video on the history of storm chasing (with appropriate warnings has been put on the Web by Jacob Swegle,

https://www.youtube.com/watch?v=uRQ-nTTCazo

Let's not forget hurricanes, described and explained by Kerry Emanuel in his book, ***Divine Wind: The History and Science of Hurricanes*** (2005)! Other professional meteorologists, many from NOAA's Hurricane Research Division, became hurricane hunters, flying into the heart and through the eye of these fearsome storms beginning in 1943 to document their structure, evolution, and awesome beauty. Information about the decades of flights into hurricanes, including photos of cosmic-feeling scale appear on the website,

https://www.aoml.noaa.gov/data-products/#hurricanedata

All these adventurers, motivated by love of the power and beauty of the atmosphere, are heroes of sorts, and must be recognized for their dedication and persistence, involving themselves in discomfort and even danger to witness and record nature at her most spectacular.

We have been lucky and grateful to have joined in some of these adventures and to have had many of the abovementioned adventurers as colleagues and friends. Others too deserve more than the brief mentions we give them here in enriching our lives.

For Stan: In addition to the names mentioned above, Mentors and Professors Harold Stolov, Victor Starr, Jule Charney, Norman Phillips, Edward Lorenz, Earl Kindle, plus many others: Long-time friends, colleagues and collaborators William Donn, Al Ehrlich, Jerome Spar, Willard Pierson, Zev Levin, Shermane Austin, George Siscoe, Nambath Balachandran, James White, Dan Smiley, Steven Richards, Tony Gordon, Mary Brady, Paul Neiman, and especially Edward Hindman, and James Lawrence: In atmospheric optics, James Lock, Javier Hernandez Andres, John Adam, Charles Adler, and Jari Piiki: In hurricanes, Robert Burpee, Hugh Willoughby, Frank Marks, Michael Black, Peter Dodge, Jason Dunion and, John Gamache: At Weatherwise Magazine, Patrick Hughes, Jeffrey Rosenfeld, Kimbra Cutlip, Doyle Rice, Margaret Benner, and Robert Ryan: Student collaborators turned colleagues, Robert Rilling, Jeffrey Rosenbaum, Robert Arnold, Xiaoping Zhang, Elaine Lewis, and Kwan-yin Kong.

For Jan: Gerd Wendler, Carlyle Wash, Tony Bergantino, Nolan Doesken, Chris Daly, Don Day, Michael Hayes, Phil Pasteris, Stan Gedzelman, and Syun-Ichi Akasofu.

Then there are the (here) unnamed thousands of scientists who have explained the workings of the atmosphere, transformed weather forecasting to a science, and who have collected, analyzed, and dispensed data that we use throughout this book to document the atmospheric conditions for the photographs and videos.

Data sources we make frequent use of throughout the book include

Landsat Gallery:
https://landsat.visibleearth.nasa.gov/

Current Weather Data
https://www.weather.gov/
https://weather.rap.ucar.edu/

Soundings (vertical profiles)
https://www.spc.noaa.gov/exper/soundings/

Archived weather mostly North America
https://vortex.plymouth.edu/myowxp/

Weather maps and soundings based on computer model runs
https://www.ready.noaa.gov/HYSPLIT.php

NASA MODIS and other satellite images since 2000
https://worldview.earthdata.nasa.gov/

NOAA GOES 14-day Archive of Images plus Storms since 2019
https://www.star.nesdis.noaa.gov/GOES/index.php

With all that as background…Let's get going.

Wonders of the Atmosphere

Chapter 1: The Sun and Light

Fig. 1-1. The Sun seen through a smoke filled atmosphere from forest fires 20 minutes before sunset at Cheyenne, WY, 01 Aug 2021. JC.

Wonders of the Atmosphere
Chapter 1: The Sun and Light

1.1 The Sun's Output

All the wonders of the atmosphere – its colors, clouds, storms, rainbows, etc., even the atmosphere itself, start, and will end, with the Sun (Fig. 1-1) and its gift of light.

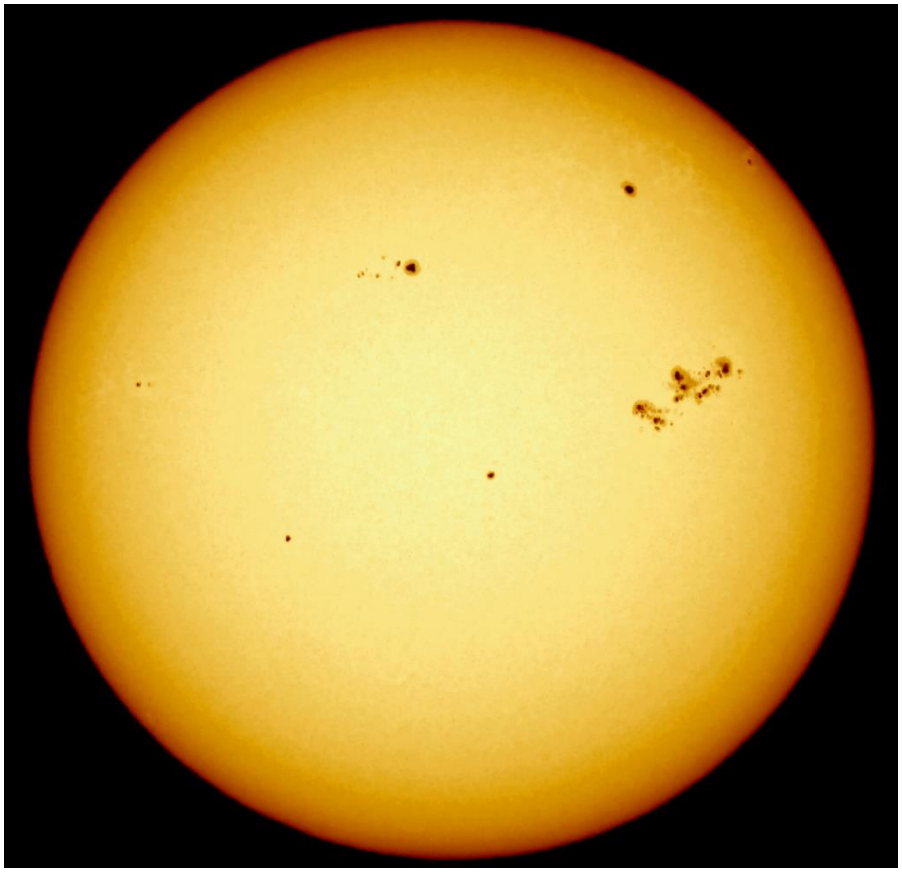

Fig. 1-2. The Sun showing sunspots and a red limb, 26 Mar 2024. JC.

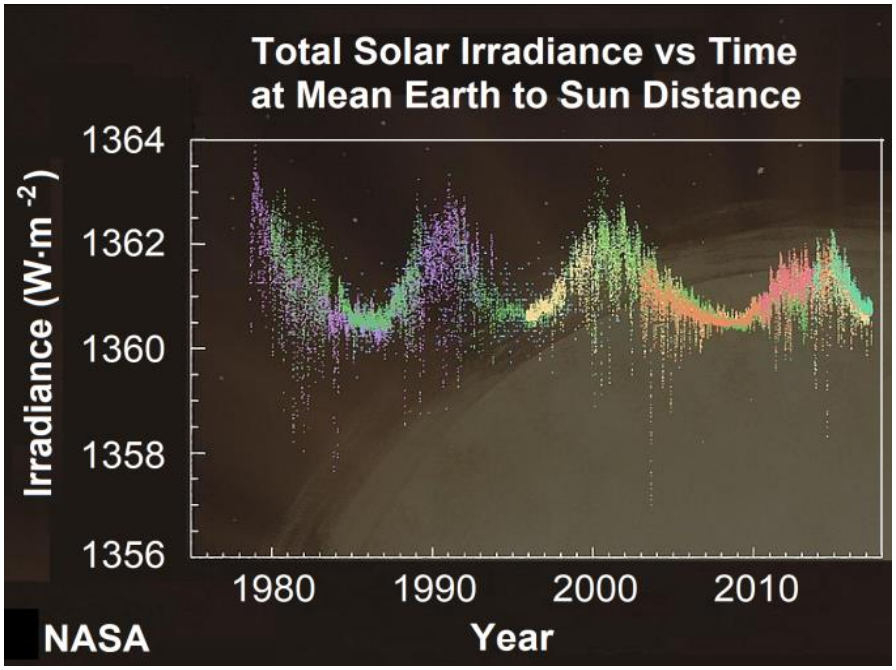

Fig. 1-3. Total Solar Irradiance vs time at mean Earth to Sun distance measured by seven NASA satellites.

Astronomers assure us that the Sun is a mediocre dwarf yellow star, blotched by sunspots some theologians would have denied (Fig. 1-2). We owe our existence to the Sun's mediocrity and to its near constancy. A much hotter, blue Sun would have burned out long ago, far too soon to allow life to evolve. It would have made Earth so hot the oceans would have boiled away and its excessive ultraviolet (UV) radiation would have proven lethal to life. A much smaller, cooler red Sun would have left Earth a frozen planet and its inadequate UV would not have had the energy to start and sustain life processes.

The Sun shines patiently with an average surface temperature of about 5750 K at an almost constant rate, as it has day after day (and night after night), and year after year, etc., etc., though it has slowly increased by 33% (and continues increasing) since settling down shortly after it and the rest of the Solar System formed some 4.6 billion years ago. That almost constant solar output is a requirement for us and for all life on Earth. Large variations in solar output would have alternately frozen and boiled away the atmosphere and oceans, and would have incinerated all life.

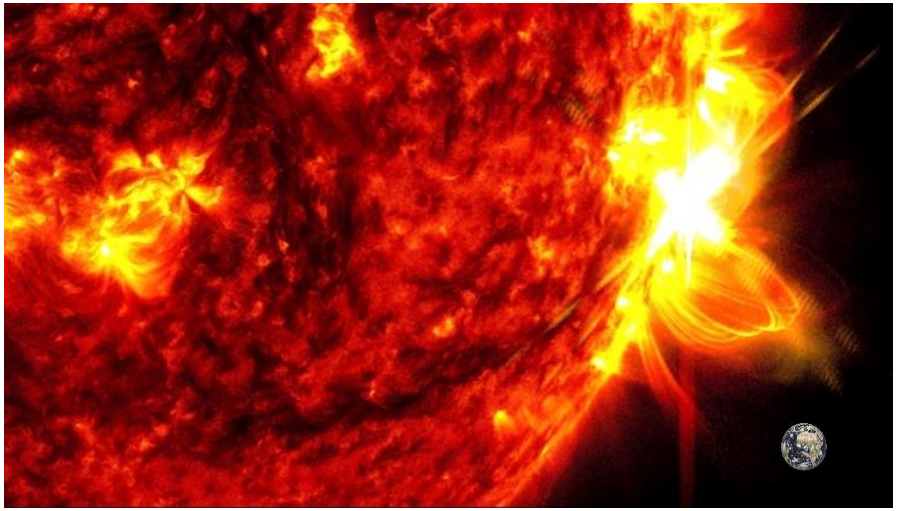

Fig. 1-4. Solar flare (white flash) of 14 May 2024 above Coronal Loops in extreme Ultraviolet. NASA/SDO. Earth shown by comparison.

The Sun's output, or irradiance, averages 1361 Watts per square meter (W/m^2) just before entering the atmosphere when Earth is at its mean distance to the Sun (149.5 million km) (Fig. 1-3). That is more than enough to power an average American household (1215 W).

The Sun's main variation of irradiance, a mere 2 W/m^2 (0.15%) occurs over the roughly 11-year sunspot cycle. The Solar Wind, the relentless outflow of protons and electrons, is another story. This flow increases greatly when Solar Flares erupt from the Sun's Corona. When these Coronal Mass Ejections aim toward us, Earth's magnetic field redirects some to the night side sky. There, the protons and electrons, spiral down and smash into the atmosphere where they spark auroras (Chapter 3). But even the most powerful Solar Flares, which are so large they dwarf the Earth (shown by comparison in Fig. 1-4), nudge solar irradiance by less than 0.2% and typically last less than an hour.

Auroras are an exception. All the atmosphere's other optical phenomena (except lightning) are produced when the Sun's light interacts with its molecules, aerosol particles, or hydrometeors (water or ice particles). Rainbows, halos, coronas, glories, and the light and colors of the sky and clouds result when the path of light is selectively absorbed (extinguished) or scattered (deflected). Scattering includes light not only spread like buckshot but highly directed by reflection, refraction, and diffraction. Let's consider these simpler processes, starting with reflection and refraction.

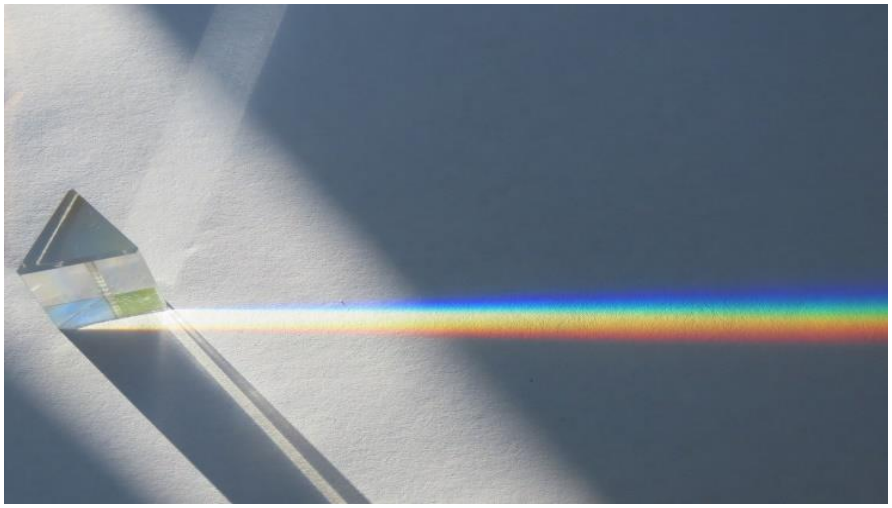

Fig. 1-5. A sunbeam striking a prism. Some light is reflected (e. g., toward upper right) and some is refracted into a spectrum. SDG.

1.2 Reflection and Refraction

When sunlight strikes a glass prism, some reflects and some bends or refracts abruptly as it enters and exits. (The fractions of reflected vs. refracted light, so important for rainbows and halos, are given by Fresnel's Law for water (see Fig. 9-17), and ice. Color hardly changes

for light reflected from a prism but the refracted light splits into a beautiful rainbow-like spectrum of colors that range in order from the least to most refracted, red, orange, yellow, green, blue, and violet (Fig. 1-5).

Raindrops and ice crystals are the atmosphere's prisms. Rainbows (Chapter 9) are the spectra produced when a veil of raindrops refracts and reflects sunlight. Halos (Chapter 11) are the spectra produced when a veil of ice crystals refracts and/or reflects sunlight.

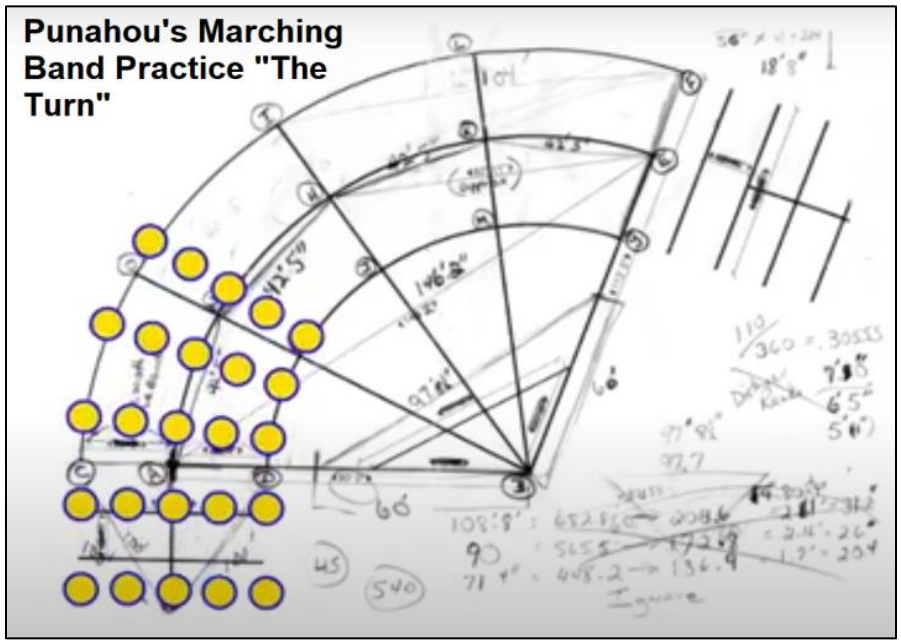

Fig. 1-6. Punahou's Marching Band practicing a turn illustrates refraction. Players on the outside of each line walk faster, making the line turn. https://www.youtube.com/watch?v=DGjfCVEg6qA

What causes refraction? In 1690, Christiaan Huygens showed that any wave refracts when one part of it moves more slowly than another. You can see this by videos of marching bands making a turn, or in Fig. 1-6, where each row of players or yellow circles represents a moving wave crest. The players on the outside of the turn must always move faster than those on the inside. Thus, ***Refracting waves always bend toward the region where they move more slowly***.

For example, water waves slow down as water gets shallower. When waves approach a shore obliquely, the parts of the waves nearest the shore in the shallowest water slow, so the waves refract more and more directly in towards shore. It was from observing ocean waves refracting as they approach the shore and comparing it to light refracting as it passed into and out of prisms that Huygens concluded that light consists of waves. Robert Hooke agreed, but Newton, his arch rival, didn't and this became the source of a great controversy. It would take more than a century to prove that light consists of waves.

In a vacuum, the speed of light is almost exactly 300 million meters per second (3×10^8 m·s^{-1}), but it is slower in all substances, which is why light bends or refracts when it enters a substance obliquely. Even in air, the speed of light is slower than in a vacuum, though only by about 0.03% at sea level. Refraction of light that travels between air and water is therefore almost the same as between a vacuum and water. Even so, light sometimes refracts enough in the atmosphere to cause mirages (see §2.8).

In water, the speed of light is about 2.25×10^8 m·s^{-1}, or about ¾ of its value in a vacuum or in air. Therefore, when light passes obliquely from air to water it slows markedly and refracts by a noticeable angle. In ice, the speed of light is slightly faster than in water, or about 2.29×10^8 m·s^{-1}, mostly because ice is less dense than water. In glass, the speed of light is only or about 2×10^8 m·s^{-1} or about ⅔ of its value in a vacuum. In diamond, the speed of light is about 1.24×10^8 m·s^{-1}, or only about 41% of its value in a vacuum. That is just about the slowest that light travels in any natural substance,

Sometimes it is easier (math-wise) to turn things up-side down. This is the case with refraction. The *index of refraction*, ***n***, measures how much faster light moves in a vacuum than in a substance. For example, since light travels through water about ¾ the speed it does in a vacuum it travels about 4/3 as fast in a vacuum than in water, so the index of

refraction of water, ***n***(H_20) ≈ 4/3 ≈ 1.33. *The larger the index of refraction of a substance the more light slows and therefore the more it bends on passing from a vacuum to the substance.*

The following inset contains just about the only equations in the book,

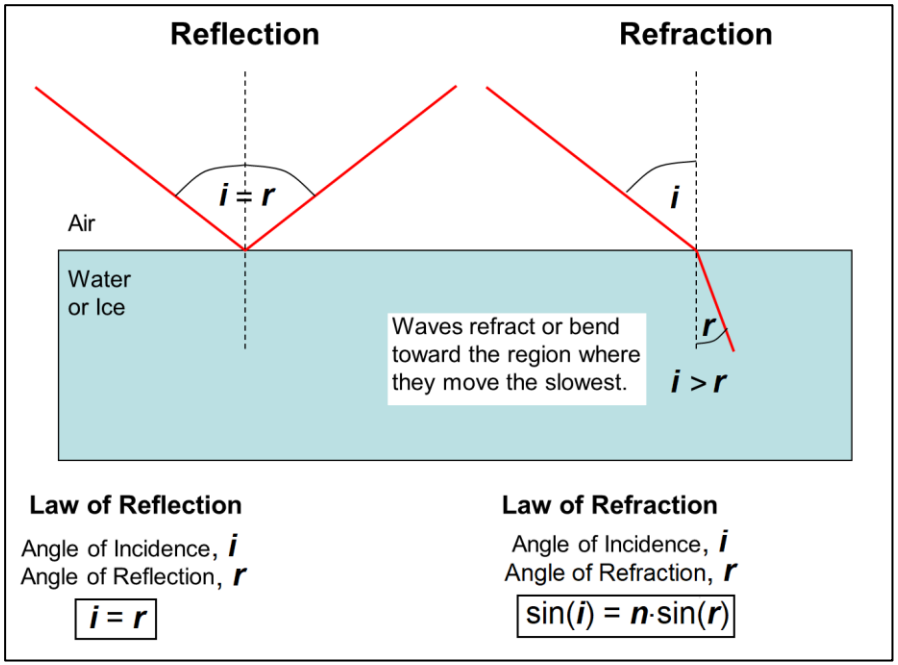

Fig. 1-7. Illustration of the Laws of Reflection and Refraction. SDG.

the laws of reflection and refraction, illustrated in Fig. 1-7.

The Law of Reflection, known even before Ancient times, is simply that the angle of reflection, ***r***, equals the angle of incidence, ***i***, or,

$$i = r$$

Snell's Law of Refraction, first discovered by Ibn Sahl in 984 CE, but rediscovered by Snell in 1621 is,

$$\sin(i) = n \cdot \sin(r)$$

Here, ***i*** is the angle of incidence in a vacuum, ***r*** is the angle of refraction in the substance, and ***n*** is the index of refraction of the substance.

Example 1: Light strikes water at ***i*** = 60°. Find the angle of refraction, ***r***, and the Deviation angle, ***D***.

For water, n ≈ 4/3 ≈ 1.333. To solve for angle ***r*** divide the Law of Refraction by ***n*** and then take the inverse sine.

$$\sin(r) = \frac{\sin(i)}{n} \approx \frac{\sin(60°)}{4/3} \approx 0.65 \rightarrow r \approx 40.5°$$

Light is deviated by the difference of the angles, ***D*** = ***i*** - ***r*** = 60° - 40.5° = 19.5°.

The deviation angle is important in locating optical phenomena such as rainbows, halos, and coronas (Chapters, 9, 11, and 14).

Example 2: If a light beam is aimed from water to air above the critical angle, r_{crit}, it will be totally internally reflected and not be able to enter the air. Find the critical angle for water.

Approach: At the critical angle, the light in air just grazes parallel to the water surface so, ***i*** = 90º. Therefore, from the Law of Refraction,

$$sin(r_{crit}) = \frac{3}{4} \times \sin(90°) \rightarrow r_{crit} \approx 48.6°$$

The critical angle limits the range of Sun elevation angles that can produce various ice crystal halos (see Chapter 11).

In each substance, the speed of light varies slightly with color, so that the angle of refraction varies with color. This variation, called *dispersion*, is the source of spectra. In most substances, including air, water, ice, glass, and diamond, the speed of light is slowest in violet light and fastest in red light. That is why violet light is refracted the most and red the least of the visible colors. In water, the speed of light

decreases from a maximum of about 2.254×10^8 m·s^{-1} in red light to a minimum of 2.240×10^8 m·s^{-1} in violet light. In other words, the index of refraction of water increases from $\boldsymbol{n}_{red} = 1.331$ to $\boldsymbol{n}_{violet} = 1.339$. (The index of refraction for ice increases from $\boldsymbol{n}_{red} = 1.307$ to $\boldsymbol{n}_{violet} = 1.317$.)

When, for example, a narrow beam of sunlight strikes water at an angle of $\boldsymbol{i} = 60°$ from vertical, the red light bends by as little as 19.41° while the deepest violet bends by up to 19.70°, a difference of only 0.29°. Because refraction occurs when light both enters and exits a prism, the spectrum that results is about twice as wide, or about 0.58°. Incidentally, the beautifully colored glints that you see when you turn a faceted diamond ring in sunlight are tiny bits of spectra resulting from dispersion. No surprise that the facets of diamonds are cut at angles to maximize this glitter.

It was from the spectra produced by glass prisms that Isaac Newton first gave us some understanding of the nature of colors hidden in sunlight. Here is how he described his discovery.

> In the beginning of the Year 1666…I procured me a Triangular glass-Prism, to try therewith the celebrated Phenomena of Colors…and made a small hole in my window-shuts, to let in a convenient quantity of the Suns light, I placed my Prisme at his entrance, that it might be thereby refracted to the opposite wall. It was at first a very pleasing divertissement, to view the vivid and intense colors produced thereby; but after a while…**I became surprised to see them in an oblong form**.

The spectrum's elongated, oblong form was the key that led Newton to his discoveries about the nature of light and color. Using a second prism or a lens, Newton showed that the oblong spectrum of colors could be recombined into a circle of white light but the individual colors could never be further separated (though each color could be widened). So each color was connected to a particular range of refraction angles.

Newton, of course, realized that raindrops act like prisms and wrote, "Why the Colors of the Rainbow appear in falling drops of Rain, is also from hence evident." This was just one of the many properties of light that he described in the 1672 letter, along with the many experiments that he performed and urged others to perform to duplicate and hence validate his findings. Newton also realized that the *dispersion*, or different refraction of each color of light through glass, was the source of chromatic aberration, which limited the accuracy of refracting telescopes. To eliminate this problem, Newton invented a reflecting telescope using a mirror shaped like a parabola because all colors of light obey the law of reflection, namely, they are reflected at the same angle they struck the mirror ($\boldsymbol{i} = \boldsymbol{r}$).

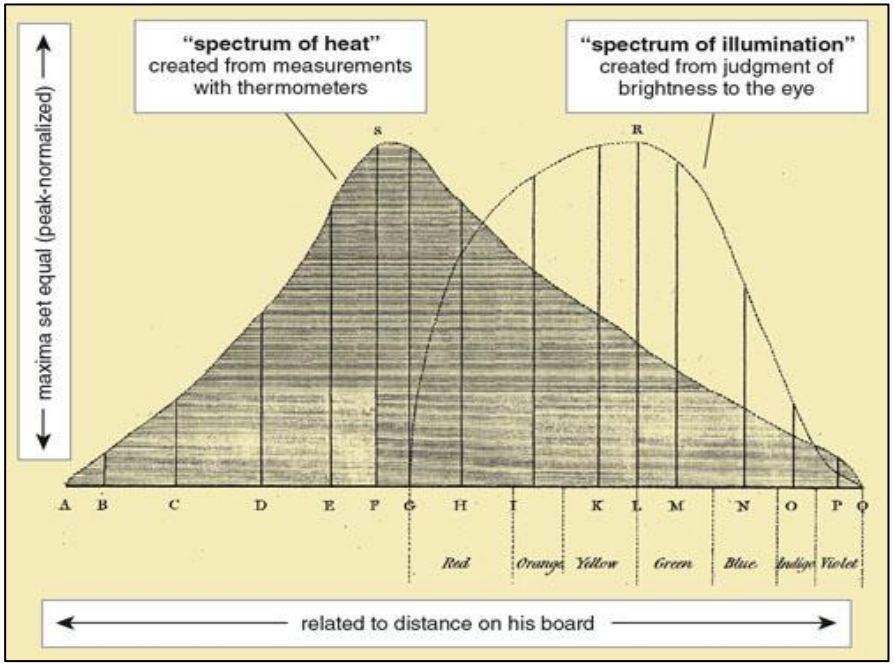

Fig. 1-8. Herschel's diagram illustrating the heating and the sensitivity of human vision as functions of the solar spectrum.

Incidentally, Newton's discovery of chromatic aberration led several people to design a compound lens made of two different kinds of glass to minimize chromatic aberration, naturally followed by a series of lawsuits over who was first.

Sir William Herschel made the next major advance on Newton's experiments with the refraction of sunlight. As an amateur astronomer (he was a professional musician and composer) whose many discoveries included double stars and the planet, Uranus, Herschel found the light blinding when he tried to examine sunspots. To mute the light he used filters of several different colors and noticed that while yellow *appeared* brighter red *felt* hotter.

That inspired Herschel in 1800, at the tender age of 61, to make the first attempt to measure the Sun's energy spectrum by measuring the temperature increase by placing one thermometer in the light of each color of the spectrum and noting how much warmer it was than a second thermometer in the dark part of the same room.

The warming increased through the visible spectrum from 1°C for violet light to almost 4°C for red light (Fig. 1-8). (Note: Because Herschel made his measurements when the Sun was only 29° above the horizon, the atmosphere had already scattered much of the violet and blue light out of the direct sunbeam and around the sky.) Current measurements of the irradiance of the solar spectrum both above the atmosphere and at sea level are shown in Fig. 1-9, and are compared to the theoretical curve (with spectral colors) derived by Max Planck in 1900 for a perfect radiator (black body) the same size as the Sun and at a temperature of 5750 K.

Because the warming increased continuously from violet to red, Herschel was inspired to move the thermometer to the dark region right next to the edge of the red light. Even though no light was visible, the warming peaked there at almost 8°F. He drew three original conclusions from these experiments, 1; The Sun emits what he jokingly called 'invisible light', and what we now call Infrared (IR) Radiation, 2: Light and Heat are both forms of radiant energy – just that our eyes are not designed to detect all forms of radiant energy and, 3: The human eye's sensitivity to color is greatest in the middle of the visible spectrum for yellow light and diminishes to zero at the violet and red ends of the spectrum.

Herschel also placed a thermometer just outside the violet region but did not detect any warming. A year later, in February, 1801, Johann Ritter exposed sensitive photographic paper beyond the violet end of the spectrum, which then turned from silvery to black. He thereby discovered Ultraviolet Radiation. Thus, ***visible light is just one part of the much larger spectrum of electromagnetic radiation***, which includes from short to long waves, X-Rays, Ultraviolet Radiation, Visible Light, Infrared Radiation, Microwaves, and Radio Waves.

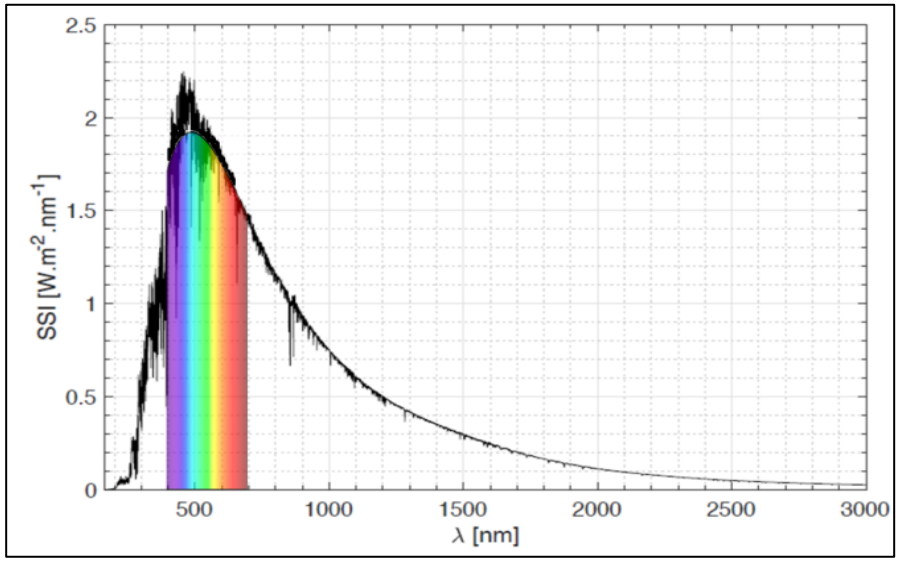

Fig. 1-9. Solar irradiance vs. wavelength above the atmosphere (black curve) vs. Black Body (Planck) irradiance at 5750 K for the visible light spectrum sandwiched between UV and IR radiation. European Space Agency.

1.3 Light Waves: Interference and Diffraction

When a rainbow appears in the sky a second bow often appears outside it. The outer or *secondary* bow is almost always fainter than the inner or *primary* bow, with colors in opposite order. In 1637, Descartes explained both the primary and secondary bows in terms of *geometric optics* – refraction, reflection and the circular cross section of

Fig. 1-10. Double rainbow with supernumerary bows (most pronounced on the left) inside the primary, Vail AZ, 21 Sep 2023. Supernumerary bows result from interference of light waves striking raindrops and are more pronounced the smaller and more uniform in size the drops. See Fig. 9-27. JC.

raindrops. But inside some primary bows, as in Fig. 1-10, are extra, pastel color bands called *supernumerary rainbows* (see §9.5) that cannot be explained using geometric optics because they result from the interference of light waves emerging from small raindrops.

Coronas (Chapter 14), the rings of colored light that appear around the Sun or Moon in thin, often smooth-edged clouds, also can only be explained in terms of light waves. Indeed, it was the corona, or 'Crowns of Colors' that Newton acknowledged in the first page of his classic Treatise, ***Optics*** (1704) he was unable to explain.

> The Crowns of Colors, which sometimes appear about the Sun and Moon, I have endeavored to give an Account of; but for want of sufficient Observations leave that Matter to be farther examined.

That's not all. In the next sentence Newton mentioned another phenomenon he could not explain.

> The Subject of the Third Book I have also left imperfect, not having tried all the Experiments which I intended when I was about these Matters, nor repeated some of those which I did try, until I had satisfied my self about all their Circumstances. To

communicate what I have tried, and leave the rest to others for farther Enquiry is all my Design in publishing these Papers.

That subject, described by Francesco Grimaldi and published in 1665, two years after he died, was the widening of the shadow and the color bands that appear through a pinhole of sunlight.

Grimaldo has informed us, that if a beam of the Sun's Light be let into a dark Room through a very small hole, the Shadows of things in this Light will be larger than they ought to be if the Rays went on by the Bodies in straight Lines, and that these Shadows have three parallel Fringes, Bands or Ranks of colored Light adjacent to them.

Fig. 1-11. Waves diffracting around both sides of a dock. SDG.

Both of these phenomena result from the wave nature of light, a conclusion that Newton did not accept. There are two main reasons it took scientists so long to prove that light consists of waves. First, whereas we can see water waves and watch their behavior, we cannot see light waves, we can only see light and color. Second, light waves are very short (too short to see) and this made it difficult to devise experiments about light waves.

Since we can see water waves and observe their behavior, we use them to illustrate two related wave phenomena – Interference and Diffraction. Interference is the adding or subtracting of waves from two or more sources. Diffraction is the curving of waves around a barrier. Fig. 1-11 shows waves curving or diffracting into the lee of a floating dock for kayaks.

When particles such as bullets pass through a narrow opening, they continue to travel in straight lines. That is not possible for waves. If waves did not spread when they passed through narrow openings impossible discontinuities of height for water waves, (Fig. 1-12), pressure for sound waves, and electromagnetic field for light waves would result.

Interference is also easy to illustrate with water waves. In the top photo of Fig. 1-13 a single, continuous train waves was made in a calm lake by dipping one cup into and out of the water at the edge of a dock with a frequency of about twice a second. With only one wave train there was no interference.

In the bottom photo of Fig. 1-13 two intersecting wave trains were produced by dipping two cups about 3 feet apart with the same frequency. The two interfering wave trains produce a pattern of alternating wavy bands where the crests and troughs from each train coincide to reinforce each other (constructive interference) and flat bands where the crests of one train coincide with the troughs of the other to cancel each other (destructive interference).

Newton was well aware of these patterns in water waves but did not think they applied to light. In his 1672 letter, he stressed that although he had indeed found many *properties* of light, and though he thought that it consisted of some type of corpuscles and recognized it had undulatory properties, he acknowledged that he remained in the dark regarding the *nature* of light, and the wondrous process by which our eyes and brains transform light into the beauty of the colors.

But, to determine more absolutely, what Light is, after what manner refracted, and by what modes or actions it produces in our minds the Phantasms of Colors, is not so easy. *And I shall not mingle conjectures with certainties.*

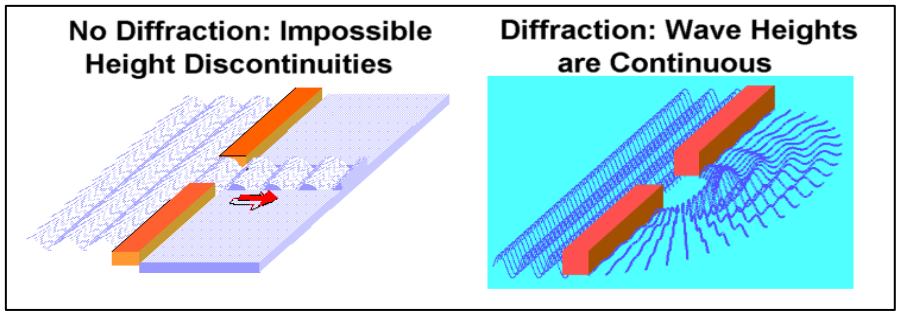

Fig. 1-12. Water waves passing through an opening. Waves that don't spread cause impossible height discontinuities (left). Therefore waves must spread or diffract (right). SDG.

But, in fact, Newton did conjecture that light consists of some form of corpuscles and for more than a century most scientists elevated Newton's conjecture to an almost inviolable doctrine.

Thomas Young therefore exhibited courage as well as insight when he went beyond conjecture to override doctrine. Trained as a physician, Young was fascinated by how we perceive light and sound. He was well aware of diffraction and interference of water waves, of beats caused by two different frequencies of sound waves and, of the problems attempting to explain supernumerary rainbows. Guessing that light consists of waves, he devised an experiment to prove it. In May, 1801 he demonstrated that each color of the spectrum consists of waves with a unique wavelength. The final form was the double slit experiment (Fig. 1-14), in which, 1: a narrow beam of sunlight is sent into a dark room, 2: passes through a prism, then, 3: through a narrow slit allowing only one color from the spectrum through, continues, 4: through two close parallel slits and finally, 5: onto a screen.

If light consisted only of beams of particles the screen would have shown two narrow bright beams. But instead, it showed a wide,

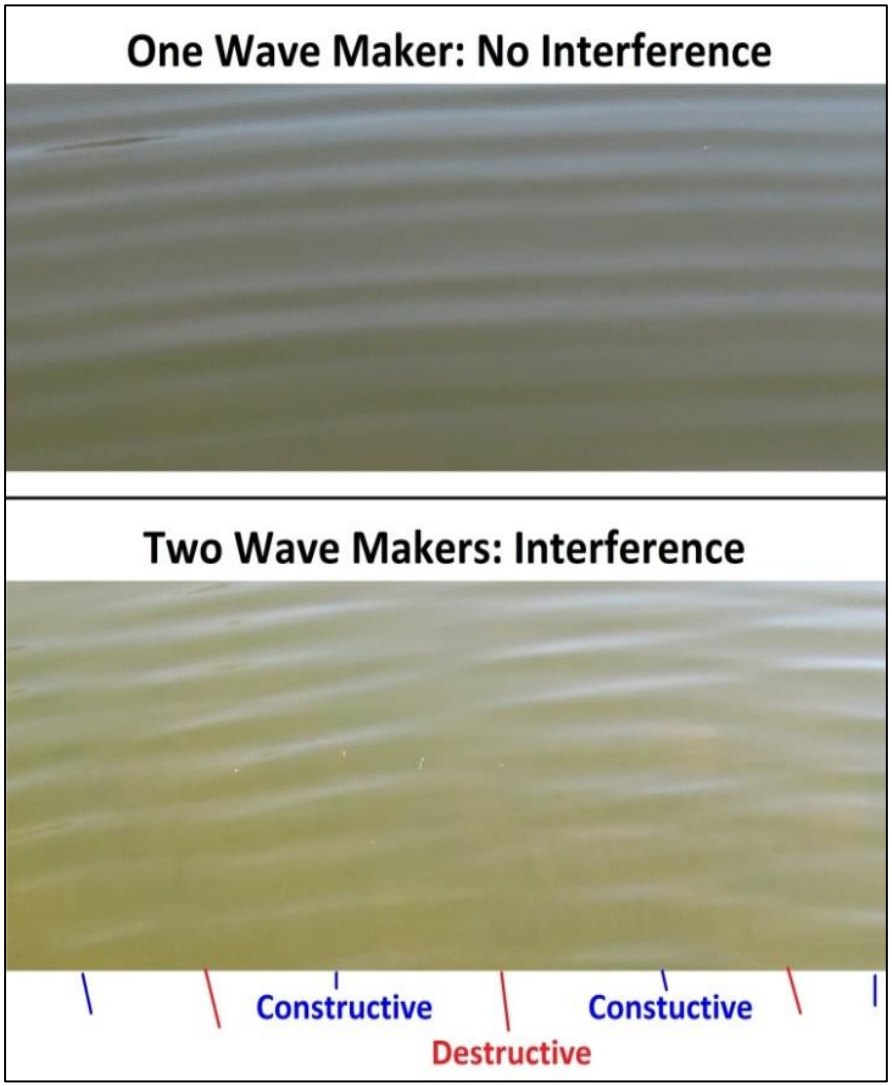

Fig. 1-13. Wave trains produced by repeatedly dipping one cup (top) and two cups (bottom) in a calm lake. In the bottom photo calm and wavy bands alternate as the result of interference. SDG.

spreading pattern of alternating light and dark bands that could only have been caused by the diffraction (spreading) and interference of a wave train from each of the slits as they crossed paths, either adding or cancelling each other.

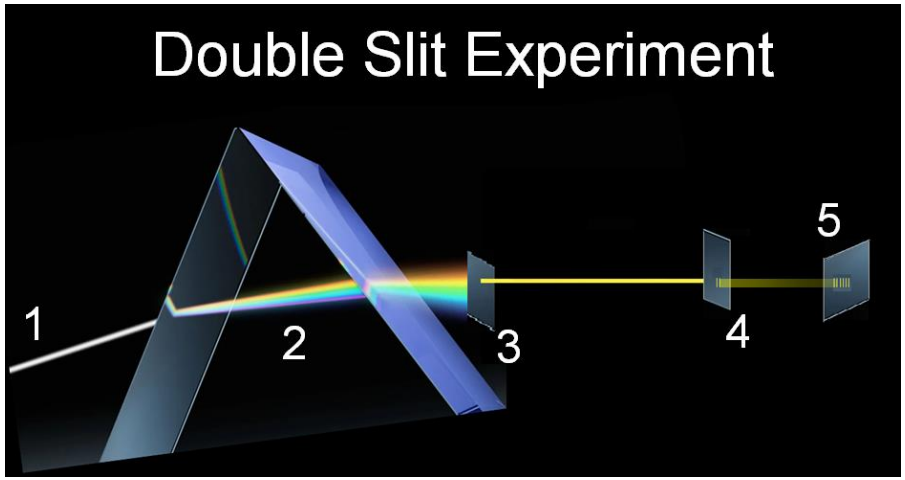

Fig. 1-14. Young's double slit experiment. When a narrow beam of one color of sunlight passes through two close parallel slits it produces a banded pattern of light, proving light consists of waves. SDG.

Because the diffraction pattern (the spacing of the bands) is a unique function of the 1: known distance between the slits, 2: known distance from the slits to the screen, 3: known spacing of the bands, and, 4: wavelength of the light (the only unknown), Young was able to calculate the wavelength of each color of light in the spectrum from violet, the shortest waves of visible radiation (as short as 0.4 micrometers) to red, the longest (as long as 0.7 micrometers). Since a *micro*meter is one millionth of a meter that means that there are 2.5 million waves of short violet packed in every meter of a light beam.

Since the speed of light in a vacuum is almost exactly 300 million meters per second ($\approx 2.998\times10^8$ m/s), 7.5×10^{14} or 750 trillion violet light waves pass by every second. That is a frequency of 750 terahertz (trillions of cycles per second). The longer the wavelength of light, or properly electromagnetic radiation, the fewer waves pass by each second so the lower the frequency. Thus, FM and even longer AM radio waves, both much longer than light waves, have lower frequencies measured respectively in millions (megahertz) and thousands (kilohertz) of waves or cycles per second.

An extraordinary follow-up to Young's double slit experiment occurred some 125 years later, when a beam of electrons was aimed at a double slit and produced a diffraction pattern. That proved that not only are electrons particles, they are waves as well. Some twenty years earlier, in 1905, Einstein proved that the photoelectric effect showed that light has properties of particles (called *photons*) as well as waves. Together they comprise the so-called wave-particle duality that adds to the wondrous and sometimes exquisite nature of reality.

1.4 Light Waves: Scattering

The brightness and colors of all the atmosphere's optical phenomena start with the visible light spectrum of the Sun and arise because scattering and absorption vary with the wavelength of light, the relative size of the scattering particle and the angle light is scattered.

The word, scattering may create the mistaken impression that it is chaotic. No chaotic process could produce the coherent range of sky colors and precisely patterned rainbows, halos, and coronas.

Scattering is the general term for all the processes that occur when light strikes an object such as a raindrop or a medium such as air or water. These processes include transmission, reflection, refraction, diffraction, scattering in all directions, and absorption (extinction).

Scattering is governed by Maxwell's Equations of Electrodynamics, whose mathematical solution depends on the nature, shape, and size of the particles. The math is complicated but, lo and behold, Ludvig Lorenz in 1890 and Gustav Mie in 1908 independently derived the all-encompassing solution for scattering of light by spheres. While Lorenz's work was overlooked, Mie's got instant recognition, so now we usually call the solution *Mie Scattering*.

Mie Scattering comes with bad news and good news. The bad news is that 1: even for spheres, the simplest geometric form, the math is extremely long and complicated, and, 2: it provides little physical

insight. The good news is that, 1: air molecules, cloud droplets, and raindrops are close to spheres, 2: computer codes have been written to produce photorealistic images of sky color, coronas, rainbows, halos, etc. and, 3: simple scattering processes, such as reflection and refraction, dominate over large ranges of particle size (Fig 1-15).

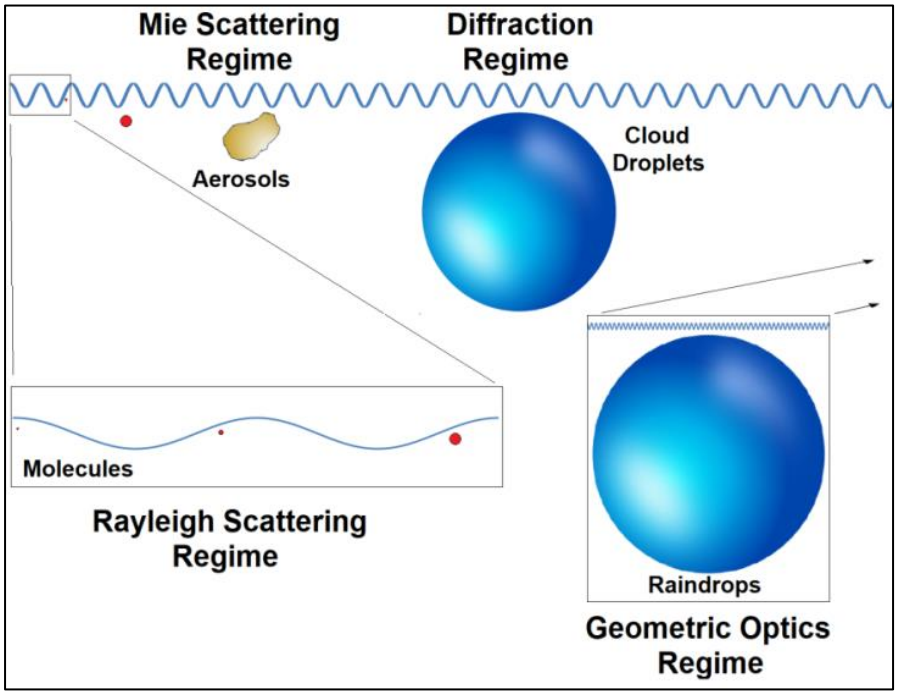

Fig. 1-15. Regimes of scattering processes as a function of the particle size relative to the wavelength of light. SDG.

Particles that are tiny compared to the wavelength of light, such as air molecules with diameters less than 1/1000th the wavelength of light, scatter light very inefficiently but obey a simplified law called Rayleigh scattering, by which scattering efficiency is *inversely* proportional to the 4th power of the wavelength. Many features of the light and color of the sky with a molecular atmosphere can be explained in terms of Rayleigh scattering (Chapter 2).

Scattering is most complicated when the particle size is comparable to the wavelength of light. This is the case for the smallest cloud droplets and ice crystals, which can produce cloud iridescence. It is also the case for small aerosol particles, which because of their varied shape and chemistry are near impossible to solve. In the atmosphere, the dominant impact of aerosols is to bleach the sky and increase haziness, and alter the global climate in complex ways that torment climate scientists.

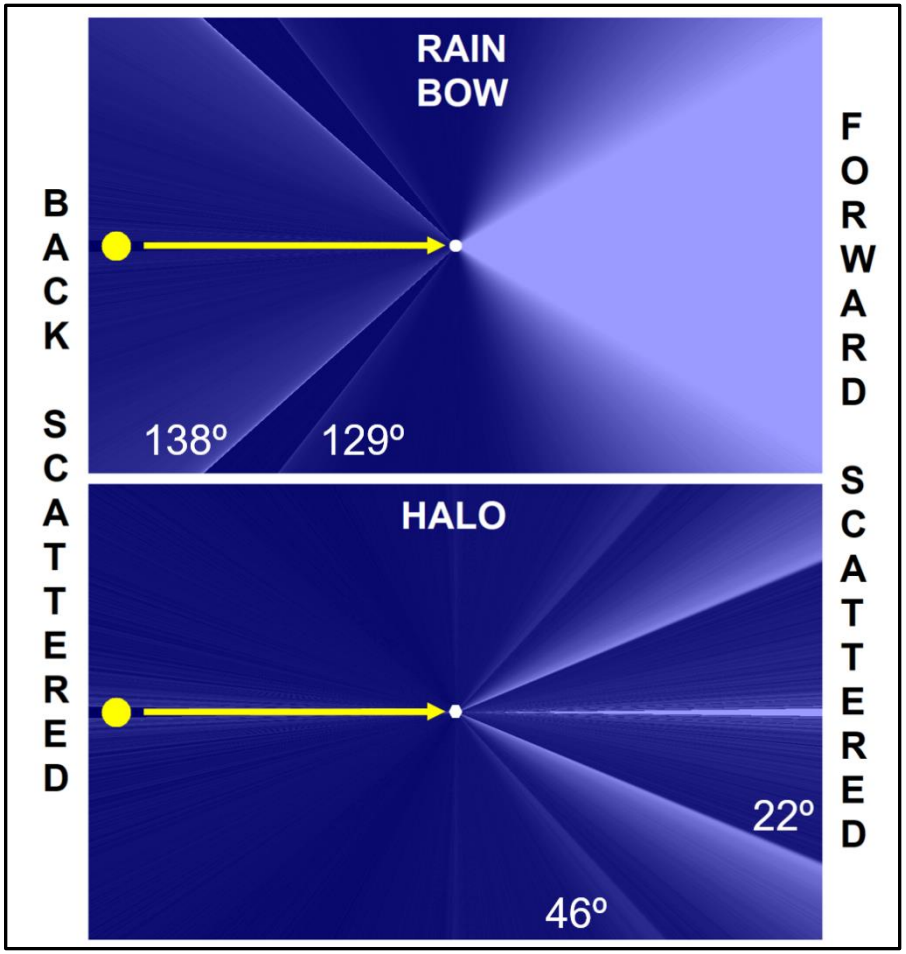

Fig. 1-16. Angular variation of brightness of scattered light for large raindrops (top) and hexagonal ice crystals (bottom) showing distinct backscattered peaks for rainbows and forward scattered peaks for halos. Yellow circle is Sun. SDG.

Diffraction represents an accurate approximation for scattering by particles from about 10 to 200 times the length of light. Cloud droplets and small ice crystals fall in this size range. Diffraction phenomena include coronas (Chapter 14) and supernumerary rainbows (Chapter 9).

Geometric optics (refraction and reflection) accurately describes scattering by large particles, at least 500 or so times longer than light waves, such as raindrops and many ice crystals. It therefore explains many features of rainbows (Chapter 9) and ice crystal halos (Chapter 11). Fig. 1-16 shows the relative brightness of light scattered by large spherical raindrops (top frame) and by tumbling thick hexagonal plate ice crystals (bottom frame) as a function of the angle of scattering. Peak brightness for both raindrops and ice crystals occurs for light scattered forward by small angles, which means that they brighten the sky right around the Sun.

Rainbows and halos in Fig. 1-16 correspond to the distinct peaks of brightness further from the Sun. For scattering by raindrops, the distinct peaks occur 138º away from the Sun for the primary rainbow and 129º away from the Sun for the much fainter secondary rainbow. For scattering by ice crystals, the distinct halo peaks occur 22º and 46º away from the Sun.

The busy Fig. 1-17 serves as a master diagram of scattering for the atmospheric optical phenomena. It shows the relative intensity of scattered light vs the deflection or scattering angle and the optical phenomena produced for air molecules (**blue**), cloud droplets with radius, r_{DROP} = 8 μm (**green**), large spherical raindrops (**red**), randomly oriented thick ice crystal plates (**black**), and horizontally oriented thin pencil ice crystals when the Sun is overhead (**purple**).

Most of the scattering curves in Fig. 1-17 have pronounced peaks, which correspond to specific optical phenomena. Particles that are tiny compared to the wavelength of light, such as air molecules (**blue curve**), have no pronounced peaks. They scatter light with almost constant intensity in all directions, and are responsible for the light and color of the clear sky (Chapter 2).

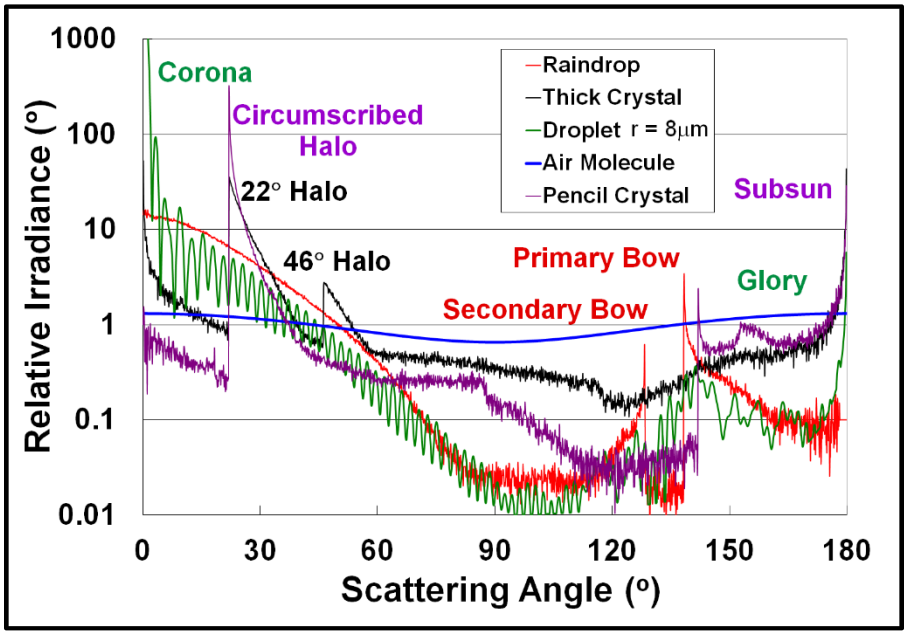

Fig. 1-17. Scattering intensity vs angle for air molecules (blue), cloud droplets (green), raindrops (red), tumbling thick ice crystal plates (black), and thin, horizontal ice crystals (purple). Peaks in intensity correspond to optical phenomena labelled in Figure and in text. SDG.

Particles that are similar in size or somewhat larger than the wavelength of light, such as cloud droplets (**green curve**) or aerosol particles, scatter most light by small angles (forward scattering), which is why the sky is blinding bright around the Sun whenever it is hazy or when thin clouds are near the Sun.

The multitude of regular waves in the scattering curve of light with wavelength, λ = 0.55 μm by spherical cloud droplets of radius, r_{DROP} = 8 μm correspond to coronas and iridescence near the Sun and glories opposite the Sun (Chapter 14). Aerosol particles of the same size would have pronounced forward scattering peaks but due to their irregular shapes would not have the neatly organized waves. Thus, they would not produce brilliant coronas or iridescence near the Sun but would simply glare with a blinding brightness (Chapter 2).

Raindrops (**red curve**) also have a pronounced forward scattering peak because much light passes through the drops with small deflection. That however is of much less interest to optics lovers than the two scattering peaks for raindrops at 138º and 129º (as we have just seen in Fig. 1-16), which correspond to the primary and secondary rainbows (Chapter 9).

The two peaks for randomly oriented thick hexagonal plate-shaped ice crystals (**black curve**) correspond to circular halos, 22º and 46° from the Sun (as we have also seen in Fig. 1-16). Because ice crystals are basically hexagonal and not spherical, variations of their shape and orientation give rise to a multitude of halos (Chapter 11), some which have peaks of much greater irradiance in certain directions than for the randomly oriented crystals. Thus, for example, when the Sun is at the zenith, long pencil crystals (**purple curve**), that fall horizontally, produce a circumscribed halo that coincides with the 22° halo, but is 8 times brighter and narrower than it. And, when the Sun is low in the sky, horizontally falling thin plate crystals produce a blinding bright subsun in the clouds below.

Fig. 1-18. A hawk flies across the Sun. 21 Aug 2020. JC.

Skylight both taints and forms the background in which all these shining optical phenomena appear. So, next, let's see what happens to sunlight as it passes through clear air.

Wonders of the Atmosphere
Chapter 2: The Clear Atmosphere: Sky Colors and Mirages

Fig. 2-1. Into the Blue. Hot air balloons rise into a clear blue morning sky as part of the Great Reno Balloon Race at Reno, NV, 6 Sep 2014. SDG.

Fig. 2-2. Twilight sky 55 minutes before sunrise over Cheyenne, WY, 29 Jun 2019. JC.

Fig. 2-3. The other side of Twilight: Earth's Shadow with rising full Moon in the Belt of Venus over Cheyenne, WY, 21 Nov 2018. JC.

Wonders of the Atmosphere
Chapter 2: The Clear Atmosphere: Sky Colors and Mirages

2.1 The Colorful Canopy of Atmosphere

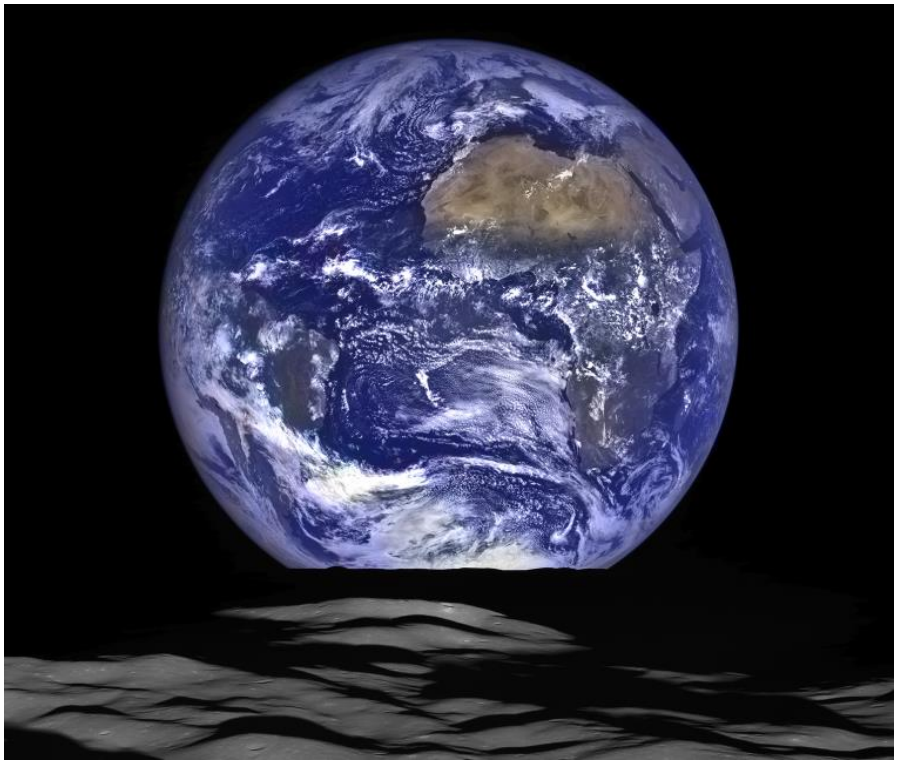

Fig. 2-4. View of Earth in the black sky over the Moon on Oct 12, 2015. NASA/GSFC/Arizona State University.

The clear blue sky of morning provided a beautiful backdrop for the Great Reno Balloon Race of 2014 (Fig. 2-1). "**Why *is* the sky blue**?"

At the 2nd International Conference on Light and Color (1984) Bob Greenler presented a demonstration that suggested how the colors of the sky and the Sun arise. In a darkened room, he shone a circular light beam from a projector through a tank of clear water and onto a screen. The beam made a bright white circle on the screen. Then, drop-by-drop he added skim milk to the water. As the milky water brightened, the circle of light on the screen dimmed. Soon though, colors emerged. The milky water turned pale blue (somewhat like the sky) and as it did the circle of light on the screen turned orange (like the Sun at sunset).

"I've just made a sunset," said Bob, "and if you're not quite convinced…" At that precise moment, Bob simultaneously turned off the projector with the beam and turned on a second projector, with a photograph of the setting Sun on the screen that coincided with and matched the orange circle perfectly.

This experiment provokes a question. How can adding white skim milk to pure water produce both blue and orange without a chemical reaction simply by shining a white light through it?

Let's go back in time. The first serious attempt to explain why the sky is blue was given by none other than Leonardo da Vinci, who noted,

> "**that the blueness we see in the atmosphere is not intrinsic color**…. as an illustration of the color of the atmosphere I will mention the smoke of old and dry wood, which, as it comes out of a chimney, appears to turn very blue, when seen between the eye and the dark distance. But as it rises, and comes between the eye and the bright atmosphere, it at once shows of an ashy grey color" ***Theory of Colors***.

Leonardo wrote this at least 150 years before Newton discovered that white light is a mixture of all the colors of the spectrum. Over 150 years after Newton's discovery John Tyndall, in 1869, made a similar observation with fuller understanding of the nature of light and color.

"On windless days [in Killarney] the columns of smoke rose above the roofs of the cottages. The lower part of each column was shown up by a dark background of pines, the top part by the light background of clouds. The former was blue because it was mainly seen through dispersed light the latter was reddish because it was seen through transmitted light.

Fig. 2-5. As the blue atmospheric canopy thins to the vacuum of space, it tints only the bottom of the Moon blue, 08 Aug, 2001. NASA ISS002.

Tyndall stood on the doorstep of explaining why the sky is blue. He correctly distinguished between light that is transmitted and light that is scattered (he called it dispersed). Thus, the sky is blue because of a form of color segregation in the atmosphere. Blue light is more likely to be scattered in all directions in the atmosphere while red light is more likely to be transmitted through the atmosphere. Tyndall, a great experimental scientist, 'prequelled' Greenler's demonstration. He shone a light through a glass tube, which he slowly filled with smoke and noted that the smoke turned blue and the light that penetrated dimmed and turned red. But Tyndall drew the wrong conclusion. He thought that aerosols were the atmosphere's scattering particles. Also, he couldn't explain why blue was scattered and red transmitted.

Two years later, beginning in 1871, Lord Rayleigh proved that the sky is blue due to preferential scattering of short light waves by air molecules by deriving the law for what we now call Rayleigh scattering in his honor (see §2.3). He also proved that aerosols and other larger particles reduce the blue (see §2. 6).

Fig. 2-6. Left: The clear sky over the Grand Canyon, AZ, 01 Apr 2001. Right: Same photo except with a vertical stripe of sky up-side-down. SDG.

Using Rayleigh scattering, we can also explain the varied colors of the twilight skies both toward (Fig. 2-2) and opposite (Fig. 2-3) the Sun, and why the sky on the Moon is black (Fig 2-4).

The sky on the Moon is always black because there is nothing, no air, no clouds, no dust to scatter the sunlight. As a result, sunlight blazes right to the Moon's surface with a brilliance and intensity and stark contrast with the black sky that shocked the Astronauts who landed there even though they knew what to expect before landing.

The great canopy of atmosphere that the Earth drags along as it whirls through the vacuum of Space (Fig. 2-5) is responsible for the all the optical phenomena we see in the sky, starting with the multicolored sky itself. Cloud cover turns it gray, smoke from forest fires turns it red, and twilight gives birth to a whole range of sky colors. At every single moment, color varies over the entire sky.

Even on the clearest day the deep blue sky overhead grades to almost white at the horizon, as in Fig. 2-6, where a vertical strip of sky over the Grand Canyon has been has been turned up-side down in the twin photo on the right to emphasize how pronounced the normal vertical gradation of sky color is, and how we normally don't even notice it.

2.2 Molecular Atmosphere: Rayleigh Scattering

Rayleigh scattering applies to particles that are tiny compared to the length of light waves, such as air molecules. The diameters of Nitrogen (N_2), Oxygen (O_2), Argon (Ar), and Water Vapor (H_2O), which constitute 99.96% of all air molecules, are, respectively 0.346, 0.364, 0.196, and 0.265 nm (nanometers or billionths of a meter). All are less than one thousandth the shortest wave of visible light (400 nm = 0.4 μm micrometers or millionths of a meter).

The law of Rayleigh scattering states that a tiny particle of a given size scatters light with efficiency *inversely* proportional to the 4^{th} power of the wavelength. For example, when wavelength doubles tiny particles scatter only $(½)^4 = {}^1/_{16}{}^{th}$ as efficiently.

Therefore, air molecules scatter violet light with up to $(7/4)^4 \approx 9.4$ times the efficiency they scatter red light. As a result, whereas sunlight peaks in the middle of the visible light spectrum, skylight is a highly selective mixture that decreases with increasing wavelength, hence successively less violet, blue, green, yellow, orange, and red (Fig. 2-7). Combining this mixture with the sensitivity of the human eye, which is greatest in the middle of the visible light spectrum, and the daytime sky we see is blue.

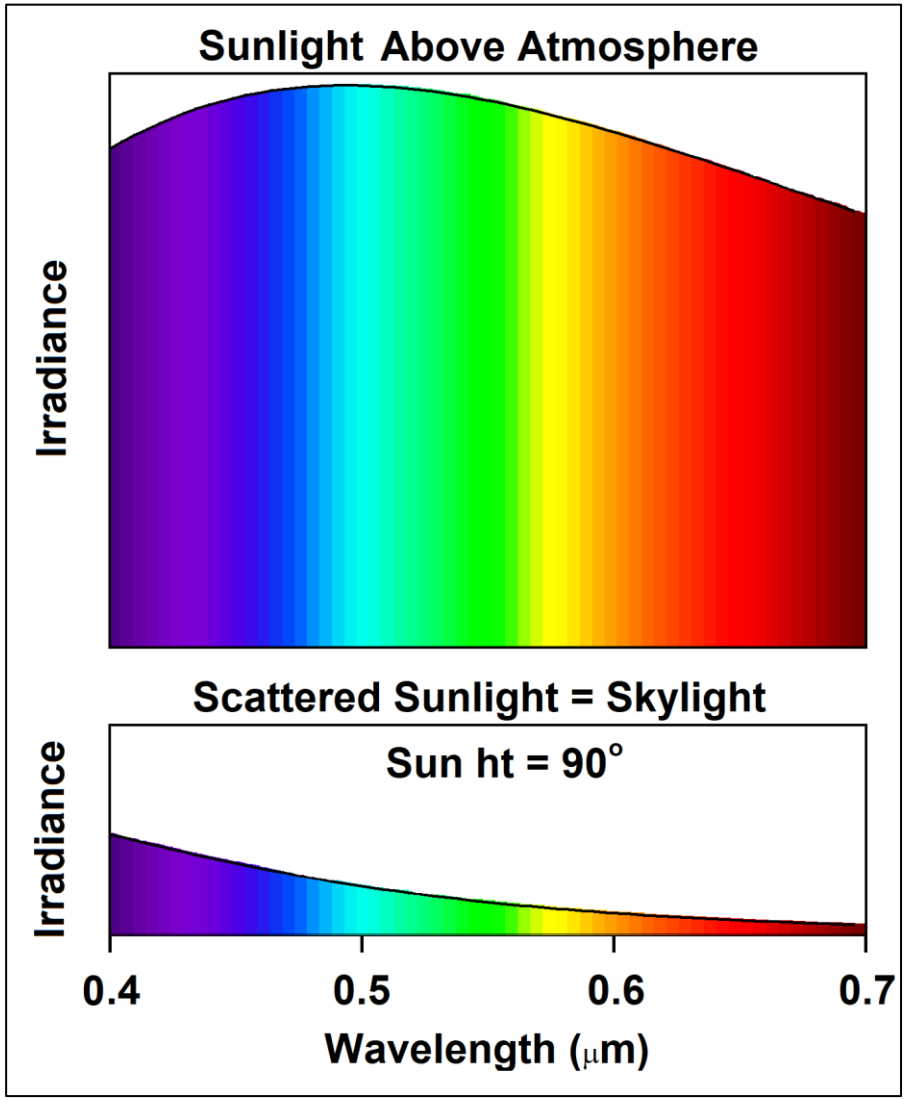

Fig. 2-7. Top: Black Body Irradiance at 5750 K approximates sunlight atop the atmosphere. Bottom: Skylight scattered from a sunbeam reaching sea level when the Sun is at the zenith. SDG.

Rayleigh scattering doesn't quit at night. It also works by the light of the silvery Moon, turning the night sky as blue as the daytime sky,

Fig. 2-8. The sky at night with a full Moon over Cheyenne, WY, 0330 MDT, 27 June 2021. JC.

though only ≈ 1/400,000th as bright when the Moon is full, which is why we can't see it. But with a long enough exposure, photographs reveal its color (Fig. 2-8).

So, when someone asks,

Question 1: "Why is the sky blue?"

The simple answer is,

"Rayleigh scattering!"

But what if someone asks the next logical question,

Question 2: "Why do the Sun and Moon turn orange or red at the horizon (Fig. 2-9)?"

Then the simple answer is,

Fig. 2-9. Moonrise sequence 13 Oct 2019 at 2½ minute intervals. The closer the Moon to the horizon the redder, and dimmer it appears. JC.

"*More* Rayleigh scattering!"

That is because Rayleigh scattering both giveth and taketh.

Imagine a photon of light 'trying' to get through the atmosphere but forced to run a gauntlet of molecules armed with paddles. Each time a paddle hits the photon it scatters it in some other direction, so that it becomes skylight. Rayleigh scattering means that long (red) photons are better at evading the paddles than short (blue) photons, so they travel further before being hit (scattered).

In a tenuous atmosphere, such as on Mars, with few molecules and paddles, almost all photons get through, so the color of the Sun or Moon is scarcely altered. Most of few photons that get hit and scattered are blue, as in the bottom panel of Fig. 2-7. Hence the sky is blue.

Fig. 2-10. Earth's wafer-thin atmosphere at sunrise, 25 Nov 2009. The sky fades to black above about 50 km, though the atmosphere exists and continues thinning for several thousand km. NASA.

In a thick atmosphere such as on Venus, a furnace with a surface temperature of 465°C and a surface pressure 90 times that at sea level on Earth, even if it were clear and not cloud-covered, with many molecules and paddles, very few photons get directly through without being hit, and most of the photons that get through are red. Hence the Sun or Moon would be dim and turn red.

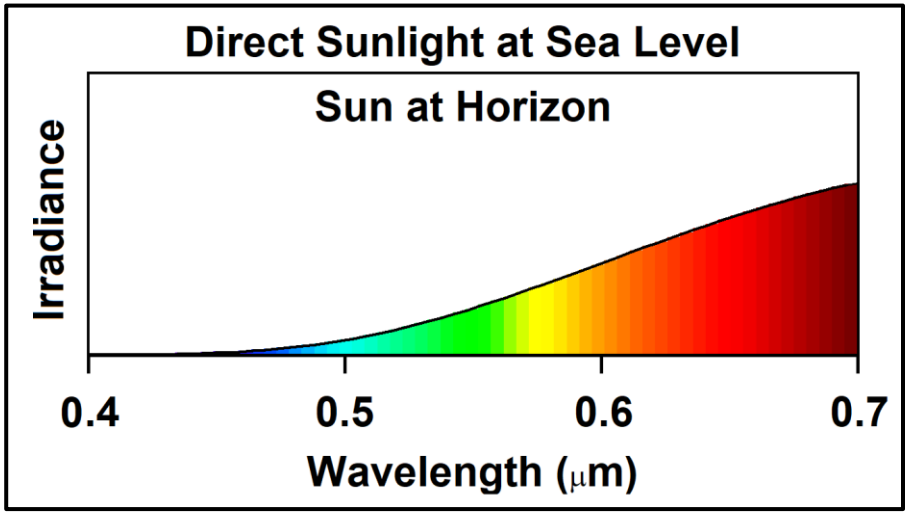

Fig. 2-11. Spectrum of direct sunlight at sea level in a pure molecular atmosphere when the Sun is at the horizon. (Compare to Fig. 2-7). SDG.

What about Earth's atmosphere? Ah, this is where it gets interesting! Geometrically, the bulk of Earth's atmosphere, relative to its radius, is thinner than the glaze on a donut (Fig. 2-10). The height at which the sky grades to the blackness of space is only about 50 km (not including the aurora), less than 1% Earth's radius (6370 km). Clearly, a vertical path through the atmosphere is much shorter than a horizontal path.

The result is that Earth's atmosphere behaves as if it is thin when the Sun is overhead, but as if it is thick when the Sun is at the horizon. For example, Fig. 2-11 shows the spectrum of direct sunlight reaching sea level when the Sun is at the horizon. After passing through about 38 times as much air as when the Sun is overhead, almost no violet or blue remains in the direct sunbeam, while orange and red dominate. Little wonder the Sun or Moon turn orange at the horizon.

2.3 Earth's Thin Atmosphere and its Layers

How fast does the air thin? At 5.5 km air pressure is half that at sea level where air is too thin for any human to live long. Pressure goes on decreasing for several thousand more km, halving every 5.5 km when temperature is 0°C, and more rapidly when the air is colder and denser.

Fig. 2-12 illustrates the fate of solar radiation as it beams down through the atmosphere. Starting around 700 km, the shortest wave lethal ultraviolet radiation ($\lambda < 0.2$ μm) strikes and is absorbed by the widely separated molecules, splitting them into atoms of O, N, and H, and ionizing some. This raises ***T*** to 1000°C at quiet times, and perhaps 2000°C when the Sun is active. Virtually all of this lethal radiation, which would easily destroy life's huge, far less stable DNA and RNA molecules, is absorbed and extinguished above 100 km.

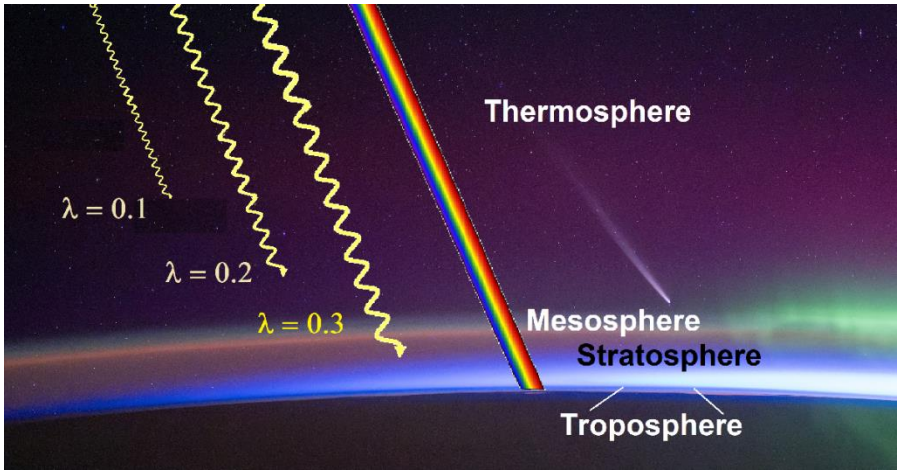

Fig. 2-12. Penetration of solar radiation and layers of the atmosphere with a comet and an aurora. Diagram, SDG. Photo, NASA/Matthew Dominick.

Longer, but still lethal UV radiation (0.2 μm $< \lambda <$ 0.32 μm) penetrates deeper into the atmosphere, where it is absorbed by ozone (O_3 is produced when O atoms drift down and combine with O_2 molecules) mainly from 60 to 30 km. That raises temperature to a maximum of about 0°C (except in the Polar Night Winter) at about 50 km. Much longer UV and visible light reach the troposphere, where some is scattered and some reaches the ground, heating it and causing sunburn.

Thus, there are three heights where the atmosphere is heated and tends to be warm – 1: above 100 km, 2: around 50 km and, 3: at the ground. Between these are two levels where it is cold because there is little heating – 1: around 85 km, and 2: between about 8 and 18 km. The result is four distinct layers in the atmosphere.

1. **The Troposphere** is the lowest layer of the atmosphere, the layer where all life, all weather and almost all clouds occur. The hot ground heats the air, which then rises, cooling as it rises, to make clouds and weather. The turbulent rising and cooling cease at the **tropopause**, about 8 km near the Poles and 18 km near the Equator, where temperatures typically range between -50°C and -80°C. The tropopause forms a cap that only thunderstorms briefly puncture.

2: **The Stratosphere** lies directly above the tropopause. Except in the dead of winter at high latitudes, temperature increases with height to about 0°C at 50 km. The stratosphere is a clear region of no storms or clouds, except in winter at high latitudes, where it gets so cold that thin, iridescent, nacreous Polar Stratospheric clouds may form (see Chapter 14).

3. **The Mesosphere** lies directly above the stratosphere and extends to about 85 km. The top of the mesosphere is the coldest place in the atmosphere, occasionally getting so cold at higher latitudes (mainly in summer!) that extremely tenuous Noctilucent clouds form.

4. **The Thermosphere** extends from 85 km up to about 700 km. This is where Auroras form (see Chapter 3) when protons and electrons expelled from the Sun collide with the atmosphere's gases. Ions form when these collisions and the Sun's UV radiation strip electrons from air molecules or atoms to produce a layer called the **Ionosphere**, which extends from the thermosphere to the top of the mesosphere.

2.4 Sky Color and Optical Thickness

When the Sun is overhead, its path down through the thin atmosphere is so short that air molecules scatter only a modest fraction of sunlight (Fig. 2-7) and most reaches the ground directly when it is clear. In other words, the atmosphere is optically thin for visible light, i. e., it has a small *optical thickness*, τ, or *optical depth* (usually defined as the optical thickness for vertical light beams).

Optical thickness, τ, is the standard measure of the fraction of photons in a light beam that penetrate a medium without being disturbed. The greater the optical thickness of a medium, the smaller is the fraction of light that passes through it without being scattered or absorbed. When optical thickness is great most photons will be scattered multiple times.

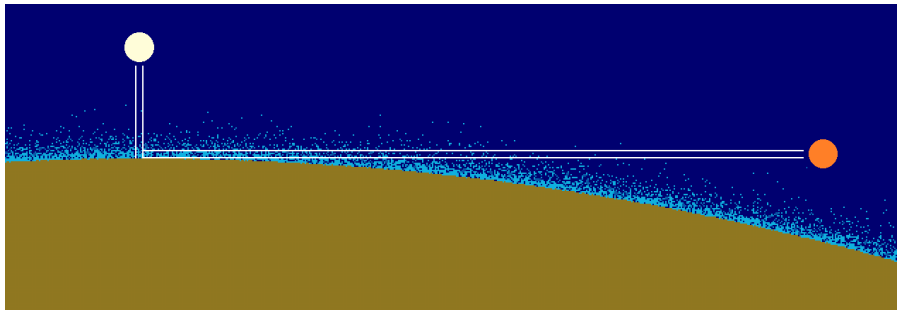

Fig. 2-13. Path length through the atmosphere for Sun at the zenith and at the horizon. The longer the atmospheric path the redder lights appear. SDG.

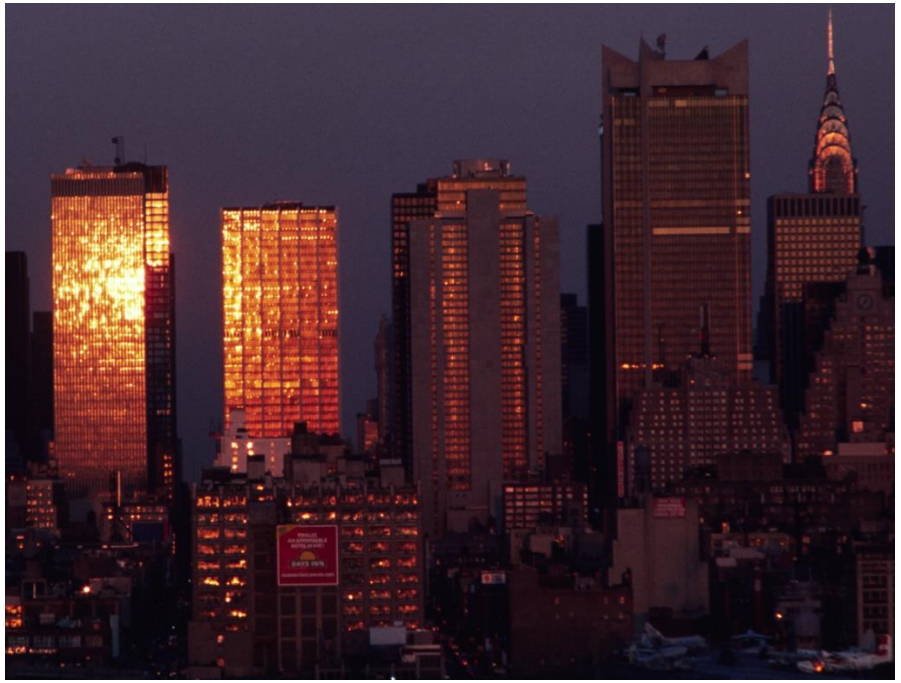

Fig. 2-14. Windows of Manhattan's skyscrapers reflect the orange light of the setting Sun. SDG.

Mathematically, optical thickness is expressed in exponential terms using the Euler number, $e \approx 2.718$. The fraction of photons in a light beam that pass directly through a medium is $e^{-\tau}$. The remaining fraction, $(1 - e^{-\tau})$, is either scattered or absorbed. When optical thickness, $\tau = 1$, $e^{-1} \approx 36.8\%$ of the light passes directly and 63.2% is scattered or absorbed. When optical thickness, $\tau = 3$, $e^{-3} \approx 5\%$ passes through and 95% is scattered or absorbed.

In a pure, molecular atmosphere the optical thickness for a vertical light beam reaching sea level is $\tau = 0.36$ for violet light of wavelength, $\lambda = 0.4$ μm, meaning $e^{-0.36} \approx 69.8\%$ penetrates directly and $(1 - e^{-0.36}) \approx 30.2\%$ is scattered. For red light of $\lambda = 0.7$ μm, $\tau = 0.0364$ so that only 3.6% is scattered and 96.4% penetrates. The mean optical depth of the pure molecular atmosphere averaged over the visible spectrum, is $\tau \approx 0.09$, so that only ≈ 9% is scattered or absorbed and ≈ 91% reaches sea level directly. Aerosols and clouds can greatly increase the atmosphere's optical thickness (see §2.6).

Fig. 2-15. The Alpenglow. Southern Iceland's cliffs, brown with a thin cover of green grass during the day, glow red at sunset, 30 Sep 2024. SDG.

Because the atmosphere is a geometrically thin veneer enveloping the Earth, the lower the Sun or Moon in the sky the longer the light path through the atmosphere (Fig. 2-13), the greater the optical thickness, the more light is scattered (perhaps multiple times) and the less penetrates. As mentioned above, a sunbeam from the horizon must penetrate about 38 times as much air to reach sea level as a sunbeam from the zenith, so that the optical thickness is about 38 times greater. Thus, $e^{-(0.0364\times38)} \approx 25\%$ of red light with $\lambda = 0.7$ μm remains in the direct sunbeam, but only a teeny $e^{-(0.36\times38)} \approx 1.15\times10^{-6}$ or little more a millionth of violet light of $\lambda = 0.4$ μm remains in the direct sunbeam.

Thus, the Sun and Moon (Fig. 2-9) turn red at the horizon. The Sun may still *appear* white at the horizon on clear days because it is still so blinding bright it oversaturates our eyes and most camera settings. One way to tell the true color of the horizon Sun is by its reflection on sunlit objects such as windows of skyscrapers (Fig. 2-14), though they too can be blinding, clouds (see §4.2 and §12.2), and snow, which appears pink or even rosy due to a mixture of blue skylight with the reddened sunlight. On mountains, this reddening effect is called the Alpenglow (Fig. 2-15) and it is most pronounced when twilight reigns in the lowlands while high peaks such as Everest, Denali, or the Matterhorn still lie bathed in sunlight.

Fig. 2-16. Sunlit clouds appear white if near, pink if distant. SDG.

Even during the day, bright, sunlit objects, such as clouds, which appear white when close, appear reddened when seen through a great optical thickness of atmosphere (Fig. 2-16) because Rayleigh scattering removed a substantial fraction of the shorter waves. That, of course, goes for skylight as well. Thus, we have the general rule,

All bright lights seen through a great thickness of air are reddened.

Shaded objects also change color in the atmosphere. On clear days, shaded white snow appears blue as in Fig. 2-17, because it is illuminated by blue skylight. In this scene snow had melted everywhere on the deck except in a strip where the shade of the railing remained almost still for several hours around noon. The Impressionists especially loved playing with the contrasting colors of sunlit and shaded snow.

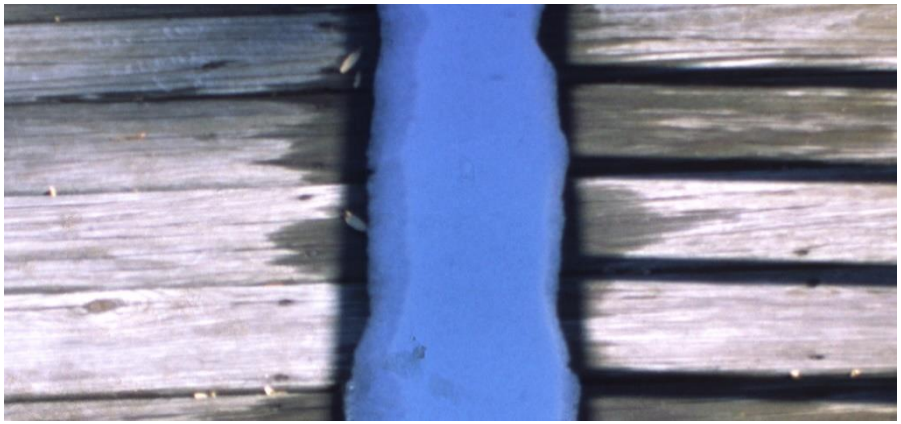

Fig. 2-17. Skylight turns a strip of shaded snow blue. SDG.

2.5 Reddened Skies

Now we are ready to answer Question 3,

What causes all the sky colors around sunrise, sunset and twilight (Fig. 2-2 and Fig. 2-3)?”

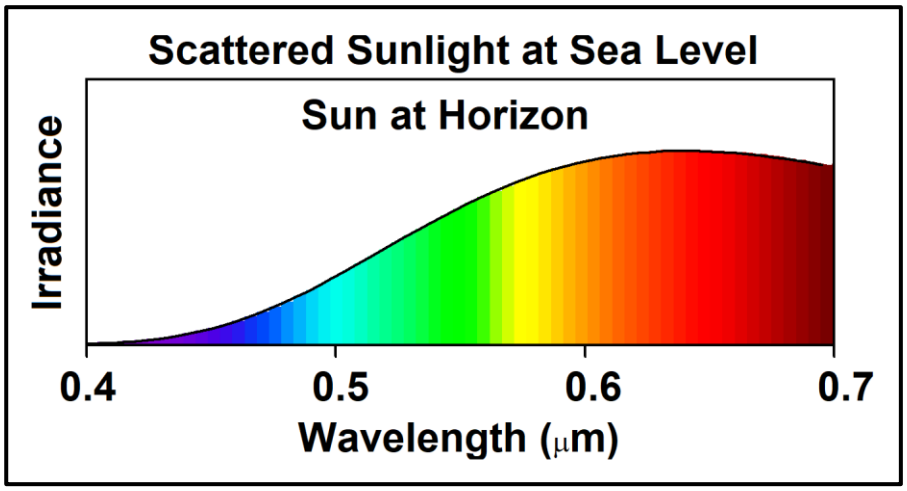

Fig. 2-18. Spectrum of sunlight scattered at sea level in a pure molecular atmosphere when the Sun is at the horizon. SDG.

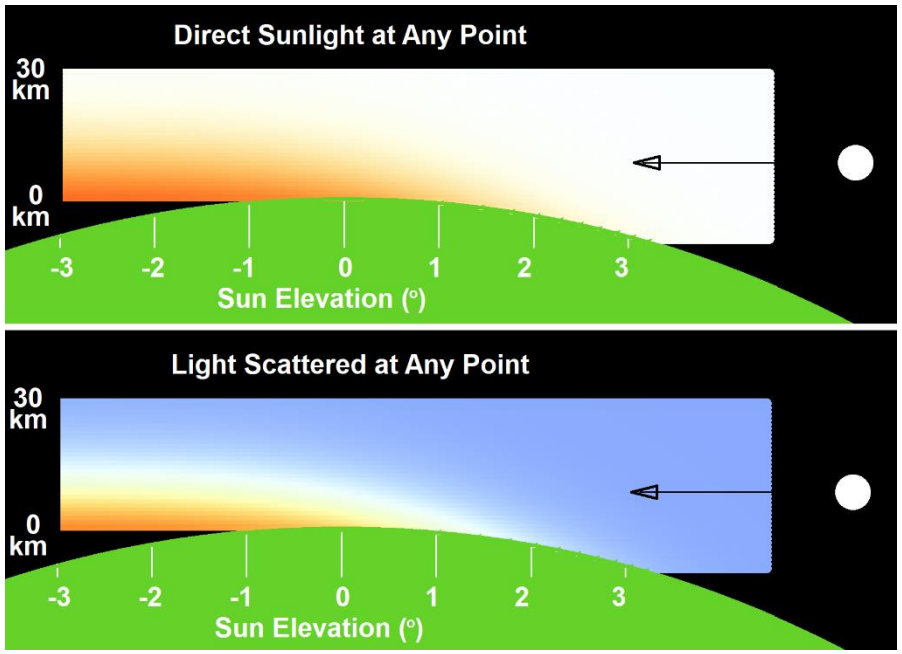

Fig. 2-19. The color of direct sunlight (top) and sunlight scattered (bottom) at any point in the molecular atmosphere when the Sun is near the horizon. SDG.

The answer is, multiple Rayleigh scattering in an optically thick atmosphere. Blue photons get hit so many times by the molecular 'paddles' that almost none reach the ground. Even most red photons get hit multiple times but since they are not hit as often, they have a higher probability of reaching the ground. Thus, just as sunlight reddens as it passes through the atmosphere so does skylight, and the greater the optical thickness each must penetrate the redder each gets.

In Earth's atmosphere, the spectrum of direct sunlight that reaches sea level when the Sun is at the horizon (Fig. 2-11) is so deficient in violet and blue that even the light scattered at that point (Fig. 2-18) contains mainly yellow, orange, and red.

The progressive changes of color of direct sunlight and scattered light as sunbeams penetrate the atmosphere from right to left are shown in Fig. 2-19. Direct sunlight (top panel) is initially white but turns orange and red as it moves through the molecular atmosphere. Scattered sunlight (bottom panel) is initially blue, but it too reddens after it has penetrated a distance through the lower atmosphere, and eventually it too turns red on the twilight side of the Earth if it passed close enough to Earth's surface, where air is densest.

Now we can explain why even on the clearest days when the Sun is overhead skylight grades to almost white (i. e., reddens) at the horizon (Fig. 2-1 and Fig. 2-6). The beam of skylight coming from the horizon is a mixture of nearby blue scattered sunlight and optically distant scattered sunlight that was initially blue but was depleted and reddened when a second Rayleigh scattering event preferentially removed the violet and blue light on its way through the atmosphere to the observer.

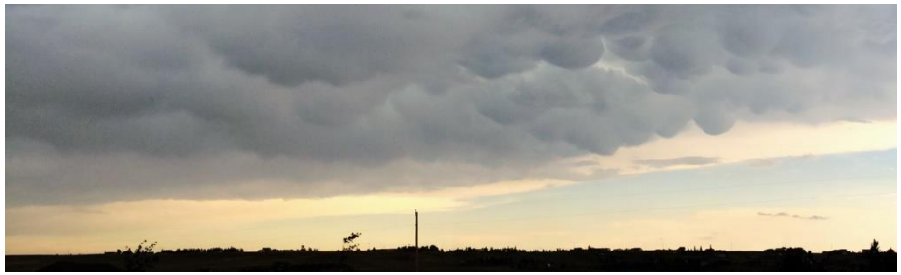

Fig. 2-20. As a dark cloud cover extends further away toward the left the near horizon sky reddens, Cheyenne, WY, 29 Jul 2016. JC.

Fig. 2-21. Sky color near the horizon during the total solar eclipse, 09 March 2016 seen from 12 km. ©Rachael C. & Sofia S., flight attendants.

If a dark thunderstorm comes overhead, covering all but the distant horizon and blotting out all nearby blue skylight, it can turn the horizon sky of a molecular atmosphere orange even at noon. (Dust stirred up by the gusty thunderstorm winds can make the sky redder.) In Fig. 2-20 the horizon sky reddens toward the left as the overcast extends further into the distance. (Conversely, distant thunderstorms that only block distant, reddened skylight turn the horizon sky bluer!)

The reddening of the daytime horizon sky is even more pronounced during a total solar eclipse. Fig. 2-21 was taken from an Alaska Air flight diverted into the umbra of the 09 March 2016 eclipse at an altitude of 12 km. For an observer in the center of the umbra the closest point of the atmosphere that receives direct sunlight is as much as 125 km away, and that sunlight comes from only the thinnest crescent of the Sun. That reddens the horizon sky further because light coming from crescent edge of the Sun is redder than light coming from the center of the Sun's disk (Fig. 1-2).

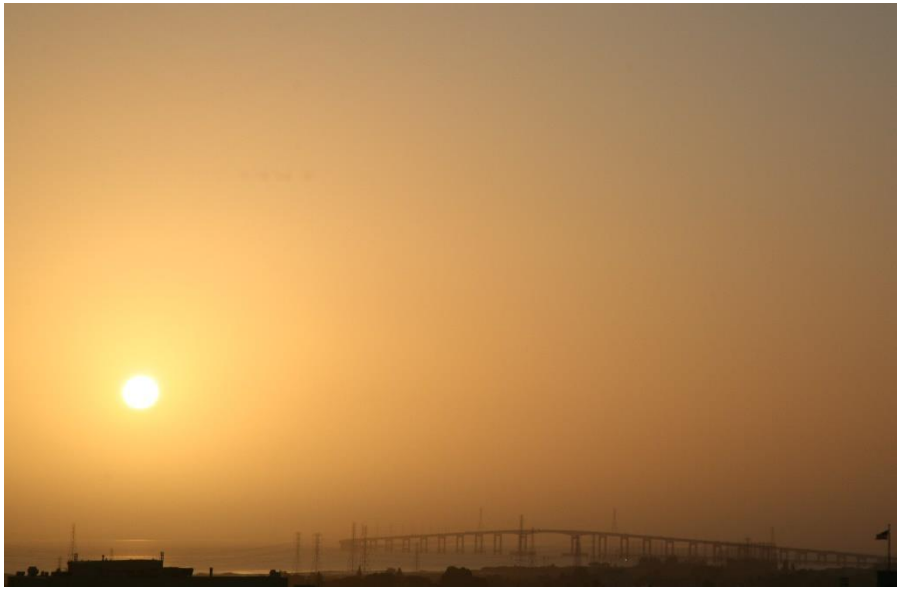

Fig. 2-22. An orange sunrise sky over San Mateo, CA, 01 Jul 2016. SDG.

Fig. 2-23. Yellow sunrise sky over Rincon Mountain, AZ, 18 May 2018. JC.

Fig. 2-24. Sky color from twilight red to orange dawn to blue day over NYC. SDG.

Of course, reddened horizon skies occur far more frequently – twice a day. Around sunrise and sunset the optical thickness sunbeams must penetrate to reach the surface is large enough to turn the horizon sky of a molecular atmosphere yellow or orange, as in Fig. 2-22 and Fig. 2-23, *but not red*. Only deep in twilight is the optical thickness large enough in a molecular atmosphere to turn the horizon sky red, as in Fig. 2-2 or the left panel of. Fig. 2-24. The three panels of Fig 2-24 show the progression of sky color near the horizon over NYC starting from deep red twilight more than 30 minutes before dawn, to orange dawn, to daytime blue.

Fig. 2-25 shows vertical panels of skylight for three situations, which together encompass a wide range of common sky colors. The panels from left to right face the Sun during twilight (from Fig. 2-2), face opposite the Sun during twilight (from Fig. 2-3), and face SW on a clear early afternoon at the Beartrail Ridge Overlook on the Blue Ridge Parkway, 12 Sep 2025 (see Fig. 2-59). Each panel is accompanied by its colorimetric analysis of Red, Green, and Blue (RGB) values (which range from 0 to 255).

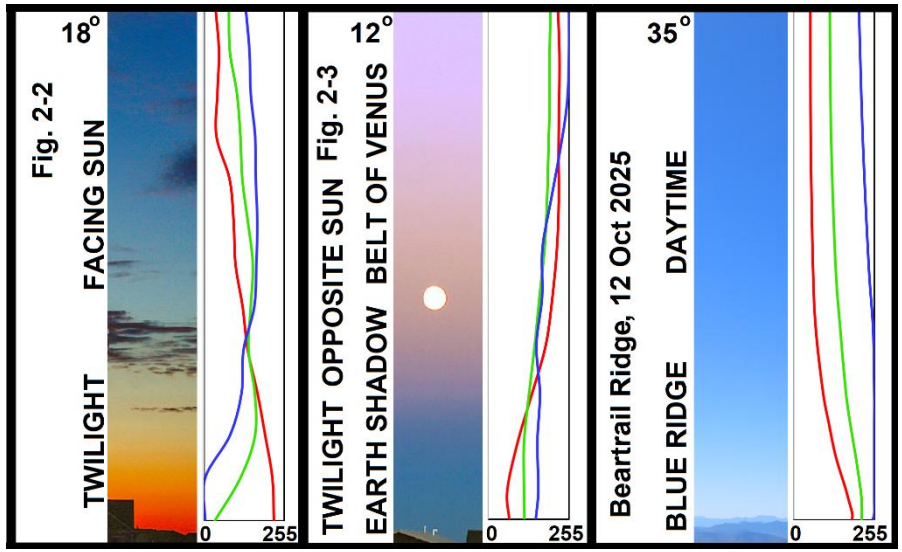

Fig. 2-25. Vertical strips of sky and RGB colorimetric analyses of twilight scenes facing the Sun from Fig. 2-2 (left), opposite the Sun from Fig. 2-3 (center) and daylight from Fig. 2-59 (right). JC and SDG.

Twilight sky colors facing the Sun tend to be appear in near spectral order from the horizon to the zenith. The colorimetric analysis shows that near the horizon the red component dominates and the blue is smallest, but the opposite is the case higher in the sky. Opposite the Sun the blue shadow of the Earth hugs the ground and grades upward into the more pastel anti-twilight arch or Belt of Venus, where the green component tends to be the smallest, so that the spectrum of skylight aloft tends to have blue and red peaks. Pastel colors imply a complicated cause because purple (not violet, which is spectral) and rose represent mixtures of red and blue. The red component in the Belt derives from the feeble red remains of sunlight scattered just above the Earth's shadow. Blue in the Belt derives from the blue scattered light

Fig. 2-26. A twilight sky with pink and purple tones and crepuscular rays over Cheyenne, WY, 18 minutes before sunrise on 24 Sep 2019 following the eruption of Raikoke, one of Russia's volcanic islands in the Kuril Chain. JC.

of less depleted sunlight at higher altitudes. Videos that animate the changes in the Earth's shadow and the Belt of Venus include,

https://www.flickr.com/photos/cloud_spirit/31866557182/in/album-72157664743046092/lightbox/

and

https://www.flickr.com/photos/cloud_spirit/32926187245/in/album-72157664743046092

The daytime sky panel grades from deeper blue aloft to near white at the horizon, just above the distant blue mountains. The colorimetric analysis reveals this primarily as an increase in the red component. Sky brightness also increases rapidly toward a maximum just above the horizon as a direct result of the increased optical thickness of the path through an optically thin atmosphere. In optically thick atmospheres the red component at all viewing angles is larger but the optical thickness is so large that the sky darkens toward the horizon.

In summary, single Rayleigh scattering makes tenuous atmospheres blue, *multiple* Rayleigh scattering makes thick atmospheres yellow, orange, or red, and atmospheres with intermediate thickness, such as

Earth's, where multiple scattering plays a varied role, display the most wondrous range and play of sky colors.

2.6 Aerosols, Skylight and Color: Mie Scattering

Many features of sky color involve more than a pure molecular atmosphere. For example, aerosol particles help produce the pink and purple of volcanic twilights (Fig. 2-26) and enhance the blue-tint of the distant Blue Ridge Mountains (Fig. 2-27).

Looking into the distance from the Wolf Mountain Overlook on the Blue Ridge Parkway in North Carolina, each successive ridge looks bluer and brighter. This feature is by no means unique. It has given its name to the Blue Mountains of Jamaica, the Blue Mountains west of Sydney, Australia, the Blue Mountains of Oregon and Washington, and several others.

Leonardo da Vinci reasoned correctly that the blue tint of distant dark mountains occurs because,

> The medium lying between the eye and the object seen, tinges that object with its color, as the blueness of the atmosphere makes the distant mountains appear blue…

Intervening skylight brightens dark, often shaded, landscape features and turns them bluer as the distance and optical thickness to them increases, although with enough distance, they turn almost as white as the horizon sky and may ultimately disappear in haze.

The blue of the distant Blue Ridge Mountains is most pronounced on days when the sky is hazy and the humidity is high. The haze is due to aerosol particles, some of which grow from organic molecules called isoprenes and terpenes (some of which are marvelously fragrant) exhaled by the thick forests that cover the Blue Ridge Mountains.

Fig. 2-27. Blue Ridge Mountains facing SW at Wolf Mountain Overlook, height, 1650 m on the Blue Ridge Parkway, 11 June 2024 at the time of the light green spring flush and bloom of rhododendrons. SDG.

Aerosol particles vary widely in size, shape, concentration, and chemistry. Salt particles fizz up from the ocean when waves break or bubbles burst. Dust or soil particles are swept up from the ground by brisk winds. Plants spew pollen into the air (which can produce pollen coronas – Chapter 14). Smoke is lofted into the air by forest and brush fires. Major volcanic eruptions blast ash and noxious gases high into the stratosphere. The Earth and biosphere exchange innumerable gases with the atmosphere. Meteors provide a constant influx of materials

from space that burn up upon entering the atmosphere. And now, human activity provides more than half the aerosols injected into the atmosphere.

Hydrometeors – cloud droplets, raindrops, ice crystals and other ice particles – also greatly affect the light and color of the sky. Hydrometeors in fog and clouds can block the Sun completely if they are numerous enough or, when conditions are just right, may produce optical wonders including rainbows (Chapter 9), halos (Chapter 11), and coronas, iridescence, and glories (Chapter 14).

Aerosols and hydrometeors span a wide range of sizes. Particle size is important in atmospheric optics because it affects the efficiency of scattering and how long the particles remain in the atmosphere. For reference, recall that air molecules are ≈ 0.0003 μm in diameter, or less than 1/1000th the wavelength of violet light, which places them in the Rayleigh scattering regime. Most long-lived aerosols range in size between 0.1 and 2.0 μm in diameter, which places them in the Mie scattering regime. Aerosols smaller than 0.1 μm quickly coagulate while aerosols larger than 2.0 μm start to fall out of the atmosphere.

The fall speed of particles less than about 100 μm in diameter is proportional to the square of the diameter. An aerosol 1 μm in diameter requires 1 year to fall 1 km while an aerosol 100 μm in diameter takes only about 1 hour to fall 1 km. Because smoke particles from forest and brush fires tend to be about 0.3 μm in diameter they fall so slowly they can travel around the world many times if rain or snow does not wash them out of the air. Aerosols in dust storms and especially sandstorms fall out much faster because they tend to be 10 μm or larger. Pollen grains range from 5 to over 100 μm in diameter and rarely remain airborne for more than a few hours though ragweed pollen, the source of hay fever, can remain airborne long enough to reach human nostrils because it is only about 30 μm in diameter.

Hydrometeors are larger on average than aerosols. Most cloud and fog droplets range from about 10-20 μm in diameter and fall between 0.3 and 1,2 cm/s, which is slow enough so that clouds float by and do not fall out of the sky. Ice crystals are larger on average – 50 to 1000 μm long and fall up to about 1 m/s, producing long trails. Raindrops range from 200 to over 2000 μm in diameter, fall up to 10 m/s and leave visible rain swaths. Hailstones have reached 20 cm in diameter, and these lethal monsters whiz out of the sky at up to 50 m/s or 160 kph.

Size not only affects how long particles remain in the atmosphere, it determines how far they can get into our lungs when we inhale them, and how they interact with light. Particles less than 2.5 μm in diameter (PM 2.5) pose the greatest threat to health because their tiny terminal velocity means that they tend to be swept along with the airflow and hence penetrate deepest into the lungs.

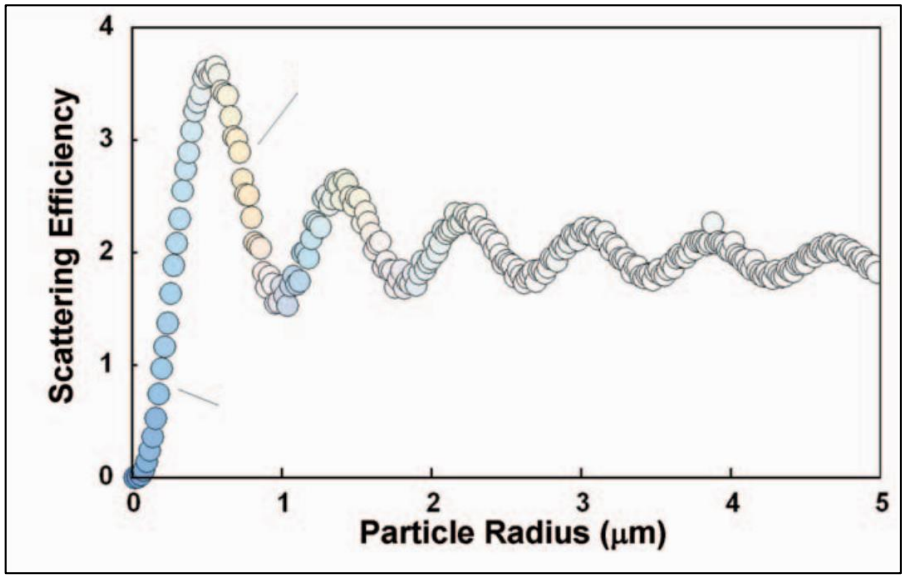

Fig. 2-28. Color of Mie scattered light and light scattering efficiency as a function of particle size. SDG.

The size of particles critically affects their *scattering efficiency*, the area of the light that is scattered divided by the cross-section area of the particle (Fig. 2-28). Scattering efficiency increases rapidly with particle size up to about 1 μm. Tiny particles such as molecules are extremely inefficient scatterers of light. If you hold a dinner plate horizontally a few feet over the ground when the Sun is overhead, the

shadow of the plate will have almost the exact same area as the plate itself. Thus, its scattering efficiency is 1. But if you could do this with an air molecule, its 'shadow' would have less than one trillionth the area of the molecule! In other words, the scattering efficiency of an air molecule is less than one trillionth! An analogy to the molecule's low scattering efficiency is that when you swim in the ocean beyond the surf, the waves pass by you on their way to the shore as if you scarcely existed because they are much longer than you.

Despite the miniscule scattering efficiency of molecules, the sky is bright because there are so many air molecules. At sea level, every cubic centimeter contains about 27 billion-billion (2.7×10^{19}) molecules. Even with this enormous number, Rayleigh scattering by molecules reduces the irradiance of sun beams by only about 10% after passing through 10 km of air at sea level.

If molecules scattered light with 100% efficiency (like the plate), about 90% of a sunbeam would be scattered before it passed through a single centimeter of air at sea level. Air molecules would have a high scattering efficiency if light behaved like tiny meteors instead of waves. Then, molecules would 'burn up' sunbeams much as they burn up meteors that streak through the atmosphere, which collide with every air molecule in their path. But unlike corpuscles or meteors, waves have the remarkable ability to skirt tiny particles.

The scattering efficiency of tiny particles increases with their size. Rayleigh scattering of a fixed wavelength increases as radius, $\boldsymbol{r}^4$, while area increases with $\boldsymbol{r}^2$ so when radius doubles, scattering efficiency increases by a factor of $2^4 / 2^2 = 4$. As particles approach the size of the wavelength their efficiency increases more gradually, then oscillates, and their color behavior becomes more complex.

One important consequence of the rapid increase of scattering efficiency with small particle size is that hazy air may not contain *more* aerosols it may just contain *larger* aerosols. When relative humidity rises above about 70% hygroscopic aerosols get wet (*deliquesce*), just as salt crystals do, and begin to swell (see §4.3), scattering light more efficiently. Thus, hazy days may just be more humid than clear days.

When particle diameter approaches about one tenth the wavelength of light Mie scattering takes over. Scattering efficiency reaches a peak when particle diameter is about three times the wavelength of light. As particle size continues to increase, scattering efficiency begins to oscillate, and eventually levels off for particles much larger than the wavelength of light (Fig. 2-28). Scattering efficiency greater than 1 occurs because waves that bypass particles are also deflected and bend into the particle's shadow.

H_2O molecules are the only molecules in Earth's atmosphere that cluster and condense to droplets or ice crystals to form fog and clouds. O_2 and N_2 have much lower boiling points and remain gases.

So long as water remains a vapor (a gas) light waves from the Sun bypass H_2O molecules even more easily than other air molecules because H_2O molecules are smaller. And since water vapor is a minor constituent of the atmosphere, averaging only 0.33% of all air molecules, its total optical thickness is quite small. But if all that water vapor condensed into typical fog-size droplets with diameters about 15 μm, its optical thickness would increase to 300 and so little light would get through the fog or cloud to the ground that the sky would be almost pitch black!

When Mount Pinatubo had its great explosive eruption on 15 June 1991 it shot 20 million tons of sulfur dioxide plus ash up to 35 km into the normally clear stratosphere. Large particles quickly fell out of the stratosphere, and were then washed out of the atmosphere by rain and snow, but tiny aerosols and the water vapor that combined with the sulfur dioxide to form tiny droplets of dilute sulfuric acid remained aloft for up to several years. The scattering caused by these particles reduced the sunlight reaching the ground by 10% and cooled the global climate by about 0.4°C for more than a year.

Pinatubo's cloud of droplets also produced wondrous red twilight skies (Fig 2-29) similar to those seen after other major eruptions such as Tambora in 1815 (which inspired the artist, J. M. W Turner), and Krakatau in 1883. Pinatubo's cloud reached New York City by

October 1991, and one cloudless morning, almost an hour before sunrise over New York City, when the ground still lay in the shadow of night, sunlight illuminated the stratosphere and was scattered. Because the droplets were about 1.5 μm in diameter, they were just the right size to scatter red light more efficiently than blue, as Fig 2-28 shows, so the sky turned a brilliant crimson red.

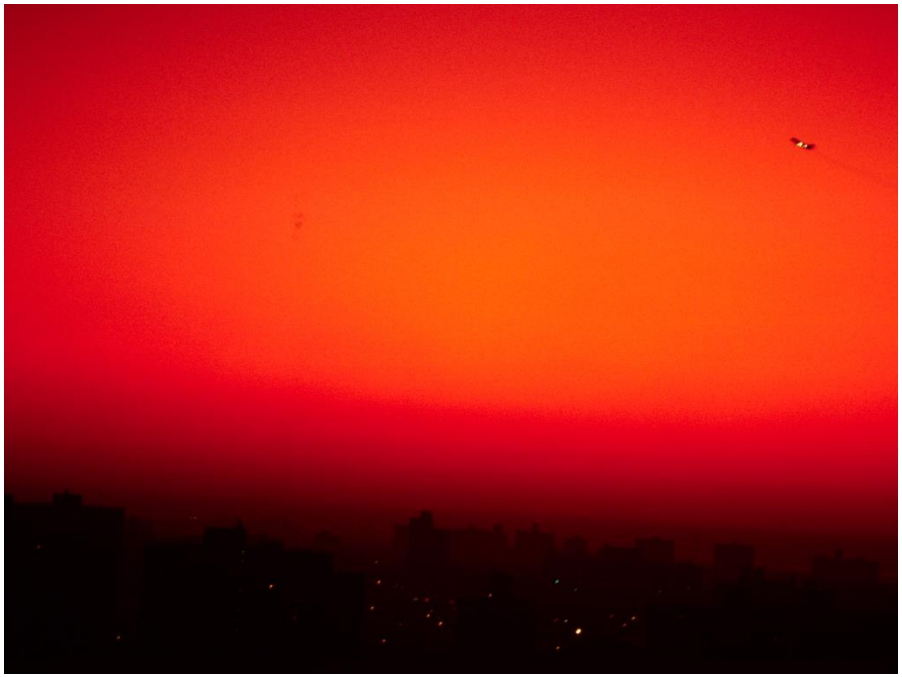

Fig. 2-29. A plane takes off into a crimson red predawn twilight over NYC in October, 1991 due to Pinatubo's stratospheric cloud of droplets ≈ 1.5 μm in diameter, which scatter long waves more efficiently than short waves. SDG.

Closer to dawn, the Sun reaches the Jet stream level where blue scattered skylight adds to the red stratospheric light This somewhat unusual combination, which leads to the occasional volcanic purple twilight facing the Sun, peaks when the Sun is about 5° below the horizon, as in Fig 2-26. Volcanic purple is only seen near the Sun because aerosols scatter light mainly by small angles. Further from the Sun the twilight sky aloft is blue.

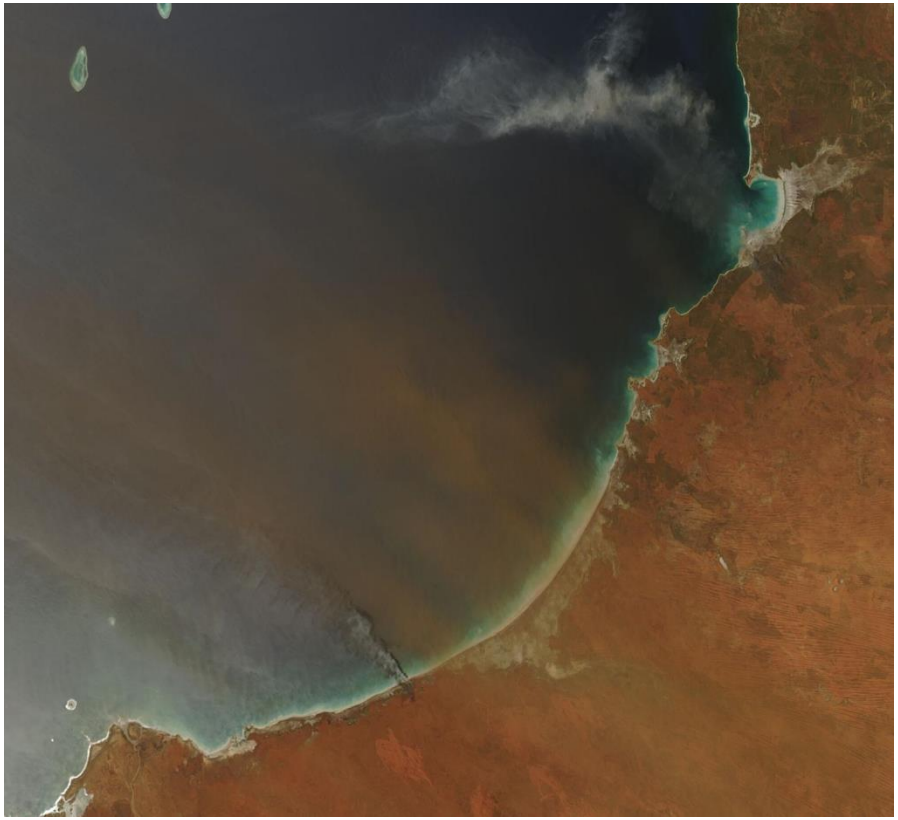

Fig. 2-30. Plume from the dust storm of 10 Dec 2023 over western Australia consisted of brick-red aerosols swept to the NW over the sea from the brick-red surface. Two gray plumes from fires are also seen. NASA MODIS image.

Red volcanic twilights may last a couple of years in extreme cases. Less than a year after Pinatubo erupted the red was gone because only the tiniest aerosol particles and droplets remained in the stratosphere. Too small to produce red twilights, these aerosols scattered all colors of light with comparable efficiency. Thus they produced a near white haze that muted the blue of pristine skies for at least two years until they fell out of the stratosphere and were quickly washed out by rain.

Smoke from dust and sand storms and from forest fires also turn the sky red, but each for a different reason. The red of dust storms and sandstorms is largely due to sunlight reflected by large grains of sand and soil colored red by iron oxide abundant in the parent rocks of the

desert. An exemplary case was the dust storm of 10 Dec 2023 in Western Australia, where the dust in the large brick-red plume was soil lifted from the deep, brick red ground. (Fig 2-30). Fig. 2-30 also shows gray smoke plumes from fires north of Broome (near the top-right) and further southwest (just left of center near the bottom) extending from Eighty Mile Beach. From satellite most smoke plumes from fires look bluish gray where they are optically thin and have a reddish cast where they are optically thick.

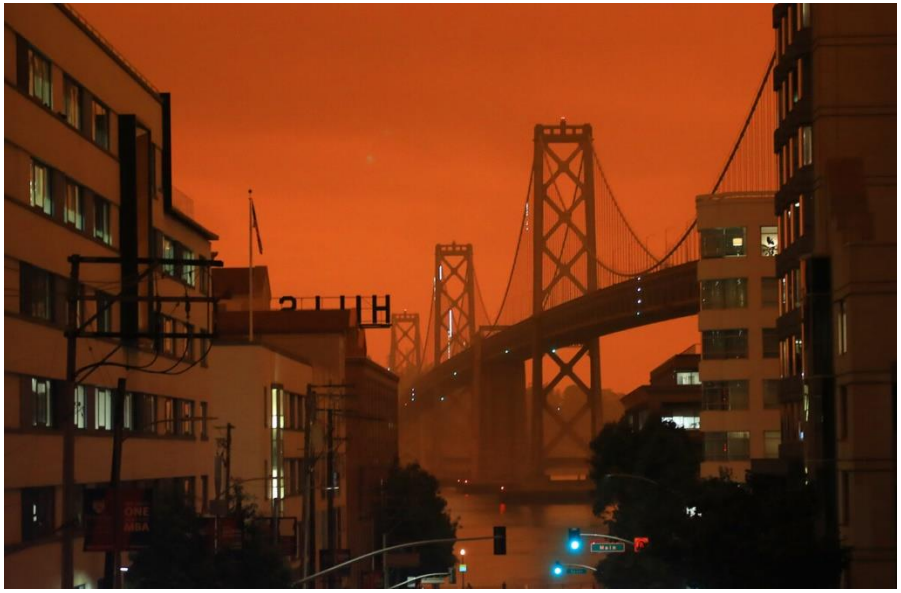

Fig. 2-31. Wind carried smoke from extensive forest fires in North California over San Francisco and turned the sky blazing red on 9 Sept 2020. NYT.

On the ground, smoke from forest and brush fires always has a reddish cast. If the smoke is optically thick it can turn a cloudless sky deep red even at noon, as on 10 Dec 2020 in San Francisco (Fig. 2-31), or make it as dark as night. Aerosols from forest fires are generally less than 0.5 μm in diameter, so they scatter short waves with somewhat higher efficiency than long waves, but to the first or second power of wavelength as opposed to the 4^{th} power of Rayleigh scattering. Hence the washed out, gray-blue color. Look at a thin smoke, as Leonardo da Vinci did, and you will see that it is a blue-gray. But, just as in the case of pure, molecular air, if smoke is optically thick enough, almost all

Fig. 2-32. A hazy day in Hong Kong seen from Sky Terrace 428. Water bloated aerosols bleach the sky and reduce visibility. SDG.

Fig. 2-33. Aerosols make the sky whiter and brighter, especially near the Sun. The scene is in Madrid, 12 Jan 2008, a day that was only slightly hazy. SDG.

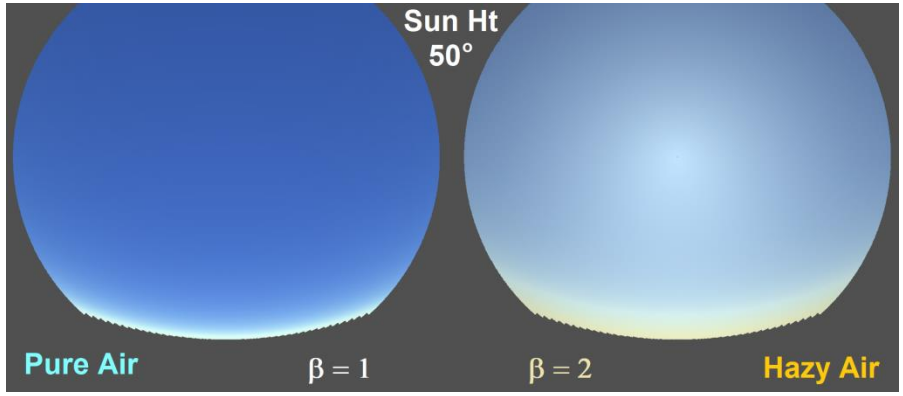

Fig. 2-34. Simulated deep blue sky light in pure air (left) gives no hint of sun's location, In hazy air (right) the sky is whiter and brighter, especially around the Sun, and redder near the horizon. SDG.

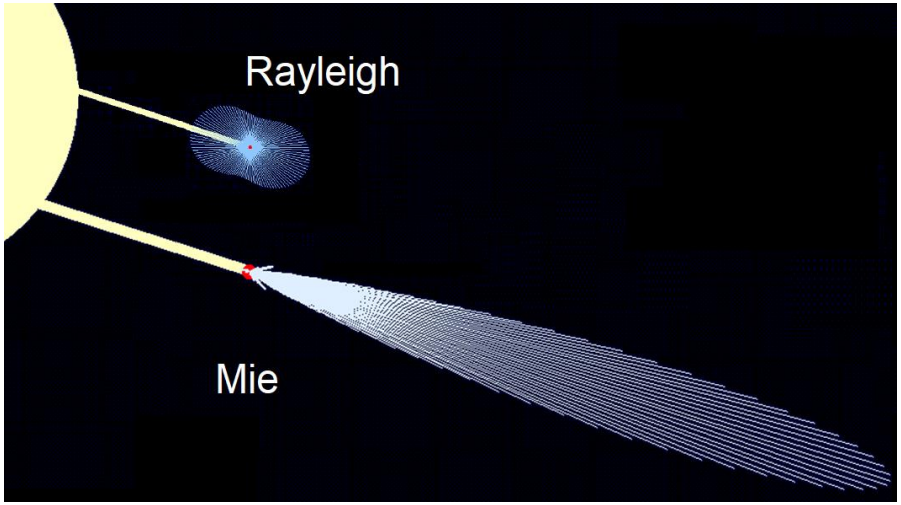

Fig. 2-35. Tiny particles scatter mainly blue light in all directions. Large particles scatter all colors more equally but mostly by small angles. SDG.

the blue light has been scattered and the light that is able to penetrate is primarily red.

Aerosols seldom produce the dramatic skies of dust storms and forest fires, which result from such extremely large injections of particles that they increase the atmosphere's optical thickness by a factor of 10 to 100, or even more. The normal impact of aerosols is to reduce visibility, give everything a hazy appearance, and bleach the sky's pristine blue, and, so long as they do not increase optical thickness too much, brighten the sky (Fig. 2-32), especially right around the Sun (Fig 2-33). One aesthetically pleasing feature is that aerosols often enrich sunset colors. On very hazy days, the Sun will turn deep red and may even disappear when still above the horizon.

Fig. 2-34 shows two computer simulations that compare sky light and color for a pure, molecular atmosphere (left panel) and for an atmosphere where aerosols double optical thickness (*turbidity*, $\beta = 2$) (right panel). With pure air, the sky is deep blue aloft and grades to a thin white strip near the horizon. Sky color and light give no hint of where the Sun is because Rayleigh scattering spreads almost evenly in all directions. When aerosols double the optical thickness, the sky is notably brighter and whiter, especially around the Sun, and the sky just above the horizon is orange even though the Sun in these simulations is 50° above the horizon.

The differences in clear sky appearance are largely due to differences between Rayleigh scattering by the tiny molecules, and Mie scattering by the much larger aerosols. Mie scattering is much more efficient and much more uniform across the visible light spectrum than Rayleigh scattering, but deflects light by much smaller angles on average (Fig. 2-35). Hence it is Mie scattering that makes the sky near the Sun appear brighter and whiter. Similarly, the glare from a dirty window can be blinding when facing the Sun.

2.7 Polarization

In the molecular atmosphere, skylight is almost completely polarized 90° away from the Sun. Light waves are transverse by nature. That means the electric field always points at right angles to the direction of light beams. If the light beam is vertical, the electric field points horizontally. When a molecule scatters light from a vertical light beam to the East, the electric field of the scattered light will point NS and still be horizontal. Thus, scattering at right angles to the Sun in a molecular atmosphere reduces the electric field from two dimensions

to one dimension. Aerosol particles, being more complex and irregular do not polarize sunlight well.

Fig. 2-36. Near identical photographs of the sky, except a polarizing lens has been used to maximum effect on the left. SDG.

Fig. 2-37. Polarized panorama photo from NW to E creates unrealistic light and color differences in the sky above Fairfield Lake, NC, 10 Oct 2025. SDG.

Because the molecular atmosphere is almost completely polarized about 90° from the Sun the sky on pristine days free of pollution is noticeably darker and deeper blue than near or opposite the Sun. If you aim a camera equipped with a polarizing lens at the polarized part of the sky, you can turn the lens until light with the one remaining direction is almost completely extinguished, so that the sky turns quite dark and deep blue. All other objects darken, but if they are not polarized they will darken by less than 50% and stand out against the darker sky As a result, clouds brighter than the sky stand out in polarized photographs of the sky about 90°from the Sun (Fig 2-36) and are visible at a greater distance than photographs taken without a polarizer.

There are disadvantages of using a polarizer. If the cloud is darker than the sky a polarizer reduces the contrast between cloud and sky. Wide angle, panoramic photographs cover such large angles that they result in unrealistic differences of sky light and color (Fig. 2-37).

The primary rainbow is also highly polarized (see §9.2), and because it covers such a large angle, polarized views brighten some parts of the bow and dim others.

2.8 Mirages: Refraction Gone Awry

Mirages are visual distortions and displacements of objects caused by refraction of light in the atmosphere. In that sense these optical illusions are much like the distorted images seen in curved mirrors at amusement parks. But mirages are much subtler. Light waves traversing the atmosphere never bend by much more than 1° because even in the densest air the speed of light is only about 0.04% slower than in a vacuum. Bending by an angle of 1° may seem tiny, but since our eyes can distinguish angles as small as 0.01° we can easily detect mirages.

The most well-known and perhaps most common mirage is the desert mirage or *inferior mirage* (inferior because the image appears below the object), which also occurs over level, superheated roads. When you look down the road at a glancing angle (Fig. 2-38) the image you see seems like a pool of water in the road. The real ‘object’ you see is the

sky. And since the superheated, light air is buoyant, it swirls up turbulently, imparting a shimmering appearance of wavy water. The inferior mirage is illustrated in the top frame of Fig. 2-39, where the rays of light bend upward. Any object located in the region where rays of light overlap will be accompanied by an upside-down image of the object in the 'water'.

Fig. 2-38. An inferior mirage. The 'water' on the road complete with inverted images is actually refracted light of shimmering air. © David Lynch.

Inferior mirages have one additional intriguing property. Since the rays of light waves curve upward, there is a distance beyond which objects on or just above the ground disappear from sight. That is also why distant thunder cannot be heard from what is called 'heat' lightning (see Chapter 8). Cars crossing this point into the invisible (or silent) zone will simply vanish. Such vanishing combined with shimmering desert air may explain why the fleeing Israelites thought Pharaoh's army was swallowed up by the Sea all around them while they walked on the dry land of the desert.

In the case of the inferior mirage, the air touching the road is so much hotter than the air only a few feet above that it is less dense. That represents the anomalous situation in which air density increases with height, which only occurs for a short height above superheated ground. Everywhere else in the atmosphere density decreases with height, so light waves curve downward.

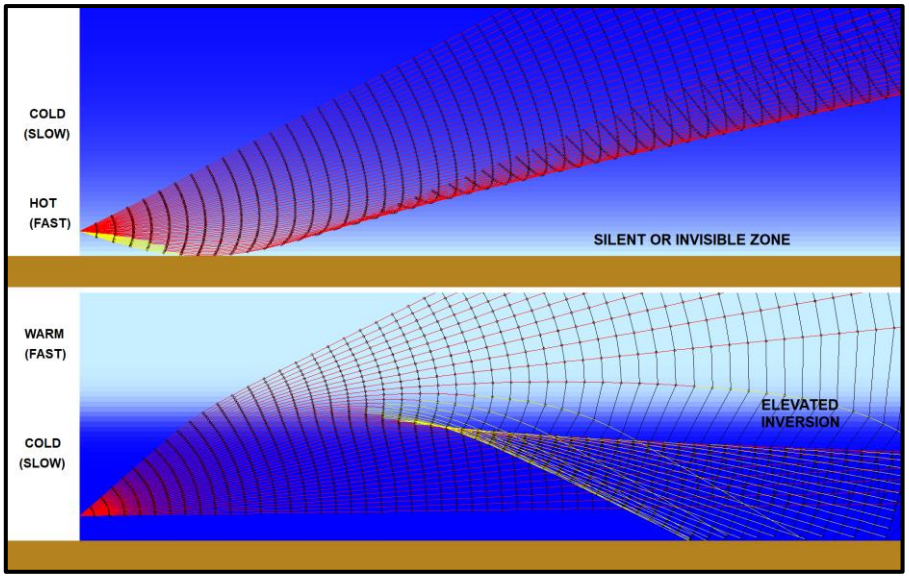

Fig. 2-39. Temperature structure and meshes of light rays (red or yellow lines) and wave fronts (black lines) for inferior (top) and superior (bottom) mirages. An observer at left will see inverted images of objects located anywhere in the regions where rays overlap. SDG.

Fig. 2-40. A superior mirage over Finland's cold waters. Images of sand bars appear as forested hills in the air. ©Pekka Parviainen.

Superior mirages occur when the surface is much colder than the air above so that air density decreases (and the speed of light increases) at

an unusually rapid rate with height. Then, light rays bend downward, making images appear *above* the objects, sometimes like castles in the sky (Fig. 2-40). And, when the angle of the rays between the top and bottom of the image is larger than the angle between the rays between the top and bottom of the object, the object will appear magnified.

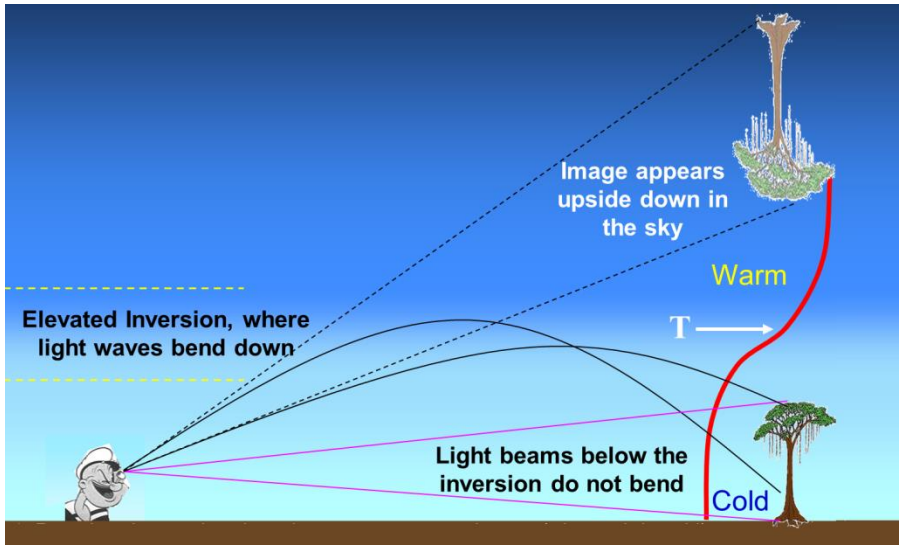

Fig. 2-41. Path of light beams and elevated, inverted superior mirage of a Palm tree with an elevated inversion. Curvature is exaggerated. SDG.

Superior mirages are most dramatic when there is an elevated inversion, a zone above the observer's eyes where temperature increases with height. An elevated inversion acts like a mirror on the ceiling to produce an up-side down image of an object you can also see straight ahead (Fig. 2-41). Superior mirages have tricked Arctic explorers into reporting nonexistent islands such as Crocker Land, named to extract funds from a wealthy banker. On clear, cold, calm nights sound waves curve down much the same way as light waves with superior mirages, forming sound channels that allow sound to be heard from great distances.

One superior mirage occurs without fanfare twice each day that has sunrise and sunset. When the Sun and the Moon appear to rest atop the horizon, 1: their true (astronomical) positions are just *below* the horizon and, 2: they look flattened. Refraction of light beams passing almost horizontally through the atmosphere, curve much as in the bottom panel of Fig. 2-39 and Fig. 2-41 and make the Sun and Moon appear higher in the sky than their astronomical positions. The angle of bending increases rapidly toward the horizon as the beams pass through a rapidly increasing optical thickness of atmosphere to reach ground level. The increase is so rapid that when the Sun or Moon rests on the horizon refraction lifts the bottom by 0.6° but only lifts the top by 0.48°. This makes the horizon Sun and Moon appear squashed by the difference, which is 0.12º, which is about 24% of their average apparent diameter of 0.517º.

Fig. 2-42. Flattened moonset from the International Space Station, 16 Apr 2003. Don Pettit, NASA.

From space or from a jet plane, the bending of the Sun or Moon seen at the horizon is at least double that seen from sea level and the flattening is exaggerated to the absurd. This is shown in the photo montage of Fig. 2-42, taken by Don Pettit from the International Space Station. Note also that the setting Moon first turns bluer and then redder as it is progressively squashed approaching the invisible horizon (see §2.10).

The superior mirage of the Sun near the horizon makes the Sun rise earlier and set later than the astronomical times of sunrise and sunset.

Since the Sun moves across the sky at the rate of 15° per hour (360° per day) or 0.6° in 2 minutes, daylight is increased by 4 minutes each day at the equator, where the Sun path is vertical and by more at higher latitudes, where the Sun rises and sets more obliquely. At the North and South Poles, for example, sunset into the Polar Night winter is delayed by 36 hours!

The protracted (once a year) sunrise and sunset at the Poles makes them the best place in the world (if you can get to them) to view the Green Flash.

2.9 The Green Flash and the Blue Flash

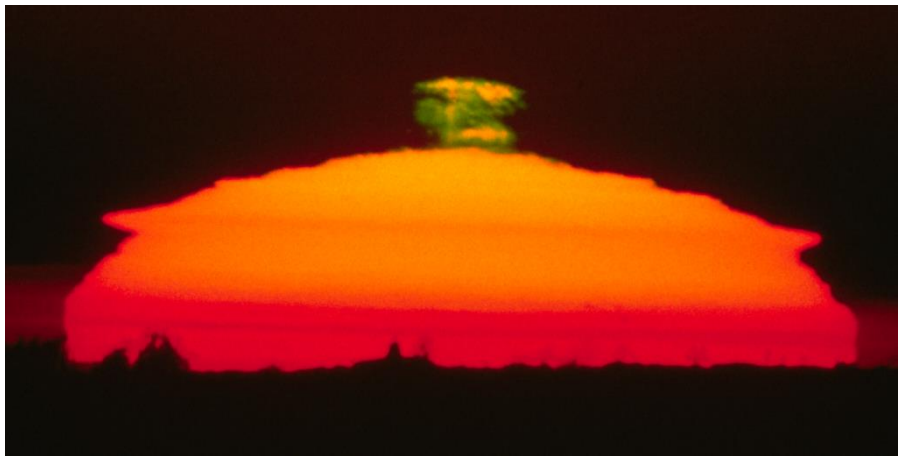

Fig. 2-43. The green flash with the Chinese lantern effect of a refraction-squashed and distorted Sun. ©Pekka Parviainen.

Elevated inversions at sunrise or sunset produce extra bending that can prolong day even more but also distort the image of the Sun in strange ways, so that it may break in pieces or resemble a Chinese lantern, as in Fig. 2-43. The extra bending can also make the atmosphere behave like a prism, separating the colors at sunrise and sunset. Since shorter waves are refracted more, they will appear elevated above the main body of the setting Sun.

Fig. 2-44. Blue Flash and Green Flash fragments atop the setting Sun 2000 m above sea level near Cheyenne, WY 30 Jan 2024. JC.

This is the origin of the Green Flash, linked to the legend that those who have seen the Green Flash can never err in matters of love. (That does not hold for seeing a *photograph* of the Green Flash.).

Shouldn't there be a Blue Flash above the Green Flash, and a Violet Flash above the Blue? Indeed, the Blue Flash exists, but almost never at sea level, because virtually all the blue light has been scattered out of the direct sunbeam at the horizon before it reaches sea level (bottom panel of Fig. 2-7). The Blue Flash is reported on rare occasion on land at least about 2000 m above sea level, where the optical thickness of the setting (or rising) sunbeam is small enough for some blue light to be transmitted (Fig 2-44). We don't know a report of a Violet Flash.

2.10 Light of the Eclipsed Moon and Ozone

The refraction of sunbeams into Earth's shadow at twilight has another beautiful optical effect. During Lunar Eclipses the Moon lies in the Earth's geometric shadow and should be invisible except for any starlight it blocks. But during most Lunar Eclipses the Moon is quite visible, as in Fig 2-45 because it doesn't lie in the shadow of Earth's

atmosphere (Fig. 2-46). The Moon is lit by sunlight that refracts as it penetrates the atmosphere, skirting above the Earth's surface, and bending by up to about 1.2° into the Earth's shadow. That is almost twice the bending of sunlight at sunrise or sunset because the path through the atmosphere to reach the Moon is almost twice what an observer at sea level sees at sunrise or sunset. The optical thickness the sunlight must pass through is also doubled, with the result that the red of the Moon during a Lunar eclipse is much deeper than the red of the Moon at sunrise or sunset.

Fig. 2-45. The Moon exiting Earth's shadow, 21 Jan 2019. At far right the Moon has emerged from Earth's shadow. Immediately to the left the Moon is tinted blue while further left and deeper into the shadow the Moon is red. JC.

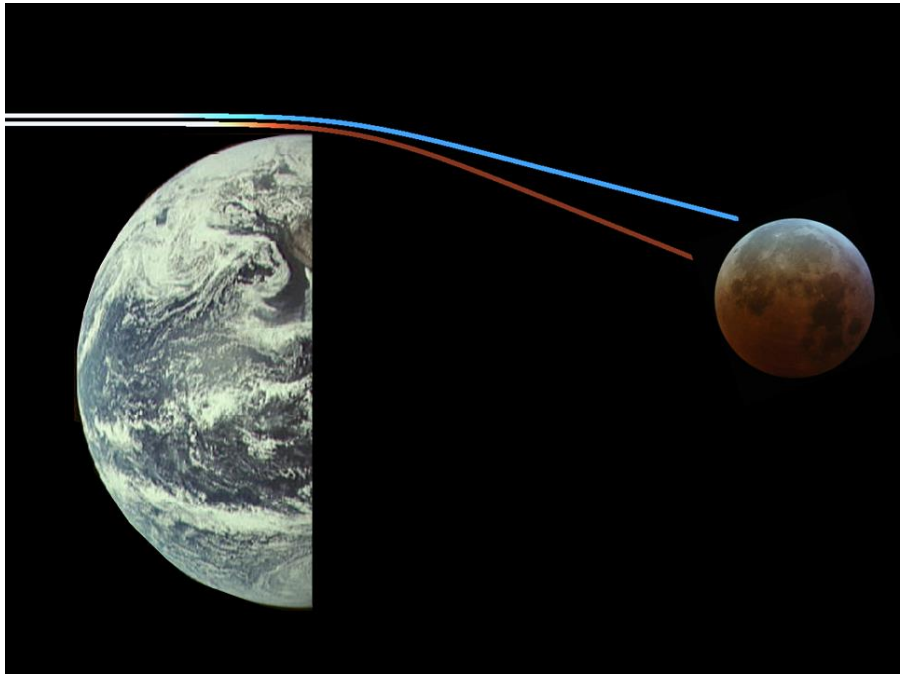

Fig. 2-46. Sunbeams changing color as they pass through the atmosphere and refract into the umbra. The higher beam turns blue as orange light is absorbed by ozone in the stratosphere. The lower beam refracts more and turns red as short waves are scattered more in the troposphere. Refraction is exaggerated. SDG.

There are times the Moon does disappear during a Lunar Eclipse. Following the eruption of Pinatubo, the atmosphere's optical thickness increased so much that the eclipsed Moon was blotted out for up to two years. The Moon's color and brightness during a Lunar eclipse provides a measure of stratospheric pollution.

As the eclipsed Moon enters or exits Earth's shadow a fringe of blue light often appears on the part of the Moon at the shadow's edge. The blue color results from a competition in which absorption dominates scattering. As this blue light beam grazes by the Earth, its closest approach is 12 or more km above sea level, (Fig. 2-46). The result is less scattering in the thin air of the stratosphere and more absorption by Ozone (O_3), which is concentrated in the stratosphere. The red beam passes closer to Earth's surface.

Ozone is the only atmospheric gas that absorbs visible light appreciably, and it absorbs with a great preference for orange light with wavelength, $\lambda \approx 0.605$ μm. The amount of ozone in the atmosphere is tiny—about 1 part per 2 million—so that if it were all brought to sea level, it would form a layer only about 3 mm deep (300 Dobson Units), on average and up to 6 mm over the Arctic. The 3 mm of ozone absorbs about 1.5% of the orange light but only 0.3% of the blue or violet light when the Sun is at the zenith, but more than 25% of the orange light when it is at the horizon, and more than 50% of the light that passes back out of the atmosphere on the way to the Moon.

The blue fringe is sensitive to the amount of ozone. If the sunbeam grazes the Arctic at a time of high ozone content, the blue is deep, but if it passes through the Antarctic ozone hole, it would not turn blue.

By absorbing orange light, ozone is also what keeps the sky near the zenith sky blue when the Sun lies on the horizon. And it deepens the blue of the sky of deep twilight (see §12.2). Never did a blue sky owe so much to so little.

2.11 Simulating Sky Color

Computer models can simulate and produce realistic images of every one of the features of sky light and color discussed and shown above. The special virtue of the models is that they can be used to create a plethora of scenarios and show how sky color and light are altered by changing quantities such as the Sun's height in the sky, atmospheric pressure, humidity, aerosol content and height, cloud cover, and ozone content.

The simple model used to produce the vertical sky panels in the three figures below treat 61 wavelengths spanning the visible spectrum of sunlight scattered into beams at 84 elevation angles aimed toward an observer. Each beam is divided into 100 segments starting at the 'top' of the atmosphere, and proceeding to the observer. In each segment light already in the beam but scattered out in the tiny section is subtracted while sunlight scattered into the beam is added. A simple, approximate formula is used to include already scattered light that enters the beam (i. e., multiply scattered light). This approach provides an accurate approximation of the light and color of the sky in most situations because the optical depth of the atmosphere is small. Though the process sounds laborious with all the wavelengths, beams, and segments, it is done so fast on the computer that an image of a vertical panel of sky is produced in a second.

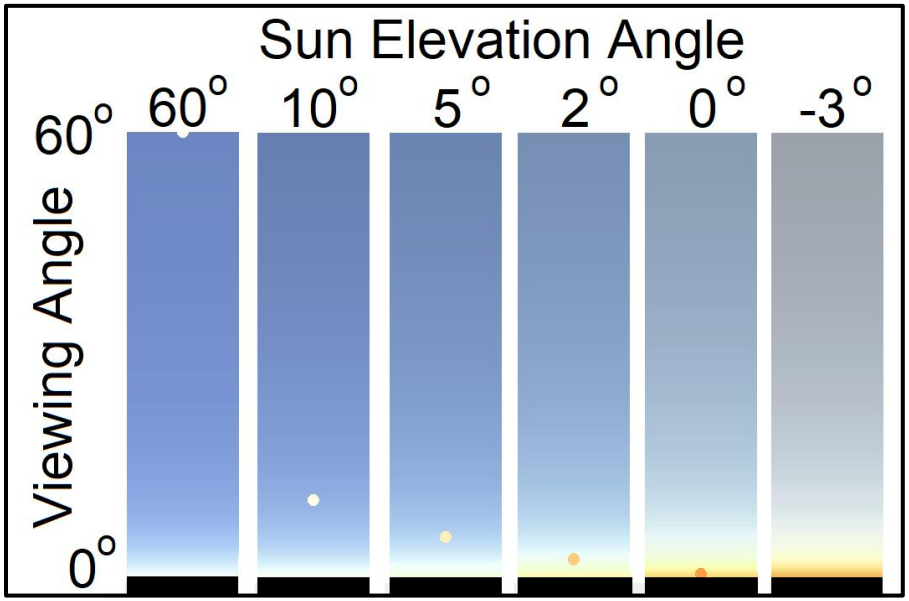

Fig. 2-47. Simulated sky color at sea level in the vertical plane of the Sun for a molecular atmosphere as a function of Sun elevation angle. SDG.

On days the air is pure and the Sun is well above the horizon, the sky appears sparkling blue and imparts a gleaming quality to the entire landscape. Near the horizon the sky grades rapidly to near white. The sparkling quality remains even as the Sun heads toward the horizon late in the afternoon, and both Sun and sky at and just above the horizon turn yellow and then orange, though the blue of the sky aloft decreases notably. All of this is shown in the simulations of Fig. 2-46, which even captures the pale green color from about 3 to 7º above the horizon when the Sun is 3º below the horizon.

Although aerosol particles are complex entities with widely variable optical properties their general impact on sky color and brightness is that when they increase in number or grow, they reduce the blue and brighten the sky, especially around the Sun (recall Fig. 2-33 and Fig. 2-34). Fig. 2-48 shows the impact of increasing aerosol optical thickness by doubling and then quintupling the total optical thickness of the atmosphere (i. e., the turbidity) for the typical case where aerosols scatter light with an efficiency inversely proportional to wavelength, are most concentrated at the ground and decrease to a fraction, $e^{-1} \approx 0.368$ each height increase of 2.5 km. The blue is washed out and in turn the sky assumes a brownish orange color that appears dirty. At large enough turbidity, the Sun turns red well above the horizon and disappears in the haze or smoke.

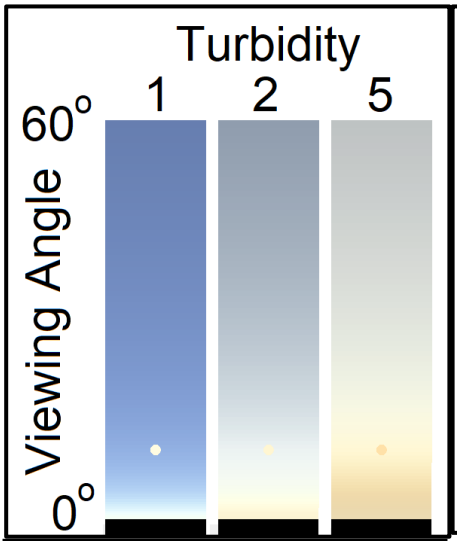

Fig. 2-48. Simulated sky color at sea level as a function of aerosol content in terms of atmospheric turbidity for Sun elevation angle = 10°. SDG.

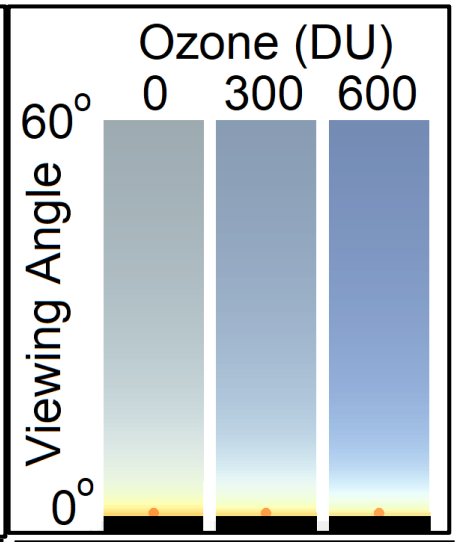

Fig. 2-49. Simulated sky color at sea level as a function of Ozone content in the stratosphere when the Sun is at the horizon. SDG.

Stratospheric ozone has little impact on sky color when the Sun is high in the sky. When the Sun is near or below the horizon, scattering increases so much across the visible spectrum that the sky would lose its blue color without ozone, which preferentially absorbs orange light. Fig. 4-49 show the profound impact that increasing the atmosphere's tiny ozone content has on deepening blue at sunrise, sunset, and during twilight.

This sampling indicates the power and beauty of computer simulations of sky light and color. Creating simulated skies is a most enjoyable game to play on gray, overcast days or long winter nights not illuminated by stars or by auroras (Chapter 3).

2.12 Meteor Trails

Meteors check in but don't check out. Millions enter the atmosphere each day, adding their mass to our planet. Most are microscopic. Those that are larger than sand grains blaze colorful, fiery trails as they burn up, usually between about 50 and 95 km above sea level. Meteors larger than about 1 m in diameter have a good chance of making it all the way to the ground. The asteroid that struck Earth 66 million years ago was between 10 and 15 *km* in diameter. It blasted the Chicxulub crater just north of the Yucatan Peninsula and caused such devastation it eliminated the dinosaurs and paved the way for us.

Most meteors are part of the debris field of comets or asteroids. Every year Earth passes through several debris fields to produce meteor showers including the Leonids (17 Nov peak), Perseids (12 Aug peak), and Geminids (14 Dec peak). Most meteor showers originate from comets; the Geminids originate from an Apollo asteroid named 3200 Phaethon.

Several meteor trails were captured over Cheyenne, WY on the night of 13-14 Dec 2025, the peak of the Geminid Meteor shower. Color can be seen in several of the trails. The color is mainly due to the meteor's chemical composition. Iron makes yellow trails, sodium, yellow-orange trails, and calcium, blue-green trails. Atmospheric nitrogen and oxygen produce red trails.

Fig. 2-50. The Geminid meteor shower over Cheyenne, WY on the night of 13 Dec 2025. Total elapsed time was 11 hours. JC.

2.13 Clear Sky Color Gallery

In this chapter we restricted our views to colors of the clear sky, or how clouds alter the light and color of the clear sky. In Chapters 4, 7, 12, and 14, we treat the light and colors of clouds. We do include one trick photo here. The deep blue 'sky' that remains deep blue right down to the 'horizon' in Fig. 2-51, in fact shows neither the sky nor the horizon. The photo was taken inside the crater Mount Mazama looking down to Crater Lake.

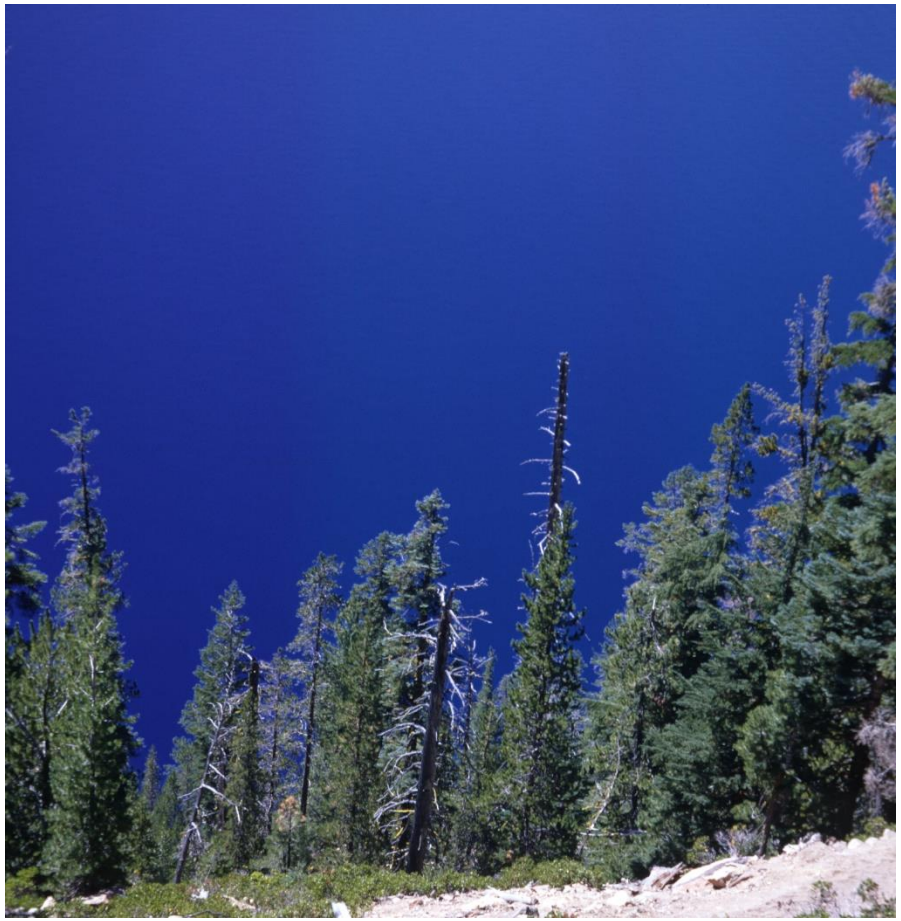

Fig. 2-51. A trick photo. A view down into deep blue Crater Lake on 1 Aug 1966, not the sky, which always grades whiter near the horizon. © Robert Gedzelman.

Fig. 2-52. World Trade Center Towers emerge from haze layer. © Aaron Wasserman.

Fig. 2-53. A black smoke trail released from a coal burning building in New York City reveals wavy flow in the air as it drifts over New Jersey. SDG.

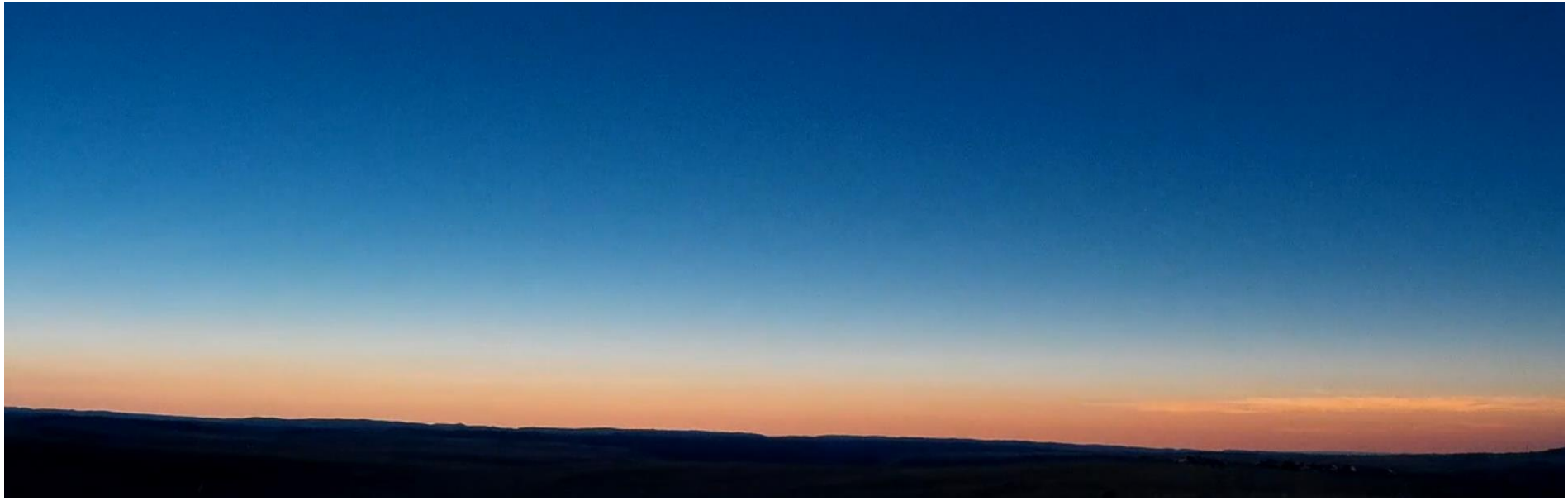

Fig. 2-54. Sky at the depth of the total solar eclipse 11:46:33, 21 Aug 2017, east of Glendo State Park, WY. JC Video at https://vimeo.com/236354795

Fig. 2-55. A purple twilight sky over Cliffside Park, NJ. SDG

Fig. 2-56. Being overtaken by Earth's shadow of night 20 Mar 2015. SDG.

Fig. 2-57. Noon sky downwind from Mullen Fire, Cheyenne, WY, 26 Sep 2020. JC.

Fig. 2-58. Twilight sky after El Chichon, Siesta Key, FL, Dec 1982. SDG.

Fig. 2-59. Clear day over Beartrail Ridge Overlook, Blue Ridge Parkway, NC, 12 Oct 2025. SDG. See also Fig. 2-25, right panel.

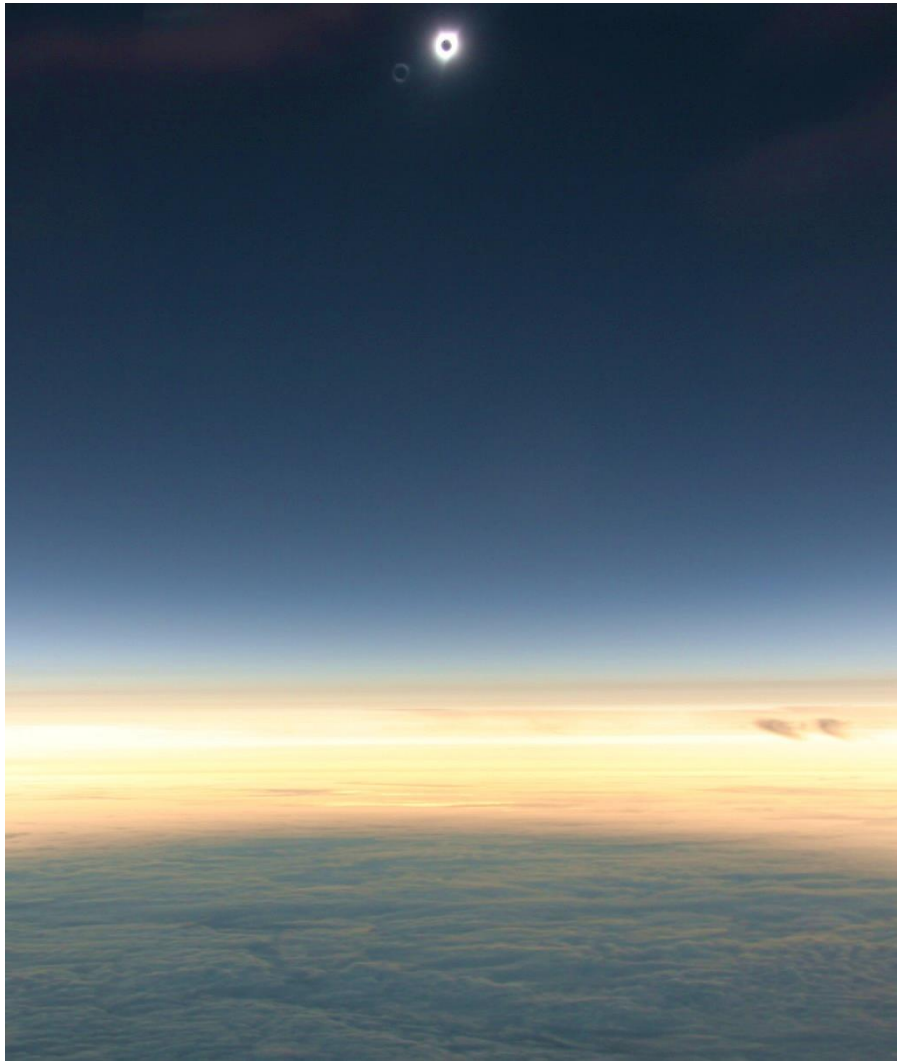

Fig. 2-60. Sky during the 21 Aug 2017 total solar eclipse 12 km over the Pacific Ocean facing east with shadow of Moon advancing eastward. SDG.

Fig. 2-61. Sky during the 2 Jul 2019 total solar eclipse over La Silla Observatory, Chile. © R. Lucchesi.

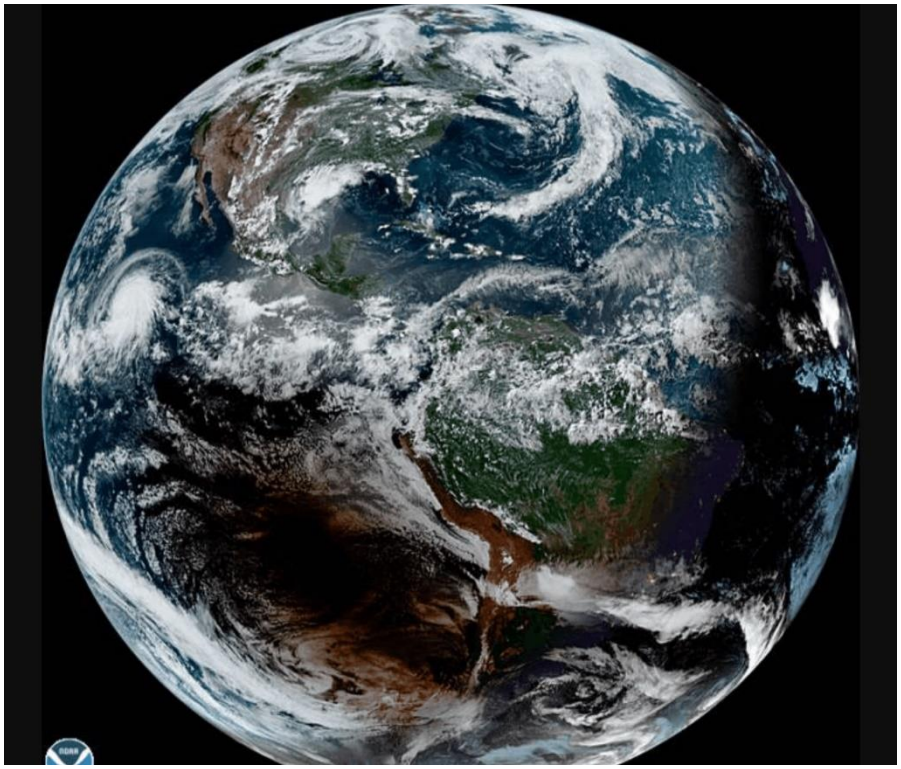

Fig. 2-62. GOES East image, 2 Jul 2019, showing the Moon's shadow reddening and darkening the clouds and the Atacama Desert. Hurricane Barbara swirls in the Pacific Ocean north of the equator as do two extratropical cyclones over Canada and over the North Atlantic Ocean (see Chapter 5).

Fig. 2-63. Inferior mirage near Stovepipe Wells, CA makes the road look wet and bumpy, 12 Apr 2019. ©FKRS

Wonders of the Atmosphere
Chapter 3: Auroras

Fig. 3-1. Aurora over Quartz Lake, AK, 06 Sep 1996. JC.

Fig. 3-2. Auroras over Fairbanks, AK. JC.

Wonders of the Atmosphere
Chapter 3: Auroras

3.1 Auroras and the Solar Wind

Of all the wonders of the atmosphere, the Aurora Borealis and Aurora Australis are perhaps the most awe-inspiring, lighting the otherwise dark night sky with fantastic moving displays of vivid colors (Fig. 3-1, Fig. 3-2). Much like snowflakes, no two auroras have the identical color, shape, and evolution, but all follow a similar cycle of growth, expansion and recovery. The importance of studying auroras goes beyond their beauty. They are caused by the same disturbances on the Sun, namely, Sunspots (Fig. 3-3), solar flares, and Coronal Mass Ejections (CME) that can present a hazard to electronics, disrupt communications, destabilize low satellite orbits, cause power grid electrical surges and upset GPS navigation.

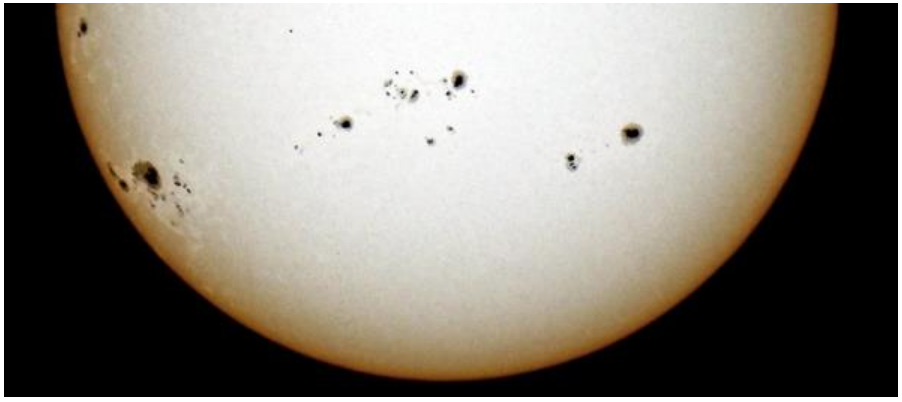

Fig 3-3. Sunspots near solar max, 5 August 2024. For scale, the Earth would be about the size of the smallest spots. The huge sunspot at left eventually produced a strong geomagnetic solar storm and many auroras. JC.

The aurora is the beautiful product of complex interactions between the solar wind, Earth's magnetic field, and the atmosphere. The solar wind consists largely of electrons and protons (i. e., ionized or split hydrogen atoms) that stream out to Space from the Sun's Corona in. The Earth is bathed in this solar wind, which would smash directly into Earth (eventually stripping away Earth's atmosphere) except that the electrically charged electrons and protons, are corralled and deflected by Earth's magnetic field into the shadow zone of night.

The vast majority of auroras occur when highly energetic electrons, approach the Earth's surface close enough to smash into the atoms and molecules of the upper atmosphere. The rare proton auroras (see §3.7) are restricted to major solar and geomagnetic storms.

During quiet times the solar wind is a modest flow. At the distance of the Earth, mean proton speeds average almost 200 km/s. The velocity and concentration of the solar wind increases enormously during disturbances that are much more common and stronger around the peaks of the Sun's cycles. Sunspots, solar flares, and CME's expel torrents of protons and electrons from the Corona. The strength of an incoming CME is measured by the speed and density of the solar wind. Usually if the speed is ~500 km/s auroras may be visible at high latitudes. If the speed exceeds 1000 km/s, the mid-latitudes may see the lights. Huge solar outbursts travel up to 3000 km/s reaching us in 15 to 18 hours and the number of energetic protons reaching the Earth every second can increase by a factor of over 100,000 from the background rate. It is during these times that the most spectacular and widespread auroras occur.

3.2 Auroras and Earth's Magnetic Field

As the electrons and protons approach the Earth they encounter its magnetic field. Earth's magnetic field is created by convective and spinning motions in the liquid iron and nickel outer core. The field is

closely but not exactly aligned with the geographic poles and drifts over time, now moving around 60 km/yr. (In 2024, the North Magnetic Pole was calculated to be at 85.9° N latitude.) The strength of the field averages about 0.5 gauss, or only about 0.5% the strength of magnets used as stickers on refrigerators. Near the Earth the shape of the field resembles that of a bar magnet and is close to a classical dipole (Fig. 3-4). Further out from the Earth, in the magnetosphere,

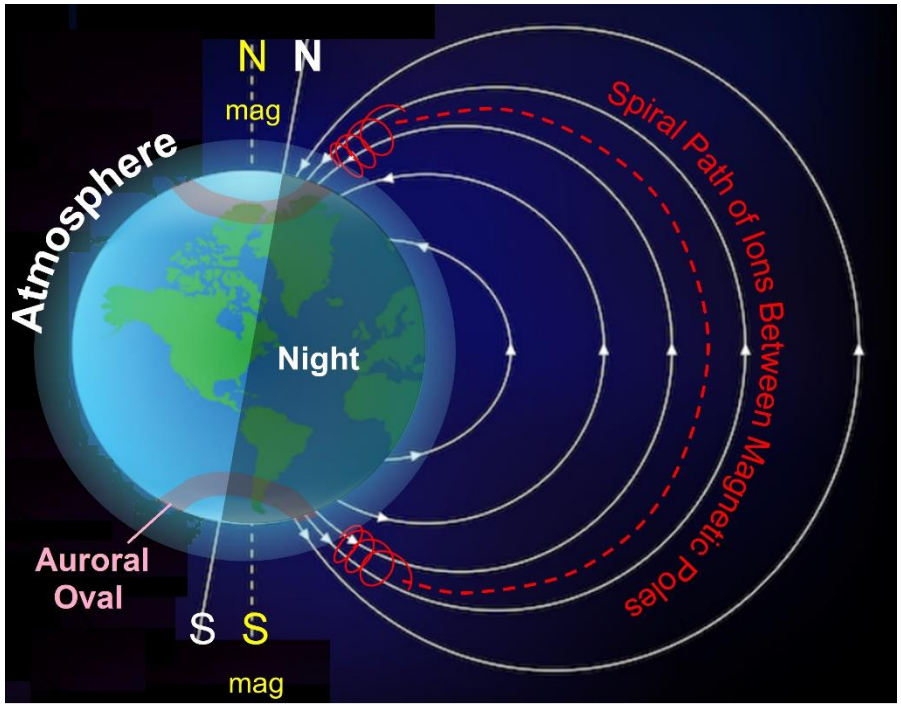

Fig. 3-4. The aurora, auroral oval, and Earth's magnetic field with spiral path of electrons along magnetic field lines between the magnetic poles. SDG.

Earth's magnetic field interacts with and is distorted by the solar wind and the interplanetary magnetic field it drags our from the Sun (Fig. 3-5).

When CME's approach the Earth they bombard the magnetosphere, distorting and strengthening it, and causing geomagnetic storms as well as auroras. The distorted magnetic field in turn deflects and accelerates the flow of electrons and protons, which have the best chance of pouring into the tail of the magnetosphere on the night side of the Earth when the interplanetary magnetic field (***B***z) aims southward (opposite Earth's magnetic field) breaking and reconnecting the two fields to produce auroras, as illustrated in Fig. 3-5 and by the video,

https://vimeo.com/1001472030

The enhanced magnetic field during peak solar activity also reduces the rate at which harmful cosmic rays approach Earth's surface, which in turn reduces the production rate of radioactive Carbon-14 (^{14}C). Since plants ingest ^{14}C and are often preserved long after they die, they serve as proxies in the geologic record of past solar activity.

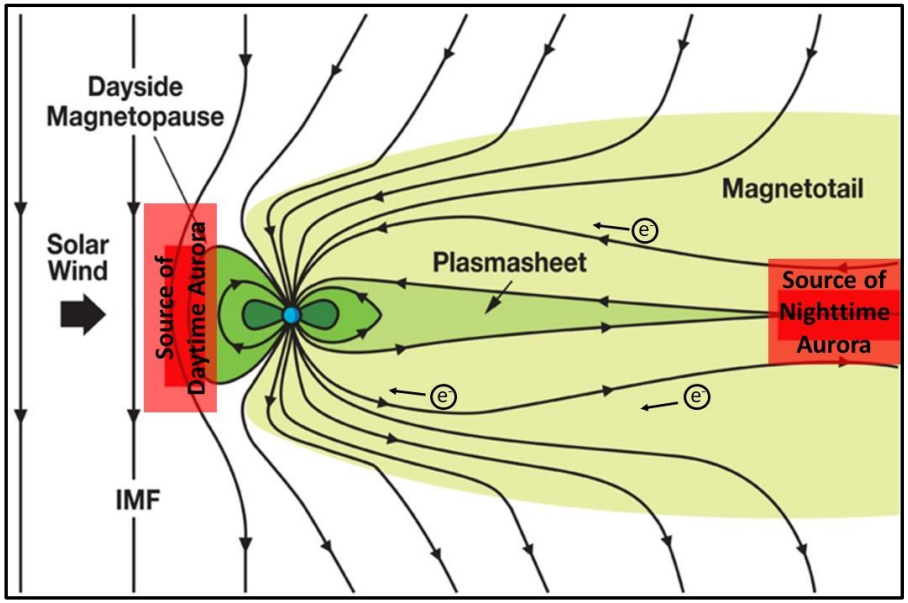

Fig. 3-5. Magnetosphere dynamics and auroras. (credit: ESA/ATG medialab)

After entering the magnetosphere, the electrons and protons are compelled to spiral along the magnetic field lines (as in Fig. 3.4) much like moths spiral around lights at night. For much of their stay, they remain so high above the Earth's surface that they essentially move through a vacuum. But the ions that have become trapped to

spiral in the magnetic field lines that slope or dip sharply downward toward the magnetic poles plunge down into the ionosphere and smash into its rarified gases.

This happens in the *auroral oval*, a ring around the magnetic poles that is confined to the high geomagnetic latitudes during quiet times, but broadens and spreads as solar activity increases, reaching the middle latitudes during huge CME's. A false color image of the auroral oval from an ultraviolet aurora around Antarctica was captured by NASA's IMAGE spacecraft on 11 Sep 2005 following a major CME (Fig. 3-6).

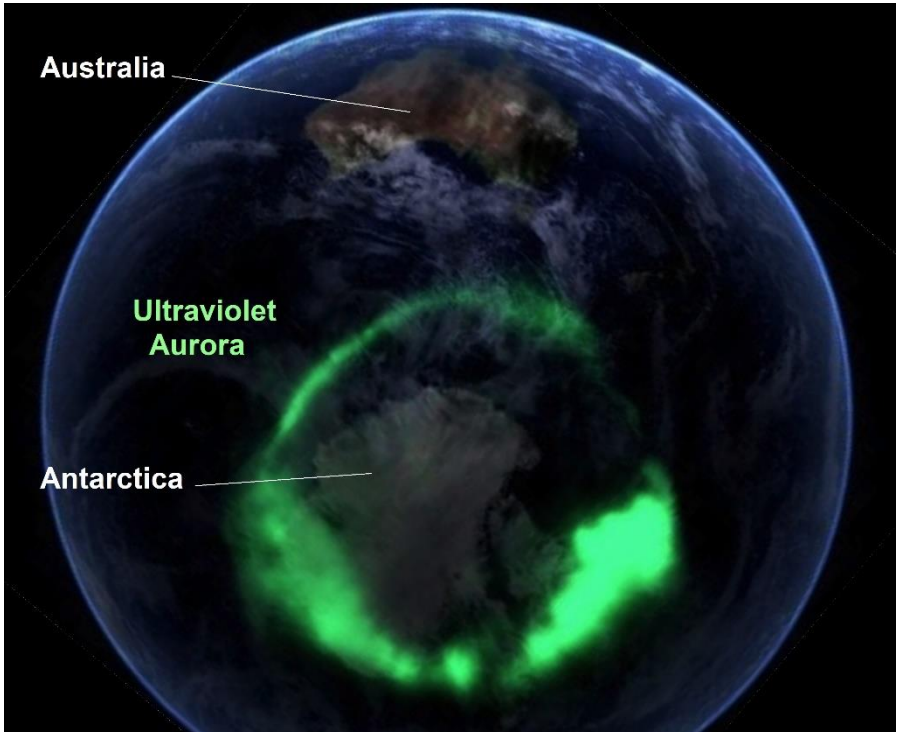

Fig. 3-6. False-color image of ultraviolet aurora australis around the auroral oval 11 September 2005. NASA IMAGE satellite, digitally overlaid onto The Blue Marble composite image.

Aurora *borealis* means *Northern* Dawn because in the middle latitudes it is most often seen reddening the sky at night just above the northern horizon. An example is the 'Deep Sky' aurora of 31 Dec 2024 in Cheyenne, WY (Fig. 3-7), which was accompanied by a rare Stable Aurora Red (SAR) arc. Deep sky auroras are barely visible to the unaided eye, but are revealed by time exposures of cameras.

Fig. 3-7. A "Deep Sky" aurora just above the horizon with a rare Stable Aurora Red (SAR) arc above, Cheyenne, WY, 31 Dec 2024. JC.

Numerous space and terrestrial sensors are used to predict when and where auroras may be visible. The quantities they measure include the flow and speed of protons, and the interplanetary magnetic field's direction and disturbances.

The mean southern limit of the aurora is related to the Geomagnetic Storm Index, G, which ranges from 1 to 5, and the K-index of the outburst (Table 3-1). The K-index a measure of the maximum fluctuations of Earth's magnetic field observed on a magnetometer during a three-hour interval. It ranges from 0 to 9, with 5 or more indicating a geomagnetic storm. The planetary 3-hour-range index, ***K***p, is the mean standardized K-index from 13 geomagnetic observatories between 44° and 60° geomagnetic latitude.

Geomagnetic Storms

Scale	Description	Effect	Physical measure	Average Frequency (1 cycle = 11 years)
G 5	Extreme	**Power systems:** Widespread voltage control problems and protective system problems can occur, some grid systems may experience complete collapse or blackouts. Transformers may experience damage. **Spacecraft operations:** May experience extensive surface charging, problems with orientation, uplink/downlink and tracking satellites. **Other systems:** Pipeline currents can reach hundreds of amps, HF (high frequency) radio propagation may be impossible in many areas for one to two days, satellite navigation may be degraded for days, low-frequency radio navigation can be out for hours, and aurora has been seen as low as Florida and southern Texas (typically 40° geomagnetic lat.).	Kp = 9	4 per cycle (4 days per cycle)
G 4	Severe	**Power systems:** Possible widespread voltage control problems and some protective systems will mistakenly trip out key assets from the grid. **Spacecraft operations:** May experience surface charging and tracking problems, corrections may be needed for orientation problems. **Other systems:** Induced pipeline currents affect preventive measures, HF radio propagation sporadic, satellite navigation degraded for hours, low-frequency radio navigation disrupted, and aurora has been seen as low as Alabama and northern California (typically 45° geomagnetic lat.).	Kp = 8, including a 9-	100 per cycle (60 days per cycle)
G 3	Strong	**Power systems:** Voltage corrections may be required, false alarms triggered on some protection devices. **Spacecraft operations:** Surface charging may occur on satellite components, drag may increase on low-Earth-orbit satellites, and corrections may be needed for orientation problems. **Other systems:** Intermittent satellite navigation and low-frequency radio navigation problems may occur, HF radio may be intermittent, and aurora has been seen as low as Illinois and Oregon (typically 50° geomagnetic lat.).	Kp = 7	200 per cycle (130 days per cycle)
G 2	Moderate	**Power systems:** High-latitude power systems may experience voltage alarms, long-duration storms may cause transformer damage. **Spacecraft operations:** Corrective actions to orientation may be required by ground control; possible changes in drag affect orbit predictions. **Other systems:** HF radio propagation can fade at higher latitudes, and aurora has been seen as low as New York and Idaho (typically 55° geomagnetic lat.).	Kp = 6	600 per cycle (360 days per cycle)
G 1	Minor	**Power systems:** Weak power grid fluctuations can occur. **Spacecraft operations:** Minor impact on satellite operations possible. **Other systems:** Migratory animals are affected at this and higher levels; aurora is commonly visible at high latitudes (northern Michigan and Maine).	Kp = 5	1700 per cycle (900 days per cycle)

Table 3-1. The strength and frequency of occurrence during the ~11 year Hale (sunspot) cycle is shown as an index of storm impacts.

In the extreme cases when ***Kp*** = 9 the auroral oval is filled to overflowing so that auroras can be seen down to even lower latitudes, where they have stupefied people in ways that cannot be overrated. For example, George Siscoe has argued in ***Unleashing Yahweh: Ezekiel's Vision and the Northern Lights*** (2023) that the description of Ezekiel's Vision matches many of the features of the aurora, and its appearance was such a wondrous event it firmed the faith among the Israelites then banished in Babylon.

Modern sightings of the aurora at Honolulu, Hawaii (latitude 21°N) and even Colombia during the Carrington Event that peaked on 1-2 Sep 1859 (making the sky bright enough to read and causing fires in telegraph stations) confirmed the possibility of Ezekiel's sighting.

The contour lines in Fig. 3-8 give the mean equatorward position for ***K***p-index of a geomagnetic storm where the aurora borealis will fill the northern half of the sky. The aurora fills the sky at all locations where the ***K***p-index is greater than the contoured value. If the ***K***p-index is slightly less than the contoured value, the aurora may still appear low on the horizon; however, a perfect viewing location and good eyes are usually required to see it. This is when a camera is helpful to pick up fainter "Deep Sky" aurora displays.

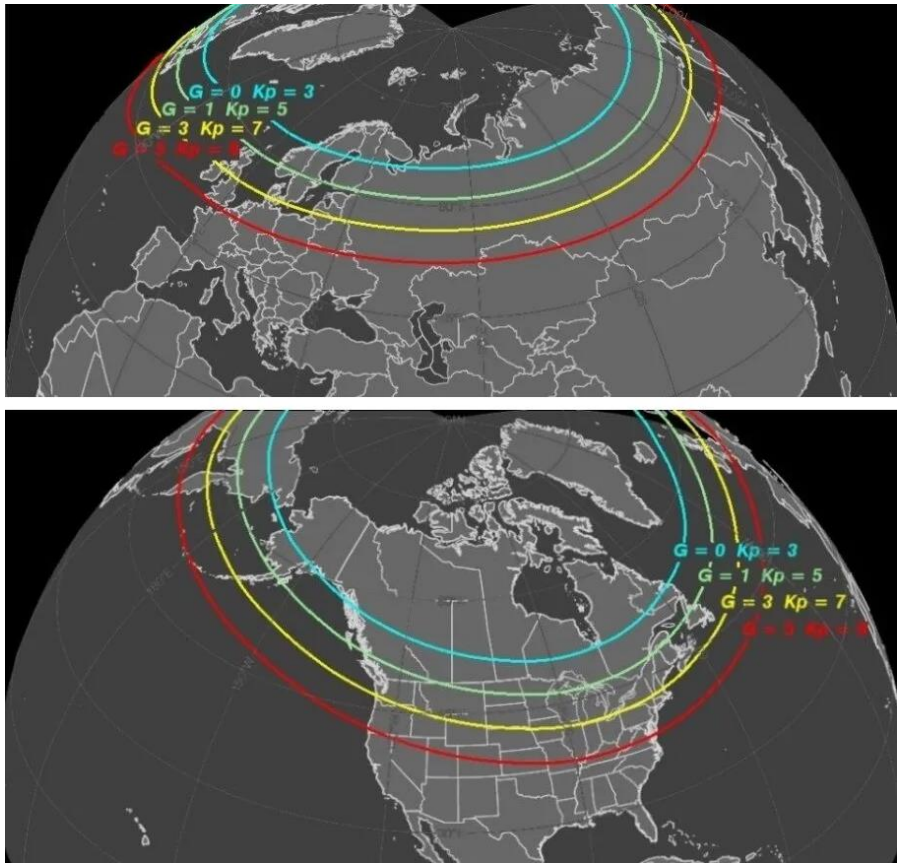

Fig. 3-8. Furthest south the aurora can be seen as a function of the Kp index. Source SWPC/NOAA, https://www.theaurorazone.com/nuts-about-kp/

The appearance and intensity of the aurora vary over the course of the night. Soon after the Sun sets in the west the aurora appears low on the eastern horizon. On average, the aurora appears highest and is brightest around midnight. As dawn approaches and the Sun begins to light the eastern sky, the auroras fade last near the western horizon. Of course, in the land of the midnight sun, auroras often brighten at noon although midnight remains the major peak time of the daily cycle.

3.3 Auroras and the Atmosphere

Auroras occur in the ionosphere, high above the Earth's surface. At the Earth's surface, even though air seems so light, molecules are packed so closely that a particle can only move about $1/10^{th}$ of a micrometer before colliding with an air molecule. Light waves can skirt around the molecules but particles have no such ability and strike any other particle in their path. As electrons spiral from great heights down to the Earth, the rarified air is finally dense enough for collisions to occur about 300 km above the Earth's Surface, and even the most energetic electrons and protons in the strongest CME's are stopped by about 60 km above the Earth's surface.

Before the era of rockets and satellites the height of the auroras could only be determined by laborious triangulation of observations at several different, widely spaced locations. Now, of course, auroras are observed in their full glory from top to bottom by astronauts in the International Space Station, which orbits the Earth at 400 km. Fig. 3-9 captured the full height of the aurora of 29 Aug 2014 from its green base to its red top, and showed how far it formed above the paper thin, dense lower atmosphere indicated by the blue stripe. The aurora's dynamism was captured in the video,

https://www.youtube.com/watch?v=WDmNsX6Y2wo

3.4 Colors of the Aurora

The aurora's light and color arise after the electrons from Coronal Mass Ejections (CME's) smash into the molecules, atoms, and ions

Fig. 3-9. Aurora 29 Aug 2014 from the International Space Station. Alexander Gerst, ESA astronaut. ESA/NASA.

in the ionosphere and energize or excite them. The collisions can split molecules into atoms, strip electrons to ionize the atoms, or simply raise the electrons' energy levels or orbitals of the electrons. Photons of light are emitted when the electrons deexcite or return to lower energy levels. The wavelength or color of the emitted light is determined by the energy change between the orbitals.

As might be expected, the atmosphere's two most abundant gases, Nitrogen (78%) and Oxygen (21%) are responsible for most auroras. Two of the major wavelengths or colors of the aurora are green, at 557.7 nm and red, at 630 nm. Both are produced by atomic oxygen.

There is, however, a limiting complication that restricts the height of all auroral colors but red in particular. Collisions that include the

energized particles disrupt their electron transitions. The times of orbital transition are very short but so are the times between collisions of particles in the atmosphere. The red transition is so slow that it is disrupted by frequent collisions in the denser atmosphere below 240 km. Hence red appears mainly at the top of auroral displays, above 240 km. The slow deactivation also makes the red part of the aurora seem to move more slowly than the green.

Much below 100 km, atomic oxygen is rare, so the green aurora fades. Nitrogen molecules produce a range of blue and red auroral light, with blue at 428 nm the dominant wavelength. Other colors arise as the result of differing combinations of the spectral colors.

Our eyes cannot always detect the colors in faint auroras. Lining our retinas are rod-shaped and cone-shaped photoreceptor cells. About 95% of our photoreceptors (about 100 - 125 million) are rods. They are great at helping you see in dim places, but they are not as good at fine details, and they cannot detect colors. Cones can detect colors but since they require more light to activate than rods, faint auroras often appear white to the naked eye. The sensitivity of the human eye varies with wavelength or color, being lowest at the violet and red ends of the visible spectrum and greatest near the center. As a result, red auroras are about 10 times more difficult to observe by the human eye (though not by digital cameras) than green auroras.

We begin our voyage of color starting with the highest auroras, which normally extend upward to about 400 km but may range as high as 1000 km. We then proceed to the lowest auroras, which cut off sharply at a minimum height around 80 km.

Blue and Violet [300-400+ km]: Hydrogen and helium release blue and violet light at the top of the aurora. However, these colors are relatively faint and are not usually visible except under very dark skies or with strong solar storms. Also, because these gases are relatively rare, the light is diffuse. One particular aurora color is the result of excited nitrogen being further excited by sunlight. This "sunlit aurora" typically occurs at twilight and can be seen as a purplish color at the top of the auroral rays (Fig. 3-10).

Figure 3-10. Blue and violet auroral tops during astronomical twilight over Fairbanks, AK. JC.

Fig. 3-11. A high-altitude red aurora during a major solar storm over Cheyenne, WY, 10 Oct 2024. JC.

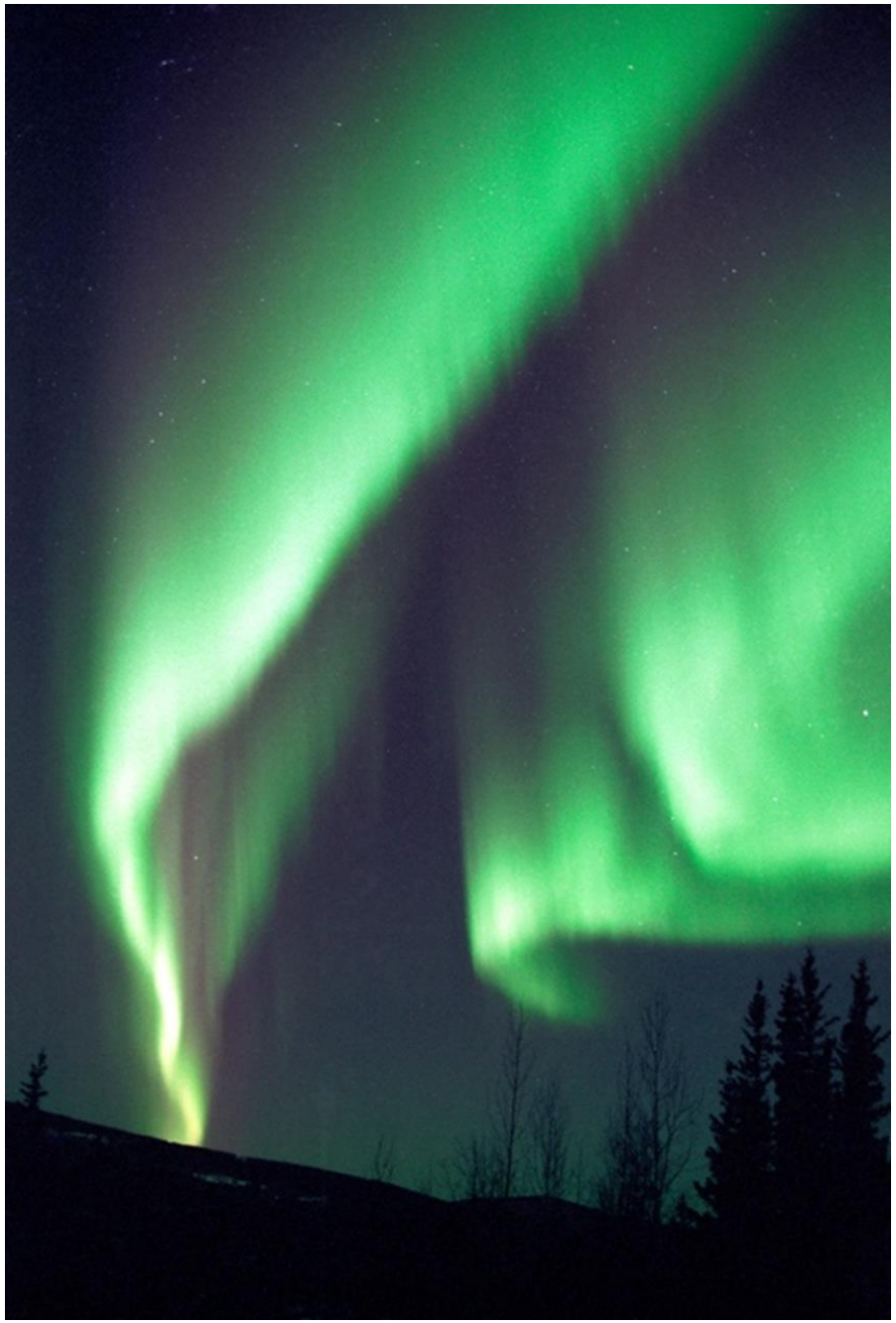

Fig. 3-12. Common yellow-green aurora at Fairbanks, AK. JC.

Fig. 3-13. An unusual blue aurora at Fairbanks, AK. JC.

Fig. 3-14. An unusual low deep red aurora that occurs very briefly during extremely active displays. At twilight at Fairbanks, AK JC.

Red [240-400+ km]: Red light at the top of an aurora comes from slow deexcitation of O atoms. In the mid latitudes, sometimes only the red appears above the horizon line (Fig. 3-11).

Yellow-Green [100-300 km]: Vivid lime green is the most common color of the aurora. It comes from rapid deexcitation of O, and penetrates to the base of the ionosphere because collisions are too infrequent to disrupt it (Fig. 3-12). Much below 100 km there is so little atomic oxygen the green aurora often ends sharply.

Blue [100-300 km]: Excited nitrogen molecules (N_2+) release blue light when they return to a more stable energy state. Whether an aurora is blue, blue-green, or yellow-green depends on the interplay of light from nitrogen ions and oxygen atoms (Fig. 3-13).

Fig. 3-15. Black "anti"aurora in Alaska. The "E" pattern shows voids that have eluded explanation until recently. ©Todd Salat / AuroraHunter.com)

Fig. 3-16. White aurora at Fairbanks, AK. JC.

Deep Red [100 km]: A deep red color at the base of the aurora comes from deexcitation of N_2 (Fig. 3-14). The red fringe often changes color that last less than a second, making it difficult to image. Purple or vivid pink results when the red combines blue-violet light from deexcitation of N_2^+ ions. Orange results from the admixture of lime-green.

Fig. 3-17. Full spectrum aurora at Kõnnu Suursoo, Estonia. ©Andres Papp.

Black "anti" auroras (Fig. 3-15) are small-scale features embedded in the diffuse background aurora, typically occurring post-substorm after magnetic midnight and with an eastward drift. Black auroras show a significant reduction in optical brightness compared to the surrounding diffuse aurora and can appear as slow-moving arcs or rapidly moving patches and arc segments. The dark regions likely come from electric fields in the upper atmosphere that block electrons from interacting with gases.

White auroras are very rare (even considered to be a hoax). However, this original un-processed image (Fig. 3-16) also observed, clearly shows that it exists and is the result of a perfect mix of many rarified atmospheric gases. Perhaps, digital camera sensors are unable to capture white aurora whereas film can. However, this still doesn't explain why visual sightings of pure white are not reported.

Multiple color auroras are the result of mixtures of the spectral colors to produce secondary colors (e. g., purple) and tertiary colors (e. g., vermilion - teal - chartreuse - amber). Thus, blended colors occur in strong geomagnetic storms. (Fig. 3-17).

3.5 Auroral Morphology and Structure

Auroras can be diffuse or discrete. Discrete auroras take on a range of shapes that extend into the fantastical including arcs, bands. curtains, coronas, and pillars or rays.

Arcs possess long graceful curves from horizon to horizon. They are the most common shape, seen in times of low solar activity. During times of more intense solar activity, they become more active and rippled or distorted. In mere minutes, arcs can change to bands and curtains.

Bands and Curtains are like arcs but appear with more curves. These wavy, ribbon-like aurora formations are the ones most people hope to see. When conditions get really intense, they may look like curtain folds blowing in the wind.

The changes from arcs to bands to curtains occur as hydromagnetic Alfven waves in the plasma of charged particles in the magnetic field form and grow in amplitude (Fig. 3-18). The series of photos in Fig. 3-20 illustrates the amplification of waves in the aurora.

The apparent shapes of an aurora also depend on the viewing angle and the distance from it (Fig. 3-19). Thus, for example, distant curtains may appear bandlike while curtains directly overhead will appear as coronas.

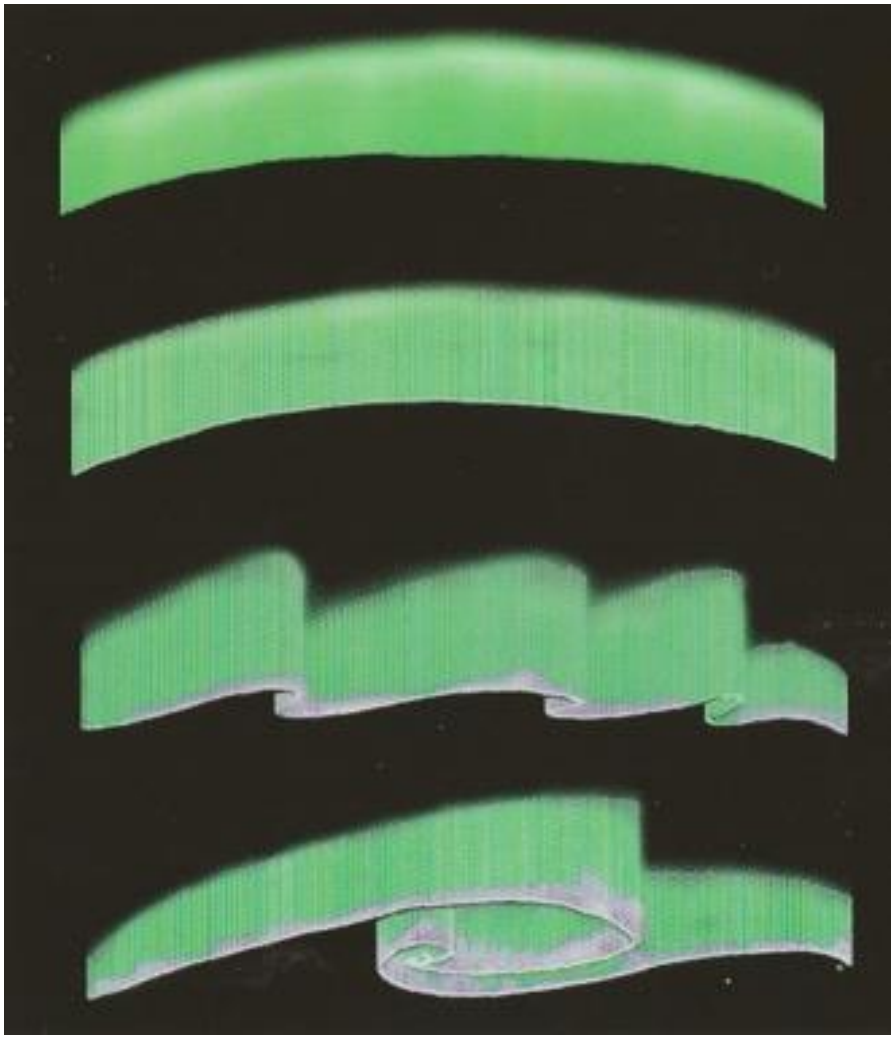

Fig. 3-18. Growth of waves changing an aurora shaped like band to an arc to a curtain. ©S. I. Akasofu.

Coronas are the most impressive of all auroras and have been the form most sought after by aurora chasers (at least until the discovery of dunes). This crazy, colorful vortex effect appears directly under a display of pillars. When it happens, the base of the aurora is only about 80-90 km directly overhead. People have described coronas as looking like angels or butterflies or dragons.

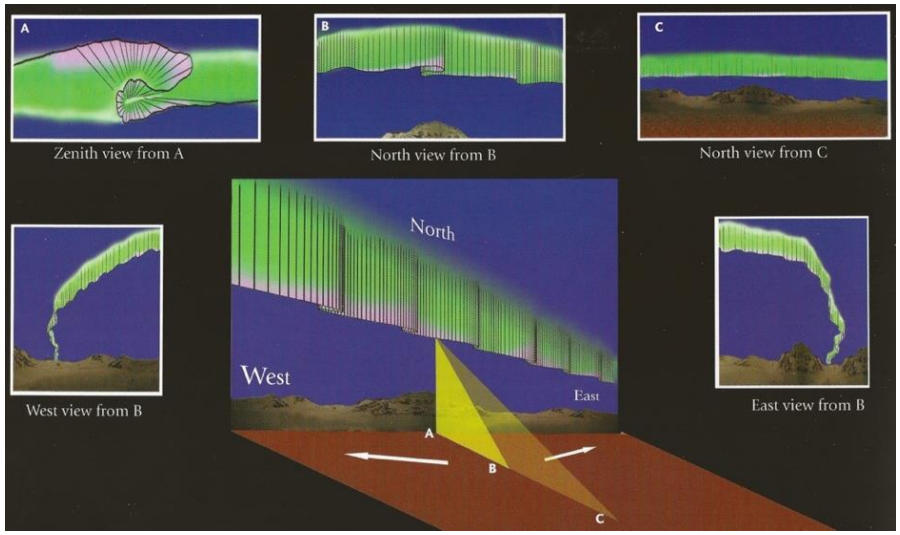

Fig. 3-19. Auroral curtain seen from various viewpoints and distances. ©S. I. Akasofu.

Since few auroras occur directly overhead, especially in the mid latitudes, corona auroras are rare. At high latitudes they are seen sporadically during periods of intense solar activity. In the mid latitudes they are only seen during exceptional, major solar events.

The sequence of photos in Fig. 3-21 captured a corona formation that developed directly overhead at Fairbanks, AK over a period of 30 seconds as auroral rays converged to the magnetic zenith.

The ephemeral corona-shaped auroras usually coincide with the peaks of strong magnetic (or auroral) substorm events. The time lapse video of the Great 10-11 May 2024 substorm,

https://www.flickr.com/photos/cloud_spirit/53726786058

taken at Glendo, WY, captured changes of the corona-shaped aurora every 10 seconds.

Fig. 3-20. Auroral arcs transitioning into bands and curtains via growth of waves in the magnetic field lines and plasma. Fairbanks, Alaska. JC.

Pillars, also called beams or rays, can be seen alone as a streak or two, or as a cluster of streaks. They can also be features of active arc, band, or corona auroras. These are the vertical bars of light that seem to reach upwards (Fig. 3-22). They can sometimes be as tall as 600 km from the green base to the purple canopy. Their apparent upward convergence is largely a consequence of linear perspective.

Picket Fence auroras (Fig. 3-23) are of short duration and typically fast moving. They manifest as lines of separate parallel rays. They are often seen above a non-aurora event called STEVE (see §3.7).

Pulsating auroras can change in appearances and intensity over a wide range of time scales, with periods of 2–20 seconds being typical. However, the changes may occur so slowly as to be difficult to notice, or too rapidly for the brain to detect. The flickering rate of 10 times per second is well known, but recent measurements show that auroras flicker at up to 80 times per second. A case of pulsating aurora was captured over a 20 s period during the peak of a G4 substorm on 10 Oct 2024 over Cheyenne, WY (Fig. 3-24).

3.6 Auroral (Magnetospheric) Substorms

During solar storms, the magnetosphere fills to overflowing. Excess electrons then pour as from a tipping bucket as pulses corralled within the auroral oval down toward the Earth's surface. These pulses, called magnetospheric or auroral *substorms*, last several hours and produce auroras that fill the sky within the auroral oval towards the magnetic poles. They have a typical life cycle of three phases, mapped in Fig. 3-25 and described below as if they take place over the course of a night, though they may occur several times in a night and even overlap.

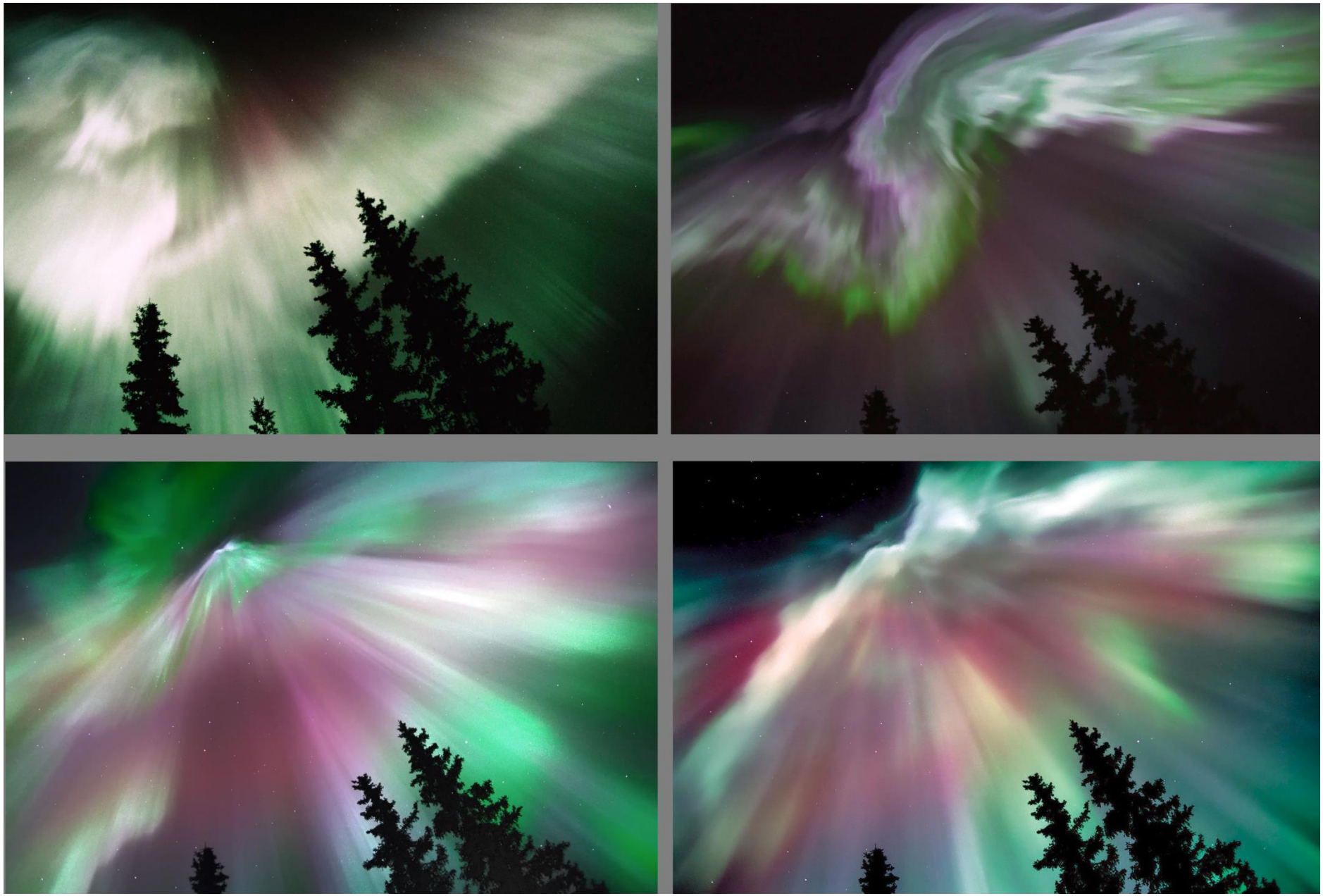

Fig. 3-21. Evolution of a corona aurora during a period of 30 s directly over Fairbanks AK. JC.

Fig. 3-22. A pillar aurora minutes apart with a cluster of streaks at Fairbanks AK, 30 Mar 2001. JC.

Fig. 3-23. Two cases of picket fence auroras lines of parallel rays, Fairbanks, AK. JC.

Fig. 3-24. Pulsating aurora during the peak of a G4 substorm on 10 Oct 24 over Cheyenne, WY, 20 seconds apart. JC.

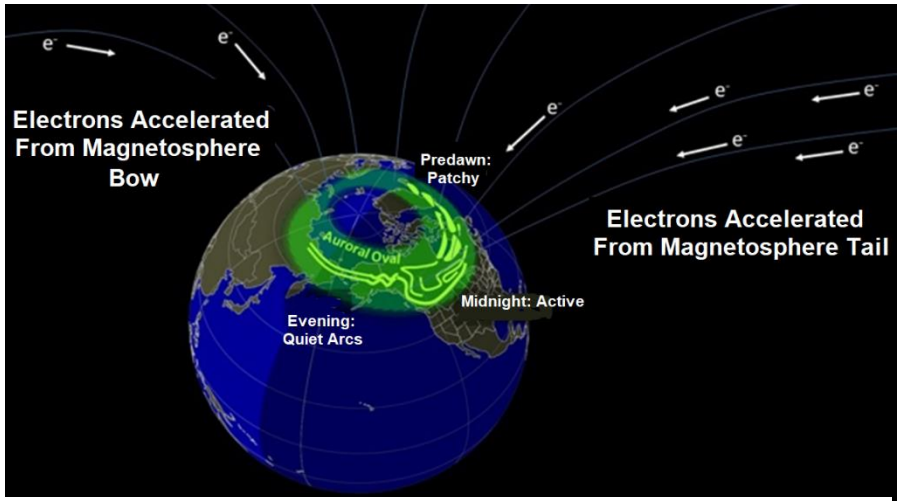

Fig. 3-25. Map of an auroral substorm that takes place over the course of a night. SDG.

Fig. 3-26. Diffuse aurora at start of a substorm JC.

Growth Phase (Evening): Shortly after sunset the aurora often appears as a diffuse arc (Fig. 3-26) spanning east-west from horizon to horizon. Sometimes there are several discrete parallel arcs (Fig. 3-27 left). Often, they appear as bundles of tall rays that resemble a hanging curtain. The evening arcs tend to fill the sky towards the poles to a degree that depends on the level of geomagnetic activity (Fig. 3-27 right). The motion of the auroras is initially east to west. It slows by midnight, after which it reverses direction and accelerates as the auroral oval sinks to the western horizon.

Expansion Phase (Midnight): A few hours before midnight, depending on the level of geomagnetic activity, the aurora can show signs of increased activity in the form of waves or ripples that develop and move along the auroral arcs (Fig. 3-28 left) much like someone running their hand along a curtain. During periods of moderate to high geomagnetic activity, there can be a series of

Fig. 3-27. Aurora becomes more structured and spreads from the east horizon to its highest point in the sky around local midnight. JC.

geomagnetic substorms that greatly enhance the complexity and brightness of the aurora for several hours around midnight. The aurora can rapidly expand poleward. Great swirls and bright features appear. Each substorm is associated with a "Westward Traveling Surge" (Fig. 3-28 right) where structures move toward the western horizon at several km/s.

Fig. 3-28. Expansion phase. Waves amplify and move along auroral arc (left). Complex structures form and move rapidly to the west (right). JC.

Fig. 3-29. Diffuse patches of aurora at Chena Hot Springs, AK. JC.

Recovery Phase (Toward Dawn): After the substorms pass overhead, the aurora becomes less active, more diffuse and 'patchy' (Fig. 3-29). The patches often pulse on and off every 10 seconds (though they could strobe up to 80 times per second) and usually continue doing so until dawn. The 10 second period is too slow to create the sense of a pulsating patch except with time-lapse videos. As the substorm ends, the aurora dims and fades and is no longer so distinctive, sometimes resembling a predawn sky (Fig. 3-30).

Fig. 3-30. Diffuse auroral glow (not twilight) at end of substorm. JC.

3.7 Auroral Outliers

Dune Auroras

Most auroras intrude themselves into a relatively passive atmosphere. Occasionally, winds can be so fast and waves so pronounced near the base of the mesosphere that they alter the shapes and motions of the auroras. This is the case with recently discovered (2016) dune auroras, which have distinctive shapes that resemble dunes (Fig. 3-31). Their shape and motions, animate in the video

https://www.youtube.com/watch?v=OMgsOyIuebc

are driven by gravity waves that rise from below, curve into the mesosphere and get trapped in anomalous temperature inversions between about 90 and 100 km The trapped waves then become supercritical and resemble tidal bores. The first documented case of dune auroras occurred on 20 Jan 2016. It was photographed by

Fig. 3-31. Dune aurora (left) at 100 km altitude with an auroral arc at Laitila, Finland 07 Oct 2018. ©Kari Saari.

scientist observers from Finland to Scotland, so its velocity could be calculated (to the WSW at 200 m/s).

STEVE

Fig. 3-32. A purple and green searchlight beacon of STEVE (possibly the southernmost case) on 17 May 2017 east of Cheyenne, WY. JC.

Fig. 3-33. A stable Auroral Red Arc on 10 Oct 2024 at Boulder, CO. ©Bill Bowman.

In 2016, more than fifty citizen science observations described what was an aurora look-alike they named STEVE, for "Strong Thermal Emission Velocity Enhancement". STEVE is not an aurora though it most often occurs in conjunction with picket fence auroras. It has been observed on and off for centuries, though was not named before 2016. STEVE occurs at an altitude of 450 km and consists of long, narrow (~25 km wide) purple and green ribbons (Fig. 3-32) of superheated plasma (***T*** ~3300 K) well above the typical high temperatures of ~2000 K in the excited thermosphere. The air is accelerated from typical speeds of 10 m/s to 6 ***km***/s. At that speed, collisions can split molecules. One hypothesis for the purple color is the energy released when nitrogen and oxygen combine to form nitric oxide. A video of the STEVE event of 17 May 2017 over Cheyenne, WY reveals an apparent clockwise spinning (opposite that of most tornadoes) of the pillars or beams.

https://www.flickr.com/photos/cloud_spirit/34869601832

Much remains to be discovered about the causes and mechanisms of STEVE. In recent years, it has been observed that STEVE may develop from Stable Auroral Red (SAR) arcs.

Stable Auroral Red (SAR) Arcs

Unlike the aurora which is generated by electrons smashing into Earth's atmosphere, Stable Auroral Red (SAR) arcs are generated by extreme thermal and kinetic heating from energy conducted from the electromagnetic field around Earth to the ionosphere. SAR arcs appear as relatively stationary east-west arcs. For unknown reasons, only oxygen is heated up during a SAR, which means these phenomena always emit the exact same shade of red. The SAR of Fig. 3-33, seen over Boulder, CO occurred during the strong G4 geomagnetic storm and associated aurora event of 10 Oct 2024. It appeared as a stationary red band rising from the west, distinct from the pillars of auroral color moving across the northern sky.

Proton Auroras

Ironically, the far more massive and higher energy protons in the solar wind play only a minor role in the aurora. They form only during major solar (and resulting geomagnetic) storms but otherwise differ from the much more frequent electron auroras in almost every respect.

Proton auroras tend to be much fainter than electron auroras. They lack the beautiful structures such as curtains and appear instead as amorphous, usually green, blobs that pulse and fade. Fig. 3-34 shows six frames of the pulsing proton aurora embedded in the red aurora over Cheyenne, WY that occurred during the major solar and geomagnetic storm of 11 Nov 2025

https://www.flickr.com/photos/cloud_spirit/54918987439

The proton auroras sometimes seem to tear themselves apart. They also tend to occur at lower latitudes as a result of their distinct formation process. Whereas electrons tend to spiral between the

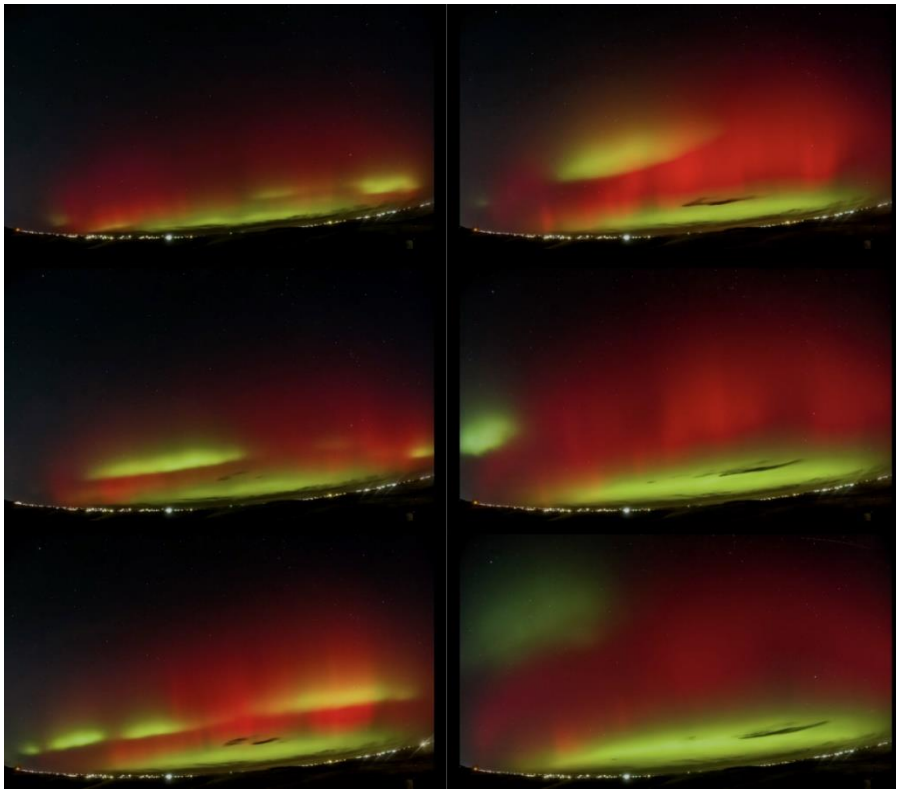

Fig. 3-34. Six frames including the proton aurora appearing as transient green blobs embedded in an electron aurora over Cheyenne, WY during the major solar storm of 11 Nov 2025. JC.

magnetic poles (Fig. 3-4), protons tend to spiral from east to west (opposite Earth's rotation) in a ring current around the magnetosphere. It is during extreme solar storms that protons overflow the ring current and pour down toward the Earth's surface to produce the proton auroras.

3.8 The Great Auroral Storm of 10-11 May 2024

On 08 May 2024 the world's aurora watchers were put on high alert as a giant X1-class flare and several other large solar flares burst out of the Sun producing Coronal Mass Ejections aimed toward Earth.

The intensity of solar activity only grew more severe over the next several days, with an X4-class flare and giant CME's blasted out on 10 May that promised great things.

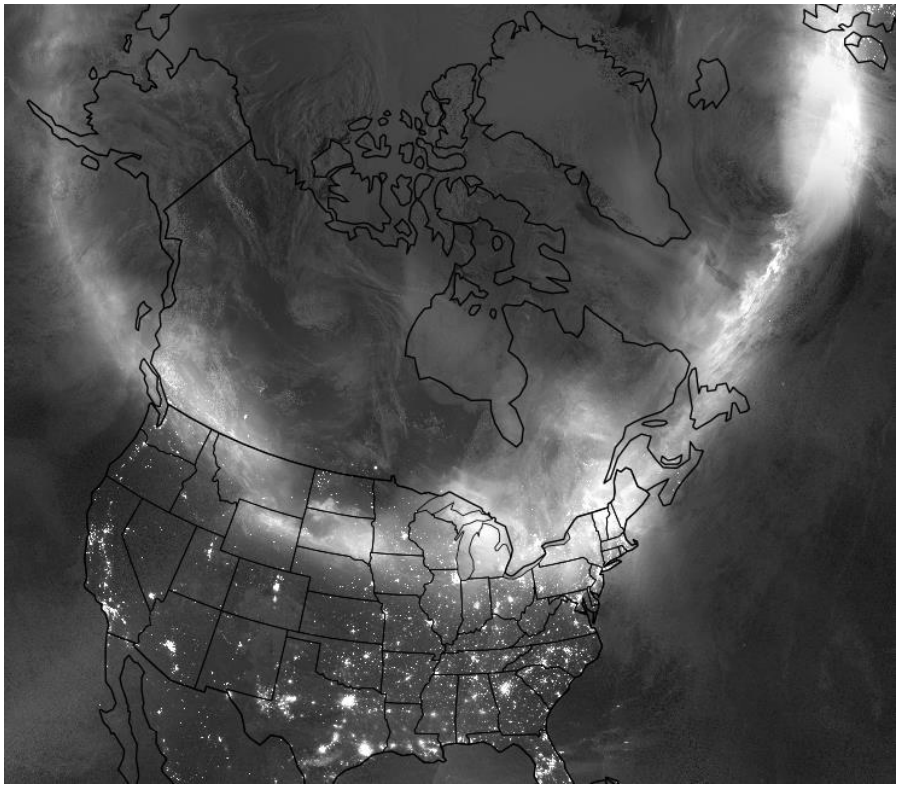

Fig. 3-35. Auroral oval on the night of 10-11 May 2024. VIIRS image.

The night of 10-11 May lived up to its promise, producing the greatest and most widespread auroral display and the highest class of geomagnetic storm (G5) in decades. The aurora was seen as far south as the Yucatan, Jamaica, Cuba, and Hawaii, but, of course, the greatest displays were seen along the peaks of the auroral oval (Fig. 3-35), for example in Wyoming, South Dakota, Michigan, New York, and northern New England. And the Moon was 'cooperative' It was only two days past new so that it was only 12% as bright as a full Moon and set just before midnight.

Jan: "Anticipating a major aurora, I drove to Glendo State Park, WY, at the edge of Glendo Reservoir, 160 km north of Cheyenne, where it was dark 5 km from the nearest town lights, and with a good view to the horizon. Setting up with multiple cameras that ran through the night until heavy dew fogged up the lenses after 0305 MDT, I recorded one of the greatest shows on Earth in an unintended selfie (Fig. 3-36) and in the video,

https://www.youtube.com/watch?v=3pcji9Tz20Y&t=67s

On another almost cloudless night, about four months later on 16 Sep 2024, a many-colored aurora decorated the predawn sky over Cheyenne, WY, with its costar, the Big Dipper (Fig. 3-37).

Cloudless skies are what aurora and eclipse aficionados wish for. But clouds, in their proper place, have their own beauty, as we will begin to see in Chapter 4.

3.9 Gallery

Needless to say, there are an overwhelming number of extraordinary images of the aurora. Here are just a few

Fig. 3-36. Aurora and selfie at Glendo State Park, WY, on the night of 10-11 May 2024. JC.

Fig. 3-37. Aurora's coat of many colors with Big Dipper (handle upper left) over Cheyenne, WY, 16 Sep 2024. JC.

Fig. 3-38. Pink-fringed aurora over Tok, AK, 20 August 2017. © Katy Turk.

Fig. 3-39. Aurora resembling a dragon over Iceland, 6 Feb 2019. © Jingye Zhang.

Fig. 3-40. Aurora and airglow (around 90 km) over Canada with Manicouagan Crater (lower right), 3 Feb 2012. NASA International Space Station Photograph.

Wonders of the Atmosphere
Chapter 4: Clouds and Fog: Composition and Forms

Fig. 4-1. Growing Cumulus Congestus Cheyenne, WY, 2000 UTC 01 Jun 2025. Cumulus clouds are blobs of buoyant, rising air, which when large have bright cauliflower tops and dark, shaded flat bases at the level condensation begins. JC.

Fig. 4-2. Cirrus uncinus over Vail, AZ at sunset, 15 Nov 2022. Cirrus are trails of falling ice crystals twisted by the wind. JC.

Fig. 4-3. Stratus opacus, Gstaad, Switzerland, 20 Aug 2007. SDG. Stratus clouds are layers of rising or cooling air that cover most or all the sky and turn it gray.

Wonders of the Atmosphere
Chapter 4: Clouds and Fog: Composition and Forms

4.1 The Composition of Clouds

Clouds, the phantom apparitions of the sky, range from pearly patterns and woven lace to menacing monsters, chaotic dealers of darkness, destruction, and death. Clouds come in wondrous varieties of color, lighting, shade, size, and form. Their forms are named. Buoyant blobs of rising air with flat bases and cauliflower tops are *Cumulus* (Fig. 4-1). Trails of falling ice crystals twisted by the wind are *Cirrus* (Fig. 4-2). Sky-covering layers of rising or cooling air are *Stratus* (Fig. 4-3).

Amid this show of wondrous variety, clouds and their ground-hugging siblings, fog, are simply assemblages of tiny water droplets and/or ice particles that block our vision in a region of the atmosphere.

Cloud droplets are spheres (my dears), not tears. Drops are only tear-shaped when they adhere to a surface such as your skin. Otherwise, droplets in mid-air and even droplets that condense on spider webs (Fig. 4-4), or even on insects, are almost perfect spheres.

Cloud droplets, drizzle drops, and raindrops form a trio based on size. Cloud droplets range up to 100 μm in diameter but are typically between 10 and 20 μm in diameter. Drizzle drops range between 100 and 500 μm in diameter. Raindrops, range between 500 μm and about 5000 μm or 5 mm in diameter. Thus, raindrops are typically about 50 to 100 times wider than cloud droplets, much as most insects' compound eyes are typically about 50 to 100 times wider than the tiny pixel lenses (ommatidia) that make up their eyes.

How much do cloud droplets weigh? That depends on their size. A single gram of water in a cloud would consist of 240 million cloud droplets 20 μm in diameter, or, because volume is proportional to the cube (third power) of the diameter, that gram would consist of 1.92 billion droplets 10 μm in diameter.

Fig. 4-4. Droplets are spheres, even when they hang on a spider web. SDG.

How much do clouds weigh? The typical liquid water density in clouds ranges from 0.1 to 1 g/m^3 or from 100 to 1000 kg of liquid water per cubic kilometer, which is a typical volume of a small cumulus cloud, and which at 1000 kg of water would contain 240 *trillion* droplets.

Why don't clouds fall? The fall speed or terminal velocity of a droplet 20 μm in diameter is about 1 cm/s or 0.03 kph. Thus, it would take 30 hours for a droplet 20 μm in diameter to fall 1 km below cloud base, and long before that the droplet would have evaporated and most clouds would be long gone.

Large cloud droplets 100 μm in diameter fall about 25 cm/s, which is fast enough to fall from the cloud and possibly reach the ground. It is also fast enough to fall on smaller droplets and join or *coalesce* with them, much like large droplets sliding down a foggy bathroom mirror coalesce with smaller, stationary drops in their path. Coalescence is one of the processes by which cloud droplets grow to raindrop size.

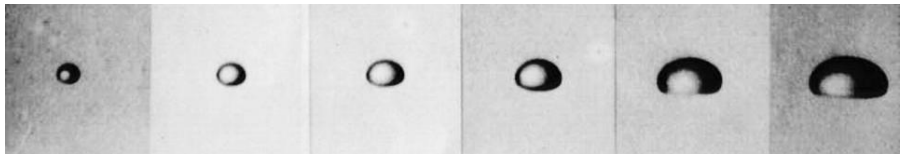

Fig. 4-5. Raindrop shape vs size from 1.35 to 4 mm. ©Pruppacher and Beard.

Small drops are spheres because they are held tightly by surface tension and because a sphere has the smallest surface area per volume of any shape. Surface tension is a small-scale force that is less effective for larger raindrops, which also fall faster. Drops larger than ≈ 280 μm in diameter begin to flatten on bottom (Fig. 4-5). Drops larger than about 3 mm in diameter are so flattened they resemble hamburger buns. They also distort, wobble, and break, much like large soap bubbles break, especially if two collide.

Ice particles in clouds come in a wondrous variety of shapes. Some are crystals. Some are cloud droplets that have frozen. Droplets that collide with ice crystals often stick and freeze in a process called riming. Most crystals are hexagonal in the form of flakes, plates, pencils, needles, bullets, etc. (Fig. 4-6). They may be quite narrow but can exceed 1 mm in length. A typical fall speed for crystals in clouds is about 0.5 m/s or 1.6 kph. That is much faster than typical cloud droplets fall and is why crystals fall out of clouds, leaving long trails.

Fig. 4-6. A sample of ice crystal forms, plates, pencils, dendrite stars, and more.. https://www.snowcrystals.com/ ©Ken Libbrecht.

The fact that you can walk through a fog and jets fly through clouds proves that clouds are not solid objects even though they may appear solid from a distance. In a typical cloud, droplets or crystals occupy less than 1 millionth of the volume. And, because most cloud droplets are so tiny that they are passively swept along with any gentle air currents it is possible to walk through a cloud or fog (a cloud touching the ground) without getting wet.

4.2 Light and Colors of Clouds

Many clouds seem solid when viewed from afar because they reflect light as well as or better than most solid objects. The fraction of light that is reflected from an object is called its *albedo*. Thick clouds have an albedo up to 90%, much like snow. The albedo is about 15% for forests, 5 - 15% for most rocks, 45% for dry quartz sand, but only about 5% for water unless the Sun is near the horizon (see Fig. 9-17).

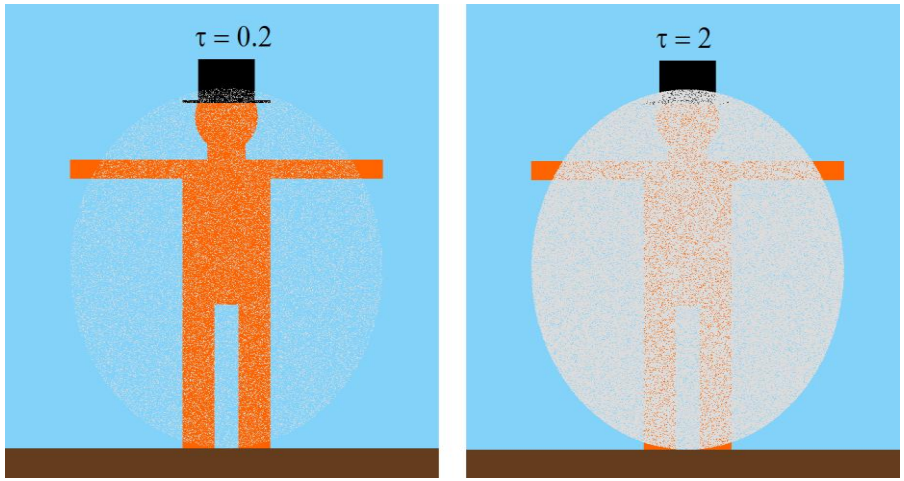

Fig. 4-7. Visibility of and through a barely visible cloud with optical thickness, $\tau = 0.2$ and an almost opaque cloud with $\tau = 2.0$. SDG.

Clouds have high albedos because their water is separated in myriad droplets or crystals, much like a smashed ice cube is bright white in sunlight. Sunlight entering a cloud quickly strikes droplets or crystals and is repeatedly scattered. A cloud with 1 g/m^3 of liquid water with

Fig. 4-8. Thin fog reduces visibility of objects gradually with distance in Saddle River, NJ. SDG.

Fig 4-9. Growing cumulus congestus looks solid and white where sunlit. SDG.

droplets 20 μm in diameter will scatter 15% of a sunbeam in a single meter. Such a cloud will have an optical thickness, $\tau = 1$ if it is 6 m across, $\tau = 10$ if it is 60 m across, and so on. (Recall the treatment of optical thickness in §2.4.) Most light that enters a cloud with $\tau = 1$ will pass through it, but most light that enters a cloud with $\tau = 10$ will be scattered so many times that it will not penetrate the cloud, but instead will reemerge in an incoherent fashion from the same side it entered and be reflected.

Fig 4-10. Towering cumulus cloud with silver lining, dark core, and a crepuscular ray. SDG.

The apparent solidity of a cloud depends on its optical thickness (Fig. 4-7). When optical thickness, $\tau \leq 0.2$ the cloud blocks so little light it is barely visible while a person behind the cloud appears clearly. At $\tau = 2$, the cloud is easy to see but almost masks the person. For $\tau \geq 3.5$, the person is invisible because the human eye cannot detect differences of light and color less than 2%.

Fig. 4-11. Underside of a thunderstorm (with mamma) lit by the setting Sun over Cheyenne, WY, 20 May 2020. Colors grade from near white above to near red on the smooth arcus cloud near the surface at left. Scuddy clouds at lower right are dark because they are shaded. JC.

The concentration of droplets or crystals at cloud edge also impacts the impression of solidity. Evaporating or slowly forming clouds and much fog (Fig. 4-8) appear amorphous and indistinct because they have fewer and smaller drops at the edges, so you can see a good distance into them, though with fading clarity.

Ice crystal clouds and rain or snow fall streaks also tend to appear fuzzy rather than solid because they contain fewer (though larger) particles than water droplet clouds. For a given water content, optical thickness varies inversely with droplet (or crystal) diameter.

Rapidly growing clouds, such as cumulus congestus and cumulonimbus appear solid because they have a high concentration of vision-blocking droplets right to the outer edges of their turrets. When such clouds punch up into clean, dry air, the visual contrast redoubles their impression of solidity (Fig. 4-9). They can have optical thicknesses that range up to 1000 or more, which is why it gets so dark when they come overhead.

Clouds near the Sun increase to a blinding bright maximum as optical thickness increases to $\tau \approx 2.5$ because 1: the fraction of scattered light increases to over 90%, 2: most of the light scattered light by cloud droplets and ice particles is only deflected by small angles (much like dirty windshields facing the Sun)) and, 3: the light is only scattered at most a few times so that it penetrates the cloud. This is the case with optically thin altocumulus, cirrocumulus and cirrus and with the silver linings of the thin fringes of thick cumulus clouds (Fig. 4-10).

As τ continues to increase above ≈ 2.5 multiple scattering dominates and blocks most light from penetrating the cloud directly. For $\tau > 20$

less than 10% of the scattered light penetrates. No wonder the *cores* of thick cumulus clouds ($\tau >> 100$) are very dark.

The *colors* of sunlit clouds close to an observer closely match the colors of the light that strikes them because droplets and crystals are large enough to scatter all wavelengths of light with nearly equal efficiency. When the Sun is high in the sky thick sunlit clouds and optically thin cloud layers that transmit much sunlight appear white because the Sun is white. Shaded clouds and the bases of optically thick clouds appear dark gray simply because little light reaches them.

When the Sun is near the horizon, nearby sunlit clouds that are high in the sky, where the air is thin, may still be white while clouds close to the ground appear golden or red because the sunlight that has reached

Fig. 4-12. A yellow thunderstorm lit by the setting Sun over Cheyenne, WY, 22 Jul 2017. The color grades from pale yellow at cloud top through yellow to orange-red at cloud base. The cloud at extreme lower right is purple due to a mixture of blue skylight with red sunlight. JC.

Fig. 4-13. Distant view of the top of a thunderstorm at twilight facing East near Cimarron, NM, Aug 1985. SDG.

them is golden or red after it passed through a great optical thickness of atmosphere. At that time, any cloud that extends from near the ground to great heights will experience a gradation of color from red at base to yellow to white at the top (Figs. 4-11, 4-12).

The colors of distant clouds are altered by scattering in the intervening atmosphere. Distant sunlit clouds are tinted pink even when the Sun is high in the sky (recall Fig. 2-16), and yellow, orange, or red when the Sun is near the horizon. Fig.4-13 is a distant view of the top of a sunlit towering thunderstorm at twilight (so that the sky is already black) that is not only reddened by its long optical path to the thunderstorm but also by its long path through the atmosphere back to the observer.

The shaded sides of clouds often turn purple when the Sun is near or below the horizon (Fig. 4-14). Because purple is not one of the spectral colors, but rather a combination of blue and red light, any time purple appears in the sky (recall twilight skies of Fig. 2-3, Fig. 2-26, and Fig. 2-55) or on clouds (lower right of Fig. 4-12) the explanation must consist in how red and blue light combine. For example, a cloud that is optically thin will transmit to the shaded side some of the sunlight that hits it, which is red. An optically thick cloud transmits very little light, so its shaded side is illuminated by skylight, which is largely blue. In that setting, the purple cloud is the one with an intermediate optical thickness, which transmits an amount of red sunlight almost equal to the blue skylight it reflects.

Twilight colors of structured layer clouds are the focus of §12.2.

4.3 Formation of Clouds and Precipitation

In this section we present Cloud Physics. If you find the going tough and long, focus on the indented blue text, which summarizes essential highlights without the details.

Clouds form much the same way that dew and frost form. When the ground and the grass cool at night, some of the water vapor in the air condenses to water drops, just as a fog of droplets condenses on the cool surface of the mirror when you take a hot shower in a cold bathroom, or on the outside of a glass of ice-cold drink on warm, humid days. Frost forms as ice crystals in the same way, except on window panes at temperatures below freezing.

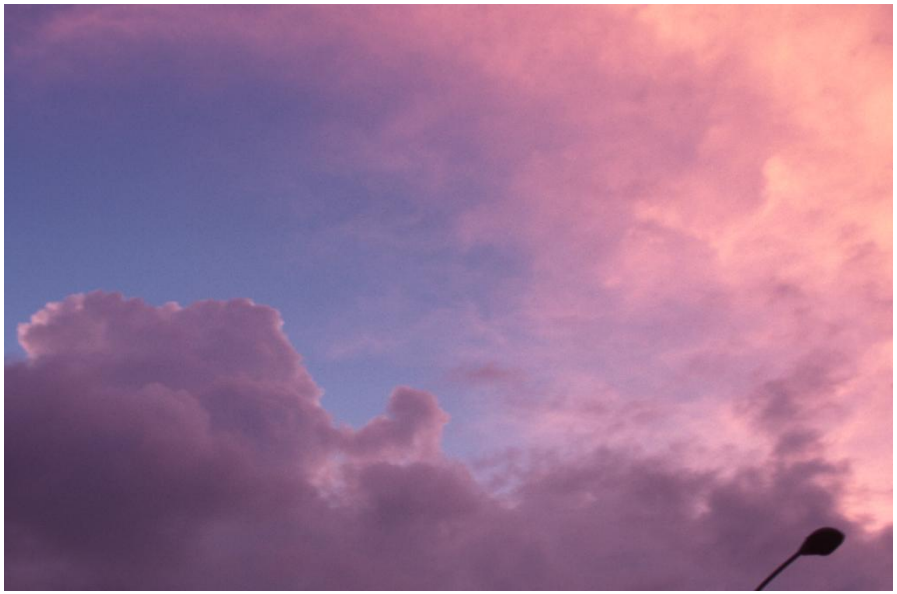

Fig. 4-14. A partly cloudy sunset or twilight sky with pink and purple shaded clouds and blue sky. SDG.

When the Sun comes up in the morning and heats the ground, dew evaporates and frost sublimes back to vapor. Likewise, no droplets ever condense on the hot outside of a cup of boiling water even when steam wafts up from the boiling water. Clothes dryers work on the same principle by heating the air and effectively creating wind in the dryer by tumbling the clothes to enhance evaporation. Clouds and fog form and dissipate in the same way.

Clouds form when air cools enough for water vapor to condense to cloud droplets or ice crystals. Clouds dissipate when air warms enough so droplets and crystals evaporate.

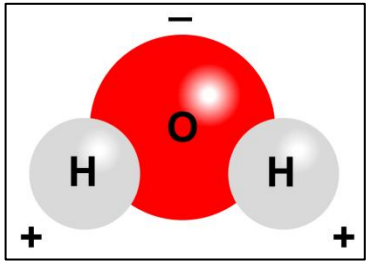

Fig. 4-15. An H_2O molecule and its electric charges. SDG.

It pays to think of these changes in terms of molecules. First, H_2O molecules are attracted to each other by hydrogen bonds, which result from the asymmetric shape of the H_2O molecule and its electric charges (Fig. 4-15). The two hydrogens are positively charged on one side while the oxygen is negatively charged on the opposite side. Since opposite electric charges attract, the hydrogen atoms of one H_2O molecule attract the oxygen atom of a nearby H_2O molecule. By contrast, because molecules of N_2, O_2, and CO_2 form straight lines and do not have such asymmetrical charges, their attractive forces are much smaller and as a result they do not condense to liquids until the temperature is much, much lower.

Think of moving molecules to explain how H_2O molecules overcome the hydrogen bonds that hold them together. In water vapor, a gas, molecules move freely in all directions, and with a wide range of speeds. The higher the temperature, the more energy molecules have and the faster they move on average. The mean speed of molecules is comparable to the speed of sound, which is ≈ 331 m/s in air at 0°C.

When temperature is very low H_2O molecules have so little energy and move so slowly that they are locked together in solid ice, though they can vibrate in place. As ice is heated, the molecules vibrate more and more rapidly until finally they have enough energy to slide around their neighbors and melt into liquid water, but they don't have enough energy to break free of the mass. As the temperature continues to rise, the molecules continue to speed up until they have enough energy to completely break free from all other molecules and evaporate or boil into water vapor (a gas) and fly around space.

How then can water vapor and liquid water, and sometimes ice, exist at the same time and place? At any temperature molecules have a wide range of energies and speeds. Thus, there are always a few molecules with enough energy to escape water or ice and float in the air as water

vapor, but the lower the temperature the fewer molecules have that critical energy.

Fig. 4-16 illustrates many of the important concepts about water vapor and condensation. The terms it involves include *Saturation*, *Vapor Capacity*, given by the solid line and expressed in units, grams of vapor per kilogram of air at sea level pressure, *Relative Humidity*, ***RH***, and *Dew Point Temperature*, $\boldsymbol{T}_d$.

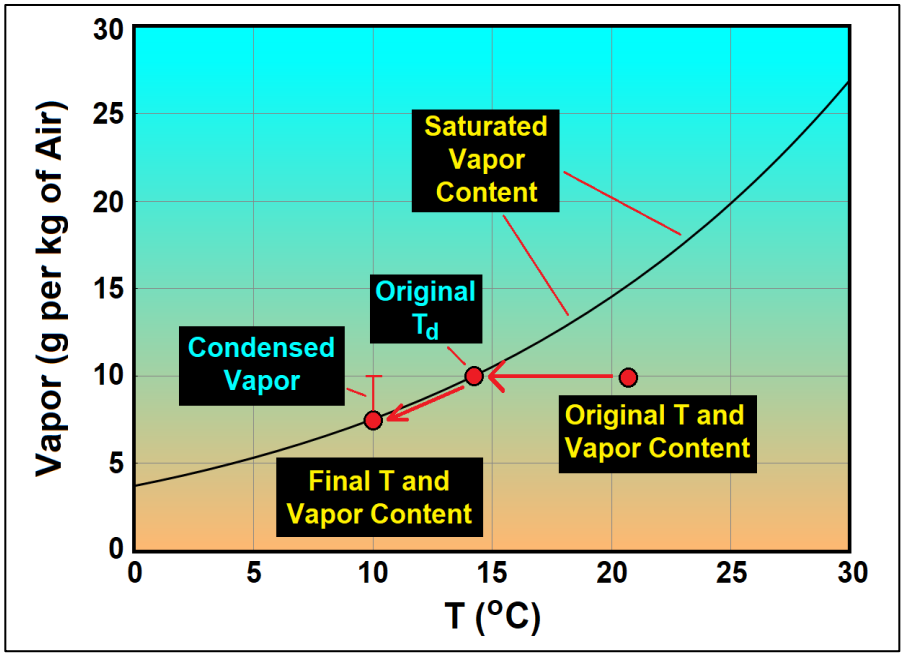

Fig. 4-16. Saturated Vapor content (i. e., vapor capacity) vs Temperature. Changes to air cooled from T = 21°C and vapor content = 10 g/kg (air) to T = 10°C, described in text. SDG.

- *Saturation* occurs when vapor content equals vapor capacity. When air is saturated with vapor H_2O molecules enter water or ice at the same rate they exit.
- *Relative Humidity*, ***RH*** is vapor content divided by vapor capacity, expressed as a percent. When ***RH*** = 100% vapor content equals vapor capacity. When ***RH*** = 50% vapor content is half of capacity.
- *Dew Point Temperature*, $\boldsymbol{T}_d$, is the temperature at which air becomes saturated when it is cooled without evaporation or change of pressure. It is called the dew point because this is the temperature at which dew will begin to condense on objects.

In Fig. 4-16, air initially at $\boldsymbol{T}$ = 21°C with vapor content, 10 g/kg (air) is cooled to $\boldsymbol{T}$ = 10°C. At $\boldsymbol{T}$ = 21°C vapor capacity = 15 g/kg (air). Therefore, ***RH*** = (10/15)×100 ≈ 67%. The air becomes saturated once it is cooled to $\boldsymbol{T}$ ≈ 14°C; therefore $\boldsymbol{T}_d$ ≈ 14°C. Further cooling forces vapor to condense. At $\boldsymbol{T}$ = 10°C the vapor content has been reduced from 10 g/kg (air) to the vapor capacity ≈ 7.5 g/kg (air) so that 10 – 7.5 = 2.5 g/kg (air) condensed.

The solid curve in Fig. 4-16 also shows that

Water vapor capacity doubles for roughly every 9 °C increase of temperature.

Fig. 4-17. Hole punch clouds of cirrus fall streaks in supercooled altocumulus on 12 Dec 2014 in Boynton Beach, FL. Compare satellite image in Fig. 5-7. SDG.

Conversely, vapor capacity halves for roughly every 9°C decrease of temperature, so ***RH*** doubles for roughly every 9°C decrease of

temperature. This is why relative humidity usually rises to a daily high around dawn, the coldest time of day, and sinks to a daily low in mid-afternoon, the hottest time of day.

Thin layers of patterned cloud elements or cells (e. g., altocumulus) sometimes have circular or long, straight clearings with streamers of cirrus cloud that fall from and curve toward their centers (Fig 4-17). These hole-punch or fall streak clouds, which were never reported before aviation (and are most often seen near major airports), illustrate a curious but important phenomenon. They are produced when a plane flies through altocumulus clouds at temperatures typically between about -15°C and -25°C that consist of *supercooled* liquid water (below 0°C). The temperature in the cloud in Fig. 4-17 was ***T*** = -23°C.

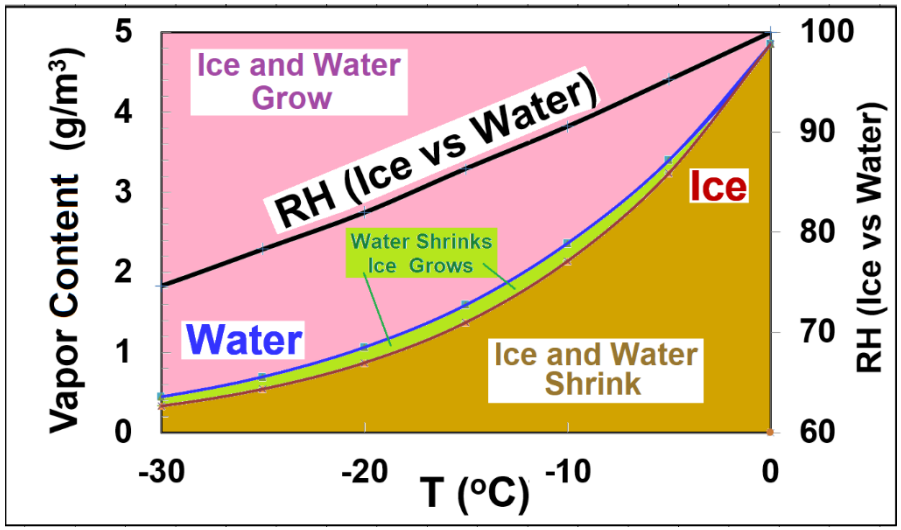

Fig. 4-18. Curves of vapor capacity of supercooled water and ice vs. *T*, RH of ice vs water (black curve) and regions of growth and shrinkage of ice and supercooled water. SDG.

Clouds made of supercooled droplets are surprisingly common. Planes cool and disturb the air enough at the wing tips to freeze the droplets into ice particles, which then grow and fall, and are driven toward the center by the flow of wing-tip vortices in the plane's wake. The cloud hole is near circular if the plane penetrated the cloud steeply and it is a long line if the plane flew through the cloud almost horizontally.

How is supercooled water possible? Crystals melt automatically above 0°C, but droplets must overcome an energy barrier to freeze when temperature drops below 0°C, much as you must tug very hard to start a gas-powered lawn mower. In fact, it is possible to cool a tiny cloud droplet of pure water down as low as -38°C before it must freeze! When water freezes to ice it expands to form hexagonal crystals. Moving H_2O molecules apart and in line requires more energy than tiny droplets have to overcome their mutual attraction.

On average, molecules have less energy in ice than in supercooled water at the same temperature, and therefore require more energy to escape from ice than from supercooled liquid, so fewer do escape. Hence vapor capacity is lower when ice is present (Fig. 4-18), and,

Vapor capacity with respect to ice decreases about 9% for every 10° C below 0° C below vapor capacity with respect to water.

For example, air at ***T*** = -20°C that is saturated with respect to ice ($\boldsymbol{RH}_{ICE}$ = 100%) has $\boldsymbol{RH}_{LIQ}$ = 82% with respect to supercooled water. This difference has great significance for producing precipitation particularly in the green zone of Fig. 4-18 where *ice crystals will grow and cloud droplets will evaporate*. In general,

When T < 0°C ice crystals grow at the expense of droplets.

Ice or no ice, if air is cooled enough vapor capacity will decrease below the vapor content. The excess vapor above capacity must then condense to droplets or crystalize or deposit to ice.

And that leads to the secret of clouds and rain.

All clouds and precipitation are produced by lowering air temperature until vapor capacity falls below vapor content.

Three processes operate in the atmosphere to lower temperature.

1. Contact with a cold surface
2. Loss of heat by radiation
3. Depressurization of air as it rises.

The first two of these cooling processes are relatively slow, seldom more than 2° C per hour, and are confined to thin layers of the atmosphere, for example just above the ground. They can produce fog and create or enhance thin cloud layers but they never produce thick, towering clouds, or precipitation.

Rising air in storms cools much faster and through a great thickness of the atmosphere. Depressurization cools rising air adiabatically (without any loss of heat) at 9.8°C/km if it is unsaturated and between about 4 and 9.8°C/km depending on the vapor content once it is saturated (see §6.2). Since air typically rises 0.5 km/h in winter storms and at least 20 km/h in thunderstorms, cooling rates due to rising air in storms range from at least 2°C/h to more than 100°C/h (although air in thunderstorms seldom rises for more than 10 or 15 minutes, by which time it nears cloud top). Therefore…

Most clouds (other than fog) and all precipitation are produced by rising air,

This process is illustrated in Fig. 4-19. After sugar is extracted the cane is routinely burned. This makes the smoky air hot enough to rise. If it rises and cools enough it will reach the condensation level where droplets begin to condense from vapor. The resulting cloud is called pyrocumulus, a cloud form that has become increasingly common due to the panflagration of huge forest and brush fires in the Western United States and many other seasonally dry places around the world.

But droplets and crystals do not form automatically once RH rises above 100%. Just as supercooled water must overcome a barrier to crystallize as ice, cloud droplets must overcome the energy barrier imposed by surface tension to cluster and condense from vapor. If an H_2O molecule joins a tiny cluster with few H_2O molecules, it will produce a noticeable expansion. Surface tension opposes this because it 'tries' to minimize surface area. This effect is much greater for tiny droplets than for large droplets with zillions of molecules, when adding a molecule does not produce a noticeable expansion. For example, the expansion of surface area caused by adding a molecule to a small droplet is 100 times *greater* than the expansion of surface area caused by adding a molecule to a droplet 1,000 times larger.

Fig. 4-19. Pyrocumulus forms when hot (smoky) air from burning vegetation rises and cools enough to initiate condensation and form a cloud. Everglades, FL, Jan 1984. SDG.

The barrier surface tension imposes on droplet formation would, if acting alone, require RH to exceed 300 or 400%! But in the atmosphere, surface tension has an opponent.

Aerosols, the atmosphere's impurities, are what overcome the energy barriers to droplet and crystal nucleation, Water droplets readily condense on water-loving (hydroscopic) gases and particles, such as salt. For example, table salt (NaCl) becomes wet (deliquesces) once RH exceeds 75%. Hygroscopic aerosols reduce the energy barrier on

cloud droplet growth imposed by surface tension from a few hundred percent to a few hundredths of a percent above 100% RH.

Ice crystals nucleate more easily on aerosol particles with templates that help the H_2O molecules align properly, such as clay particles. Even with these aerosols nucleation is not easily activated in the atmosphere until the temperature falls below about -15°C, which is why thin altocumulus clouds at or above that temperature consist entirely of supercooled droplets if no jet disturbs them.

Once the cluster grows beyond its barrier growth proceeds by the steady statistical process of diffusion, in which there is a net drift of vapor molecules toward the droplet or crystal.

Diffusion is the fundamental and ubiquitous process by which quantities drift from regions of higher concentration to regions of lower concentration. Diffusion is the great leveler. If diffusion reigned supreme the universe would become uniform and inert.

Diffusion in the air is due to the random motion of molecules. It is a discrete process but because there are so many molecules it appears continuous. Statistics ensures that more molecules will move from where concentration is greatest to where it is smallest. An example is that any smelly gas emitted in one part of a room gradually spreads around the entire room by diffusion without the slightest wind.

Condensation and evaporation are the diffusion processes connected to growth and shrinkage of tiny droplets and crystals. They grow by diffusion of when the vapor density (or vapor pressure) of the surrounding air is greater than right at their surfaces. Since the vapor concentration or density just outside a droplet or crystal is close to the saturated value, in order for droplets or crystals to grow, the ambient air must be slightly supersaturated. Cloud droplets shrink by diffusion and will eventually evaporate completely when the surrounding air is subsaturated, i. e., when the relative humidity is less than 100%.

Diffusion is the dominant growth process for tiny droplets and crystals. But the larger droplets and crystals grow, the slower they expand by diffusion. In fact, the expansion rate due to diffusion varies inversely with the droplet's or crystal's radius. In winter storms over land, where air contains so many nucleating aerosols and so many droplets it would take about two days for a droplet to grow to the size of a drizzle drop, 400 μm in diameter, by diffusion alone. That is too slow to produce precipitation in a timely manner, and another process is needed to grow the droplets to raindrop size.

At sea, air is much cleaner on average and contains fewer aerosols and therefore fewer droplets than over land. Each droplet gets a larger share of the available water and will grow faster and larger by diffusion and can reach drizzle drop size much sooner than over land.

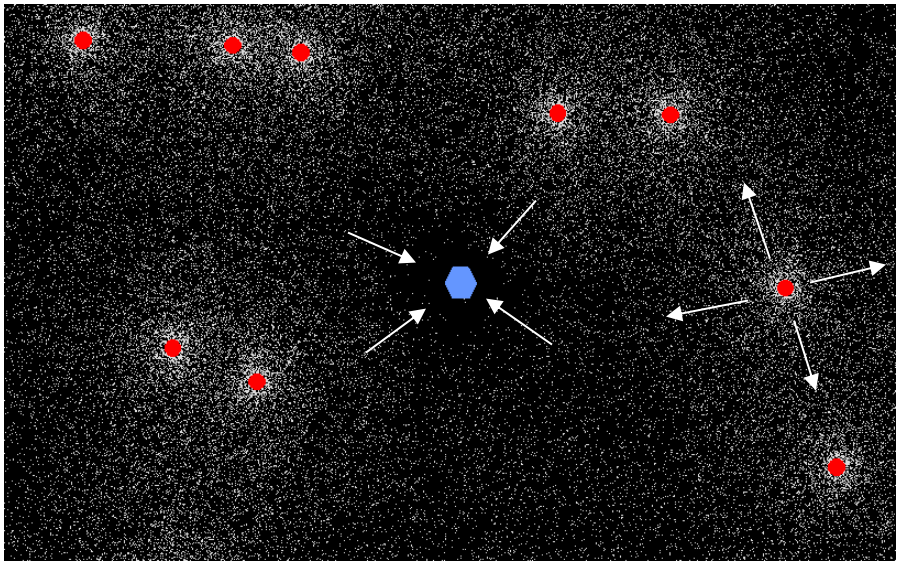

Fig. 4-20. Wegener-Bergeron-Findeisen process. In this supercooled cloud, droplets (red circles) shrink and crystals (blue hexagon) grow as vapor molecules (white dots) diffuse (arrows) from where they are most (the surface of droplets) to least concentrated (the surface of ice crystals). SDG.

Ice is almost inevitably what helps particles reach raindrop or snowflake size. In the first place, ice crystals are a far rarer breed than droplets. Since there are far fewer crystals in an ice cloud than droplet in a water cloud (even at sea), each crystal gets a larger share of the available water and will grow faster and larger by diffusion.

The elephant in the room regarding ice in a cloud of supercooled droplets is the lower saturation vapor density above ice (Fig. 4-18). Not only will ice crystals grow much faster than supercooled droplets, they will, as in hole punch clouds, grow at the expense of the supercooled droplets (Fig. 4-20). The importance of this process for producing precipitation was first theorized in 1911 by Alfred Wegener, the founder of the theory of Continental Drift, and later documented in the atmosphere by Tor Bergeron and Walter Findeisen.

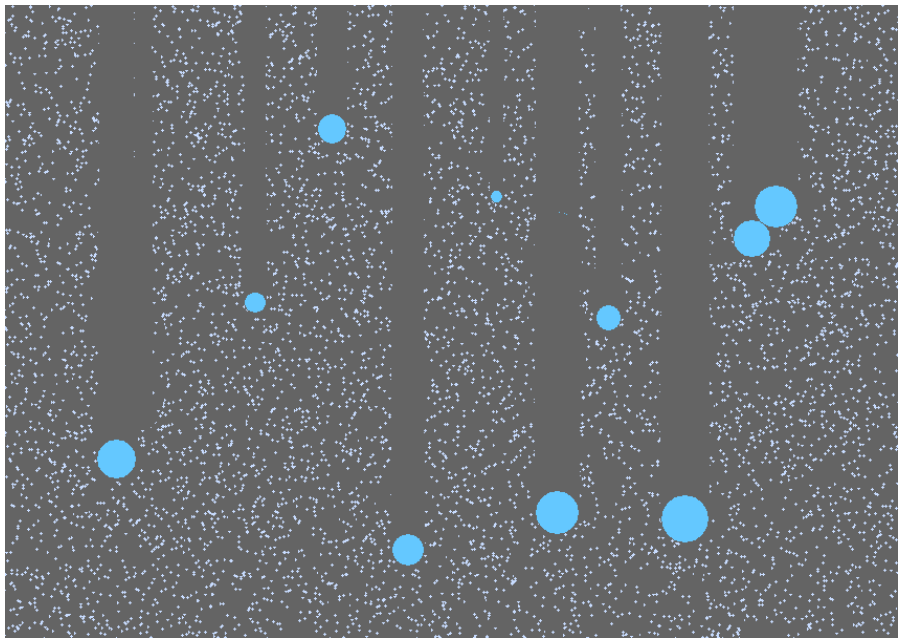

Fig. 4-21. Coalescence growth. Raindrops collect cloud droplets in their path. At upper right a larger drop is about to overtake and collect a smaller drop. SDG.

The faster diffusional growth rate of ice particles allows them to grow large enough to fall fast enough to either reach the ground growing solely by diffusion (sometimes as beautiful crystal flakes), or after gathering other crystals and droplets in their path by the process of accretion or coalescence (Fig. 4-21).

Accretion is the term used when snowflakes collect ice crystals or when hailstones collect drops. *Riming* is the term for ice crystals that collect droplets and look covered by parasites. *Coalescence* is the term for drops that collect and merge with other drops or droplets.

Growth by diffusion adds one molecule at a time. Growth by accretion adds zillions of molecules from another particle all at once. The finite growth in an instant by accretion is particularly important in jump-starting the process when the collecting particles are only slightly larger than the rest of the crowd.

As droplets and crystals grow, the rate of growth by accretion occurs ever faster because the larger droplets and crystals are 1: the faster they fall and, 2: the larger the area they sweep out. The growth rate of the particle radius by accretion is roughly proportional to the radius. As a result, for particles larger than about 50 to 100 μm in diameter growth by accretion takes over and gets raindrops, snowflakes and especially hailstones to their final size.

Thus, in the final stages, raindrops and snowflakes grow somewhat like planets. The craters on Mercury, Mars, the Moon, and Earth were produced by the impacts of meteors. Each meteor buried itself in the body it struck and added its mass to the mass of the body although some mass may "splash" away. This process of collision and collection, known as *accretion* in the case of planets, is the process by which the Moon and all the planets grew.

To produce rain by accretion, most clouds must be at least 3 km thick to allow enough collisions to grow droplets and crystals to the size of raindrops and snowflakes that can reach the ground as precipitation.

Once drops and crystals grow large enough (≥100 μm) they fall out of the cloud and begin to evaporate in the dry air below cloud base. If precipitation is light enough and cloud base is high enough, they will evaporate completely before reaching the ground and leave a trail called *virga* that ends in mid-air (Fig. 4-22). When precipitation is heavy enough it will reach the ground as rain or hail streaks (Fig. 4-23). Their appearance depends on lighting. Sunlit virga and rain or hail streaks appear white; shaded streaks that block skylight appear dark.

Fig. 4-22. Sunlit virga from stratocumulus clouds. Ice crystals formed in the mostly supercooled liquid cloud over Cheyenne, WY, 17 Dec 2021. JC.

Fig. 4-23. Dark, shaded rain streaks falling from a backlit thunderstorm over Cheyenne, WY, 31 May 2017. JC.

Cloud Name	Cld	Definition
Cirrus	**Ci**	Detached clouds in the form of white, delicate filaments or white or mostly white patches or narrow bands, with a fibrous appearance, and/or a silky sheen.
Cumulus	**Cu**	Detached clouds, generally dense with sharp outlines (perhaps ragged), developing vertically in the form of rising mounds, domes or towers, whose bulging upper part often resembles a cauliflower. Their sunlit parts are mostly brilliant white; their bases are relatively dark and nearly horizontal.
Stratus	**S**	Generally grey layer with a fairly uniform base, which may give drizzle, snow or snow grains. The Sun may be visible through the cloud. Stratus does not produce halo phenomena except, possibly, at very low temperatures.
Cumulonimbus	**Cb**	Heavy, dense cloud with considerable vertical extent, in the form of a mountain or huge towers. At least part of its upper portion is usually smooth, or fibrous or striated, nearly always flattened and often spreads out in the shape of an anvil or vast plume. Under the base, which is often very dark, there are frequently low ragged clouds either merged with it or not, and precipitation sometimes in the form of virga.
Nimbostratus	**Ns**	Grey layer, often dark, that blots out the Sun. Its appearance is made diffuse by more or less continuously falling rain or snow, which in most cases reaches the ground. Low, ragged clouds often occur below the layer, and may merge with it.
Stratocumulus	**Sc**	Grey and/or whitish patch, sheet or layer that almost always has dark parts, composed of tessellations, rounded masses, rolls, etc., which are non-fibrous (except for virga) and which may be merged; most of the regularly arranged small elements have an apparent width of more than 5°.
Altocumulus	**Ac**	White and/or grey patch, sheet or layer, generally with shading, of laminae, rounded masses, rolls, etc., which are sometimes partly fibrous or diffuse and which may be merged; most of the regularly arranged elements usually have an apparent width between 1° and 5°
Cirrocumulus	**Cc**	Thin, white patch, sheet or layer of cloud without shading, composed of very small elements in the form of grains, ripples, etc., merged or separate, and more or less regularly arranged; most of the elements have an apparent width of less than 1°.
Altostratus	**As**	Greyish or bluish cloud sheet or layer of striated (grooves or channels in cloud formations, arranged parallel to the flow of the air), fibrous or uniform appearance, totally or partly covering the sky, and having parts thin enough to reveal the Sun at least vaguely, as through ground glass or frosted glass. Altostratus does not show halo phenomena.
Cirrostratus	**Cs**	Transparent, whitish cloud veil of fibrous or smooth appearance, totally or partly covering the sky, generally producing halo phenomena.

Table 4-1. Names, abbreviations, and definitions of the 10 cloud genera modified from the World Meteorological Organization.

4.4 Cloud Forms

For eons it was customary to view clouds as protean mists that blur or hide objects, and as bringers of life that water the Earth or takers of life that drown or immobilize. Few knew that clouds could be viewed as solid objects with distinct forms, other than artists, who, centuries ago provided graphic but mute testimony about the unnamed entities they painted so accurately (see §15.1, §15.2).

With all the attention that clouds draw it is mind-boggling that they were not named until 1802 when Jean Baptiste de Monet Lamarck in France and Luke Howard in England independently classified them following Linnaeus's ***Systema Naturae*** (1758). Lamarck's scheme, which emphasized cloud forms (e. g., dappled clouds) was essentially ignored, but Howard's original articles, ***On The Modification of Clouds*** (1803), attracted attention and won praise, and constitute the core of the currently accepted system of cloud classification.

The significance of Howard's (and Lamarck's) work was assessed cogently by Johann Wolfgang von Goethe, who wrote that Howard,

> was the first to hold fast conceptually the airy and always changing forms of clouds, to limit and fasten down the indefinite, the intangible and unattainable and give them appropriate names.

The system accepted by the World Meteorological Organization has 10 genera (Table 4-1), which use only five words either alone or in combination, *cirrus* → curl, *cumulus* → heap, *stratus* → layer, *alto* → moderately high and *nimbus* → precipitation, plus numerous species and varieties. The genera are classified by the heights of their bases as either low (*Cu*, *S*, *Ns*, *Sc*), with bases below about 2 km above ground level, middle (*Ac*, *As*), with bases between about 2 and 6 km, and high (*Ci*, *Cs*, *Cc*), plus clouds of vertical development (*Cb*)

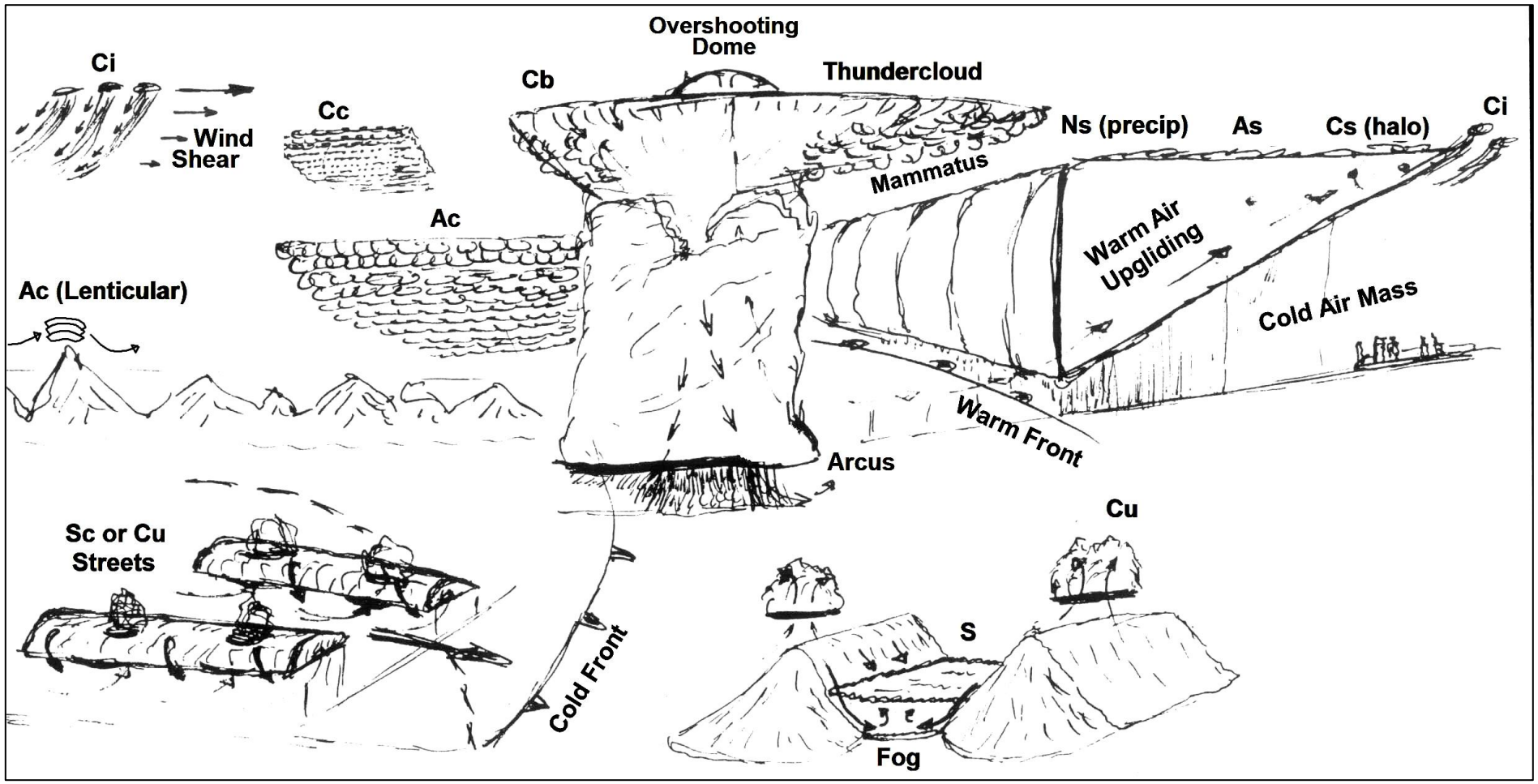

Fig. 4-24. Cloud chart showing typical forms, heights, airflow, and settings, particularly in relation to the fronts of extratropical cyclones. SDG.

Cloud charts show the cloud genera in cartoon form (Fig. 4-24) and in photos (Fig. 4-25). Fig. 4-24 indicates their relative positions, heights, and sizes with one major exception that it exaggerates by a factor of about 50 the slope of the warm frontal surface separating the upgliding warm air mass over the dome of cold air, and at the same time, shrinks the horizontal extent of layer clouds, which in reality are larger by the same factor of about 50.

Fig. 4-24 also shows some of the air motions that produce and shape the clouds. For example, at center left it shows the smooth lenticular altocumulus clouds that form at the crests of wavy airflow when winds cross mountains.

Clouds are shaped by the flow of air. Most cloud particles, and especially cloud droplets, fall so slowly that they are swept along by the wind and act as tracers. Thus,

Clouds are the signatures of the winds. Their forms are due to the patterns of rising and sinking air.

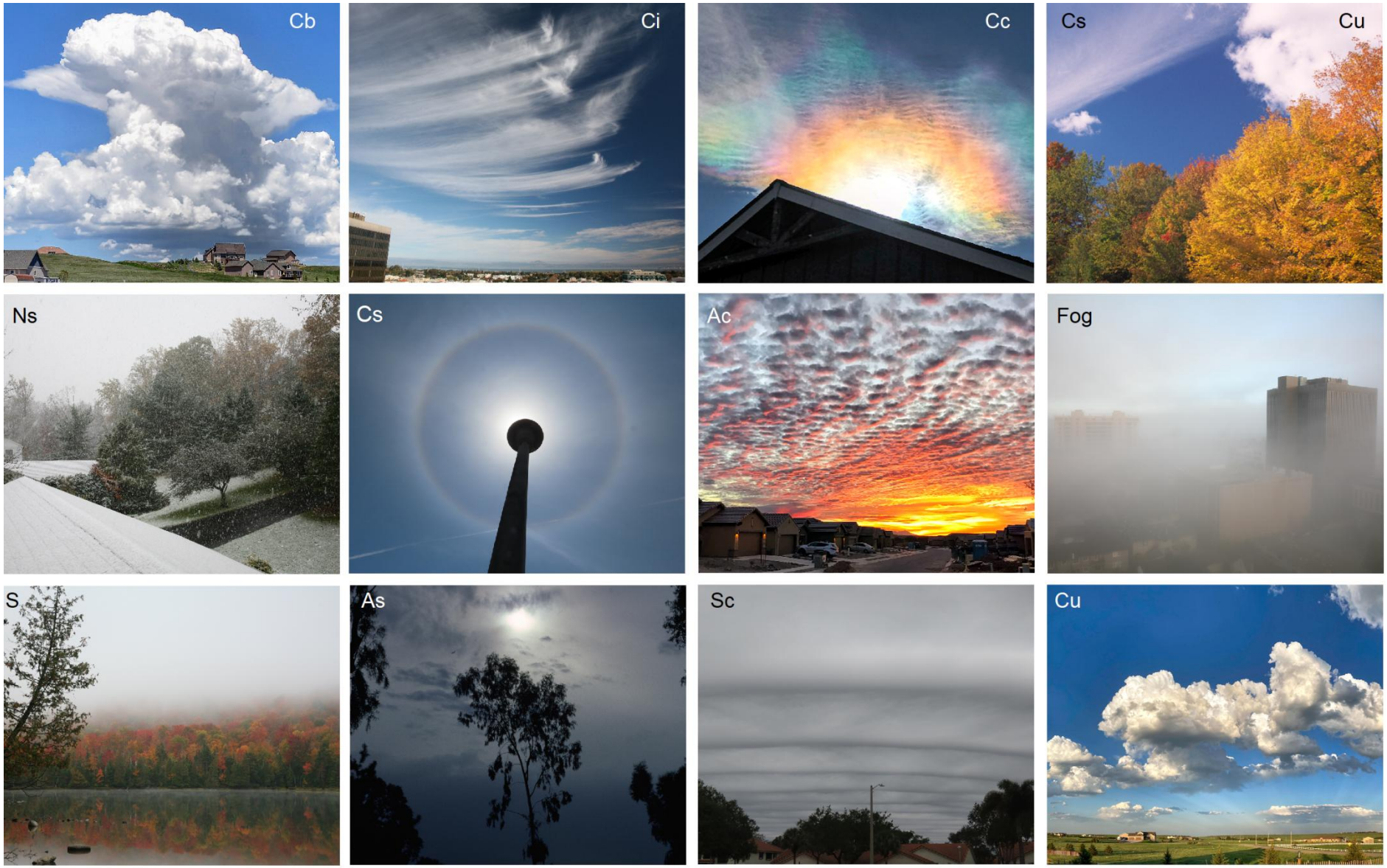

Fig. 4-25. The cloud genera. Cirrostratus often has a halo. Cirocumulus near the Sun often has a corona or is iridescent. Altostratus often has a 'watery' Sun. Top right photo shows a sky with two distinct genera. Right center photo is ground fog. JC and SDG.

Exceptions to the rule occur when particles grow large enough to have substantial fall speeds. Rain shafts extend beneath clouds because raindrops fall between 1 and 10 m/s. Cirrus streamers extend below the generating cell because ice crystals fall speeds around 1 m/s. Thus,

Cirrus clouds are trails of falling ice crystals twisted by the winds.

There are only a few basic cloud forms because there are only a few distinct patterns of air motions. Thus,

- When a hot, buoyant puff of air (thermal) rises like a hot air balloon through otherwise quiescent air, the resulting cloud, a cumulus, looks like a puff.
- When a layer of warm air glides over a cold air mass, as on a conveyer belt with a slope of about 1/100, the resulting cloud complex (S, Ns, As, Cs) covers the sky.
- When waves form in the air, the resulting clouds (Sc, Ac, Cc) appear like waves or ripples, with clouds at the crests and clearings at the troughs.

Identifying clouds takes practice but here are some hints.

- Cumulus is a lumpy cloud that often has a flat base and a top that resembles a cauliflower.
- Cumulonimbus, when seen at a distance looks like a huge cumulus, but with a top that resembles an anvil or a gigantic mushroom and with rain or hail falling from its base.
- Cirrus, sometimes called mares' tails, often looks like a pony tail.
- Stratus tends to be formless, but turns the sky from blue to gray. If it rains or snows the stratus is a nimbostratus.

Altostratus and cirrostratus are progressively higher and thinner versions of stratus that cover the sky but with distinguishing marks.

- Altostratus are gray, but the Sun is often dimly visible through it, as if seen through smoky glass. When air below the cloud is dry and no precipitation is falling from the cloud, the base may appear wavy, corrugated, or mottled, and it is common to see cloud fragments below and dark silhouettes of higher clouds.
- Cirrostratus is so tenuous that the sky often appears milky blue. Its signature is the ice crystal halo. There are many halos (see Chapter 11), but perhaps the most common is a circular ring 22º in all directions from the Sun or Moon in the center (about the width of an outstretched hand at arms' length).

Stratocumulus, altocumulus, and cirrocumulus all appear as sheets of flattened cells, bands, or ripples, usually with blue sky between. These three genera can be distinguished by a rule of thumb, that is, use your thumb. When your arm is outstretched,

- Stratocumulus cells or ripples appear wider than your thumb.
- Altocumulus cells or ripples appear smaller than your thumb but larger than your pinky nail.
- Cirrocumulus cells or ripples appear smaller than your pinky nail.

Cloud height is difficult to estimate visually unless the base intersects some known landmark such as a hill or a skyscraper. *Soundings*, vertical profiles of temperature, humidity, and wind of the ambient atmosphere, provide data on cloud height and thickness. Soundings give a picture like sticking a straw down through a layer cake, or a core drilled down into the ice caps of Greenland or Antarctica, or through tree trunks to see their rings. It is from soundings that we know which altocumulus clouds are supercooled (e. g., -23°C in Fig 4-17), and how high fog extends above the ground.

4.5 Fog

Fog is defined as a cloud that touches the Earth's surface and reduces visibility below 1 km. In most cases, fog is produced when air is cooled by the surface below. It therefore extends very little above the surface, from a meter or so (as ground fog) up to perhaps a little more than 1 km. As a result, fog is usually classified as a stratus cloud.

The definition and properties of fog hide a great variety of forms that it can assume, causes that produce it, and emotions it can arouse given that fog is often a creature of the night, which adds mystery, fear, and even terror to its obscuration, but also beauty.

Fig. 4-26. Radiation fog at San Mateo, CA, 1500 UTC 07 Nov 2014. SDG.

The different forms of fog are named for their cause or their location. *Radiation fog* forms when the surface radiates heat out to space most rapidly, namely when, 1: the air aloft is cloudless and dry, 2: the wind speed just above the surface is slow or calm, 3: the ground is wet and, 4: the difference at sunset between the temperature and the dew point temperature, $\boldsymbol{T} - \boldsymbol{T}_d$ is small just above the surface. Under these conditions, the air just above the surface cools rapidly by close contact to form a classic nocturnal inversion and reaches the dew point so that condensation begins and fog forms. Because the cold, foggy air is denser than the air aloft it hugs the ground, and friction slows it even more, sometime to a dead calm. If the radiation fog is so thin an observer on a small rise can see above it, it is called ground fog.

These were the conditions at San Mateo, CA on the morning of 07 Nov 2014 (Fig. 4-26). The sounding at 0700 PST (Fig 4-27, left side) shows a temperature inversion from $\boldsymbol{T}$ = 12°C at the surface to $\boldsymbol{T}$ = 17°C at 600 m. The air at the surface had cooled to the dew point and remained humid up to about 350 m. Higher up, the air was clear and extremely

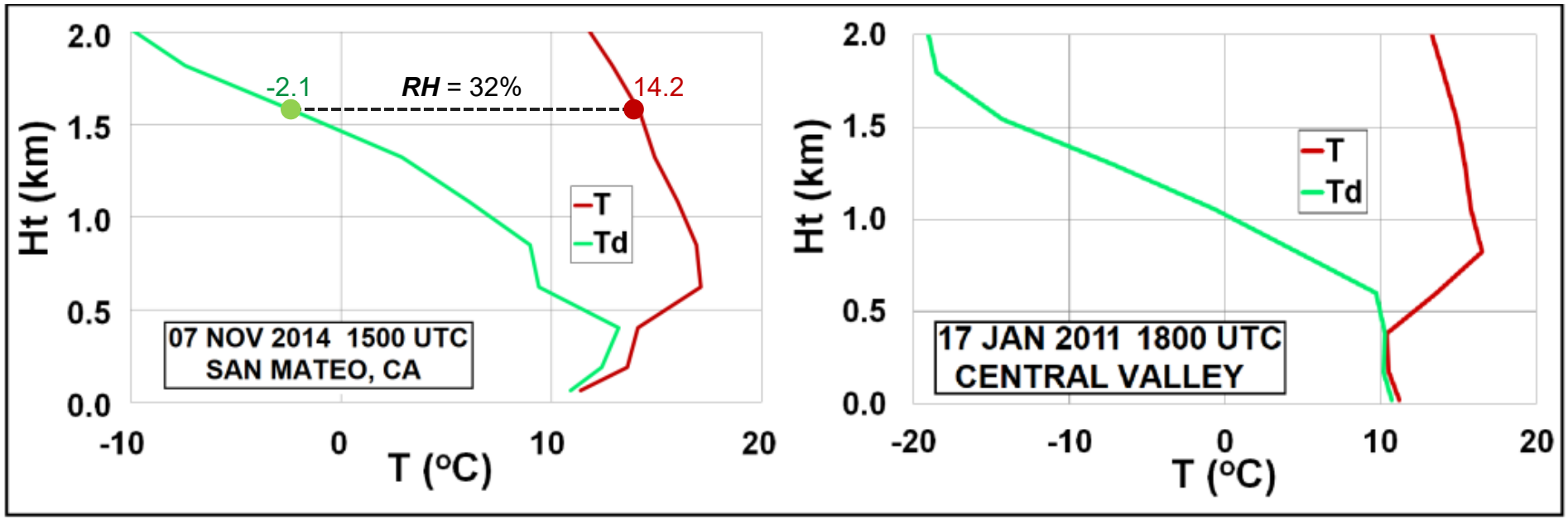

Fig. 4-27. Soundings during radiation fog at (left) San Mateo, CA, 1500 UTC 07 Nov 2014 and (right) the Central Valley, 1800 UTC 17 Jan 2011. SDG.

dry. At 1568 m, ***T*** = 14.2°C and T_d = -2.1°C, so ***RH*** = 32%. At 3 km (not shown) ***RH*** dipped below 1%.

Under similar conditions of clear, calm winter nights following ground-soaking rains (with similar soundings) California's Central Valley can fill with a radiation fog called *Tule Fog*, named for the tule grass widespread in the valley (see right panel, Fig. 5-7). The sounding for 17 Jan 2011 from the midpoint of the Central Valley (Fig. 4-27, right side) closely resembled that of the San Mateo sounding, with a nocturnal inversion just above the surface, saturated air in a thin layer just above the surface, clear, dry skies aloft, and almost calm surface winds (not shown).

Fig. 4-28. Advection fog pours through the Golden Gate as a long tongue covering all of the Golden Gate Bridge except the top of the north tower (indicated by the yellow arrow), Aug 1966. ©Robert Gedzelman

Because the Tule fog covers such a large area (at times it extends westward to San Francisco), and because the valley is almost entirely hemmed in by mountains (except at San Francisco), it may persist for days until a strong wind blows it away and dissipates it. In addition to the low, weak winter sun and short winter days that provide little heating to burn off the fog, the high albedo of the extensive fog adds to its persistence, because reflected sunlight is wasted in that it does not contribute to warming and evaporating the fog.

Advection fog forms when warm, moist air blows over a cold surface. It is the type of fog that so often covers San Francisco. It blows in from the Pacific through the Golden Gate, often extending a long tongue 'clear' across the San Francisco Bay, as in Fig. 5-19 and Fig. 4-28, where it covers all of the Golden Gate Bridge but the tippy top of the north tower (indicated by the yellow arrow).

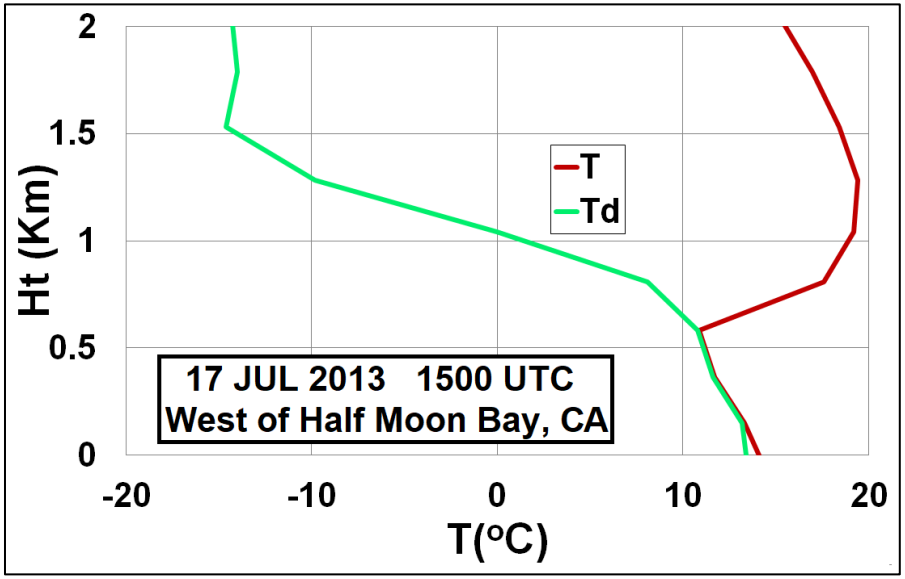

Fig. 4-29. Sounding for the advection fog of 17 July 2013 at 1500 UTC west of Half Moon Bay, CA. SDG.

California's advection fog and low stratus can extend up more than 1 km. That is high enough to pour over the Coast Range and then cascade as an enormous but harmless tsunami of fog when the wind has a component from the west.

That was the case on the morning of 17 July 2013. The sounding (Fig. 4-29) shows that the fog topped out at almost 600 m, just above the summit of Montara Mountain, the highest point on the Coast Range between San Francisco and Half Moon Bay. The fog can be seen cascading down the slopes after surmounting the crest of the Coast Range just east of Half Moon Bay (Fig. 4-30), and indeed, it moved fast enough to be seen in real time. The long, parallel stretch lines were likely caused by horizontal roll vortices similar to the roll vortices that produce cumulus cloud streets (see §6.5). They reveal the direction of

Fig. 4-30. Advection fog pours over the coast range from Half Moon Bay on 17 July 2013. After crashing like a breaking wave it rebounds on the right. SDG.

the moving fog as it plunged downslope and then, like the splash of a breaking wave, rebounded on the right before evaporating completely. The rough, corrugated outlines of the fog testified that the flow was turbulent.

San Francisco's advection fog is just one case of the persistent fogs and low clouds that form off the west coasts of all the continents from about 15° to 45° latitude. These fogs and low clouds form when persistent winds of initially warm air blow over persistent cold coastal ocean waters upwelled from the depths by those same persistent winds (see §5.5).

Another notable example of advection fog occurs over the cold Labrador Current on the Grand Banks of Newfoundland when air blows from the warm waters of the Gulf Stream just to the south over the cold waters. The Grand Banks and Point Reyes, CA are among the foggiest places in the world with fog over 200 days a year.

Upslope fog is the only type of fog that forms or is enhanced by rising air. When air rises up mountain slopes, it can produce a range of cloud genera including cumulus, cumulonimbus and altocumulus lenticularis (mountain wave clouds) when seen from a distance, as at Machu Picchu on 29 Dec 1999 (Fig. 4-31), where cumulus covered the surrounding mountain tops. But observers located just below cloud base can see right in front of their eyes wispy shreds of fog condensing out of thin air and sweeping upward into the cloud. Of course, observers above cloud base will be in fog and not see much of anything.

A combination of upslope and radiation fog occurs on clear nights when the wind blows uphill over lands that may seem level but, in fact, gain in elevation over a long enough stretch. One notable case of such fog occurs when winds blow from the east over the Great Plains, which rise about 1.5 km in altitude from the Mississippi River to the Front Range of the Rocky Mountains.

Fig. 4-31. Upslope fog forming as cumulus clouds that cover the mountains surrounding Machu Picchu 29 Dec 1999. SDG.

Steam fog forms when cold air settles or blows over warm streams, rivers, ponds, lakes, seas, and oceans. It is the most complex and dynamic type of fog with only two ingredients – cold air and warm water. The favorite season for this to happen is fall, when 1: waters retain the warmth accumulated during summer, 2: lengthening nights give time for increased cooling of the air, and 3: polar air masses behind cold fronts bring the first frigid air to previously warm areas.

A striking scene of steam fog covered the Hudson River on the morning of 12 Dec 1988 (Fig. 4-32). The fog boiled up turbulently, reaching heights up to 20 or 30 m before evaporating into the clear air above.

The fog followed a cold front passage overnight that drove temperature down from 13ºC to -15°C. Prior to that the weather had been unseasonably warm for weeks and the Hudson River had been made even hotter by the massive outflow of hot water ejected from the reactors of the Indian Point nuclear power plant.

Steam fog formed over Fairfield Lake in Sapphire, NC on eight consecutive nights in late October, 2024 when a high-pressure dome of polar air with clear skies and calm winds stalled over the SE United States. On several still mornings, including 24 Oct 2024 steam fog boiled up while much of the lake remained mirror smooth (Fig. 4-33). The boiling steam fog gleamed in the morning Sun, lasting for several hours after sunrise until the air warmed. Under these conditions radiation fog may occur nearby and drift downslope over the lake (see Fig. 4-38 and Fig. 15-18).

Fig. 4-32. Arctic Sea Smoke over the Hudson River, 12 Dec 1988. SDG.

Dramatic cases of steam fog, known as Arctic Sea Smoke, occur when Arctic air behind cold fronts or frigid, downslope, katabatic winds from the Greenland and Antarctic Ice Sheets pour over the ocean. The Arctic Sea Smoke in Fig. 4-34 occurred on 11 Feb 1986 when polar air flowed over the Gulf Stream east of Cape Hatteras, NC. The research plane flew in the clear space just above the tops of the steam fog but below the bases of the cumulus clouds.

Fig. 4-33. Steam fog rising in turbulent eddies but calm morning winds over Fairfield Lake, NC, 24 Oct 2019. SDG.

Fig. 4-34. Arctic Sea Smoke as Arctic air pours over the Gulf Stream east of Cape Hatteras, NC, Feb 1986, during the GALE Experiment. SDG.

This wild, epic-appearing scene had an almost curious cause. The rising plumes of fog, some of which swirled up as steam devils (e. g., Fig. 4-35) which are akin to dust devils, evaporated within about 100 m of the sea surface but the still buoyant air continued rising as invisible plumes before ultimately reaching the condensation level,

where the cumulus formed. All this occurred under conditions of gale-speed winds that amplified the chaotic appearance.

Fig. 4-35. Steam devil over Fairfield Lake, NC, 03 Oct 2025. SDG.

The turbulent motions and chaotic appearance of steam fog contrast sharply with the smooth outline of radiation and advection fogs, where the airflow is laminar (except when it cascades over a ridge and into a valley) because it is cooled from below and lacks buoyancy.

What is the complex process by which steam fog forms?

As pointed out above, the encounter of cold air with warm water is the first step in the formation of steam fog. The second step involves what happens to the cold air when it encounters the warm water surface. Steam fog would never occur if the warm surface were dry because warming alone can only cause evaporation. But since the warm water surface is wet it not only heats the air, it charges it with vapor, which increases the relative humidity.

That leads to the third step in the formation of steam fog. No sooner does the humidified, heated air swirl up from the water surface, than it encounters colder, drier air aloft and mixes with it.

Fig. 4-36 illustrates the surprising fact that the **mixture** of two **un**saturated samples of air can be **super**saturated (above the saturated curve) provided the temperature difference between the warm, humid source air and the frigid ambient air is large enough. As the warm, humid but unsaturated air moves away from the source it mixes with more and more ambient air and is progressively diluted and cooled. Supersaturation is due to the fact that the **saturated** vapor content of the source air decreases exponentially as it is cooled and diluted while the **actual** vapor content of the mixture decreases linearly.

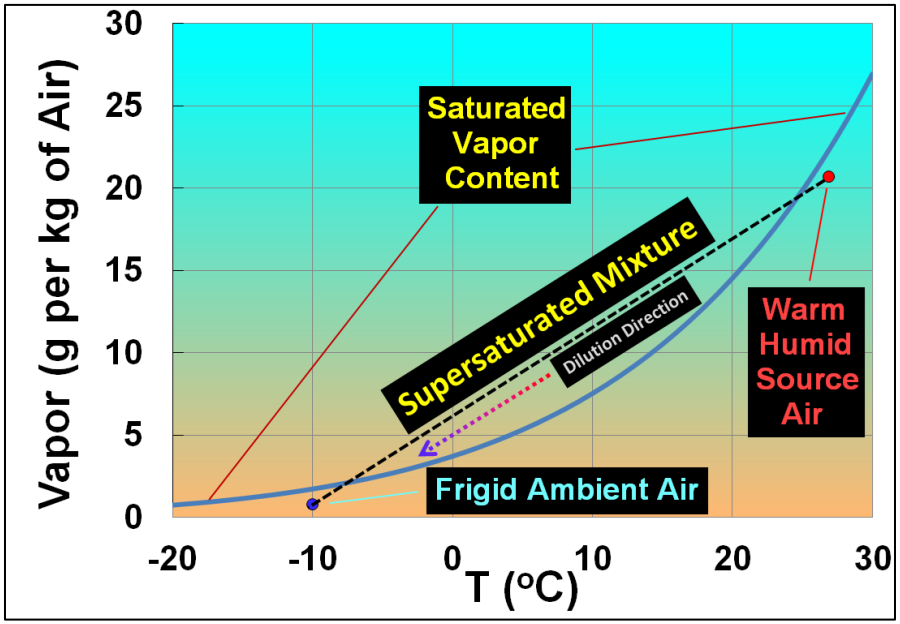

Fig. 4-36. Saturated vapor content and the formation process of steam fog. The mixture of enough warm, humid, but unsaturated source air with frigid, dry ambient air can be supersaturated. SDG.

The following example, from Fig. 4-36, illustrates the principle. Mix 1 kg of warm, humid source air at T = 27°C and vapor content = 21 g/kg (red dot) with 1 kg of frigid, ambient air at T = -10°C and vapor content = 1 g/kg (blue dot). Each kg of the resulting mixture air has

the average ***T*** = 8.5°C and vapor content = 11 g/kg. But at ***T*** = 8.5°C vapor capacity = 6.7 g/kg, so several grams of vapor will condense.

Maximum condensation occurs when the mixture contains roughly equal parts of source air and ambient air. Ultimately, as the warm, humid source air continues rising it mixes with ever more cold, dry ambient air, diluting the mixture until it resembles the ambient air and becomes unsaturated so that the steam evaporates and disappears.

Even though steam fog almost always forms overnight and evaporates by midmorning, there is at least one situation in which it forms in the heat of the day. Falling rain from afternoon sun showers not only cools the air as it evaporates it also wets the hot blacktop pavement of roads. So, once again we have the classic conditions for steam fog which lasts till the pavement dries – a hot, wet surface and much cooler air above.

Fig. 4-37. Steam fog made by throwing powdered dry ice in a tub of hot water advances across the table top and cascades down the edge. SDG.

We also produce steam fog simply by exhaling when the air is cold enough. When we inhale, the air in our lungs and windpipe is heated to near body temperature (37°C) and humidified by contact with the wet lungs, windpipe and mouth. The steam does not appear immediately upon leaving our mouths but only after mixing begins, a few cm away from our mouths. Then, as the source air becomes progressively diluted it disappears, usually within a meter or two.

The densest of all steam fogs results by powdering dry ice (to increase its surface area) and throwing it into a tub of hot water (Fig. 4-37). As the mixture bubbles furiously, each initially frigid bubble of CO_2 gas is heated and humidified as it passes through the hot water. The temperature difference between dry ice (-78.5°C) and the hot water (40°C) is so great that an enormous number of tiny fog droplets forms in each bubble and when shot in the air can reduce visibility to 1 cm.

A bonus feature of dry ice fog is that it makes air motions visible. When the dense, dry ice fog reaches the end of the table top, it cascades down over the edge, ultimately evaporating. Before that, as the fog spreads out atop the table it curls up at the leading edge, where lobes form in the unstable flow (Fig. 4-38 and see Fig. 7-5). The same flow pattern occurs at the leading edges of thunderstorm outflow boundaries, cold fronts, fog banks (Fig. 4-39), and sandstorms or *haboobs* (Fig. 4-40). Views of clouds and fog from above (Chapter 5), offer similar perspectives.

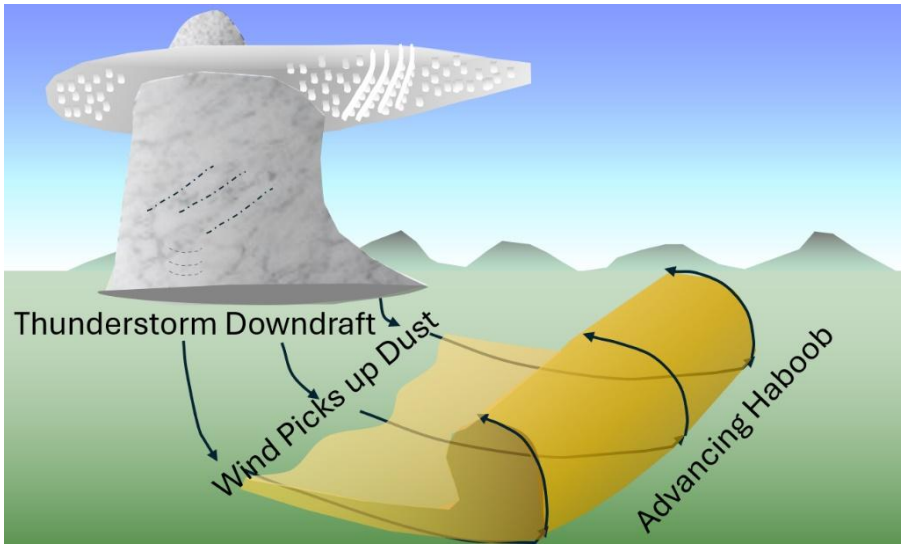

Fig. 4-38. Air flow at leading edges of haboobs, fog banks, and cold fronts. SDG.

Fig. 4-39. Fog bank with rising air at the leading edge, Cheyenne, WY, 29 Jul 2018. This was one of several outflow boundaries from thunderstorms in Nebraska. JC.

Fig. 4-40. Haboob in Lubbock, TX, 5 Jun 2019 driven by downdraft and outflow from a line of thunderstorms with ascending air at leading edge. © Matt Sutkoski.

Fig. 4-41. Radiation fog sinks towards Fairfield Lake, NC, 19 Oct 2018, as steam fog boils up over the warm water. Condensation trails (*contrails*) crossing the sky are reflected in the still water. SDG.

4.6 Cloud and Fog Gallery

Fig. 4-42. Cirrus uncinus off to the races over Boynton Beach, FL 30 Jan 2024. SDG.

Fig. 4-43. Cloud color vs height and viewing angle Cheyenne, WY, 28 Aug 2024. The optical thickness of the light path from Sun to cloud to observer is shortest for the white cirrus, intermediate for the near horizon golden clouds and longest for the underlit red base of the stratocumulus. JC.

Fig. 4-44. A field of cumulus mediocris and its reflection at Fairfield Lake, NC 26 Jul 2025. SDG. Usually when cumulus are present the wind is gusty and ruffles the water.

Fig. 4-45. Shade vs. Light, Cheyenne, WY 08 Jun 2018. The shaded protuberances under the optically thick cumulonimbus are almost black while the sunlit clouds near the horizon are white. JC.

Fig. 4-46. Altocumulus stratiformis undulatus with clouds at wave crests and clearings at troughs Boynton Beach, FL,10 Jan 2023. SDG.

Fig. 4-47. (Above) Valley fog and stratus Mont Blanc Massif, 17 Aug 2007. SDG.
Fig. 4-48. (Below) Moonlit ground-valley fog, Veliki Vrh, Bloke, Slovenia, 29 Sep 2023. © Stefano Zerauschek.

Wonders of the Atmosphere
Chapter 5: Cloud and Storm Systems: The View From Above

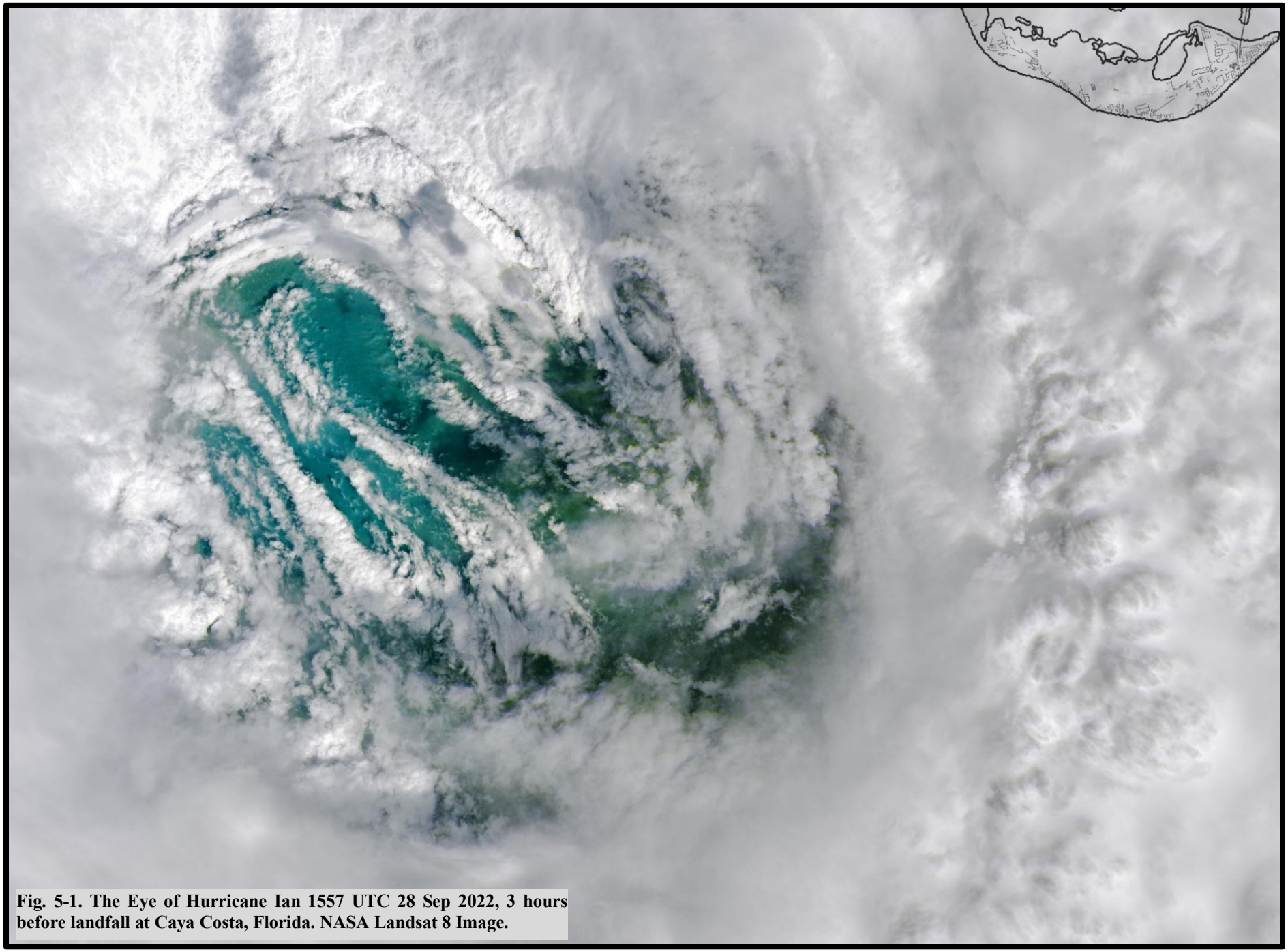

Fig. 5-1. The Eye of Hurricane Ian 1557 UTC 28 Sep 2022, 3 hours before landfall at Caya Costa, Florida. NASA Landsat 8 Image.

Wonders of the Atmosphere
Chapter 5: Cloud and Storm Systems: The View From Above

5.1 The View from Above

Throughout history humans have almost exclusively looked at clouds from below. That gave us little idea of their place and patterns in large scale storm and circulation systems. Now, with the conquest of the air and of space we routinely see clouds from above with a perspective that adds to our knowledge of the atmosphere, as, for example, the swirling cloud bands of Hurricane Ian's eye (Fig. 5-1).

Fig. 5-2. Flying amidst towering Cumulus over NC, 16 May 2009. A subsun is the bright spot directly below the Sun, indicated by the arrows. SDG.

The view from the commercial jets is more extensive than from the ground yet remains intimate and detailed. Nearby sights are fleeting but endlessly new. The view from space is less intimate, depending on the satellite's resolution, but so grand and extensive, even global, that we now see at a glance cloud and storm systems that took scientists centuries to suspect and then arduously piece together.

It is a joy to fly among the clouds, in the canyons between them, and to rise above them. Breathtaking, close-up views of the turrets of cumulus, the anvils and mamma of thunderstorms, the streamers of cirrus, the mottled and wavy sheets of altocumulus, and a host of optical phenomena including 360° rainbows and a range of halos, some only seen from above. In Fig. 5-2 the jet has just emerged into a clearing almost walled in by towering cumulus, while a subsun, a mirror image reflection of the Sun made by ice crystals that fall like horizontal mirrors appears as a bright dot indicated by the arrows.

Fig. 5-3. Valley Fog in San Mateo, CA on the morning of 24 Nov 2016. SDG.

5.2 Small-Scale Systems: Valley Fog

Fig. 5-4. Clear rifts in the fog at the centers of valleys in the Peruvian Andes 16 Jul 2015. NASA Earth Observatory, LANDSAT.

Even before aviation and space travel, anyone who climbed hills or mountains could look down upon a sea of fog filling the valleys (Fig. 5-3, and §15.2). Valley fog, essentially a form of radiation fog, forms best on clear, calm nights as the slopes radiate heat out to space and the cold ground cools the air just above by contact.

Fig. 5-5. The final ribbon of valley fog hugs the hillside. The view faces WSW to the Obaiu from Corps, France, around 10 AM, 03 Aug 1978. SDG.

The chilled, dense air sinks down the slopes as a mountain breeze, often in spurts, where it accumulates in the valleys and continues cooling as the valley floor also radiates heat out to space. If the air cools enough to become saturated, droplets condense to form valley fog. The top surface of the fog then radiates heat out to space and cools even more rapidly so that the fog becomes self-enhancing. At the same time, sinking air clears the sky over the summits.

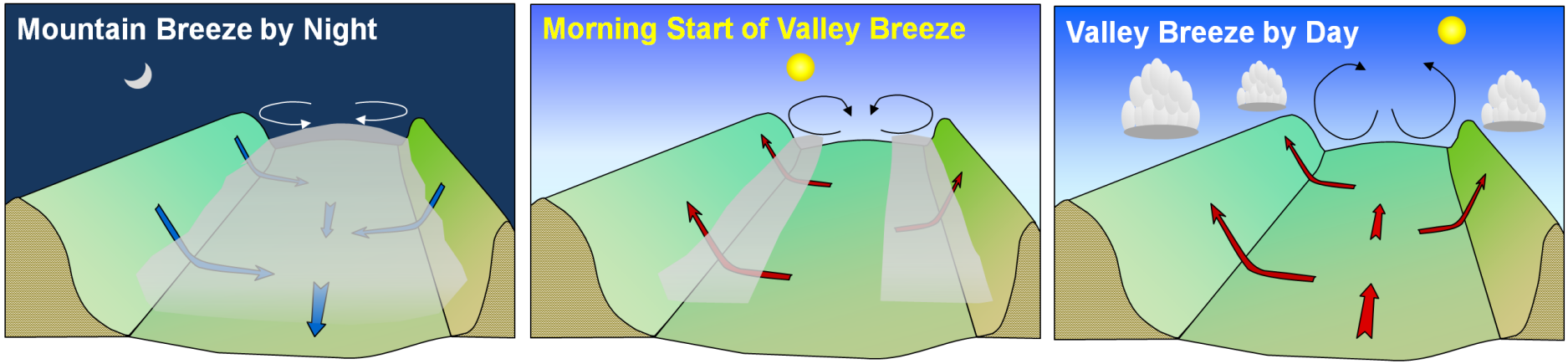

Fig. 5-6. The daily cycle of valley and mountain breeze circulations. Valley fog forms at night and evaporates from valley center outward as the Sun rises. Cumulus clouds form over the hilltops and summits during the day. SDG.

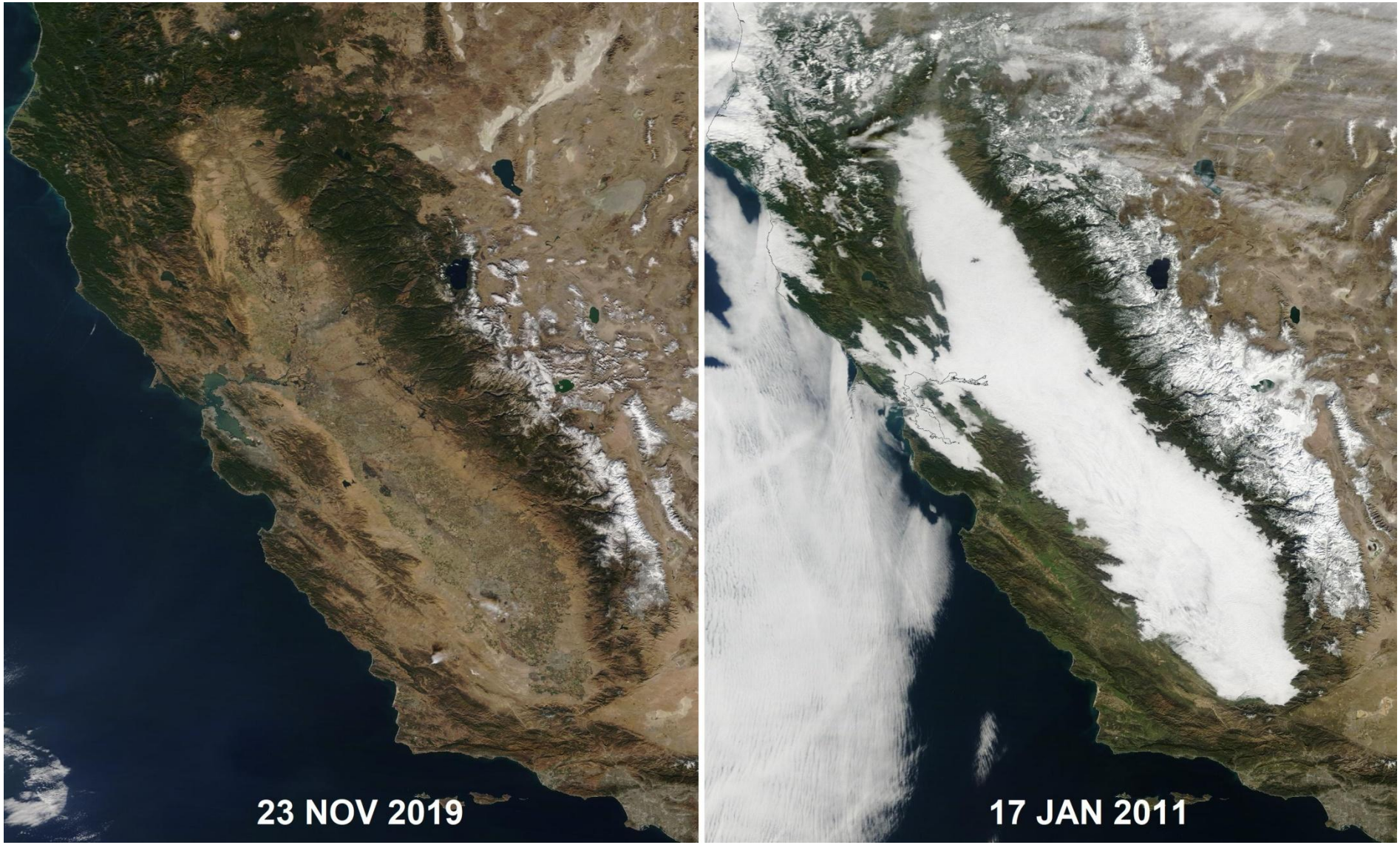

Fig. 5-7. Left: The Central Valley of California on 23 Nov 2019 during a dry period with a brown rim (NASA MODIS Terra). Right: The Central Valley filled with Tule Fog, which extends to the adjacent valleys including the San Francisco Bay on 17 Jan 2011, after a soaking rain. The visible parts of the rim are green and snow cover is greater. Advection fog, crossed by ship tracks, covers a large area of the Pacific Ocean.

As the morning Sun rises and heats the slopes, valley fog begins to 'burn off', but it does so in a curious way revealed by satellite images (Fig. 5-4). A clear rift in the fog opens along the center line of each valley and gradually broadens until the last remnants of fog hug the slopes like ribbons (Fig. 5-5).

This manner of clearing, from valley center outward, results because the circulation reverses direction. As heated air over the slopes slides upward as a valley breeze, cooler air in the center of the valley sinks, warms, and makes the fog evaporate faster.

As the day goes on if the air is heated and rises enough it will produce cumulus or even cumulonimbus clouds over the summits. The daily cycle of mountain and valley breeze circulations and the resulting daily cycle of fog and cumulus are illustrated in Fig. 5-6.

Fog can also fill valleys on a grand scale, especially during winter's short days and low, weak Sun. Fig 5-7 contains two contrasting NASA MODIS Terra images of the Central Valley of California, one on 17 Jan 2011, when it was filled by a Tule Fog that followed a soaking rain. In this case, as in others, the fog persisted unbroken for several days and nights even though it was quite shallow as the sounding at that time (Fig. 4-25) shows.

The Central Valley is so wide that Mountain Breezes play only a secondary role in the formation of the Tule Fog; cooling by radiation of heat to space by the ground is the primary driver. And, once the fog forms, it tends to be locked in by the surrounding mountains until a strong wind drives it out of the valley and dissipates it.

Without the rains, the Tule Fog seldom forms, as on 23 Nov 2019. A give-away of the dry conditions is the brown rim of the non-irrigated slopes around the valley. And, since drought has prevailed much of the past decade in California the slopes have more often been brown and the Tule Fog less frequent and less extensive.

5.3 Satellite Pixel Size: Limits of Resolution

The extensive view provided by the meteorological satellites often comes at the cost of resolution. If you zoom ever closer in the attempt to see fine details of small features, the features either become blurred or morph into fields of pixels (i. e., squares). An example of the visually unpleasant limitation of resolution is shown in Fig. 5-8, which compares two side-by-side images of cumulus and cirrus clouds over the Kimberly Region of Australia on 31 Oct 2021.

The cumulus clouds are of order 2 km wide. The Landsat 9 image on the left shows the fine scale structure of the clouds. The MODIS (**MOD**erate resolution **I**maging **S**atellites) Terra image on the right shows the cumulus clouds as blurry with individual pixels visible.

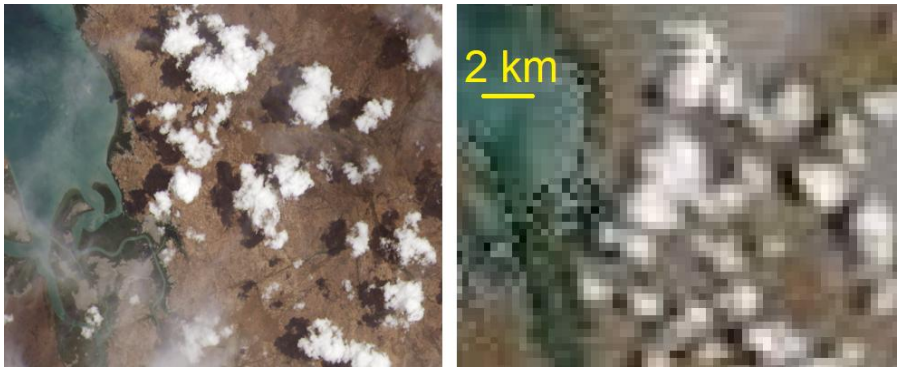

Fig. 5-8. Landsat 9 (left) vs MODIS Terra image (right) of cumulus clouds over the Kimberly Region of Australia on 31 Oct 2021, showing improvement of 30 m over 250 m pixels.

The smallest *discernable* feature of any object must wider than the pixel size. Minimum pixel size for the geostationary satellites such as GOES that hover 35,686 km over the equator is 1 km (but only for the red band). Minimum pixel size for Polar orbiting, MODIS Terra and Aqua satellites, archived at

https://worldview.earthdata.nasa.gov/

is 250 m, but for only 2 of the 36 wavelength bands, 500 m for 5 bands, and 1 km for the others. Landsat images, with their pixel size for color images of 30 m, resolve much finer scale features of clouds. Unfortunately, Landsat images are not routinely available on the Web and require the hopeful viewer to perform special processing, available at,

Fig. 5-9. Hole punch cirrus in altocumulus from Florida to the Bahamas, 12 Dec 2014. Cloud base at 6000 m at *T* = -20ºC. NASA MODIS Terra image.

https://glovis.usgs.gov/

No image including the beautiful images of the MODIS satellites must be looked at too closely Even their 250 m pixel size can only resolve the largest cells and ripples of altocumulus clouds. For example, the tiniest cells and ripples visible in Fig. 5-9 are 500 m, and if the image is zoomed too much individual pixels will appear.

Many cloud elements we see in detail from the ground are less than 250 m wide. An altocumulus cell 3 km above ground level that appears 5º wide (by definition, the maximum angular width of altocumulus elements) to a viewer on the ground is only 262 m wide. Cirrocumulus cells or ripples are even smaller. A cirrocumulus cloud element 10 km above ground level that appears 1º wide (by definition, the maximum angular width for cirrocumulus elements) is only 175 m wide. The individual strands or fibers in cirrus can be even narrower. Typical cumulus humilis clouds are wide enough to be seen, but without any detailed structure.

That is why most satellite images of sheets of stratocumulus, altocumulus, and cirrocumulus clouds give little or no hint of the beautiful fine scale cells and ripples. It is why cirrus clouds with beautiful streamers when seen from the ground appear fuzzy or gossamer smooth in most satellite images. It is also why cumulus humilis clouds appear as mere dots in most satellite images. By contrast, the much larger anvils of cumulonimbus clouds do appear in most satellite images to resemble popcorn or cotton balls if they are almost circular, and long smoke plumes if rapid winds in the upper troposphere stretch them downwind.

When pixel size is 30 m, as for Landsat images, more details of cirrus streamers and altocumulus cells are clearly visible. The false color image of Fig. 5-10 was processed for a study of hole-punch clouds. Temperature in the altocumulus sheet over West Virginia on 11 Dec 2009 ranged between -5 and -20°C, yet it consisted entirely of (false color) pink supercooled water droplets until some time after is was punctured by a plane that led to the (false color) turquoise ice crystal cirrus in its center.

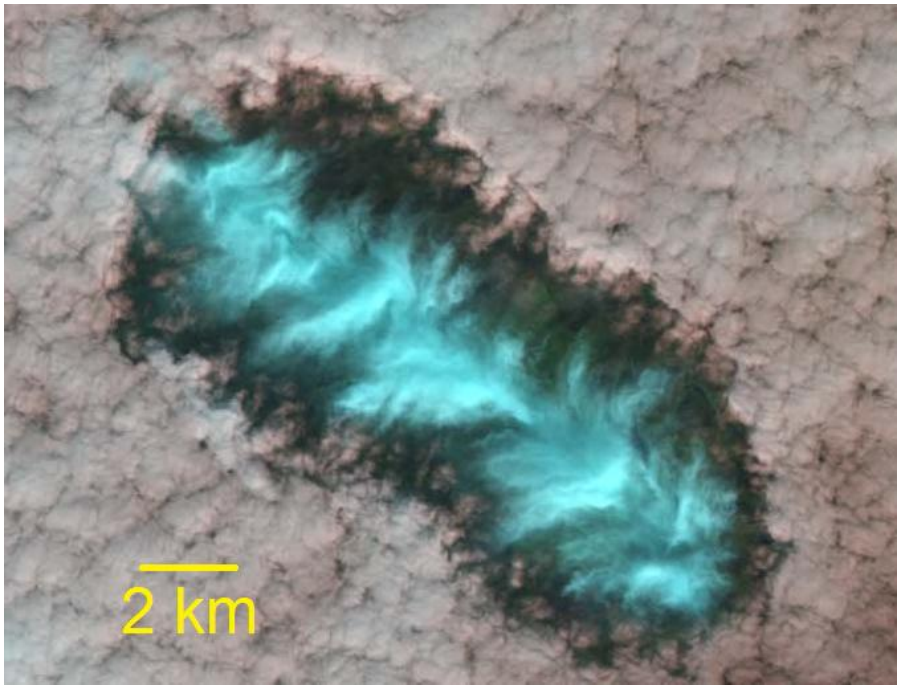

Fig. 5-10. Landsat 5 image with 30 m pixels of hole punch cloud of 11 Dec 2009 showing ice crystal Ci (blue) in the midst of supercooled water Ac (pink).

Many meteorological satellites now distinguish water and ice clouds. This is done by comparing the signals at several different wavelength bands given that the optical properties of water, such as reflection and absorption, vary with wavelength differently from those of ice.

Even though most satellites do not have such high resolution one look at the images constitutes proof that they give us breathtaking and informative views of the panoply of the clouds that grace the skies, and clothe the land. And many cloud features have a large enough scale so that the panoramas provided by satellite are superior to what we can see from the ground.

5.4 Small-Scale Systems: Sea Breeze

Fig. 5-11. A field of cumulus covers the land north of Tampa, FL while the sky is cloudless over the waters of the Gulf of Mexico. SDG.

Flying over coastlines on many spring and summer afternoons reveals a striking but common pattern. In Fig 5-11, a field of cumulus covers the land on the west coast of Florida just north of Tampa while clear skies reign over the Gulf of Mexico. Cumulus clouds sprout up almost every day of the year over the land and some grow into cumulonimbus, making afternoon showers a byword in the tropics.

This pattern is caused by the *sea breeze*, another classic local wind system with a daily cycle (Fig. 5-12). During the day all year long in much of the tropics and during spring and summer in many locations outside the tropics, the land quickly gets hotter than the sea and the hot, buoyant, air rises over the land. Cooler, denser air over the sea

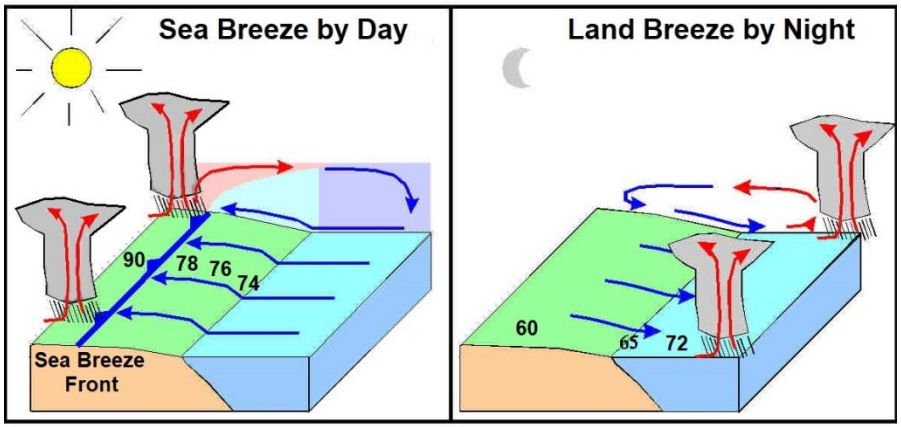

Fig. 5-12. The daily cycle of sea breeze and land breeze circulations. Clouds form over the land during the day and over the water at night. SDG.

then blows in from the sea near the surface. The sea breeze typically penetrates 10 km or more inland before it is warmed enough to rise buoyantly, sometimes forming a sea breeze front with enhanced cloudiness. After rising between about 500 or 1000 m (except higher in cumulus) the wind aloft returns to the sea and sinks over the ocean to complete a circulation cell and produce a clear aisle.

Fig. 5-13 illustrates these features to a tee! The near symmetry of clouds around the Yucatan on 16 Aug 2024 indicates that the large scale winds are weak. The sea breeze cleared skies over the coastal waters and a short distance inland. Dots of cumulus are spread across the interior of the Yucatan but are enhanced at their perimeter by the rising air at the inland edge of the sea breeze. A much larger popcorn cumulonimbus cloud has formed over the NE corner of the Yucatan, where colliding sea breezes from two coasts enhance updrafts.

In most cases, the fuzzy, thin anvil edges thin out to Ci, and show that the anvils are composed of ice crystals and other frozen particles.

Myriad satellite images show the sea breeze and its clouds. Cuba is so narrow that sea breezes from north and south clash, often producing a

Fig. 5-13. The Yucatan Peninsula covered by cumulus dots and popcorn cumulonimbus, illustrating the sea breeze, 16 Aug 2024. NASA MODIS AQUA image.

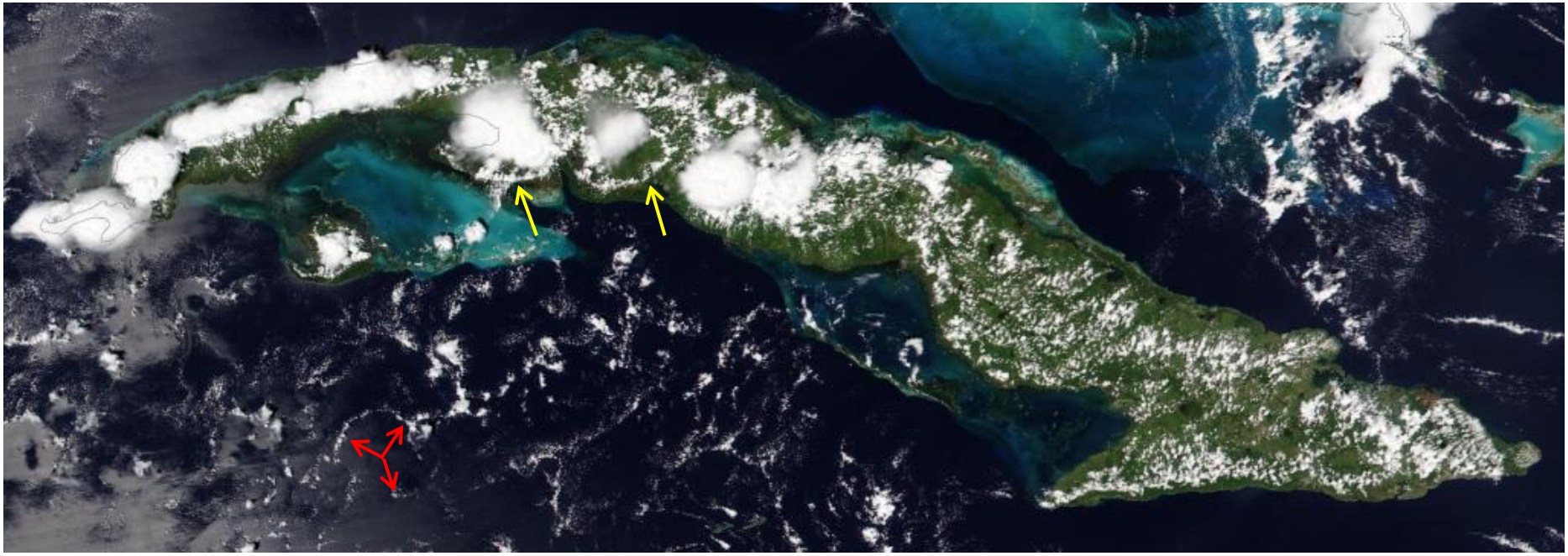

Fig. 5-14. Popcorn cumulonimbus and dots of cumulus rise over the heated land of Cuba, 09 Sep 2023. Rings of cumulus form at the outflow boundaries south of two cumulonimbus clouds (yellow arrows). Rings of cumulus dots mark the perimeters of open convection cells (red arrows). NASA MODIS AQUA image.

string of popcorn cumulonimbus clouds over the land while the coastal strip remains mostly clear, as on 09 Sep 2023 (Fig. 5-13).

Fig. 5-14 contains at least two other interesting features. 1: Dotted rings of cumulus clouds form south of two cumulonimbus clouds (Yellow arrows). They mark outflow boundaries of thunderstorm downbursts, where air turns up and rises, as in Fig. 4-37 and Fig. 4-38 (see also Fig. 7-5), and 2: Narrow, broken rings of cumulus dots with clear centers in the Caribbean south of Cuba (red arrows) represent open convection cells often seen over warm waters (see §12.3).

At night the land gets colder than the sea, cumulus and cumulonimbus subside and evaporate, and the direction of circulation reverses to form a land breeze. The land breeze is generally weaker and shallower than the sea breeze, but if the ocean waters are warm enough, cumulus or cumulonimbus can form over the water while the sky over the land remains clear, as in the NOAA image at 1300 UTC on 01 Sept 2019 (see Fig. 5-28). Then, as the land warmed up during the day, cumulonimbus clouds sprouted up over Cuba and the Florida Peninsula by 2200 UTC (see Fig. 5-29), where they were displaced to the west coast by easterly winds of Hurricane Dorian's periphery.

5.5 Large Scale Wind, Storm, and Cloud Systems

Large scale wind and storm systems determine the locations and dominant forms of clouds around the globe. Satellite images put these systems on display for up to the full globe in several ways, each with advantages and disadvantages. Full disk visible light images of the geostationary satellites put cloud and storm systems on display at any given moment for up to half the globe, as in Fig. 5-15, though systems near the limb appear at glancing angles. Stitched visible light images of the polar orbiting satellites can display the entire globe, as in Fig. 5-16, but they transpire over 24 hours and the stitching is never perfect.

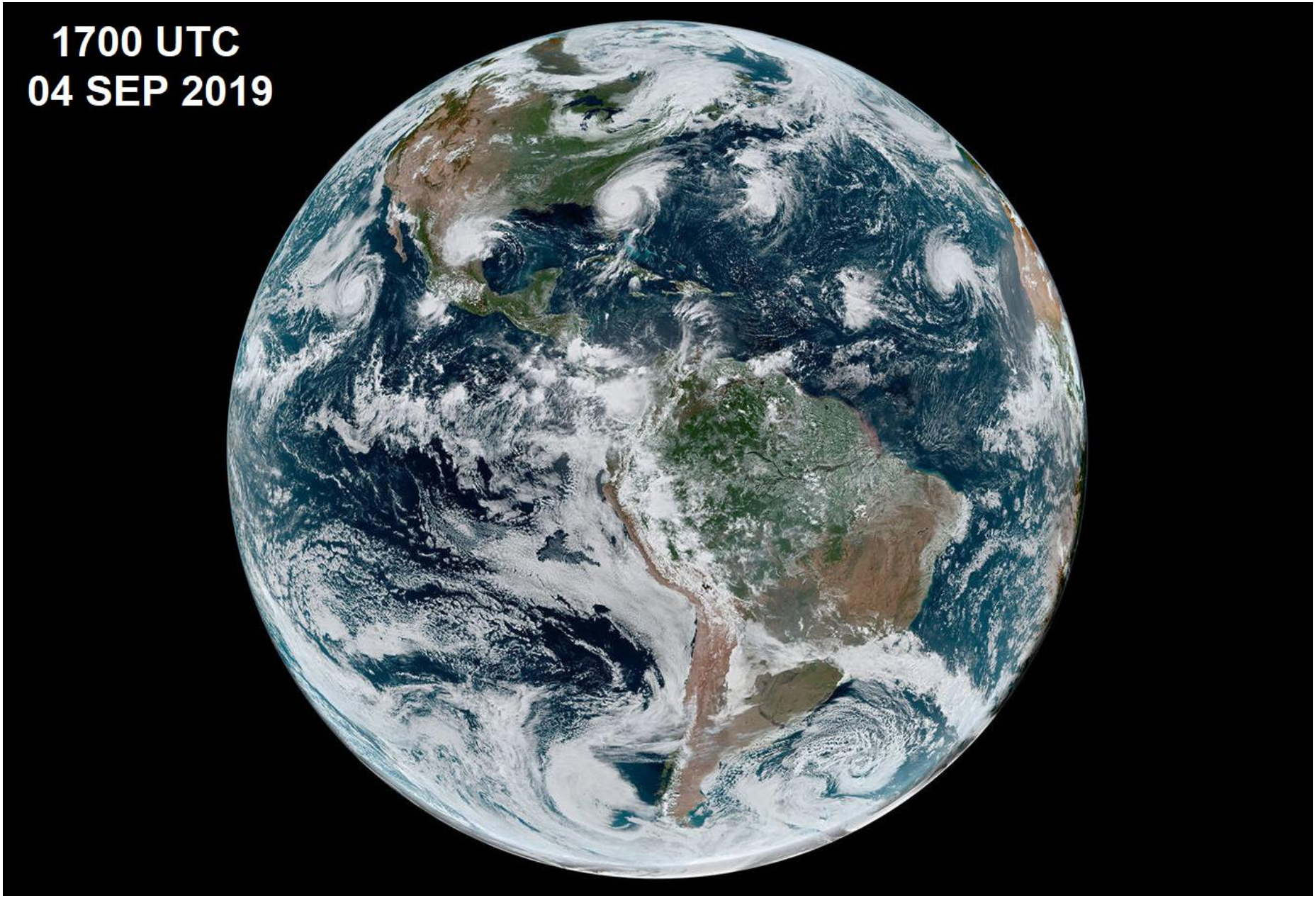

Fig. 5-15. Full Disk NASA GOES Image 4 Sept 2019 with many cloud genera and systems. Spiral pinwheels in the tropical oceans are Hurricanes Dorian and Juliette, and Tropical Storms, Fernand, and Gabrielle. Cloud swirls at higher latitudes ae extratropical cyclones. Dotted clouds over the Amazon Basin are cumulus and cumulonimbus. Cloud field over the Pacific Ocean west of the Atacama Desert are cellular stratocumulus clouds.

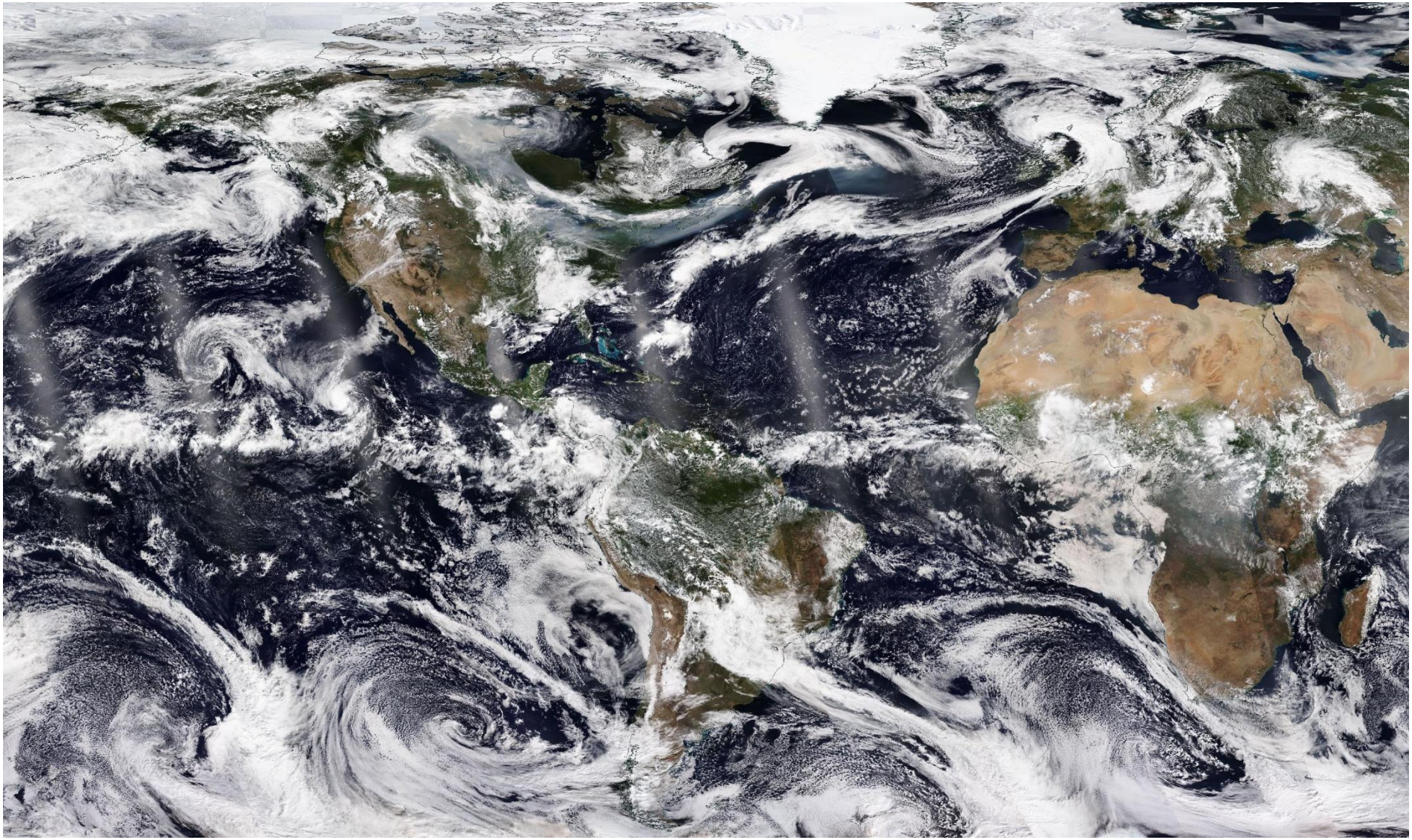

Fig. 5-16. NOAA 20 VIIRS collage of 24 hours of stitched orbits, 4 Aug 2025. Prominent features include extratropical cyclone wave trains in each hemisphere, the band of convective clouds of the ITCZ stretching EW across the entire image north of the equator, smoke plume extending from Boreal forest fires in Canada and Tropical Storm Henriette over the eastern Pacific Ocean.

We chose the full disk image of 4 Sept 2019 (Fig. 5-15) because it contained four storms resembling spiral galaxies over the subtropical oceans – Hurricanes Juliette in the East Pacific and Dorian just east of Florida and Tropical Storms Fernand in the Gulf of Mexico and Gabrielle off the coast of Africa. The stitched image of 4 Aug 2025 contains only one Tropical Storm, Henriette, some 2000 km west of Baja California, but it shows some of the other cloud and storm systems to greater advantage.

A list of the systems includes,

- Tropical cyclones, which often resemble pinwheels or spiral galaxies, and which form over the subtropical oceans during the warm water season.
- Extratropical, frontal cyclones, the cloud spirals or masses at mid and high latitudes with comma-shaped extensions in the Northern Hemisphere (up-side down in the Southern Hemisphere).
- Abundant dots of cumulus and cumulonimbus over the green tropical rainforests.
- Patterned subtropical stratocumulus clouds extending westward from the west coasts of the continents, mainly in summer.
- The InterTropical Convergence Zone (ITCZ), the wavy, broken line of cumulonimbus clouds parallel to the equator.

The ITCZ is the low-pressure belt that girdles the globe, drifting north and south of the equator in pursuit of the Sun. It is where the Trade Winds converge and rise, for the most part in cumulonimbus clouds. The rising cumulonimbus towers of the ITCZ produce ample precipitation and result in tropical rainforests. After rising to the upper troposphere, the air aloft moves away from the tropics and sinks in the

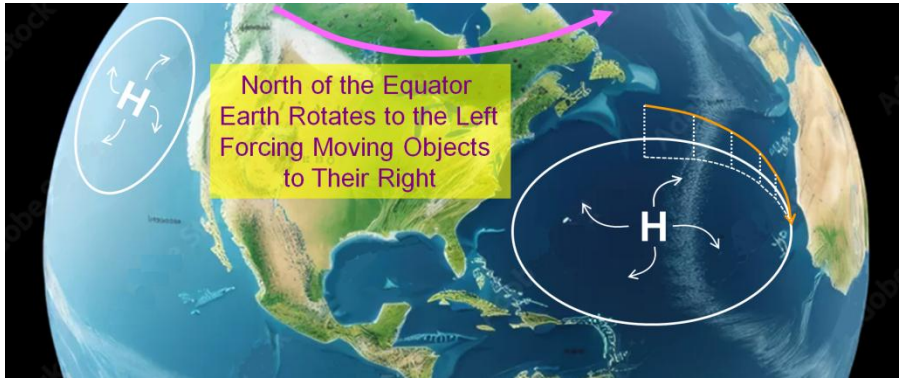

Fig. 5-17. Earth's rotation and wind around the Subtropical Highs. SDG.

subtropics, typically between about 20° and 30° latitude, producing mostly clear skies and the world's subtropical deserts.

Away from the equator, the large-scale surface winds are organized into spiraling high- and low-pressure areas. Air near the surface spirals out of highs (anticyclones) and air aloft sinks to replace it to form mostly clear skies. Air spirals into lows (cyclones) and rises to form abundant clouds and precipitation with the distinctive patterns mentioned above.

The Earth's rotation via the Coriolis force is what causes the wind to spiral around the highs and lows. *North* of the equator, when viewed from space, every point turns to its left, indicated by the purple arrow in Fig. 5-17. This turning deflects all moving objects in the Northern Hemisphere to their right (as in the winds in Fig. 5-17), so that

> **North of the equator, wind spirals 1: counterclockwise in toward the centers of cyclones, and 2: clockwise out from the centers of anticyclones.**

Since the sense of the Earth's rotation *south* of the equator is to the right, all moving objects are forced to their left, and winds spiral in the opposite direction from lows and highs in the Northern Hemisphere.

Large, semi-permanent high-pressure areas centered at about 30° latitude dominate the world's subtropical oceans. Because the air tends to sink, skies are generally clear and the climate is generally dry. But the subtropical highs have great east-west asymmetry. The air on their eastern sides blows from the direction of the poles, is usually cool and the tendency to sink is particularly strong, so there is little precipitation, though fog and low clouds often hug the coasts, as at Peru, Chile, and California.

On the western sides of the Subtropical Highs, air blows from the direction of the equator and tends to be warm and humid. Sinking motion prevails but is weak enough so that cumulonimbus clouds pop up to produce adequate precipitation. Quite often, the wind aligns the cumulus clouds, as over Florida (Fig. 5-18) and satellite loops reveal the motion. In the season of warm waters, tropical cyclones form and move around the highs' equatorward and western periphery.

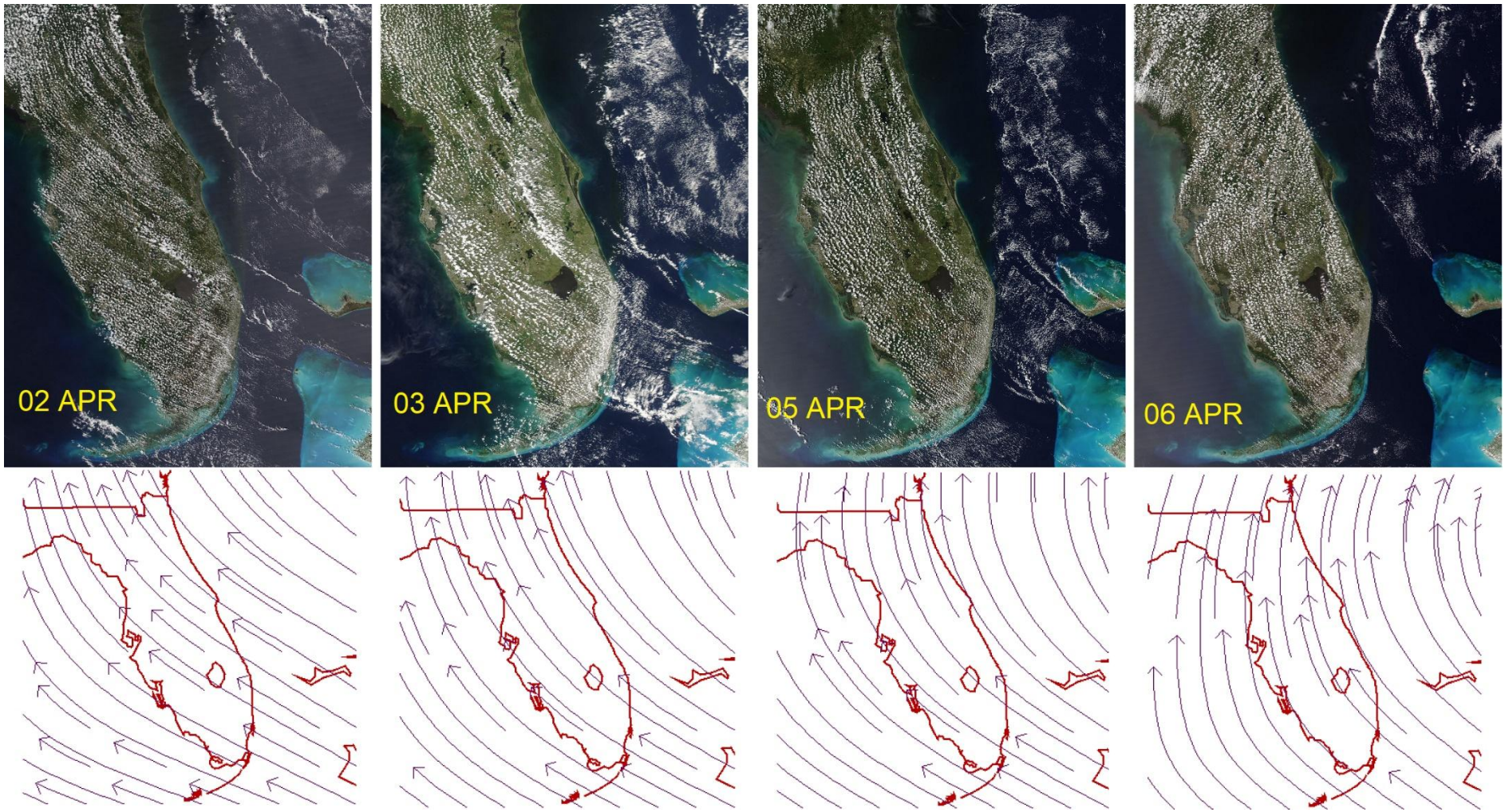

Fig. 5-18. Southerly winds on the western side of the Bermuda-Azores High frequently (as from 02 to 06 Apr 2025) align cumulus clouds in long rows. Note that the cumulus clouds form and are confined to the land and they are suppressed downwind from the still cool April waters of Lake Okeechobee. NASA MODIS images.

The east-west asymmetry is enhanced by the interaction between the wind and the ocean currents. The wind drives the ocean currents but in an unexpected way, again because of the rotation of the Earth.

It is natural to think that ocean currents would be blown directly downwind, but this is not the case. The Earth's rotation forces the surface ocean currents to move to the right (left) of the wind in the Northern (Southern) Hemisphere, and thus away from the west coasts of the continents from about 10° to 45° latitude.

As the surface water moves away from the west coasts, frigid deep ocean water upwells (Fig. 5-19) and chills the air near the surface. That enhances the tendency of the air to sink so that cumulus and cumulonimbus clouds cannot form, which are absent over the coastal waters, and often for 100 km or more inland.

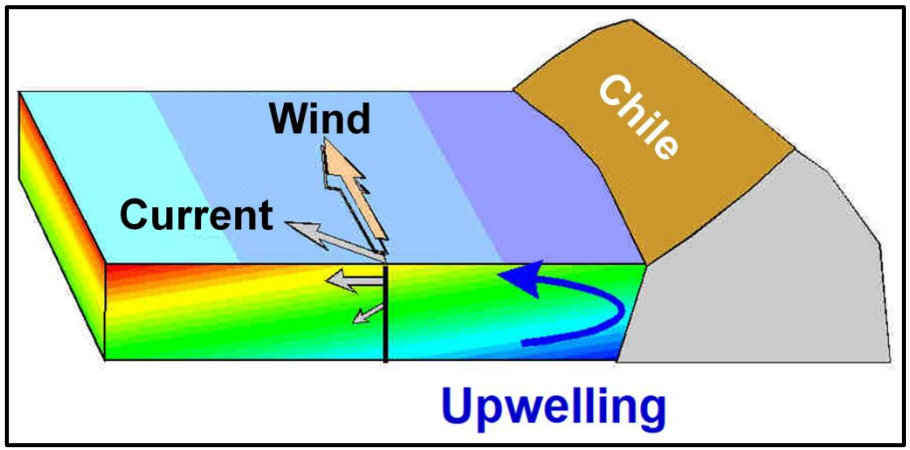

Fig. 5-19. Wind driven currents move to the left of the wind south of the Equator and force upwelling of cold, deep water. SDG.

The air over the coastal waters west of the continents in the subtropical and middle latitudes is not only cooled but also charged with water vapor. This leads to the widespread subtropical stratocumulus clouds, and stratus, and fog, that often bank up against the coast, especially during summer, as at San Francisco, even though the tops seldom reach 2 km. Patterns in the cloud field are produced when mountainous islands deflect the winds (see §12.6).

Any time the large-scale wind has an inland component (often enhanced by the sea breeze) it drives the fog inland over coastal hills and makes it pour through valleys or straits such as San Francisco's Golden Gate. On 26 Jul 2023 (Fig. 5-20), a long tongue of the stratocumulus cloud field extended across San Francisco Bay all the way to Oakland (recall Fig. 4-24). On this day the fog topped out at about 350 m so it was blocked by the Coastal Range, but on the days the fog layer is thick enough, it will top the Coastal Range and pour down into the lowlands (Fig. 4-25 and Fig. 4-26).

Fig. 5-20. Fog and low clouds lodge against the Coast Range and pour through the Golden Gate as an extended tongue on 26 Jul 2023. NASA Modis image.

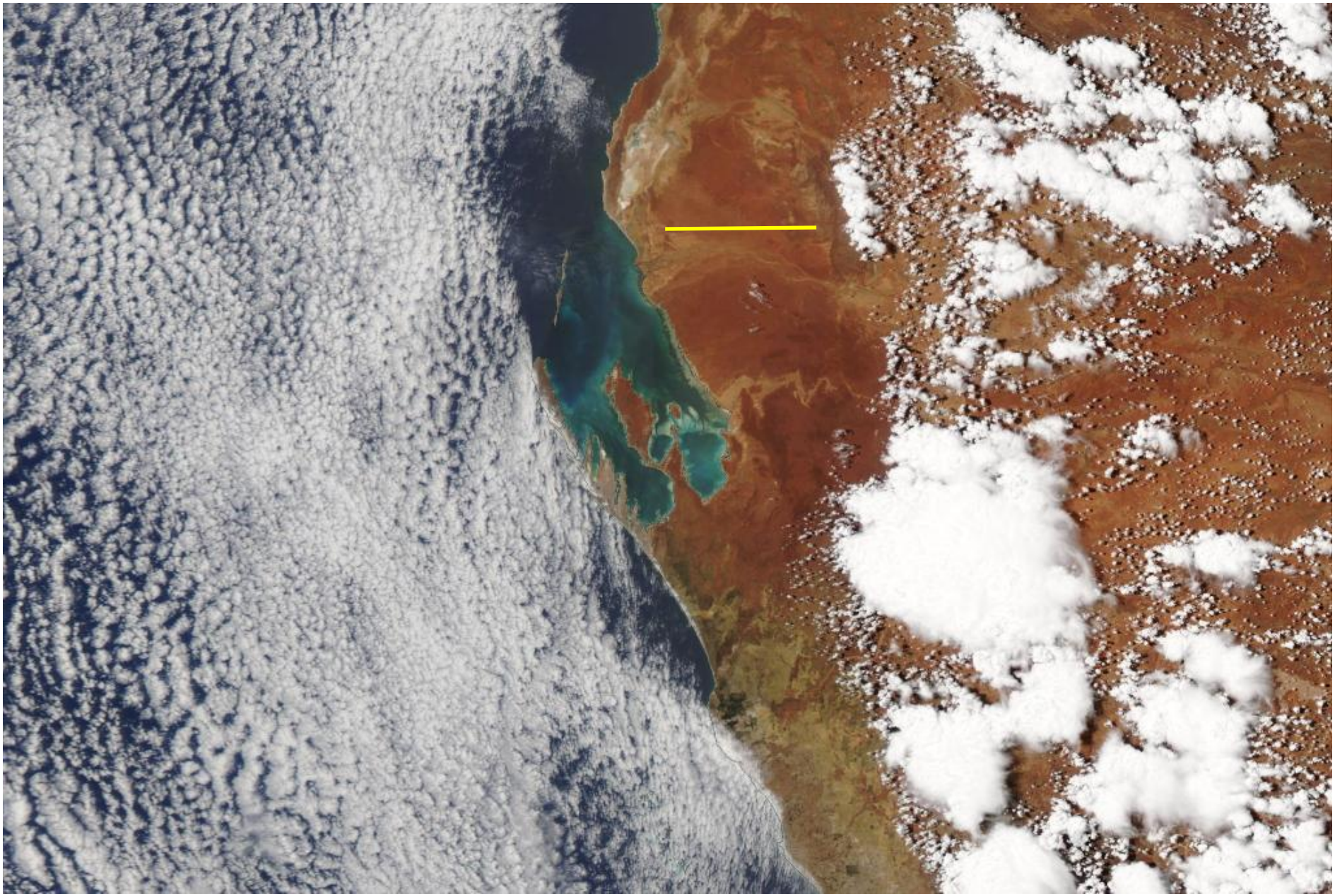

Fig. 5-21. A thin sheet of stratocumulus cells cover the cool Indian Ocean. Inland, cotton-ball cumulonimbus and dots of cumulus rise over the hot Great Sandy Desert, Australia, 29 Jan 2015. NASA MODIS Aqua image. Yellow line is 100 km long.

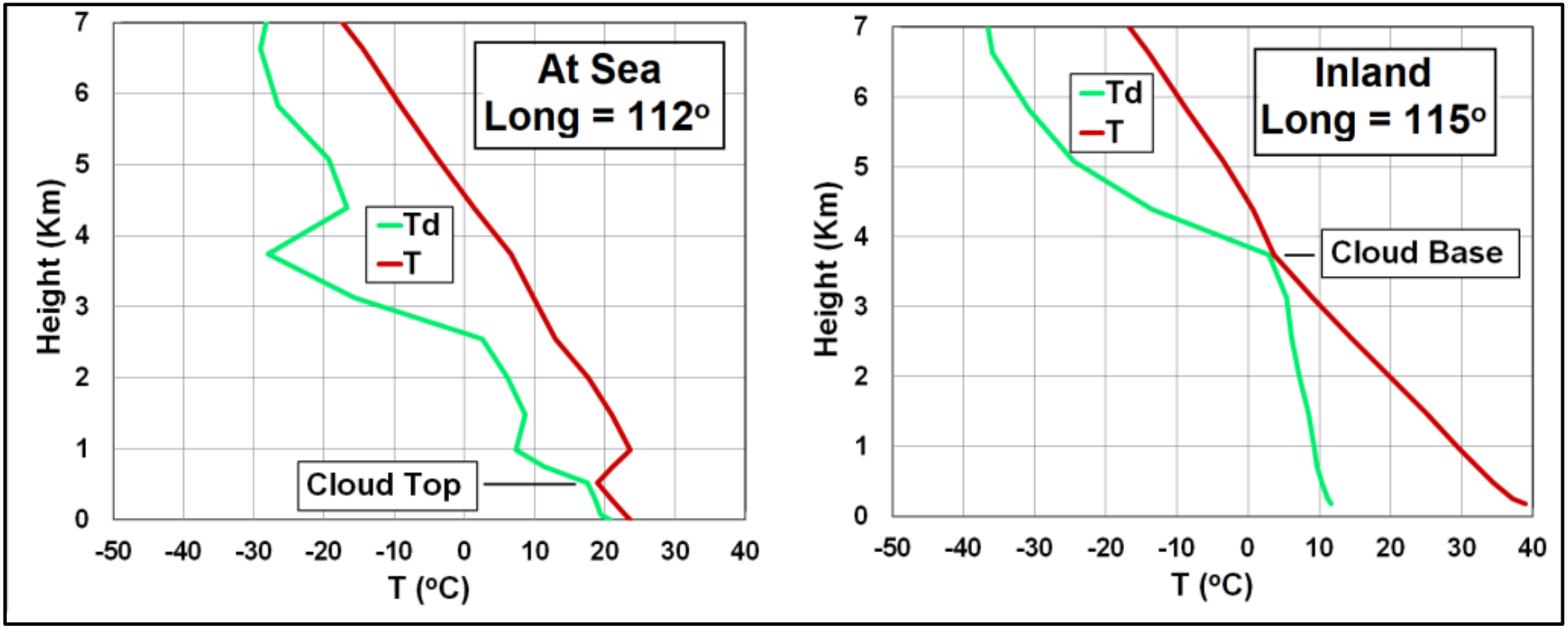

Fig. 5-22. Soundings at longitude 112° over the cool Indian Ocean with stratocumulus cloud cells (left), and inland at longitude 115°, over the hot Great Sandy Desert with cumulus and cumulonimbus (right) 29 Jan 2015. SDG.

When cool ocean air from the subtropical highs drifts inland during the day it is heated and the stratocumulus clouds and fog evaporate. If the air continues moving inland it can be heated enough to produce cumulus and cumulonimbus clouds. This was the case over Australia's Great Western Desert on 29 Jan 2015 (Fig. 5-21). An extensive, patterned sheet of stunted stratocumulus cloud cells whose tops barely reach 500 m. above sea level covered the cold, cobalt blue Indian Ocean water west of Australia.

As cool, humid ocean air along the coast blew inland it was heated over the dry, desert land. Skies cleared and remained clear until the air had moved far enough inland so that it was heated and buoyant enough to rise and form cumulus dots and popcorn cumulonimbus that towered above the deep red surface of iron-rich rock and sand and lighter colored sediments of the meandering, dry stream beds.

This image of striking visual contrasts is mirrored by contrasting soundings over the sea and inland (Fig. 5-22). Air just over the sea had $\boldsymbol{T}$ = 23°C and $\boldsymbol{T}_d$ = 21°C, so $\boldsymbol{RH}$ = 90%. Cloud top was capped by an inversion at 500 m, above which $\boldsymbol{T}$ and $\boldsymbol{T}_d$ diverged abruptly. The sounding over the desert 300 km to the east was markedly different. The air at the surface, at $\boldsymbol{T}$ = 40°C and $\boldsymbol{T}_d$ = 12°C, was warmer and drier than when it had been over the sea. The sounding shows that temperature decreased with height at a rate near 10°C/km while the dew point decreased with height at a rate near 2°C/km. Both of these lapse rates match the adiabatic cooling rates of rising, unsaturated air (recall §4.3). Cloud base occurred at 3.6 km above the surface, where $\boldsymbol{T} = \boldsymbol{T}_d$. Though the ambient air was dry above this height cumulus and cumulonimbus clouds were buoyant and continued to rise.

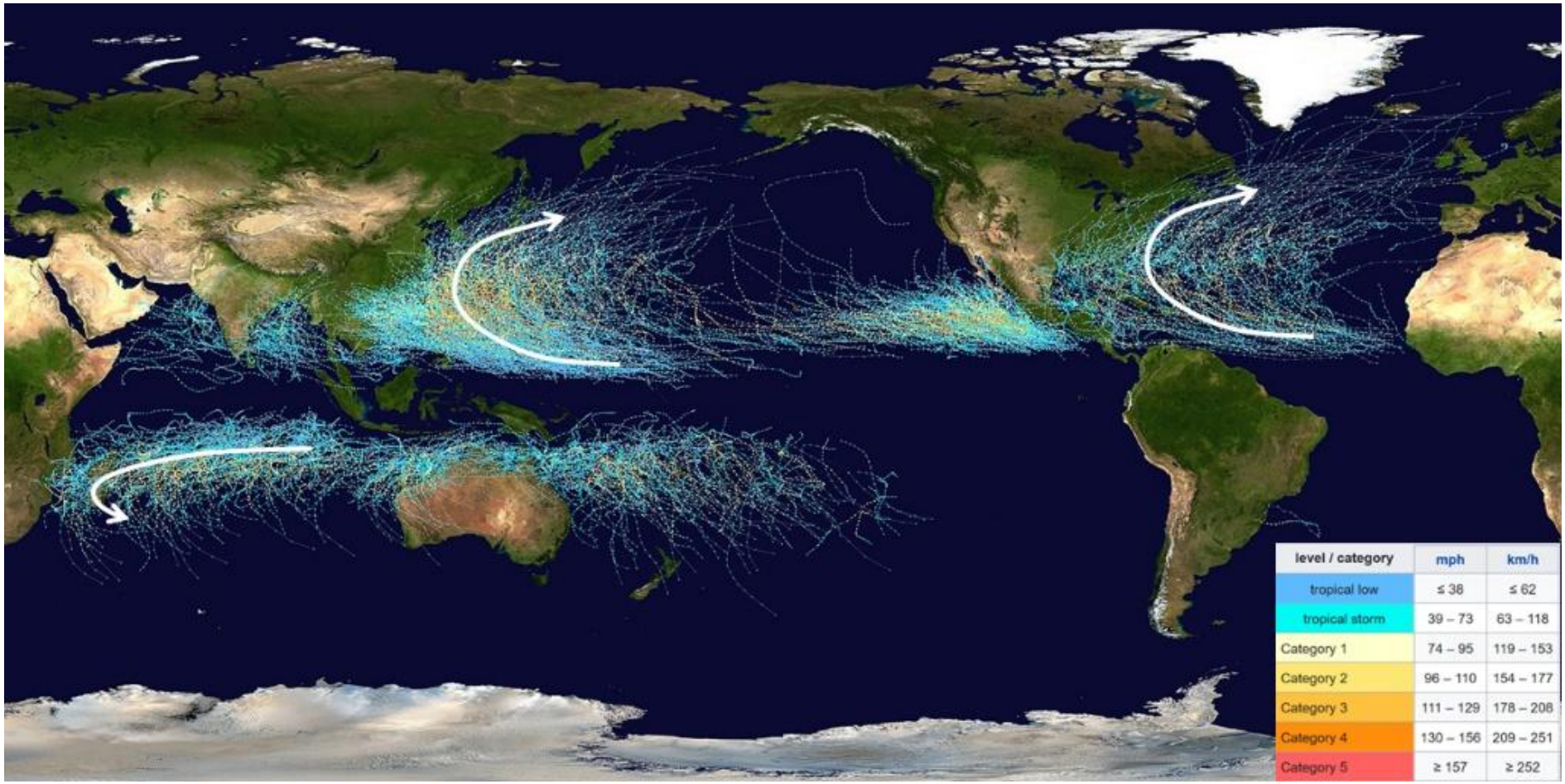

Fig. 5-23. Tropical cyclone tracks and intensity 1985-2005. White arrows show representative tracks around the subtropical highs. NASA image.

5.6 Tropical Cyclones

At the same time that fog and low clouds refrigerate summers on the eastern edges of the subtropical highs, towering spiral-galaxy shaped cloud systems of tropical cyclones roil the atmosphere and the warm sea surface waters that energize them on the tropical and western sides of the same highs. Tropical cyclones have various names depending on location but are all basically the same. They are called *hurricanes* in the North Atlantic and East Pacific Oceans, *typhoons* in the West Pacific, *baguios* around the Philippines, and *cyclones* in the North Indian and South Atlantic Oceans.

Tropical cyclones are intense low-pressure areas between about 300 and 1500 km in diameter that rage over all the world's tropical and subtropical oceans given by the spaghetti trails in Fig. 5-23. (The South Atlantic, long an exception to the rule, got its first cyclone in memory in 2004 – Cyclone Caterina.) Tropical cyclones form over warm waters (T > 26.5°C), mainly from late summer to early autumn from about 3° to 33° latitude, avoiding the equator where there is no Coriolis force.

To qualify as a hurricane or typhoon the surface wind speed must reach at least 118 km/h somewhere in the storm, though many greatly exceed that minimum standard with peak winds over 200 km/h. Hurricanes are ranked by maximum wind speed on the Saffir-Simpson scale from Category 1 to Category 5 (super typhoon) (Fig. 5-23). Storms of Category 3 or more are considered major. The greatest 1-minute sustained *surface* wind speed ever recorded in a tropical cyclone was 345 km/h in Hurricane Patricia (2015) in the eastern Pacific Ocean.

Tropical cyclones are the deadliest of all storms and, given that an average of almost 100 form every year, they are collectively the costliest of all natural disasters. They mete out damage in a range of ways. They can ravage the coasts, raising sea level in a storm surge typically 2-3 m but up to 10 m or even more, and produce enormous waves on top of the storm surge. At sea the waves may exceed 15 m high. Inland, torrential tropical cyclone rains up to about 2 m transform babbling brooks into raging rivers and submerge wide swaths of lowlands, while their ferocious winds mow down forests. For example, Hurricane Maria (2017) transformed emerald green Virgin Islands and Puerto Rico in its path into mountainous morasses of mud. Adding insult to injury, rotating thunderstorms, mostly on the hurricanes' advancing right quadrants can generate scores of tornadoes.

Hurricane Helene (2024), a Category 4 storm at landfall is a case-in-point. Its storm surge exceeded 2 m along the Gulf Coast of Florida and topped out at almost 5 m in the sparsely populated panhandle region. Rainfall totals exceeding 25 cm occurred from Florida to Virginia and topped out above 50 cm in the Blue Ridge Mountains of western North Carolina, where Helene was preceded by a front that produced a separate 25 cm. These enormous rainfall totals led to cataclysmic flooding in the river valleys, as around Asheville. Fierce winds toppled trees by the millions, blocking highways and knocking out electricity for days. Helene spawned a documented 33 tornadoes, most of which, fortunately were weak. The death toll from Helen exceeded 200 and monetary damage was almost $100 billion.

As furious as the whirling tropical cyclones are, they are guided by gentle winds to move around the giant subtropical highs that envelop them. Eventually, they make landfall and/or move to higher latitudes, often merging with or transforming into extratropical cyclones, where they do further damage.

These storms, which on the ground can be so devastating and leave behind scenes of almost unimaginable destruction, appear as wondrous, aesthetic objects when viewed from the air or from space. For example, the beautiful satellite image of 03 Sept 2010 (Fig. 5-24) shows four distinct cloud systems and their relative sizes. Hurricane Earl, centered over the warm Gulf Stream waters east of Virginia, was moving up the coast. It appeared in the pincers of the fronts of a larger extratropical cyclone centered in Ontario. A cumulonimbus whose anvil was larger than Lake Okeechobee covered SE Florida, showing how much smaller thunderstorms are than cyclones. Far to the west, an extensive blanket of low stratus and fog covered the Pacific Ocean west of California and pressed against the Coast Range.

Tropical cyclones are so destructive that it is essential for forecasting purposes to obtain the most accurate data about their precise location, movement, and strength. This is done by flying into and through the heart of even the most violent hurricanes with instrumented airplanes. What these adventurers see may be the most awesome of the atmosphere's sights – the eye of the hurricane (Fig. 5-1 and Fig. 5-25).

To enter the eye, the plane must penetrate the storm's most violent weather, the eyewall There it can be subjected to accelerations up to 6 g's with zero visibility in gushing rain or ice pellets.

The panoramic view inside the eye is called the stadium effect because it resembles the inside of a giant stadium**, only some 300 times higher and wider than the Colosseum in Rome**. When the eye is open, usually as the storm approaches maximum intensity, the sky overhead is deep blue. A circular wall of cloud rings, much like tiers in a stadium, extends from near the roiled sea surface to a height of 15 km. Inside the eye shortly above the sea surface cloud vortices whirl (Fig. 5-1). All these features be seen flying inside the eye of Hurricane Katrina (Fig. 5-25), except that the photo, magnificent as it is, conveys little idea of the scene's immensity.

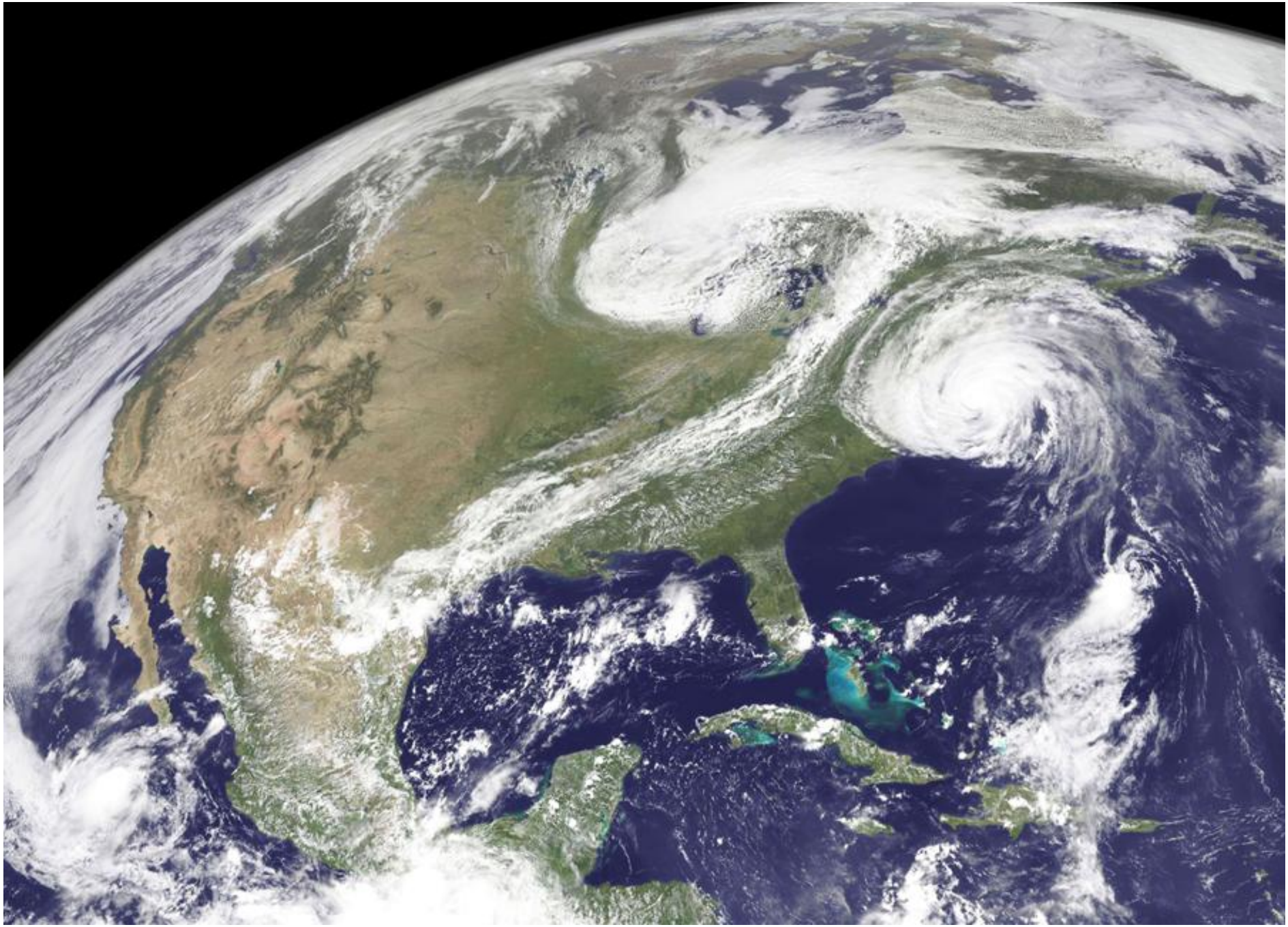

Fig. 5-23. Hurricane Earl in the warm sector of an extratropical cyclone. An extensive field of stratus and stratocumulus clouds cover the ocean west of California, 03 Sep 2010. Popcorn cumulonimbus and dots of cumulus cover Florida, Cuba, and the Yucatan Peninsula. NOAA GOES image.

Fig. 5-25. Hurricane Katrina Eyewall with cloud bands inside the eye. NOAA Photo Library Fly 00449 28 Aug 2005.

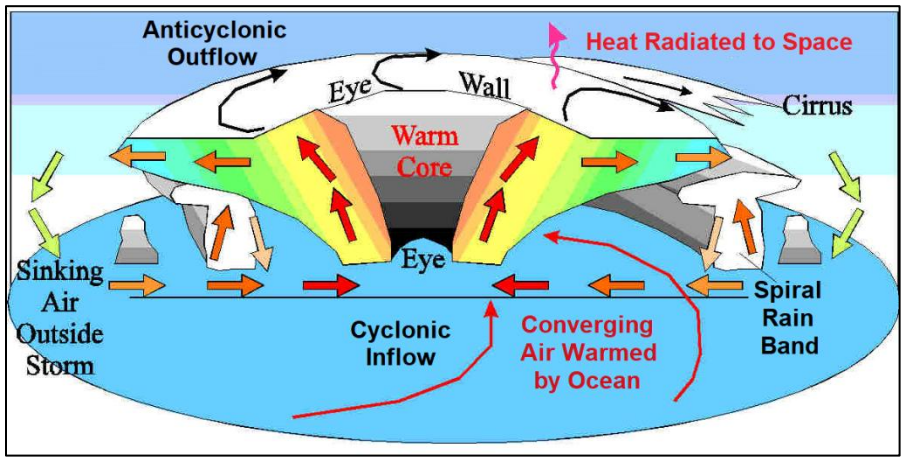

Fig. 5-26. Major structural features of tropical cyclones. SDG.

Tropical cyclones can only form and exist some distance from the equator because to spiral, the winds require that the Coriolis force have a horizontal component, which is zero at the equator. The spiraling winds and clouds organize into a pattern whose features are illustrated and named in Fig. 5-26 and bear an almost uncanny resemblance to the features of spiral galaxies. The eye, which ranges from 10 to 100 km wide, a crude analog to the galaxy's central black hole, marks the low-pressure center. Moving out from the eye, the eyewall forms the inner edge of the central dense overcast, the region with the storm's fastest winds and heaviest precipitation. That corresponds to the dense central bulge of spiral galaxies, a region packed with old stars. Extending out to the periphery of the storm, spiral bands of cumulonimbus clouds with gusty winds alternate with quieter regions of partly cloudy skies. Like the spiral arms of galaxies, which are wavelike regions where mass converges to favor new star formation, the hurricane's spiral bands are wavelike regions where surface winds converge and rise to favor thunderstorm formation. Thunderstorms in the spiral bands (especially over the land) may spout tornadoes since they are immersed in the hurricane's rotating environment.

The hurricane can be considered a thermodynamic heat engine that generates the kinetic energy of winds. Air at the surface spirals in toward the low-pressure center spinning ever faster until it spins so fast it cannot approach the center any closer. Hence the eye! As the converging air approaches that point, it turns up and rises in the central dense overcast. The hurricane has two main heat sources. The first is contact with the warm sea surface that keeps the converging air at an almost constant temperature despite the pressure decrease that would normally cool it by about 5 to 10°C.

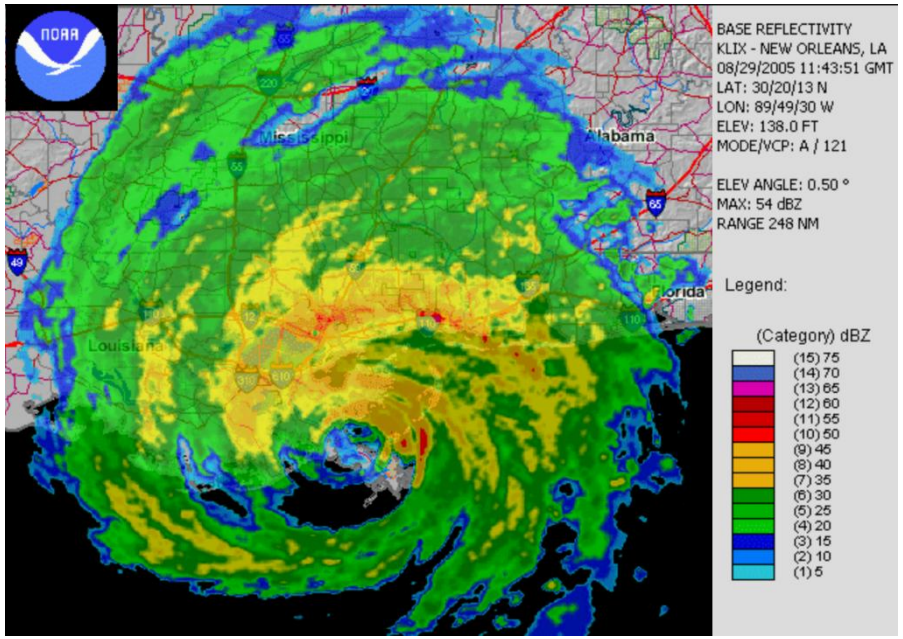

Fig. 5-27. Radar image of Hurricane Katrina at landfall on 29 Aug 2005, showing the eye and the banded nature of precipitation. NOAA.

Condensation in the rising air of the central dense overcast releases enormous quantities of latent heat into the air, ensuring that the hurricane is a warm-core storm, and that it is a high-pressure area at its top. Therefore, as the rising air in the central dense overcast approaches the stratosphere it is forced to turn outward. The air spins slower as it diverges, until beyond a certain distance the direction of spinning reverses and the air continues diverging anticyclonically (clockwise in the Northern Hemisphere). At the leading outer edge of the overcast the clouds may thin to beautiful bands of cirrus, especially as the storm is intensifying. The contrast between the cyclonic rotation of the converging air near the surface and the anticyclonic rotation of

the diverging air and cirrus clouds aloft is displayed in magnificent fashion in animations of satellite images.

Radar images, such as that of Hurricane Katrina at 1200 UTC on 29 Aug 2005, the time it made landfall (Fig. 5-27), shows the partly rainy eye, surrounded by the eyewall and rainbands (which were first discovered by radar). Such images reveal the intensity of rainfall and the detailed structure of rainbands throughout the storm. These features are masked in satellite images by the almost uniform white cloud cover of the central dense overcast.

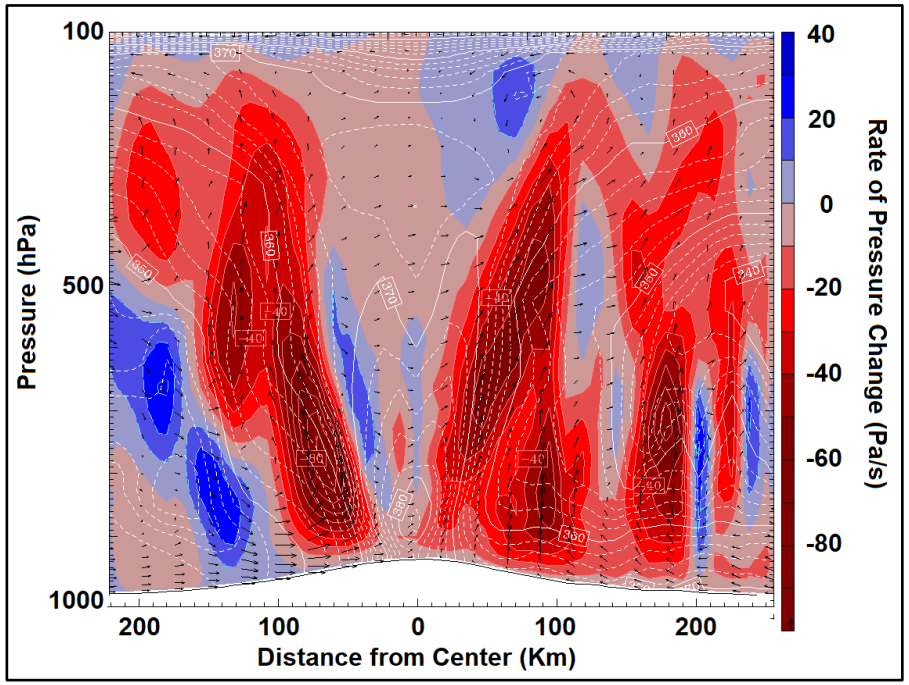

Fig. 5-28. Cross section view of vertical velocity (as rate of pressure change) for Hurricane Katrina prior to landfall. NOAA WRF Model.

An EW cross section or panoramic profile of Katrina, produced by the WRF hurricane model (Fig. 5-28), shows the calculated ascent rate (color contoured and expressed as a rate of pressure change) and the equivalent potential temperature (dashed white lines), a measure of the air's total heat content. Zones of rapidly rising air (deep red) of the eyewall surround the eye, tilting upward and outward, while a rainband of rising air appears about 180 km east of the storm center.

Morning (Fig. 5-29) and afternoon (Fig. 5-30) satellite images show Dorian, the most intense hurricane ever to strike the Bahamas, at its maximum intensity on 01 Sep 2019, Maximum sustained surface wind speed was 295 km/h. Minimum pressure, 910 mb was 10% below mean sea level pressure, and more like pressure 1 km above sea level!

Both images show the open eye spreading to a diameter about 50 km at the top (the size of Lake Okeechobee). The eyewall clouds were steep enough, given the low Sun to produce shadows on the eastern side of the eyewall angle at 1300 UTC and on the western side of the eyewall at 2200 UTC.

In each image, Dorian's eye was surrounded by a wide, solid white ring of clouds of the central dense overcast. Here, the cirrus tops masked hints of structure, but in some storms, bands and even waves can be seen. Spiral bands extended from the central dense overcast to the storm's edge. Cumulonimbus clouds with nipple tops emerged from the cover of fuzzy cirrus to give some hint of the structure below. In the afternoon image, distinct streamers of cirrus, fanned out in the radial direction, to indicate efficient venting, a characteristic during intensification. Near the surface, open convection cells (see §12.3), bounded by rings of cumulus clouds, covered the warm Gulf Stream waters north of Dorian and were blown over the Florida peninsula by Dorian's easterly winds.

The main difference between the morning and afternoon images was the intensity and location of convection. At 1300 UTC, a broad line of cumulonimbus clouds covered the warms waters just south of Cuba though the anvils spread over the otherwise mostly clear land. The skies over the Florida peninsula and a band of waters to the west were also mostly clear. By 2200 UTC, popcorn thunderstorms covered the heated land of Cuba but were restricted to only the west side of Florida's peninsula, because of the combined action of the sea breeze and the easterly winds on Dorian's northern fringe.

Fig. 5-29. Hurricane Dorian at 1300 UTC, 01 Sep 2019. NOAA Photo Library.

Fig. 5-30. Hurricane Dorian at 2200 UTC, 01 Sep 2019. NOAA Photo Library.

5.7 Extratropical Cyclones = Winter Lows

So long as tropical cyclones remain in the tropics, they are reasonably symmetric storms with warm cores embedded in uniformly warm environments. But when they move out of the tropics, they are likely to encounter cold air. When they do, they entrain the cold air on their poleward and western sides. In that process they become asymmetrical and increasingly take on the characteristics of extratropical cyclones.

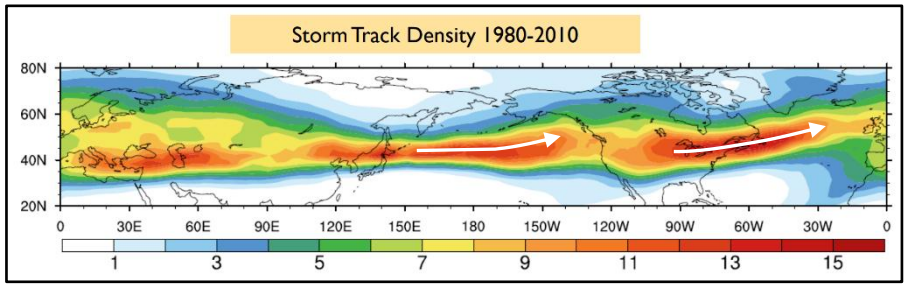

Fig. 5-31. Extratropical cyclone track density in the Northern Hemisphere from Dec through Feb of the winters 1980-2010. Cyclone locations are further north from Jun through Aug. ©Katherine Lukens.

Extratropical cyclones, often called winter storms, are large, asymmetric storms between about 500 and 2000 km in diameter that form on the border of tropical and polar air (Fig. 5-31) and derive much of their energy as the cold, polar air sinks and the warm, tropical air rises over it. The storms move generally from west to east with a component towards the Poles at variable speeds averaging roughly 40 km/h. The structure and typical weather sequence, which typically lasts for about a day, are described on the next pages.

Extratropical cyclones are not only larger, but far more numerous than tropical cyclones, so that almost any point in the mid latitudes will be at least touched by some part of one about once a week. Extratropical cyclones, in association with thunderstorms they help generate, provide the middle latitude belt with most, if not all, of its precipitation in the winter half of the year. Though their precipitation intensity and winds (except in supercell thunderstorms) are much lower on average than in tropical cyclones, there are monster extratropical cyclones that are a match for hurricanes.

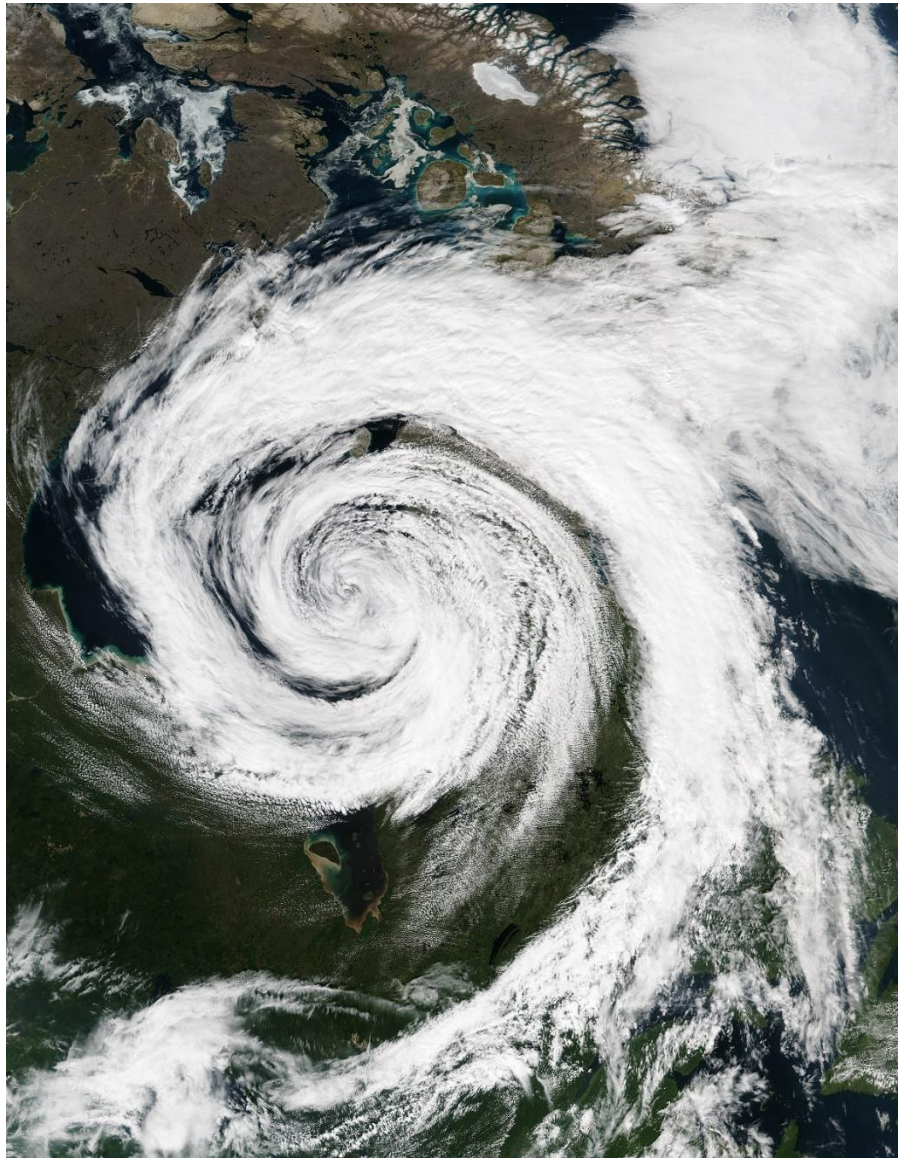

Fig. 5-32. The spiral cloud pattern of a dissipating extratropical cyclone centered over Hudson Bay, Canada on 10 Aug 2016. NASA VIIRS image.

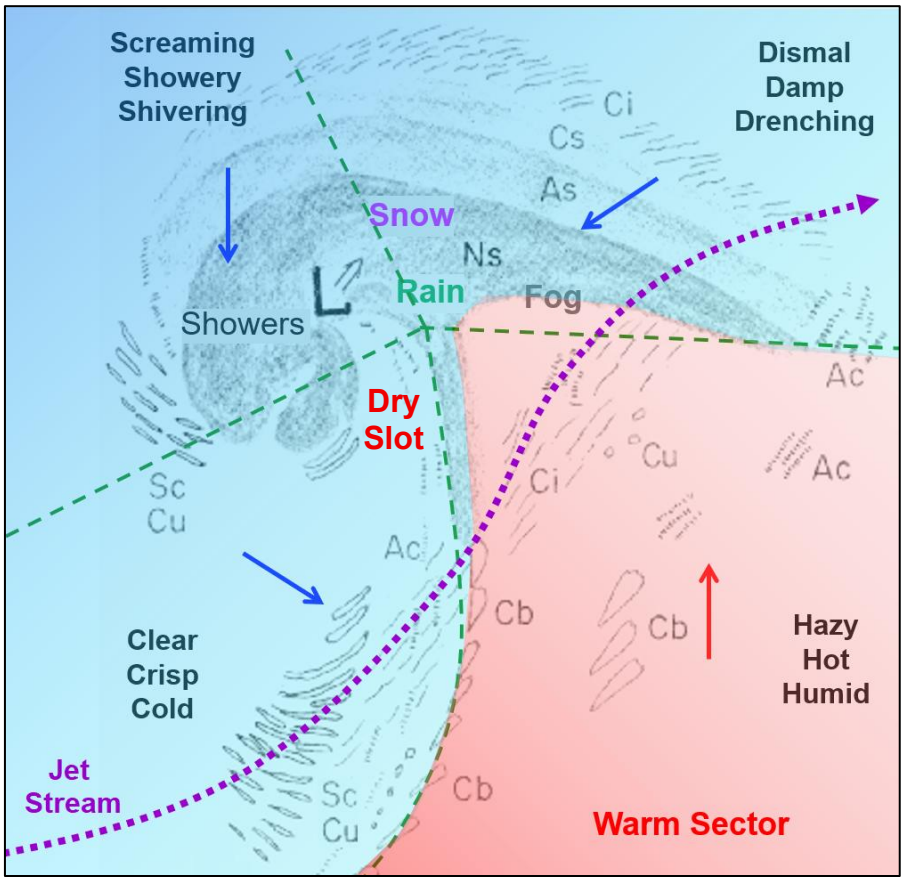

Fig. 5-33. Floor plan of clouds, wind, and weather sectors for a mature extratropical cyclone. Double arrow shows this storm moves to the NE.SDG.

Blizzards are extratropical cyclones with wind speeds faster than about 56 km/h and prolonged driving snow. They typically produce 10 to 40 cm of snow but have produced snow totals that greatly exceed 1 m and raised drifts over 5 m high. Sometimes, a short distance from where blizzard conditions are raging, the same cyclone produces ice pellets (sleet) and freezing rain. Freezing rain is rain that freezes on contact. It can crack tree limbs, down trees and exposed power lines, and cover the ground with a layer of almost frictionless black ice that brings everything to a complete standstill. The coating of ice often gleams brilliantly in the sunshine after the storm has passed. What irony! And further equatorward, the same extratropical cyclone can spawn supercell thunderstorms with large hail and tornadoes!

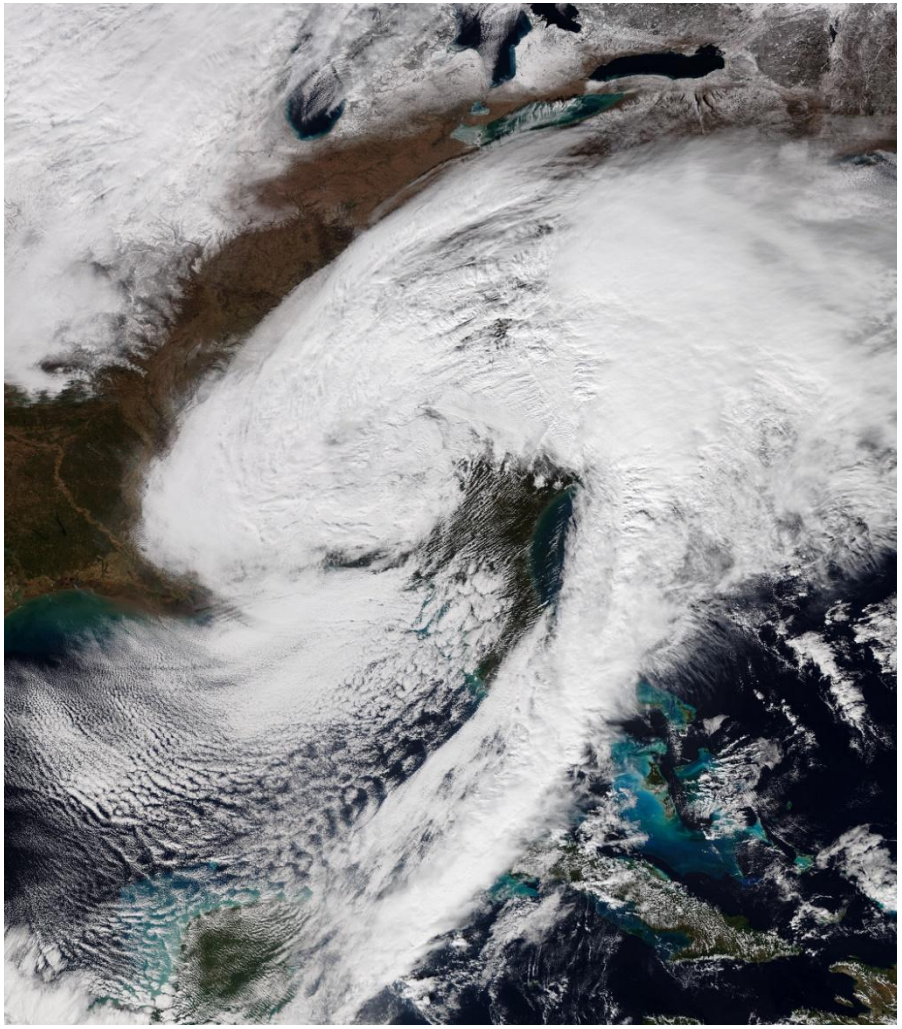

Fig. 5-34. Winter Storm Izzy, 16 Jan 2022. The snow-covered ground around the Great Lakes and forested Adirondack Mountains at upper right are from previous storms. NOAA VIIRS.

Extratropical cyclones form in conjunction with and directly under the polar jet stream, which cooperates to drive or steer the cyclones from west to east. The polar jet stream is the wavy band of the fastest mostly west to east winds near the top of the troposphere that girdles the globe in the middle latitudes of each hemisphere where the poleward temperature gradient is largest. It is a direct product of that temperature

gradient due to a curious consequence of Earth's rotation and the Coriolis force called the thermal wind such that,

> The west wind increases with height at a rate proportional to the gradient of poleward temperature decrease.

As air swirls around an extratropical cyclone, polar air on its western side sweeps equatorward, advancing on the tropical air and, being denser, undercuts it and wedges it aloft at the boundary called a cold front. At the same time, on the storm's eastern side, tropical air advances on the retreating polar air, and being lighter, rides over it at the warm front. All this occurs as the storm continues rotating, winding the cloud pattern in an ever-tightening spiral, as in Fig. 5-32 before all the tropical air has either moved aloft or mixed with the polar air, and the entire system ultimately dissipates.

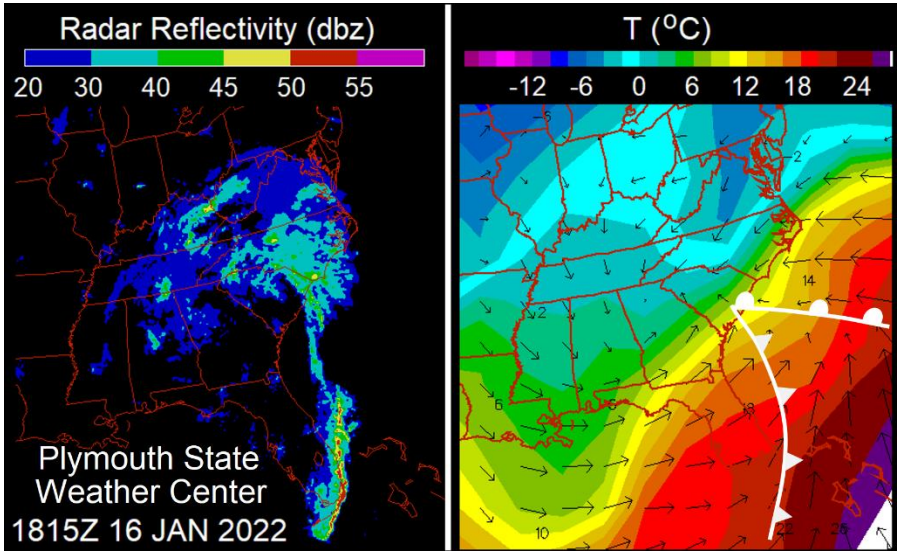

Fig. 5-35. Radar summary chart (left) and (right) surface weather map with wind arrows, fronts, and temperature for Winter Storm Izzy, 1800 UTC, 16 Jan 2022, modified from Plymouth State Weather Center charts.

The classic, mature extratropical cyclone averages about 1000 km in diameter and extends from the ground to the base of the stratosphere. As air spirals toward the storm center, the tropical and polar air masses are brought into ever closer contact, forming distinct fronts. The storm's floorplan map (Fig. 5-33), closely matched by the satellite image of Winter Storm, Izzy on 16 Jan 2022 (Fig. 5-34) shows its classical pattern of clouds and weather.

The radar and weather charts (Fig. 5-35) of Winter Storm Izzy at 18 UTC, 16 Jan 2022 also closely match the features drawn in the classical floor plan (Fig. 5-33). The entire pattern bears resemblance to the human brain (the main cloud mass) and comma-cloud spinal column (the cold front).

Izzy's comma-shaped cold front, with a line of largely hidden, embedded thunderstorms over Florida, advanced to the south and east. In its wake, long parallel streets of stunted cumulus clouds formed as the polar air poured over the warm waters of the Gulf of Mexico, and was charged with water vapor and heated enough to become buoyant. The broad cloud mass that covers the cold, wet and the showery sectors contained a wide area of snow and rain north of the warm front and the storm center. The poleward edge of the stratiform cloud shield was covered by cirrus and cirrostratus clouds. Finally, a dry slot of sinking, warm air injected itself into the showery sector, just west of the storm center

Two small but telling features appear outside the poleward fringe of Izzy's cloud shield. 1: Cumulus streets appear over the open waters of Lake Erie, as tracers of the frigid north wind and, 2: The Adirondack Mountains near the NE corner of the image appear as a relatively dark region surrounded by white, snow-covered fields. This is a frequent sight in satellite images of the Adirondack region during winter and is due to the largely forested nature of the Adirondack Park that covers the white ground.

The extratropical cyclone's floor plan of Fig. 5-33 divides the storm into four quadrants or sectors, with fronts acting as two of the boundaries. The storm's vertical motions and relation to the fronts are shown in Fig. 4-24, with at least one caveat (already mentioned) that the slope of the warm frontal surface and associated ascent rate of the air is too large and its width too narrow (each by a factor of about 50).

Each sector is filled by a giant conveyer belt of moving air. The cold, dry sector, located SW of the low-pressure center is filled by the polar conveyer belt from the northwest. It sinks as it wraps around the western side of the low to produce mostly crystalline skies, of clear, crisp, cold weather, though streets of cumulus or stratocumulus clouds can form if daytime heating is sufficient or when the polar air pours out over the ocean. And, with the jet stream overhead near the cold front, mid and high clouds, which may be especially beautiful in this sector, are possible.

The warm sector, located SE of the low-pressure center and which extends into the tropics, is filled by a warm conveyer belt of tropical air. Weather of the warm sector tends to be hazy, hot, and humid. Mostly clear skies prevail, though mid- and high-level clouds are possible, and afternoon thunderstorms can develop from cumulus clouds, especially during spring and summer. Lines of possibly severe thunderstorms, with large hail and tornadoes, can develop near the western boundary of the warm sector, where the advancing cold front gives an extra upward shove to warm, unstable air.

The cold, wet sector, located north and east of the storm center, contains two conveyer belts, separated by the warm frontal surface that slopes upward towards the Poles. Below the frontal surface a conveyer belt of polar air slithers in from the NE. Above the frontal surface, the conveyer belt of tropical air from the warm sector ascends the dome of cold air, turning east as it does so to ultimately join the jet stream. The tropical air ascends at a gentle slope of about 1/100, spreading layer clouds that grade from nimbostratus near the surface warm front, with stratiform precipitation, to altostratus to cirrostratus across an area several hundred km wide, and finally thinning out to cirrus at the NE edge of the storm (**Ns→As→Cs→Ci**). The weather of this sector might well be termed dismal, damp, and drenching. It is where the majority of the prolonged rain, snow, and freezing precipitation occur.

In the showery and shivering sector north and west of the center of mature extratropical cyclones, the cold conveyer belt, previously soaked by the precipitation falling through it, final emerges and joins with the polar conveyer belt from the NW. The resulting weather is varied, but most often, especially in winter, can be described as screaming, showery, and shivering. Yet despite its threatening appearance, its intense showers tend to be brief and it is a region of generally lifting and clearing skies as the storm moves off to the east. And, as intense storms wrap up, a dry slot of clear skies whose air was warmed by sinking from jet stream levels, can protrude poleward into the cold air like a long tongue just west of the storm center.

The storm's typical eastward motion transforms the classical ***pattern*** of clouds and weather to a classical ***sequence*** in time (in the reverse order, namely, **Ci→Cs→As→Ns**) for any fixed location. Thus, the classical sequence of clouds and weather as storms approach from the SW begins with cirrus (now often preceded by jet contrails), followed in order by cirrostratus (often with a halo), altostratus (with a 'milky' Sun), and nimbostratus (often starting as snow, perhaps with a period of sleet and freezing rain, followed by rain). The halo has been recognized for millennia as a classical warning sign of an approaching winter storm (and hurricane), memorialized in poems such as Henry Wadsworth Longfellow's ***Wreck of the Hesperus***, and often appearing as a ring around the Sun or Moon some 6-24 hours before precipitation begins.

Extratropical cyclones are usually not soloists. They often form as the wave crests on a cyclone wave train, below waves in the jet stream. The connections are most distinct over the oceans where they are not masked and interrupted by mountains. For example, on 09 Nov 2024 Winter Storm Anya (Fig. 5-36), which had dumped snow in the Rocky Mountains and sported a pronounced dry slot over the Central Great Plains and a gossamer veneer of sentinel cirrus over the western Great Lakes, was attached by a long umbilical like cold front from the coast of Georgia to a cyclone far out over the Atlantic Ocean. Behind that cold front cold, dry air poured from the Eastern seaboard over the Atlantic Ocean, producing cumulus cloud streets and open convection cells. In the warm sector, which extended into the tropics, cumulus clouds were dotted over all the land bordering the Gulf of Mexico and the Caribbean as well as over Cuba and Florida. At the same time, purely by chance (?) the remnants of Hurricane Rafael, swirling to its demise in the Gulf of Mexico, just happened to join the party.

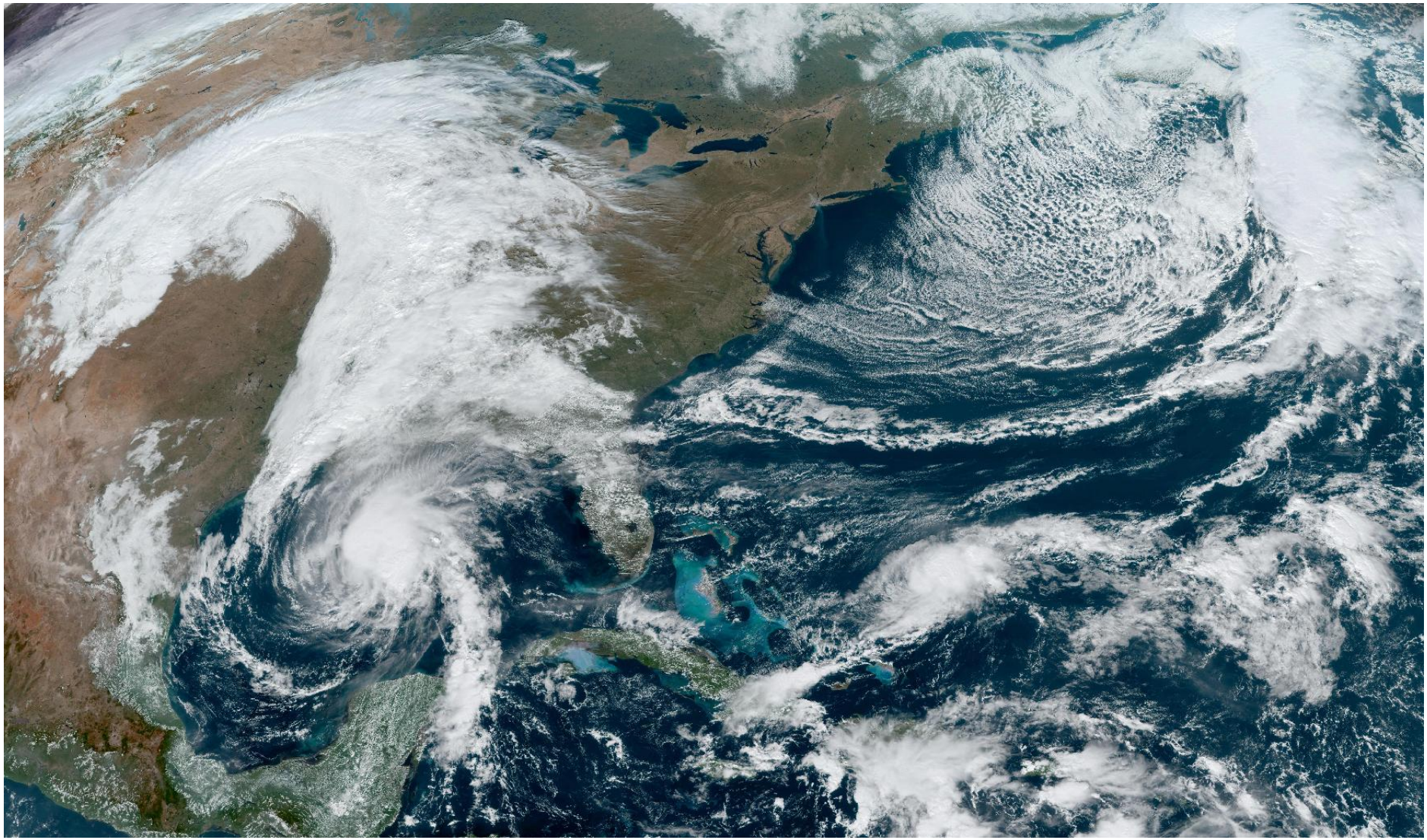

Fig. 5-36. Winter Storm, Anya over Kansas at 1800 UTC on 09 Nov 2024, connected by a cold front to a cyclone over the Atlantic Ocean, with the remnants of Hurricane Rafael over the Gulf of Mexico. NOAA VIIRS image.

With this brief overview of the world's cloud and storm systems it is time to return to terra firma and look more closely at clouds and the optical phenomena they host. We begin in Chapters 6 and 7 with closeup views of this Chapter's cumulus cloud dots and popcorn or cotton ball cumulonimbus

5.8 Gallery

But before returning to terra firma, take a few moments longer to marvel at a sample of the wondrous variety of clouds viewed from above.

Fig. 5-37. Flying above a field of cumulus and below cirrus over the red earth south of La Mancha, Spain 22 Aug 2007. SDG.

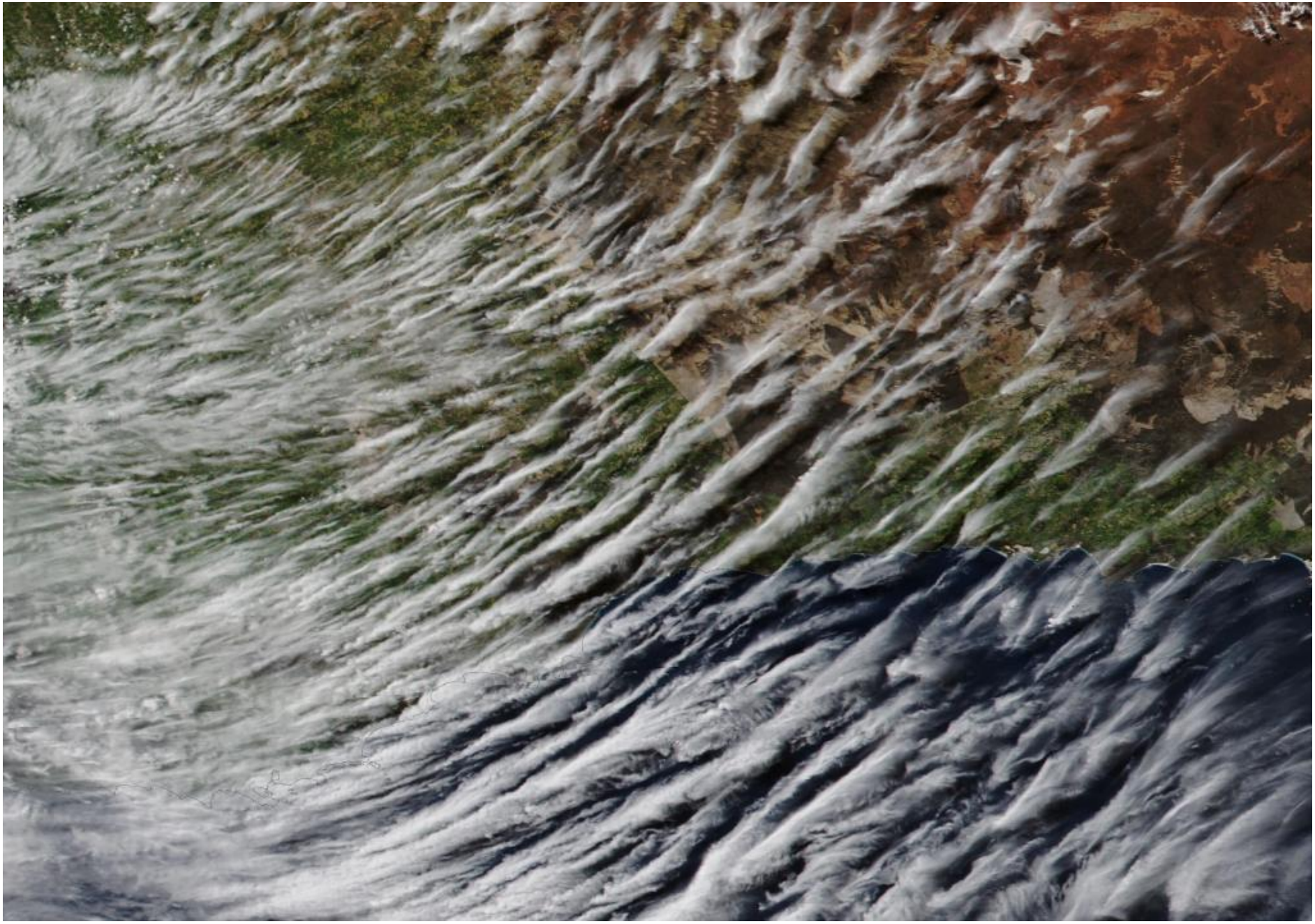

Fig. 5-38. Cirrus invasion over SW Australia, 09 Sep 2020. NASA MODIS.

Fig. 5-39. Anvil-topped cumulonimbus with overshooting domes, 31 Jul 2016. NASA Photo ID: ISS048-E-046902.

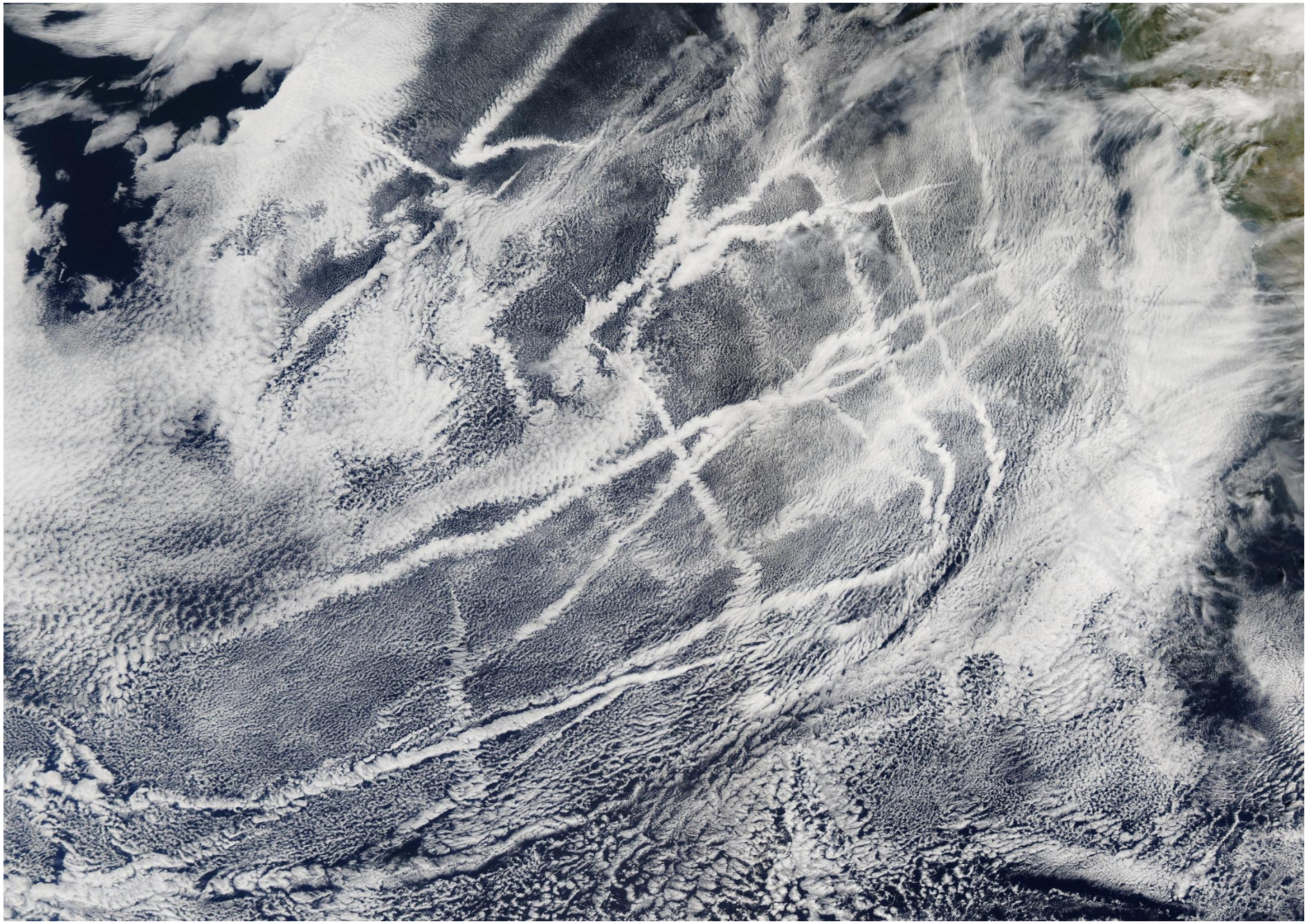

Fig. 5-40. Ship tracks embedded in stratocumulus cloud field west of California, 21 Feb 2012. NASA MODIS Aqua Image.

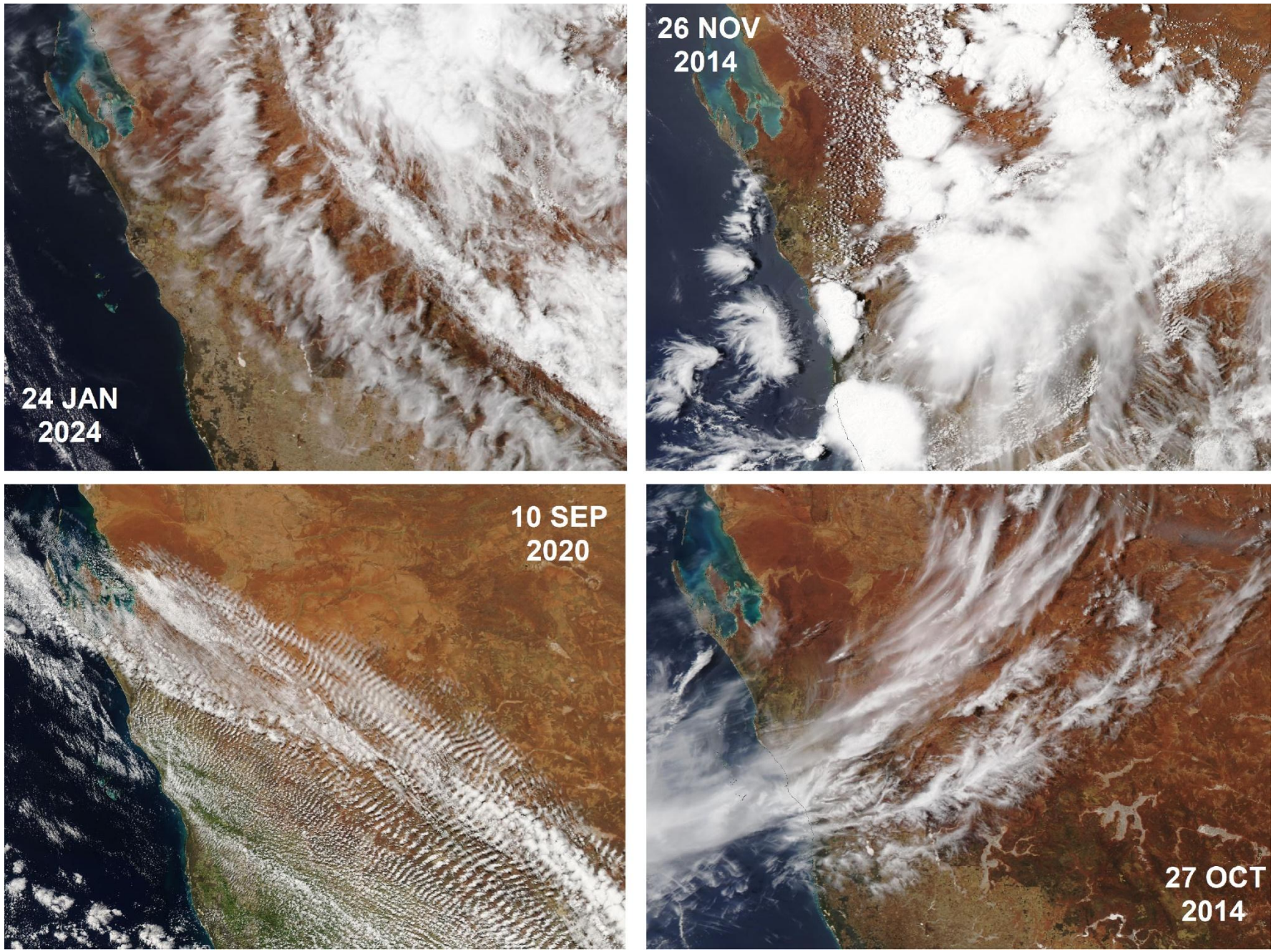

Fig. 5-41. Cloud festivals over Western Australia. Clockwise from top left, 1: Cyclone with cirrus bands, 2: Cumulus, cumulonimbus, and cirrus outflow, 3: Cirrus and, 4: Stratocumulus undulatus. NASA MODIS Images.

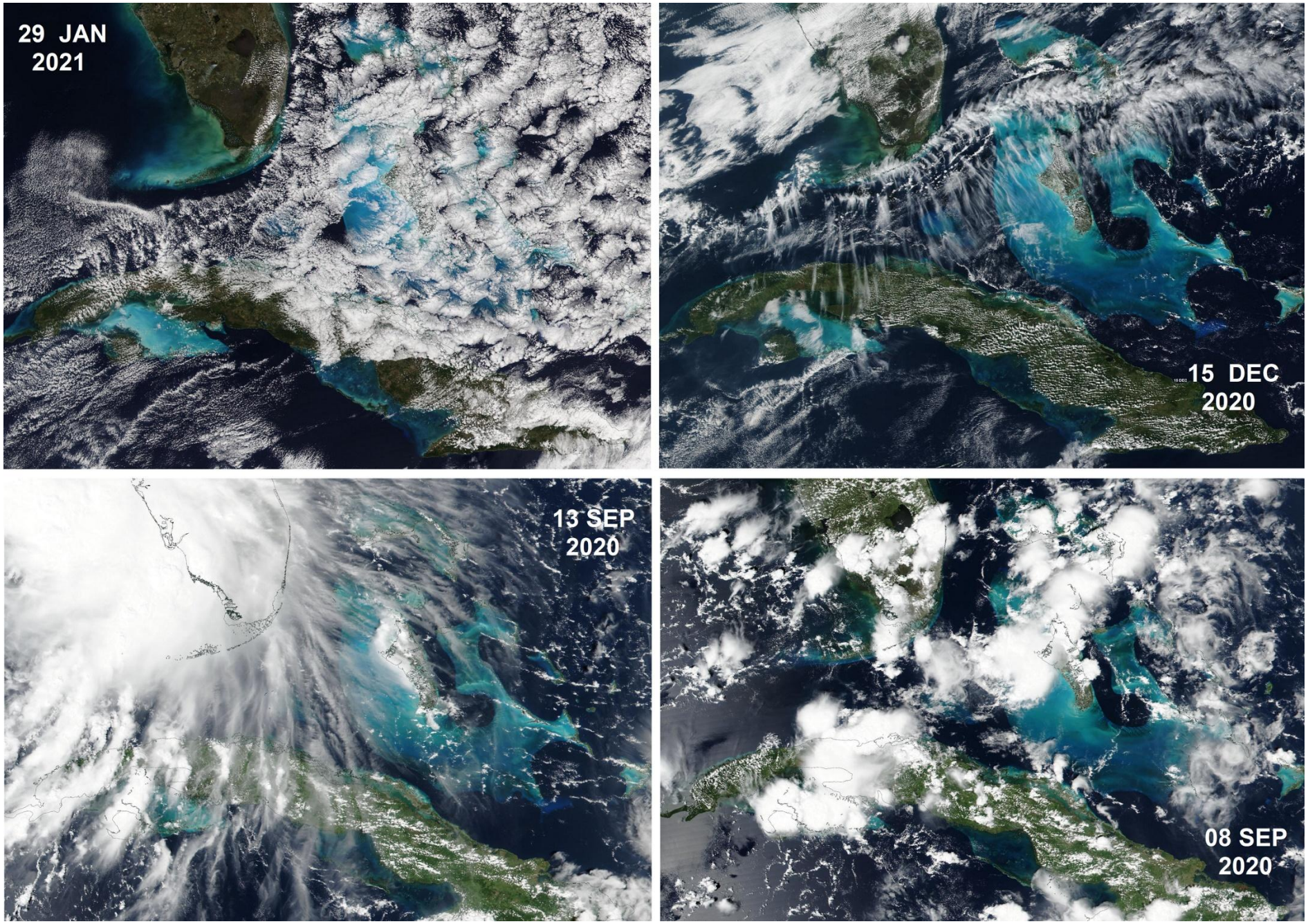

Fig. 5-42. Cloud festivals over Florida, the Bahamas, and Cuba. Clockwise from top left, 1: Closed-cell stratocumulus, 2: Serpentine line of cirrus vertebratus SE of Florida, stratus and fog west and over Florida plus cumulus dots over Cuba, 3: Cumulonimbus and, 4: Cirrus outflow from Hurricane Sally. NASA MODIS Images.

Wonders of the Atmosphere
Chapter 6: Penetrative Clouds and Their Motions

Fig. 6-1. A field of cumulus humilis over City College of New York, 15 Sep 2008, about six hours after a cold front passed. SDG.

Fig. 6-2. Explosive towering cumulus congestus, with flat base and small pileus cap over Cheyenne, WY, 07 Jul 2019. JC.

Wonders of the Atmosphere
Chapter 6: Penetrative Clouds and Their Motions

6.1 Cumulus: The Nature of Penetrative Clouds

"Ice cream castles in the air." Joni Mitchell.

Cumulus clouds are buoyant blobs of rising hot air made visible by droplets. They are the clouds drawn by almost every child, and adult.

At dawn the sky is clear. As the rising Sun heats the ground, which heats the air above it, great numbers of classic fair weather *cumulus humilis* clouds arise, (Fig. 6-1). By mid-afternoon most of these have disappeared but a few have grown to towering cumulus *congestus*, with classic cauliflower tops everyone notices and flat bases few people notice (Fig. 6-2). These have won the battle of Survival of the Fittest. After a few more hours of afternoon heating, one or two of the growing cumulus congestus may have swelled to gargantuan size with tops that spread out into enormous anvils as the monarchs of all clouds, the cumulonimbus or thundercloud (§6.3, Chapter 7).

Cumulus clouds are mainly daytime clouds that tend to congregate over heated places such as hills, dark or paved surfaces, forest fires, and where polar air behind cold fronts pours over warm waters. They are least likely over cool landscape features such as valleys, lakes, rivers, snow-covered ground, or the Polar Ice Caps.

Stratocumulus, cumulus, and cumulonimbus are penetrative clouds. Their hot, buoyant blobs (*thermals*) or fountain-like plumes puncture and rise through the quiescent surrounding (*ambient*) atmosphere. On occasion, they may penetrate other clouds. The towering cumulus congestus *velum* over Fairfield Lake, NC (Fig. 6-3) punctured a pre-existing smooth altocumulus cloud veil.

Fig. 6-3. A towering cumulus (with a tiny pileus cap) penetrates a veil of altocumulus to form a cumulus velum, Sapphire, NC, 30 Aug 2022. SDG.

Thermals are invisible (if not smoke filled, as in Fig. 4-15) until they reach the *lifting condensation level* or ***LCL***. That is where droplets begin to condense and the flat base of a penetrative cloud forms. The cloud then extends as high as the thermals rise.

6.2 Changes of T and T_d in Rising and Sinking Air: Soundings and Stability

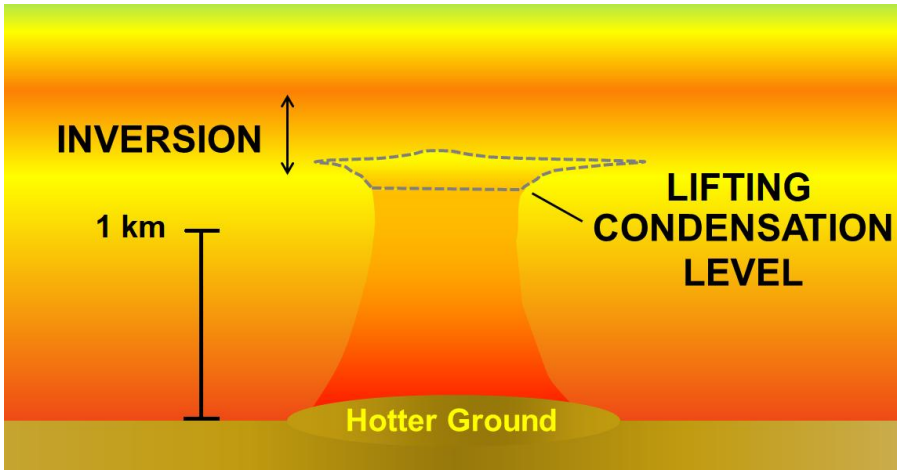

Fig. 6-4. Pancakes of stratocumulus (in dotted outline) are all that can form when an inversion occurs just above the lifting condensation level, *LCL*. SDG.

Thermals rise buoyantly so long as they are warmer and less dense than the quiescent ambient atmosphere. Once they penetrate warmer surroundings, such as when they encounter temperature inversions (where ambient temperature ***in***creases with height) they lose their buoyancy. From that point they decelerate, reaching some maximum height, like fountains do, and then sink back to the equilibrium level where they have the same density as the ambient atmosphere.

If thermals enter warmer surroundings just above the *LCL*, as in Fig. 6-4, the resulting clouds will be vertically stunted stratocumulus, and may resemble pancakes. If, however, the rising thermals remain warmer than the ambient atmosphere from the *LCL* all the way up to the base of the stratosphere, as in Fig. 6-5, the resulting clouds will be towering cumulonimbus, often with fountain-like, overshooting domes that spread into wide anvils.

There is one complication. The temperature, ***T***, and dew point, $\boldsymbol{T}_d$, of rising air decrease at rates set by physical processes (recall §4.3). Thus, to determine whether a rising thermal is warmer than the ambient air at any height, and therefore how high a cloud will rise, requires comparing the ambient temperature of the particular *situation*, to the temperature determined by set physical *processes*.

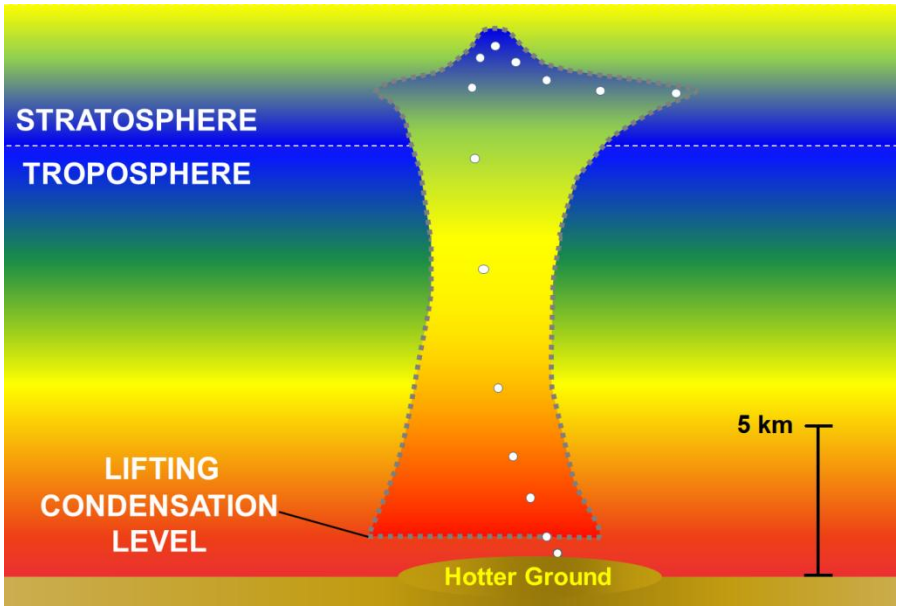

Fig. 6-5. Cumulonimbus with overshooting tops can penetrate the stratosphere when the atmosphere is unstable (lifted thermal *T* warmer than ambient *T*) through the troposphere above the *LCL*. SDG.

Soundings of situations where penetrative clouds develop provide *direct* information only about the vertical profiles of ***T***, $\boldsymbol{T}_d$, and wind in the ambient atmosphere. Information inside penetrative clouds must be inferred by adding process lines that depict the physical processes of changes of ***T*** and $\boldsymbol{T}_d$ in rising or sinking air.

What are the processes that make ***T*** and $\boldsymbol{T}_d$ change when air rises or sinks? When air rises it expands as pressure decreases, doing work that decreases ***T*** and $\boldsymbol{T}_d$ with no loss of heat – *adiabatically*. Adiabatic cooling also occurs when air escapes from a pressurized tire or tank or when a person blows air out under pressure. The temperature drop can be understood on the level of molecules. When a molecule inside a pump strikes a piston it pushes the piston out so the molecule rebounds more slowly. **Temperature, a measure of the kinetic energy of the molecules, decreases as molecules slow.** If vapor molecules slow enough, they will clump together (i. e., condense as droplets or crystalize as ice).

So long as rising air remains unsaturated (i. e., $T > T_d$), no condensation occurs and both T and T_d cool at their respective constant, *dry adiabatic cooling or lapse rates* (recall Chapter 4),

T decreases ≈ 9.8°C/km
T_d decreases ≈ 1.8°C/km

Once T cools to T_d the air becomes saturated. If the saturated air continues rising and cooling, excess vapor condenses. $T = T_d$ and both cool together at the *Saturated (or Moist) Adiabatic Lapse Rate*, which is slower for T than the dry adiabatic lapse rate because condensation releases latent heat into the air.

Every gram of vapor that condenses in 1 kilogram (kg) of air warms the air by 2.5°C.

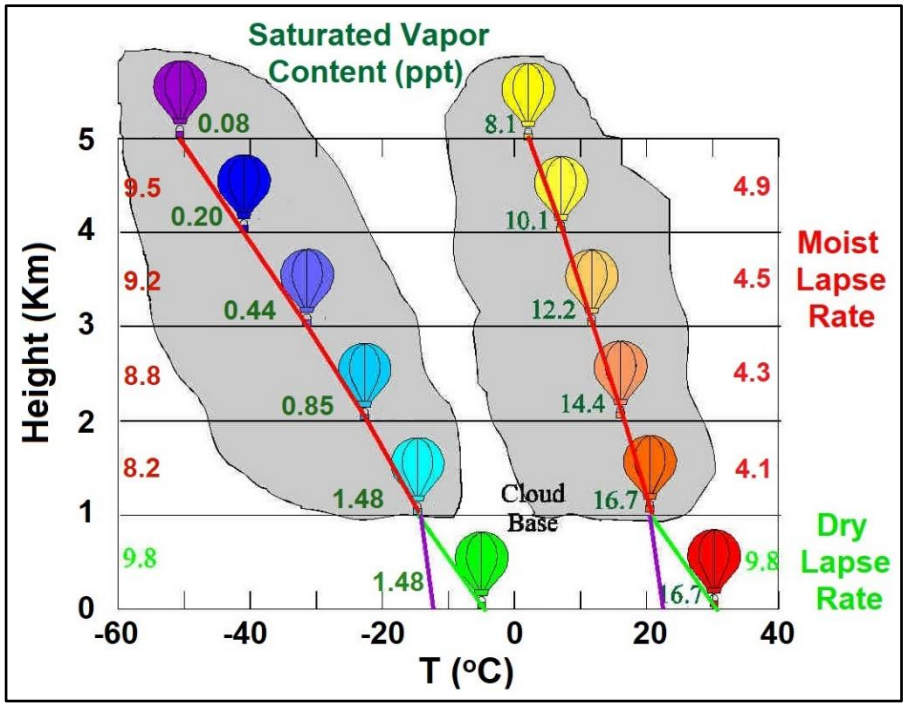

Fig. 6-6. Dry (green line) and Moist (red line) Adiabatic lapse rates and vapor content (T_d, purple line) for warm and cold rising thermals. SDG.

The added latent heat of condensation partly offsets the cooling due to expansion. Unlike the *dry* adiabatic lapse rate, which is a constant, the *saturated* or *moist* adiabatic lapse rate varies with temperature. The warmer saturated air is, the larger its vapor content and capacity and the larger the rate of condensation. This is shown for two rising air parcels in Fig. 6-6, and calculated in Table 6-1 from 1 to 2 km.

Both rising air parcels start at sea level (0 km). The warm parcel starts at T = 30°C and the cold, at T = -4°C. Both cool at the dry adiabatic rate (9.8°C/km) as they rise to the *LCL* at 1 km, where both become saturated, cloud base forms, and condensation begins. Above 1 km the two parcels differ. The warm parcel starts with much more vapor, so, much more condenses, which adds much more latent heat, reducing the net or moist adiabatic cooling rate more for the warm parcel (4.1°C/km) than for the cold parcel (8.2°C/km).

Sample	Vapor 1 km	Vapor 2 km	Liquid grams	Latent Heating	Dry Lapse Rate	Moist Lapse Rate
Warm	16.7	14.4	16.7-14.4 = 2.3	2.3×2.5 = 5.7°	9.8°	9.8 - 5.7 = **4.1**°
Cold	1.48	0.85	1.48-0.85 = 0.63.	0.63×2.5 = 1.6°	9.8°	9.8 - 1.6 = **8.2**°

Table 6-1. Changes for warm and cold parcels from 1 to 2 km.

As parcels continue rising, less vapor remains and less condenses, so they cool more rapidly, gradually approaching the dry adiabatic rate.

When will a penetrative cloud be produced and how high can it rise? Lift a parcel along its process lines and compare its temperature to that of the ambient air. If the lifted parcel is cooler and denser than the surroundings, it will sink back and oscillate around its original level when released. This situation is statically stable and it will not produce penetrative clouds. If, however, the lifted parcel is warmer than the surroundings, it will be less dense and buoyant (like a hot air balloon) and accelerate upward. This statically unstable situation will produce a penetrative cloud that will rise until it enters warmer surroundings and comes to a halt.

The sounding for Fig. 6-1 (Fig. 6-7) reveals why it has only humble cumulus humilis, and the sounding for Fig. 6-2 (Fig. 6-8) reveals why it has a towering cumulus congestus.

First, note that both soundings have large spreads between the ambient ***T*** (**solid red line**) and T_d (**solid green line**). That indicates that the ambient atmosphere is unsaturated and clear.

Second, compare in each sounding the *relative* positions of the *ambient* ***T*** to the *process* ***T***(cld) (**dashed blue line**) of the lifted parcel for a possible convective cloud. Note that in Fig. 6-7 the *process* ***T***(cld) is colder than the *ambient* ***T*** while in Fig. 6-8 it is warmer through much of the sounding.

What are these process lines?

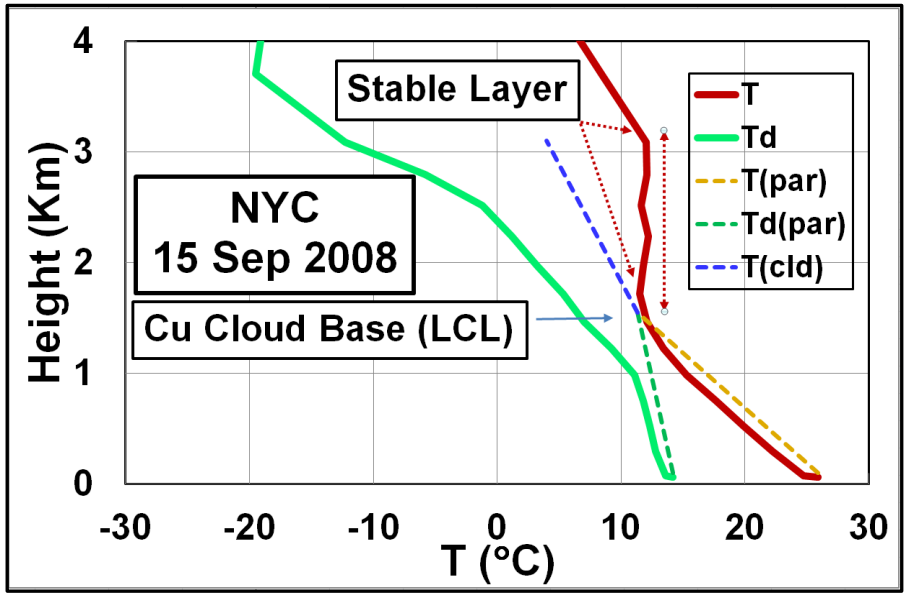

Fig. 6-7. Sounding for cumulus humilis at 1500 UTC 15 Sep 2008 of Fig. 6-1 including the dashed process lines for dry adiabatic lapse rate for *T* (orange dashed line) and T_d (green dashed line) and moist adiabatic lapse rate for *T* and T_d (blue dashed line) above cloud base. SDG.

For unsaturated air below cloud base there are two process lines.

T decreases at the dry adiabatic rate (**dashed orange lines**).
T_d decreases at the rate (**dashed green lines**).

Moving up, the two lines converge to a point. Cloud base occurs at the lifting condensation level, *LCL*, where parcel $T = T_d$.

For saturated air above cloud base there is one process line.

T and T_d cool at the moist adiabatic rate (**dashed blue lines**).

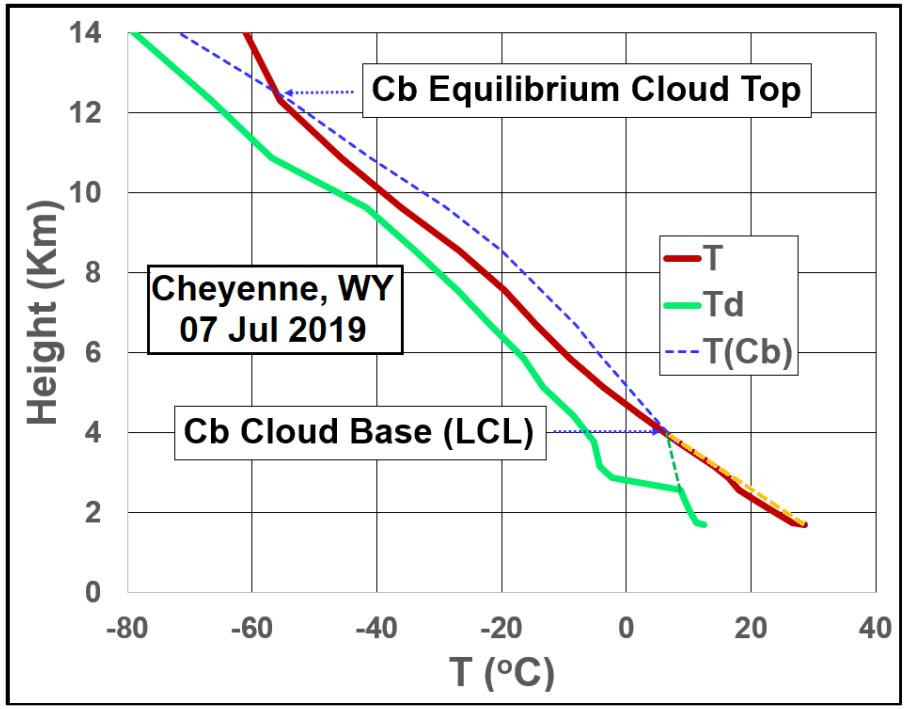

Fig. 6-8. Sounding for towering cumulus at 2100 UTC 07 Jul 2019 of Fig. 6-2 with same process lines as Fig. 6-7. SDG.

In both cases strong solar heating at the ground renders the rising thermals warmer than the ambient atmosphere below the lifting condensation level. Hence the heated thermals are buoyant and rise and the surface boundary layer is unstable. That, however is where the similarity ends.

The difference between the two soundings occurs above cloud base. For the cumulus humilis of Fig. 6-1 and Fig. 6-7, the ambient atmosphere almost immediately above the *LCL* is marked by an inversion from 1.5 km to 3 km, and the rising parcels are cooler than the sounding. They arrive at the *LCL* with some velocity and quickly decelerate so that the clouds can only rise a short distance further.

By contrast, for the cumulus congestus of Fig. 6-2 and Fig. 6-8, the rising parcels remain warmer than the ambient atmosphere up to 12.3 km, above which they are cooler than the ambient air and decelerate.

Now we can begin to understand…

6.3 The Realm of Penetrative Clouds

Fig. 6-9. Pancake stratocumulus above cold waters. SDG.

The realm of penetrative clouds extends from wafer-thin stratocumulus clouds that top out or settle back to just above the condensation level to towering cumulonimbus that puncture the stratosphere. Weak heating and/or a stable, 'repressive' atmospheric regime lead to stratocumulus. Strong heating and an unstable, 'permissive' atmospheric regime lead to cumulonimbus.

Whenever the surface is cold, no penetrative clouds rise from it. This is the case on clear, calm nights, when the ground radiates heat to space and cools the air just above. If cooling is sufficient, fog and low stratus may form, but they will utterly lack buoyancy and hug the ground. For the same reason, penetrative clouds are almost completely absent over the refrigerated Polar Ice Caps.

The cold, upwelled ocean waters on the east side of the Subtropical Highs, and off the west coasts of the continents are only slightly less repressive to penetrative convection. They chill and humidify the air in the lowest kilometer enough to produce extensive sheets of fog, stratus, or stratocumulus clouds bounded by a capping inversion that separates them from much warmer and drier sinking air above.

Fig. 6-10. Pancake stratocumulus over San Mateo, CA, 17 July 2011. SDG.

This can be seen both from the air (Fig. 6-9) and from the surface. The repressed environment of the sky over San Mateo, CA on 17 Jul 2011 served up a flattened layer of stunted, pancake stratocumulus (Fig. 6-10). The clouds were driven inland from the cool Pacific Ocean because the wind around the subtropical North Pacific High had a westerly component.

Wind shear can elongate the cells and orient them in parallel ribbons, as in Fig. 6-11 over the cold Pacific waters west of Oregon on 17 Aug 2017. The clouds in this case were capped by an inversion 800 m above the sea surface.

Fig. 6-11. Aerial view of elongated cells of stratocumulus clouds capped by an inversion at 800 m, 100 km west of the Oregon coast, 1830 17 Aug 2017. SDG.

All soundings for such convectively driven but capped stratocumulus clouds look alike.

The sounding (Fig. 6-12) of the San Mateo case (Fig. 6-10) reveals two distinct air masses separated by a transition zone from 500 m to 1200 m, where the two air masses mixed. Maritime air that had been cooled and humidified by contact with the cold sea surface occupied the lowest 500 m of the atmosphere. The clouds were confined to the thin layer of saturated air between 250 and 500 m in this layer. Above 1200 m, warm air, with very low ***RH***, marked by the large difference between ***T*** and T_d, filled the atmosphere. The extreme dryness of this air indicates that it had sunk from the upper troposphere as it coursed around the North Pacific High. The upper part of the transition zone was marked by a temperature inversion between 800 and 1200 m that no clouds could reach let alone penetrate.

The dashed blue line of moist adiabatic ascent in the sounding of Fig. 6-12 shows why the clouds were so flattened and stunted vertically. If lifted above 500 m cloud air would be colder than the ambient (solid red line). Thus, even if cloud air were thrust upward, for example, forced by the wind to cross over the Coast Range, it would quickly sink back to its equilibrium level on the downwind slope.

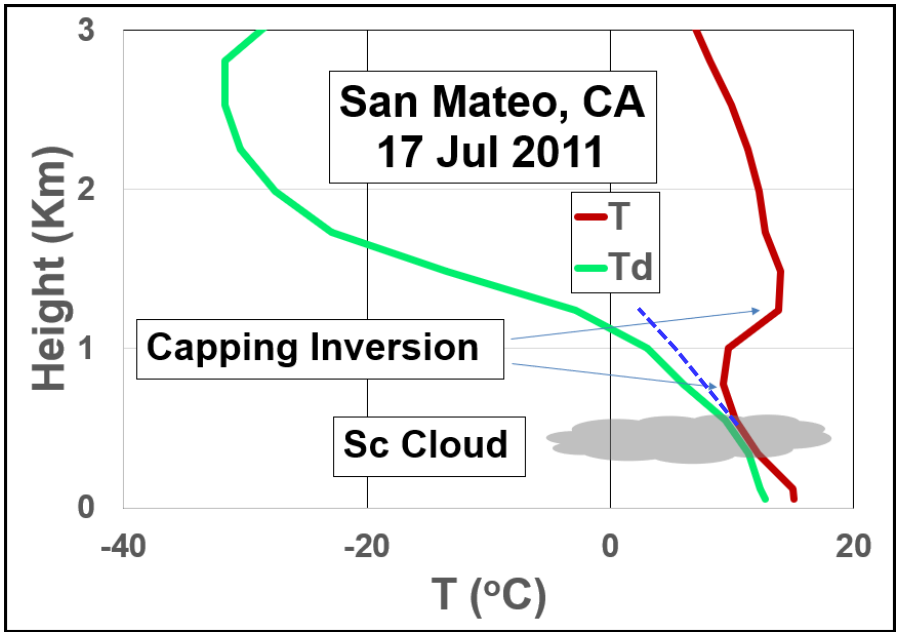

Fig. 6-12. Sounding for the San Mateo stratocumulus of Fig. 6-10 capped by an inversion. SDG.

Stratocumulus is also the most likely form of penetrative cloud when daytime heating is weak or late afternoon heating is fading, even if the atmospheric regime is not so repressive. Stratocumulus is a common afternoon cloud in the mid and high latitudes during autumn, when the Sun remains low in the sky and the days are short.

Fig. 6-13. Sunset stratocumulus clouds are the dying embers of cumulus earlier that afternoon over Catalina Mountain, AZ, 16 Mar 2023. JC.

Stratocumulus clouds often form as the degenerating, disintegrating remnants of late afternoon cumulus losing their struggle for life, first shrinking and flattening and ultimately evaporating as they mix with dry, ambient air. Even so, stratocumulus clouds can be quite pretty when lit by the colors of sunset, as in Fig. 6-13 where convection is still simmering, and even glorious, as in Fig. 6-14, where convection is almost dead, the cloud is no longer penetrating, and evaporation has taken over. The last remnants of stratocumulus often persist into twilight, as in Fig. 6-15, though they vanished within an hour after the photo, leaving the sky cloudless.

Twilight does not always sound the death knell of penetrative clouds. Thunderstorms sometimes thrive through much of the night, as witnessed by many of the best photographs of lightning (Chapter 8) and, of course by experience. Evening and nocturnal late spring and summer thunderstorms are often the rule on the lee side of mountain ranges including the Rockies. As the Sun sets the eastern slopes of the Rockies cool, and cool downslope mountain breezes form. These breezes crash into the still warm air over the Great Plains, forcing it to rise despite the absence of Sun. The thunderstorms follow the convergence zone and race off eastward, into the shadow of night. Far from the mountains, organized thunderstorm families or complexes, called *Mesoscale Convective Systems* also often bubble away through the night.

The appearance of convective clouds depends on factors such as their optical thickness, density of droplets or crystals near the cloud edge, the viewing angle from the Sun, and the Sun' height in the sky. The sunlit sides of stratocumulus clouds as in Fig. 6-9 or Fig. 6-10 may appear bright until compared with the sunlit sides of nearby towering cumulus or cumulonimbus clouds, which almost always have much greater optical thickness and which reflect up to 90% of the incident sunlight.

Fig. 6-14. Evaporating stratocumulus at sunset, Cheyenne, WY, 23 Dec 2020 JC.

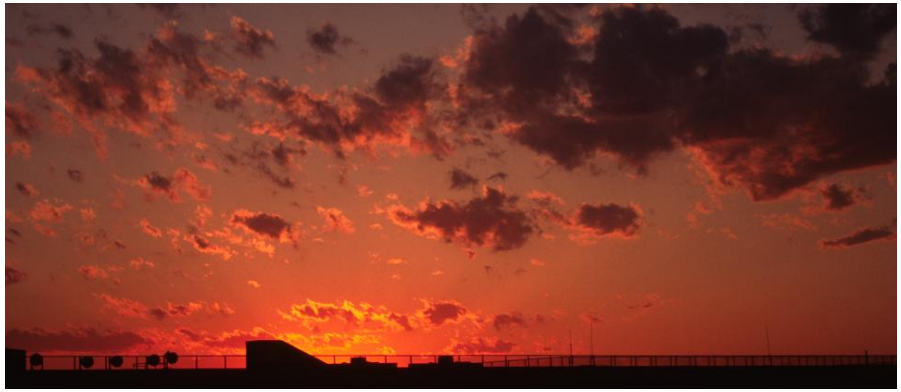

Fig. 6-15. Shriveled stratocumulus at sunset over CCNY. SDG.

Clouds that block or appear near the Sun are dark if optically thick but can gleam blindingly bright if optically thin, as with the field of cumulus in Fig. 6-16. In such clouds lighting dominates form.

Form dominates lighting for the curious anvil-topped line of cumulus mediocris in Fig. 6-17. The modest height of the clouds shows that the unstable layer is shallow, but the anvil indicates that, 1: the degree of instability is large enough so that the air rises rapidly until, 2: it reaches a sharp capping inversion, where it slows and spreads abruptly.

Fig. 6-16. Sunlit field of optically thin cumulus at Boynton Beach, FL, 13 Feb 2014. SDG.

Fig. 6-17. An anvil-topped cumulus street over the Bronx. SDG.

The small cumulus turrets that rise slightly above the otherwise level top represent miniaturized versions of the overshooting dome tops seen in growing cumulonimbus clouds, as in Fig. 6-18.

Fig. 6-18. Thunderstorm with an overshooting dome above the anvil at the equilibrium level, over Kimball, NB, 08 Jul 2018. JC.

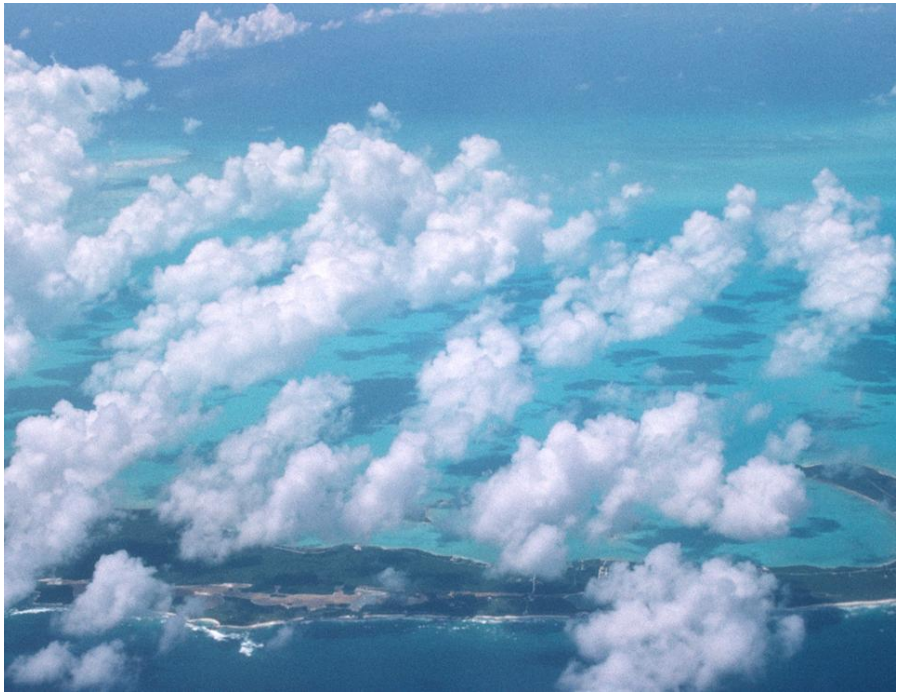

Fig. 6-19. Trade wind cumulus over the Bahamas on the way into Hurricane Hortense, 11 Sep 1996. SDG.

Fig. 6-20. A field of cumulus humilis with white sunlit sides and gray shaded bases over Cheyenne, WY, 23 Apr 2019. JC. Note the similarity to Fig. 6-1.

Overshooting domes occur in growing, active thunderstorms when the rising thermals or plumes have large upward velocities at the equilibrium level, marked by the anvil. Their momentum carries them as much as a kilometer or two higher before they sink back down.

The height of the overshooting dome above the equilibrium level depends on three main factors, 1: the range of height through which the parcel is warmer than the surroundings, 2: the parcel's mean temperature excess over that range and, 3: the ambient temperature profile above the equilibrium level. The first two factors combine as a measure of the potential energy that is available to be converted to kinetic energy of the updraft. This quantity, called the Convective Available Potential Energy (CAPE) helps to estimate the maximum updraft speed at the equilibrium level and the storm's ferocity. The ambient temperature profile above the equilibrium level determines how rapidly the rising parcel decelerates.

In the Trade Wind belt unusually narrow cumulus burst upward for some distance, buoyed by the large release of latent heat of condensation in the otherwise stable air. A pretty case occurred over one of the Bahama Islands, flying on the way to Hurricane Hortense on 11 Sept 1996, whose outer winds tilted the clouds (Fig. 6-19).

Not only does intense, prolonged heating lift thermals and plumes, it destabilizes the entire atmosphere. This is illustrated by the daily time sequence of cumulus, noting that even the most towering and formidable thunderstorm starts from a successful cumulus humilis that was born only a few hours earlier (Fig 6-1 and Fig. 6-20).

Fig. 6-21. Cumulus humilis Fairfield Lake, NC, 06 Oct 2023. SDG.

Fig. 6-22. Cumulus mediocris over Boynton Beach, FL, 03 May 2024. SDG.

Fig. 6-23. Cumulus Congestus enhanced by orography Vail, AZ, 18 Aug 2018. JC.

Fig. 6-24. Stand-alone growing cumulus congestus with cauliflower protuberances and flat, dark shaded base Ranchettes, WY, 05 Sept 2016. JC.

Fig. 6-25. Cumulonimbus, the thundercloud with flat base, fuzzy cirriform anvil and growing cauliflower towers over Ranchettes, WY, 22 June 2023. JC.

Let's repeat the daily biography of cumulus using Fig 6-21 to Fig. 6-25. Start with a cloudless sky at dawn. After a few hours the surface air has been warmed enough to produce thermals that rise above the *LCL* and produce small, humble *cumulus humilis* that may resemble powder puffs (Fig. 6-21). Each small cloud mixes with the environment and many die within minutes, but the when the droplets pumped aloft evaporate they not only increase the ambient RH they also destabilize the air by cooling it aloft. This enables subsequent cumulus to rise faster and higher, and last longer before evaporating.

After a few more hours of intense, mid-day solar heating the cumulus clouds have grown wider and higher, and cover a larger fraction of the

sky. They have now become *cumulus mediocris* clouds (Fig. 6-22) and, unless large vertical wind shear tilts and distorts them, they almost always have marked flat, dark bases.

If the atmosphere is unstable through a deep layer of the troposphere, a few of the 'fittest' cumulus clouds win the 'struggle' for survival and continue widening and rising to towering cumulus congestus with growing cauliflower shaped tops, in Fig. 6-23 and Fig. 6-24.

A cumulus congestus that continues growing will ultimately be stopped by a stable layer such as the stratosphere at a height between about 8 and 18 km, where it spreads out into a great anvil cap and metamorphoses into a cumulonimbus or thunderstorm (Fig. 6-25 and Chapter 7). The large quantities of water and ice that condensed and accumulated in the cloud weigh the air down, and produce rain or hail filled downdrafts that hurtle toward the ground.

Warning: This Book is an Active Deception Site

Almost all photos in this book are deceptive in that they are highly selective. For example, enormous time and patience are needed to capture such model cumulus that stand separately or solo in pristine, deep blue skies of unlimited visibility. Even over isolated peaks, such as Mt. Fuji, stand-alone, towering cumulus are not common; over flat ground they are exceptional. Fig. 6-24 is a case in point. For half an hour, the nearest cloud in the line of cumulus remained unobstructed, with no nearby clouds on either side as well. Simply extraordinary!

The vast majority of cumulus skies contain a chaotic jumble of clouds at all stages of development that make it difficult to see the complete outline of any cloud, as the the fields of cumulus of Fig. 6-16 and Fig. 6-26 (over Melk, Austria). Shreds of juvenile clouds appear side by side with mature growing beauties and aged dissipating clouds. Such clouds are spread around the sky almost like buckshot, which befits their unstable, turbulent nature indicated by cauliflower corrugations. (All doubts about the turbulent nature of towering cumulus are dispelled the moment a jet flies through one and undergoes violent shaking.) Furthermore, fields of cumulus clouds often arise in hazy air of high humidity, which further limits visibility and mars the clouds' potential beauty.

Fig. 6-26. Overlapping cumulus over Melk, Austria, 07 May 2018. SDG.

6.4 Mountains: Orographic Cumulus

Mountains act as elevated heat sources on sunny days. Even though temperature decreases with height, the air on the sunlit mountain slopes is warmer than the air in the free atmosphere at the same height. The heated air slides up the slopes from the valley as a valley breeze (recall Fig. 5-6). If the ambient wind is slow enough and the air rises high enough, the first place a cumulus cloud will form is above the peak, as with the new, baby cumulus humilis over Mount Coe in Baxter State Park, ME on 28 Aug 2005 (Fig. 6-27).

Such *orographic* clouds can grow to towering heights and result in thunderstorms over the mountains (Fig. 6-28) while the lowlands remain clear. That would not be the time to celebrate a climb at the peak. Thus the saying, "mountains make their own weather."

Fig. 6-27. Orographic cumulus over Mount Coe, ME, 28 Jul 2005. SDG.

Fig. 6-28. Orographic cumulus over Rincon Mt., AZ, 15 Oct 2018. JC.

Fig. 6-29. Flat-based orographic cumulus over the Alpine peaks east of Zermatt, Switzerland, 12 Jun 2004. SDG.

Fig. 6-30. Orographic cumulus over Rincon Mt., AZ, 20 Aug 2022. JC.

When cloud base is below the peak, young, growing orographic cumulus clouds can be seen rising up the slopes, as around Zermatt, Switzerland (Fig. 6-29) and Rincon Mountain, near Vail, AZ, where a complex humidity structure in the valley and on the slopes produced cloud bases at various heights (Fig. 6-30).

Fig. 6-31. Orographic cumulus cloud street 160 km long over Cheyenne, WY. 23 Dec 2020. JC.

Fig. 6-32. Stratocumulus lenticularis over Cheyenne, WY, 29 Mar 2021. JC.

Uplift by winds that cross ridges of even modest height can generate cumulus when the atmosphere is unstable. On 23 Dec 2020 near Cheyenne, WY (Fig. 6-31) a NW wind crossing a low ridge at a 90° angle coupled with an unstable sounding up to about 3 km provided sufficient lifting to produce a line of cumulus 160 km long that persisted in place for 2 hours. On 29 March 2021 a west wind crossed the same ridge when the atmosphere was stable and produced laminar stratocumulus lenticularis in the same place (Fig. 6-32). Lenticular, mountain wave clouds are the subject of Chapter 13.

Cloud lines sometimes form when the wind crosses the modest Palisades, a cliff 90 m high at Fort Lee, NJ. If the atmosphere is stable, as it tends to be with an east wind. the cloud line is smooth and laminar at top and bottom, but when the atmosphere is unstable, as in Fig. 6-33, buoyant cumulus turrets bubble up turbulently from the flat-based cloud line.

Fig. 6-33. Cumulus line over the Palisades. NJ. SDG.

6.5 Motions: Mushrooms and More

Fig. 6-34. Mushroom-shaped nuclear cloud of Ivy Mike. Skirt clouds (velum) widen the rising stem, 01 Nov 1952. Charles Wyckoff, Public Domain.

The mushroom is the iconic form of all penetrative clouds. It is, of course, associated with the cloud of nuclear explosions. Ivy Mike, which rose to over 40 km and evaporated the Pacific island, Elugelab in 1952 is just one example (Fig. 6-34).

Mushroom clouds are common and long predate nuclear explosions. They are produced by explosive volcanic eruptions, by routine explosions (often depicted in movies) and can even be distinguished in mundane cumulus clouds where, on occasion, a mushroom shape appears alone (Fig. 6-35). The reason that few penetrative clouds look like mushrooms is that thay are built by many overlapping mushroom-shaped thermals of warm, buoyant rising air. The anvil of a cumulonimbus is also a compound structure. It may start its life as a single mushroom cap, but with time accumulates the detritus of many defunct mushrooms.

Fig. 6-35. Mushroom-shaped cumulus, Boynton Beach, Fl, 05 Feb 2014. SDG.

Fig. 6-36. Auspicious cloud scroll, Forbidden Palace, Beijing captures the form and motions of growing cumulus cloud turrets and lobes. SDG.

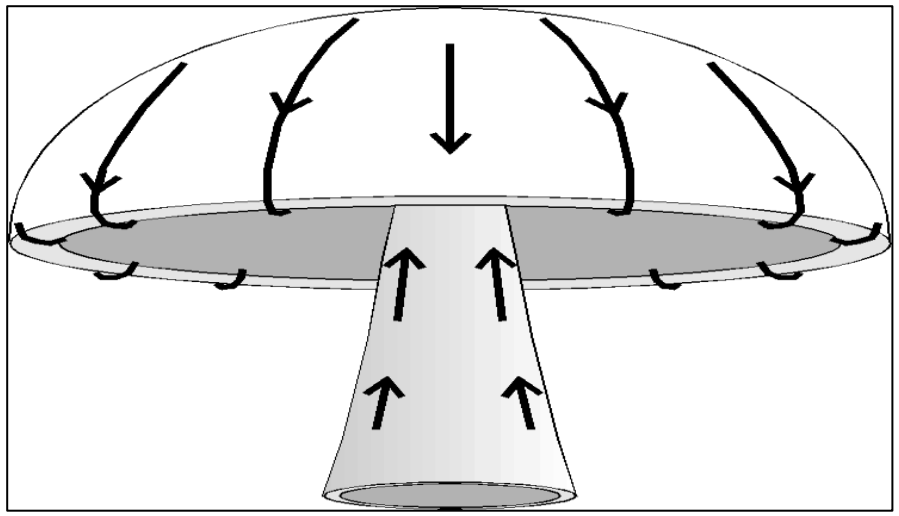

Fig. 6-37. Vortex air flow in a mushroom-capped plume. SDG.

Knowledge of the mushroom cloud shape is ancient. The Chinese auspicious cloud scroll motif (yunwen) (Fig. 6-36) dates from the Shang Dynasty 1500 BCE. It shows that Chinese artists knew the form and motions within cumulus. Pliny the Younger, watching the eruption of Vesuvius in CE 79 reported that the cloud resembled a pine tree with a rising trunk and spreading branches.

The basic motion of the mushroom cloud is shown in Fig. 6-37. A plume of hot, buoyant air moves up the mushroom stem and then out, down, and around the cap (suppressing nearby clouds) as it encounters resistance penetrating the quiescent surroundings. This motion is a classical smoke ring vortex, with an invisible stem.

The turbulent, bubbling motions of cumulus are models of the complexity omnipresent in clouds. Simultaneous telephoto and wide-angle views of cauliflower turrets look similar and betray a fractal, nature. Large corrugations have smaller corrugations on them, almost in the manner of the infinite series of Jonathan Swift's poem,

> Big fleas have little fleas upon their backs to bite them,
> And little fleas have lesser fleas, and so ad infinitum.

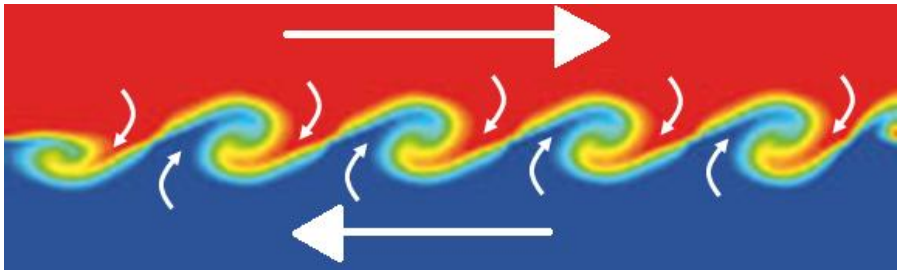

Fig. 6-38. Motions in breaking Kelvin-Helmholtz waves. SDG.

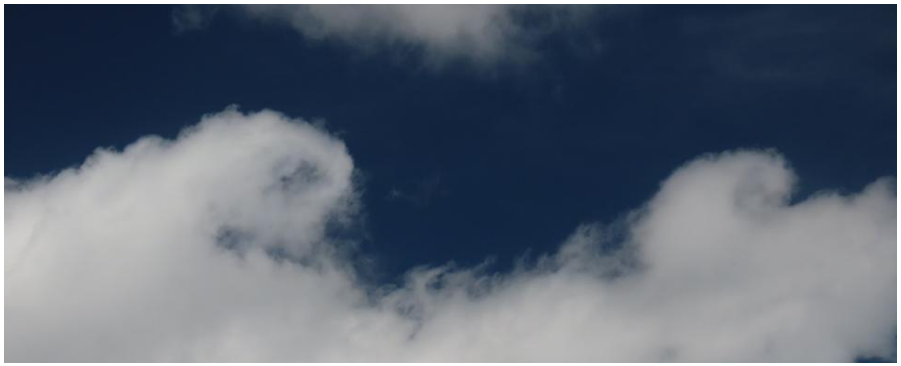

Fig. 6-39. Breaking Kelvin-Helmholtz waves atop Cu *fluctus* in strong wind shear, 10 Aug 2023 Fairfield Lake, NC. SDG.

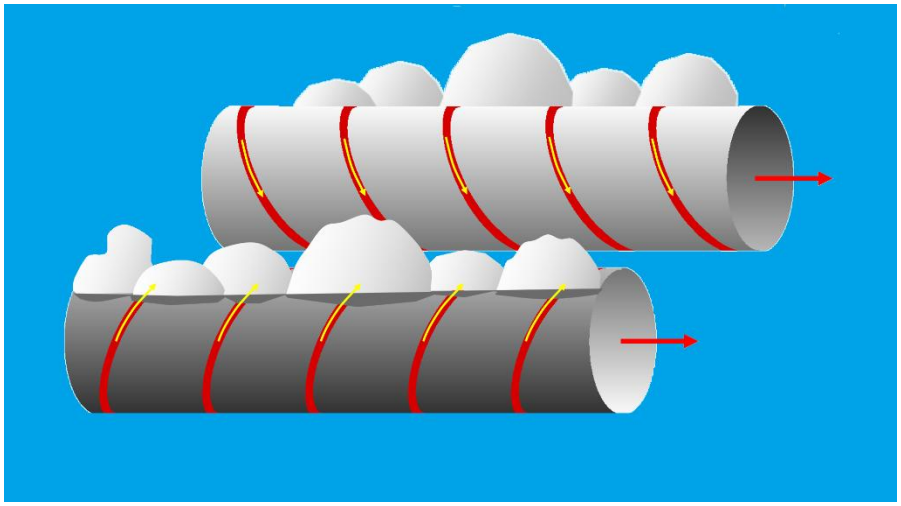

Fig. 6-40. Helical flow produces long parallel cumulus streets alternating with clear lanes, both parallel to the wind. SDG.

Kelvin-Helmholtz waves, another simple flow pattern, (Fig. 6-38) form on the interface of two fluid layers moving relative to each and grow like breaking ocean waves at the shore. They occur at the tops of clouds where there is large vertical wind shear, such as the cumulus *fluctus* cloud of 10 Aug 2023 over Fairfield Lake, NC (Fig. 6-39).

Helical (corkscrew) flow with a vertical axis spirals upward like strands of a DNA double helix.to produce waterspouts and tornadoes (Chapter 7). When the axis is horizontal, rows of rising and sinking air alternate (Fig. 6-40) to produce long streets of cumulus that alternate with clear lanes, all aligned with the wind.

Cumulus cloud streets, seen in satellite images, occur almost every time advancing Polar air behind cold fronts pours over warmer waters. A classic case occurred on 16 Nov 2008, filling the Gulf of Mexico and extending north off the Atlantic coast (Fig. 6-41).

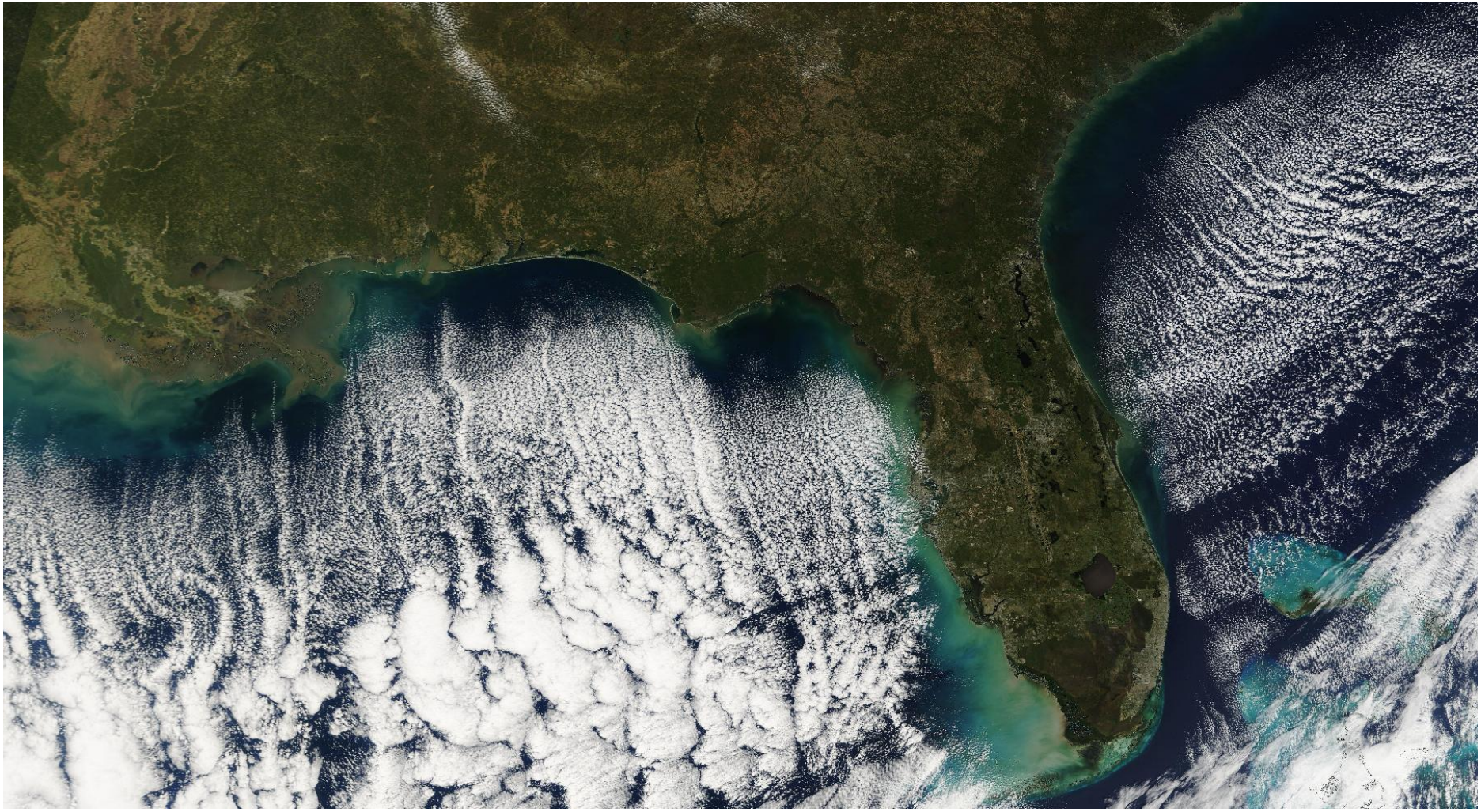

Fig. 6-41. Cumulus cloud streets over the Gulf of Mexico and the Atlantic Ocean behind a cold front while the land is clear on 16 Nov 2008. NOAA GOES.

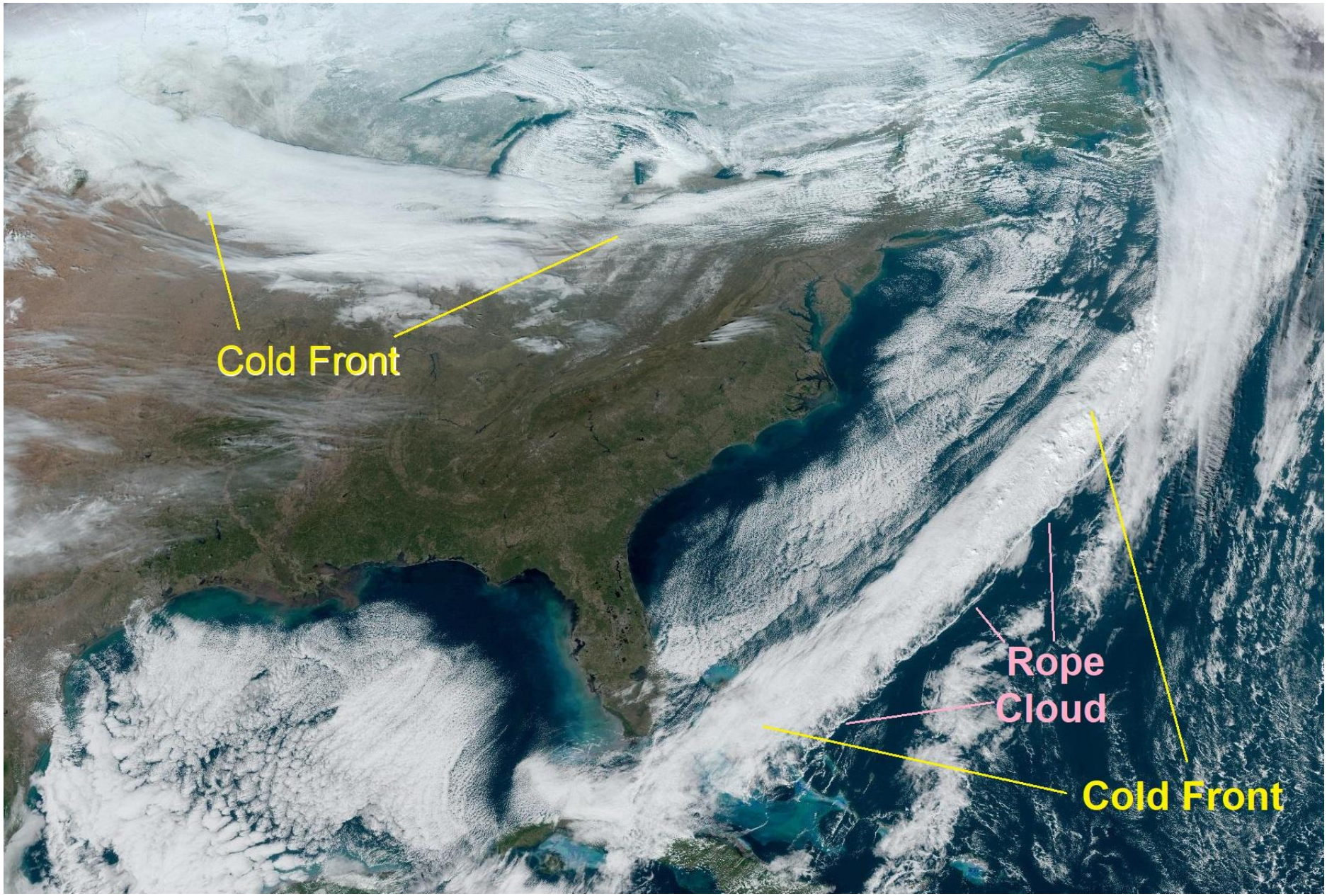

Fig. 6-42. Cumulus cloud streets behind a rope cloud, and over Lakes Superior and Michigan behind a secondary cold front, 1800 12 Dec 2024. GOES 16.

As is typical, the sky is clear over land and over a strip of coastal

waters typically 50 or more km wide before the cold, dry air acquires enough heat and water vapor to begin to form clouds. Similar features occurred on 11 Dec 2024 (Fig. 6-42), when cloud streets formed behind a cold front extending from the Gulf of Mexico south of Texas to the Atlantic Ocean south of Nova Scotia, Canada, and also behind a second cold front over Lakes Superior and Michigan.

Fig. 6-43. Post cold front cumulus cloud street capped by an inversion at 2.5 km, Grand Turk, 19 Dec 2013. SDG.

Cloud streets seen from Space, resemble lines of puffs. Views from the ground reveal that the puffs are cumulus turrets, which may be linked or separate. Fig. 6-43 shows a cloud street over the waters near Grand Turk on 18 Dec 2013 behind a cold front.

When the Polar air has travelled far enough over the warm waters to begin to rise, the unstable layer is still quite shallow so cumulus cloud streets typically top out below 2 km until they are far out to sea. This leads to a classical sounding for these cases, marked by an unstable layer that is saturated at top and capped by an inversion. Fig. 6-44, the sounding for the case of 16 Nov 2008, is typical. It is, in fact, the combination of a thin unstable layer of air flowing over a warm surface confined by a capping inversion that produces the helical flow pattern of cumulus cloud streets.

Cumulus cloud streets also occur over land, as in Fig. 6-45. They have the same basic sounding except that the air must be humid to start with, and they may require assistance from topography (recall Fig. 6-31). If it is cold enough, the cloud droplets may freeze, giving the cloud a fuzzy appearance, and snow may fall (Fig. 6-46).

Another distinctive flow and cloud feature associated with cumulus is *pileus* (felt cap). Pileus is a smooth, arched, often veil-like attendant cloud that forms when the top of a rising cumulus approaches a thin moist layer aloft and forces it above its condensation level (Fig. 6-2 and Fig. 6-3). On 29 Oct 2016, at San Mateo, CA, (Fig. 6-47) two

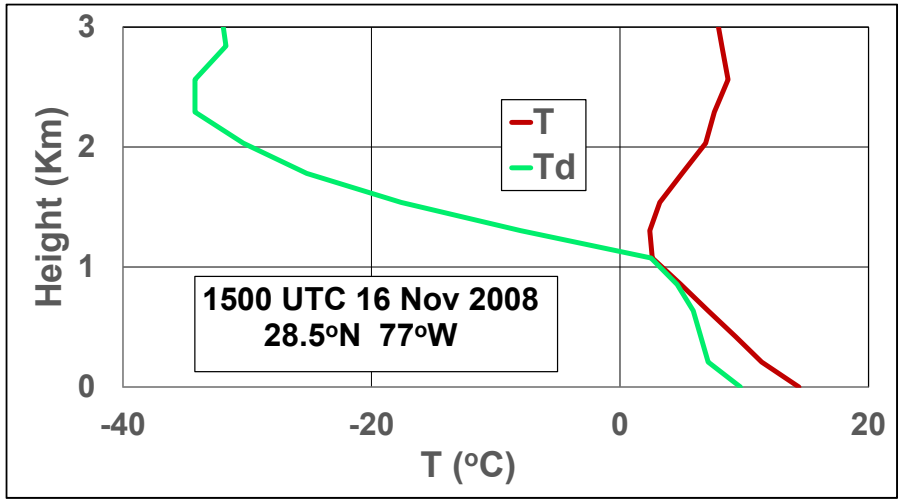

Fig. 6-44. Sounding for cumulus cloud streets at latitude, 28.5°N, longitude 77°W at 1500 UTC 16 Nov 2008. The unstable layer is 1.1 km thick. SDG.

pileus caps formed over the highest turrets of a modest, cumulus cloud street capped by an inversion.

Pileus, discussed in more detail in §13.2, is similar to mountain wave clouds, with two main differences. 1:, the rising mushroom cloud turret serves the role of a very short-lived mountain, 2: pileus can form

without vertical wind shear, as in Fig. 6-47, because the rising cloud forces the ambient air to rise. No mountain rises so fast.

Fig. 6-45. Cumulus cloud streets over CCNY. SDG.

Fig. 6-46. Glaciating, snow-producing cumulus cloud streets over Cliffside Park, NJ with T = -12°C at the surface. SDG.

Both mountain wave clouds and pileus are smooth because the forced flow of the stable ambient air is smooth and laminar. Pileus lasts but moments. It evaporates as soon as the cumulus turret sinks or when the rising turret punctures it (to form a skirt) and the sinking air around the periphery forces it back down to its original level.

Fig. 6-47. *Pileus* atop cumulus turrets over San Mateo, CA, 29 Oct 2016. SDG.

The skirt cloud, or velum (recall Fig. 6-3) is less common than pileus but lasts longer because it forms when a growing cumulus punctures a preexisting cloud sheet that does not require further lifting.

6.6 Time Lapse Views of Cloud Motions

If a picture is worth 1000 words an animation is worth (and often contains) 1000 pictures.

Even the most rapidly developing cumulus clouds evolve too slowly for all but the most patient eyes, once possessed only by a few Chinese artists and few others, to visualize the lifespan and motions of clouds. One time-honored way to speed up time and dramatize motions that mimic aspects of growing cumulus is to pour a thimble of milk into a tank of water. As the milk hurtles (not curdles) to the bottom of the tank it forms up-side down thermals with turrets and lobes. When the milk reaches the bottom of the tank it spreads out along the bottom,

curling up at its outer edge in a vortex ring of a thunderstorm downburst, as in the spreading dry-ice created fog of Fig. 4-37.

Time-lapse videos and animated loops of satellite images now speed up time and show the dynamism of real clouds and cloud systems. In this section we show videos mostly of penetrative clouds. Videos of other clouds are presented in the appropriate chapters. More than 1100 videos are available at the album labelled, ***Time Lapse***, at

https://www.flickr.com/photos/cloud_spirit/albums/

Even with a sequence of still photos at one second intervals (Fig. 6-48) it is difficult to visualize the growth of the stem and the motions around the mushroom cap of the atom bomb cloud that is obvious almost immediately and without effort watching the animation loop

https://www.youtube.com/watch?v=yvGNP6AzyCY

Other videos of nuclear mushroom clouds are on the Web under the names, Operation Tumbler-Snapper, Operation Buster-Jangle, and Operation Ivy.

It requires even more diligence to track the much slower evolution of two mushroom thermals in the cumulonimbus cloud of 02 June 2017 east of Cheyenne WY from life or from individual frames in Fig. 6-49, whereas the motions and evolution of thermals in the towering anvil-topped cumulonimbus incus are obvious in the video, ***Explosive Thunderstorm Development***,

https://www.flickr.com/photos/cloud_spirit/35022437616/in/album-72157667543992515

The rising and expanding mushroom-shaped thermal or plume described and illustrated in the last section is only an outline of the first stage in its life cycle. As the rising mushroom cap advances through the clear, quiescent ambient air it experiences resistance and must force its way. This slows its upward progress, with air in the mushroom stem still rushing upwards so that the cap is forced to spread outward. It is a violent, unstable flow, which means that even miniscule irregularities grow and self-distort into lobes at all scales, hence the cauliflower appearance. The smaller lobes are driven by the flow of the larger mushroom cap. They appear at the top center of the cap, move out, around, and down under it.

Fig. 6-48. Nevada Atom Bomb Test. from time, 27s to 33s. Red lines show the sinking movement of one lobe down the outside of the mushroom cap.

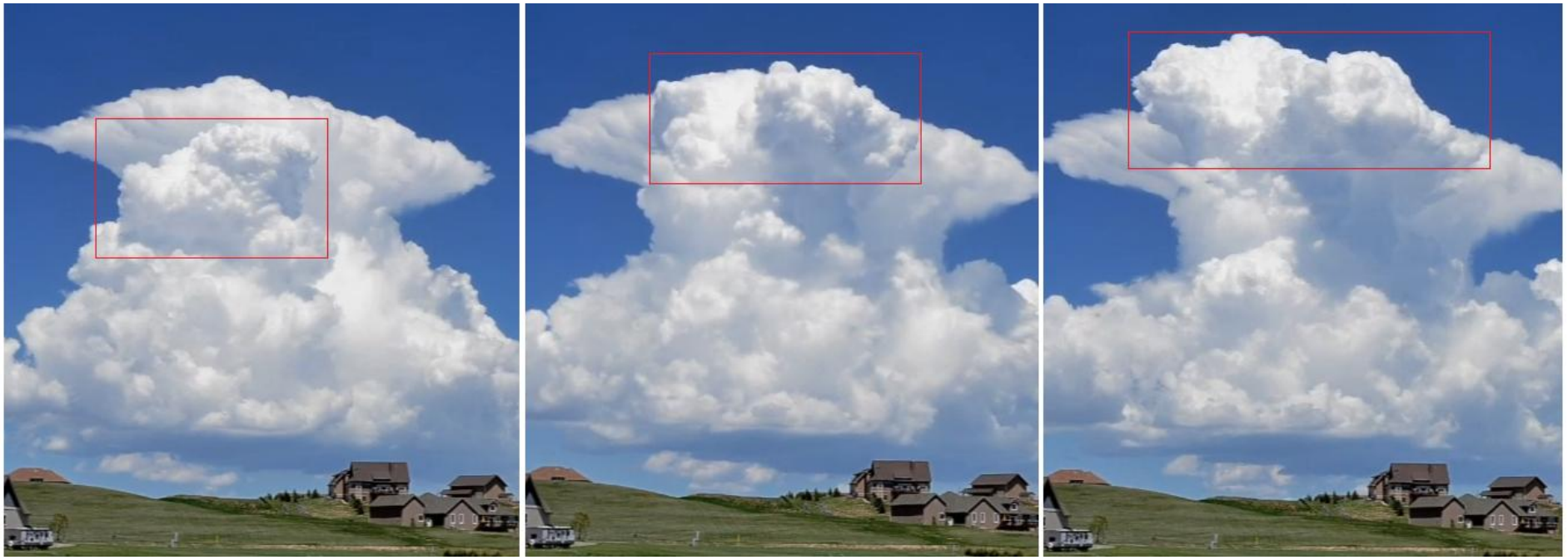

Fig. 6-49. Three frames of a cumulonimbus on 02 June 2017 east of Cheyenne, WY showing a rising and spreading thermal (in the red boxes). JC.

So long as the cap rises its outline contrasts sharply with the background clear sky because of the high concentration of droplets or ice particles right to the outer edge. Eventually, the supply of warm air is exhausted and/or the thermal rises into warmer surroundings. Then, aided by the weight of condensed water and ice that adds to its density, it begins to sink. The flow direction of the entire cap reverses and it collapses from the center outward, warming as it sinks so that the drops and crystals, especially at the outer edge, evaporate. As they evaporate progressively larger lobes vanish until the entire cap disappears. That renders the motion of the dying, infolding cap invisible though it is still turbulent.

Successful and successive mushroom thermals that reach a stable layer (such as the base of the stratosphere) with considerable momentum do not disappear but rise as overshooting domes and then 'bounce' back down to (and often oscillate about) their equilibrium level, where they spread out much further to form and contribute to an expanding anvil. A high-speed ambient wind sweeps the bulk of the anvil downwind in a long plume, though the strong outward flow of thermals at the upwind end of the storm tilt a small part of the anvil backward against the wind.

Amidst all the dynamism of boiling motions at the tops of growing cumulus and young cumulonimbus clouds, the flat base, which corresponds to the lifting condensation level, remains in place almost unmoved as the one static feature in time lapse videos. An excellent case that occurred on 05 Aug 2013 was captured in the video,

https://www.flickr.com/photos/cloud_spirit/25162008824/in/album-72157662969788496/lightbox/

Of course, cloud base only remains fixed until the precip-weighted downdraft pierces it and helps provide dynamism to it and all features near the bottom of the storm. But that is the subject of Chapter 7.

Videos captured the evolution of the cloud photos of Fig. 6-2, Fig. 6-23, and Fig. 6-24 (among others). The teeny, inconspicuous pileus atop the main cloud of Fig. 6-2 appears for just the brief moment before the rapidly rising thermal that produced it engulfs it in the video,

https://www.flickr.com/photos/cloud_spirit/48227039931/in/album-72157664743046092/lightbox/

Fig. 6-23 captures just one moment in the life of the growing cumulus congestus that minutes later developed an anvil in the video,

https://www.flickr.com/photos/cloud_spirit/30352758818/in/album-72157664743046092

The solitary cumulus congestus of Fig. 6-24 bubbled away for about half an hour in an otherwise clear sky in the video,

https://www.flickr.com/photos/cloud_spirit/29380390452/in/album-72157664743046092/lightbox/

Convection typically weakens in the late afternoon as the Sun sinks toward the western horizon. Cumulus tends to shrink and flatten to stratocumulus before ultimately evaporating around sunset. Sunset stratocumulus can be quite pretty, as in Fig. 6-13 where convection is only flickering, and Fig. 6-14, where evaporation dominates, though videos that show shrinking and vanishing stratocumulus lack the drama of videos of young, burgeoning cumulus.

Ground-based time-lapse videos of the penetrative clouds, with their dynamism, contrast with the static nature of videos of most other cloud genera. The cells and ripples of sheets of altocumulus or cirrocumulus and the streamers of cirrus tend to cross the sky with little change in shape because the circulations inside the cells and ripples and the fall speed of crystals in the streamers are very slow compared to the wind speed. For example, wind speed at the level of cirrus is typically of order 50 m/s while most ice crystals fall less than 1 m/s. Thus, a streamer may move out of sight before it can lengthen or descend much, especially when old crystals at a streamer's tail evaporate as fast as new crystals form at its head.

Time lapse videos or loops of satellite images span enough time and space to show how cirrus and altocumulus evolve. One example is cirrus streamers that form in the lee of mountain ridges and extend downwind.

Even though little dynamism is apparent in time lapse videos of cirrus and altocumulus, they still provide awesome and surprising views. Optical phenomena, such as halos and coronas, can flash on and off.

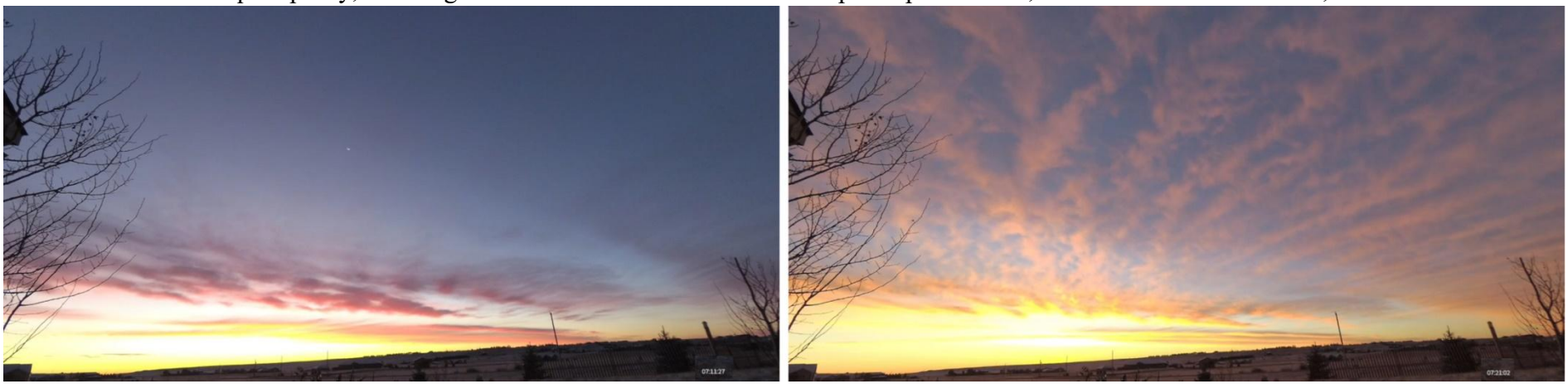

Fig. 6-50. Thin deck of altocumulus at dawn east of Cheyenne, WY 04 Nov 2018 appears suddenly when sunlit. Left 0711 MDT, Right, 0721 MDT. JC.

Changes of illumination during sunrise and sunset can cause cloud veneers to appear or disappear in minutes. The video, ***Perfect Sunrise*** is a perfect example of a sunrise surprise.

https://www.flickr.com/photos/cloud_spirit/43902575520/in/album-72157673924732027/

Fig. 6-50 shows two frames of the video 10 minutes apart. In the left frame at 0711 MDT the sky appears to be mostly clear except for a broken layer of golden and rich red altocumulus above the horizon. By 0721 MDT (right frame) an extensive sheet of altocumulus (that was there all along) appeared laced across much of the sky.

Its surprise appearance took place over only two minutes. The cloud sheet was invisible before the Sun illuminated it because its optical depth was so small that skylight from above passed through it almost undiminished. However, once the Sun struck the thin but wide cloud sheet broadside much sunlight was scattered and the cloud lit up. The layer then scarcely changed shape as it traversed the sky. Much later, with the Sun high in the sky, thin sheets of altocumulus fade from view once again because sunlight passes through them with little scattering. In a sense, these often near invisible thin clouds are much like some recently discovered 'missing' matter in the universe, which was invisible until viewed in the proper light.

6-7. Pyrocumulus and Pyroanvils

Sunset often makes the sky and clouds *seem* to be on fire. Sometimes they are! Between 2000 and 2020, average annual wildland fire area in the United States more than tripled to an average of about 30,000 km^2. Lightning (Chapter 8) sparks many of the fires. But those, fires and also rouse thunderstorms, or at least cumulus (recall Fig. 4-19).

On the days around 12 Aug 2015, in the worst fire year in the USA since comprehensive records were first kept in 1983, with just over 40,000 km^2 burned, the normally pristine air and deep blue skies

Fig. 6-51. Pyrocumulus north of Crater Lake, OR 12 Aug 2015. SDG.

Fig. 6-52. Pyroplume over Cheyenne, WY, 11 Jun 2018. JC.

around Crater Lake, OR were tarnished by fires. Some of them burned so hot in the unstable air they generated towering pyrocumulus clouds, as in Fig. 6-51. On occasion pyrocumulus clouds grow into pyrocumulonimbus and produce enough rain to quench the fires that gave them birth, but alas, not often enough.

Too often, of course, wildfires fail to produce clouds, but in strong winds do lead to long plumes or anvils, as with the Badger Creek Fire

of 11 June 2018 photographed and videoed at Cheyenne, WY, 200 km east of the fire (Fig. 6-52).

6-8. Gallery

Fig. 6-53. Cumulus humilis reflected by Fairfield Lake, NC, 29 Sep 2023. SDG.

Usually, surface winds are gusty enough to rustle lake waters by the time cumulus clouds have formed, but somehow, the convection that produced the field of cumulus humilis of Fig. 6-53 was too weak over Fairfield Lake to disturb its still waters. Far more often, early morning scenes with steam fog have almost calm winds and hence the lake surface appears like a mirror, as in Fig. 4-33 and Fig. 4-38.

Cloud bases are shaded during the day and may be quite dark if the clouds are optically thick (Fig. 6-54). As a result, their fine details are mostly masked. Cloud bases are illuminated only in the minutes after sunset (Fig. 6-55) and before dawn (Fig. 6-56), casting a spotlight on their normally masked, rippling fine scale structure.

Fig. 6-54. Cumulus mediocris with almost black bases over Cheyenne, WY, 22 Dec 2020. JC..

Fig. 6-55. Underlit stratocumulus deck 5 minutes after sunset over Cheyenne, WY, 26 May 2020. JC.

Fig. 6-56. Underlit Stratocumulus minutes before dawn east of Cheyenne, WY 27 June 2018. JC.

Fig. 6-57. Unpolarized (left) and polarized views of a cumulus cloud street facing west from CCNY, 21 Oct 2010. Polarized view shows distant clouds. SDG.

Fig. 6-58. Sea breeze front cumulus advancing across Boynton Beach, FL, 08 Feb 2014. SDG.

Fig. 6-59. Cumulus sampler. Clockwise from top left. Fall in Ramsey, NJ 16 Oct 2010, Twilight at Fort Lauderdale, FL 18 Dec 2010, Cloud canyon over Boynton Beach 18 Dec 2021, cloud field Panama Canal 1 Mar 2017. SDG.

Fig. 6-60. Line of cumulus and cumulonimbus over Cheyenne, WY, 23 May 2021. (Try waiting on this line!) JC.

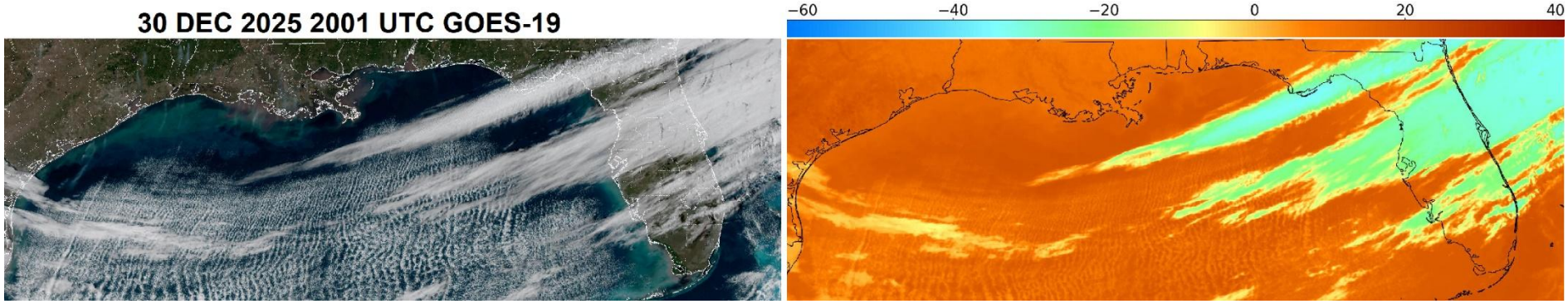

Fig. 6-61. Cirrus (in the Jet Stream) above cumulus cloud streets seen in visible light (left) and infrared (right), 2001 UTC, 30 Dec 2025. There is often little contrast between white cirrus and white cumulus in visible images, so animation brings out the contrast with the streets moving to the south and the cirrus moving to the east. The infrared channel is essentially a map of surface and cloud-top temperatures. Cirrus clouds stand out in infrared because they are much colder than the tops of the cumulus, which are only slightly cooler than the surface and hence almost invisible. NOAA GOES-19 Images.

Fig. 6-62. Pyrocumulus, El Dorado, NM, 11 June 2013. JC.

Wonders of the Atmosphere
Chapter 7: Thunderstorms

Fig. 7-1. Severe thunderstorm with cirrus at the edge of the anvil, a dark shelf cloud and rain fall streaks south of Cheyenne, WY, 21 Jul 2023, JC.

Fig. 7-2. Mamma hanging down from the underside of the anvil of a cumulonimbus with rain in the distance over Cheyenne, WY, 12 Jun 2016. JC.

Fig. 7-3. Underlit arcus of an impending hailstorm over Cheyenne, WY at sunset, 18 Jun 2021. Pastel colors belie the storm's fury. JC.

Wonders of the Atmosphere
Chapter 7: Thunderstorms

7.1 Thunderstorm Facts and Statistics

Cumulonimbus, the thunderstorm cloud, is the monarch of the sky. It metamorphoses from a cauliflower-topped cumulus congestus that bursts up until it encounters a stable layer near or at the top of the troposphere. Then, like a butterfly spreading its wings for the first time, it sprouts an anvil top. From a distance, as in Fig. 6-19 or Fig. 7-1, a thunderstorm is a thing of beauty, an awesome sight that dwarfs mountains. As it approaches, the anvil overhead may be underlain by mamma (Fig. 7-2). Still closer, the arcus, sometimes resembling a plow and near pitch-black unless lit by the setting Sun (Fig. 7-3) threatens death and destruction

As the thunderstorm draws overhead, its fury typically rises to a quick peak captured by composers. Furious cold winds, splaying out from the downburst, lead intense rain or hail by mere moments, while all is accompanied by lightning (Chapter 8), deafening, earth-shaking thunder, and perhaps a tornado that sweeps all into ruin. No surprise that the thunderstorm god, the hurler of thunderbolts, was the king of the Gods in so many ancient religions. But the havoc seldom lasts half an hour before it gradually subsides and skies clear again, perhaps with a parting a rainbow (Chapter 9) to grace the sky.

The great energy of this powerhouse largely goes to waste. Too bad, for its average of 1 trillion watts would be enough to power 40 million homes during the brief time it lasts. But its rains sustain life.

Thunderstorms are towering but narrow storms, typically 6 to 18 km high and 8 to 40 km wide. They resemble umbrellas in the sense that all activity occurs in a narrow shaft, where updraft speeds range from 5 to as much as 50 m/s, all covered by a much wider canopy anvil.

Despite their fury, most thunderstorms do not cause significant damage or death. Violent downbursts, large hail, and tornadoes are almost exclusively confined to the class of severe, organized thunderstorms. Each year in the United States thunderstorms kill an average of about 15 people due to lightning, 50 people due to tornadoes and 200 people due to Flash Floods. (Death tolls used to be higher but for the most part, Americans have wised up.)

Thunderstorms are as common as popcorn. Globally, there are about 2000 at any moment, 45;000 per day, and 16 million per year.

The global map of lightning flashes (a good proxy for *thunder*storms) measured by satellite (Fig. 7-4) shows that thunderstorms occur most frequently in the tropics, where sunlight is intense all year, and over land, which the Sun heats more rapidly than it heats water. Thus the saying, “Convection craves continents and lightning loves land!” Central Equatorial Africa is the world thunderstorm capital, and their electrical effects are conducted around the world. Java and Maracaibo have equal or even greater peaks but over smaller areas. In the United States central Florida is the thunderstorm capital due to the boost to convection given by converging sea breezes from both the Atlantic Ocean and the Gulf of Mexico. In most of the middle latitudes, thunderstorms are most common in late spring and summer and least common in winter

Thunderstorms are uncommon over cold ocean currents such as those on the eastern side of the subtropical high pressure areas, at Polar latitudes, and they are almost nonexistent over the ice caps of Greenland and Antarctic.

Thunderstorms also have a strong diurnal cycle. In many inland locations peak time is late afternoon, shortly after the hottest time of the day. Most thunderstorms fade away as the land cools at night, or they move down from mountain ranges towards valleys, following the zone where mountain and upslope valley breezes converge. Nocturnal thunderstorms also form over warm coastal waters, where they are aided by the land breeze.

7.2 Thunderstorm Structure and Features

All mature thunderstorms share four core features, namely,

1. A deep layer with a conditionally unstable lapse rate.
2. A lifting mechanism
3. Strong updrafts of buoyant warm, moist air.
4. Cold, precipitation laden downdrafts.

All thunderstorms undergo a similar life cycle. In youth they consist entirely of buoyant updrafts. As droplets and ice condense in the rising air they weigh the air down, producing downdrafts. In maturity a precipitation laden downdraft typically lies side by side with the updraft (Fig. 7-5). Evaporating rain and melting ice cool the air and accelerate the downdraft, sometimes causing a rain gush and

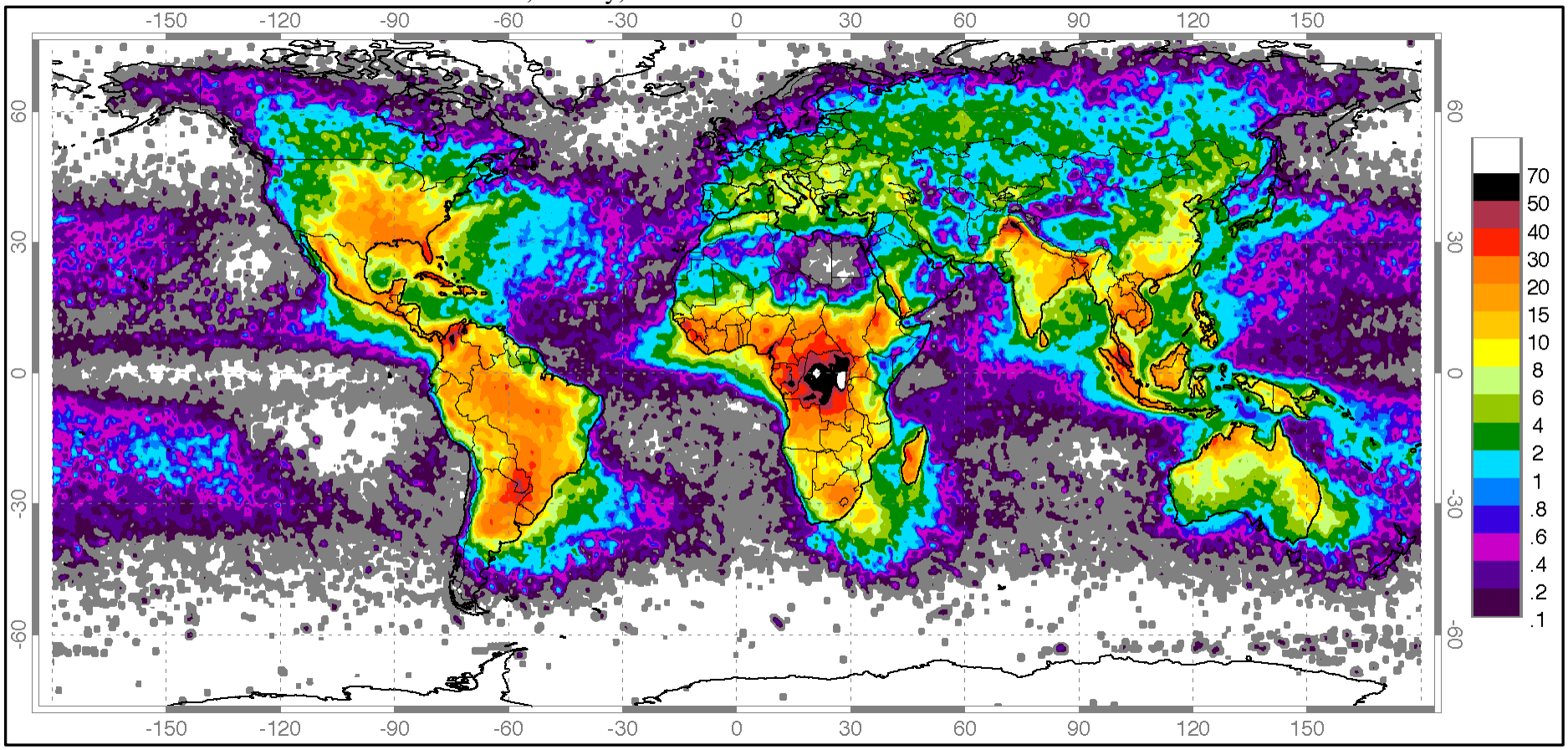

Fig. 7-4. Global map of annual lightning flash frequency per km^2. Concentrations are greatest over land and in the tropics, almost absent over the Poles. NASA.

downburst, which splays out on hitting the ground, as in the video,

https://www.youtube.com/watch?v=a_G2KRzha7o

Nothing good lasts forever. Old age encroaches when the supply of nearby warm air is exhausted. Once the hot air supply is exhausted the updraft dies, usually from bottom up so that the anvil is the last remnant of many storms. Without an updraft the production of liquid water and ice ends. That, in turn, weakens the downdraft, which persists a little while longer with only light rain. Remnants of the anvil blow downwind, detach from the dying storm, and evaporate to produce humid layers aloft that may later (mainly at night) recondense as cirrus or sheets of altocumulus or cirrocumulus.

Despite this basic plan and life cycle, there are enough differences to divide thunderstorms into at least four distinct types. In order of increasing severity they are,

1. Single cell, air mass thunderstorms.
2. Multicell, air mass thunderstorms.
3. Squall-line thunderstorms.
4. Supercell thunderstorms.

Air mass storms are the least intense form of thunderstorms because they form with little organization and little vertical wind shear (change of wind speed and/or direction with height). Lacking the support of the larger scale winds, air mass storms only draw from the nearby, local supply of hot air, and which the shading of sunlight by the anvil helps to reduce. Severe thunderstorms – squall-line storms and supercell storms – are more intense and last longer because they are embedded in larger scale flow that provides a large and protracted supply of hot, humid air.

Severe thunderstorms form in settings with

1. Marked instability
2. Sustained warm air supplies
3. Approaching cold fronts or jet stream troughs
4. Significant vertical wind shear.

Vertical wind shear adds to a thunderstorm's intensity by tilting the updraft so that condensed water and ice do not fall back into it, weigh it down, and choke it on its own precipitation. (Excessive wind shear will shred the updraft.) The downdrafts increase the strength of the updrafts by undercutting them and wedging them aloft. The video,

https://www.youtube.com/watch?v=Ur4k8cAuQUY

animates many motions of severe thunderstorms' features.

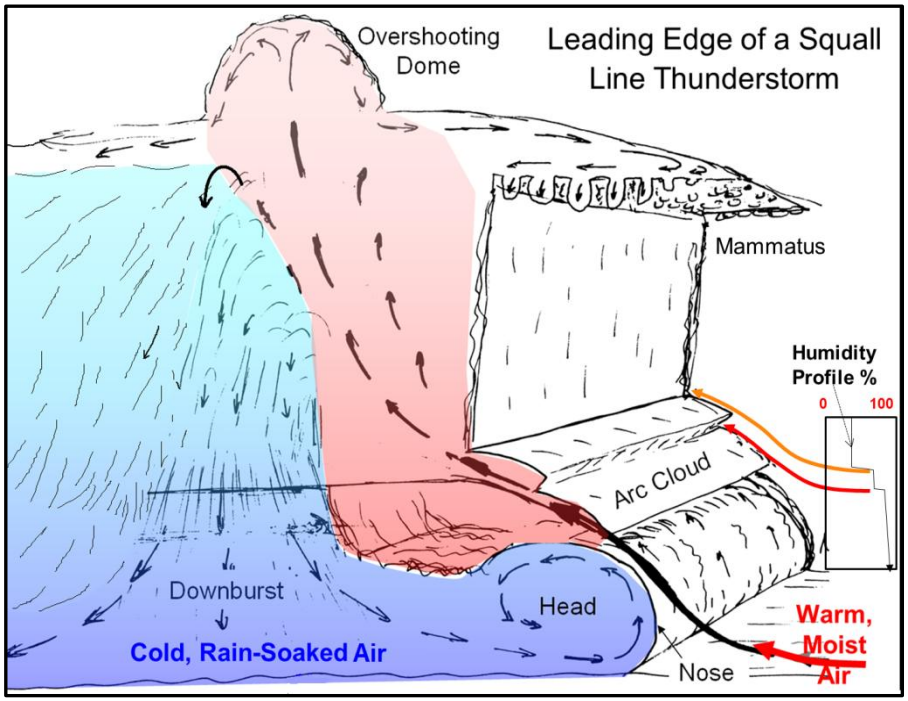

Fig. 7-5. Structure at front end of a mature squall line thunderstorm with attendant features including an overshooting dome, mammatus, an arc or shelf cloud, and a downburst with a vortex ring at its head. SDG.

The main structural features of squall line thunderstorms are illustrated in Fig. 7-5. A long-lasting supply of warm, moist air (pink) enters the updraft, tilted by the vertical wind shear. Precipitation forms and falls to the side of the updraft, weighing the air down and cooling it by evaporation to produce a downdraft

Fig. 7-6. A tornadic supercell thunderstorm, 75 miles SE of Cheyenne, WY, 23 Jun 2023, with Ci streamers and mamma lined up under the anvil. JC.

(blue). The downdraft splays out on striking the ground, moving ahead of the cloud and forces the warm air aloft, often before it is buoyant. This leads to a convex plow-shaped arcus cloud at the leading edge of the squall line thunderstorm. The rising air soon becomes buoyant and results in an updraft of great intensity.

Though squall line thunderstorms form in atmospheres with significant wind shear, the wind direction does not change much with height. Supercell thunderstorms the greatest and most severe of all thunderstorms can cover an enormous area, as did the storm of 23 Jun 2023 over the Pawnee National Grassland, CO (Fig. 7-6). They form when wind speed both increases and turns consistently with height. This helical motion, which resembles a double strand of DNA in the process of zipping (Fig. 7-7) adds to the storm's potential severity and is what provides the initial rotation for tornadoes.

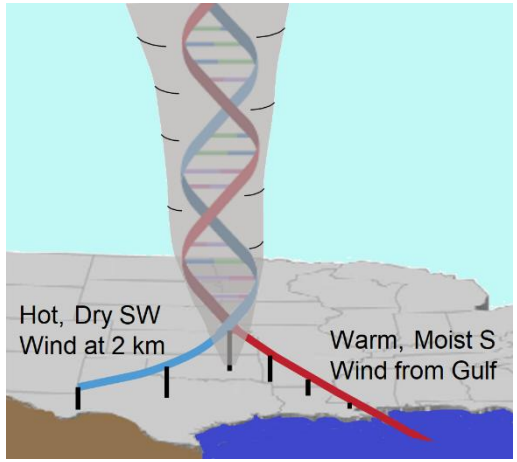

Fig. 7-7. Helical flow approaching a tornado resembles zipping of a double helix of DNA. SDG.

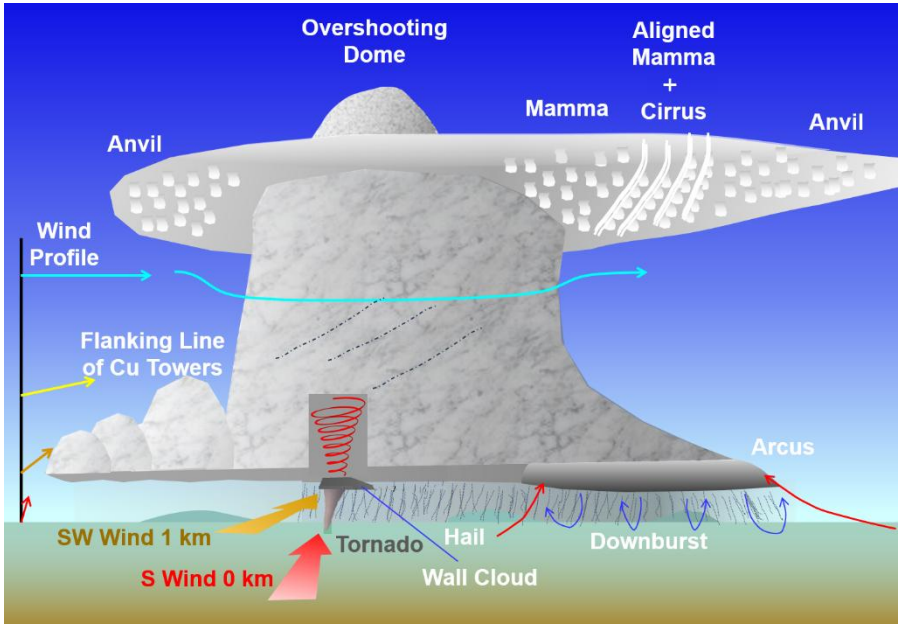

Fig. 7-8. Structure and environment of supercell thunderstorms. SDG.

The main structural features and larger scale environment of supercell thunderstorms are illustrated in Fig. 7-8. The larger scale environment of the supercell consists of a 3-layer sandwich,

1. Warm, humid air from the S in the lowest km or so,

2. Hot, dry air from the SW at about 1-3 km,
3. Cold, dry jet from the W in the mid and upper troposphere.

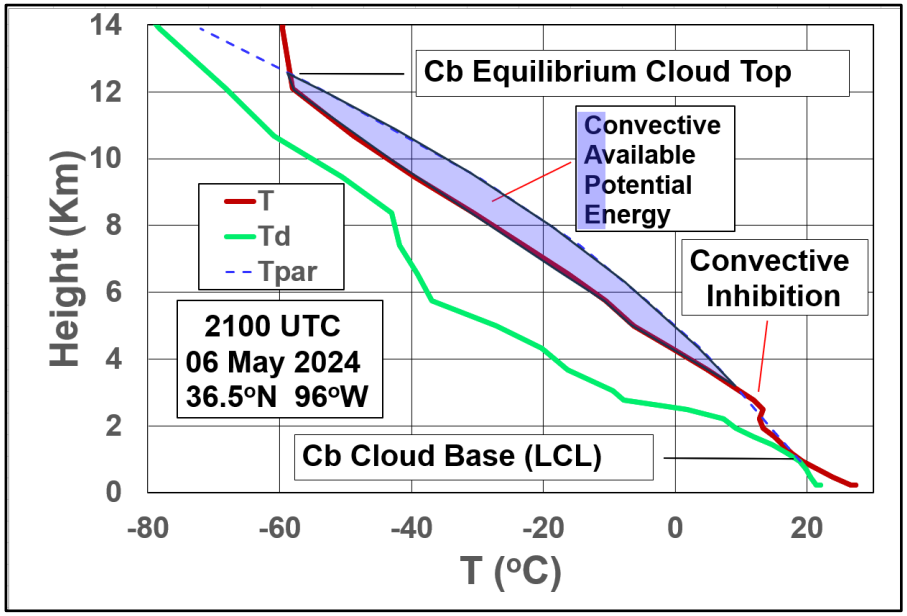

Fig. 7-9. Sounding just before tornado outbreak of 06 May 2024. SDG.

The bottom layer is the storm's moisture source. In American supercells on the Great Plains, it is a wide river of warm, humid air 1 to 2 km thick streaming up from the Gulf of Mexico. The humid layer is capped by an inversion topped by a layer of hot dry air blowing from the SW. This inhibits the convection until potential instability increases to frightening levels and later enhances the intensity by evaporative cooling.

For a supercell to form the capping inversion must be large enough to be impenetrable until major heating has built a huge potential instability. If the inversion is flimsy, convection will break out prematurely everywhere but will only produce storms of modest intensity. If it is too large it will completely suppress convection.

In the ideal scenario the capping inversion is only punctured in a few isolated places to maximize the supply of hot, humid air for each storm. Then thermals and plumes of the warm, moist air can rise into the top layer of cold dry air. The rising fountains of the warm moist air will be so much warmer and lighter than the cold dry air aloft they will race upward at speeds of perhaps 50 m/s. For supercells (and all thunderstorms), the wind shear will be large enough to tilt the updrafts so that precipitation falls off to the side but not so large that it shreds the updrafts.

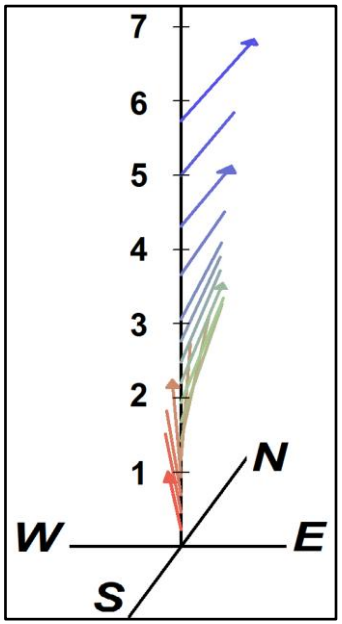

Fig. 7-10. Hodograph just before the tornado outbreak of 06 May 2024. SDG.

The sounding (Fig. 7-9) and wind profile *hodograph* (Fig. 7-10) at 2100 UTC of 06 May 2024 (three hours before the outbreak of supercell thunderstorms that spawned 33 tornadoes including an EF4 monster (see §7.5) that struck Barnsdale and Bartlesville, OK) fit the above description to a tee. The inversion extending from 2 to 2.7 km represented the region of convective inhibition, which weakened in the hours following the sounding. The lavender shaded area, where the parcel temperature exceeded the ambient temperature represents the ***C***onvective ***A***vailable ***P***otential ***E***nergy (CAPE) for the storm, a value (> 3600 J/kg) great enough to produce an updraft speed of 60 m/s (if not slowed by friction and mixing). The hodograph for the same time showed the wind from the SSE at the surface and from the SW aloft and therefore possessed significant helicity (corkscrew motion).

These general conditions persisted for the next four days over a large region that stretched and drifted eastward from Oklahoma, Iowa, and Texas, to Pennsylvania and Georgia. The result was that severe and tornadic supercell thunderstorms continued breaking, out ultimately producing 179 tornadoes.

Fig. 7-11. Thunderstorm over Africa with pancake-shaped anvil top and overshooting dome seen from the International Space Station ESA/NASA.

The concurrence of the large scale features conducive to severe weather, shown by the soundings and hodographs and therefore, the general region severe weather will break out can often be predicted days in advance. For examples, the first notices of potential severe weather for the 6 May 2024 outbreak were given a week in advance, on 29 April, and as the days went by the warnings became progressively more certain and more dire. The situation was so classic in its signature that the National Weather Service gave a rare tornado-driven high risk outlook on the morning of 6 May.

Forecasting the precise location of each supercell is much more difficult than forecasting the general region of severe weather. Indeed, it is much like forecasting which kernel of popcorn will pop first. That can only be forecast as the convection begins to develop.

7.3 Accessory Features of Thunderstorms

Thunderstorms, and particularly when severe, have several accessory features that add to their majesty and beauty. They include 1: the anvil, topped by an overshooting dome, and with undersides graced by 2: mamma and cirrus, 3: an arcus (arc or shelf cloud) attached to the advancing cloud base, or leading it as a roll cloud, 4: rain/hail shafts that may appear green or blue, and, 5: tornadoes. Lightning (Chapter 8) and rainbows (Chapter 9) are two attendant phenomena.

The mature anvil is the thunderstorm's crown. It is mostly accumulated detritus of mushroom-shaped overshooting domes that spread at the equilibrium level (recall §6.3 and §6.5). Viewed from

Space, it often resembles a pancake topped by an overshooting cauliflower dome if the updraft is active (Fig. 7-11). Circular waves may propagate out along the anvil's top when new domes puncture it.

The bulk of the mature anvil has a mostly smooth, even fibrous appearance because it consists mainly of ice particles (crystals and frozen drops) that evaporate as the air sinks down the anvil's sloping underside toward the parent storm. It takes its classic asymmetric shape (Fig. 7-12) when strong upper level winds blow it downwind to warn a thunderstorm is on the way. Videos show that motions in the anvil are, no longer turbulent or penetrative. An example is the runaway anvil of an active storm at Cheyenne, WY on 29 Jun 2025,

https://www.flickr.com/photos/cloud_spirit/54622678729/in/album-72157664743046092

The smooth base of the anvil is not featureless. Cirrus cloud tassels may form at the anvil's outer edge, with tails that tilt inward along the anvil's underside following the airflow toward the parent storm. The cirrus clouds may be separate from the anvil's base, or more often, are attached and give it a ribbed appearance, as in Fig. 4-12, Fig. 7-6, and Fig. 7-12. An example of such evolving cirrus is shown in the video,

https://www.flickr.com/photos/cloud_spirit/35292977813/in/album-72157664743046092/lightbox/

The anvil's base also may be marked by a much more prominent type of protuberance

Fig. 7-12. Thunderstorm with anvil-shaped anvil, east of Cheyenne, WY 2008 MDT 22 Jul 2017. JC.

Fig. 7-13. (Top) Sunlit mamma with rainbow and anticrepuscular rays, 12 June 2016 . (Bottom) Shaded mamma, 09 May 2018. Both at Cheyenne, WY. JC.

Mamma, smooth, breast-like pouches of sinking cloud air that hang down from anvils as in Fig. 7-2, Fig. 7-6, and Fig. 7-13. Their shape and motions are illustrated in Fig. 7-14. Mamma are more likely to form where the anvil is thick and laden with water and ice, and the air under the anvil is dry. That produces a positive feedback loop of evaporation and cooling, so that the sinking motion becomes unstable and wavelike. For the same reasons, mamma sometimes form below dense cirrus spissatus (see Fig 10-26), altocumulus or stratocumulus. Mamma appear smooth because the hydrometeors at their edges have largely evaporated. Time lapse videos show their bases disappear as they sink, as in

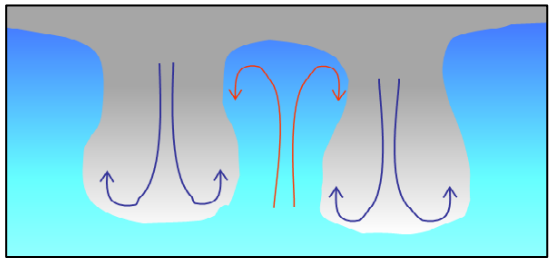

Fig. 7-14. Air motions in mamma. SDG.

https://www.flickr.com/photos/cloud_spirit/41732019035/in/album-72157671673645956

Sunlit mamma appear bright white if the Sun is not near the horizon, as in the top image of Fig. 7-13, where the scene is enriched by a double rainbow crossed by anticrepuscular rays (see Chapter 9). At sunrise and sunset, sunlit mamma reflect the light of the horizon Sun and appear yellow, orange, or deep red, as in Fig. 7-6.

Shaded mamma can appear almost pitch black, as in the almost cosmic scene in the bottom photo of Fig. 7-13. The parent cloud in that case was the optically thin remnant of what had been at most a weak thunderstorm. Mamma are often so optically thin, especially at their bottoms, that when viewed horizontally they are translucent (see Fig. 10-27). Thus, even though mamma are often associated with severe thunderstorms, they are, in and of themselves, harmless. Mamma are sometimes aligned like pearls on a string of the cirrus streamers that wrap under the anvil, as on the left side of the anvil of the supercell in Fig. 7-6, and give evidence of wavelike behavior.

Since mamma hang from the anvil they can be seen from great distances. That makes them either an early warning sign that a thunderstorm is approaching or an indicator that it is departing.

As thunderstorms draw closer, features attached to or rolling ahead of the base, come into view. These include arcus, shelf, or roll clouds), rain and hail shafts, rainbows, and tornadoes.

Arcus clouds form over or in front of the leading head of cold rain or hail-soaked downbursts that have struck the ground, splayed out ahead of the storm and curled up in ring vortices illustrated in Fig 7-5 and Fig. 7-8. Arcus clouds are harmless in and of themselves despite their awesome and even ominous appearance. However, since they form at the leading edge of the advancing thunderstorm's severe weather, the onset of the storm's fury occurs as they pass overhead, as can be seen and heard in the video of the thunderstorm that passed over Cheyenne, WY late on the afternoon of 06 Jul 2025.

https://www.flickr.com/photos/cloud_spirit/54638208522/in/album-72157667543992515

Because downbursts splay out ahead of the rain and hail, they are normally invisible unless they stir up dust. And so, without any warning they caused many aircraft fatalities before they were identified, understood, and now mostly avoided.

The arcus often resembles a smooth, gray convex plow on top, as in the top image of Fig. 7-15 and Fig. 7-16. By contrast, the underside of the arcus often appears ragged and highly convoluted, especially so in the bottom image of Fig. 7-15. The top of the arcus is smooth when the head of the advancing vortex ring at the leading edge of the downburst undercuts warm, moist air approaching the thunderstorn and forces it to rise above its condensation level before it is buoyant, because the forced flow is laminar. The underside of the arcus is ragged because it is in direct contact with highly turbulent flow of the vortex head and downburst.

Fig. 7-15. Approaching arcus with marked blue tint and rain below, Cheyenne, WY 06 Jul 2025. Ragged underside is due to turbulent flow JC.

Fig. 7-16. An arcus with smooth top and ragged bottom beneath the thunderstorm over Cheyenne, WYT 02 Aug 2023. The rain shaft is the dark gray area within the arcus. JC.

As an arcus draws overhead, the sky often becomes incredibly dark and remains so until it has passed by and rain or hail begins in earnest, whereupon the sky often brightens noticeably. This can be seen in the thunderstorm of 26 Aug 2021 (Fig. 7-17) and is apparent in the video of the 06 Jul 2025 thunderstorm.

It can be so dark under the arcus that street lights turn on even in the middle of the day. The darkness is due to the huge total cross section area or optical thickness of the myriad tiny newly formed droplets in the rising air of the arcus plus the droplets and ice particles in the main cloud above it. The rain/hail shaft is much brighter because even in a deluge the total cross section area (and hence optical thickness) of large raindrops and hailstones is minute compared to that of an equal mass of tiny droplets.

That may sound impossible, but the following example shows why it is true. A raindrop 1 mm wide is 100 times wider than a 10 μm wide cloud droplet and has 1 million times the mass. But since, for a given total mass of droplets, surface area and optical thickness is inversely proportional to radius, 1 million of those tiny cloud droplets have 100 times the total area and hence 100 times the optical thickness and light scattering power of that one large raindrop.

Fig. 7-17. Bright rain streaks behind a black arcus Cheyenne, WY 26 Aug 2021. JC.

Fig. 7-18. Chaotic thunderstorm sky Cheyenne, WY 16 Jul 2025. JC.

The turbulent flow under the approaching thunderstorm at Cheyenne, WY on 16 Jul 2025 produced patterns so chaotic and lighting contrasts so extreme (Fig. 7-18) that would make El Greco proud (see his ***View of Toledo***, Fig. 15-15). The video of the 16 Jul storm,

https://www.flickr.com/photos/cloud_spirit/54661210650/in/album-72157667543992515

brings all its chaos to life. The video starts with a distinct helical flow amidst the swirling. A cumulus line at left moves away from the camera while the overcast above moves toward the camera from the left. Soon thereafter a rippled low-lying cloud sheet moves in from the right while an arc cloud just above the distant horizon approaches. The sky darkens as the roll cloud nears, then brightens as it races overhead with bubbling motions, heavy precipitation, and a distinct blue tone.

Fig. 7-19. A roll cloud ahead of a hailstorm in Cheyanne, WY on July 04, 2023. Note distinct blue-green tone behind the roll cloud. JC.

Sometimes, the vortex outflow moves well out ahead of the parent thunderstorm, just as a smoke ring self-propagates across a room with no wind. The arcus can then detach from the parent storm, riding like a surfer on the updraft at the head of the outflow vortex as a *roll* cloud.

The roll cloud in Fig. 7-19, was produced by a strong thunderstorm that crossed Cheyenne, WY at 70 kph. As the roll cloud passed overhead the wind gusted to 80 kph and 0.6 cm of rain mixed with

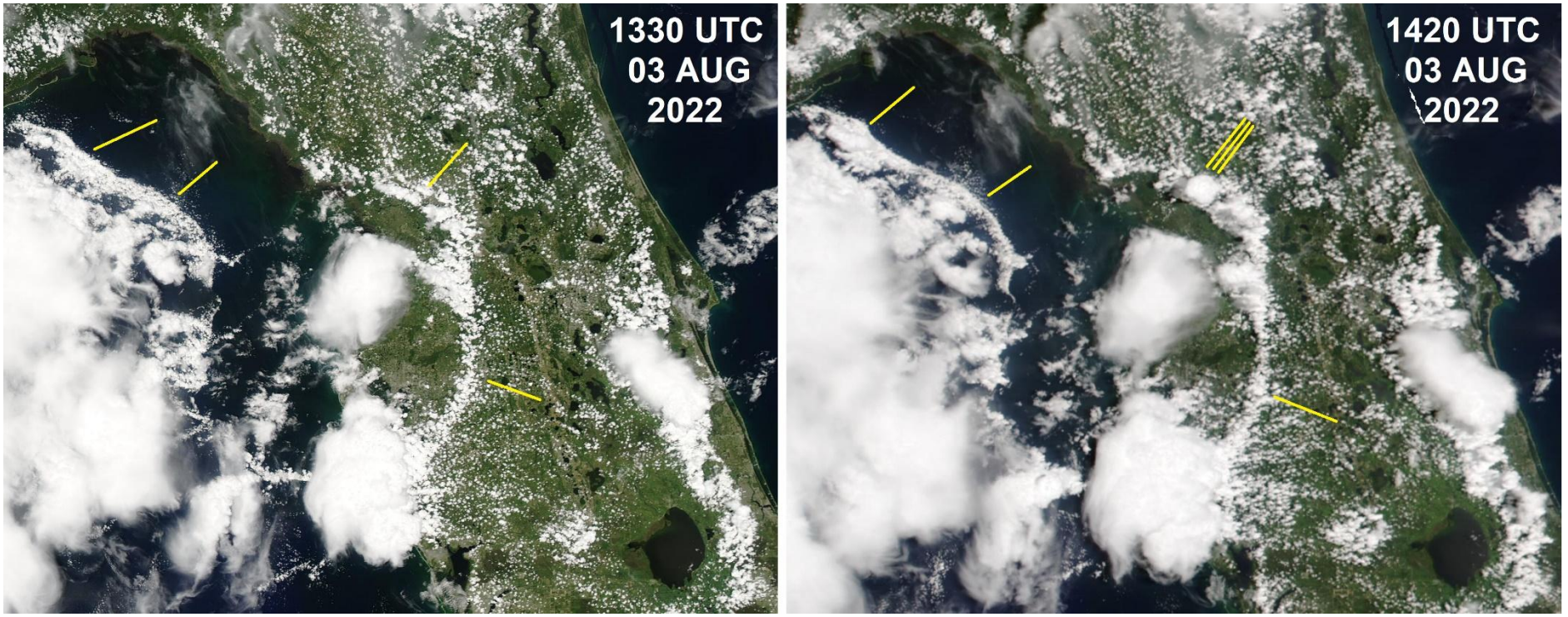

Fig. 7-20. NASA MODIS AQUA (left) and NOAA VIIRS 20 (right) views including roll clouds from thunderstorms (indicated by yellow lines) on 03 Aug 2022. The roll cloud's updraft at the leading edge of the outflow boundary boosted a cumulus cloud to develop into a new cumulonimbus at the triple yellow line.

pea-size hail fell in less than 10 minutes.

Roll clouds may appear ominous as they advance across the sky but are harmless by themselves. However, they may provide critical extra uplift needed to grow any cumulus mediocris they collide with into a new thunderstorm. This occurred in the satellite images of 3 Aug 2022 over central Florida (Fig. 7-20). Several of the cumulus clouds began to develop into cumulonimbus once boosted by the roll cloud's updraft. Satellite images with thunderstorms show that outflow boundaries, marked by roll clouds, are surprisingly common.

Similarly, if the air in the forced updraft of an arcus has a significant upward speed when it reaches the level where it becomes buoyant, it will strengthen the resulting thunderstorm updraft.

7.4 Green Thunderstorms and Rain/Hail Shafts

The rain and hail shaft behind the roll cloud of Fig. 7-19 has an unmistakable green-blue color, as does the rain shaft behind the arcus of the 06 July 2025 thunderstorm in Fig. 7-15. Other cases at Cheyenne, WY include the thunderstorm of 20 Jul 2016 (Fig. 7-21) where the the green rainshaft appears luminous in contrast with the almost pitch black underside of the turbulent arcus, and the almost blue rain-hail shaft of the thunderstorm of 08 Jun 2024 (Fig. 7-22). An extraordinary, almost bizarre case of a green thunderstorm is shown in Fig. 7-23. The hail shaft is a deep green while the bright gaps between the black blobs of the arcus that penetrate into the cloud above are turquoise.

Fig. 7-21. An arcus with dark ragged bottom and green rain/hail shaft beneath the thunderstorm at Cheyenne, WY, 20 Jul 2016. JC.

Fig. 7-22. A blue rain/hail shaft beneath the thunderstorm at Cheyenne, WY, 08 Jun 2024. JC.

Fig. 7-23. A green and blue shaft. ©Grundlesquatch.

These are the so-called green thunderstorms, though the photos show that the color varies and often contains blue. Green thunderstorms are rare enough and so distinctive that they come as a surprise. What could be their cause? Perhaps it should not be surprising. We are not surprised to see the distinctive turquoise color of shallow water. And the colored part of green thunderstorms is always the bright rain or hail shafts behind dark arcus clouds.

Fig. 7-24. Water color vs depth Paradise Island Nassau, 31 Dec 2008. SDG.

Green and blue thunderstorms occur because both water and ice preferentially absorb red and orange light, allowing green and blue light to scatter and pass through. But water's color, which grades with depth from turquoise to cobalt blue as in the Bahamas (Fig. 7-24) does not begin to emerge until the depth exceeds 10 cm (Fig. 7-25).

Fig. 7-25. Blue color deepens with water depth in pool. Each step is about 15 cm. Depth at the top step at right is only 3 cm. SDG.

The difficulty in explaining the color of green thunderstorms is that even the most prolific thunderstorm never contains much more than a depth of 10 cm of liquid water or ice. The solution is that the water in a cloud is subdivided into drops and hailstones. Scattering by the largest hydrometeors lengthens the effective optical path by at least a factor of 10 over a water body. That is more than enough to turn the beams turquoise or blue and still allow enough light through to be bright. If the 10 cm depth of hydrometeors were as small as cloud droplets they would block so much light the rain/hail shaft would be darker than the arcus. This difference is illustrated by the contrast between the luminous turquoise color of the bright gaps of the turbulent, black underside of the arcus in Fig. 7-23. The color of green thunderstorms is enhanced by skylight that penetrates the rain/hail shaft.

The apparent color of green thunderstorms changes with distance to the rain/hail shaft. Rayleigh and Mie scattering in the intervening atmosphere scatters away the blue and makes rain/hail shafts further than about 10 km tend appear green rather than blue. Rain/hail shafts close to the observer are the bluest.

Few rain/hail shafts are green or blue but even without color they can still appear almost cosmic. If shaded and if they block the light from the clear sky or sunlit clouds behind, they can be almost pitch black. If sunlit they gleam with the same color as the sunlight that strikes them, and stand out from the dark, shaded cloud base. For example, numerous sunlit rain shafts brightened the otherwise dark underside of the thunderstorm of 24 Sep 2018 (Fig. 7-26).

The thunderstorm of 14 Aug 2021 (Fig. 7-27) popped up rapidly after 1900 MDT. It produced 1 inch hail and a double rainbow. The rain/hail shafts were sunlit and bright and slightly reddened both because the Sun was only 18° above the horizon (determined by the rainbow) and by Rayleigh and Mie scattering in the intervening atmosphere. Jan noted, “The video not only showed many storm features, it showed me getting pelted by hail as I rescued a camera.”

https://www.youtube.com/watch?v=11jkffhxNd8

When shaded rain/hail shafts block bright skylight or blindingly bright reflected cloud light in the background behind a thunderstorm they can give the impression of the 10th Plague of Egypt descending from the heavens, as in the thunderstorm of 31 May 2017 (Fig. 7-28). This is a case when appearances are deceiving. The video,

https://www.flickr.com/photos/cloud_spirit/34980434346/in/album-72157667543992515

shows that while some of the streamers reached the ground as rain gushes others evaporated harmlessly before reaching the ground as *virga*. In this respect though they almost obliterate the background lighting and appear black by contrast they can be compared to opaque but delicate streamers of cirrus.

The not-so-delicate, pitch-black rain shaft of the thunderstorm on 03 Jul 2019 (Fig. 7-29) sported a *rain foot*, a rain shaft whose leading edge tilts outward from the storm. The tilt is caused by wind flowing out from thunderstorm downbursts at speeds up to 50 m/s, sweeping raindrops sideways because they only fall at about 7 m/s.

Hailstones, a product of some severe thunderstorms, can grow much larger than raindrops. Stones about 2.5 cm in diameter fall at about 12 m/s. It is the really large stones, 8 cm or more in diameter that fall 50 m/s or more and have been lethal. The largest measured hailstone was 20 cm across and weighed 760 grams (Fig. 7-30). It fell on Vivian, SD on 23 Jul 2010.

How in the world can the atmosphere produce such monsters? The answer is rapid updrafts, which only occur in severe thunderstorms, can suspend the hailstones for perhaps half an hour at levels high in the atmosphere where it is cold enough for supercooled drops to strike them and freeze to them. When they finally do fall from the cloud through the warmer air below melting must be minimized. This is why hailstorms tend to occur in elevated locations such as Wyoming and Kenya and why hail is so rare in tropical lowlands or places like Florida despite abundant thunderstorms.

Fig. 7-26. Sunlit rain shafts from the thunderstorm at Cheyenne, WY, 24 Sep 2018. JC.

Fig. 7-27. Sunlit hail and rain shafts from the thunderstorm at Cheyenne, WY, 14 Aug 2021. JC.

Fig. 7-28. Shaded rain shafts and virga appear almost black in contrast with sunlit background at Cheyenne, WY, 31 May 2017. JC.

Fig. 7-29. Rain/hail foot, Cheyenne, WY, 03 Jul 2019. JC.

Fig. 7-30. Vivian, SD record hailstone with ruler marked in inches. NOAA.

Fig. 7-31. Tornado (EF5) of 22 Jun 2007 at Elie, Manitoba with debris. ©Justin Hobson.

7.5 Tornadoes

Tornados are the umbilical cords of thunderstorms, attaching them to Mother Earth, but bringing death instead of life.

It should be no surprise that the thunderstorms with the awesome updrafts needed to produce large hail also produce the atmosphere's single most terrifying phenomenon, the tornado. (To supplement this brief section, we highly recommend Chapter 5 in ***The Architecture of Clouds*** by Howard Bluestein.)

The United States, because of its particular geography, is the tornado capital of the world, with an average of about 1200 per year. Tornadoes are graded on the EF (Enhanced Fujita) scale, originally devised by Tetsuro Fujita. The scale is based on the maximum 3-second wind gust speed (EF3 > 215 kph, EF4 >265 kph, EF5 > 320 kph) and closely linked to the severity and nature of the damage. EF4 and EF5 tornadoes can do incredible damage, obliterating solid brick homes, levelling forests, stripping bark from trees left standing, and ripping away the soil to the bare rock below.

The highest wind speed ever recorded on or near the surface of the Earth was 517 kph during the Moore, OK tornado of 03 May 1999. It was measured remotely by a mobile doppler radar unit. (Another lethal EF5 tornado hit Moore on 20 May 2013.)

Tornadoes are rendered visible both by the debris they lift and swirl in the air and by condensation due to reduced air pressure in the vortex by up to about 10% of the ambient atmospheric pressure. This enough to make the tornado visible at the ground from a cloud with base 1 km. One irony is that as the tornado intensifies, the visible tube may descend to the ground all the while the air spirals upward.

The classical funnel cloud (Fig. 7-31) or *tuba* is narrowest at the ground and widens the closer it gets to cloud base because as the air spirals upward $\boldsymbol{T}$ approaches $\boldsymbol{T}_d$ and only requires a smaller pressure decrease within the vortex to produce condensation. Thus, the visible vortex cloud is only the inner, visible part of the tornado vortex; the outer, invisible part of the vortex can still blow you away.

Fig. 7-32. 1.6 km-wide EF4 Tornado Binger, OK, 22 May 1981. NSSL Photo.

The width of tornadoes varies from about 10 m to 4 km and the path length ranges up to 1000 km. In general, the more violent the tornado the wider it is and the longer its path on the ground. The typical EF0 tornado is about 20 m wide, has a path length of 1 km and a maximum wind gust of 120 kph. The typical EF4 tornado is about 500 m wide, has a path length of 40 km and a maximum wind gust over 265 kph! Ironically, the extreme width of many EF4 and EF5 tornadoes plus the enormous airborne debris makes them less photogenic than many much less intense tornadoes.These "wedge" tornadoes resemble short, wide black tubes extending down from cloud base that obliterate any sight of the ground. The 1.6 km wide Binger Tornado of 22 May 1981 (Fig. 7-32) was one terrible example

Weak tornadoes (even the weakest have wind gusts of 104 kph) can have smooth outlines and will appear light or dark like all clouds, depending on whether they are sunlit or shaded. The short-lived sunlit tornado of 17 Jun 2017 to the NE of Cheyenne, WY (Fig. 7-33) was captured in the video,

https://www.flickr.com/photos/79387036@N07/33711850968/in/dateposted/

Fig. 7-33. Tornado 10 km NE of Cheyenne, WY, 17 Jun 2017. JC.

One of the most celebrated photographs of a sunlit tornado was taken by storm chaser, Eric Nguyen and was at the correct angle (42° from the antisolar point) to include a rainbow (Fig. 7-34). The white dots and vertical streaks are hailstone tracks. Why the streaks (which also appear during rainstorms)? During the time of the exposure, typically $1/250^{th}$ of a second a hailstone that falls at 25 m/s will fall 10 cm and consequently look vertically elongated if near the camera.

Some supercell thunderstorms generate several tornadoes during their lifetimes of several hours. On rare occasion, a supercell will spout two tornadoes at the same time (Fig. 7-35).

The airflow in tornadoes is so rapid and has such large shear that it may become unstable and generate smaller, short-lived vortices that

Fig. 7-34. Sunlit tornado of 12 Jun 2004 near Mulvane, KS with rainbow and white hail streaks. ©Eric Nguyen.

whirl around the main vortex like whirling dervishes. Multiple vortex tornadoes (Fig. 7-36) are not seen often but are more common than would appear because the narrow, short-lived vortices are easily visible only during clear intervals when the main vortex is not filled with a funnel cloud.

Fig. 7-35. Double tornado (EF4) near Pilger, NE, 16 Jun 2014 Ethan Schisler/NOAA Weather in Focus Photo Contest 2015.

Fig. 7-36. Multiple vortex EF4 tornado of 09 May 2016 near Katie, OK. Justin Cox, KFOR TV, OKC. https://www.youtube.com/watch?v=T5Et2iIzdgI

Tornadoes are more likely to develop multiple vortices when the swirling speed is much greater than updraft speed. The secondary vortices or 'suction' vortices make multiple-vortex tornadoes potentially the deadliest because wind speed is increased in the places where the wind of the small vortices adds to the wind of the main vortex. The deadly Xenia, OH tornado of 03 Apr 1974, at times a wide, 'wedge' tornado and certainly no pretty sight (Fig. 7-37) was perhaps the most notorious multiple vortex tornado. It killed 32 people, destroyed much of Xenia, and, with wind speeds estimated up to 500 kph was among the strongest tornadoes ever recorded.

Fig. 7-37. Xenia OH tornado, 03 Apr 1974, laden with debris. ©Fred Stewart, Xenia Hospital.

It is mind boggling that almost all that is known about severe thunderstorms and tornadoes was unknown until quite recently, and long after the nature and properties of atoms were discovered. Storm chasing is a relatively new activity, begun by Roger Jensen in 1953 and David Hoadley in 1956, neither of whom were professional meteorologists. Tetsuro Fujita was among the early researchers, who worked in good part by analyzing damage patterns left by the storms some time after they had ended. Serious professional storm chasers did not begin work until the 1970's. Over the years, and especially

inspired by the film, Twister (1996) more and more people took up storm chasing. Now, professional and amateur storm chasers crowd the roads every time severe weather is forecast and provide images, videos, and measurements of these awesome storms, The increase of attention and knowledge also inspired people unwittingly living in the path of these storms to photograph and video them, sometimes putting themselves in extreme danger.

It might seem a crazy thing to chase tornadic storms given that tornadoes have killed so many hapless people in their paths, and certainly it is dangerous even when great care is taken. But there is a science to it that turns the odds in the savvy storm chasers' favor.

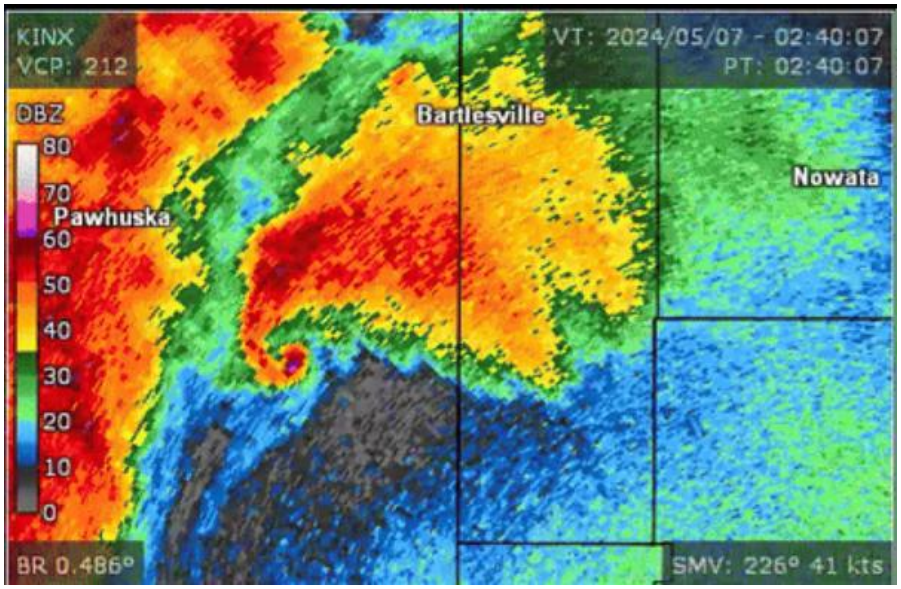

Fig. 7-37. Radar image of Bartlesville, OK tornado of 07 May 2024 showing classic 'hook' echo at SW and debris echo at the tip of the hook. NOAA.

The classic supercell thunderstorm (Fig 7-5) places the tornado at its southwest corner. Storm chasers will therefore try to place themselves under clear skies if possible, south of any promising supercells. They must know the roads well, should have a vehicle designed for storm chasing, and have access to current forecasts and, of course, live radar imagery.

Weather radar provides a way to 'see', quantify, and provide life-saving, short-range forecasts of supercell thunderstorms and the tornadoes they spawn. Doppler radar, which records the line-of-sight speed (toward or away from the radar) of hydrometeors can often detect rotation within supercells before the tornadoes extend and appear below the cloud and touch down on the ground. The classic radar signal of a tornado is a hook echo, the end of which is sometimes an echo of lifted debris, as in the Bartlesville, OK tornado of 07 May 2024 (Fig. 7-37). The hook occurs because large, radar reflecting raindrops and hailstones take time to grow and are only present in the region of the storm surrounding the core of the main updraft (called the bounded weak echo region), which mainly contains small droplets and ice particles that have not had the time to grow large enough to reflect the microwaves efficiently.

Photos and videos of thunderstorms, spectacular as they are, can never convey a full idea of their awesome nature. Only direct experience can do this. Seeing is believing, but more than seeing – all the senses can be involved. The locomotive roar of the wind that can not only blow you down but toss you around and vault you into the air or ram a piece of straw through solid wood, the whistling and impact of large hailstones crashing into objects on the ground are difficult to believe if not experienced (and survived). Indeed, you need hear just one crash of thunder from the explosive expansion and contraction of air due to a nearby bolt of lightning to get some idea of how terrorizing thunderstorms and their attendant phenomena can be. And after the storm has passed and you view the storm's magnificence as it moves off into the distance, a brilliant rainbow may arc across the sky to impart a feeling of reverence for the wonder of nature that a thunderstorm is.

A few hours later, when only remnants of the anvil remain of the once glorious and terrifying storm, now disintegrated and vanished into the thin air it congealed out of, a sense of wonder persists, that mere air can do all this!

7.6 Cumulonimbus Gallery

Fig. 7-38. Cumulonimbus entraining low-level moist air and dark attendant cloud Cheyenne, WY, 07 Jul 2019. JC.

Fig. 7-39. Twilight of the Gods, Cheyenne, WY, 20 May 2020. JC.

Fig. 7-40. Dying cumulonimbus with aligned mamma at Cheyenne, WY, 27 May 2022. JC.

Fig. 7-41. Rare cumulonimbus with classical anvil shape and overshooting dome 50 east of San Mateo, CA, 1 Oct 2015. SDG.

Fig. 7-42. Cumulonimbus at sunset over Cheyenne, WY, 13 Jun 2021. JC.

Fig. 7-43. Mamma at dawn over NYC facing west (left) and east (right) on 19 Oct 2011. SDG.

Fig. 7-44. Mamma in altocumulus over San Mateo, CA, 7 Oct 2013. SDG.

Fig. 7-45. Mushroom-shaped mamma in cirrus, Boynton Beach, FL, 13 Feb 2024. SDG.

Top frame. Fig. 7-46. Blue hail core of thunderstorm near Stratford, TX, 18 May 2023. Hail was up to the size of tennis balls. © Kyle Cutler. Bottom frame. Fig. 7-47. Triple twilight thunderstorm, Cheyenne, WY, 7 Jul 2025. JC.

Fig. 7-48. Color-graded twilight cumulonimbus. NOAA Weather in Focus Photo Contest 2015. Jeremy Bower.

Wonders of the Atmosphere
Chapter 8: Lightning

Fig. 8-1. Lightning at sunset with rain fall streaks over Cheyenne, WY, 21 July 2020. JC.

Fig. 8-2. Lightning illuminating its thunderstorm during the 'blue hour' of twilight more than 30 min after sunset over Cheyenne, WY, 13 Jun 2021. JC.

Wonders of the Atmosphere
Chapter 8: Lightning

8.1 Thunderbolts

Fig. 8-3. Lightning strike less than 300 m away, Oracle, AZ, 10 Aug 2022 JC.

In distant thunderstorms, lightning (Fig. 8-1, Fig. 8-2) often puts on a silent light show for the viewing pleasure of spectators. Careful though, for a little later, with no warning, a blinding flash of lightning (Fig. 8-3) zaps down to the ground perilously close, turning night into day for an instant. A fraction of a second later, the concussion of thunder's sonic boom rattles, terrorizing and deafening people and animals on the ground who barely escaped death.

Thunder may well be the atmosphere's most terrifying natural phenomenon and it is certainly is the most startling because of its sudden, deafening sonic boom, enough to make anyone jump out of their skin. Thunder can deafen and stun, but the lightning that causes it is the real culprit, killing by electrocution. Little wonder that almost every ancient religion had its god of lightning and thunder, often the chief god, who threw thunderbolts. That includes Yahweh and Allah.

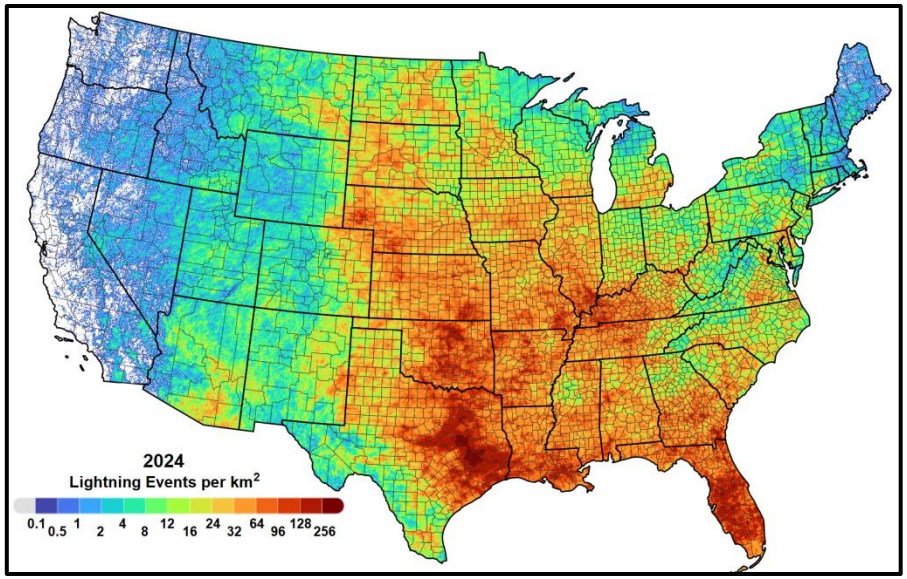

Fig. 8-4. Lightning strikes per km² in the United States 2024. Vaisala

Throwing lightning bolts must keep the gods quite busy for, in righteous anger as lessons to the wayward, they throw some 1.4 billion bolts a year (Fig. 7-2 and Fig. 8-4) or 45 per second. At least once, however, Zeus was sad he had to throw a bolt.

When Phaethon, son of a mortal woman, discovered that his father was Apollo, the Greek God of the Sun, he extorted a gift from his father to drive the Chariot of the Sun across the sky for just one day. Almost immediately on the steep climb after dawn, Phaethon lost control of the horses that drew the chariot, which went awry across the sky creating the Sahara Desert among other disasters. Zeus had to throw his bolt, killing the poor lad, who fell to Earth as a shooting star.

On 24 Dec 1971, 17-year old Juliane Koepcke fell to Earth but survived after a lightning bolt struck Lansa Flight 508 on its way to Pucallpa, Peru in the Amazon Rainforest. Lightning hits planes so often they are designed with an outer metal shell to direct it away harmlessly. But on 24 Dec 1971 the plane's shell failed. The plane broke apart 3 km above the rainforest and ejected the passengers in midair.

Juliane survived the fall by a freakish combination of events. She was strapped to her seat, which acted like a parachute that was likely slowed further by the thunderstorm updraft. Finally, the impact was buffered by shredding through the rainforest canopy. Fourteen other passengers survived the fall, but only Juliane, trained in survival techniques, made it out alive despite multiple injuries.

Lightning claims between 2000 and 24,000 lives annually around the world (Estimates vary widely.) The situation has become much better in the United States. Up until the early 1950's lightning used to claim between 200 and 400 American lives annually, but since then Americans have become much more lightning savvy, and the death toll has fallen to only about 15. This means that in the United States, less than 1 in a million lightning flashes results in a death. More than 10 times as many are struck by lightning but survive, though often with debilitating physical and psychological injuries.

The impossibility of predicting precisely when and where a bolt will strike increases its danger by surprise. This was illustrated by a video taken during a soccer match in 2024 in Peru. The unsuspecting players were walking calmly across the field during a break in the match and simply fell over like pick-up sticks as the lightning ran invisibly along the ground (though it sometimes leaves scars as in Fig. 8-5) and through them. One player never got up.

An earlier event that drew international attention to what can happen if you stand out in the open or under a tree during a thunderstorm took place on 28 June 1975 when the golfing great Lee Trevino and two others were struck by lightning that ran along the wetted ground on the 13th hole. Each survived but was seriously injured. Trevino needed two spinal surgeries and it was a few years before he played competitive golf again. Alerted by this incident, American deaths from lightning strikes dropped below 100 for good that year.

Fig. 8-5. A hole in one. Radial damage pattern from a lightning bolt that struck the flag. Posted by @RickShielsPGA, 14 Jul 2020.

Exposed sites such as open fields, golf courses, beaches, and especially water bodies such as lakes, increase one's vulnerability. Standing under a solitary tree, hoping for protection from a thunderstorm, is now widely known as a dangerous thing to do. A recent video, posted 04 Jul 2023 of 31 cattle killed while huddling under a tree during a storm in Cullman County, AB illustrates that danger.

https://www.youtube.com/watch?v=_dy65dpH_IY

> Jan: "In preparing photographs and videos, I have been within 30 m of a lightning strike a half dozen times despite beating strategic retreats. Once I was knocked over and deafened for ten minutes by a nearby bolt that shattered the small tree I was

standing near moments earlier. At a different time and place, several of my relatives were struck but survived a nearby bolt that traveled along the wet ground."

Fig. 8-6. Panorama of thunderstorm with lightning, 100 km east of Cheyenne, WY, 20 May 2021. JC.

Fig. 8-7. Last gasp lightning striking ground from a dying thunderstorm over Tucson, AZ, 16 Aug 2018. JC.

Now, with lightning detectors as simple as AM radios and extreme vigilance few Americans mess around with lightning. In Sapphire, NC, one of countless places around the United States, as thunderstorms near, sirens, tripped by lightning detectors, go off requiring people to get out of Fairfield Lake, away from the beach, and out of local pools. Discretion is the better part of valor.

Lightning statistics have become quite accurate over the past 25 years as sensor technology has improved and spread. The National Lightning Detection Network recorded an annual average in the United States of 23 million flashes, 55 million strokes (the visible bright, flickering light we see) and 36.8 million ground strike points. During the peak lightning month (June), about 3.7 million strikes occur. Florida, the nation's thunderstorm capital, has the highest concentration of strikes at 116/km^2. The West Coast, chilled by the cold California current that suppresses convective activity, has the lowest strike rate of < 1/km^2 (Fig. 8-4).

Fig. 8-8. Chaitén eruption cloud 03 May 2008 and its lightning bolts including a rare green bolt. ©Carlos Gutierrez UPI/Landov.

Thunderstorms produce the vast majority of lightning strikes (e. g., Fig. 8-1, Fig. 8-2, Fig. 8-6, and Fig. 8-7). Ash-laden *pino* (pine tree shaped) clouds from volcanic eruptions produce abundant lightning strikes but major eruptions occur much less often than thunderstorms. The eruption cloud of Chaitén (Satan), Chile on 03 May 2008 (Fig. 8-8) produced myriad lighting strikes, at least one of which was bright green, by discharging O atoms much as in the aurora. Sandstorms and major earthquakes also can produce lightning.

Lightning has been both a curse and a blessing. In the Western United States lightning is the cause of more than 50% of the wildfires because it often strikes dry ground with desiccated vegetation as tinder. It may have been in the lightning burned areas of the African Savannah where early humans foraged that lighting's spark first taught humans to save and perhaps even create fire by striking rocks together and later, learning to strike flint and iron pyrite together to create a spark that would ignite dry tinder.

8.2 Lightning and Thunder Characteristics

Lightning is a giant electrical spark. Even those who know the numbers remain impressed. The core temperature of a lightning bolt may exceed 30,000°C, making it brighter and bluer than the Sun. The typical flash packs a wallop of 300 million volts and 30,000 amps, and extreme bolts may exceed 1 billion volts and 200,000 amps. Compare this to typical American household electricity of 110 volts and circuit breakers of 25 or 50 amps. Each bolt releases between about 50 and 1500 kilowatt hours of energy, depending on the type of lightning[6]. That is enough to power the typical American home between about 2 and 50 days. If only we could capture that energy!

The typical length of a lightning bolt is of order 10 km but some can be much, much longer. The longest documented single bolt stretched 766 km from Texas across Louisiana to Mississippi. And the bolts can emanate from the thunderstorm anvil, far from all the weather on the ground and literally strike as a bolt from the blue.

Anyone who has seen lightning knows it travels fast. When a bolt is forging its path its typical speed is 300,000 km per *hour*. Once the lightning channel is established the bolts travel much, much faster, at up to one third the speed of light, or about 100,000 km per *second*. Since sound travels much slower – 1 km in just under 3 s, hearing thunder 3 s after seeing a lightning flash (whose light travels at the speed of light) means the nearest part of the bolt was 1 km away.

The near instantaneous enormous heating of the air along the channel of the bolt produces the explosive, supersonic expansion shock wave that is thunder. The thunder's sound is intimately connected with the pressure wave of the expanding air, which can certainly produce temporary deafness and even damage the ear drum.

Thunder can vary from a deafening and shocking clap that can scare the wits out of anyone to a prolonged rumble. It may start with a preliminary hiss, then a bang, and can echo or reverberate for what seems to be an eternity but rarely lasts 30 seconds. Of course multiple closely spaced and timed bolts can prolong the noise considerably.

The peak decibel level of thunder depends on the power of the lightning bolt, its distance, and its orientation. Thunder from bolts that strike close by tend to be louder because sound weakens as it spreads with distance. The decibel level is higher and lasts a shorter time when the bolt is oriented at near right angles to the observer so that all the noise reaches at almost the same time. Jan's recording of such a booming thunderbolt with follow-up reverberations can be heard along with the lightning that produced it at,

https://www.flickr.com/photos/79387036@N07/51417257579

8.3 Discovering the Nature of Lightning

How do thunderstorms manage to produce lightning? Discovering the nature of lightning and how it forms took centuries, even after the

Scientific Revolution, and is now at last mostly but still not fully answered.

Understanding lightning began with the realization that it might be a giant spark. The same electrical buildup and breakdown via sparks, but on a much smaller scale than lightning, occurs when you strike flint against pyrite or rub amber against fur as the Ancient Greeks did. (Little wonder that the words, electron and electricity were taken from ēlektron, the Greek word for amber.) More commonly, sparks occur when you remove sweaters, walk across a carpet in dry weather, or rub a balloon against your hair. As the opposite charges build, extending your hand toward the doorknob or bringing the balloon close can create a spark (or cause your hair to stand on end). The spark can sting, but holding a metal key so that the electric charge goes through the key to the doorknob or balloon (which may pop) eliminates the pain, somewhat like a lightning rod.

Rubbing produces static electricity by a *triboelectric* effect (tribo = rubbing) that transfers negative charge from your hair to the balloon. Exactly how and why electric charge is transferred by rubbing or striking two objects, in particular when both objects are made of the same material, is still not fully understood.

Scientists and aficionados began to investigate electricity seriously in the 1600's. In 1746, Pieter van Musschenbroch invented a device to store electric charges he generated with a friction machine. Benjamin Franklin called the storage device a Leyden jar and built his own, for experiments and entertainment such as electrocuting a turkey. On his first attempt, Franklin almost killed himself by accidentally giving himself the shock designated for the turkey.

Franklin had more in mind than mere entertainment. The repulsion of the two strands of the Leyden jar led to his discovery that there are positive and negative electric charges, with like charges repelling and opposite charges attracting. And, of course, his famous 1752 kite experiment during a thunderstorm, which did give him small shocks, proved that lightning is a giant electrical spark.

The lightning rod was Franklin's great life-saving contribution. Though it might capture more strokes by sticking up above the main structure, it guides the current safely into the ground. It took several decades for Franklin's invention to be widely adopted. In that interval, many lives were needlessly lost. Perhaps the paradigm case was when in 1769 lightning struck the unprotected Church of St. Nazaire in Brescia (now Italy), which served as a repository for 100 tons of gunpowder. The resulting explosion destroyed $\frac{1}{6}^{th}$ of the city and killed 3000 people. That event went a giant step toward replacing church bell ringers (many of whom were electrocuted) with lightning rods as a more effective form of protection from lightning.

8.4 How Thunderstorms Generate Charge

Thunderstorms are in effect combined electric generators and capacitors, both building and storing electric charges until the air can take it no longer, and a sudden discharge occurs.

The electrification process begins with a background electric field. Cosmic rays (mainly protons) that bombard Earth from Space give the ionosphere a positive + charge while the Earth has a negative – charge. The atmosphere's potential or voltage gradient averages 100 V/m and though positive charges constantly leak down from the ionosphere to the ground, the air is normally an insulator that easily withstands the average voltage gradient. But thunderstorms raise the voltage gradient by orders of magnitude, causing the air to break down as an insulator and become a conductor.

How does a thunderstorm act as a friction machine and capacitor? The rubbing that in a thunderstorm is the collision of hydrometeors. The great hint that ice is involved is that thunderstorms only produce lightning when the cloud top temperature is below about -20°C. Ice particles also tend to separate after colliding, which is necessary for separating electric charges. In the sub-freezing region, the hydrometeors consist of a mix of supercooled droplets, ice crystals,

graupel (ice particles that have accreted a community of droplets), and hail.

The primary charging occurs when graupel and crystals collide. Warning: The sign of the charging depends on condensed water and ice content, collision rates, and temperature. When these values are

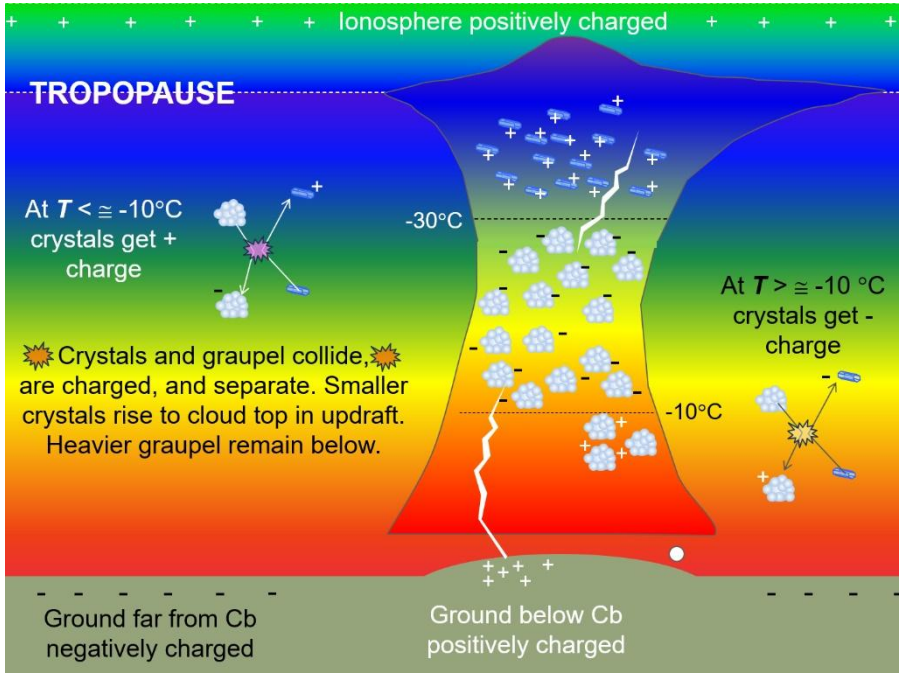

Fig. 8-9. Lightning (cloud to cloud and cloud to ground) and the generation of electrical charges in a thunderstorm. SDG.

1: low, collisions give ice crystals + charge and graupel – charge. This charging dominates most thunderstorms for -30°C < ***T*** < -10°C.

2: high, collisions give ice crystals – charge and graupel, + charge. This charging dominates most thunderstorms for -10°C < ***T*** < 0°C.

The resulting situation and electrification charging processes are illustrated in Fig. 8-9. Inside the thunderstorm, crystals with + charge dominate the upper part of the cloud, usually where ***T*** < -30°C. Graupel with – charge dominate in the middle heights of the cloud between about -30°C < ***T*** < -10°C. A smaller region of graupel with + charge dominates nearer the cloud bottom for -10°C < ***T*** < 0°C.

The segregation of + from – electric charge into separate regions in a thunderstorm occurs because ice crystals and graupel segregate. Most ice crystals are smaller and lighter and have a slower terminal velocity than most graupel, so the crystals get swept up high in the cloud by the updraft while the graupel remain below.

This explains why cumulonimbus is the by far the main cloud genus to produce lightning. If there is no strong updraft extending high in the troposphere, there is no charge separation and no lightning. That is why cumulus humilis, stratocumulus, altocumulus, cirrocumulus, cirrus, stratus, altostratus, and cirrostratus, all with their gentle updrafts or circulations and little or no accretion do not produce lightning. Lightning and thunder do occur in the stratiform shields of organized thunderstorm clusters, or Mesoscale Convective Systems (MCS) and intense winter storms and but only in or associated with embedded thunderstorms. In blizzards it is called thunder snow.

Lightning bolts represent the attempt to neutralize + and – charge concentrations in the separate regions of the cloud that have grown excessive and at the same time reduce excessive electric field gradients.

Since the two major repositories of charge are the + charged crystals high in the cloud and the – charged graupel lower in the cloud, more than ⅔ of all lightning flashes occur within the cloud or between two nearby thunderstorm clouds. Less than about ⅓ of all lightning bolts occur between the cloud and the ground.

8.5 The Life of a Lightning Bolt

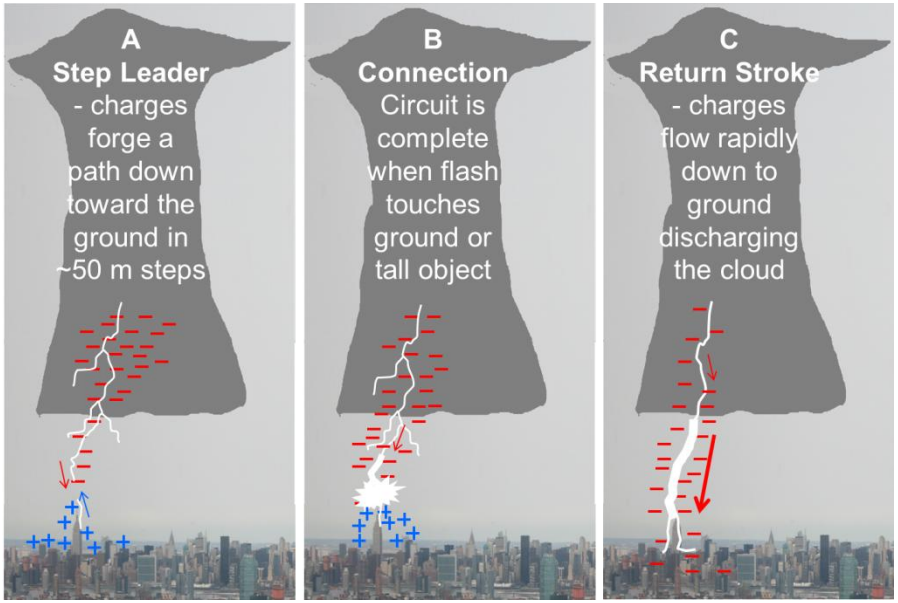

Fig. 8-10. Stages in cloud to ground lightning stroke. A: Step leader, B: Connection, C: 'Return' stroke. SDG.

Fig. 8-11. Step leader. A stack of 100 frames over 0.25 s on 31 Jul 2022. JC. In any single frame the leads look like short, isolated meteor trails.

Lightning bolts evolve in a series of stages, illustrated in Fig. 8-10 for the case of cloud-to-ground lightning. As the predominantly – charge region lower in the thunderstorm forms, it repels the normally small – charge on the ground enough so that the ground beneath thunderstorms becomes + charged. The + charges on the ground, attracted to the – charges in the cloud, concentrate on any high point such as a mountain, a hill, a tall building or church steeple, a tree, or even a flag on the green of a golf course.

Fig. 8-12. The change between the step leader (top) and the bright return flash for cloud-to-ground lightning, Cheyenne, WY, 26 Aug 2023. JC.

As the charges in the cloud continue building, the electric field gradient eventually surpasses the insulating capacity of the air and a conducting channel of – charges begins moving away, either toward the + charge region above (which will produce cloud to cloud lightning) or down to the ground. This is called the step leader because it occurs in steps of roughly 50 m, with branching paths (most failing) as the insulating property of the air is overcome.

In its effort to forge a conducting channel (essentially a wire of ionized air), the step leader zigzags downward with many failed leads of short, rapidly fading meteor-like trails in a 'forked' pattern, (Fig. 8-11) hence it is sometimes called *forked lightning*. As the step leader nears the ground, it is attracted to a streamer, a channel of positive charge reaching up, usually from a tall object, such as a tree, house, telephone pole, or the Empire State Building.

Step leaders reach the ground in a millisecond, so quickly that the human eye cannot distinguish them from the main, return strokes that follow though ultrafast photography can, as in the stack of 100 closely spaced frames over 0.25 s on 31 Jul 2022 (Fig. 8-11) which make the leaders appear continuous. These frames are part of the video

https://www.flickr.com/photos/79387036@N07/52256821316/

The video animates 15 minutes of intense lightning activity, slowing for each event. It highlights the step leader's erratic advance and explosive change to the main, *return stroke* after leader and streamer connect. The return stroke propagates upward at up to ⅓ the speed of light (100,000 km/s). Its enormous current and voltage make it ill-advised to stand under or near a tall object during a thunderstorm! The two photos in Fig. 8-12 capture the change that occurred from the step leader to the main stroke. The video's final bolt almost knocked Jan to the ground.

The visible flash of the main, return stroke propagates upward as the negative charges move downward. This seeming paradox results from the difference between wave propagation and the motion of matter. Analogies abound. Earthquake waves propagate around and through the world but the plates move up to 50 m. After a dam bursts, water rushes downstream but the wave of depression in the reservoir propagates upstream. And, as cars start moving forward when a traffic light turns green the wave of openings propagates backward.

A single return stroke seldom discharges the cloud completely. Up to 30 return strokes may occur within a half second after the initial discharge to complete the job until the charges rebuild.

Fig. 8-13 Five cloud-to-ground (CG) strikes in 2.5 min within 5 miles from an approaching storm at Cheyenne, WY on 30 Sep 2023. JC.

8.6 Inventory of Lightning Types

Lightning bolts connect regions of opposite charge. Believe it or not, there are several different types of bolts. The most common are intracloud bolts followed by cloud-to-ground bolts that transport – charges downward (–CG). Less common are cloud-to-ground bolts that transport + charge downward (+CG), ground-to-cloud bolts, cloud-to-cloud bolts (CC) and cloud to air (CA) bolts.

Negative Cloud to Ground (–CG) **Lightning** starts from the main region of – charged graupel. It is distinguished by its downward diverging branches that accompany the main strokes, as in Fig. 8-3, Fig. 8-7, Fig. 8-12, and Fig. 8-13. This type of lightning tends to occur later in the lifespan of a thunderstorm, specifically after it has developed strong downdrafts, which increase the electric field gradient near the ground by transporting negative charges downward. Just think of getting a shock from a spark when you bring your hand closer to a doorknob after walking across a rug on a dry day.

Fig. 8-14. A single +CG strike 300 m away with branches not reaching the ground, Cheyenne, WY, 26 Aug 2021. JC.

Positive Cloud to Ground (+CG) **Lightning** gives the ground a positive charge by transporting the more mobile negative charges upward. +CG starts with a downward-moving positively charged stepped leader from the region of positive charge near cloud base or high in the cloud, particularly from the anvil. It is usually associated with organized, severe thunderstorms including supercells, the trailing stratiform precipitation regions of squall lines, and mesoscale convective systems.

Sprites (see §8.7) are usually associated with (+CG) lightning.

Fig. 8-15. A bolt from high in the cloud out into clear air. ©MarianMalaquin

Fig. 8-16. Ground to cloud lightning is identified by the divergence of strikes up from the ground, south of Santa Fe, NM, 3 Aug 2012. JC.

+CG lightning bolts represent less than 5% of all cloud to ground strikes but are on average 10 times more energetic than –CG lightning. The features that distinguish +CG bolts include,

Fig. 8-17. Stacks of frames showing cloud-to-air lightning (top) and Anvil crawlers, (bottom) with a few distant cloud-to-ground bolts, Cheyenne, WY. 29 May 2020. Stacking prevents blurring and reduces overexposure but can weave separate bolts. JC.

1: branches tending not to reach the ground,
2: often a single strike,
3: great brightness,
4: loud thunder with a series of deep, low-frequency sonic booms.

Sometimes, long, bright +CG bolts extend from high in the cloud or the base of the anvil miles out into clear air (Fig. 8-15), striking by complete surprise, hence the saying, "out of the blue".

Ground to Cloud (GC) Lightning (Fig. 8-16) is distinguished by upward diverging branches, though some upward-moving lightning is branchless below the cloud base. It often emanates from elevated points on the ground where it is often seen extending up from the tops of skyscrapers. Negative charge may move up or down.

Cloud-to-Air (CA) Lightning is a discharge that jumps from a cloud into clear air and terminates abruptly, sometimes as a branch of the main channel of cloud to ground lightning (Fig. 8-17).

Fig. 8-18. Intracloud lightning stays within the confines of the cloud, Cheyenne, WY, 13 Jun 2021. JC.

Intracloud (IC) Lightning is the most common type of discharge (⅔ to ¾ of all strikes) and refers to lightning embedded within a single storm cloud, which jumps between opposite charge regions in the same cloud (Fig. 8-18 and Fig. 8-19). Early in the thunderstorm's life IC is by far the dominant form of lightning. However, once strong downdrafts form, which transport negative charges closer to the ground CG lightning increases and IC lightning subsides.

Sheet Lightning is a term used to describe clouds illuminated by lightning discharges where the actual lightning channels are either inside the cloud or below the horizon (i.e. not visible to the observer). Although sheet lightning is often associated with IC lightning, it includes any lightning bolts blocked from direct view by clouds, terrain, or the Earth's curvature (Fig 8-19).

A related term, *heat lightning*, is any lightning or lightning-induced illumination too far away for thunder to be heard (recall Fig. 2-39 top). Heat lightning got its name because it is often seen on hot summer nights with distant thunderstorms.

Fig. 8-19. Sheet lightning with an isolated distinct bolt at right, east of Cheyenne, WY, 16 Jul 2018. JC.

Fig. 8-20. Anvil crawlers move horizontally along the base of the anvil while CG strikes are usually vertical, Vail ,AZ, 16 Aug 2018. JC.

Fig. 8-21. Anvil crawler over Cheyenne, WY, 03 Jul 2019, 25 minutes after sunset. JC.

Cloud-to-Cloud (CC or Intercloud) Lightning travels between two or more clouds. It is a less common form but certainly the form of the record longest lightning bolt. *Spider lightning* refers to long, horizontally moving flashes often seen on the underside of the stratiform region of squall lines and MCS's (Fig. 8-17, Fig. 8-20, and Fig. 8-21). Such lightning bolts are often referred to as *anvil crawlers*, which are animated in the video referenced above in §8.5 connection with Fig. 8-11 on 31 Jul 2022.

Fig. 8-22. Ribbon lightning with three adjacent ionized paths displaced by high winds displaced on 27 Jul 2014 (left) and three distinct ionized paths on 20 May 2020 (right). JC.

Ribbon Lightning occurs in thunderstorms with high cross winds and many return strokes. As the wind blows each successive is displaced sideways giving the appearance of parallel ribbons. The bolt in the left panel of Fig. 8-22 on 27 Jul 2014, which struck ground a mere 300 m away, consisted of three strokes that graded continuously from dark to bright magenta to white from left to right. The bolt in the right panel occurred on 20 May 2020, and consisted of three distinct but closely spaced parallel strokes. Faster cross winds and longer intervals between strokes help ribbons separate. (Camera movement during the capture of a series of return strokes can also produce a similar effect.)

Fig. 8-23. The last instant when a lightning discharge dissipates. JC.

Bead Lightning is the name given to the decaying stage of a lightning channel, which cools after a return stroke, and its luminosity breaks up into segments (Fig. 8-23). It describes the dying gasp of a normal lightning discharge.

Staccato lightning is a short-duration CG lightning stroke that often appears as a single very bright flash with considerable branching. It occurs in strong thunderstorms and is a fearsome sight to witness. (Fig 8-24).

Ball Lightning is one of the best-known natural phenomena that few have seen. Jan: My great uncle told me that as a teen ha witnessed ball lightning during an intense lightning storm. Seeking shelter under a rural underpass with a small stream that was fenced off, a glowing orb about 6 inches in diameter hissed as it seemed to move on top of the fence after a CG strike nearby. After perhaps 15 seconds, it exploded with a loud bang. Years later, he realized the odor he smelled was that of ozone.

Fig. 8-24. Stack of staccato lightning bolts during an intense thunderstorm, 5 Sep 2019. JC.

We will pass on this elusive phenomenon until there are certifiable photos or videos, as there now are for…

8.7 Transient Luminous Events: Sprites, Etc.

One glance at the red sprite in Fig. 8-25 might make you ask, “What in the world is this and why haven’t I seen anything like this before?” Indeed, red sprites are relatively rare and can only be seen under specific and optimal conditions. An Jin (Angel An) joined a scientific

Fig. 8-25. Red sprites grading to blue at bottom above a mesoscale convective complex over India and Nepal 19 May 2022, seen from near Lake Pu Moyongcuo at altitude 5000 m. ©An Jiu (Angel An).

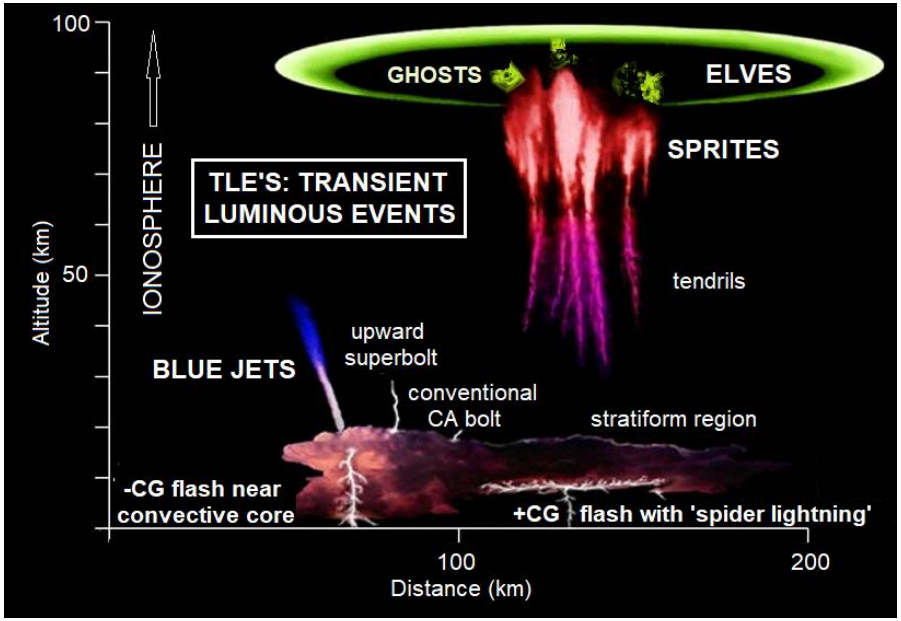

Fig. 8-26. TLE's and the Thunderstorms they are associated with. NOAA Adapted from Carlos Miralles (Aerovironment) and Tom Nelson (FMA).

expedition to Lake Pu Moyongcuo 5000 m above sea level on the Tibetan Plateau hoping to encounter and photograph sprites. Her hopes were more than realized when a large mesoscale convective system formed over northern India on the night of 18-19 May 2022, producing the natural fireworks she captured in Fig. 8-25.

Red sprites are just one of several distinct phenomena of Transient Luminous Events or TLE's that occur above thunderstorms Other TLE's include blue jets, halos, elves, and green ghosts (Fig. 8-26).

The first announcement of luminous meteorological phenomena extending high above thunderstorms was published with no fanfare as a single paragraph in the 16 January 1886 issue of ***Nature***.

> Leaving the port of Kingston, Jamaica, at dusk on November 23, 1885 the night was fine and starlit overhead but about 8 p. m. a heavy bank of cloud [thunderstorm] obscured the island and all around the upper edges of this cloud-bank brilliant flashes of light were incessantly bursting forth…while intermittently would shoot vertically upward continuous darts of light displaying prismatic colors…. Sometimes these darts of light were projected but a short distance above the cloud-bank but at others they ascended to a considerable altitude, resembling rockets more than lightning." T. Mackenzie.

A century passed with only occasional, haphazard notice of TLE's. For example, Jan noted,

> In 1976, while stationed in the navy in Norfolk, Virginia, I used to attend star parties south of Virginia Beach along the very dark Atlantic coastline. Occasionally, the group would notice a flash without seeing any signs of lightning (thinking it was a meteor explosion, distant heat lightning or naval ship artillery exercises). Twenty years later, while working at the Geophysical Institute in Fairbanks, AK, I learned that the flashes were, in fact, TLEs. It turns out that these elusive atmospheric phenomena occur off the mid-Atlantic coast in a kind of ground zero frequency max.

TLE's became a rage with lightning speed after R. C. Franz took the first serendipitous photograph on 06 July 1989 of a red sprite, only named later for its fleeting, fairy-like appearance using the ingenious acronym, Stratospheric Perturbations Resulting from Intense Thunderstorm Electrification (even though it mainly occurs in the Mesosphere). Since TLE's occur above thunderstorms and since they are too dim to see during the day, they are best seen on clear dark nights either from space or from the ground at least 100 km and up to about 500 km from the thunderstorms they are associated with.

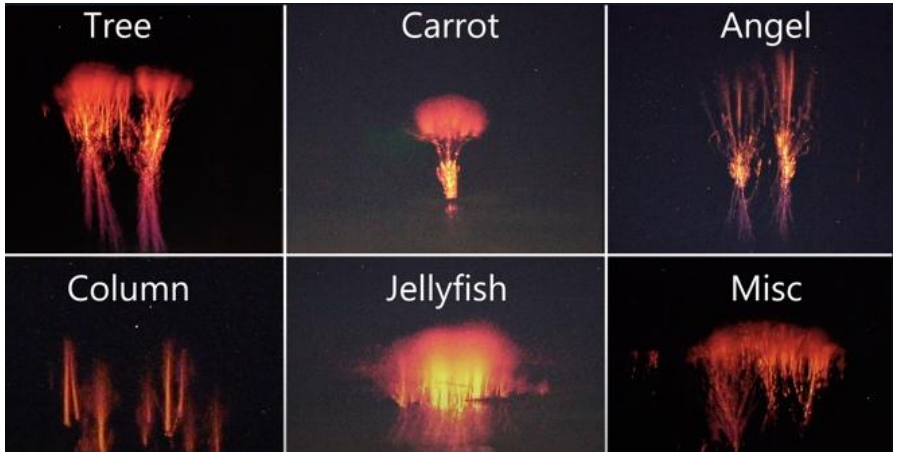

Fig. 8-27. Different shapes of sprites.

Red Sprites are electrical discharges (but not lightning) that form in the lowest part of the ionosphere, extending through much of the mesosphere, from 50 to 90 km. They are typically 50 to 100 km across. Despite their size and potential drama, they only last up to about 300 milliseconds. They exhibit a variety of characteristic shapes resembling trees, columns, and angels, etc., illustrated in Fig. 8-27. Most sprites are faint, as in Fig. 8-28, and, as with the aurora, the light intensity is so low that most appear as white to the naked eye. Only the brightest appear red. All are best captured with high ISO camera setting used in low light photography.

Red sprites are mainly associated with +CG bolts of great horizontal extent in severe, organized thunderstorms or Mesoscale Convective Systems, the latter which often persist through the night. The +CG bolt transfers negative charge upward to the thunderstorm top. This increases the voltage difference between the top of the thunderstorm and the positively charged ionosphere to the point it initiates the red sprite. However, the red sprite is not a lightning strike. It is a cooler phenomenon akin to the aurora in which the electrons in N_2 are excited and raised to more energetic orbitals. The energy emitted as the excited electrons return to ground state corresponds to red light near the top of

Fig. 8-28. Selected stacked images taken over several minutes showing clusters of sprites well above a mesoscale convective system about 250 km east of Cheyenne, WY, 07 Aug 2017. JC.

the mesosphere and blue light near its base. The color gradient occurs (as with the aurora) because the slower red transition dominates in thin air where it has adequate time to occur between collisions of molecules. In the denser air lower in the mesosphere where collisions

occur so rapidly they disrupt the red transitions the weaker but more rapid blue transitions emerge.

Fig. 8-29. Blue jet emanating from an upward bolt above a thunderstorm over Big Bend National Park, TX 28 Jul 2022. ©Matthew Griffiths

Blue jets shoot up from thunderstorm tops, often emanating from upward lightning bolts (Fig. 8-29). They extend up in narrow cones, fan out at top, typically reach 40-55 km and last a fraction of a second. Sometimes a blue jet extends so high it creates and is topped by a red sprite to form a **gigantic jet**, as above a thunderstorm near Shikengkong Mountain, China on 13 Aug 2016 (Fig. 8-30).

Astronauts are now attuned to the chance of seeing TLE's and have taken numerous photos of them. On 03 Jul 2025, astronaut Nicole Ayers captured a **gigantic jet** with nearby thunderstorm tops lit by lightning and the airglow above the distant horizon (Fig. 8-31).

Elves are rapidly expanding disk-shaped glowing regions up to 500 km in diameter. They last less than a thousandth of a second and occur above areas of active +CG lightning. They may result when an energetic electromagnetic pulse from a blue flash extends up into the ionosphere as a shock wave that lasts but an instant (Fig. 8-32).

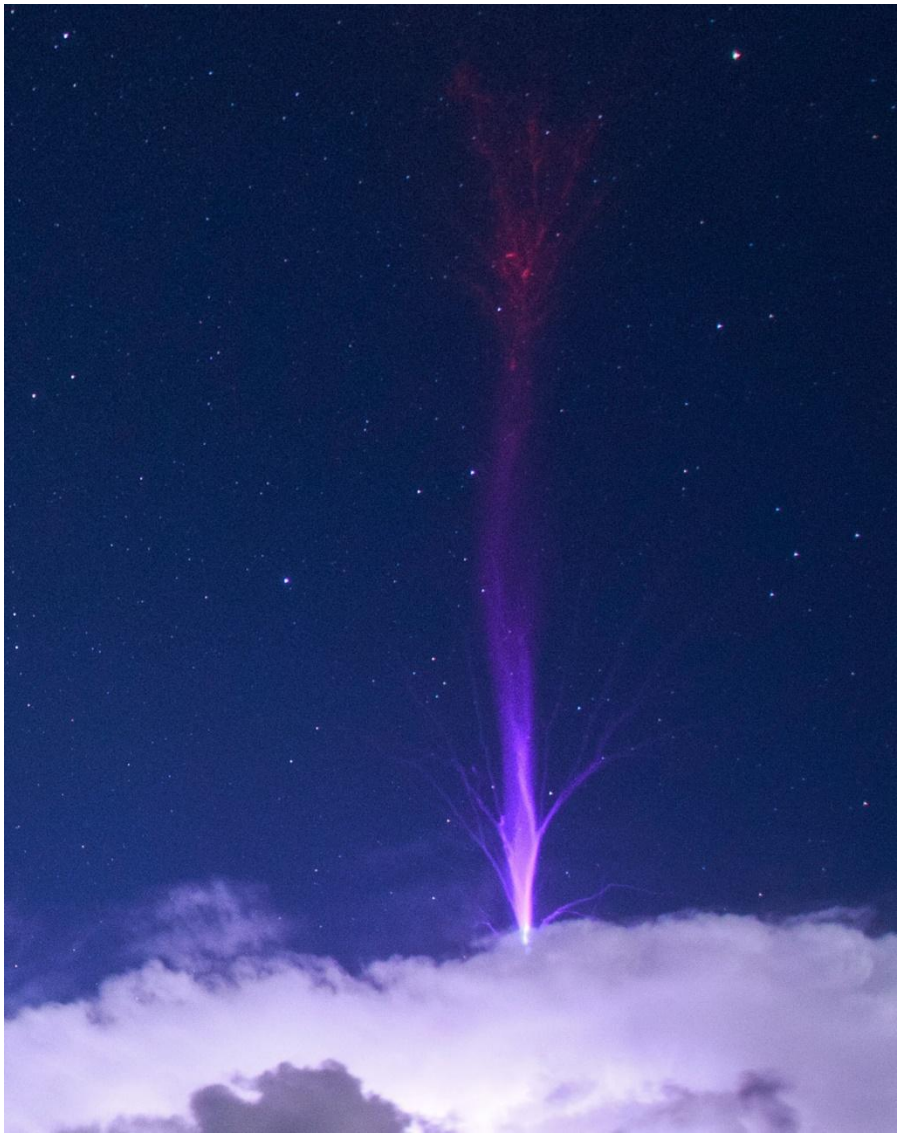

Fig. 8-30. Gigantic jet above a thunderstorm near Shikengkong Mountain, China 13 Aug 2016. ©Phebe Pan.

Fig. 8-31. Gigantic Jet above Mexico from the ISS, 03 Jul 2025. White regions are tops of lightning-lit thunderstorms. The faint green glow above the horizon is the airglow. Nicole Ayers, astronaut.

Fig. 8-32. Blue jet with expanding elf ring 26 Feb 2019 central Pacific near Nauru, DTU Space, Daniel Schmelling/Mount Visual

Green ghosts have only been recently observed. They occur on rare occasion atop active red sprites and their color is due to excited O atoms returning to ground state, just as with the green aurora. We recommend the video by Pecos Hank,

https://www.youtube.com/watch?v=sIaYOdujmz4

TLE's have generated enormous excitement, perhaps in part because they are so rare and so transient. They are so brief that the photos must almost invariably be extracted as lucky single frames from videos and they show details the naked eye cannot fully capture but now cannot be denied or ignored as they were for so long.

Thus, not only do lightning bolts and TLE's light the skies, they light our lives. So do rainbows and crepuscular rays (Chapter 9).

8-8 Gallery

Fig. 8-33. Lightning on the links, Westin Kierland Golf Course, AZ, 11 Aug 2018. Don't stand under that tree! © Jeremy Willetts.

Fig. 8-34. Lightning at sunset over Cheyenne, WY, 30 July 2016. JC.

Fig. 8-35. Lightning bolt out of the blue, Wyamo, WY, 14 Aug 2019. © Kevin Porter.

Fig. 8-36. Lightning strike nearby. Shell, WY, 12 Jul 2024. © Kevin Porter.

Fig. 8-37. Lightning from eruption of Sakurajima, 13 May 2012. ©Mike Lyvers.

Wonders of the Atmosphere
Chapter 9: Rainbows, Fog Bows, and Rays

Fig. 9-1. Double rainbow in the rain shaft beneath the thunderstorm east of Cheyenne, WY, 23 Jul 2018. JC.

Fig. 9-2. Double rainbow crossed by anticrepuscular rays at Cheyenne, WY, 08 Jun 2024. JC.

Wonders of the Atmosphere
Chapter 9: Rainbows, Fog Bows, and Rays

9.1 Observations and Properties of Rainbows

Tranquility reigns and the blue sky gleams because the late afternoon thunderstorm of 23 July 2023 shown in Fig. 9-1 has moved off to the east of Cheyenne, WY. The Sun, low in the western sky, illuminates the retreating cumulonimbus cloud. In the darker, but sunlit rain shaft beneath the cloud a bright segment of a rainbow appears, red on the outside of the arc and almost spectral, though deficient in blue. That is the primary rainbow. A faint secondary bow with colors in the opposite order, appears outside (to the right of) the primary bow.

How can it now be so peaceful when just minutes before it was so dark, so terrorizing, and so destructive beneath that same cloud? It is fitting that such an observation was memorialized and given great significance in the Book of Genesis of the Bible.

> I have set My bow in the cloud, and it shall be for a token of a covenant between Me and the earth…and you and every living creature of all flesh; and the waters shall no more become a flood to destroy all flesh. ***King James Bible***, ***Genesis***, Ch. 9.

Forgetting for the moment that rainbows appear in the rain shafts below the clouds it is true that outside the tropics rainbows are usually seen after the storm and all its fury have passed because, 1: most thunderstorms occur in the afternoon, when the Sun is in the west, 2: rainbows appear opposite the Sun and, 3: the prevailing wind aloft outside the tropics drives thunderstorms from west to east. In the tropics, rainbows have been taken a warning of impending doom because the prevailing winds aloft blow in the opposite direction – from east to west, so that rainbows are often seen just before the thunderstorm blots the sky and wreaks its havoc.

Rainbows are produced when sunlight strikes raindrops. Each drop acts like a prism and a mirror. Sunbeams are refracted upon entering a drop. They are then reflected inside the drop either once for the primary bow or twice for the secondary bow. After the reflections, the beams are refracted a second time on exiting the drops.

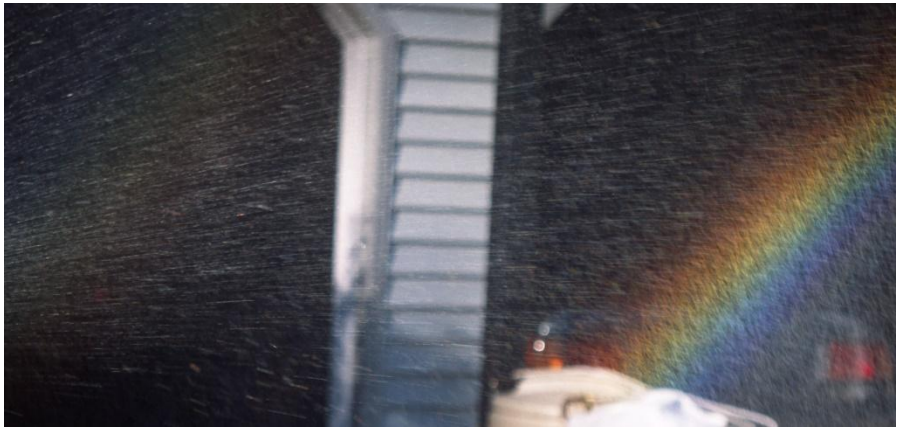

Fig. 9-3. A double rainbow from spray drops from a garden hose. SDG.

The relative intensity of scattered light striking a raindrop as a function of scattering or deflection angle was shown in Fig. 1-16 and the red curve in Fig. 1-17. It shows a deep, flat valley walled in by abrupt increases on each side – by factors of more than 100 to the peak of the primary rainbow at 138° (42° from your shadow at the antisolar point) and, more than 25 to the peak of the secondary bow at 129°. The primary bow is about 2° wide with red on the outside (at 42.5°) and violet on the inside. The secondary bow is about 3° wide with colors in the opposite order. *Anticrepuscular* rays sometimes cross the bows, always at 90° as they point to the antisolar point (Fig. 9-2).

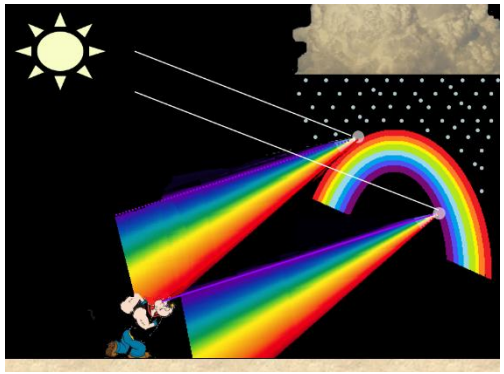

Fig. 9-4. Drops that produce the rainbow reaching PopEYE. SDG.

In spray from a hose, you can how see myriad individual drops add up to produce the bow (Fig. 9-3). The drops, which were shot out of a hose to the left of the image, appear as streaks because they moved several cm during the camera's finite exposure time. Each drop-streak produces its own minibow but appears to have the color appropriate to its location in the bow, or if the drop-streak traversed several color bands in the bow it displays those colors. Fig. 9-4 shows that each drop produces an entire spectrum but only one tiny beam of light with just one color reaches PopEYE and all other colored beams from that drop miss PopEYE.

The requirement that drops be sunlit to produce rainbows is why rainbows tend to be associated with thunderstorms, which are often surrounded by clear skies that allow sunlight to strike the rain shaft below the cloud. Nimbostratus clouds, which tend to cover the sky, only produce rainbows in rare breaks in the overcast most likely to occur in the cold, showery sector of departing extratropical cyclones.

The most vivid rainbows occur when the background is dark. In Fig. 9-3 the shaded inside of the garage provided a very dark background while the sunlit garbage pails were so bright they swamped the bow. Similarly, fountain rainbows cannot be seen in the opaque white central column, but only off to the sides in the translucent spray.

The rainbow's beauty is reduced by incoherent background light of the rain shaft, which results from multiple scattering of sunlight off many drops. When the optical thickness of the sunlit rain shaft is small, relatively little light is scattered more than once so that the coherent light that has been scattered off a single raindrop dominates and the rainbow stands out from a dark background. The greatest contrast

Fig. 9-5. Two views, minutes apart of the double rainbow east of Cheyenne, WY, 21 Jun 2018. Rainbows stand out best against a dark background. JC.

between the brightness of the rainbow and the brightness of the rain shaft occurs at optical thickness, $\tau \approx 1$. As τ continues to increase the fraction of light that is is scattered more than once increases more rapidly than the single scattered light that produces the rainbow, so contrast decreases and the rainbow is swamped.

The two images of the double rainbow in Fig. 9-5 demonstrate the crucial role played by lighting *contrast* between the bow and the

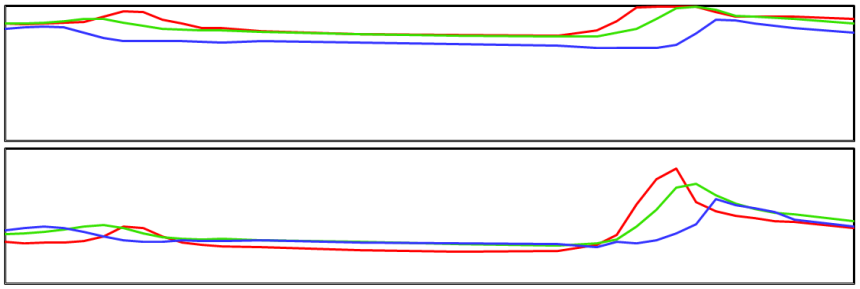

Fig. 9-6. RGB colorimetric analysis of the rainbows of Fig. 9-5. SDG.

background in creating a feeling of awe. The bottom image occurred only minutes after the top image. Both are taken from the video, https://www.flickr.com/photos/cloud_spirit/29073519338/in/album-72177720311456882/lightbox/

In the top image, a much greater optical thickness of the rain shaft was sunlit (while the foreground was shaded) than in the bottom image. As a result, the background skylight was so great in the top image that the rainbows appear washed out with poor color purity. In the bottom image, though the foreground was sunlit, much of the rain shaft and the background sky were shaded and dark. The resulting bow, just about the most dramatic that Jan ever saw, had much greater contrast with the dark background and greater color purity even though its

Fig. 9-7. Double rainbow with sunlit rain streaks east of Cheyenne, WY, 20 Jun 2017. JC.

Fig. 9-8. Primary rainbow, Cheyenne, WY, just before sunset 26 Apr 2020. JC.

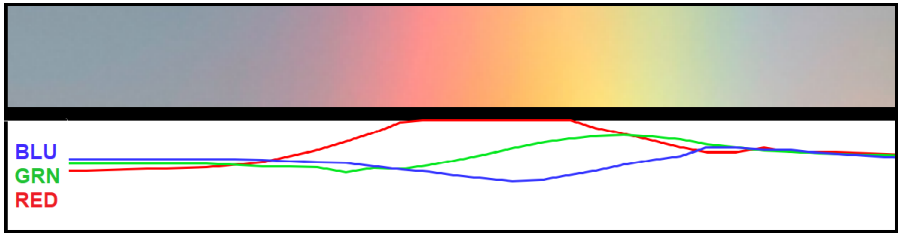

Fig. 9-9. RGB colorimetric values across the sunset rainbow of Fig. 9-8. SDG.

absolute luminosity was 30% lower than the bow in the top image! This is confirmed in Fig. 9-6, the colorimetric analysis of Red, Green, and Blue (RGB) values of the bows. The increase of red is both absolutely and fractionally much larger for the bow with the dark background, and it also has a distinct green band absent from the bow with the bright background. (Photographs provide reasonably accurate spectra if they are not under- or overexposed.)

Fig. 9-10. Rainbow, San Mateo, CA, just after sunrise 19 Nov 2016. SDG.

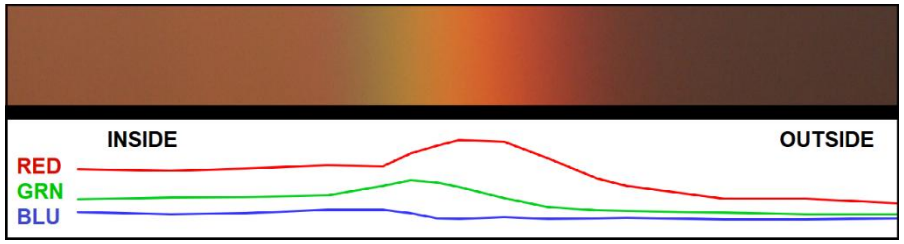

Fig. 9-11. RGB colorimetric values across the dawn rainbow of Fig. 9-10. SDG.

The complete arc of a double rainbow can be a noble sight, spanning up to almost ⅓ of the way around the horizon as on 20 Jun 2017 east of Cheyenne, WY (Fig. 9-7). The bows were so wide (a maximum of 102°) that seven panels were stitched to produce it with its curved horizon. The photo is reminiscent of Frederic Church's painting, ***Rainy Season in the Tropics*** (see Fig. 15-6) and the scene's excessive width may be one reason Church cut the space between the bows in his painting to half of what Nature demands.

In Fig. 9-7 sunlit rain streaks brighten the primary bow and the sky below it in dramatic fashion, though where they are brightest they almost swamp the bow. The contrast between the bow and the dark, clouded background on the right is much greater, than between the bow and the clear, pale blue sky on the left horizon.

As vivid as the colors of the rainbow may seem, they always fall far short of the color purity of a spectrum produced when a slit of sunlight at the zenith passes through a prism. Three main factors limit the rainbow's color purity, 1: A raindrop lacks the eyeball's narrow circular pupil and lens, which focuses a narrow beam of light on the retina in the back of the eye. As a result, because light strikes the entire raindrop it emerges in a diffuse manner with limited focusing 2: Rayleigh and Mie scattering by air molecules remove most violet and blue sunlight before it reaches raindrops, especially when the Sun is near the horizon where the optical path through the atmosphere is large, 3: Skylight and other background light 'drown' the bows and reduce the purity of their colors (as in Fig. 9-5). As a result, rainbow photos with high color purity are always doctored!

Fig. 9-12. Afternoon spray bow at Niagara Falls. SDG.

Despite the surprisingly large color range and beauty of the sunset rainbow of Fig. 9-8, it suffered from these limitations. Fig 9-9, the RGB (Red, Green, Blue) colorimetric analysis of the bow shows that even at the red peak, the color purity of the bow is modest at best and blue never dominates in the bow. Outside the bow blue skylight prevails. The only reason that this sunset bow had such a large range of colors is that Cheyenne, WY is 1850 m above sea level, where pressure is 20% lower than at sea level, so that some of the shorter waves reached the rain shaft.

At sea level, red dominates sunrise and sunset bows to a high degree because almost all the short waves have been scattered before reaching the rain shaft. The bright sunrise bow on 19 Nov 2016 at San Mateo, CA (Fig. 9-10) is a case in point. Even though we FEEL sure that the bow has a yellow and green band, red is the dominant color for the entire bow as shown in the colorimetric analysis of the RGB values across a rectangular section encompassing the bow just above the level of the apartment (Fig. 9-11). Green has its maximum value where we

Fig. 9-13. Double rainbow in Oahu from a nearby sun shower with mountains in the background. ©Rudy Fernberg.

'see' green, but even at that point, red is dominant. The optical illusion derives from the nature of human color perception, where we judge the color of some region in the vision field by the surrounding colors.

Covering all but the bow's 'green' region shows that its color is, in fact, a tone close to buff or camel.

When the Sun is not near the horizon the primary rainbow is often quite colorful. Even so, its color sequence, with red on the outside, is often ignored or blatantly reversed, as in the 1940 film, ***Fantasia***. Perhaps the artists worried that they could not violate Nature's Copyright. Perhaps they were representing the secondary bow, whose color sequence is opposite that of the primary.

Fig. 9-14. A glass bead bow in the street forms a circle around the camera. Glass bead bows are close to half the size of rainbows. SDG.

Even less often do people notice that the sky is brighter inside than outside the primary bow, For example, the sky in Fig. 9-10 is much darker outside (to the right in this case) of the rainbow, and this is confirmed quantitatively in Fig. 9-11. A more subtle observation occurs when the primary and secondary rainbows are both present, as in Fig. 9-1, both frames of Fig. 9-4, and Fig. 9-5, etc.). There, the sky is darkest between the two bows in a region called Alexander's Dark Band (which is pronounced in the 'valley' of Fig. 1-16 and Fig. 1-17), after Alexander of Aphrodisias, who described it around 200 CE.

Fig. 9-15. A 360° double rainbow in a rain shower above Cottesloe Beach in western Australia in 2013. Colin Leonhardt colin@birdseyeview.com.au

In most sightings and photographs, rainbows are cut off by the horizon. That is only because in most settings there are too few raindrops between the observer and the ground to produce a visible bow. All it takes is a view into the chasm of a waterfall such as Niagara (Fig. 9-12) or a nearby sunshower in Oahu, Hawaii (Fig. 9-13) with dark hills in the background to dispel that notion.

Without any obstacles it is possible to see the full circle rainbow. The almost full circle bow of Fig. 9-14 was produced not by rain but by the tiny spherical glass beads incorporated in traffic paint to improve its reflection. Because the index of refraction of glass, $\boldsymbol{n}_{\text{GLASS}} \approx 1.51$, the glass bead bow forms 21° from the antisolar point instead of 42° produced by raindrops. The lines were freshly spray painted, so, some glass spheres bounced outside the lines and spread around the

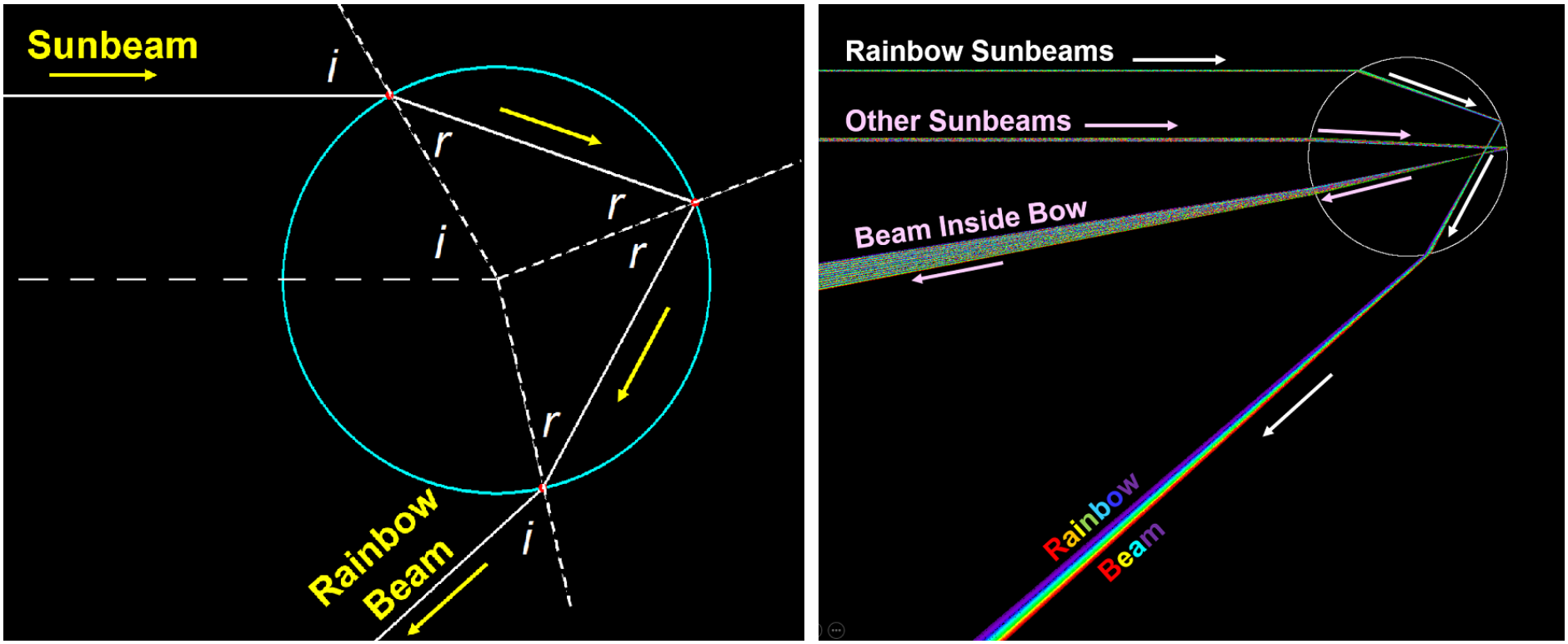

Fig. 9-16. Left: Geometric optics of the rainbow beam with incidence angle $i \approx 60°$ and refraction angle $r \approx 40.2°$. Right: Narrow bundle of rainbow beams with near spectral colors vs. broader bundle of white beams at all other incidence angles. SDG.

pavement. Glass bead street bows last until the spheres are crushed, blown away by the wind, or ironically, washed away by rain.

Full circle rainbows can only be seen from elevated vantage points such as airplanes, mountain peaks, cliffs, or near spray from a garden hose, because it is in these situations where the veil of sunlit drops can surround or envelop the observer. Fig. 9-15, taken at Colin Leonhardt's expense during a flight over Cottesloe Beach, shows the full 360° primary bow, most of the secondary bow, and Alexander's Dark Band.

9.2 The Geometric Optics Rainbow

Most features of the primary and secondary rainbows can be explained or at least modeled and simulated accurately with a few simple laws. The main simplification is to use geometric optics, which treats light as beams that obey the laws of reflection and refraction. These laws are then applied to circular cross sections that pass through the centers of spheres, a close approximation for all but very large raindrops (recall Fig. 4-4 and Fig. 4-5).

The rays that produce the primary rainbow follow the path shown in both panels of Fig. 9-16.. They strike the drop at incidence angle, ***i***, are refracted and pass into the drop at refraction angle, ***r***. The rays then proceed to the back of the drop where they are reflected inside the drop at angle ***r***. Finally, they exit the drop at angle, ***i***, after being refracted for the second time.

Sunbeams strike all over each raindrop so ***i*** can be any angle from 0° (dead center) to ± 90° (top/bottom fringe). In the left panel we set angle, ***i*** = 60°, which is very close to the beams that produce the primary rainbow. Then, angle ***r*** ≈ 40.2°.

When light strikes a raindrop and undergoes one reflection and two refractions it will return at angles between 0° and 42° from your shadow depending on where they strike the drop. For example, the light beam that hits the center of the raindrop will bounce straight back at a 0° angle from your shadow.

A problem is why only the beams that emerge at 42° contribute to the primary rainbow and exhibit colors. The right panel of Fig. 9-16 illustrates this. Two bundles of several thousand beams each, were aimed at the raindrop. The top bundle struck the drop at a small range of angles around ***i*** = 60°. It produced the focused primary bow with near spectral color segregation. The bottom bundle struck the drop at a small range of angles around ***i*** = 10°. It emerged as a broader, less focused, near-white mixture (which appears inside the primary bow).

In 1637, Rene Descartes solved one part of that problem in an appendix to ***A Discourse on Method***. He aimed a series of parallel sunbeams at a spherical globe filled with water and then used the laws of refraction and reflection to trace their paths through the drop.

> The principal difficulty still remained, which was to determine why, since there are many other rays which can reach the eye after two refractions and one or two reflections when the globe [raindrop] is in some other position, it is only those of which I have spoken which exhibit the colors.
>
> I then took my pen and made an accurate calculation of the paths of the rays which fall on different points of a globe of water to determine at what angles after two refractions and one or two reflections they will come to the eye and then I found that after one reflection and two refractions there are many more rays which come to the eye at an angle of 41° to 42° than any smaller angle, and none which come at any larger angle. I found also that, after two reflections and two refractions there are many more rays which come to the eye at an angle of from 51° to 52° than at any larger angle and none which come at a smaller angle.
>
> ***A Discourse on Method***. Appendix III ***Les Meteores***

Descartes' explanation of the primary and secondary rainbows did not include the role of colors. Isaac Newton, who was the first to explain the nature of colors (recall Chapter 1), explained the presence and order of the colors of the primary and secondary bows. He also greatly simplified Descartes' approach by using Calculus to derive a simple equation to find the rainbows' angles without needing to calculate the deflections of hundreds of rays.

"When you come to a fork in the road, take it." Yogi Berra

One well-known factor that determines the brightness of the rainbow is seldom mentioned in popular presentations. The ray approach of Descartes, colorized and improved by Newton still did not explain the intensity and brightness of rainbows. The problem occurs at every point the ray strikes the edge of the raindrop. There, the light comes to a fork in the road, so to speak, and takes it because some of the light is reflected and the rest is refracted.

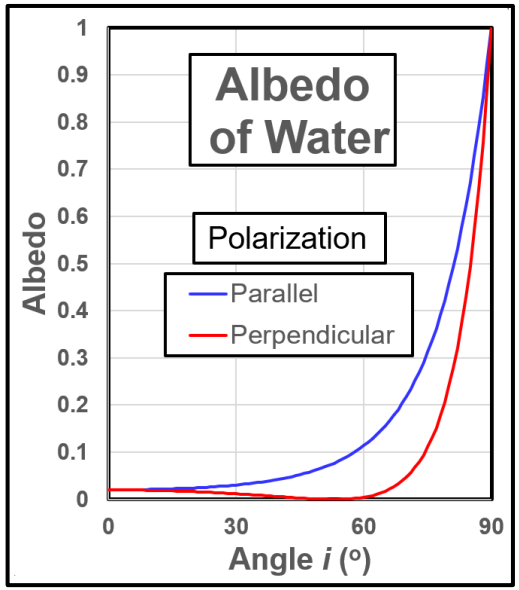

Fig. 9-17. Reflection fractions (albedo) of light passing between air and water. SDG.

In 1823, expanding on Young's finding that light consists of waves, Augustin-Jean Fresnel derived the two equations for the fraction of light reflected (i. e, albedo) at the interface between two different

media such as water and air as a function of the angle of incidence, ***i*** (Fig. 9-17). There are two equations because light waves striking the drop have two orientations (waves with electric fields either perpendicular or parallel to the drop's surface).

The percentage of reflected light remains small (< 10%) for each *polarization* when $i < 60°$, after which it increases to 100% at $i = 90°$. At $i \approx 53°$, the so-called Brewster Angle, the albedo of the perpendicular component is 0. Light striking water at the Brewster angle is completely polarized. Since the primary rainbow forms near the Brewster at $i \approx 59°$, where the albedo of the perpendicular component is only 0.35%, it is about 96% polarized.

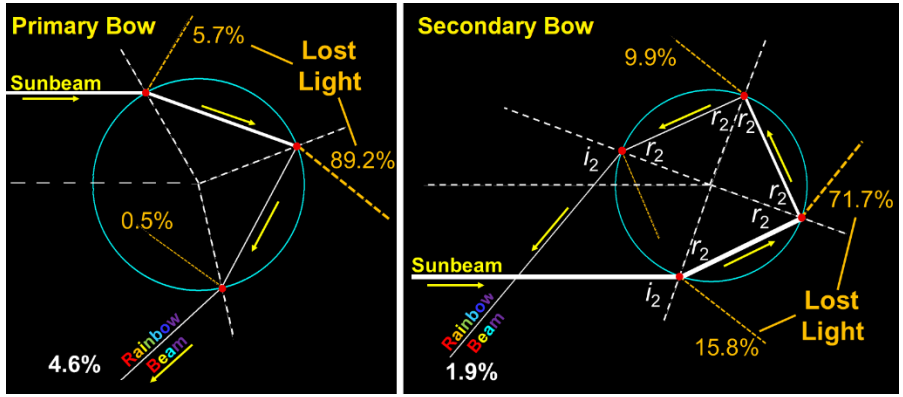

Fig. 9-18. Light beams that produce the primary (left) and secondary (right) bows and losses at each crossroad (red dots). SDG.

Fresnel's Equations bring us a giant step closer to evaluating the brightness of the primary and secondary rainbows. Fig. 9-18 shows the percent of light (the average of the two polarizations) lost or wasted at each fork and the final percent that contributes to each bow. The left panel shows the values for the primary bow. When the sunbeam strikes the drop only 5.7% is reflected or lost and 94.3% enters the drop. The largest loss to the bow occurs at the back of the drop where 89.2% of the initial light exits the drop. At the third fork, most of the remaining light, a measly 4.6% of the initial sunbeam (8.7% and 0.35% of each of the two polarized beams), forms the primary rainbow. If the back of the drop had acted like a perfect mirror the primary rainbow would be about 20 times brighter.

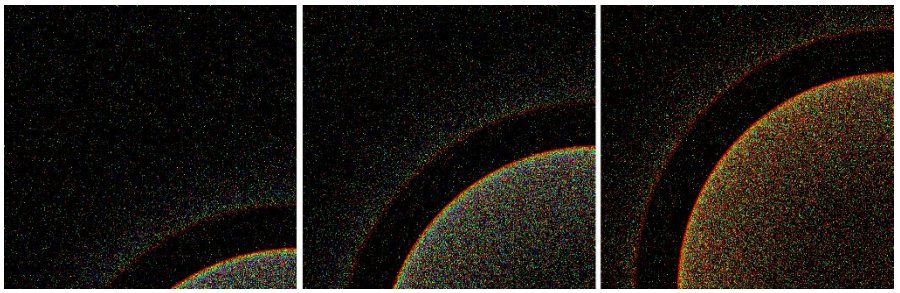

Fig. 9-19. Monte Carlo simulated rainbows for sun elevations 40° (left), 20° (center), and 1° (right) with dark background and no skylight. SDG.

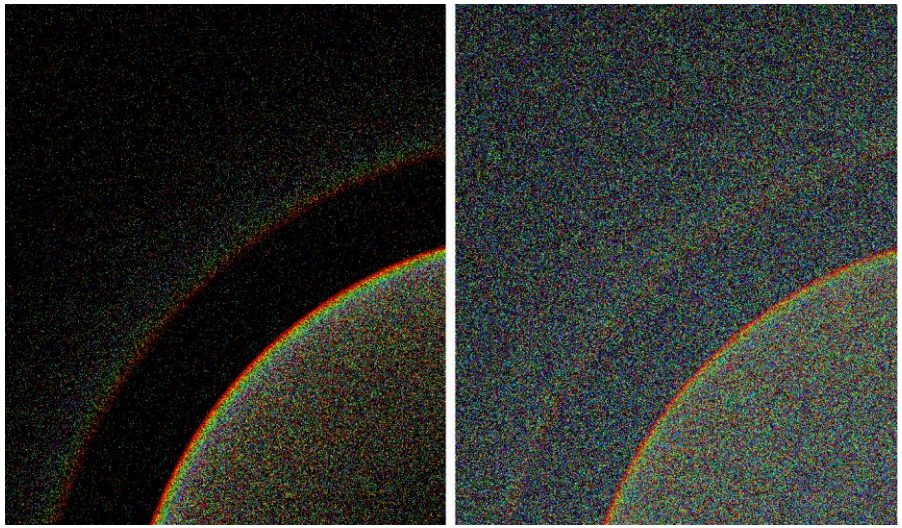

Fig. 9-20. Simulated rainbow for solar elevation 20° without (left) and with (right) skylight. SDG.

The secondary bow's path and losses at each fork are shown in the right panel of Fig. 9-18. The incidence angle for the secondary bow is $i \approx 72°$, and to produce a ray that heads down from raindrops in the sky to observers at the ground the initial sunbeam strikes the lower part of each drop. The secondary bow has four forks due to the additional internal reflection. With four forks for light to be lost, the secondary bow has only 1.9% the brightness of the initial beam.

Fig. 9-21. Reflected light from sunlit cumulus clouds brightens the glassy areas of the Caribbean Sea, 07 Dec 2014. SDG.

Rainbow simulations using the computer return to Descartes' cumbersome, lengthy Monte Carlo approach of calculating the results of aiming large numbers of beams at a raindrop. The Monte Carlo technique (briefly described in the Preface) can be pursued to any level of sophistication and detail. For the rainbow, the technique aims beams with the spectrum of Sunlight through the atmosphere where they suffer losses due to absorption and scattering. The beams hit all over the drop in random fashion. At each contact with the drop's edge Fresnel's equations determine the probability of reflection or refraction, and the laws of reflection and refraction determine the direction of the beams that ultimately leave the drop. The beams then are subject to scattering in the atmosphere on the way to the observer. Beams that reach the observer are recorded and mapped on the computer.

The three Monte Carlo simulations in Fig. 9-19 are done for rainbows that occur right in front of the observer after the beams pass through the atmosphere with an aerosol content that adds 20% to the optical thickness of the Rayleigh atmosphere at sea level with a black background at Sun elevations 40°, 20°, and 1°. In each case 5 million beams strike the drops.

At each of the Sun elevations the primary bow stands out from the black background, and especially from Alexander's Dark Band, which is almost pitch black because drops scatter little light in that range. The right panel represents a reddened sunrise or sunset bow and the sky below the primary bow is also reddened. The secondary bow is fainter and wider than the primary bow in all three panels, the colors have lower purity, and they appear in the opposite order from the color sequence of the primary bow.

Fig. 9-22. Early morning reflected sun glint from a building at the edge of the Port of Miami, FL, 12 Dec 2015. SDG.

Including background skylight in the simulation, as in the right panel of Fig. 9-20, seriously vitiates the appearance of the simulated bows. The primary bow is still distinct, though with lower color purity but the fainter secondary bow is almost camouflaged. The main change is the brightening of Alexander's dark band by skylight.

The Fresnel reflection fractions have great significance in many natural phenomena and industrial products (e. g.,thin films) besides rainbows and halos. Their impact is especially important in climate. The albedo of water is quite low until the Sun is near the horizon, which is why water bodies look dark in satellite images and in most

photographs (except for sun glint). It also means that deep water absorbs sunlight with high efficiency, except when the Sun is near the horizon. The stratocumulus clouds that cover substantial areas of the east side of the subtropical oceans (recall Fig. 5-19 and Fig. 5-20) play a major role in cooling Earth's climate because they have much higher albedo than the ocean water below, and reflect much sunlight to space before it can heat the planet. The stratocumulus clouds also emit infrared radiation to space as if they were black bodies (and to infrared eyes, clouds do appear black) at almost the same rate as the ocean waters below them.

Fig. 9-23. Red waters of the Gulf of Mexico reflecting the light of twilight at Siesta Key, FL, Dec 1987. SDG.

9.3 Rainbows to Reflect On

Reflection of light from normally dark water bodies has almost magical effects on rainbows.

Dark waters brighten and even gleam when light strikes it a glancing blow. In Fig. 9-21, the near glassy ocean reflects the white light from the sunlit side of cumulus clouds near the horizon (and even from the boat) except in the patches where the water surface is ruffled. Sun glint, even when reflected from the windows of a building (Fig. 9-22), turns the normally dark waters blinding bright. When light near the horizon comes from sunset-reddened clouds (Fig. 9-23), the waters below reflect it and appear as if the Nile waters had turned to blood.

Fig. 9-24. A rainbow and its reflection in the water of Fairfield Lake, NC, 02 Sept 2018. SDG.

Rainbows are also reflected by smooth waters. After a thunderstorm chased everyone from the small beach on Fairfield Lake, NC late on the afternoon of 02 Sep 2018 the wind calmed in time to allow the smooth water to reflect the rainbow from the departing storm (Fig. 9-24).

An oddity is that the rainbow we see reflected in the water is produced by different drops than drops producing the rainbow it appears to reflect. This is shown in Fig. 9-25, where the top of the flag and the primary rainbow both *appear* at the same height in the sky, but the flag's reflection *appears* lower in the water than the reflected bow because the primary rainbow beam always deflects light by 42°. Thus, the reflected bow is produced by drops lower in the rain shaft than the drops that produce the primary bow.

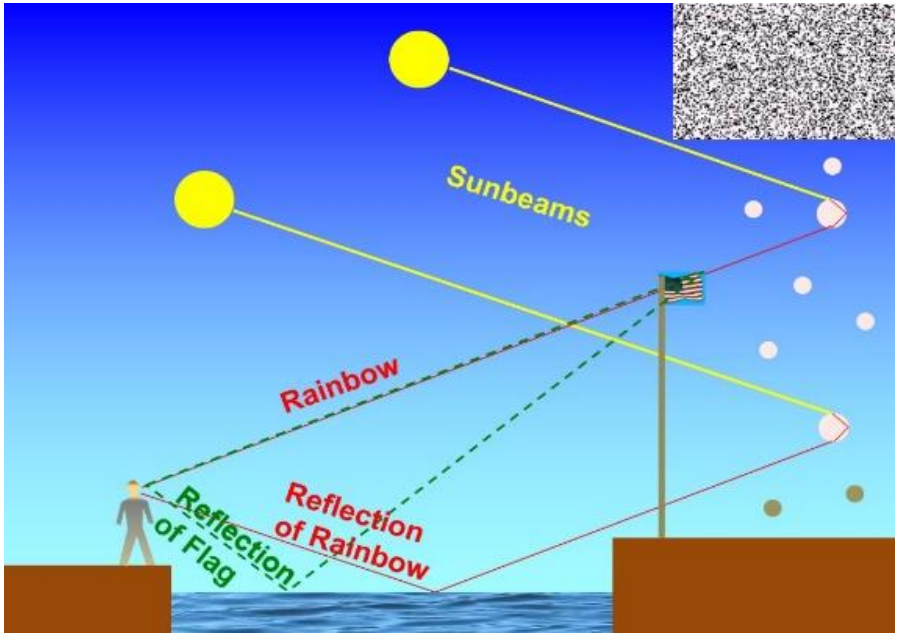

Fig. 9-25. The reflection of a rainbow in the water is produced by drops that are lower in the sky than the rainbow it appears to reflect. SDG.

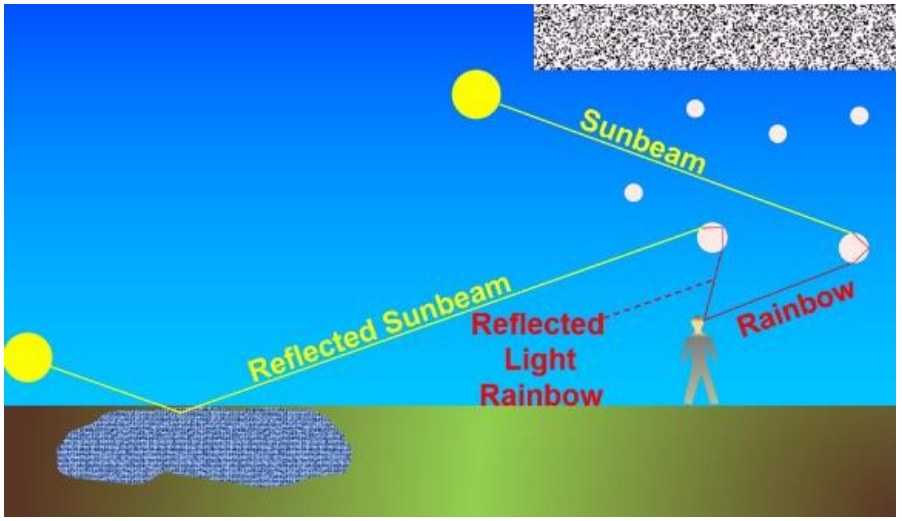

Fig. 9-26. Reflection rainbows are produced by reflected sunbeams. The water surface must be almost mirror smooth. SDG.

Fig. 9-27. A double rainbow and a double reflection rainbow in Northern Ireland. ©William Bradley

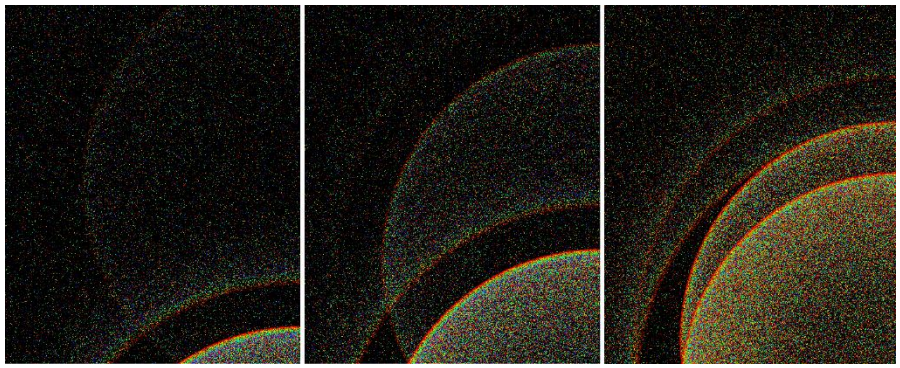

Fig. 9-28. Monte Carlo simulated rainbows and reflection bows for Sun elevations 35° (left), 20° (center), and 5° (right) with dark background. SDG.

On rare occasions four rainbows appear in the sky. Imagine standing on the shoreline shortly before sunset, gazing out to sea facing the setting Sun. The sky over the sea is clear but rain is falling to the east from a shower. The sea is unusually calm and the sun glint in the water is almost as blinding as the Sun. You turn opposite the Sun to

Fig. 9-29. Twinned rainbow (top of primary bow) produced by two different size populations of raindrops, Cheyenne, WY, 21 Jun 2018 . JC.

the rain in the east. Four rainbows tower in the sky. Attached like a Siamese twin to the primary bow at the horizon, is a bow with the same color sequence but not quite as bright. Similarly, attached like a Siamese twin to the secondary bow at the horizon is another bow with its color sequence but not quite as bright. The Sun produced the primary and secondary bows. The Sun's reflection, not quite as bright but still a blinding, real light, produced the two extra bows. Such *reflection rainbows* are illustrated in Fig. 9-26 and photographed in Fig. 9-27. The rainbows produced by the Sun form less than half circles if they are complete above the horizon. The rainbows produced by the Sun's reflection in the water form more than half circles if *they* are complete above the horizon and, spread outside the bows to which they are joined at the horizon.

All of the few photos of reflection rainbows occur when the Sun is low in the sky. This follows from Fresnel's Equations of Reflection. Water reflects a high percentage of sunlight only when the Sun is near the horizon. For example, the albedo of water is 58.4% when the Sun is 5° above the horizon, so reflection bows can be about half as bright as the normal bows. But when the Sun is 35° above the horizon, water's albedo is only 4.4%. Thus the reflection rainbow will be less than $1/20^{th}$ as bright as the normal bows even in the optimal case of mirror smooth water. The Monte Carlo dot simulations of Fig. 9-28 illustrate this difference, where the reflection bow is bright at Sun elevation 5° (right panel) but barely detectable, even with a black background at Sun elevation 35°. At Sun elevation 20°, where albedo is 13.4%, the primary reflection bow is fainter than the normal secondary bow, so

background skylight almost completely swamps it, and even with a black background, the secondary reflection bow is almost invisible.

9.4 Twinned and Disjoint Rainbows

The top of the arch of the primary bow in Fig. 9-29 is split, as if there were two primary bows. Indeed, there are. What is its cause? Up to this point we have assumed bows are produced by spherical drops. But large raindrops flatten on bottom so that the angle of refraction is altered and the primary bow will flatten on top. Why then are there twin bows instead of one flattened bow?

Fig. 9-30. Disjoint rainbow from sea spray and a fresh-water shower. Commissioned by Gunther Konnen.

If all the drops were the same size and were flattened the same way the slight flattening of the bow would be particularly hard to notice. But when there are two distinct bows – twinned bows as they are called, it implies that the bows are produced by two distinct sizes of drops, either by two distinct showers, each with different size drops, or a single shower with a split population of distinctly larger and distinctly smaller drops, (i. e., a bimodal drop size distribution).

Twinned bows are always split at their tops and never on the sides where they are near vertical. That is because the rays that produce the vertical sides of the bow go through near horizontal cross sections of the drops, which are not squashed and remain circular.

A final rainbow oddity we consider here might be called a disjoint rainbow. Gunther Konnen reasoned that since salt water is denser than fresh water and has a higher index of refraction, its primary rainbow, like that of glass spheres, will appear closer than 42° from the antisolar point. He asked a mariner friend to look for a rainbow produced by a fresh water rain shower at the same time a rainbow was produced by sea water spray from the ship and photograph the scene. The seaman took the photo (Fig. 9-30) on his very next voyage, which confirmed Gunther's prediction.

9.5 Supernumerary Bows and Fog Bows: Waves

All the rainbows photographed up to this point in this chapter, are accurately described and modeled using geometric optics. But, as noted in Chapter 1, some rainbows have extra color bands just inside the primary called supernumerary rainbows. These bands add to the width of the primary bow and also embellish it. A beautiful example is the supernumerary bow of 21 Sep 2023, shown in (Fig. 9-31), which is a closeup of the double rainbow in Fig. 1-10. Jan noted it was,

> "A crazy afternoon with slow moving and slow developing thunderstorms. This capture was taken in light rain as the thunderstorm passed to my east. The skies were clear to my back as the brilliant sunlight reflected and refracted off the nearby heavier rains. The supernumerary rainbow was as bright as I have ever seen. The secondary bow was surprisingly not as bright as I would have thought. The primary bow was exceptional."

Light rain means small raindrops. Indeed, the best supernumerary bows and fog or cloud bows are produced in rain shafts or fog with small drops of almost constant size. How so?

Fig. 9-31. Primary bow of 21 Sep 2023 at Oracle, AZ with pronounced supernumeraries, matched with Mie solution from Fig. 9-32 for drops with $r_{DROP} \approx 325$ μm (extension at right). JC.

Supernumerary rainbows and fog bows arise from the wave nature of light, As an example, consider two waves of length, $\lambda = 0.55$ μm (corresponding to green) that strike a raindrop at the two different incidence angles, $i = 47°$ and $i = 70°$. Both these waves emerge from the drop at the identical angle from the antisolar point, 38.67°, but since they travel through different lengths both inside and outside the drop they will arrive at the eye out of phase, by an amount depending on the size of the drop. If the distance differs by half a wavelength then the two green waves will interfere totally and cancel so at 38.67°, the supernumerary bow or fog bow will have no green.

These phase changes are almost random for large drops, which are more than 1000 times the wavelength of light, and hence have no impact on the rainbow. The phase changes and hence the color pattern become more consistent for successively smaller drops. The supernumerary bows begin to appear for raindrops less than 1 mm in diameter ($r_{DROP} = 0.5$ mm) and dominate increasingly for smaller drops while the primary rainbow becomes less colorful and distinct.

Ray Lee – that is Raymond Lee and not Lord Rayleigh – constructed a diagram using Mie scattering calculations that shows how the colors

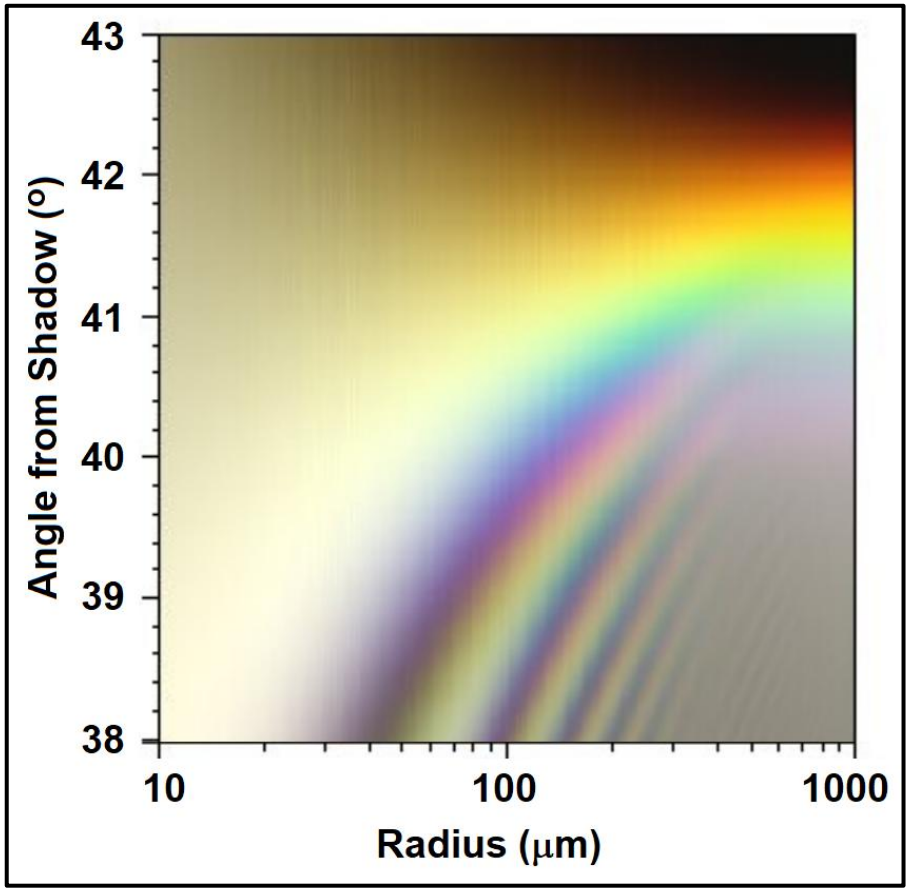

Fig. 9-32. Lee diagram of rainbow colors vs drop size and angle from shadow for a perfect Mie single scattering model. ©Phil Laven.

and deviation angles of the rainbow vary with drop radius. The Lee diagram for the primary rainbow and its supernumeraries is shown in Fig. 9-32 (calculated by Philip Laven using more than 24 hours of computer time at

(http://www.philiplaven.com/links2.html).

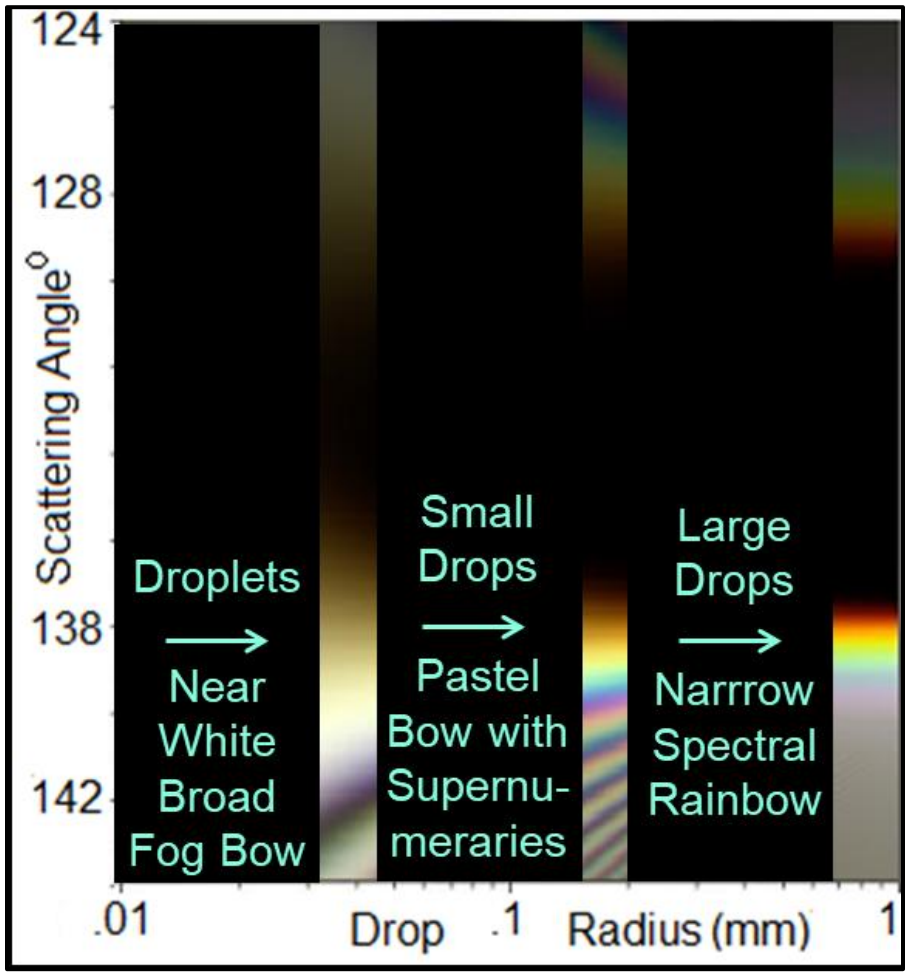

Fig. 9-33. Lee diagram showing drop-size regimes for fog bows, supernumerary bows and spectral primary bows. ©Phil Laven and SDG.

Pretty as this Lee diagram is, it may be difficult to read at first, so in Fig 9-33 we isolate three vertical stripes that correspond from left to right to small, medium, and large drops. Small drops ($r_{DROP} \approx 0.04$ mm) produce a wide, largely white fog bow or cloud bow with a few stripes of washed out colors and essentially no secondary bow. Medium size drops (($r_{DROP} \approx 0.2$ mm) produce multi-ringed supernumerary bows inside a broadened primary, and a wide secondary bow. Large drops (($r_{DROP} > 0.6$ mm) produce a bright, near spectral primary bow and a distinct secondary bow.

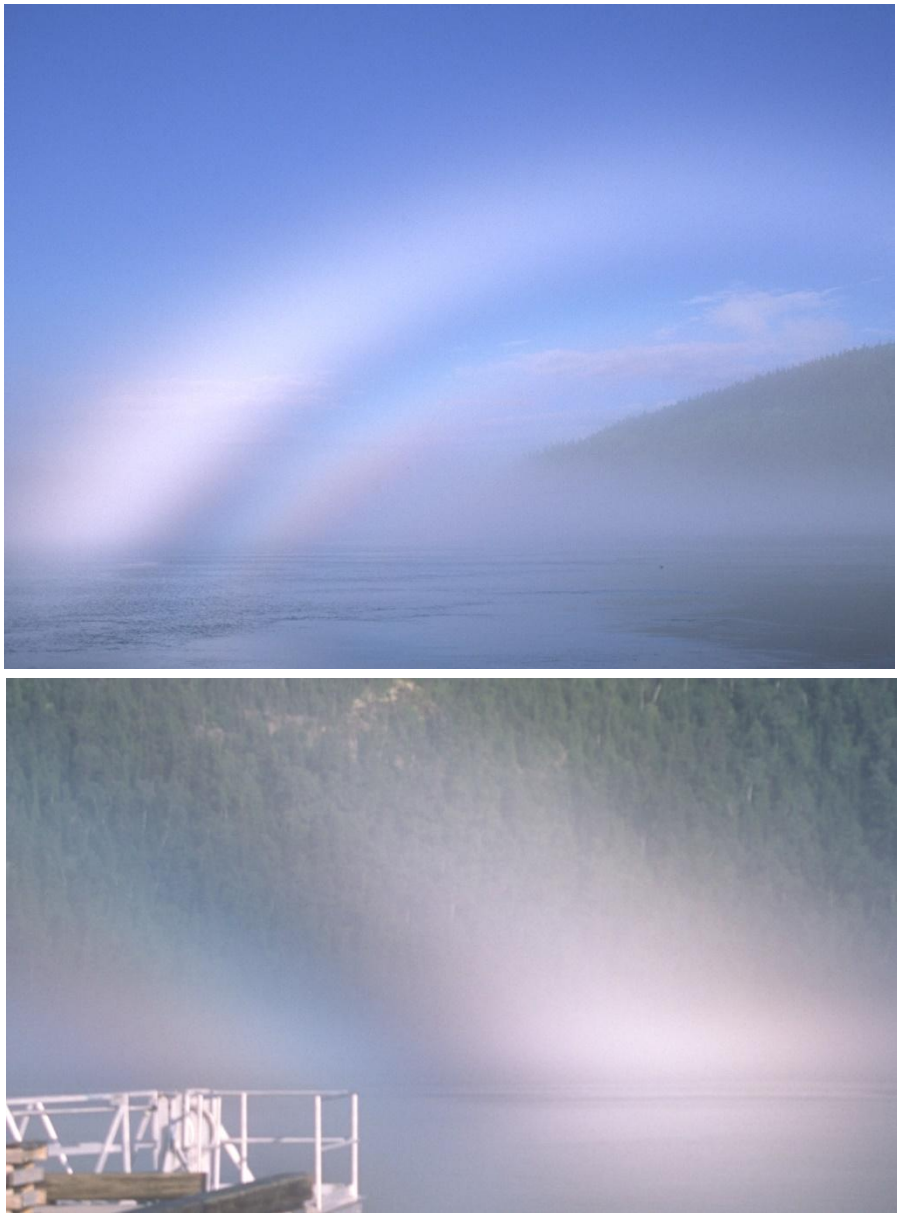

Fig. 9-34. Fog bows at Fenêtre sur le Saguenay, QB, Canada, a few minutes apart on 13 Aug 2005. The darker background of the bottom panel brings out the weak colors. SDG.

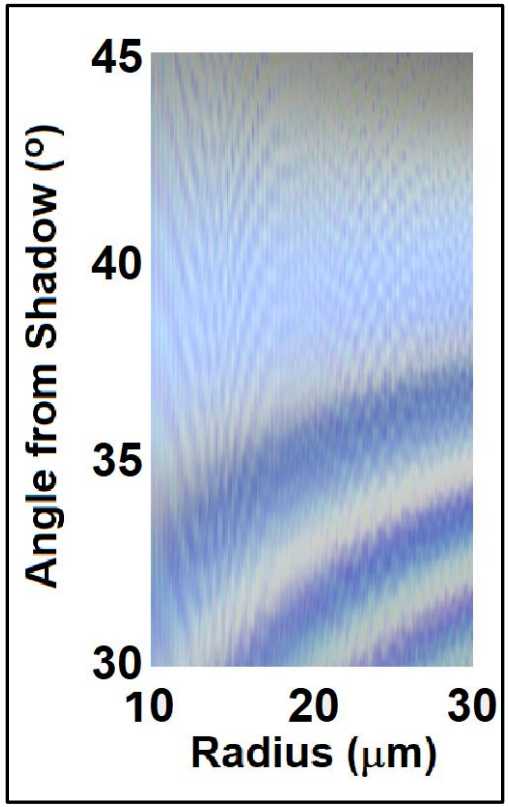

Fig. 9-35. Lee diagram for fog bows of small droplets. SDG.

Fig. 9-36. Fog bow in the Redwoods 31 May 2021. ©Bill Young.

Matching photos of bows to vertical slices of the Lee diagram provides a way to estimate the drop size. For example, the best match between the supernumerary bow of 21 Sep 2023 (Fig. 9-31), occurs for drops with $r_{DROP} \approx 0.325$ mm. The discrepancies between photo and model (at right) are due to the model's neglect of skylight and the range of drop sizes that always occurs in any rain shaft or fog.

The difference between fog bows and rainbows is striking. The fog bow of Fig. 9-34. which lit up in stunning fashion as fog and drizzle began clearing around 1630 ADT, 13 Aug 2005 at Fenêtre sur le Saguenay, Quebec after a raw, rainy day. Whereas the geometric optics rainbow is about 2º wide, this fog bow was about 10º wide and consisted of two very broad, almost blinding bright white bands. Its faint color sequence became distinct minutes later (bottom panel) when seen against a dark forested hillside. Its width and strange color sequence matched cloud bows made by droplets with $r_{DROP} \approx 18$ μm in the Lee diagram of Fig. 9-35. Tiny variations of droplet size (which Nature always provides) eliminate the fine scale variations of the mathematical Mie scattering solutions of Fig. 9-35.

The most beautiful photo of a fog bow we've ever seen (Fig. 9-36) was captured by Bill Young one morning in the Redwood forest. The teeny sunlit space was the optimal setting for uniform size droplets, which comparison with Fig. 9-35 shows, $r_{DROP} \approx 27$ μm. A precious few minutes later the Sun evaporated the tiny droplets and the bow vanished.

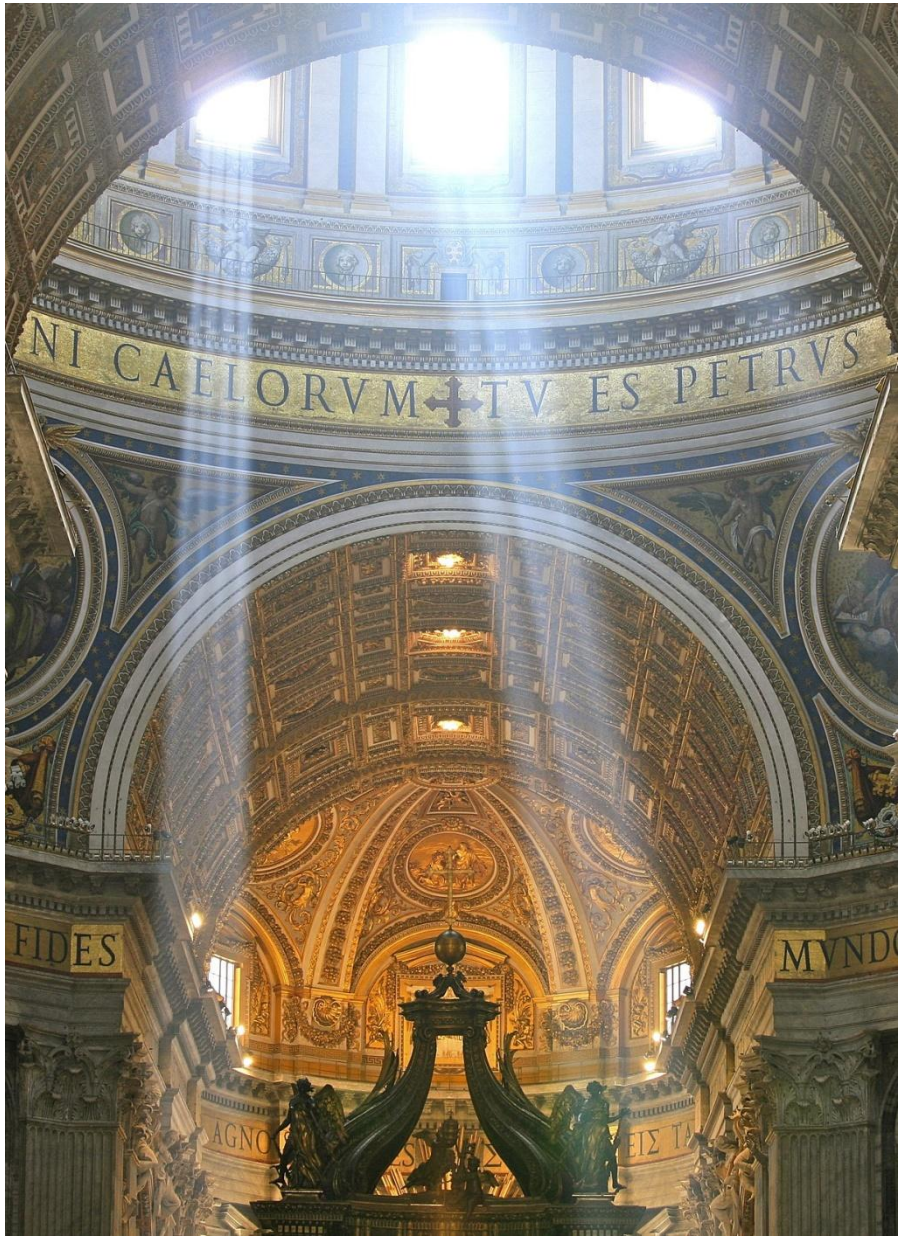

Fig. 9-37. Crepuscular rays, a divine symbol, shine through the windows of the dome in St. Peter's Basilica, Vatican City. Inside air quality is suspect, or perhaps the humidity is high. ©Alex Priomos.

9.6 Crepuscular and Anticrepuscular Rays

By placing gods in the sky, ancient religions attributed atmospheric optical phenomena to divine sources. Foremost among these are crepuscular rays, which appear to emanate from the Sun, sometimes beaming down to reveal sanctity, as in St. Peter's Basilica (Fig. 9-37), and sometimes spreading in all directions (Fig. 9-38).

Fig. 9-38. Crepuscular rays emerging in all directions from the Sun east of Cheyenne, WY, 16 Jun 2020,. Smoke from numerous Western US forest fires enhanced the rays and allergies. JC.

What causes crepuscular rays and what gives them their appearance? An impressive demonstration illustrating the nature of crepuscular rays is to aim a laser beam across a dark room. Nothing can be seen except for a red dot at the point on the wall the beam strikes. But the beam suddenly lights up the moment chalk dust or flour is sprinkled along it. Crepuscular rays can also be seen when a shade is opened a mere slit in a dark room. In that case, you can see individual dust particles light up. Smoke from barbeque grills also works (Fig. 9-39).

Fig. 9-39. Crepuscular ray from sunlit smoke of a BBQ grill. SDG.

Crepuscular rays are sunbeams scattered by dust, aerosol particles, and air molecules.

Crepuscular rays can also be the shaded regions between two sunlit rays. In fact, sunlit and shaded crepuscular rays often alternate. Opaque clouds that provide dark shadows but only cover part of the sky, such as cumulus or cumulonimbus clouds are usually the objects that cause the shade, but mountains or trees also work.

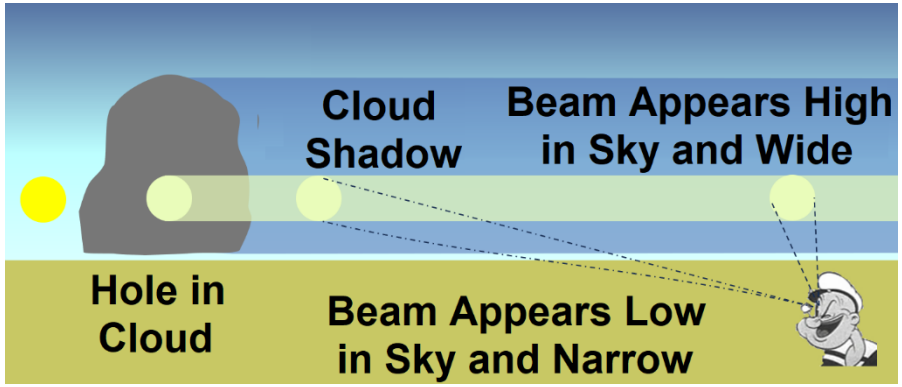

Fig. 9-41. When the Sun is at the horizon a horizontal sunbeam passing through a hole in a cloud produces a crepuscular ray that appears to spread as PopEYE looks higher in the sky. SDG.

The apparent spreading of crepuscular rays, which point in all directions is a consequence of perspective. All sunbeams striking the Earth are almost parallel and only aim downward during the day. This is shown in (Fig. 9-40) which displays the Sun and Earth to scale except that the almost invisible blue dot representing the Earth (just to the right of where the sunbeams converge and midway between the two white arrows) is 15 times too *large*! The Sun, whose diameter (1.4 million km) is 108 times the diameter of Earth, appears as a tiny circle in the sky, only 0.53° wide compared to its distance to Earth, an average of 149.5 million km. As a result, all sunbeams reaching Earth at any moment spread by a maximum angle of 0.53°.

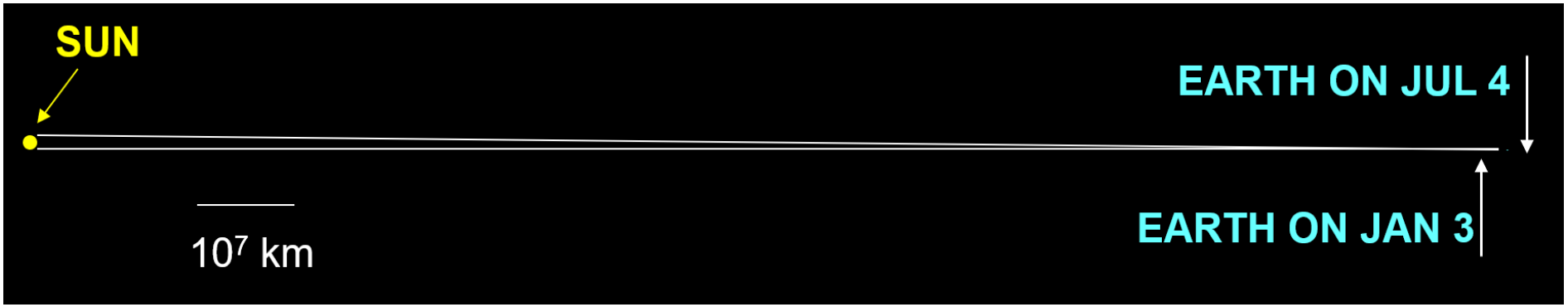

Fig. 9-40. Relative size of the Earth, Sun, and the distance between them. Sunbeams reaching Earth are all almost parallel, varying by a maximum of 0.53°. SDG.

Fig. 9-41 illustrates how crepuscular rays appear to diverge from the Sun and can appear to aim up. It shows the Sun at the horizon blocked by a distant cumulus cloud except for one hole that allows the horizontal sunbeam through, which passes directly over the observer. The part of the beam near the cloud appears low in the sky. It is much further from the observer than the part of the beam directly overhead, so, by linear perspective, it appears to broaden with elevation angle.

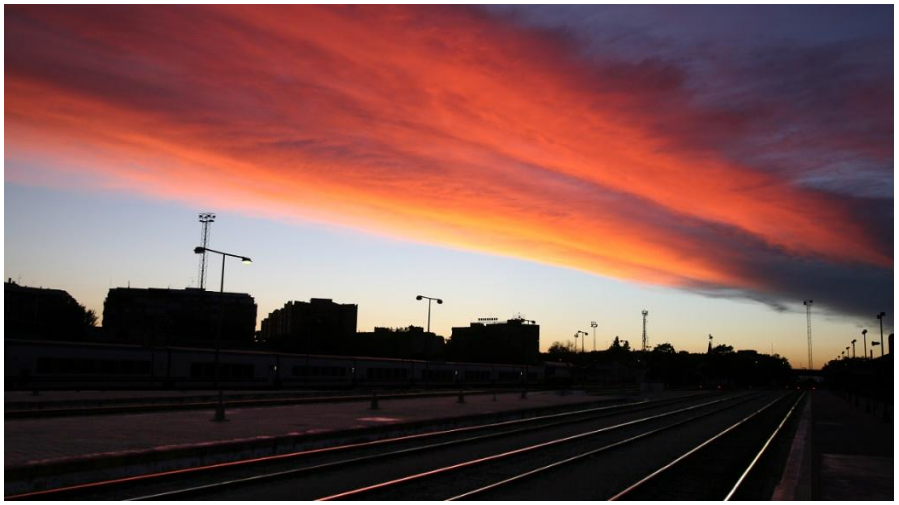

Fig. 9-42. Parallel crepuscular track rays and parallel altocumulus cloud bands at sunset in Granada, Spain, 11 Oct 2007, appear to converge in the distance because of linear perspective. SDG.

The same illusion of broadening due to perspective is illustrated by train tracks, which we know are parallel, as at the Train Station in Granada Spain at sunset on 11 Oct 2007 (Fig. 9-42), which also contains parallel bands of altocumulus clouds seeming to narrow in the distance.

Crepuscular rays can appear faint or striking depending on the cloud's optical thickness and on the quantity and character of the aerosol particles. Cumulus and cumulonimbus produce crepuscular rays with the greatest contrast between light and dark rays, as in Fig. 9-43, Fig. 9-44, and Fig. 9-45, because they are so optically thick almost no light penetrates them and hence they cast the darkest shadows. Optically thinner and smaller clouds such as the delicate cells and ripples of altocumulus, allow more light through as in Fig. 9-46, and so, tend to produce faint and fine crepuscular rays.

Fig. 9-43. Crepuscular rays at the edge of a cumulonimbus cloud, Cheyenne, WY, 15 Jul 2023. Rays are brighter at right center, near the Sun. JC.

A pure molecular atmosphere tends to produce feeble, blue crepuscular rays. Add aerosols from pollution, fires, or airborne dust from distant dust storms, or swell them in high humidity and perhaps even add fog droplets in the morning mist, and crepuscular rays light up. Impressive crepuscular rays in the dry air of Wyoming, as on 15 Jul 2023 (Fig. 9-43), are more likely due to dry smoke particles from forest fires. Impressive crepuscular rays in the SE United States are more likely due to aerosols bloated by deliquescence in humid air (Fig. 9-44, Fig. 9-47).

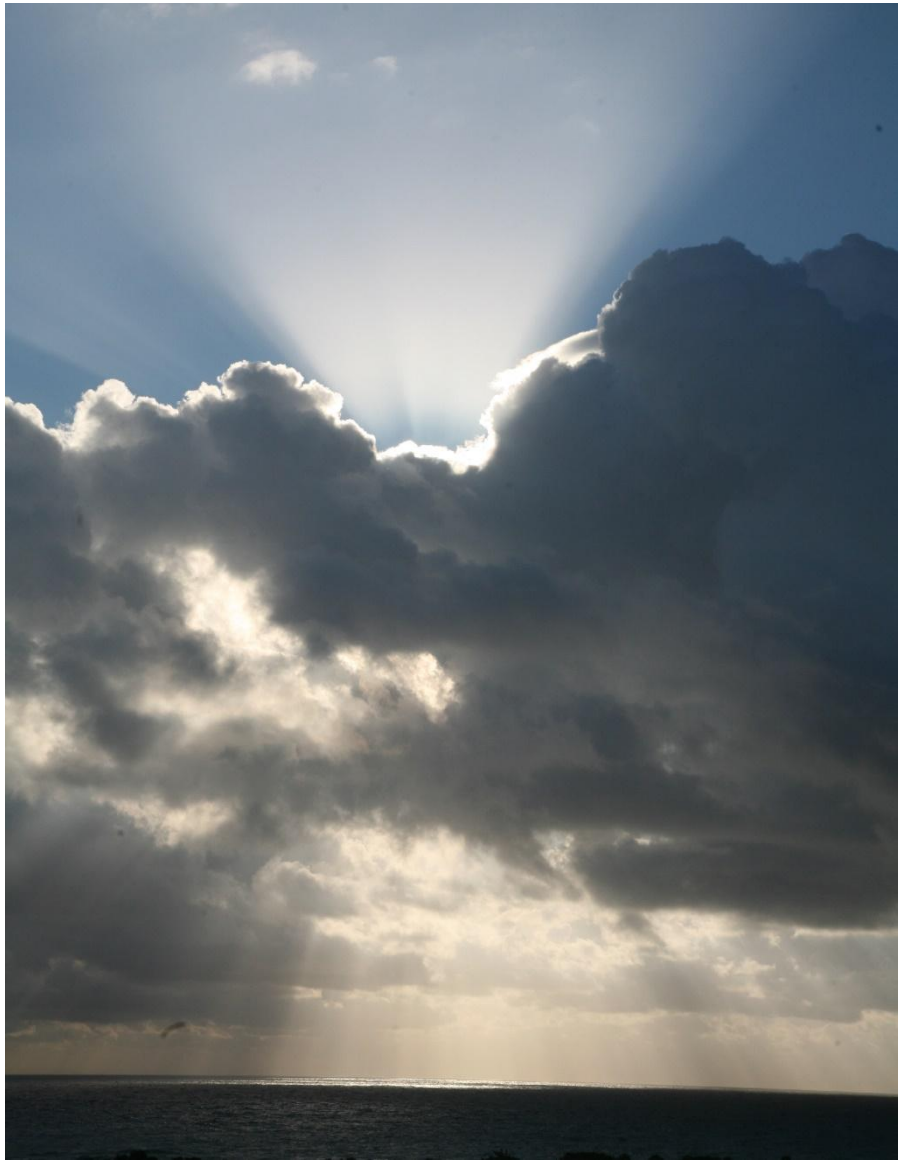

Fig. 9-44. Crepuscular rays from Cu illuminate the humid morning air and the distant sea surface, Fort Lauderdale, FL, 20 Dec 2011. SDG.

Fig. 9-45. Crepuscular rays beaming through a hole in a field of cumulus in Cliffside Park, NJ. SDG.

Fig. 9-46. Crepuscular rays from a sheet of altocumulus cloud cells in smoky air, east of Cheyenne, WY, 17 Jul 2017. JC.

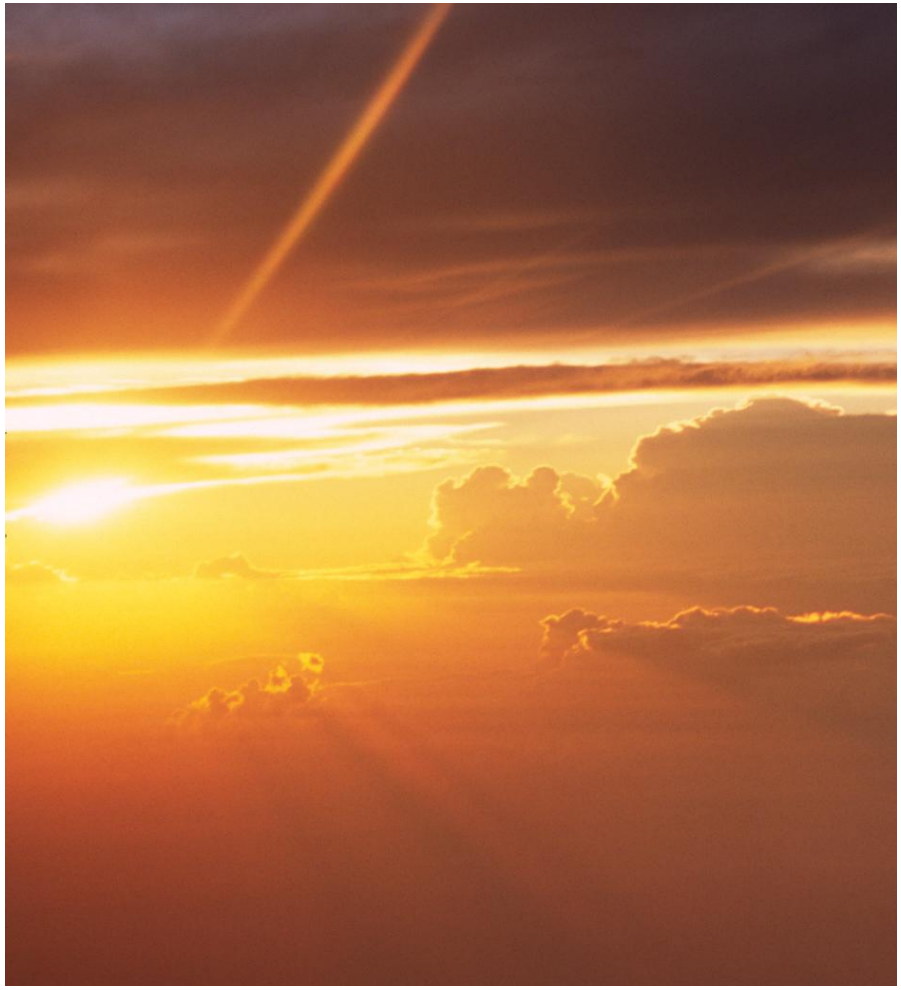

Fig. 9-47. Golden crepuscular ray searchlight beam at sunrise flying north over Florida. Even though the ray appears to brighten upward it is only by contrast with the darkening sky. The ray's *measured* luminosity decreases upward. SDG.

Crepuscular rays fade with angular distance from the Sun because most aerosols scatter light by small angles with much greater efficiency than by large angles (Recall Fig. 1-17, Fig 2-35, and Mie scattering). Even though the ray in Fig. 9-47 appears to brighten upward it is only by contrast with the darkening sky. The ray's *measured* luminosity decreases upward! For the same reason, the aerosols on dirty windshields produce a blinding and hence unsafe glare when facing the Sun, but not when lit from behind.

The principles governing crepuscular rays may be simple but their variations are prolific. They result from all the different sizes, opacities, and shapes of the clouds (or other obstacles including mountains), each with with unique, multiple indentations, ever-moving around the ever-moving Sun, and endless variations of the atmosphere's aerosol content, concentration, and distribution. For example, the crepuscular rays of Fig. 9-43 that emerged from the side of a cumulonimbus cloud are bright where the edge is close to the Sun and deep blue where it is far enough away to cast a wide shadow in relatively clean air. Time lapse videos show crepuscular rays moving like searchlight beams, as openings in the cloud move and change, and as the Sun moves. One example, for sunlight beams, is,

https://www.flickr.com/photos/cloud_spirit/51426097845/in/album-72157673641455795

Crepuscular rays at twilight (crépusculaire means twilight in French) take on twilight colors (Fig. 9-47) and sometimes surprising color contrasts On 16 Aug 2021 (Fig. 9-48) the rising sun, surrounded by a red glow, peeps beneath a distant cumulonimbus cloud that casts a blue crepuscular ray shadow in the otherwise reddened sunlit sky.

The color and lighting differences of twilight crepuscular rays are simulated in Fig. 9-49. In the simulation, two major tricks were used and one major approximation was made. Trick #1: A skylight model was run twice – once to produce an image for a clear twilight sky and once for a beam shaded by a distant, towering thunderstorm. Trick #2: A widening wedge of the shaded beam (to mimic perspective) was grafted into the clear sky image to match a photograph taken during twilight. The approximation: No light from the sunlit sky was allowed to be scattered into the shaded beam and then scattered again to the observer. The approximation was validated by calculations and by the close match of the simulation to the photo.

Fig. 9-48. A blue crepuscular ray shaded by a cumulonimbus cloud contrasts with a bright orange sky east of Cheyenne, WY moments after sunrise, 16 Aug 2021, with Air Quality Index = 100 (borderline polluted). JC.

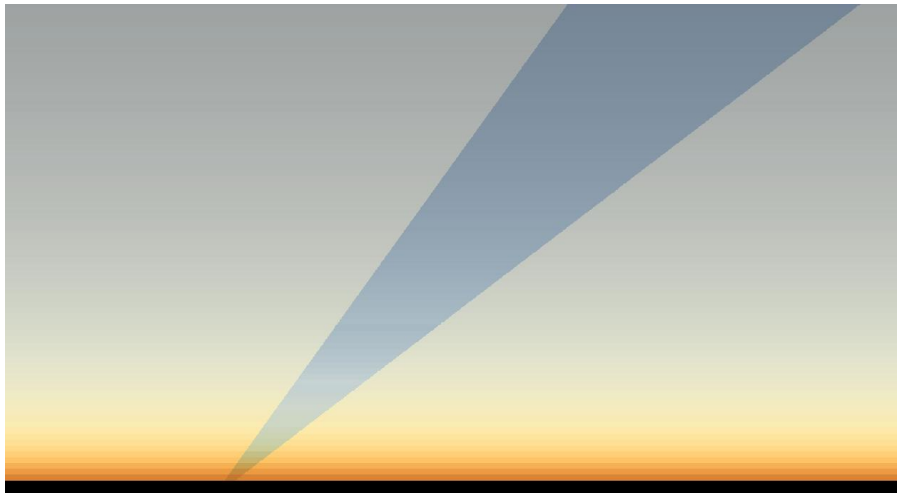

Fig. 9-49. Simulated blue crepuscular copy ray shaded by a towering cumulonimbus cloud when Sun is 1.8º below the horizon. SDG.

Fig. 9-50 illustrates why the shaded beam is bluer and darker than the surrounding atmosphere. The unshaded beam (the white line in the left panel) receives light scattered from the top of the atmosphere all the way to the ground. (recall Fig. 2-12). When the Sun is at the horizon that includes a large contribution of red light. The beam in the shadow only receives light scattered from the top of the atmosphere to the top of the cloud shadow. That light is primarily blue beause high in the troposphere, where the atmosphere is thin, the scattered sunlight is still blue.

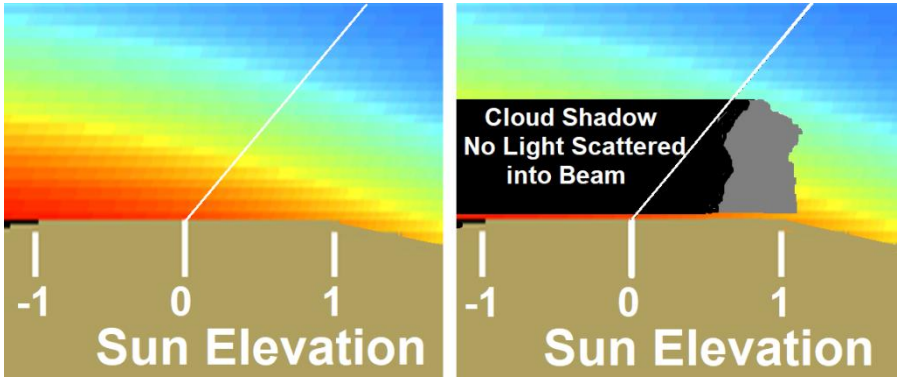

Fig. 9-50. Beam in clear air includes scattered sunlight from all heights in the atmosphere and therefore much red light from the lower troposphere. Beam shaded by a towering cumulonimbus only includes blue light from the upper troposphere. SDG.

Fig. 9-51. Crepuscular rays through foliage in morning mist USR NJ. SDG.

A walk through the woods in the early morning mist often reveals crepuscular rays, where instead of towering clouds, the trees and leaves form the obstacles (Fig. 9-51). On rare occasion, the droplets in the mist or ground fog will all be almost the same size, and in that case, the rays become iridescent.

Shortly after dawn, the crepuscular rays produced by trees can exhibit color variations normally produced by distant mountains or towering cumulonimbus clouds. On the morning of 18 Oct 2024 rays of the rising Sun peered through gaps in the forest around Fairfield Lake, NC near the bottom of Fig. 9-52. The sunlit rays, as well as the sunlit sky above were pink because the sunlight scattered by the low lying radiation fog overwhelmed the light of the blue sky above. By contrast, the shaded rays in the sky immediately above the fog-dimmed treetops

Fig. 9-52. Crepuscular rays from the rising Sun appear through and above the forest, whose treetops emerge above a thin layer of radiation fog at Fairfield Lake, NC, 18 Oct 2024. SDG.

were sky blue because they suffered no competition. A perhaps subtle feature of the blue shaded rays is that they traced out the outlines of the treetops.

Fig. 9-53. Crepuscular rays copy a cumulus outline onto a low haze layer, Boynton Beach, FL, 29 Dec 2015. SDG.

The ends of some crepuscular rays make almost perfect copies of the outlines of the clouds (Fig. 9-53), mountains, or trees whose shade caused the rays. These shaded copy rays often appear blue and higher in the sky than the objects they copy. All told it adds to the sense of astonishment.

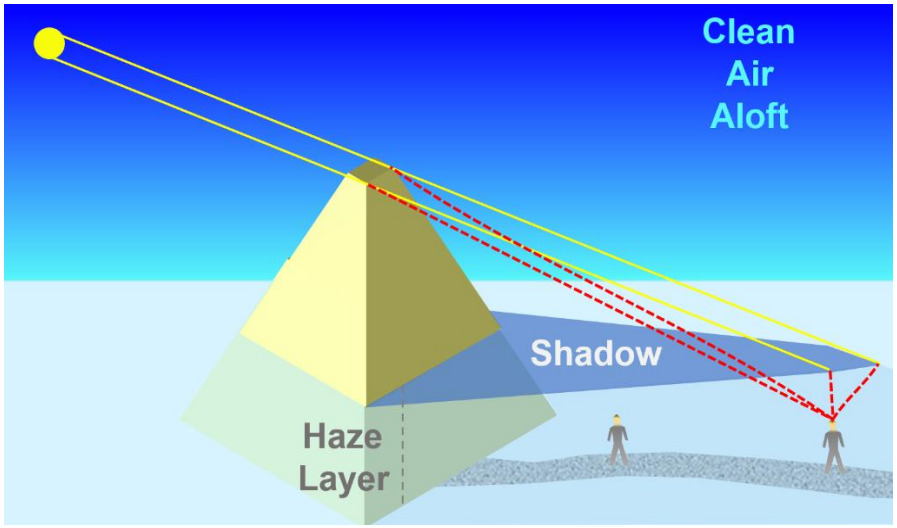

Fig. 9-54. Crepuscular copy rays of a mountain on a shaded haze layer. SDG.

This is illustrated in Fig. 9-54, where the shadow of the mountain is a perfect copy of the mountain, yet appears higher in the sky than the mountain. The copy image is often caused when the shadow-producing object extends above a humid or dusty, aerosol laden air layer near the surface and rises into clean, dry air. It then casts a mimicking shadow on the top of the humid layer below, as if it were a screen, and perspective broadens the shadow.

The shadow appears bluer than the brighter sky because that is the part of the sky where the object blocks the sunlight from striking the bleached aerosol layer.

Not all the fun is near the Sun. When crepuscular rays reign, take a moment to turn your eyes to the opposite side of the sky. There you may see *anticrepuscular* rays, which are crepuscular rays seen on the opposite side of the sky from the Sun. By perspective, anticrepuscular rays converge at the *anti*solar point.

A unique anticrepuscular ray, produced by the exhaust cloud of the Space Shuttle Atlantis shortly after the launch of NASA Mission STS-102 at 1832 EST on 07 Feb 2001, was photographed by Patrick McCracken (Fig. 9-55). Since sunset was 1807 EST, this was a twilight photograph, with the lower part of the exhaust cloud (and atmosphere) in Earth's shadow. Direct sunlight illuminated the upper part of the cloud, with red light from sunbeams that skirted just above the horizon, grading through yellow to white as sunbeams passed through thinner air aloft to reach the ever-rising cloud. The shaded, dark blue ray aimed at the antisolar point but also appeared to aim at the Moon. This was a case of serendipity because it was a Full Moon, the only time the Moon is at or near the antisolar point.

On occasion the anticrepuscular rays will cross rainbows, combining two ancient symbols of aerial divinity in a single scene. Such a scene was first ilustrated by Luke Howard. Anticrepuscular rays always cross the primary and secondary bows at right angles, like spokes on a wheel, as in Fig. 9-2, Fig. 9-56 and Fig. 7-13 (top). The rays often extend from bright or dark spots on the bow.

Fig. 9-55. Anticrepuscular ray as the shadow of the exhaust cloud of Space Shuttle, Atlantis 1832 EST 07 Feb 2001, NASA STS-102. The rays seem to point to the Moon only because it is a full Moon, which always appears opposite the Sun. Patrick McCracken.

Fig. 9-56. Spoked double rainbow with anticrepuscular rays over Cheyenne, WY, 08 Jun 2024 (moments apart from Fig. 9-2). JC.

Anticrepuscular rays are not seen often in the Eastern United States in part because the horizon is often blocked, but they are surprisingly common and sometimes quite dramatic under open skies from the Great Plains west. Like crepuscular rays, they change constantly as the clouds and Sun move, as on 30 Apr 2018 (Fig. 9-57), when, as Jan noted, "Against the backdrop of a departing thunderstorm, the Sun broke through a gap in the clouds and the sunbeams were crazy for about 5 minutes". The video of the rays can be seen at,

https://www.flickr.com/photos/cloud_spirit/26948984667/in/album-72157673641455795/

Fig. 9-57. Anticrepuscular rays seconds apart, at Cheyenne, WY, 30 Apr 2018. JC.

Anticrepuscular rays can also take on the colors of sunrise or sunset, as in fig. 9-58 just before sunset on 14 Oct 2016 when the dimly lit house confirms that the scene faces opposite the setting Sun.

At times it is difficult to know if you are seeing crepuscular rays or rain fallstreaks. Fig. 9-59 has the virtue of showing both. At other times, the obstacles producing the rays are out of sight, perhaps beyond the horizon, as in the twilight rays in the dust-filled stratosphere on 07 Sep 2019 (Fig. 9-60). Such twilights were produced for months following the eruption of Raikoke (one of the Kuril Islands east of Siberia) on 22 Jun 2019, as its tiny aerosol particles filled the stratosphere, and with no rain or snow to wash them out fell at a snail's pace.

Fig. 9-58. Colorful sunset anticrepuscular rays, Cheyenne, WY, 14 Oct 2016. JC.

Fig. 9-59. Crepuscular rays from the Sun at right crossing nearly vertical rain fall streaks, Cheyenne, WY, 04 Sep 2023. JC.

Fig. 9-60. Crepuscular rays after sunset over Cheyenne, WY, 07 Sep 2019, from ash of the Raikoke Eruption of 22 Jun 2019. JC.

9.7 Hotspots and Heiligenscheins

A curious feature, often called a hotspot, is the bright area on the ground just above the apex of the shadow of the fence pole in Fig. 9-61. A similar hotspot also appears in the grass just beyond the shadow of a house Fig. 9-57. The enhanced brightness of the ground at the antisolar point is a common observation on dry ground. It occurs because directly behind the objects all shadows of the ground cover lie hidden. At any other angle, some fraction of the shadow of objects appears, with the effect of darkening the ground.

A different type and cause of brightening occurs at and around the antisolar point when dew is on the grass or on other vegetation. The *heiligenschein* (holy glow) is due to sunlight directly backscattered from sparkling drops of dew. The drops resting on the hairs of the grass or on waxy leaves act as retroreflectors, reflecting sunlight directly backwards with increased focus, as in Fig. 9-62. The same heiligenschein occurs on street lines and road signs, because the paint is impregnated with glass spheres. (Recall the glass bead street bow of Fig. 9-14.)

Fig. 9-61. Antisolar glow on dry grass, 29 Sept 2017. JC.

The most famous description of the heiligenschein comes from the autobiography of the Renaissance goldsmith, Benvenuto Cellini.

> There is one thing I must not leave out—perhaps the greatest that ever happened to any man—and I write this to testify to the divinities and mysteries of God which he deigned to make me worthy of. From the time I had my vision till now, a light—a brilliant splendor—had rested above my head ....It can be seen above my shadow, in the morning, for two hours after the sun has risen; it can be seen much better when the grass is wet with soft dew.

Cellini took the heiligenschein as a sign that he above all others was blessed because he saw it shining only on the dew around the shadow of *his* head and not the shadows of the heads of his companions. Somehow, he never thought to ask his companions if they saw the heiligenschein around their blessed heads. He also failed to look close enough to see that it was the little dew drops that were shining.

Fig. 9-62. Heiligenschein cause by dew on the grass 05 Feb 2025. SDG.

9.8 Rainbow and Ray Gallery

Fig. 9-63. Hail streaks without raindrops blot out rainbows. Where there is only hail the bow will fail. Anticrepuscular rays cross the bow at right. Cheyenne, WY, 02 Aug 2020. JC.

Fig. 9-64. Blue sky double rainbow from dying shower facing Catalina Mountains from Vail, AZ, 22 Jun 2022. JC.

Fig. 9-65. Blue shaded crepuscular rays in smoky air, 31 Jul 2025. JC.

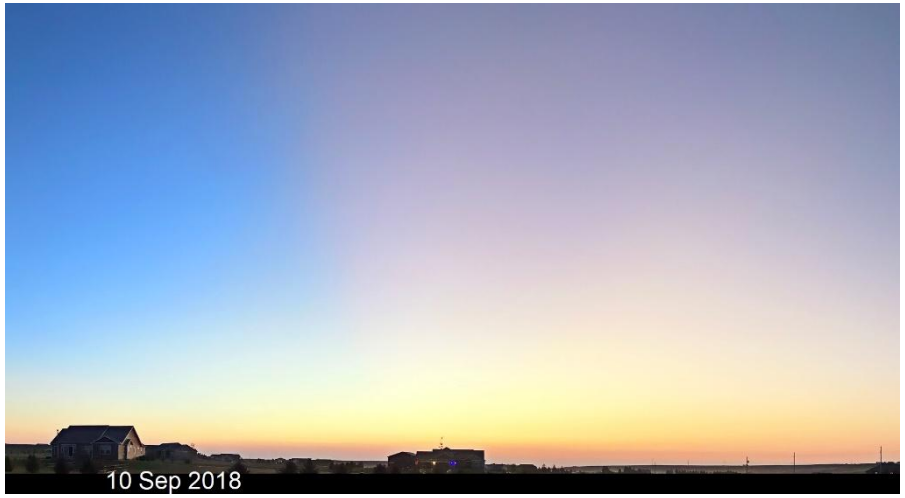

Fig. 9-66. Two color twilight sky – crepuscular ray due to shadow of thunderstorm 500 km away over the horizon, Cheyenne, WY, 10 Sep 2018. JC.

Fig. 9-67. Double rainbow with supernumeraries at sunset, Cheyenne, WY, 26 Jul 2024. JC.

Fig. 9-68. Full circle 360° double rainbow seen from the air over Vancouver, BC, Canada, 5 Nov 2025. © Martin Passchier.

Fig. 9-69. A 270° rainbow seen from the Schafberg near Wernstein, Upper Austria, 8 August 2022. © Erwin Köckerandl.

Fig. 9-70. Rainbow (with a faint secondary bow) in the rain shaft below a supercell thunderstorm outside of Dickenson, ND, June 19 Jun 2025. Note how blue the sky is below the rain-free flat cloud base on the right side of the supercell. This is largely from nearby scattered sky light. © Laura Hedien.

Wonders of the Atmosphere
Chapter 10: Cirrus and the Layer Clouds

Fig. 10-1. Cirrus uncinus fill the sky. SDG.

Fig. 10-2. Cirrus streamers over Boynton Beach, FL, 30 Dec 2016. The streamers fell from a jet's condensation trail. SDG.

Fig. 10-3. Tic-tac-toe contrails with cirrus near the horizon at 10.5 km near horizon over San Mateo, CA, 03 Nov 2016. SDG.

Wonders of the Atmosphere
Chapter 10: Cirrus and the Layer Clouds

10.1 Contrails: The Usurpers

Throughout Earth history, sentinel cirrus clouds invaded pure azure skies as the first forerunners of approaching storms (Fig. 5-30, Fig. 10-1, Fig. 10-2). Now, their role has been usurped by anthropogenic clouds left in the wake of jet planes – *cirrus homogenitus*, more commonly called condensation trails, or *contrails* (Fig. 10-3).

Fig. 10-4. Contrail with stratus, Harriman Park, NY, 04 Nov 2015. SDG.

Contrails form in air that is almost but not quite humid enough to produce natural clouds, as in Fig 10-3, where contrails and cirrus shared the sky around 10.5 km. Contrails form by two distinct processes. 1: Air pressure is lowered as it flows over the wing or flaps (Fig. 10-4), which produces adiabatic cooling. This process tends to lead to very short-lived contrails of extremely tiny droplets or ice

Fig. 10-5. A contrail is born over Cheyenne, WY, 06 Dec 2020. JC.

particles over or behind the wing that may be iridescent (see Fig. 14-28). 2: The exhausted fuel of jet engines adds both heat and water vapor. The mixing of the vapor-enriched exhaust with the colder and drier surroundings produces condensation in the manner of steam fog (recall §4.5). This process tends to leads to longer-lasting contrails in air supersaturated with respect to ice (recall §4.3) that form some distance directly behind the jet engines, as in Fig. 10-5.

The cloud canal or altocumulus *cavum* (cavity) over Boynton Beach, FL on 17 Jan 2014 (Fig. 10-6) is an example of a contrail. Temperature at cloud level was -30°C. Circular hole-punch clouds (recall Fig. 4-17) or long cloud canals are contrails that form after jets puncture or fly along patterned cloud sheets that consist of supercooled water droplets. This typically occurs at ambient temperatures between about -15°C and -35°C. The air and droplets above the wings or at wing tips are cooled enough to produce ice particles. The clear gap starts as the ice particles grow at the expense of the nearby droplets, which evaporate. The gap spreads as sinking motion in the jet's wake vortex warms the air and evaporates droplets further away.

Fig. 10-6. Contrail of ice particles making a clear lane in an altocumulus cavum of supercooled droplets over Boynton Beach, FL, 17 Jan 2014. SDG.

Airflow in the wake of jets not only affects the formation of contrails, it largely determines their shapes. A pronounced vortex develops in the wake of each wingtip (Fig. 10-7) as pressurized air beneath the wing swirls outward, up, and back inward atop the wing where air is depressurized. Tracers, such as the red smoke or droplets at cloud edges render their normally invisible flow fields visible.

A view facing the jet from behind reveals a counterclockwise vortex behind the right wing. If the photo had extended beyond the left wing and if another smoke release occurred on the left side of the plane, it would have revealed a clockwise vortex behind the left wing. Each of the twin vortices is embedded in the sinking flow of the other, so that the pair sinks with time. As the air sinks between the center lines of the vortices it warms, evaporating the droplets or ice crystals.

Fig. 10-7. A wingtip vortex revealed by smoke. NASA EL-1996-00130

Fig. 10-8. Contrails twisted by wingtip vortices. Left over Upper Saddle River, NJ (SDG). Right over Cheyenne, WY, 07 Feb 2018. JC.

Fig. 10-9. Wide contrail reflecting double vortex wake flow and snaking due to vertical shear crossing the contrail. The new contrail is still straight. SDG.

Contrails are also twisted in the wingtip vortices, as in the two cases shown in Fig. 10-8. When, in addition, the ambient wind with vertical shear crosses the twisted contrails at near right angles it gives them a serpentine shape, as in Fig. 10-9. If, for example, wind speed across the contrail increases with height from left to right, the contrail's twisted crests will be forced to the right while its troughs will be forced to the left.

The intense flow of the wingtip vortices is often unstable, so that tiny irregularities grow into a variety of pulses and waves. It also causes the distance between the vortices to form snake-like waves. This is called "Crow" instability The combination of all these motions with various profiles of ambient temperature, humidity, and wind speed and direction, contrails contain a range of fine scale features.

Almost all contrails consist of series of closely spaced beads, somewhat like strings of pearls. Periodic irregularities in the vortex flow may enlarge some of the beads, as in the top frame of Fig. 10-10. Wavy flow in the ambient air may bend the beaded contrails into a wavy shape as in the bottom frame of Fig. 10-10.

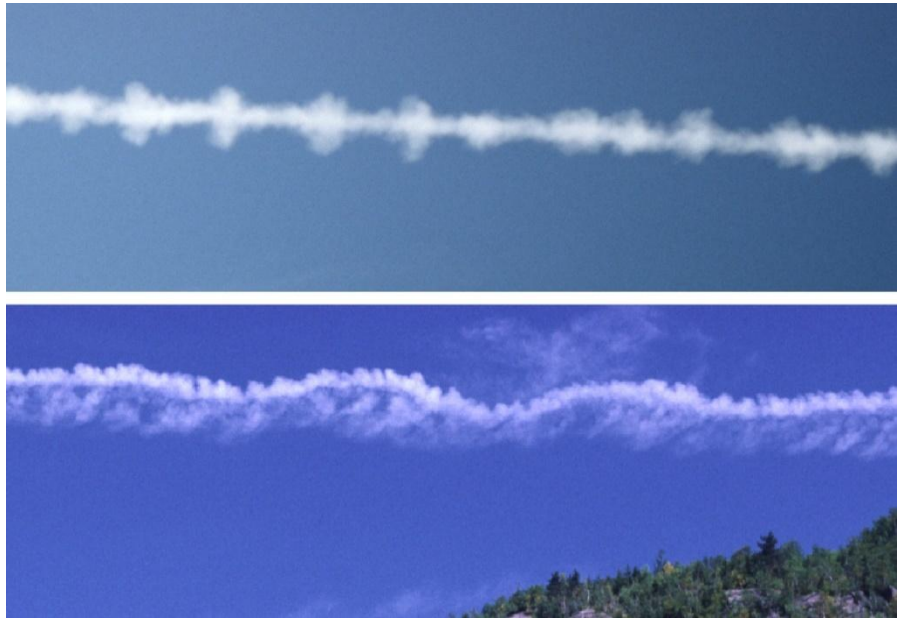

Fig. 10-10. Beaded contrails. The bottom contrail reveals waves in the air. SDG.

When a jet flies in a layer of air that has strong vertical wind shear and is stably stratified, possibly with a distinct inversion, its contrail may reveal Kelvin-Helmholtz waves, as in Fig. 10-11 and expose clear air turbulence.

Fig. 10-11. Contrail and possible natural cirrus revealing Kelvin-Helmholtz waves in a stable layer of strong vertical wind shear. SDG.

Fig. 10-12. Buoyant beaded contrails growing into species castellanus. SDG.

Fig. 10-13. Contrails with sinking mamma over San Mateo, CA, 09 Nov 2014. SDG.

When a jet flies in unstably stratified air, the contrail beads may be buoyant and rise to form cirrus castellanus homogenitus (Fig. 10-12).

Contrails that form in the descending and converging flow just above the center of the double vortex often assume the shape a V-shaped valley or trough. This shape is quite common with canal clouds, as in Fig. 10-5. The vortex flow enhances the sinking of the ice particles, with cirrus streamers and/or distinct mamma-like pouches, as in Fig 10-13. When there is little vertical wind shear beneath hole punch clouds, the falling streamers converge and take a funnel shape, as in Fig. 10-14.

Fig. 10-14. Hole punch cloud with little shear form goblet-shaped cirrus streamers over San Mateo, CA, 14 Sep 2018. SDG.

For better or worse, contrails are here to stay, so we might as well appreciate their artistry, and may even choose to embellish it (Fig. 10-15). Certainly, contrails are not mere curios. Many mutate so that after a few hours they often cannot be distinguished from natural cirrus (Fig. 10-16). They also persist and spread out to cover the sky from horizon to horizon, adding to the natural cloud cover as in Fig. 10-17 and Fig. 10-18. For three days after 9/11, when all commercial flights were halted, high cloud cover decreased (as did nighttime low temperatures).

Fig. 10-15. A photographically 'stacked' contrail at sunrise over Cheyenne, WY, 8 Dec 2020. JC.

Fig. 10-16. Cirrus uncinus homomutatus descending as streamers from stratocumulus over Cheyenne, WY, 31 Oct 2017. JC.

Fig. 10-17. Spreading contrails filling the sky over Cheyenne, WY, 10 Oct 2017. JC.

Fig. 10-18. Spreading contrails, cirrus homogenitus, curving from top left to center bottom and cirrocumulus homomutatus arching over Cheyenne, WY, 30 Mar 2022. JC.

10.2 Cirrus: Angel Hair Clouds

Cirrus, Joni Mitchell's 'Angel Hair', is the most delicate of the cloud genera, certainly in appearance. As stated in Chapter 4,

Cirrus are trails of falling ice crystals twisted by the wind.

In Fig. 10-2 the streamers fell almost straight down because the wind direction (west) and speed (32 m/s) were almost constant between 6.6 and 12.2 km, where the streamers were located. That is the exception. Far more often, wind speed increases with height so that the bottom or tail of each cirrus cloud lags behind the head, which may appear as a distinct generating cell (somewhat like a tiny cumulus) for the ice crystals, as in the cirrus *uncinus* (i. e., hook) in Fig. 10-19.

Fig. 10-19. Cirrus uncinus invading the sky over Boynton Beach, FL, 10 Jan 2023.

The comma is the most common shape for cirrus streamers, as illustrated in Fig. 10-20. The top or head of the comma is wider when it is the generating cell. The back or bottom of the tail lags further behind and is often nearly horizontal because as the crystals fall they sublimate and shrink. And as they shrink they fall more slowly, lagging ever further behind until they vanish.

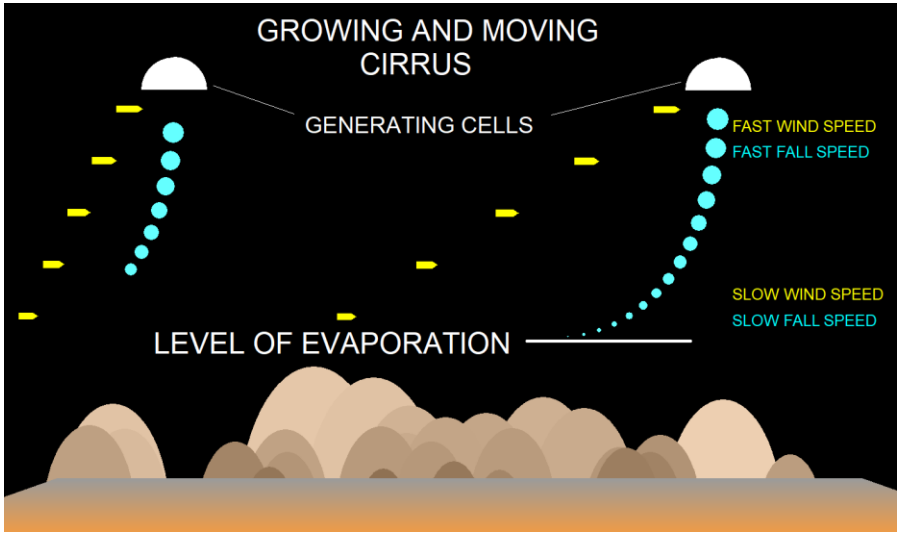

Fig. 10-20. Growing and moving cirrus. Ice crystals form in the generating cells, fall, sublimate, and fall slower as they shrink. When wind speed increases linearly with height trails take a comma shape as slower-falling crystals lag.

Fig. 10-21. Cirrus complex over Sapphire, NC, 23 Oct 2022 resembles the head and neck of some animal.

Fig. 10-22. Cirrus uncinus possibly from contrail over Ridgewood, NJ. SDG.

Be forewarned, though. Cirrus clouds seldom have such distinct streamers and heads and such simple shapes as in Fig. 10-2 and Fig. 10-19. Far more often, variations of ambient wind direction, speed, ascent rate, and humidity are complex. Then the streamers can twist, get entangled and blurred, and take on fantastic shapes. On occasion, even the least imaginative person will see animal forms in the clouds, as in Fig. 10-21, but it would take the most imaginative person to disentangle the complexities of this particular cirrus formation.

The zig-zag cirrus streamers below the generating heads in Fig. 10-22 reveal a simpler situation to disentangle. This line of cirrus streamers, possibly formed from an old contrail, reveals a nonlinear vertical profile of wind speed. The wind, blowing from right to left, decreases in speed below the generating cells to a minimum but then increases in the thin layer where the streamers bend downward to the left. Wind speed again decreases down toward the bottom of the streamers, where the downward slope to the right resumes.

Fig. 10-23. Two cases of paintbrush cirrus fibratus over Upper Saddle River, NJ, likely produced at crests of waves. SDG.

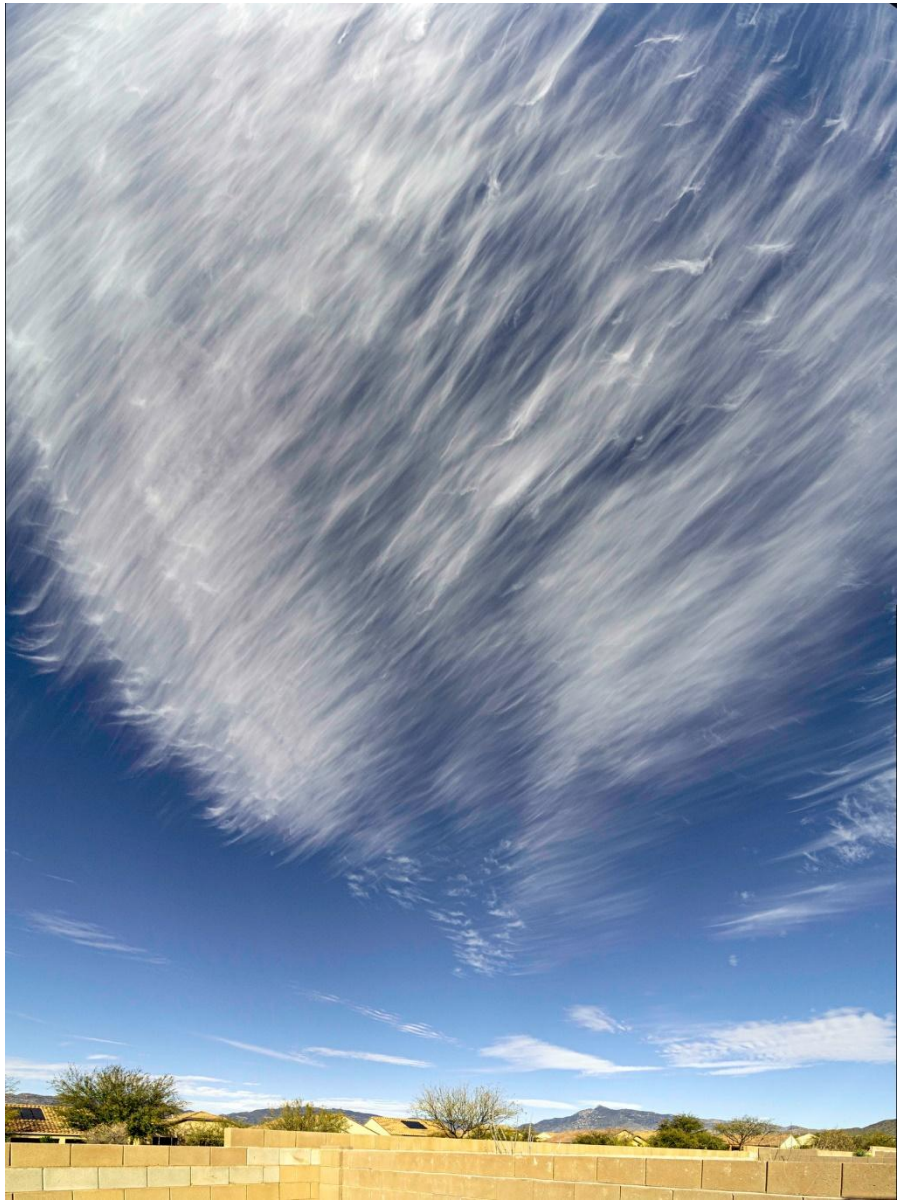

Fig. 10-24. Cirrus fibratus over Vail, AZ, 20 Feb 2020. JC.

Many cirrus clouds lack visible generating cells. Some of these look as if a paint brush were gently slid across a long section of sky, leaving a swath of parallel tracks of separate, individual fibers (Fig. 10-23). A likely cause for such *cirrus fibratus* is a gentle, laminar wave motion produced by wind shear in the ambient air. The tops of the fibers would form at the wave crests, where upward motion would have cooled a moist layer of air to the point of saturation. The shear would then align the fibers to cross the crests at angles up to 90°. A wondrous feature of cirrus fibratus is the vast number of largely distinct fibers (Fig. 10-24) almost as if mounted on a loom – a warp waiting for a woof of crossing threads.

Fig. 10-25. Cirrus floccus in a complete ring around a central tuft over Limerick, Ireland, at sunset, 22 Jul 2008. SDG.

The tufts in cirrus floccus seldom form lines. The ring of cirrus tufts with one more tuft in the center taken shortly before sunset on 22 Jul 2008 at Limerick, Ireland (Fig. 10-25), looks as if a stone were dropped into the atmosphere causing a circular wave to spread out with a central crest occupied by a tuft and circular crest occupied by a

garland of other tufts. This extraordinary formation may be the remnant of a hole-punch cloud.

Fig. 10-26. Cirrus spissatus mamma over San Mateo, CA 31 May 2015. Sublimation has made the mamma translucent. A thin layer of gray fog from the Pacific Ocean tops the crest of the Coast Range. SDG

Cirrus clouds may be translucent or opaque (i. e., optically thin or thick). Opaque cirrus spissatus (i. e., thickened) may have a large enough ice particle density to cause blobs of cloud air to sink. The sinking will be enhanced by evaporative cooling if the air below the cloud is dry. This is the optimal condition for mamma to develop beneath cirrus.

The cirrus spissatus of Fig. 10-26 formed in a humid layer at 7.4 km. With ***T*** = -24°C, it was likely for supercooled droplets and altocumulus. Indeed, one hour later a sheet of cellular altocumulus did form just above the cirrus. The mamma fell into a dry layer of air where ***RH*** fell as low as 15%. A closeup view

Fig. 10-27. Closeup of translucent mamma of Fig. 10-26. SDG.

Fig. 10-28. Cirrus radiatus vertebratus over Cheyenne, WY, 15 Feb 2017. JC.

Fig. 10-29. Cirrus vertebratus over Pacific Palisades, CA, possibly a remnant of a contrail. SDG.

shows that sublimation exacted a 'heavy' toll on the blob that sank the most (Fig. 10-27) making it translucent. Much lower, over the ridge of

the Coast Range in Fig. 10-26, ragged tendrils of gray fog from the Pacific Ocean also evaporated after cascading down the lee slope.

Fig. 10-30. Cirrus homogenitus vertebratus over Upper Saddle River, NJ, 22 Feb 2010 early in its evolution from contrails. SDG.

Sometimes cirrus takes the form of a central spine with vertebra on both sides, as in the cirrus vertebratus (i. e., jointed) of Fig. 10-28. Some cirrus vertebratus may be caused by the double wingtip vortex flow in the wake of jets, as possibly in Fig. 10-29 and certainly in Fig. 10-30. In those cases of cirrus homogenitus vertebratus, the vertebra form near the crest of each vortex and then sink, converge, and join to form the central spinal cord.

Parallel bands of cirrus radiatus will sometimes line the sky like the stripes of a flag (Fig. 10-31). The bands may be so long that they cross the sky (Fig. 10-32). When they do satellites provide an overview that may differ from the surface-based classification.

An extraordinary case of cirrus that would be identified as *radiatus* by a ground-based observer but more likely as *vertebratus* from Space occurred over the ocean south of Adelaide, Australia on 17 Oct 2017 (Fig. 10-33). The streamers, from 100 km long in the north to 200 km long in the south, were evenly spaced about 40 km apart and were

Fig. 10-31. Cirrus radiatus over Shepard Hall, CCNY. SDG.

Fig. 10-32. Cirrus radiatus crossing the sky over the Weisshorn, Switzerland, 15 Jun 2004. SDG.

oriented at almost right angles to the NW wind. The even spacing suggests waves and the sounding did contain relatively small vertical

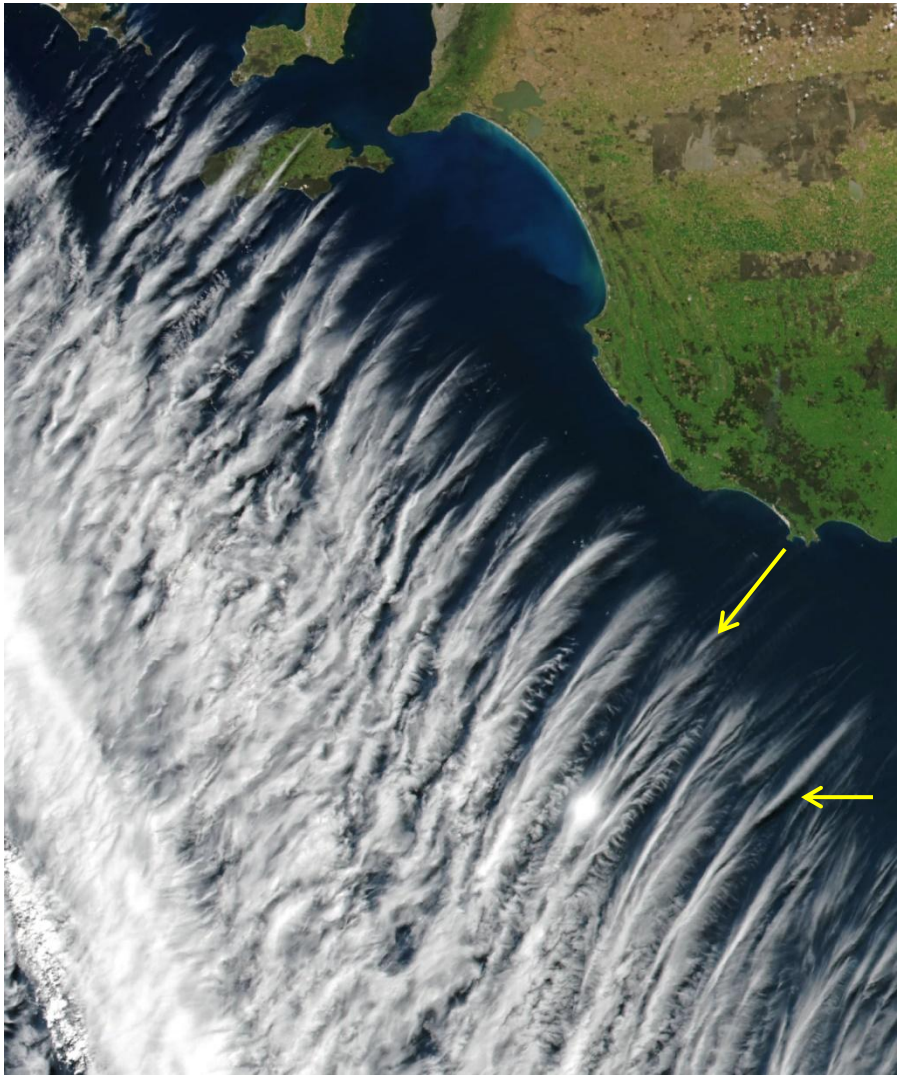

Fig. 10-33. Evenly spaced, parallel bands of cirrus south of Adelaide, Australia, 17 Oct, 2017. A subsun appears where arrows converge. NASA Suomi NPP VIIRS.

wind shear centered at 12 km, the height of the tropopause and cloud top.

A subsun can be seen toward the lower right of the image in the streamer pointing to the small cape at Portland. Subsuns occur when ice crystals (which formed at $T \approx -60°C$ in this case) fall with the top surface almost horizontal and act like tiny mirrors.

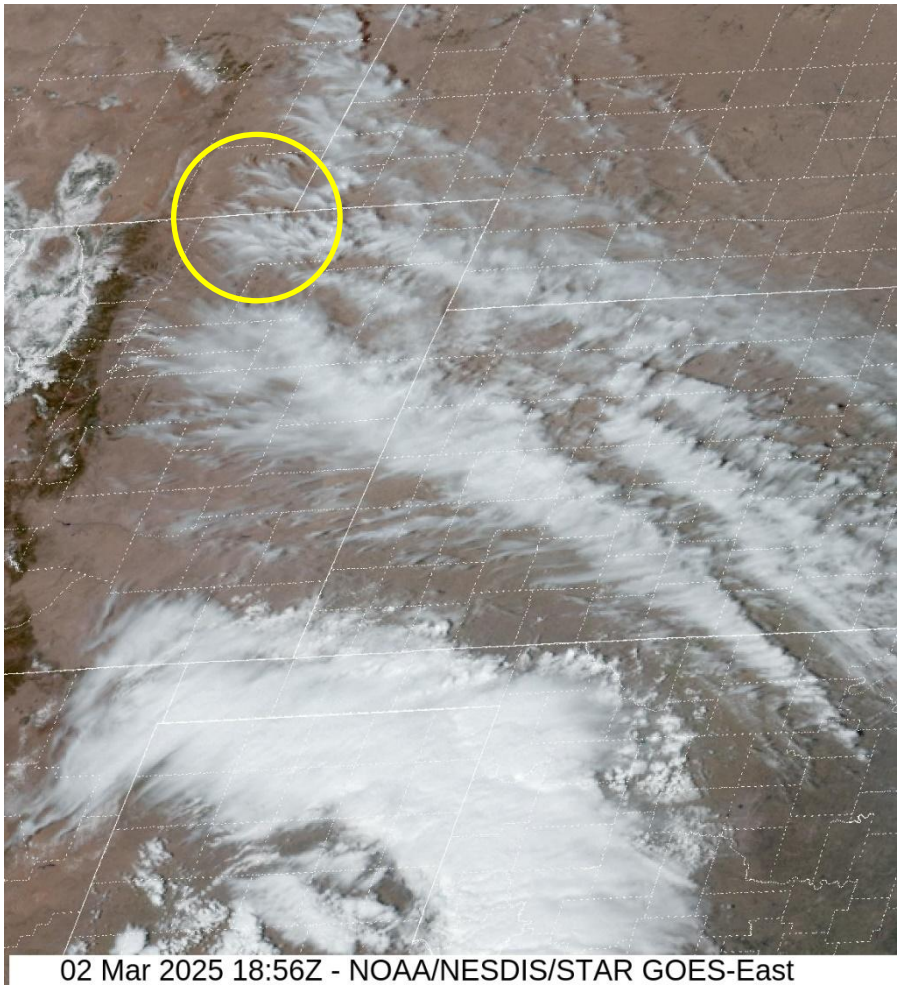

Fig. 10-34. Cirrus bands propagating ahead of a cyclone on 02 Mar 2025. Cirrus radiatus photographed from the ground appear in the yellow circle.

The drama of a similar outbreak of cirrus radiatus, though on a smaller scale, was imaged from both above (Fig. 10-34) and below (Fig. 10-35) on 02 Mar 2025. Its dynamism was captured by simultaneous time lapse GOES images and by a ground-based time lapse video (facing east) in,

https://www.flickr.com/photos/cloud_spirit/54361753915/in/photostream/lightbox/

The cirrus radiatus formed at the western edge of long bands of cirrus that stretched from Colorado and Wyoming eastward through Kansas and Oklahoma. While the satellite imagery shows the long bands

Fig. 10-35. Cirrus vertebratus east of Cheyenne, WY, 02 Mar 2025. JC.

ground-based video propagating northward out in advance of an extratropical cyclone centered over the Texas Panhandle, the ground-based video shows band after band of the feathery cirrus radiatus racing across the sky.

The reason that cirrus clouds are often forerunners of approaching tropical and extratropical cyclones as well as thunderstorms, is that all these storms expel cirrus in their outflows high in the troposphere. Hurricanes in particular generate parallel curved bands of cirrus radiatus in the anticyclonic outflow (Fig. 5-30 and Fig. 10-36). Blobby, asymmetric convection in the eye wall generates gravity waves that spiral outward. Then, instability at the periphery of the outflow produces the parallel bands of cirrus radiatus.

Gravity waves also produce cirrus bands in the outflow ahead of deepening extratropical cyclones, These bands seldom approach the symmetric beauty of hurricane outflow cirrus. An exception was developing Winter Storm Anya on 08 Nov 2024 (Fig. 10-37), which ejected two 1000-km long parallel bands that propagated so far ahead of the main cloud mass that skies cleared for hours after each passed. But the storm was on its way.

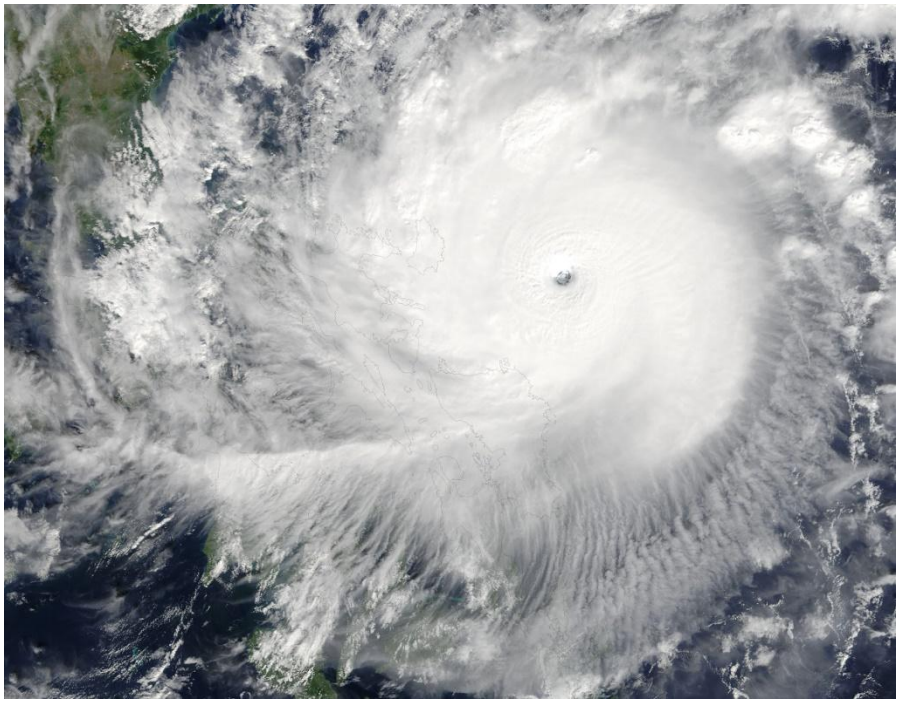

Fig. 10-36. Spiral cirrus and parallel bands of curved cirrus radiatus in the outflow of Typhoon Chaba, 03 Oct 2016.

Cirrus clouds are not always forerunners of storms. Quite often, they stand alone on their own, filling the skies for a precious few hours with beauty and grace before disappearing with nary a trace or passing over the horizon, leaving cloudless cobalt blue skies behind. While moving quietly in the background they adorn and embellish the foreground scenery. They go especially well with fall foliage (Fig. 10-38) and roses (Fig. 10-39).

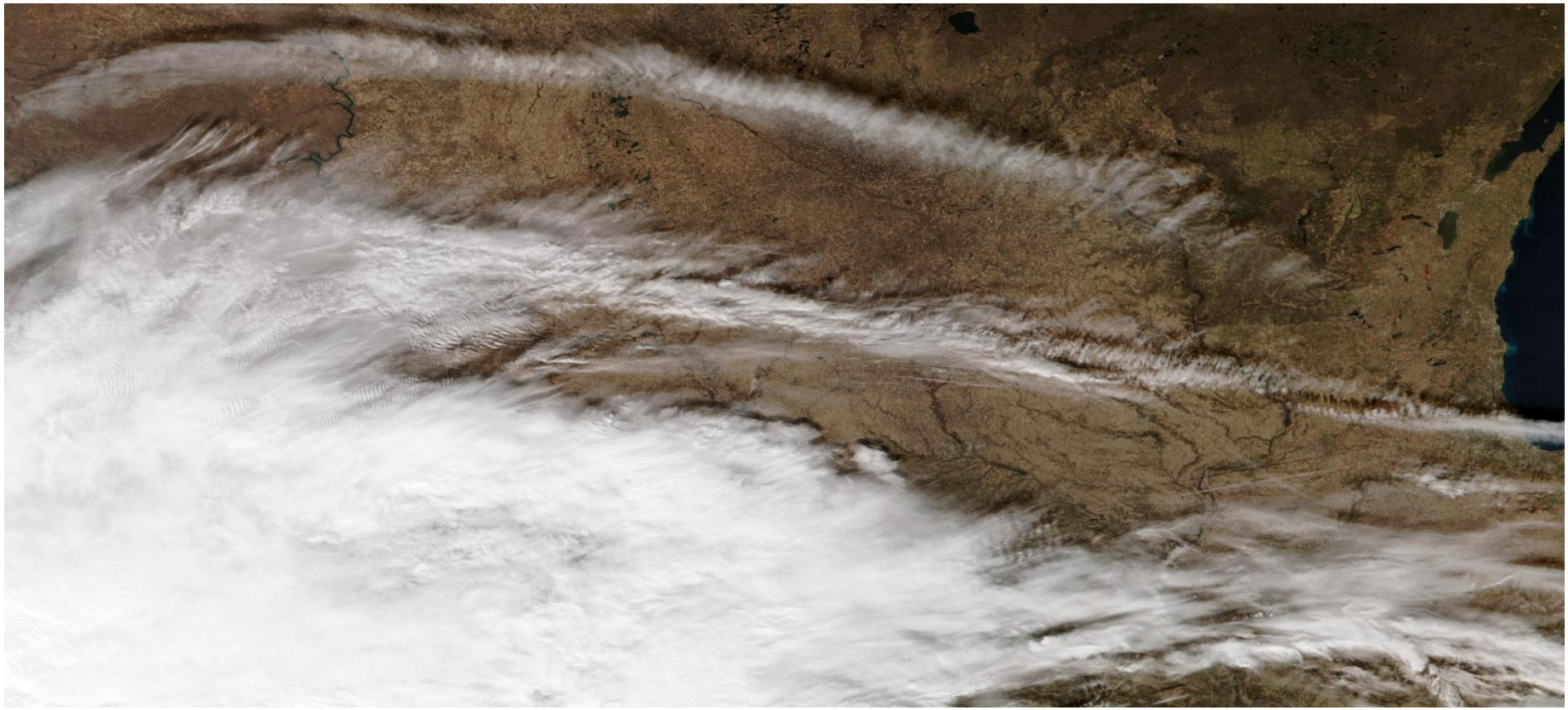

Fig. 10-37. Parallel bands of Cirrus radiatus moving ahead of the cloud shield from deepening Winter Storm Anya, 08 Nov 2024 NOAA 21 VIIRS satellite image.

Around sunrise and sunset, and sometimes almost an hour into twilight, cirrus clouds can take on colors. Because cirrus are high clouds, they bask in direct sunlight when all lower clouds are submerged in Earth's shadow. At such times, if they are optically thick, they can take on a deep red color because to reach them the Sun must pass through up to almost 80 equivalent atmospheric masses. Because of their great height, cirrus differ in color from lower clouds. Cirrus (and cumulonimbus tops) are the first clouds to turn white after sunrise and the last to remain white as the Sun sets.

Despite their great height, cirrus are seldom the best sunrise and sunset clouds. This is because cirrus tend to be scattered and optically thin. As a result, their color palette tends to be less fiery, even gentle, though the play of colors in Fig. 10-40 is quite fine.. As we will see in Chapter 12, the honor of best sunrise and sunset clouds usually goes to patterned sheets of altocumulus because of their great optical thickness to the horizontal rays of the rising and setting sun.

10.3 Overcast Layer Clouds

Layer clouds are the opposite of penetrative clouds. Penetrative clouds are short-lived, buoyant plumes. Even though they tend to form where moisture and upward motion are enhanced by the large-scale setting, they appear to act with dramatic flair as individual rogues. They are

Fig. 10-38. Cirrus radiatus over Saddle River, NJ. SDG.

Fig. 10-39. Cirrus fibratus and uncinus over the San Mateo, CA rose garden, 30 May 2012. SDG.

Fig. 10-40. (also Fig. 4-2). Cirrus sunset at Vail, AZ 15 Nov 2022. JC.

Fig. 10-41. The advancing edge of a cirrostratus veil. SDG.

narrow enough to be viewed in their entirety from the ground and so, convey a false impression that the atmosphere is deep.

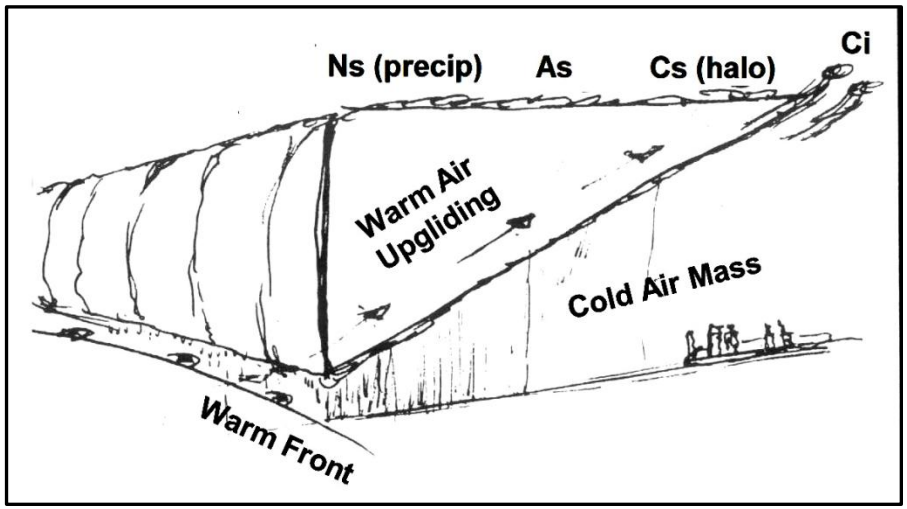

Fig. 10-42. The cloud wedge above the warm frontal surface. The typical width is 500-1000 km and the slope is of order 1/100. SDG.

Layer or stratiform clouds form from air that ascends at a gentle slope of about 1/100 and at little more than a snail's pace (typically 1 to 50 cm/s). The air may surmount broad highlands or huge domes of cold air masses as part of extratropical cyclones (Fig. 10-42, see also Fig. 4-24 and Fig. 5-36). Stratiform cloud decks act as extended units hundreds of kilometers across that operate with little fanfare but great endurance for hours or days on end. Stratiform clouds are so extensive they can only be seen in their entirety from space. In this way, they restore a proper perspective that the atmosphere is a thin veneer.

Stratiform clouds can be complex. Flying through them reveals they often contain several cloud layers with interspersed clear lamina, plus embedded convective clouds, just as a layer cake is interspersed with layers of frosting and often laced with chocolate bits.

Stratiform clouds produce most of the rain and snow outside the tropics during the cold part of the year. Even in the tropics, where thunderstorms command much of the attention, stratiform clouds often knit the anvils together, outlast the thunderstorms that created them, and produce about 40% of the rain. Bob Houze's ***Cloud Dynamics*** (2014) is an encyclopedic reference by the scientist who discovered much about cloud systems.

In extratropical cyclones, stratiform clouds form a wide wedge as tropical air slides over a dome of polar air. This is the warm conveyer belt (recall §5.7). Nimbostratus, which provides the bulk of the extratropical cyclone's rain and snow, forms as tropical air begins its ascent over the dome of polar air. Frontal fog may form when rain falls through the shallow cold air dome just poleward of the surface front. Further east and poleward the cloud thins and its base rises as the altostratus, through which the Sun or Moon may peer dimly and from which rain or snow may fall. As the air continues ascending the dome the cloud sheet thins to cirrostratus, sometimes marked by halos. With further rising, almost all the water vapor has been removed and the highest, furthest poleward and east cloud remnants are the cirrus

The entire stratiform cloud pattern becomes a sequence in time for an observer at a fixed location as it moves from west to east to provide early warning signs of the approaching storm. The highest clouds arrive first and lead to the classical lowering cloud sequence,

$$\text{cirrus} \rightarrow \text{cirrostratus} \rightarrow \text{altostratus} \rightarrow \text{nimbostratus}$$

Precipitation begins about 12 to 24 hours after cirrus appears. It typically lasts another 12 to 24 hours. Fog or a fracturing, ragged complex of clouds marks the end and then the temperature rises.

Cirrus clouds, the first in the storm sequence, and which we have just seen in §10.2 are so beautiful and delicate they rouse little suspicion of a possible storm. But high aloft they may be weaving their web silently. If you have not been watching the change, you may suddenly notice that the landscape does not seem to sparkle as it did a short time before. Looking up, you may catch the leading edge of the veil of cirrostratus advancing across remnants of azure sky, as in Fig. 10-41. More likely, you are a bit too late and the azure sky now appears milky blue. The cirrus clouds have thickened and congealed into a complete

Fig. 10-43. Cirrostratus with 22° halo over Cheyenne, WY on 18 Feb 2017. JC.

but translucent fabric of cirrostratus. The Sun still shines through cirrostratus, but it casts less pronounced shadows.

Quite often, cirrostratus provides compensation in the sky for the loss of brilliance to the landscape below. Stretch your arm out and use your outstretched palm to shield your eyes from the still blinding Sun. Look all around your hand and if you are lucky, you will see a large circular ice crystal halo, the classic insignia of cirrostratus and oncoming storms. Recall the fateful lines in Henry Wadsworth's poem, ***The Wreck of the Hesperus***,

Then up and spake an old Sailòr,
Had sailed to the Spanish Main,
"I pray thee, put into yonder port,
For I fear a hurricane.

Fig. 10-44. Leading edge of cirrostratus with 22° halo at its best over Cheyenne, WY, at noon on 24 Jan 2022. Snow arrived 12 hours later. Note that the sky just inside the halo is darker than the sky just outside. JC.

"Last night, the moon had a *golden ring*,
And to-night no moon we see!"
The skipper, he blew a whiff from his pipe,
And a scornful laugh laughed he.

Of course, the old 'Sailòr' was spot on and the skipper was dead wrong, for the 'golden' ring is the circular 22° halo, so named because its bright inside (which is reddish and not golden) appears at an angle of 22° from the Sun or Moon in all directions. The first example of an ice crystal halo we present (Fig. 10-43) is typical but is neither brilliant nor highly colorful, so that most people would not notice it. Its subdued appearance results from two factors that so often impair the potential beauty of halos and even presence of halos in cirrus and cirrostratus, namely, 1: many crystals are 'imperfectly' shaped and, 2: the cloud is optically thick.

A more alluring but still modest appearing halo (Fig. 10-44) graced the leading edge of an optically thinner layer of cirrostratus on 24 Jan 2022 over Cheyenne, WY. The time lapse video of that halo,

https://www.flickr.com/photos/cloud_spirit/51842056189/in/album-72157632749850748

shows that it faded whenever and wherever the cirrostratus got too thick.

Ice crystal halos that form from perfectly shaped and oriented crystals in clouds of optimal optical thickness with the proper Sun angle can be so stunning they can take your breath away, especially if you are immersed in them. We present views of such extraordinary halos and explain how they form in Chapter 11.

When a halo appears in cirrostratus (halos also appear in cirrus and, near ground level on frigid days, when 'diamond dust' crystals form and sparkle in clear air) there is a 50% chance of rain or snow within 24 hours. That probability rises to over 80% if the cloud cover thickens and lowers and transitions to altostratus.

Fig. 10-45. Altostratus with a watery Sun and lower scud clouds over Cliffside Park, NJ. SDG.

Fig. 10-46. Altostratus undulatus asperitas over the City College of New York and the George Washington Bridge. SDG.

Altostratus, the central cloud genus in the warm, moist conveyer belt, imparts a somber look to every scene, without a hint of blue in the gray sky. Altostratus can be translucent (Fig. 10-45), with its trademark 'watery' Sun only dimly visible through the thickened veil as through ground glass so that at best it casts faint shadows. Scud or *pannus* (shred) often forms nearer the ground. Altostratus may also be opaque, and if so, can be quite dramatic when the polar air below the frontal surface is dry. Then the strong vertical wind shear across the frontal surface produces a series of ripples and waves that can give the cloud base the almost cosmic look of asperitas, as in Fig. 10-46.

The first light rain or snow in a winter storm sometimes falls from altostratus. An indication that rain or snow may soon reach the ground is that the once distinct corrugations of the base of the altostratus have become blurred and indistinct. Then, provided the polar air below the frontal surface is not too dry rain can begin in about 15 minutes, or snow in about 30 minutes if it is cold enough. This is the time it takes

raindrops or snowflakes to reach the ground from the blurred cloud base of the altostratus, typically around 2 km above the surface.

Fig. 10-47. Nimbostratus in Chittenden, VT at the beginning of the snowstorm of 03-04 Oct 1987. SDG.

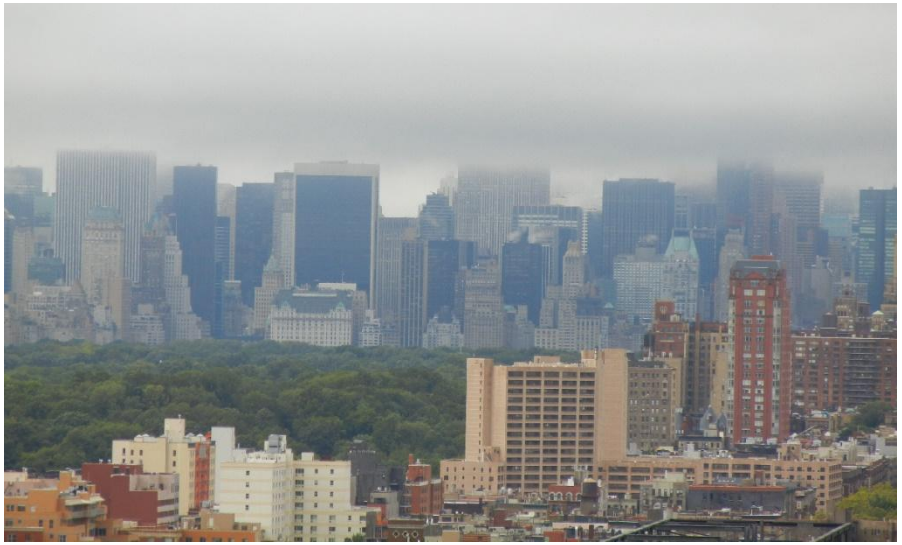

Fig. 10-48. Nimbostratus cutting off tops of skyscrapers over Manhattan, NY, 08 Sep 2011. SDG.

Fig. 10-49. Snow from nimbostratus filling the air at City College. SDG.

Steady rain or snow or freezing precipitation begins in earnest once the altostratus lowers and thickens to nimbostratus. Nimbostratus is generally almost featureless, though cloud fragments called scud sometimes appear below. The base of the amorphous cloud is almost indecipherable unless it is marked by some towering landscape feature such as a mountain (Fig. 10-47) or skyscraper (Fig. 10-48).

Light rain had just begun to fall around Vermont on 03 Oct 1987 at the moment shown in Fig. 10-47, but aloft it was cold and snowing. Over the next few hours the falling snow cooled the air as it melted, just as ice cubes cool a glass of water. In this way, snow forged its way to the surface. For the next 12 hours snow totals up to 50 cm fell, weighing down the trees, which were in fall foliage mode, breaking their limbs or felling them en masse and making the forest sounds reverberate like the cannon cracks of a pitched battle.

Moderate or heavy snow can be a beautiful sight, even if everything is gray, as in the pre-Halloween storm of 2011 in northern New Jersey and southern New York (Fig. 10-49). In very cold air, flakes tend to

Fig. 10-50. Huge, clumping wet snowflakes at start of storm at Upper Saddle River, NJ, 30 Oct 2011. SDG.

Fig. 10-51. Snow-burdened foliage adds color to a gray scene under nimbostratus clouds, Rockaway NJ, 30 Oct 2011. SDG.

be small and fine and the snow on the ground is so fluffy that a column of snow on the ground will weigh only 1/30th that of the same depth of water. When either $\boldsymbol{T} \approx 15°C$ where the flakes are shaped like branched dendrites and interlock, or especially as $\boldsymbol{T} \rightarrow 0°C$ so that the flakes begin to melt and stick, and form huge flakes several cm across, as in Fig. 10-50, snow on the ground can be slushy and almost as dense as ice. It is the heavy, wet flakes that pile on and stick to tree branches, especially those still in full leaf, that crack branches and limbs and make entire trees bow down or topple. This occurred in both the 04 Oct 1987 snowstorm from the northern border of New York and Vermont south to the gates of New York City, and the pre-Halloween 30 Oct 2011 snowstorm (Fig. 10-51) with up to 40 cm.

Fig. 10-52. Altostratus reflected by Cloud Gate, Chicago, 15 Jul 2009. SDG.

What about aesthetics, always a matter of individual taste? Stratus and nimbostratus are the classic gray, often featureless clouds that either render scenes gloomy or obscure them. All other cloud genera can be look attractive or at least distinctive without any other foreground or background features. Even altostratus exhibits some variation, as in Fig. 10-45, Fig. 10-46, and Fig. 10-52, where it is reflected by Cloud

Fig. 10-53. Stratus covering the United States Capitol, 13 Apr 2013. SDG.

Fig. 10-54. Stratus covering Yosemite Valley, CA, 16 May 2017. SDG.

Gate in Chicago. Featureless stratus and nimbostratus require foregrounds in order to appear as anything other than blank, gray slates, and then they remove all sparkle from the landmarks they cover, as with the United States Capitol (Fig. 10-53) and Yosemite Valley (Fig. 10-54).

Fig. 10-55. Same scene during Blizzard whiteout conditions Cheyenne, WY, 14 May 2021 (top), and clear sky the next day (bottom). JC.

Blizzards can cause *whiteout* conditions that make cloud and snow-covered ground look the same and obscure everything not immediately in front of the viewer, as during the height of the blizzard of 14 Mar

2021 in Cheyenne, WY (Fig. 10-55 top). The same scene gleams under clear skies just after sunrise the next morning (Fig. 10-55 bottom), with pink sunlit snow and blue shaded snow (recall the Alpenglow in §2.4).

The forms of precipitation in the great warm conveyer belt cloud shields of extratropical cyclones include snow, ice pellets (sleet), freezing rain, and rain. And, just as there is a pattern of cloud genera in the warm conveyer belt, so too, there is a pattern of precipitation forms, with snow furthest poleward, grading in order to ice pellets, freezing rain, and rain. However, freezing rain and ice pellets require special conditions.

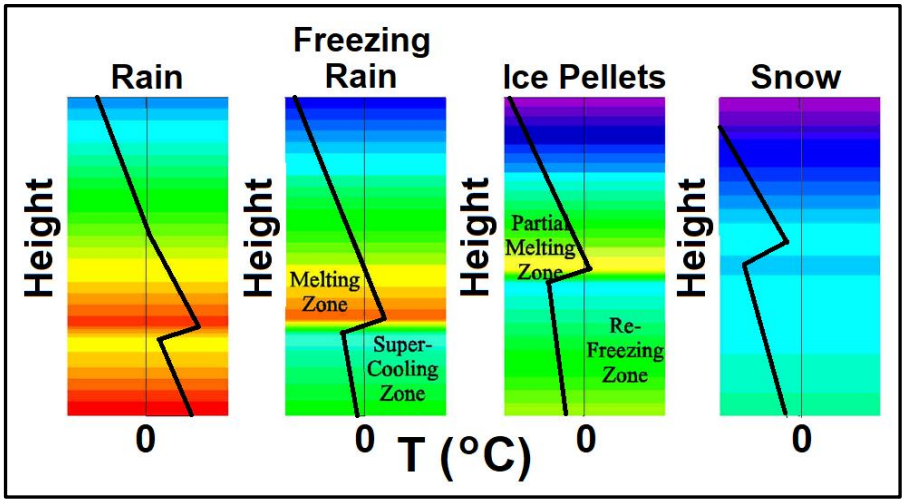

Fig. 10-56. Precipitation forms and their soundings. The sequence from left to right mimics the sequence moving poleward from the warm front. SDG.

The form of precipitation at any particular location in a storm is determined by the vertical profile of temperature and humidity that the hydrometeors form in and fall through, i. e., the sounding, and it tends to occur in order from furthest poleward to nearest the surface warm front as shown in Fig. 10-56.

In almost all cases, precipitation forms aloft as snow but melts to rain if there is a thick layer at and near the surface up where $\boldsymbol{T} > 0°C$. But if $\boldsymbol{T} < 0°C$ all the way to the surface, snow reaches the ground and sticks. Because snowflakes do not melt immediately once $\boldsymbol{T} > 0°C$, snow can also reach the ground if the lowest few hundred meters is just above freezing, particularly if RH is low, because then evaporation will dominate melting and keep the snowflakes frozen. Except in the rapid downbursts in thunderstorms, the highest temperature that snow can reach the ground is ≈10°C. Of course, if $\boldsymbol{T} > 0°C$ the snow will not stick on the ground very long.

Freezing rain and ice pellets (i. e., sleet) only form when there is a wrinkle in the sounding – a melting zone aloft (just above the frontal surface) where $\boldsymbol{T} > 0°C$ sandwiched between layers higher aloft and near the surface where $\boldsymbol{T} < 0°C$. Freezing rain dominates when the melting zone is warm and thick enough to melt snowflakes completely to raindrops, because even if the surface layer of air is extremely cold the raindrops will not easily refreeze but will become supercooled.

Ice pellets dominate when the melting zone is thin and barely above 0°C so that the snowflakes do not melt completely. The partially melted flakes collapse into tiny slush drops, which easily refreeze if the surface layer they fall into is cold enough. Once hydrometeors have largely melted, they never regain their virginal crystalline form. Instead, they refreeze as ice pellets that sting when they hit your face and often bounce like the much larger hailstones when they hit the ground.

Freezing rain is deceptively dangerous and destructive. It seems like normal rain, but since it is supercooled, it freezes upon contact with the ground, with trees, with power lines, even with eye glasses. Freezing rain turns the ground into an ice skating rink, much like the scene in the movie, ***Home Alone***, where Kevin (the boy) hosed the steps to the house, which quickly freeze so that Harry (the chief burglar) almost broke his back and Marv (the second burglar) slipped down the stairs on his back and failed in several attempts to stand up. In a film this may be hilarious, but it is accurate and not funny in real life when it happens to people who fall or to cars and trucks that slide and crash into each other, brakes being utterly useless. We both know!

When freezing rain sticks on trees it can be a beautiful sight if the freezing layer is thin (Fig. 10-57), but if it is thick it can and has downed power lines, tree limbs and whole trees. In short, nothing moves and power outages are widespread and long-lasting, even if the weather turns warm.

Fig. 10-57. Alder branches coated with a thin layer of ice and Spruce branches with snow at Fairbanks, AK, moonlit winter night, 1999. JC.

Winter storms may seem to last an eternity, but eventually they move on. Moving Fig. 5-33 in the direction of the double arrow shows the cloud and weather sequence. If the storm center passes by poleward of the observer the air begins to warm and the cloud base continues to lower, often reaching the ground as frontal fog. After that, warming continues and the sky tends to clear and often hazy.

If, however the storm center passes by equatorward of the observer, the weather remains cold and the cloud layer clears fitfully, lifting, severing and shredding in a sometimes ominous manner (Fig. 10-58) and sometimes in a hopeful manner with a setting Sun finally peeking through the western edge of the overcast (Fig. 10-59). Sometimes smooth, rounded evaporating remnants resembling cumulus but classified as fractostratus are all that remain, as at Unga Island in the Aleutians, Alaska after four days of unbroken clouds and rain (Fig. 10-60). Soon though, these vestiges also disappear, leaving behind some of the deepest blue pristine skies, the air having been swept clean of aerosols by the falling raindrops and snowflakes.

Fig. 10-58. Departing storm over Cliffside Park, NJ with altostratus above fractostratus tilted by strong vertical wind shear. Clearing occurred a few hours later. SDG.

Fig. 10-59. Lifting cloud veil at sunset with fractostratus west of New York City after a storm. SDG.

Extensive covers of stratus and fog often form far from extratropical cyclones when air passes over cold water. The fog often lifts and breaks up to fractostratus during the day as it drifts over land and gets heated, as on Inch Beach, Ireland on the afternoon of 21 July 2008 (Fig. 10-61). In such places the beauty is striking, especially when it

comes after many hours or days of gray, and with the prospect of returning as the air cools when the Sun goes down.

Fig. 10-60. Fragmenting, evaporating fractostratus after 4 days of rain on Unga Island in the Aleutians. © Margaret Winslow.

Fig. 10-61. Dissipating fractostratus, Inch Beach, Ireland, 21 July 2008. SDG.

10.4 Gallery

Cirrus is beautiful enough to make a scene all by itself or can embellish any scene.

Fig. 10-62. Cirrus uncinus, Granada, Spain, 06 Oct 2007. SDG.

Fig. 10-63. Cirrus fibratus, Boynton Beach, FL, 15 Jan 2012. SDG.

Fig. 10-64. Clear morning sky (left) vs nimbostratus afternoon with ice pellets (right), Long's Peak, CO, 01 Aug 1976. What a difference a cloud makes. SDG.

Fig. 10-65. Stratus fractus dissipating, San Francisco, CA, 13 Apr 2013. SDG.

Fig. 10-66. Sunlight breaking through stratus at Killington, VT, 28 Feb 2010. SDG.

Fig. 10-67. Cirrus uncinus and spissatus racing to the east over San Francisco, CA, 27 Sep 2015. SDG.

Fig. 10-68. Nimbostratus soaks the Alamo, 27 Feb 2012. SDG.

Fig. 10-70. Stratus with Moeraki Boulders, New Zealand, 01 Nov 2017. SDG.

Fig. 10-69. Stratus with small breaks over Kinderdijk, Netherlands, 18 May 2018. SDG.

Fig. 10-71. A contrail over fall foliage at Sapphire, NC, 17 Oct 2025. SDG.

Wonders of the Atmosphere
Chapter 11: Ice Crystal Halos

Fig 11-1. Halo complex atop Mt. Fichtelberg, 30 Jan 2014. ©Claudia Hinz

Wonders of the Atmosphere
Chapter 11: Ice Crystal Halos

11.1 Halos, Overlooked Cousins of Rainbows

Outside the polar regions or ski slopes, halos are the overlooked cousins of rainbows. Produced when ice crystals refract and/or reflect sunlight, they often form beautiful rings, arcs, or spots of light in the sky above entire unseeing populations. There are times, though that you are immersed in such a bewildering array of brilliant halos, as in Fig. 11-1, you can't help being awestruck, as Jack London was when he saw diamond dust in the Klondike gold-rush Alaska.

> It is clear and cold....And in the sky are three suns, and all the air is flashing with the dust of diamonds. ***The Sundog Trail***.

Two of these 'Suns' are not Suns at all, but brilliant halo spots directly right and left of the Sun called *parhelia*, mock Suns, or Sun dogs because they 'follow their master', the Sun (Fig. 11-2). And the flashing dust is not made of diamonds, but of ice crystals.

Just as you can see the sparkling drops that make garden-hose rainbows, if you are lucky you can see sparkling ice crystals right in front of your eyes that make up diamond dust halos. The bright spots in Fig. 11-1 are ice crystals, not stars, for it is daytime. Fig. 11-3 is a paradigm example of halos produced by diamond dust, especially in the eyebrow-shaped upper tangent arc at the top of the photo.

If you live where temperature falls far below 0°C, diamond dust may crystallize right in front of your eyes in the chilled air on clear, frigid mornings. If enough of the crystals spread around the sky, those situated where halos form with respect to the Sun will light up best.

How do you find halos if they do not find you? In warmer regions, begin your search the next time cirrostratus clouds of an approaching

Fig. 11-2. Sundogs following their master, the Sun 20 Mar 2020, 21 minutes before sunset. A sun pillar also tops the Sun. JC.

extratropical or even tropical cyclone begin to fade the sunlight. Halos can be seen on the hottest days, even at the equator, for the temperature 10 km above sea level is always cold enough for ice crystals. Of course, great care is needed not to blind yourself when looking for halos, coronas, or crepuscular rays near the Sun.

Fig. 11-3. Halo complex with 22° halo, upper and lower tangent arcs, a parhelic circle and parhelia, all lit by diamond dust crystals. ©Claudia Hinz.

Instructions for Viewing Halos: While looking down, extend your arms and cross your hands to block the Sun. Then look up around your hands, preferably with sun glasses. The 22° halo will appear about an open hand width in all directions around the Sun.

If you are ever fortunate enough to witness a spectacular halo display you may find yourself swept away by its 1: great extent, for halos may crisscross the entire sky (both above and below the horizon), 2: blinding brightness, as with the spear tip shaped lower tangent arc directly below the Sun in Fig. 11-3, 3: high color purity, as in the circumzenithal arc near the top of Fig. 11-1, and 4: incredible variety, as in Fig. 11-1. You may then judge halos more fascinating than rainbows.

Halos can cover a greater extent of the sky than rainbows, and, of course, their scale is much greater than photographs (especially wide angle shots) suggest, for photos rarely convey a sense of the scale of the scenes they portray. The 22° halo (recall Fig. 10-41 and Fig. 10-42) is an impressive sight, for when its bottom touches the horizon its top extends half way to the zenith. But in Fig. 11-1 the 22° halo is only the *inner* ring. The outer ring, a combination of several arcs, has a *radius* of over 46°, so that if its base touched the ground, its top would extend just beyond the zenith.

We now proceed as in a mystery by first presenting the incredible variety of halos and only then explaining *how* each halo forms and how the incredible halo complexes form.

11.2 The Incredible Variety of Halo Forms

As of 2022, Jarmo Moilanen and Maria Gritsevich identified and listed 119 different ice crystal halos. Fig. 11-1 offers a magnificent but partial sampling of this diversity, as does Table 11-1 and Fig. 11-4, where the simulation includes and labels 17 halo forms.

Included in this great diversity are at least nine circular halos. In addition to the common 22° halo and the rare 46° halo are the parhelic circle and the so-called odd-radius halos of 9°, 18°, 20°, 23°,

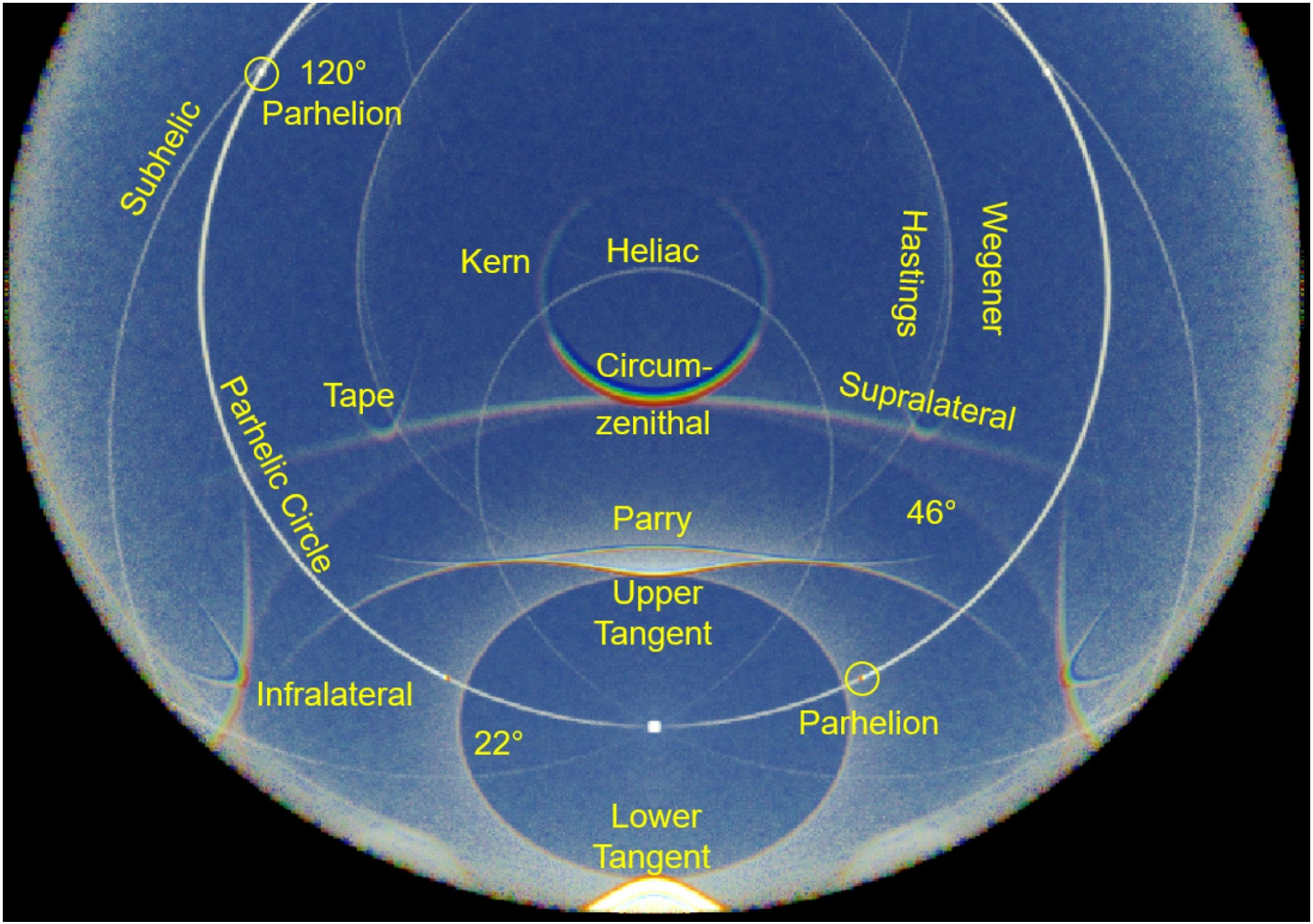

Fig. 11-4. Simulated Halo Complex for Sun height, H_{SUN} = 30° with Halo Names. There are a few more arcs opposite the Sun (not shown here). SDG.

Table 11-1. Catalog of the more common halos and their properties. H_{SUN} is the Sun's elevation angle.

Halo Name	Shape	Frequency	Intensity, Color	Crystal Shape	Orientation c-axis	H_{SUN}	Light Path
22º	Circular	High	Moderate Pale Red Inside	Plates, Pencils	Random	All	Refraction through Alternate sides
46º	Circular	Very Low	Feeble Red Inside	Thick Plates	Random	All	Refraction through 1 side and top or bottom
9, 18, 23, 35	Circular	Low	Moderate Red Inside	Pyramidal	Random	All	Refraction through at least one pyramidal face
Sundog Or Parhelion	Spot	High	Intense, Semispectral	Plates	Vertical	Below ~61º	Same as 22º halo
Tangent Arcs	Arcs at top and bottom of 22º	Medium-High	Intense, Semispectral	Pencils	Horizontal	Below ~ 40º	Same as 22º halo
Circumscribed Halo	Oval around 22º halo	Medium-High	Intense, Semispectral	Pencils	Horizontal	Above ~ 40º	Same as 22º halo
Parry Arcs	Arcs above and below 22° halo	Low	Intense near spectral	Pencils	A rectangular face Horizontal	All	Same as 22° halo
Circumzenithal Arc	Arc above Sun around part of Zenith	Medium-high	Bright, Spectral	Plates	Vertical	Below ~32º	Refraction in top hexagon out of side
Circumhorizon-tal Arc	Arc below Sun around part of horizon	Low	Bright, Spectral	Plates	Vertical	Above ~58º	Refraction in side out bottom hexagon
Parhelic Circle	Horizontal arc through Sun	Medium	Bright, White	Thick Plates Pencils	Vertical or Horizontal	All	Reflection from sides or Hexagons
Sun Pillar	Vertical arc through Sun	Medium-low	Bright, Same as Sun	Pencils, Plates Dendrites	Tilted slightly	Near Horizon	Reflection from top or bottom
Suprlateral Arc	Arc above Sun touching CZ arc	Low	Bright, Spectral	Pencils	Horizontal	Below ~32º	Refraction in Hexagon out of lower side

Fig. 11-5. Odd-radius halos of 9°, 18°, 20°, and 24° (with its upper tangent arc) over San Francisco, 1400 PST, 23 Feb 2016. The 35° halo was present but did not show in the photograph. ©Mila Zinkova

Fig. 11-6. Vertically elongated (overexposed) subsun surrounded by Bottlinger's Rings over the Rocky Mountains. SDG.

Fig. 11-7. Halo underworld: Subsun, sun pillar, 22° halo and lower tangent arc (on left) with subparhelion, subparhelic circle, and sub-22° halo (on right) on 11 Jan 2007, S. Canada. ©Bill Burton, USGS.

Fig. 11-8. Left: Orange Subsun and Sun pillar from a low Sun. Right: 22° halo, sundog, subsun, and lower tangent arc for H_{SUN} 19°. SDG.

24°, and 35° (Fig. 11-5) Most of the circular halos are accompanied by halo spots and multiple arcs. For example, the upper and lower tangent arcs are often attached to the top and bottom respectively of the 22° halo, and Parry arcs sometimes bracket them. In Fig. 11-1, Fig. 11-3, and Fig. 11-4, the upper tangent arc resembles a pair of arched wings, while the upper suncave Parry arc, (concave with respect to the Sun but not visible in Fig. 11-3) appears as an eyebrow over the upper tangent arc.

There is also a whole underworld of halos. In fact, the halo with the greatest, potentially blinding brightness is the subsun, as in Fig. 5-2, Fig. 10-33, and Fig. 11-6, where a faint elliptical Bottlinger ring surrounds the subsun. The subsun has its own set of halos, including a sub-22° halo and sub-sundogs, as in Fig. 11-7, which includes a sun pillar, the bottom of the 22° halo and a blinding, lower tangent arc. The detailed form of a less brilliant lower tangent arc, with a subsun near its bottom, 22° halo, parhelion, and faint subparhelion appears in the right panel of Fig. 11-8.

All halo arcs change shape as the Sun's elevation angle or height in the sky, $\boldsymbol{H}_{SUN}$, changes. Only the circular halos involving refraction appear with the same form and size at any $\boldsymbol{H}_{SUN}$. The parhelic circle shrinks as the Sun rises and has an angular radius equal to the Sun's zenith angle, $\boldsymbol{Z}_{SUN} = 90° - \boldsymbol{H}_{SUN}$.

As the Sun or Moon rises, the tangent arcs join to form the circumscribed halo as in the simulations of Fig. 11-9. When the Sun is low in the sky, the upper tangent arc, which touches the top of the 22° halo, resembles a pair of arched wings, and the lower tangent arc, which touches the bottom of the halo, resembles closed legs or a spear tip, as in Fig. 11-1 and Fig. 11-3. As the Sun climbs the wings relax downward and the legs spread out and up. Once the Sun is a little higher than 30°, the upper and lower tangent arcs join to enfold the 22° halo as a circumscribed halo, as in Fig. 11-10, a lunar halo!

Fig. 11-10. Halo display with H_{MOON} = 45° including the 22° halo surrounded by the circumscribed halo, the parhelia and parhelic circle and the rare infralateral arcs in Kuopio, Finland, 24 Jun 2014. ©Vesa Vauhkonen.

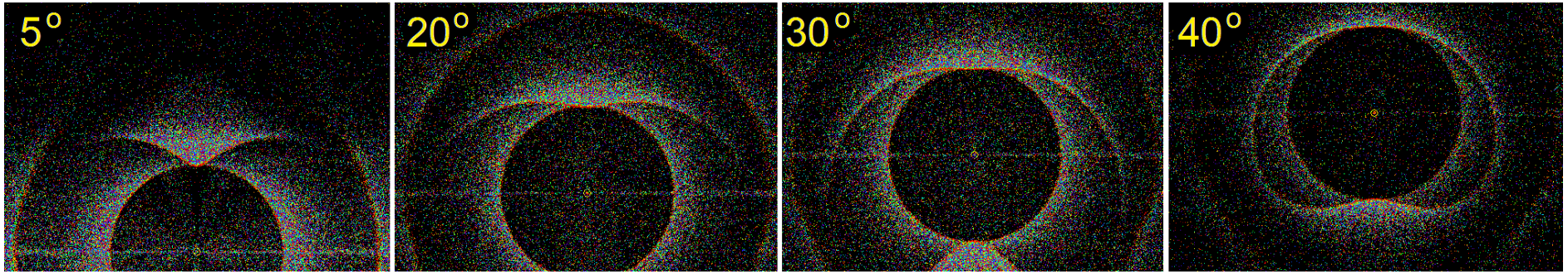

Fig. 11-9. Simulations of the 22° halo, its tangent arcs or circumscribed halo, and supralateral and infralateral arcs as functions of H_{SUN}. SDG.

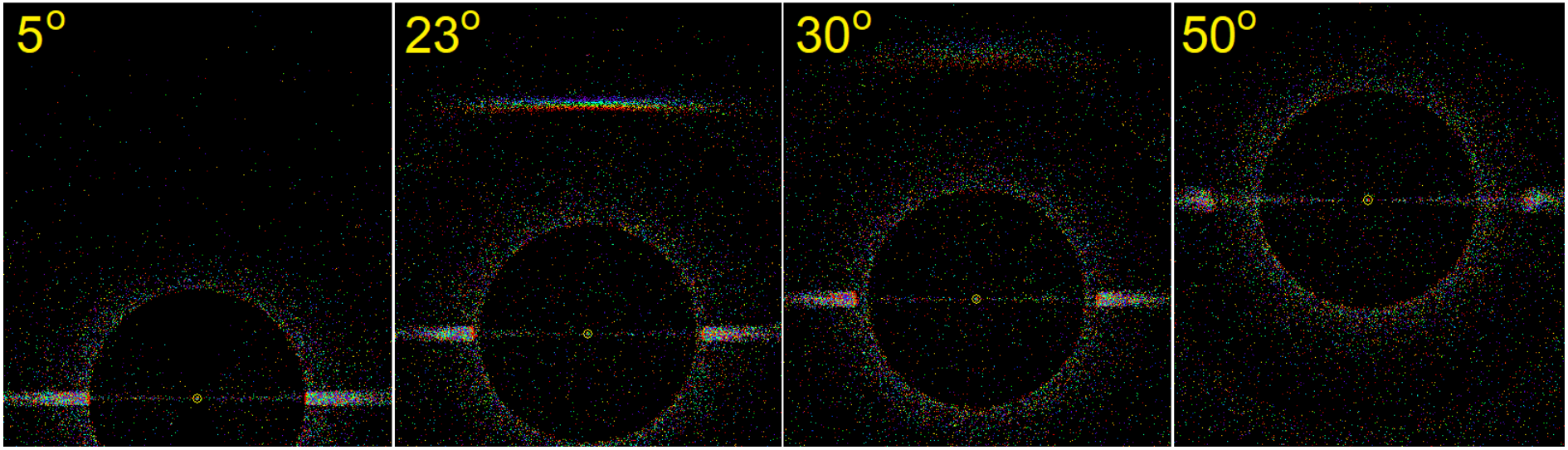

Fig. 11-11. Simulations of the 22° halo, the parhelia and parhelic circle, and the circumzenithal arc as functions of H_{SUN}. SDG.

Fig. 11-12. Parhelic circle with 120° parhelion over Old Bald Rock Mountain, Sapphire, NC, 18 Oct 2018. SDG.

The parhelia appear most often when the Sun is relatively low in the sky, though they do appear for Sun heights up to $H_{SUN} \approx 61°$. They form on both sides of the Sun at the same height as the Sun, which is why they are called sun dogs (following their master). When the Sun is at the horizon, the parhelia coincide with the 22° halo. However, as H_{SUN} increases the parhelia move further outside the 22° halo, as in the simulations of Fig. 11-12. In Fig. 11-10, where $H_{SUN} \approx 45°$ the parhelia are far outside the 22° halo and happen to coincide with the circumscribed halo (which gets closer to the 22º halo as H_{SUN} increases). The parhelia also tend to diminish in intensity the higher the Sun in the sky. Once $H_{SUN} >\approx 61°$ in the sky the sun dogs refuse to follow their master and vanish, though the parhelic circle (e. g., Fig. 11-1, Fig. 11-4, Fig. 11-10) persists and potentially brightens.

Fig 11-12 shows a piece of the parhelic circle in cirrus clouds on the opposite side of the sky from the Sun above Old Bald Rock Mountain and Fairfield Lake, NC on 18 Oct 2018 when $H_{SUN} \approx 45°$. The bright enlarged dot to the right of center in the parhelic circle is a 120° parhelion, which is always located at an azimuth angle of 120° from the Sun. Notice that both the parhelic circle and the 120° parhelion are white.

The parhelic circle and the 120° parhelia are among the halos that have no play of colors because they involve reflection with no refraction. Others include the sun pillar, the subsun, and the rare heliac, subhelic, Wegener, and Hastings arcs. Since these arcs for

solely by reflection, they are near white when the Sun is much above the horizon (at least 10°) and redden as the Sun nears the horizon. Sun pillars, which form when the Sun is near the horizon, appear tinted by the low Sun, as in Fig. 11-13.

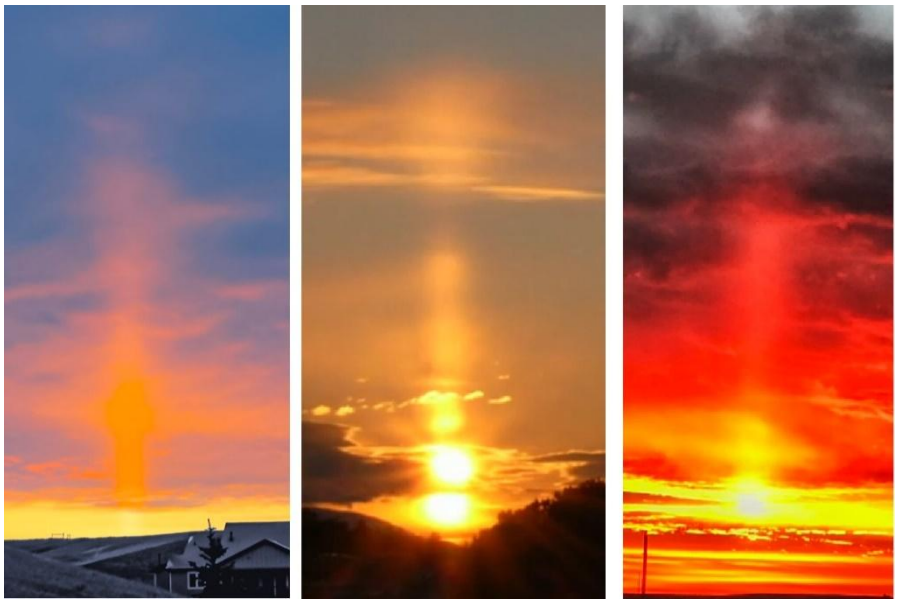

Fig. 11-13 Sun pillars hold the sky, predawn, 05 Apr 2025 (left), 28 Mar 2016 south of Santa Fe (center), and 10 Jan 2018 (right). JC.

It is nice to wake up seeing a sun pillar holding up the sky. Sun pillars are most pronounced around dawn, often appearing before sunrise and lasting until the Sun is about 5° above the horizon. They often form in conjunction with altocumulus clouds at $\boldsymbol{T} \approx$ -15°C, the optimal temperature for flat, star-shaped crystals.

Irrefutable evidence that the cirrus centers of hole punch clouds consist of ice crystal is the parhelion and segment of the parhelic circle in Fig. 11-14. Coronas and iridescence but no halos, may occur in the surrounding altocumulus cloud of supercooled droplets, though they seldom do. It is fun when hole punch clouds appear in the sky to seek out those that are properly located to host halos, or wait for a cirrus-filled hole to move to a possible halo location. The reward, of course, is when the cirrus lights up.

Fig. 11-14. Parhelion inside hole punch cloud over Boynton Beach, Fl, 02 Jan 2024. SDG.

Brightness and color are two separate properties of halos, although halos that possess color tend to be brighter when they are more colorful.

Table 11-2 lists the maximum potential brightness of several halo forms relative to that of the Rayleigh atmosphere. The parhelia are the brightest of all halos seen *above* the horizon, just as subsuns are the brightest of the infernal halos. Spots are the brightest because the scattered light is directed to the smallest area of the sky. Next come the arcs, and last, the circular halos, which spread the light over the largest area of the sky. Some rare halo forms have great potential brightness but require stringent conditions that are seldom met.

Name	Max
Parhelion	1415
120° Parhelion	1000
Tangent Arc	92
Parry Arc	80
Parhelic Circle	34
Circumzenithal Arc	25
Heliac Arc	15
9° Halo	15
Circumhorizontal Arc	9.5
22° Halo	9.5
Parry Infralateral Arc	7.5
Parry Supralateral Arc	3.5
Hastings Arc	2.6
Subhelic Arc	2.5
Infralateral Arc	2.25
Supralateral Arc	1.65
46° Halo	1.5
Clear Skylight	1.0

Table. 11-2. Maximum potential brightness of simulated halos relative to a Rayleigh atmosphere.

Fig. 11-15. Circumscribed halo, parhelic circle and circumhorizontal arc over Peru with $H_{SUN} \approx 72°$. ©Steve Gettle.

Color is, of course, one of the alluring properties of halos, with some halos much more colorful than others. Color even provides a way to distinguish halos. For example, even though the colored circular halo in Fig. 11-13 *seems to be* a 22° halo, it is, in fact, a circumscribed halo, which is near circular at $H_{SUN} \approx 72°$, and much brighter and more colorful than the 22° halo, though it is lacking in blue.

Fig. 11-16. Colorful parhelion over Boynton Beach, FL 06 Jan 2023. SDG.

The parhelia, which can be blindingly bright, never have high spectral purity. Red, which is the most prominent color of the parhelia only has modest spectral purity. Orange and yellow are progressively less pure and the 'cooler' colors are seldom seen. The parhelion in Fig. 11-16 has unusually rich colors. However, it owes its pale green and blue tones in part to the blue skylight that penetrated the optically thin cloud edge.

The most colorful halos are the arcs associated with the 46° halo, which can be seen by comparing the arcs of the 46° halo to the arcs and spots of the 22° halo in Fig. 11-1, Fig. 11-4, and Fig. 11-17, a display with the 22° halo, tangent arc, parhelia and parhelic circle, supralateral and faint infralateral arc plus the spectral circumzenithal arc. Note also that the circumhorizontal arc in Fig. 11-15 is more nearly spectral than but not as bright as the circumscribed halo.

Fig. 11-17 Halo display 13 Jan 2024, Cheyenne, WY with $H_{SUN} \approx 22°$. JC.

Fig. 11-18. Circumzenithal arc over Tolland, CT, 05 Dec 2010. SDG.

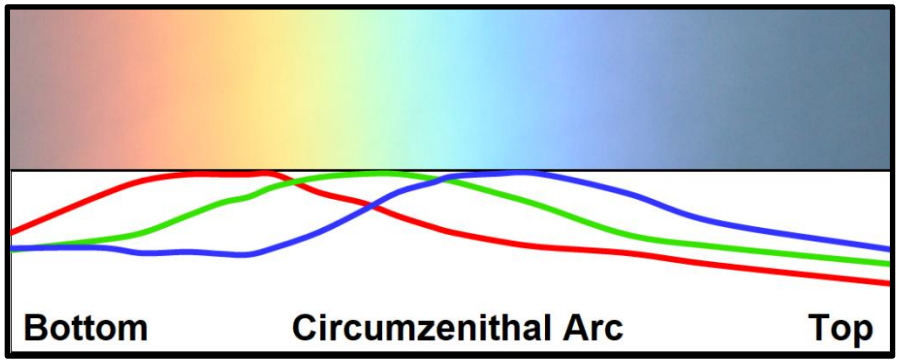

Fig. 11-19. RGB colorimetric values of vertical slice through the CZ arc of Fig. 11-18. SDG.

The two most highly spectral halo arcs are the circumzenithal (CZ) arc (Fig. 11-18 with RGB values in Fig. 11-19) and the circumhorizontal (CH) arc (Fig. 11-20 with RGB values in Fig. 11-21). Not only do they have very similar spectra, they are geometrical complements of each other (i. e., they add up to 90º). The CZ arc partly circles the *zenith* at least 46° *above* the Sun, but only forms when $\boldsymbol{H}_{SUN} < \approx 32°$ and its spectral purity is greatest when $\boldsymbol{H}_{SUN} \approx 22°$. The CH arc partly circles the *horizon* line at least 46° *below* the Sun, and only forms when the Sun is higher than $\boldsymbol{H}_{SUN} > \approx 58°$ and its spectral purity is greatest when $\boldsymbol{H}_{SUN} \approx 68°$.

The CH arc is much rarer than the CZ arc because it requires such a high Sun. In much of the world the Sun either rarely or never climbs as high in the sky as $\boldsymbol{H}_{SUN} = 58°$. On the summer solstice the highest

Fig. 11-20. Circumhorizontal arc over Nepalese Himalayas, 7 May 2011. Фтещт Нфтлщмнш.

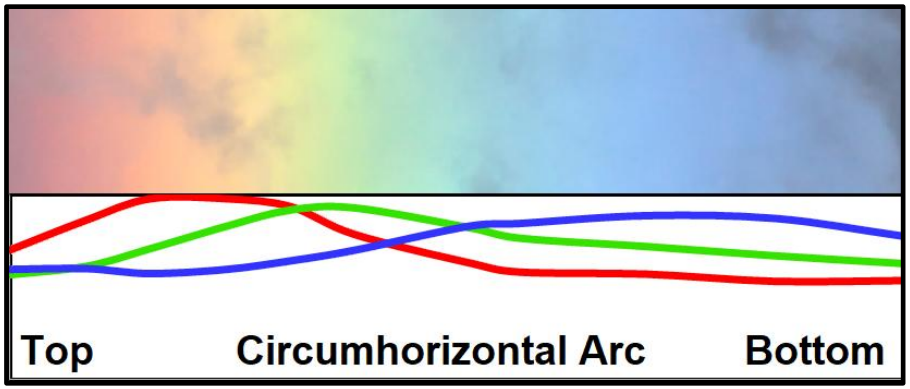

Fig. 11-21. RGB colorimetric values of vertical slice through the CH arc of Fig. 11-20. SDG.

latitude the Sun reaches that height is Lat = 55.5. On the winter solstice the highest latitude the Sun reaches that height is only Lat = 8.5º. And it only reaches that height in the hours, or perhaps minutes around noon local time. By contrast, the CZ arc can be seen any day with sunlight.

11.3 Why Halos are so Varied

We have now seen a significant number of different halos, though only a few of the 119 halos are common. The most common seen from the ground are the 22° halo and the parhelia, which are observed almost 200 days a year in Western Europe! Many halos are

quite uncommon and some, such as the Kern and Lowitz Arcs, and sun dog of the sun dog are so rare they may not be reported anywhere in a generation. Nevertheless, all these halos do exist. How can there be so many when there are only four rainbows (aside from virtually invisible higher order bows)?

Begin with the analogy between ice crystals and cut diamonds. Turn a brilliant cut diamond ever so slightly and whole series of sparkles flash on and off. The popular *brilliant cut* for diamonds was designed in 1919 by Marcel Tolkowsky using a combination of trial and error and mathematics to maximize sparkle.The multiple sparkles are due to the fact that the brilliant cut diamond has 57 facets with the optimal dimensions and angles. The most basic ice crystal plan is the hexagonal prism with only 8 facets – six rectangular side faces and two hexagonal end faces – but that's enough for starters. (Pyramidal crystals have up to 20 facets, though they are not common.) By contrast, raindrops and cloud droplets are not faceted.

The great diversity of halos arises from the large number of choices a sunbeam has upon striking a crystal. It can strike any of the facets that face the Sun and either be reflected by or refracted into the crystal. Once inside the crystal it can be refracted immediately upon striking another facet or reflected once or more inside the crystal before ultimately being refracted and leaving the crystal.

The choices available to the sunbeams and the angles of deflection derive from three geometrical factors,

1: The dimensions and facets of the ice crystals (§11.4),
2: Their orientation as they fall (§11.5),
3: The Sun's height in the sky.

These factors, along with the laws of reflection and refraction and Fresnel's Law determine 1: which facet the sunlight strikes, 2: which facet it leaves, 3: the angle, ***D***, it has been deviated by, and, 4: the fraction of light beams reflected or refracted at each facet.

The brightness of halos depends on two additional factors,

4. The size of the ice crystals,
5. The optical thickness of the path through the cloud and through the air outside the cloud.

Geometric optics is an excellent approximation for halos (§11.6) only if crystals are larger than about 100 μm. Diffraction, which only vitiates halos, (there are no supernumerary halos) is increasingly important the smaller the crystals.

The optical thickness of the path through the cloud determines the probability that light will emerge from the cloud after striking one and only one crystal (see §11.8). The optical thickness through the atmosphere outside the cloud including aerosols, diminishes the halo beam and determines the contrast-reducing background lighting.

11.4 Forms of Ice Crystals

The study of halos represents a marriage with the study of ice crystals. Almost always, the simplest ice crystals make the best halos. The most basic ice crystal form is the 8-facet hexagonal prism. It has 6 rectangular sides (prism faces) of length, ***c*** and 2 hexagonal ends (basal faces) of width, *a*. The ratio (***c***/***a***) of crystal length to width, is the aspect ratio. The direction of the crystal is defined by the c-axis, which points out from a hexagonal face, and by the angle the rectangular faces rotate around the ***c***-axis.

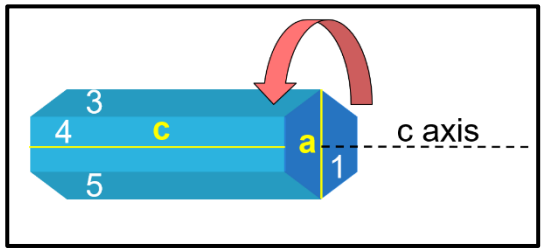

Fig. 11-22. A simple pencil ice crystal of length *c* > width a, with faces numbered. Pencil crystals often fall with c-axis horizontal and may spin around the c axis. SDG.

Pencil crystals are much longer than wide and have typical aspect ratios of about 3 to 5. Plate crystals are much shorter than wide and have typical aspect ratios of about 0.2 to 0.33. Pencil crystals often fall with ***c***-axis horizontal (as in Fig. 11-22) while plate crystals tend to form with the ***c***-axis vertical.

Fig. 11-23. Ice crystal forms. ©Kenneth Libbrecht

Crystals may grow pyramidal endings, either on one or both basal faces. The pyramids are either complete, coming to a point, or stunted and ending at a smaller basal face, in which case a bipyramidal crystal will have 20 facets. The length of a complete pyramid is always 1.63 times its width (aspect ratio = 1.63). The angle between the c-axis running the length of the prism and each of the pyramidal sides is 28°. Walt Tape (a leader in collecting diamond dust crystals that produced halo complexes at the South Pole) has dubbed this *Angle* ***x*** because it took two centuries to confirm.

Simple, solid pencil, plate, and pyramidal ice crystals are the exception. The vast majority of crystals have complex features, including capped ends, hollow insides, steps, and spiked branches (Fig. 11-23). Each of these complexities reduces the halo producing effectiveness of the crystals. Star-shaped crystals (*dendrites*), as beautiful and symmetric as they are, are so complex, with so many facets, that the only halos they can produce are subsuns and sun pillars. It should be obvious that heavily rimed and multifaceted crystal complexes, such as in Fig. 11-24, cannot produce any halos at all. For the purpose of halos, they are 'junk' ice.

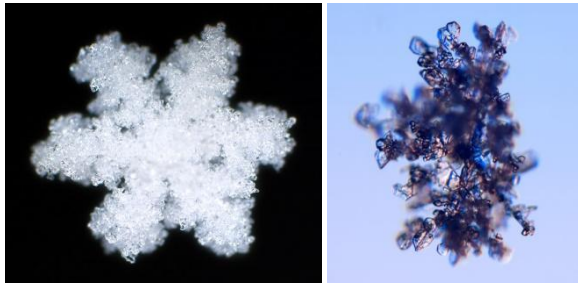

Fig. 11-24. Heavily rimed snowflake and a crystal cluster. ©Kenneth Libbrecht.

It took time to sort out the crystal forms and their properties. The microscopic study of ice crystals was pioneered by Robert Hooke (***Micrographia***, 1665). Explorer, and natural scientist William Scoresby furthered the field in around 1820 with his drawings of pristine crystals observed in the Arctic, documenting the basic forms, including plates, pencils, and pyramids or bullets in addition to the well-known star-shaped crystals.

Starting in the late 1800's and continuing up to his death in 1931 from pneumonia contacted in a snowstorm, Wilson Bentley in Vermont pioneered the microscopic study of snow crystals, photographing them resting on black velvet with great skill and selection. (He apparently rejected thousands of flakes for each one he chose.) Taking up where (and when) Bentley left off, Ukichiro Nakaya in Japan documented the ranges of ***T*** and ***RH*** under which the various forms of ice crystals dominate and illustrated them in a Nakaya Diagram (Fig. 11-25).

For example, plates dominate for the ranges, 0°C < T < -3°C and -10 < ***T*** < 20°C, while columns dominate in the range, -3°C < T < -10°C Solid plates dominate at the smallest values of supersaturation over a large range of temperature. In general, crystal complexity increases with the degree of supersaturation, with star-shaped or dendritic crystals dominating at the highest values of supersaturation, especially in the range, -10 < ***T*** < 20°C.

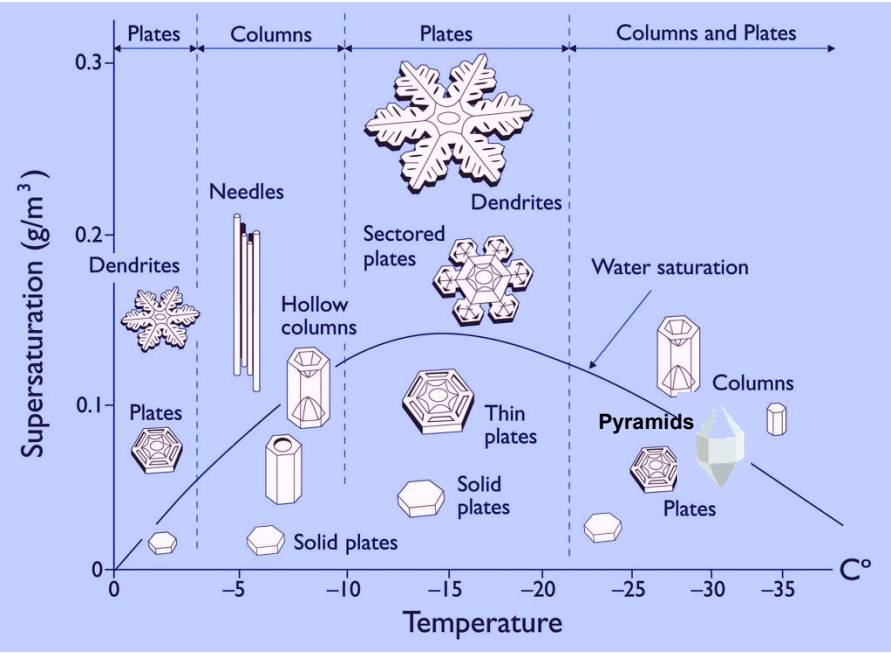

Fig. 11-25. Nakaya Diagram of ice crystal growth habit vs *T* and *RH*. ©Kenneth Libbrecht.

Kenneth Libbrecht has advanced this work by elucidating the growth mechanisms of the crystals. In order for vapor molecules to deposit on ice crystals they must overcome an energy barrier. Hexagonal faces have a different energy barrier than rectangular faces. In the temperature ranges where plates dominate, the energy barrier is smaller at the edges of the hexagonal faces, so depositing vapor molecules extend the hexagonal faces. When supersaturation is low, growth is slow and vapor molecules tend to fill in gaps in crystals, leading to solid forms. When supersaturation is high, growth is rapid and vapor molecules from the ambient atmosphere find the places where the crystal protrudes into the environment the most, hence the crystal grows branches and spikes on the branches to form stars.

The amazing symmetry amidst the profound complexity of the star-shaped crystals, with all branches almost identical, leads to a natural but bogus question, "How does each branch 'know' what the others are doing?" The fact is, the branches don't 'know' anything. What happens is that as the crystal passes through the cloud each branch is bathed in almost identical variations of temperature and saturation ratio, so that growth spurts and lulls of each branch are near identical.

In recent decades, ice particle censuses in clouds have been taken by laser cloud particle imagers on instrumented aircraft. Thunderstorm anvils contain mostly 'junk' ice thrust upward from lower in the cloud, often as droplets that froze upon contact with ice particles (rime). Even in the stratiform cirrostratus clouds of extratropical cyclones there are enough embedded convective cells to loft a substantial fraction (at least 33%) of rimed ice particles.

What this means for halo lovers is depressing. It renders the bulk of ice clouds at best poor halo producers, and the good halo producers as exceptional. This is one main reason why many of the best halo producers are the thin and often almost invisible diamond dust ice fogs that slowly grow the diamond dust on frigid days in the polar regions and on frigid winter mornings in the higher middle latitudes.

11.5 Crystal Orientation and Halo Forms

Orientation of crystals as they fall is the second factor that determines halo form. The simplest, and potentially brightest of all halo forms, especially when the Sun is low in the sky, is the *subsun* (Fig.5-2, Fig. 10-33, and Fig. 11-6) It appears directly below the Sun, and as far below the horizon as the Sun is above it, as if it ere reflected by horizontal mirrors. Those 'mirrors' are most often the hexagonal faces of plate crystals (or dendrites), which tend to be oriented horizontally as they fall (so that the c-axis is vertical).

At the same time, sunbeams reflected from the *vertical* rectangular side faces of plate crystals produce the *parhelic circle*. It appears at the same elevation angle as the Sun, $\boldsymbol{H}_{\mathrm{SUN}}$, and may circle the sky.

The orientation of falling crystals is a result of aerodynamic forces. Large objects tend to tumble turbulently in all directions as they fall. Small objects, such as ice crystals tend to fall smoothly, with the largest area near horizontal, which ironically maximizes drag. In the

land of maple trees, it is a common wonder to see the autogyrating winged seeds or *samaras*, heavy on the end with the encapsulated seed, fall like whirling helicopter wings, their flat blades almost horizontal. A simple experiment is to cut rectangular and triangular pieces of paper, about 5 cm long and 1 - 2 cm wide and watch as they fall. Within a meter of their release they settle into a stable fall pattern, spinning rapidly about their long axis, which remains almost horizontal, while their path traces out a helix.

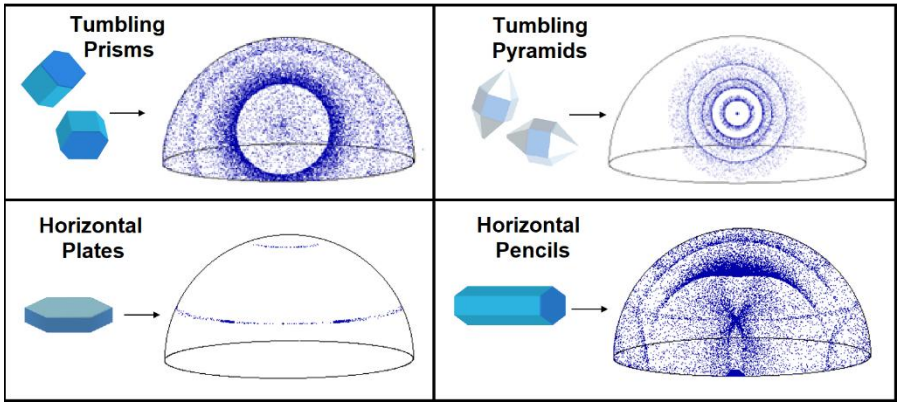

Fig. 11-26. Halo forms vs. ice crystal habit and orientation. SDG.

The main simple, ideal crystal forms, their common orientations as they fall, and the halos they produce are shown in Fig. 11-26. Thick crystals, with aspect ratios near 1, tend to tumble in all directions as they fall, scattering the light in all directions around the Sun. Therefore, randomly oriented crystals produce the circular halos. Simple, 8-faceted crystals, produce the 22° and 46° halos, while crystals with pyramidal faces produce the uncommon odd-radius 9°, 18°, 20°, 23°, 24°, and 35° halos.

Flat, plate-shaped crystals tend to fall with the wide hexagonal basal faces horizontal (the c-axis vertical). They produce the parhelia and the parhelic circle, and, depending on $\boldsymbol{H}_{\text{SUN}}$, the CZ or CH arcs and their infernal versions as well.

Long pencil-shaped crystals tend to fall with the long, c-axis horizontal. They produce the tangent arcs to the 22° halo or the circumscribed halo when the Sun is higher than ~ 40°, and the supralateral and infralateral arcs, among others, depending on $\boldsymbol{H}_{\text{SUN}}$.

Some of the rare arcs only form with extra restrictions on the fall modes of the crystals. The Parry arcs require not only that the c-axis of pencil crystals be horizontal, but that two opposite rectangular prism faces be near horizontal as well. Although there is no established aerodynamic reason why crystals should fall with a rectangular face horizontal, geometric optics calculations and computer simulations of halos have certified this double restriction on crystal orientation does in fact exist. Hypotheses include 1: pencil crystals with basal faces of unequal sided (scalene) hexagons, and, 2: Parry oriented pencils locked in a crystal cluster.

11.6 Geometric Optics of Halos

Explaining and modeling halos with geometric optics use the same laws used with rainbows – the law of reflection, the law of refraction, and Fresnel's Law. The huge difference is that rainbows are modeled using spherical (or near spherical) drops, which renders the problem almost two dimensional and the geometry simple. Halos are modeled with crystals of different forms, orientations, and complex relations to $\boldsymbol{H}_{\text{SUN}}$. These differences make the halo problem far more intricate if not more difficult.

So, let's start with the simplest of these not so simple scenarios.

1: Beam Paths for the Halos and their Arcs and Spots

The 22º halo and its arcs and spots are produced by light beams that refract on entering a rectangular face and refract a second time on exiting an *alternate* rectangular prism face (Fig. 11-27 left panel). Light beams that strike the *opposite* rectangular face and exit the crystal leave at the same angle they entered with no net refraction and no dispersion. Beams strike *adjacent* sides too obliquely to exit the crystal, i. e., at an angle larger than the critical refraction angle

(recall Chapter 1) for ice of $r_{crit} \approx 49^{o}$. Such beams are totally internally reflected and will exit some other face.

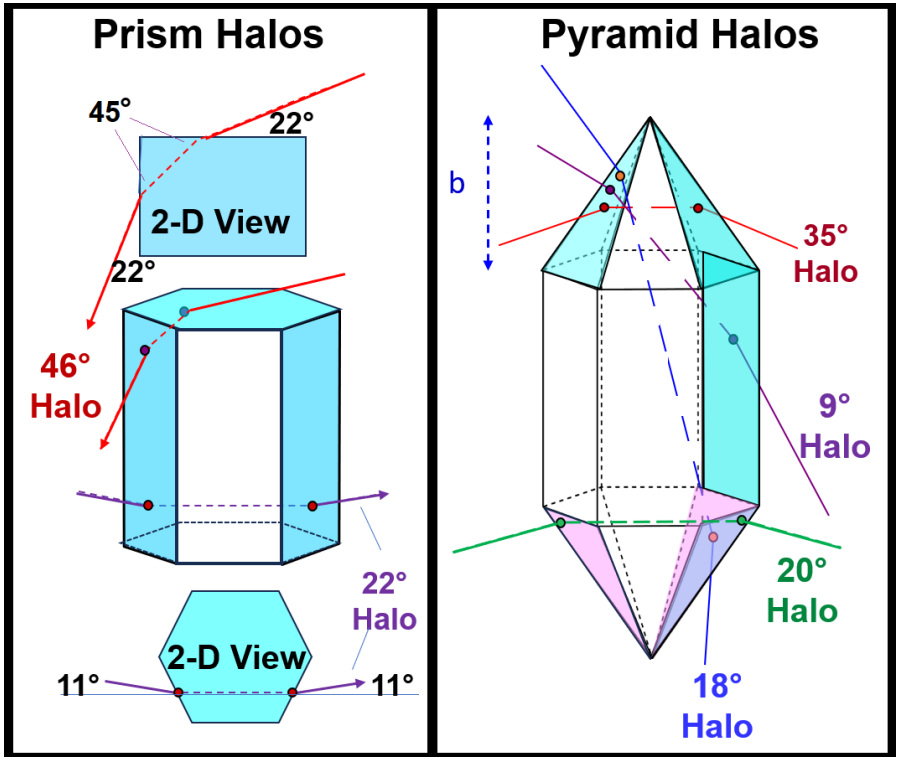

Fig. 11-27. Light beam paths for halos produced by prisms (left) and pyramids (right). For circular halos c-axis takes all values, not just vertical. SDG.

The 46º Halo and its arcs are produced by beams that refract as they pass through a hexagonal basal face and a rectangular side.

The odd-radius halos and their arcs are produced by pyramidal crystals. The right panel of Fig. 11-27 shows the paths for 4 of the 6 odd-radius halos. Beams for the 9º halo pass through a pyramidal face and the opposite rectangular prism face. Beams for the 18º halo pass through alternate pyramidal faces on opposite pyramids. Beams for the 20º halo pass through opposite pyramidal faces of the same pyramid. Beams for the 35º halo pass through alternate pyramidal faces of the same pyramid. Beams for the 24º halo pass through one pyramidal face and the opposite prism face. Beams for the 23º halo form in truncated pyramidal crystals and pass through one pyramidal face and one hexagonal basal face.

Beam paths that produce halos, arcs, and spots for plate and pencil prism crystals of various orientations are given in Fig. 11-28.

2: Minimum Deviation Angle, D_{min} → Maximum Brightness

The 22º halos in cirrostratus on 24 Jan 2022 at Cheyenne (Fig. 10-44) with -55 ºC < T < -35 ºC and in ice fog on 08 Jan 24 at the Pizon ski slope in Switzerland (Fig 11-29) are exemplary cases even though

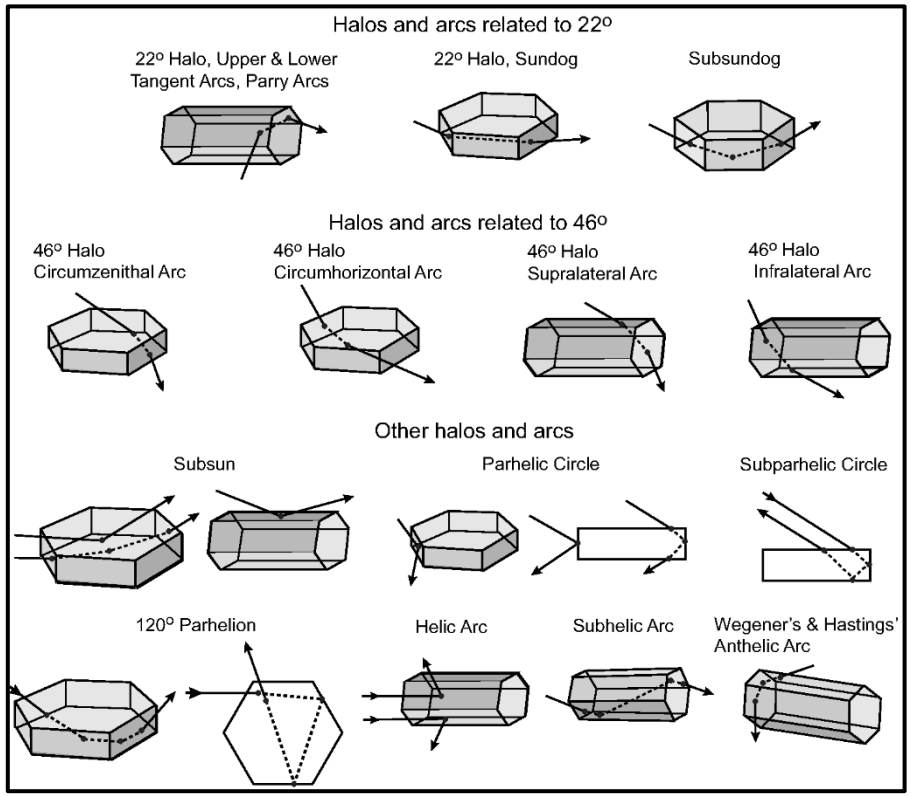

Fig. 11-28. A halo itinerary with the shapes and orientation of crystals, and the paths of light. ©Kuo-Nan Liou

they are neither blinding nor colorful. Recall from Table 11-2 that though the 22º halo is the most common halo form, its maximum brightness is tiny compared to many other halos. These halos have

the typical slightly red inside rim and one more striking feature (after it is pointed out). The sky inside the halos is darker than outside. This contrast for the 22º halo is dramatized by the Monte Carlo dot model simulations of Fig. 11-9, Fig. 11-11, and Fig. 11-30, because it excludes skylight. The right panel of Fig. 11-30 shows that at 22° the number concentration of dots rises abruptly from low values and then quickly decreases as the deviation angle continues increasing.

Fig. 11-29. 22º halo, parhelia and parhelic circle in ice fog Pizol Ski Area Switzerland, 08 Jan 2024. ©Robert Gedzelman.

The sky is darker inside the 22° halo because 22° is the minimum angle sunbeams can be deflected by when passing through alternate rectangular side faces of ice crystals. Fig. 11-31 shows that the deviation angle, $\boldsymbol{D}$ is a minimum. $\boldsymbol{D}_{min} \approx 22º$ when the angle of incidence, $\boldsymbol{i} \approx 41º$. Fig. 11-32 shows that for $\boldsymbol{D} > \boldsymbol{D}_{min}$ the relative number of beams calculated from Fig. 11-31 for each 0.1º range of $\boldsymbol{D}$ decreases by over 80% within 1º of its maximum at $\boldsymbol{D}_{min}$. The 22° halo continues fading outward until it vanishes at $\boldsymbol{D}_{max} \approx 50º$.

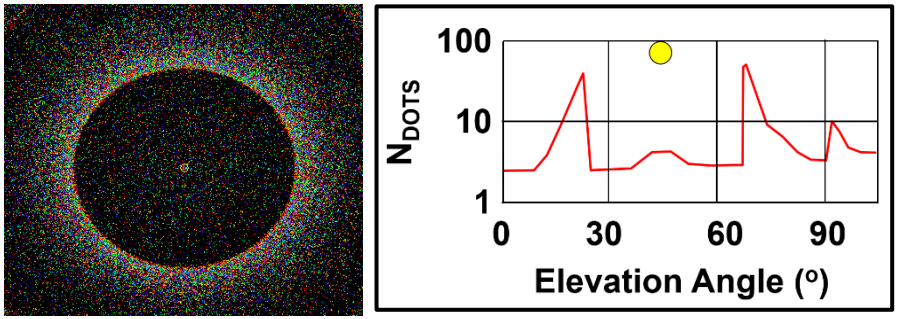

Fig. 11-30. Dot model of the 22º halo (left) and relative number of beams vs angle (right) produced by thick, random oriented plate crystals. SDG.

Color arises at the inner edge of the 22º halo because red is deviated less than the other colors. Thus, the halo is not only brightest but also most colorful near its inner edge, where the overlap of colors is minimized, as with rainbows.

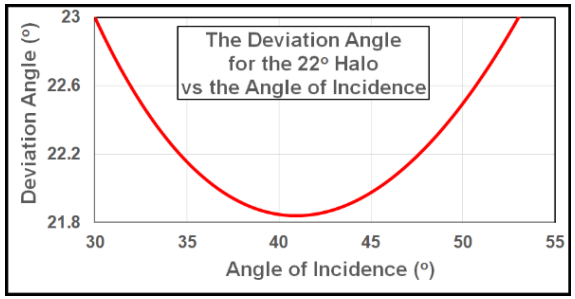

Fig. 11-31. Angle of incidence on crystal $\boldsymbol{i}$ vs deviation angle, $\boldsymbol{D}_{min}$ for the 22º Halo. SDG.

The calculations made for Fig. 11-31 and Fig. 11-32 apply to crystals with c-axis is oriented at right angles to the sunbeams. For randomly oriented crystals, the angle between the sunbeams and the c-axis takes all values from 0º to 90º, and the more obliquely the beams strike the crystal, the larger the value of $\boldsymbol{D}_{min}$.

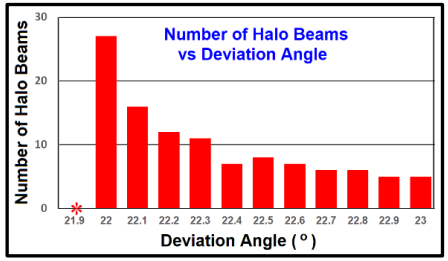

Fig. 11-32. Number of beams vs $\boldsymbol{D}$ for the 22º halo. SDG.

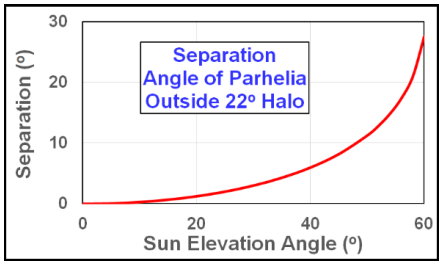

Fig. 11-33. Angle of parhelia outside 22º halo vs H_{SUN}. SDG.

Fig. 11-34. A colorful parhelion outside a faint 22º halo for $H_{SUN} \approx 28º$ over Cheyenne, WY, 10 Dec 2018. JC.

The parhelia illustrate how the minimum deviation angle, D_{min}, increases as the angle between the sunbeams and the c-axis decreases. The parhelia form when plate crystals fall with the c-axis vertical and light passes through two alternate vertical rectangular faces. The higher the Sun, the more obliquely beams strike the vertical rectangular faces and thus the larger the value of D_{min}, and the further outside the 22º halo the parhelia form (Fig. 11-33). This was illustrated in the simulations of Fig. 11-11 and by comparing how far the parhelia lie outside the 22° halo in Fig. 11-29, when the Sun is low in the sky, the halo with the colorful parhelion in Fig. 11-34 when $H_{SUN} \approx 28°$ and Fig. 11-9 where $H_{SUN} \approx 45°$.An enlarged view of the parhelion (Fig. 11-35) highlights its impressive range of colors including seldom seen blue in parhelia.

Fig. 11-35. Closeup view of the parhelion in Fig. 11-34. JC.

Parhelia are seen more often and tend to be more intense the lower the Sun in the sky (though not all the way to the horizon) for the same reason that the lower the Sun in the sky the more likely that sunlight passing into a room through a window will strike the opposite wall than the floor. The probability of striking the opposite wall also increases as the room's height to width ratio (its aspect ratio) increases. In the same way, the thicker the plate crystal in relation to its height (i. e., the larger its aspect ratio) the more likely sunbeams will strike an alternate vertical face and not the hexagonal base.

The dependence of parhelia brightness (i. e., maximum number of beams) on crystal aspect ratio is given in Fig. 11-36 for values of H_{SUN} from 5º to 50º. (These values were calculated by a Monte Carlo halo model that neglects atmospheric obscuration). It shows that when the H_{SUN} is 10º or less, 1: the parhelia can be more than 10 times brighter, and 2: can occur for much thinner plate crystals, than when $H_{SUN} > 40º$.

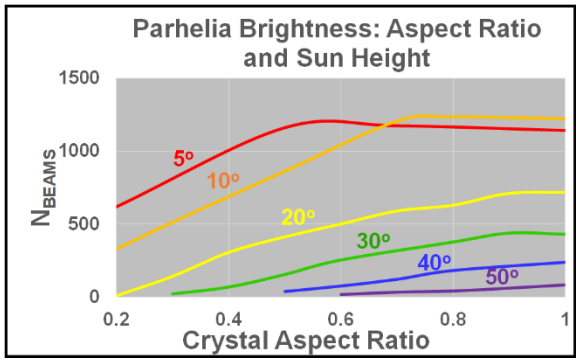

Fig. 11-36. Relative number of sunbeams for parhelia as a function of crystal aspect ratio for various values of H_{SUN}. SDG.

High-Sun parhelia suffer from a further major limitation. Since they can only be produced by relatively thick plates, and since the aerodynamic force that keeps thick plates falling with c-axes vertical is weak, thick plate crystals are more likely to tumble with all orientations. That would produce a 22º halo but no parhelia.

In any case, once $H_{SUN} >\approx 61º$ the parhelia disappear because all beams strike the alternate rectangular prism face at above the critical angle and are totally internally reflected.

The tangent arcs of the 22° halo are produced by horizontal pencil crystals that spin at all angles around the horizontal c-axis. They are tangent to the top and bottom of the 22º halo because there, the c-axis is perpendicular to sunbeams and because as the crystals spin around the c-axis all values of incidence angle, ***i***, (including $i \approx 41º$) occur for some crystals, as in Fig. 11-31. Moving to either side along the tangent arc, the sunbeams confront the crystal's rectangular sides more obliquely, so the tangent arcs wing their way further outside the 22º halo.

Fig. 11-9 shows that the higher the Sun in the sky the lower the 'wings' of the tangent arc until at $H_{SUN} \approx 32º$ the upper and lower tangent arcs join to form the circumscribed halo.

The higher the Sun in the sky, the closer the circumscribed halo approaches the 22º halo, as in Fig. 11-13, until when the Sun is at the zenith, the two merge. But there are differences. The restriction on crystal orientation for the circumscribed halo makes it narrower, more colorful and about four times brighter than the 22º halo. (Compare N_{dots} in Fig. 11-37 with the right panel of Fig. 11-30.)

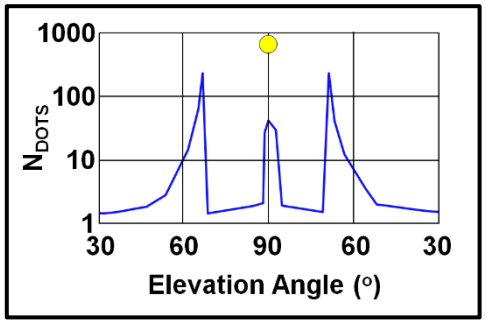

Fig. 11-37. Relative number of beams vs angle produced by pencil crystals with horizontal c-axes is 4x greater than for the 22° halo. SDG.

If, in addition, pencil crystals with horizontal c-axes have the further restriction that two rectangular sides are also horizontal (the orientation for Parry arcs), then the resultant circular halo when the Sun is at the zenith is 25% brighter than the circumscribed halo, has an almost spectral color sequence, but has an angular radius of 25º (3.1° larger than the 22° halo) because the angle between the rectangular sides the refracted beams pass through and the vertical sunbeams is 30º. In addition, the restriction imposed by the Parry orientation (with maximum 1º tilts) eliminates the spread of dots that occurs for randomly oriented crystals and crystals that can rotate around a fixed c-axis. Side-by-side comparison of Monte Carlo dot models of the 22º halo, the circumscribed halo, and the larger, brighter, spectral Parry halo in Fig. 11-38 illustrate these differences.

Parry arcs (there are several) are potentially brilliant and colorful, but

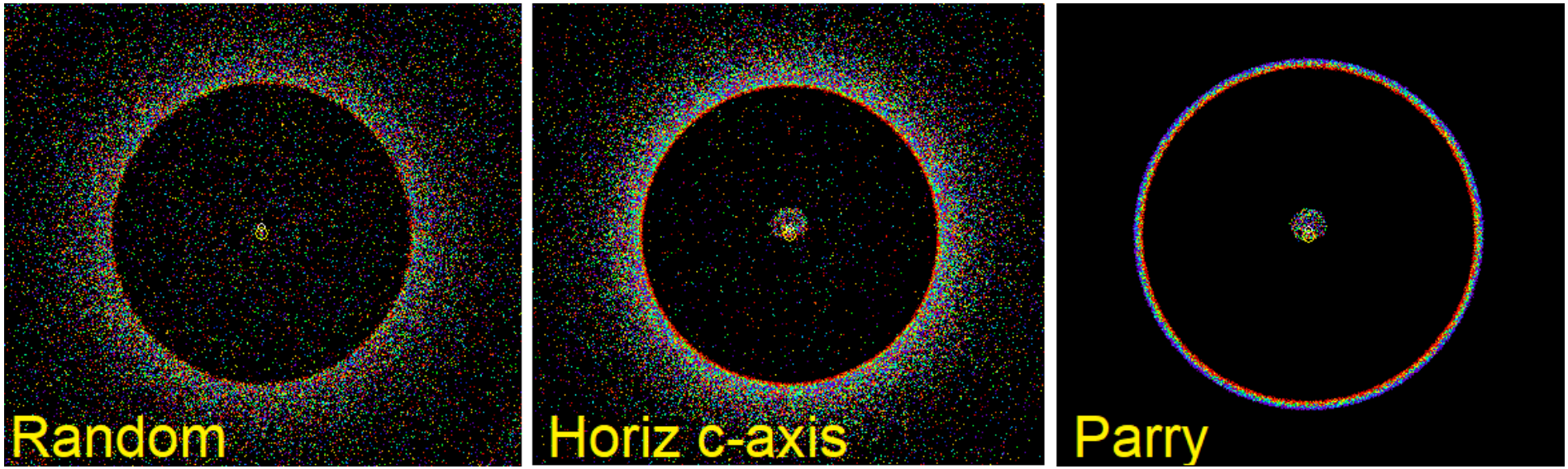

Fig. 11-38. Comparison of dot density and color purity for the 22º halo (left), circumscribed halo (center) and 25º Parry halo (right) for Sun at the zenith. SDG.

relatively rare, curious critters because of the extra restriction that two rectangular faces be horizontal. Not surprisingly, Parry arcs are prominent in the even rarer complex halo displays such as Fig. 11-1 and several in §11.7. In these displays only the eyebrow-shaped suncave Parry arc appears.

Fig. 11-39. Halo Display over Cheyenne, WY, 23 Nov 2019 for $H_{SUN} \approx 6^{o}$ with upper tangent arc, sunvex Parry arc, circumzenithal arc, 22° halo, parhelia, parhelic circle, and a seventh arc. JC.

The complex halo display of Fig. 11-39 contains both a faint suncave Parry arc and much brighter wing-shaped sunvex Parry arc. The wing-shaped sunvex Pary arc appears above and within the upper tangent arc that touches the 22° halo. The display also includes a parhelion and the parhelic circle, and the colorful circumzenithal arc. Why do both Parry arcs remain well outside the 22° halo and not touch it as the tangent arc does? It's all a matter of angles. Because the crystals that form the Parry arcs do not have the freedom of rotating around the c-axis but remain locked with two opposite rectangular side faces kept horizontal, no sunbeams can strike the crystals at the optimal angle of 41° required to produce $D_{min} \approx 22^{o}$ except when $Z_{SUN} \approx 41^{o}$.

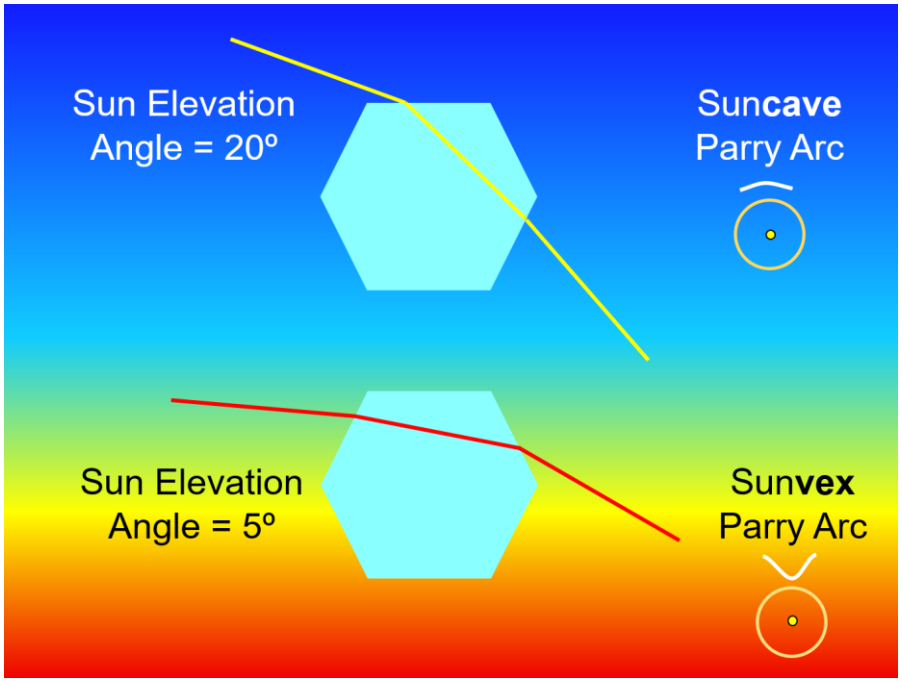

Fig. 11-40. Sunbeam paths for the upper suncave and sunvex Parry Arcs. SDG.

What makes the Parry arcs curious is that sunbeams have two distinct paths (Fig. 11-40), which leads to two distinct arcs. Sunbeams can either enter the top horizontal face to produce the suncave Parry arc, or enter an adjacent upward tilted face to produce the sunvex Parry arc. When $H_{SUN} <\approx 7^{o}$, only the sunvex Parry arc appears (unless the pencil crystals have an aspect ratio of at least 5. When $H_{SUN} >\approx 17^{o}$ (as in Fig. 11-1), only the suncave Parry arc forms. For the intermediate range of H_{SUN}, both Parry arcs are visible. These properties of Parry arcs are illustrated in the simulations of Fig. 11-41, which allow tilts of the c-axis and the rectangular side up to 1° for a range of H_{SUN} for crystal aspect ratio, 3.

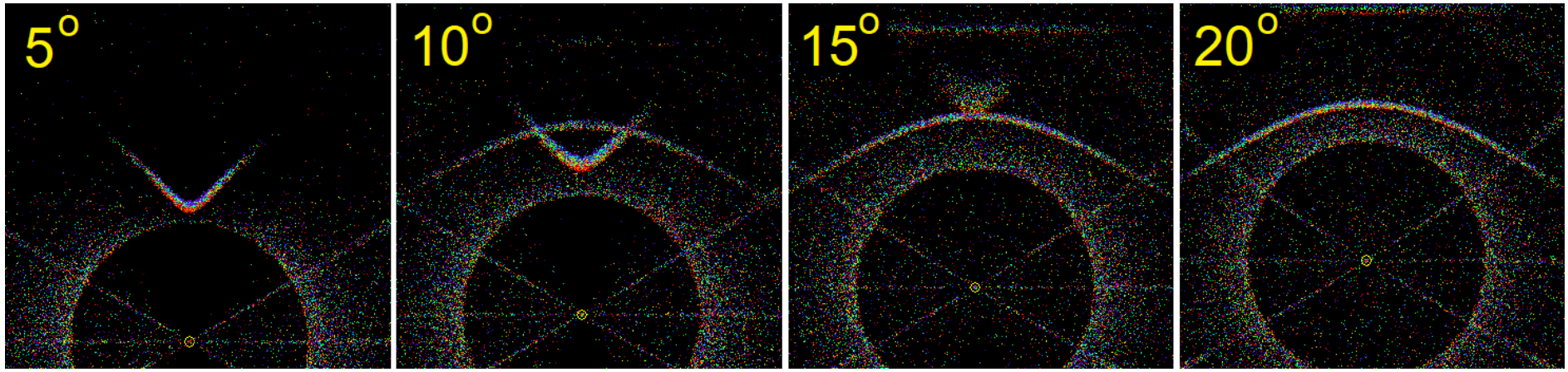

Fig. 11-41. Monte Carlo dot model simulations showing dependence of suncave and sunvex Parry arcs on H_{SUN}, with 22° halo to provide scale. SDG.

Our attempt to simulate the halo display in Fig. 11-39 constitutes a form of detective work common when simulating halos and halo complexes. The Sun's height is essential data. The display formed in a cirrostratus cloud at the top of the troposphere at $\boldsymbol{T} \approx$ -53ºC and was photographed 37 minutes before sunset, at which time $\boldsymbol{H}_{SUN} \approx 6^{o}$.

In the attempt to reproduce the display accurately on the computer, the Monte Carlo halo dot model was run many times. The first runs, assuming Parry-oriented pencil crystals with the typical aspect ratio = 3 failed to produce the suncave Parry arc. Because the mystery arc was ≈ 40° above the Sun and hence near arcs of the 35° halo, stunted pyramidal tops were added to the thin, horizontally oriented plate crystals (c-axes vertical). That succeeded in producing a suncave arc that matched the photograph except that it was too bright.

This was not satisfactory, in part because of the brightness but mainly because introducing stunted pyramidal crystals was unlikely, so more computer runs were made. Lo and behold long Parry-oriented crystals with aspect ratio at least 5 did, in fact, produce a weak suncave Parry arc that closely matched the photograph. Both alternatives (long pencils vs pyramidal capped plates) are shown in Fig. 11-42. Crystal characteristics for this simulation are listed in Table 11-4. We continue the presentation of this simulation when treating complex halo displays in §11.7.

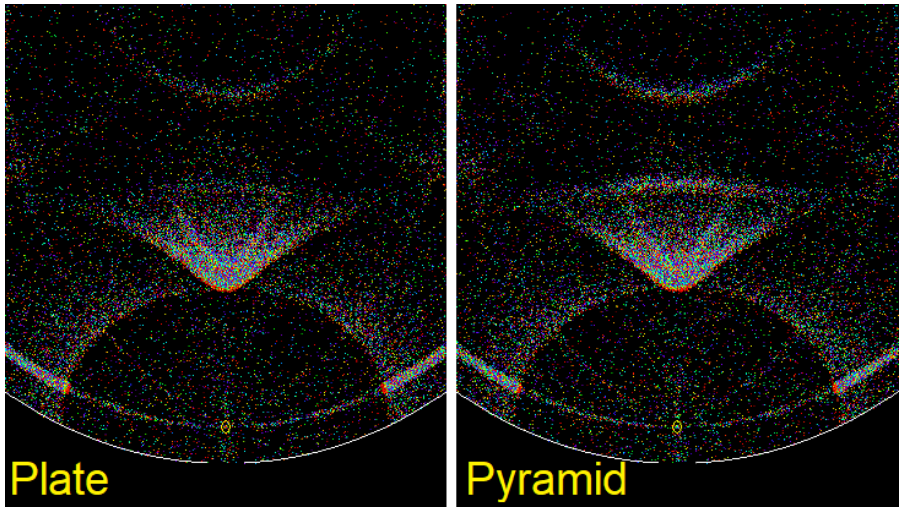

Fig. 11-42. Monte Carlo dot simulations of the halo display of Fig. 11-34 with plate crystals (left) and truncated pyramids (right). SDG.

Recall now that the 46º halo and its various arcs form when sunbeams refract through one rectangular crystal side and one hexagonal face (Fig. 11-27 and Fig. 11-28). For these arcs, $\boldsymbol{D}_{min} \approx 46^{o}$ occurs only when the plane of the beams occurs at right angles to the rectangular side face they enter or exit the crystal. Otherwise, $\boldsymbol{D}_{min}$ is larger than 46º.

The 46º halo, which forms from randomly oriented prisms, is quite rare. That is surprising considering that simulations with randomly oriented crystals show it present whenever the 22º halo appears, albeit much fainter. It is true that many crystals have hollow or stepped ends (as in Fig. 11-23) and not flat hexagons. Why then is the circumzenithal arc so much more common? Crystal orientation is the obvious answer.

The most common of the 46° halo arcs is the circumzenithal CZ) arc. Halo displays including the CZ arc often include the parhelia, implying that they are usually produced by plate crystals falling with the c-axis vertical, though they can be produced by Parry oriented crystals.

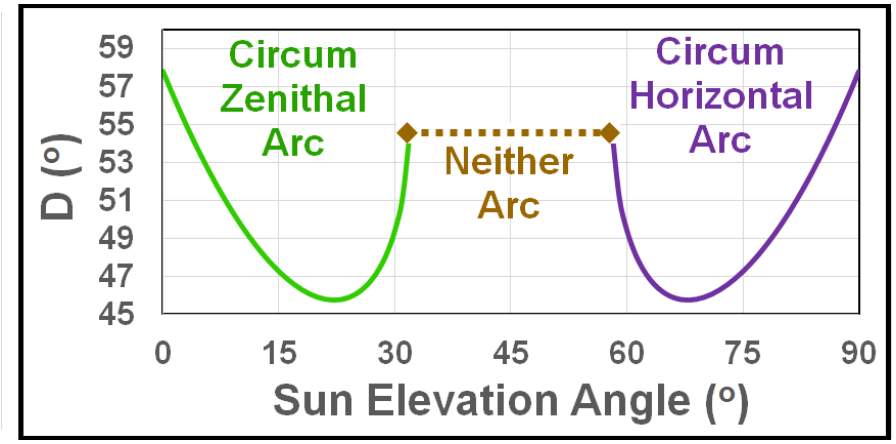

Fig. 11-43. Deviation angles of circumzenithal and circumhorizontal arcs as a function of H_{SUN}. SDG.

Both the CZ and the circumhorizontal (CH) arcs vary with H_{SUN} (Fig. 11-43). The CZ arc forms when sunbeams enter the top hexagonal end face and exit a vertical rectangular side, but it can only form when $H_{SUN} <\approx 32º$. It is brightest, most spectral and comes nearest the Sun (46°) when $H_{SUN} \approx 22º$. The CH arc is its complement in almost every way. The CH arc only occurs when $H_{SUN} >\approx 58º$ and is brightest, nearest the Sun and most spectral when $H_{SUN} \approx 68º$. It is, however almost never seen with the parhelia, which disappear once $H_{SUN} > 61º$.

As with the parhelia, the intensity of the CZ and CH arcs vary with H_{SUN} (Fig. 11-44). Also, as with the parhelia, the intensity of the CH and CZ arcs depends on the crystal aspect ratio, thin plates producing brighter CZ arcs when the Sun is low in the sky and thicker plates producing brighter CZ arcs when the Sun is higher in the sky.

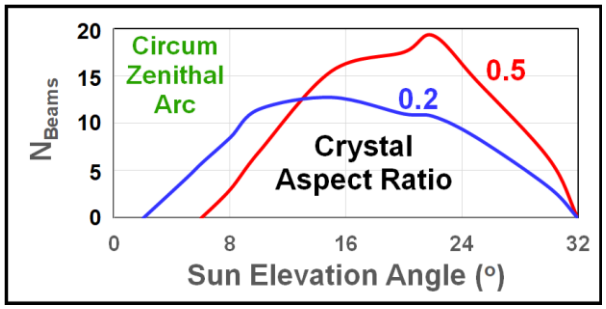

Fig. 11-44. Relative brightness of the circumzenithal arc as a function of H_{SUN} for two values of crystal aspect ratio. SDG.

3: Halo Color and Width

The greater spectral color purity of the arcs associated with the 46° halo is due in good part to their greater width than the arcs of the 22° halo. For example, the CZ and CH arcs are 1.57° wide at their maximum spectral purity, while the Parry arc is only 0.76° wide. These angular widths must be compared to the Sun's angular width (0.53°), which smudges and blurs (in a manner similar to an astigmatism) all rainbows and halos and reduces their color purity. The wider the halo arc and the greater the angular spread of the spectrum, the smaller the relative role of the Sun's smudging and therefore the smaller the reduction of spectral purity.

When comparing spectral purity of rainbows and halos, rainbows, have two advantages, while the CZ and CH arcs at their optimal Sun angles have one. Rainbows form in the rain shafts under thick clouds with potentially dark backgrounds while most halos form with sunlit skies as their background. Recall how greater background lighting detracts from rainbow appearance in the two photos in Fig. 9-5.

Celestial (above horizon) halos must pass through the ice crystal clouds they are produced in. Once the optical thickness of the cloud exceeds about 5, virtually all halos disappear. Rainbow spectra also suffer as the optical thickness of the rain shaft increases, but because

they are reflected in the raindrops and reflected from the rain shaft, they remain visible for much larger values of optical thickness. The same is also true for 'infernal' halos emerging from the clouds below, which stand out best when the surface below is dark, as it is over the ocean.

The high color purity of the CZ and CH arcs at their optimal Sun angles occurs because all rays are deflected by $\boldsymbol{D}_{min}$, which varies only by wavelength. This is also true of the Parry halo when the Sun is at the zenith (an extremely rare event).

Fig. 11-45. Halo complex in morning ice fog, Hörnli Arosa, Switzerland, 30 Nov 2019 with T = -7°C. ©Michael Schneider

11.7 Complex Halo Displays

Complex halo displays are among the atmosphere's most awesome, sights. They cross the sky with multiple halo forms that usually appear alone or in much smaller combinations, and often include rare halos. The brilliance, colors, and sculpted geometric forms that appear in thin air rivet attention from casual observers as well as halo experts.

The uninitiated may experience a sense of bewilderment, and ask, "What could possibly cause such a complex apparition in thin air?" The answer is simpler than the complex appearance. Since each halo form is produced by a specific crystal form and orientation at specific Sun elevation angles halo complexes must be produced in clouds or ice fogs that contain several distinct crystal forms and orientations, and very little junk ice when the complexes are brilliant and contain rare halos.

In our effort to connect displays with crystals we find first that the brilliant but relatively simple display of Fig. 11-15 involved two crystal forms and orientations. Horizontal plates produced the parhelic circle and the CH arc since the Sun was high ($\boldsymbol{H}_{SUN} \approx 72°$) and nearly horizontal pencils produced the circumscribed halo that might be mistaken as a 22° halo. The display of Fig. 11-17 required tumbling prisms (possibly thick plates) to produce the 22° halo and since it occurred with $\boldsymbol{H}_{SUN} \approx 22°$, horizontal plates produced parhelia just outside the halo and a brilliant spectral CZ arc. It also required a small percentage of horizontal pencils to produce the weak upper tangent arc and faint supralateral arcs.

The more complex display of Fig. 11-1 not only required the abovementioned crystals (with a much larger percentage of horizontal pencils), but also a significant fraction of Parry-oriented pencils (rectangular prism face horizontal) to produce the upper sun**cave** Parry arc, the hook-like Tape arcs on the supralateral and infralateral arcs, and the heliac arc.

Brilliant displays also require very constrained weather and cloud conditions. The conditions that led to the complex of Fig. 11-1 were documented by Claudia Hinz, who maintained and practically lived on the Deutscher Wetterdienst's meteorological observatory atop Mount Fichtelberg in Germany's Ore Mountains for more than a decade, and never (well, almost never) missed an opportunity to

photograph beautiful scenes. On the morning of 31 Jan 2014, there was a pronounced temperature inversion with a gentle but insistent wind that forced humid, cold air layer from the valley to ascend the modest peak, and cool even more as it rose. At $\boldsymbol{T}$ = -8°C and low supersaturation, the Nakaya diagram (Fig. 11-25) shows that both solid plate and solid pencil crystals form.

Thus it is no coincidence that the very similar halo complex photographed by Michael Schneider on another ski slope at another time (Fig. 11-45), occurred in a thin ice fog at $\boldsymbol{T}$ = -7°C.

Fig. 11-46. South Pole Halo Display of 11 Jan 1999. ©Marko Riikonen.

Most of the most magnificent displays contain sparkling diamond dust and blue skies, as in the South Pole display of 11 Jan 1999 photographed by Marko Riikonen (Fig. 11-46), showing they form in thin ice fogs right at ground level. Geometry requires that an object covering a large angle of the visual field is small if it is close and large if it is far. This makes it much more likely for a nearby ice fog that a viewer is immersed in to contain a narrow range of near perfect crystals than for a distant cirrostratus cloud high above the ground in the upper troposphere. Furthermore, most cirrostratus clouds extend over a wide range of heights and temperatures in storms with embedded convection, which makes it unlikely in the extreme to consist almost entirely of simple crystal forms with no junk ice.

In the case of diamond dust halos it is possible to collect the crystals responsible for a halo complex as they fall to the ground, though it remains a difficult task because crystals change rapidly when atmospheric conditions change. When Robert Greenler, Walter Tape, Marko Riikonen, and others went to the South Pole in search of complex halo displays, which form near the surface of the ice cap, they collected and photographed the delicate crystals, which change so rapidly on being collected a crystal census can only be indicative. However, even an accurate crystal census only suggests their orientations in the air.

When crystals producing a complex halo display cannot be collected and their fall mode only surmised, we have already shown that detective work involving trial and error with computer simulations is needed to solve the mystery of the mix of crystals forms and orientations needed to produce halo complexes. Computer simulations of halos answer many questions because they can produce photorealistic halos. They start by using the known connections between each halo form and the likely crystal forms and orientations and then vary the fractions of each crystal form and orientation until the simulated halo display matches photographs of the actual display. And though some uncertainty may remain, the matches can be impressive.

Table 11-3. Crystals for simulations of Fig. 11-42.

Form	%	Aspect Ratio	C-Axis Oriented	Tilt (°)	Other
Plate	20	1	Rnd		
Pencil	50	5	Vert	2	
Pencil	10	5	Vert	2	Parry Tilt = 1°
		And either			
Plate	20	0.3	Horiz	2	
Pyrmd	20	0.2	Horiz	2	Pyr Aspect Ratio = 0.2

The mix of crystal forms and orientations used to produce the simulation (Fig. 11-42) of the halo complex of Fig. 11-39 is given in Table 11-3. As pointed out, this mix was the result of many computer runs and adjustments that were made to produce the suncave Parry arc and to capture the relative brightness and color of the various halos. For example, to make the upper tangent arc suitably brighter than the sunvex Parry arc required at least five times as many horizontal pencils with random spin about the c-axis than with the Parry orientation of a rectangular face near horizontal.

11.8 Halos and Optical Thickness

Perfect ice crystal prisms and pyramids focus light to such a degree that halo spots and arcs (recall Table 11-2) sometimes appear in clouds that are invisible to the naked eye and do not impair the sky's pristine blue. Sometimes, sparkling diamond dust is the only giveaway that any ice crystals at all are present. Junk ice, which dominates thunderstorm anvils and is a significant fraction in most cirrostratus ejected from cyclones, impose the main limitation on the brightness of halos, rendering them feeble or eliminating them.

The cloud's optical thickness, τ_{CLD} is the second major factor limiting halo brightness. Recall from §2.4 that the fraction of light that penetrates a cloud or clear air depends on its optical thickness, τ, and is given by the fraction, $e^{-\tau}$. This is illustrated by the solid curve in Fig. 11-47. In optically thin clouds (e. g., $\tau <\approx 0.1$), most sunlight passes through as direct light without being scattered, but as τ increases the fraction of direct light diminishes so rapidly that at $\tau =$ 5 only 0.67% of the initial beam gets through undisturbed, and most of the initial sunlight has been scattered two or more times.

All halos (except Kern's arc and the parhelia of the parhelia) are produced by sunbeams that have been scattered once and only once. Light scattered two or more times is almost invariably incoherent and contributes to the background skylight. In optically thin clouds (e. g., $\tau <\approx 0.1$) most of the small fraction of scattered light is scattered only once, and if that light is focused on a small region of the sky it may produce a bright halo. Singly scattered light peaks at $\tau = 1$, but the fraction of multiply scattered light is already significant.

In optically thick clouds, very little sunlight passes through the cloud without being scattered, and most is scattered more than once. For example, at $\tau_{CLD} = 2.5$, 92% of the light has been scattered, but only 20% has been scattered once. At $\tau_{CLD} = 5$, 99.33% of the light has been scattered, but only 3.6% has been scattered once. Thus, as τ_{CLD} increases, the fraction of background light increases while the fraction of singly scattered light that could produce a halo decreases.

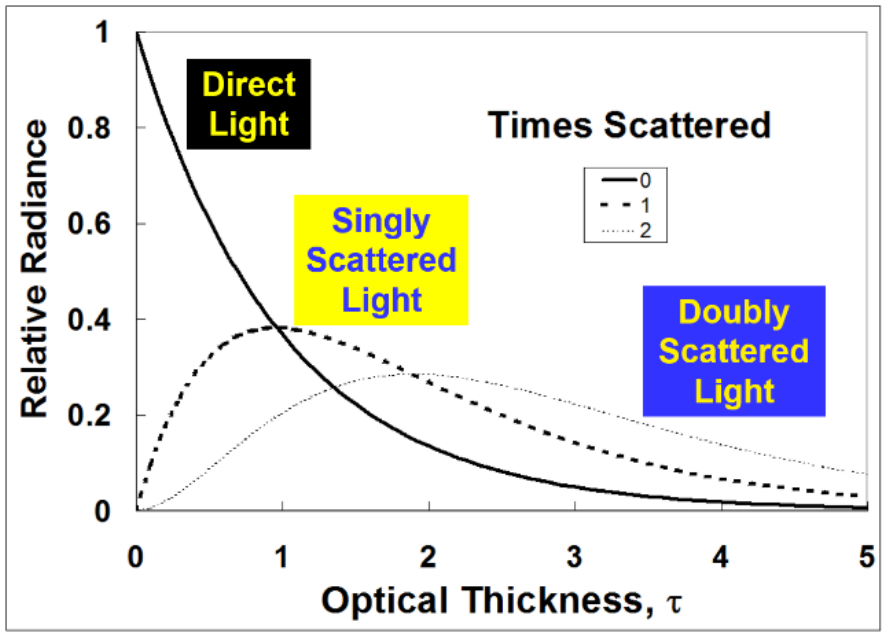

Fig. 11-47. Intensity of direct, singly, and doubly scattered light as a function of optical thickness, τ. SDG.

The simulations of Fig. 11-48 were run for $H_{SUN} = 25°$ in a slightly hazy atmosphere where aerosols add 20% to the optical thickness of the clear air. The 22° halo made by perfect thick, solid, randomly oriented plate crystals is bright when $\tau_{CLD} \approx 0.01$ (implying that the potentially brighter halo forms can appear bright at cloud optical

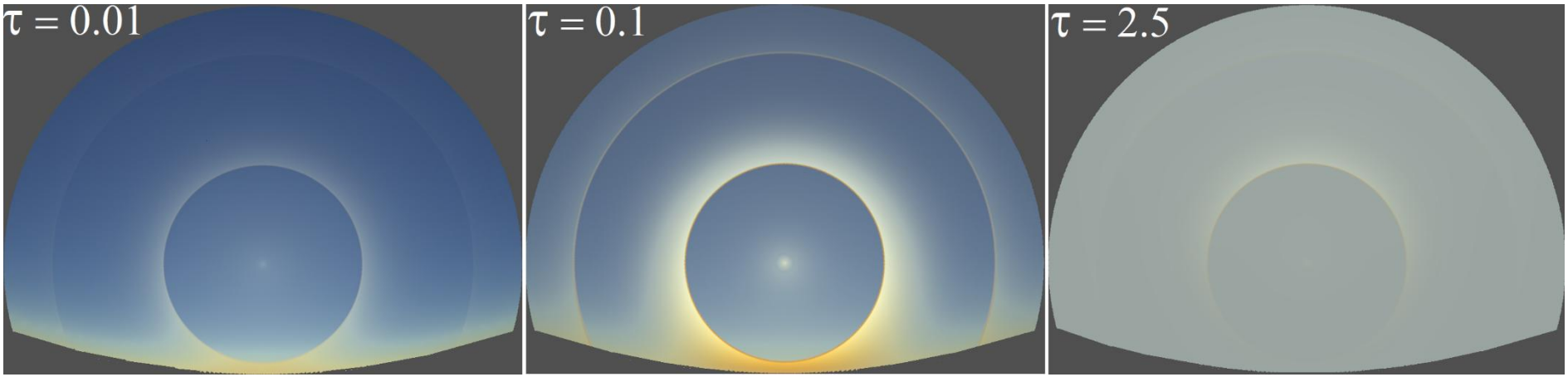

Fig. 11-48. Simulations of halo and sky brightness and color as a function of cloud optical depth (τ_{cld}) for H_{SUN} = 25º and thick plate crystals in a cloud at p = 300 hPa.

depths, $\tau_{CLD} < 0.001$). At $\tau_{CLD} \approx 0.1$, the 22º halo is brilliant, and even the 46º halo is distinct, and while the sky has lost some of its pristine brilliance, it is still deep blue except near the horizon.

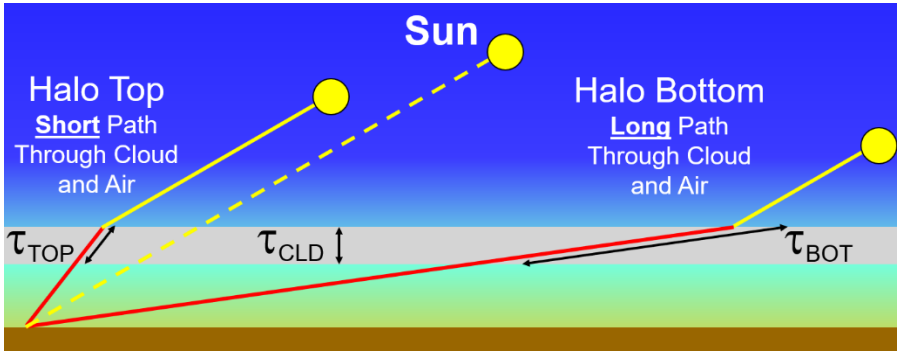

Fig. 11-49. Optical paths of halo top and bottom for a high cloud layer. When the Sun is low in the sky, $\tau_{BOT} >> \tau_{TOP}$ and halo bottoms tend to be faint.

Halos have the greatest contrast with the background sky in the range $0.2 < \tau_{CLD} < 0.5$. As τ_{CLD} continues to increase background sky and cloud light increase more rapidly than the single scattered halo beam. The right panel of Fig. 11-47 shows that at $\tau_{CLD} = 2.5$, the sky is gray, the entire 46º halo and the bottom of the 22º halo have vanished, and the top of the 22º halo is feeble. This unexciting view is quite common when the Sun is low in the sky and cirrostratus clouds are thick enough to turn the sky gray.

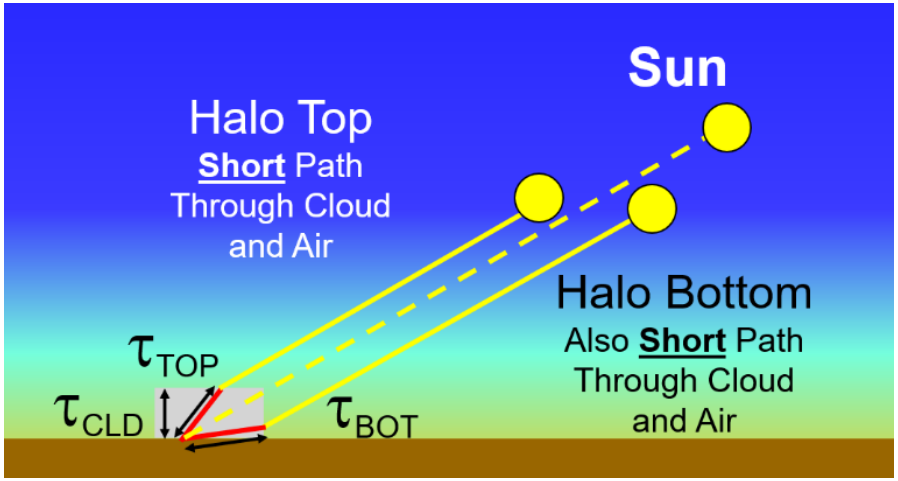

Fig. 11-50. Optical paths of halo top and bottom for a cloud at ground level.

Fig. 11-49 illustrates why halos produced in cirrostratus clouds that cover the sky from end to end in a layer fade near the horizon. Light arriving from the bottom of the halo must pass so obliquely through a high cloud layer that its path both through the cloud and the atmosphere below, is very long. If the optical depth of the cloud for a vertical sunbeam, $\tau_{CLD} \approx 2.5$, then when H_{SUN} = 25º, the optical

thickness a beam at the bottom of the halo (at $\boldsymbol{H}_{OBS} \approx 3°$) must pass through, $\tau_{BOT} \approx 19.1 \times 2.5$ is so large that no direct sunlight or singly scattered (halo) light can penetrate such a cloud.

By contrast, diamond dust halos, which are usually produced by tenuous clouds or fogs of limited width (as opposed to extensive layers) near the ground can be blindingly bright in almost pristine skies because the optical thickness of the path through the cloud and air is small (Fig. 11-50).

11.9 Simulating Halos (Photorealism)

Where nature is stingy, we can be generous.

It is a joy to create photorealistic simulations of halos and other optical phenomena. They are done using the same techniques used to create photorealistic computer images of any scene in modern animated films. And they can be done for any imagined crystal forms and tilts, all ideal if desired.

The starting point for simulations of atmospheric optical phenomena is to apply the appropriate laws of scattering to a single particle at all visible wavelengths. For example, the Lee diagram for rainbows and cloudbows (recall Fig. 9-32) was produced using Mie scattering for spherical water drops of a range of sizes. The angular distribution of the relative scattering intensity of light of a single wavelength for raindrops, randomly oriented thick ice crystal plates, cloud droplets ($r_D = 6$ μm) and air molecules was shown in Fig. 1-17.

The next step is to let the particles absorb sunbeams or scatter them around the sky. Sunbeams are aimed at random spots on a drop for a rainbow or an ice crystal for a halo, and air molecules and aerosol particles are included as scatterers in proportion to their optical thickness. In the perfect, single scattering, Monte Carlo dot model (the simplest of the models), the instant beams are scattered they are plotted as dots on the computer screen. In the early models, the dots were black; now they are colored in proportion to the solar spectrum.

The perfect, single scattering model gives a good idea of the shape, maximum possible brightness, and greatest color purity of the phenomena, but it rejects any chance that the scattered beam can itself be scattered again and removed from the rainbow or halo beam in its voyage through the atmosphere and cloud.

The next order of approximation in the hierarchy of models is to include the probability that a beam will be scattered again before reaching the observer, and remove the beams that are scattered a second time. That level of model gives an excellent approximation to halos and rainbows that appear in or through optically thin clouds.There are even good analytic mathematical formulas for such models provided the ice crystals tumble randomly, so dots are not necessary, and the halos depicted approach photorealism as in Fig. 11-42, but only for circular halos .

The most accurate model, of course, must allow each beam to be scattered as many times as necessary until it reaches the observer or is extinguished,or is scattered back out to space (where it can be seen as an infernal halo.

Photorealistic halo simulations with real sky backgrounds can be made with a six-layer, Monte Carlo multiple scattering model (Fig. 11-51). Sunbeams first pass through Layer 1, the ozone layer. The best-known impact of Ozone is to protect life on Earth by absorbing ultraviolet light. Its lesser known impact on atmospheric optics is to make the sky bluer by preferentially absorbing orange and red light in the so-called Chappuis bands (recall §2.10 and §2.11).

Layer 2 is the clear air above cloud top. Rayleigh scattering is the sole process. Elevated aerosol layers certainly do occur in the atmosphere but were not considered important for most bright halos.

Layer 3 is the cloud layer, where ice crystals of chosen form, orientation, and optical depth scatter light. This is the most time consuming part of the model, especially when the cloud's optical depth, $\tau_{CLD} >> 0.1$. Fortunately, for the purposes of computer time, almost all the best halo displays occur for small values of τ_{CLD}.

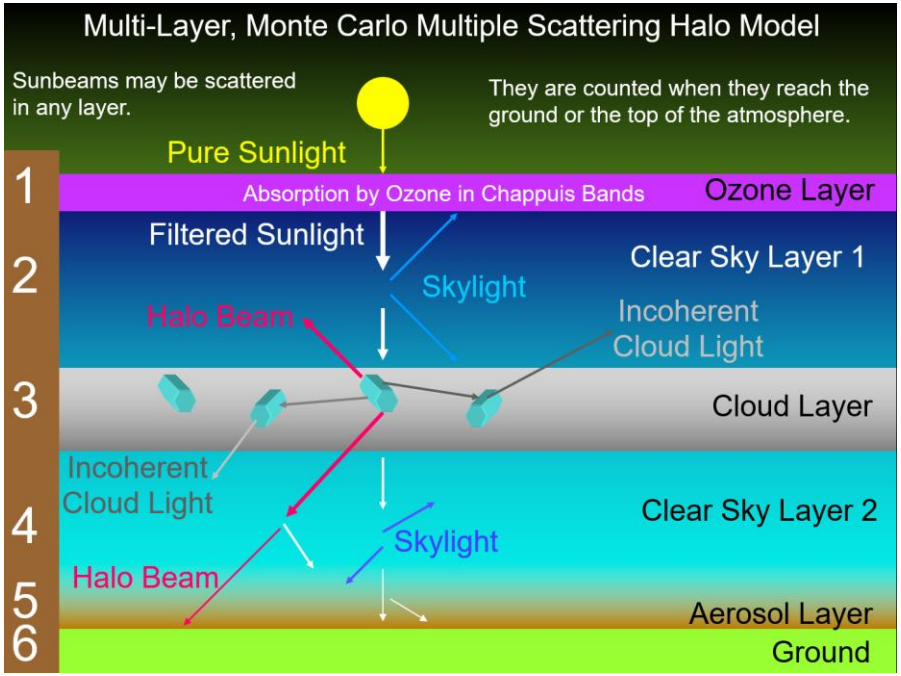

Fig. 11-51. Six-layer halo model including cloud and atmosphere. SDG.

If the cloud layer occurs above the atmospheric boundary layer, Rayleigh scattering occurs beneath cloud base in Layer 4. Layer 5, the aerosol layer is placed just above the surface since under normal conditions most aerosols are confined near ground level. Layer 6 is the ground, which can impact background sky lighting by reflecting light. This is important over snow-covered ground.

In this six-layer model, sunbeams of 61 wavelengths distributed over the visible light range in proportion to the Planck radiation curve usually set at $\boldsymbol{T}$ = 5750 and reduced by ozone absorption are 'shot' into the atmosphere and are plotted as dots and recorded in files after they reach the ground (albedo is usually neglected) or the level of an observer in a jet if the model is set to plot infernal halos.

The dot models give a good idea of the potential shape and color of the phenomena but are not photorealistic. The computer monitor is the chief limitation. In the regions of the sky, where beams are focused, for example, where the parhelia are located, the monitor quickly becomes saturated with dots and cannot become any brighter while other parts of the sky slowly become artificially brighter as the number of dots increases.

The problem of excess dots is solved by dividing the sky into tiny squares or pixels and recording the dots of each color in each pixel. Separate files are made for 1: halo dots that have struck ice crystals once or twice without striking an air molecule or aerosol particle, and, 2: sky dots, which include all other scattered dots. Dots of direct sunlight that reach the ground without being scattered are not recorded because they are too bright and not needed.

The sky dots are so sparse that to approach photorealism requires at least 10 million dots at each wavelength or computer time of several hours on a fast PC. Even then, random variations from one pixel to the next are large enough to make the sky appear spotty. That problem is reduced by a process called smoothing, which amounts to averaging nearby pixels.

Smoothing is not applied to the halo dots because 1: their number in each pixel is large enough so that smoothing is not necessary and, 2: smoothing broadens the narrow halos unrealistically but has much less impact on the broad, slowly changing background sky except right above the horizon and immediately around the Sun.

The smoothed sky dots in each pixel are then added to the halo dots and all pixels are illuminated on the monitor in proportion to the brightest pixel to produce the final image. Similar techniques have been used to create the frames for animated movies.

The difference between the dot model and the final halo simulation can be seen by comparing Fig. 11-52 to Fig. 11-4. These represent different views of a highly idealized halo situation designed to bring out a large number of halo forms and not match any particular halo complex though it does contain many of the halos seen in the complexes of Fig. 11-1, Fig. 11-45 and Fig. 11-46. Very stringent limits, indicated in Table 11-4 were placed on the crystals. All were perfect prisms, and the tilt of the aligned crystals had almost no

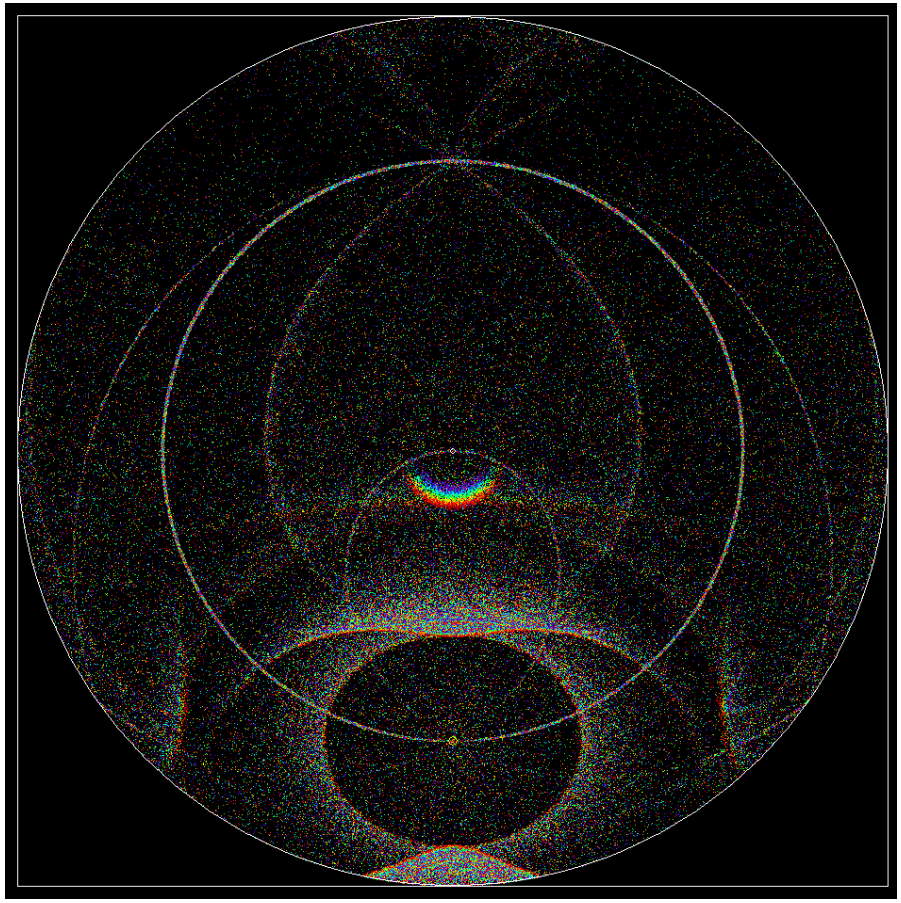

Fig. 11-52. All sky dot model version of the halo complex simulation of Fig. 11-4. SDG.

variation. The simulation was produced for $\boldsymbol{H}_{SUN}$ = 30° to make the lower tangent arc visible without having to look downslope as in Fig. 11-1, and to make the arcs linked to the 46° halo near optimum.

Table 11-4. Crystal Properties for Simulation of Halo Complex if Fig. 11-4.

Crystal %	Fall Mode	Aspect Ratio	Tilt (°)
20%	Random	1.0	0 - 90
30%	C-axis vertical	0.3	0 – 0.1
45%	C-axis horizontal	3.0	0 – 0.1
5%	Parry	3.0	0 – 0.1

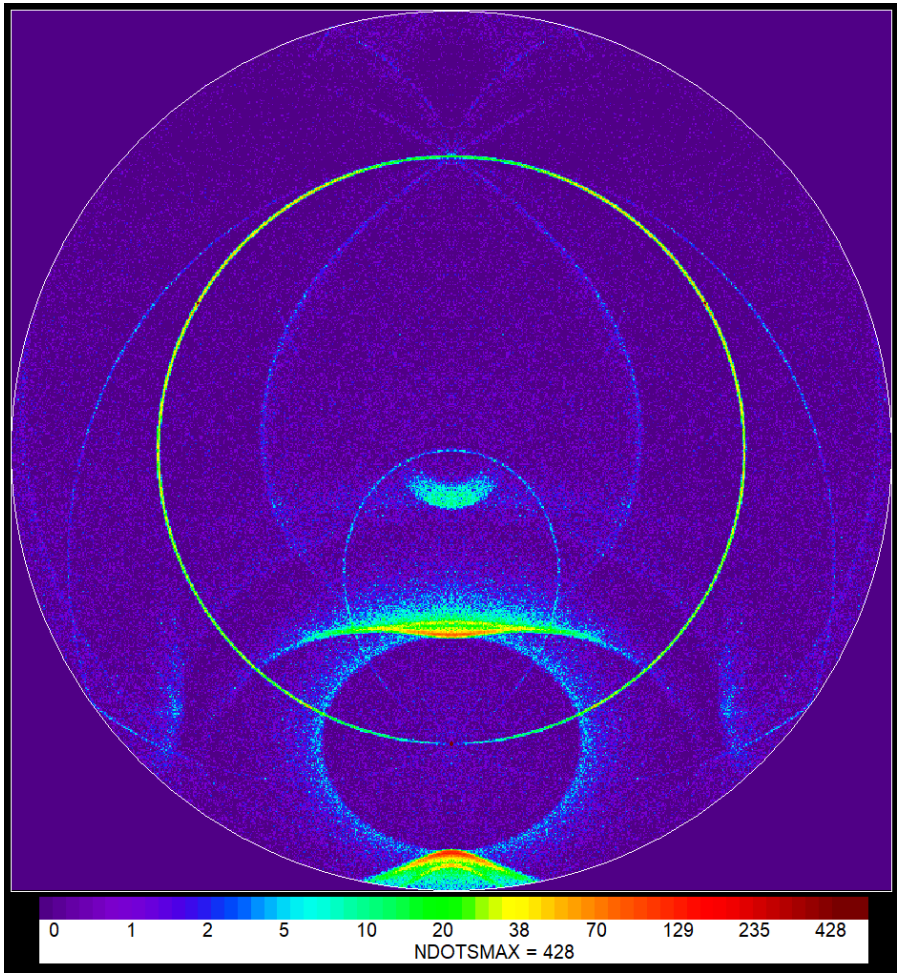

Fig. 11-53. False color image of dot density of dot model of Fig. 11-51. SDG.

The dot model of Fig. 11-52 shows most of the arcs with only 10,000 dots per wavelength, whereas the near photorealistic simulation of Fig. 11-4 required 10 million dots per wavelength, The dot model fails to show the parhelia because the tilt of the plate crystals is so small the parhelia are little more than dots immersed in the parhelic circle. The false color dot density map of Fig. 11-53 gives a better idea of the relative brightness of the halo forms, but does require a close look to see the existence of the tiny parhelia. It also highlights the lower Parry arc, easily missed in both Fig. 11-4 and Fig. 11-51.

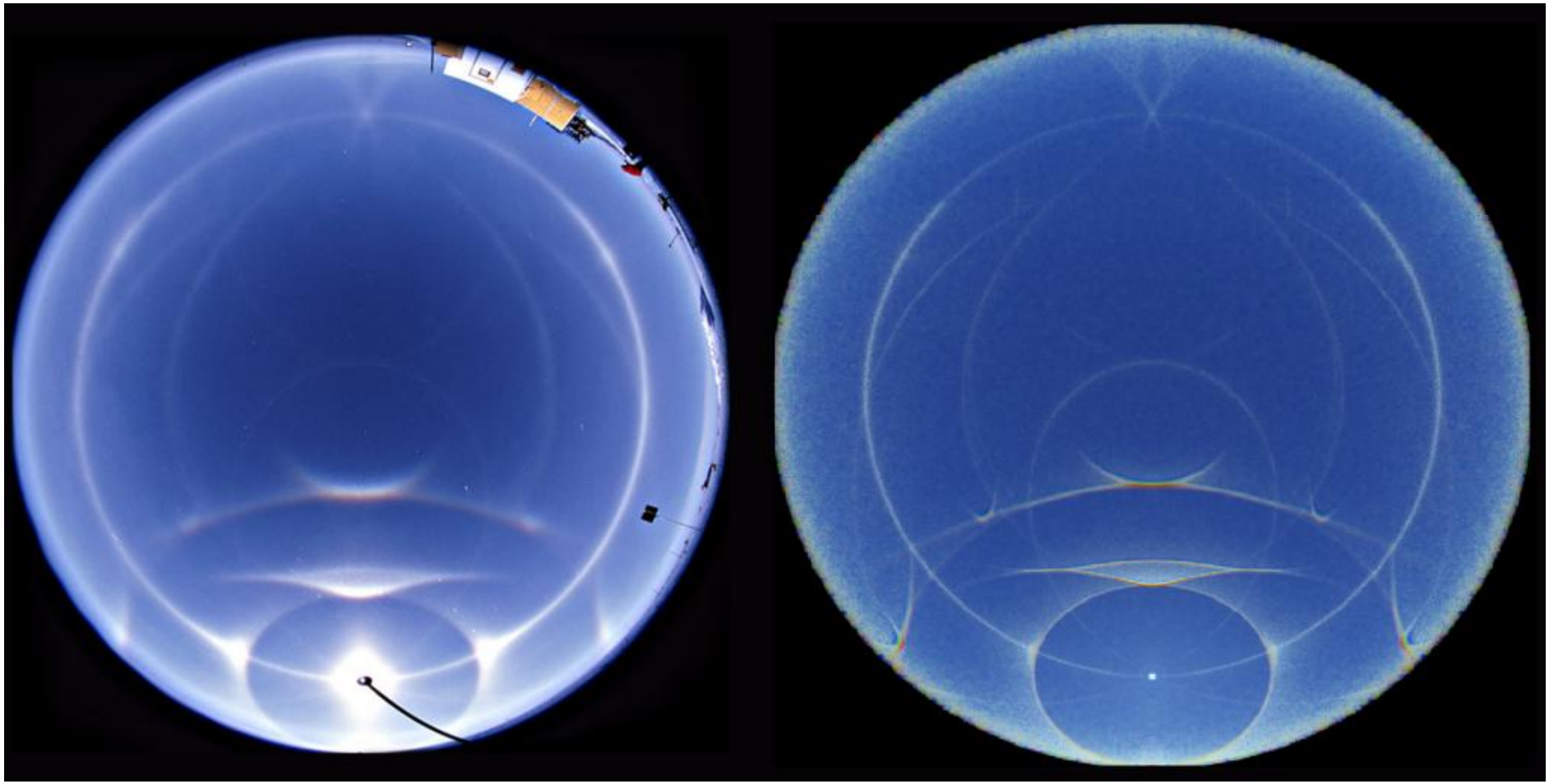

Fig. 11-54. Fisheye view of South Pole Halo Display of 11 Jan 1999. Sun and several bright arcs are broadened by overexposure. ©Marko Riikonen.

Fig. 11-55. Simulation of South Pole Halo Display of 11 Jan 1999.

Table 11-5. Crystal Properties for Simulation of South Pole Halo Display of 11 Jan 1999.

Crystal %	Fall Mode	Aspect Ratio	Tilt (°)
30%	Random	1.0	0 - 90
22.5%	C-axis vertical	0.3	0 – 5
40%	C-axis horizontal	3.0	0 – 2
7.5%	Parry	3.0	0 – 2

It is appropriate to conclude this chapter by comparing halo complexes with simulations. The South Pole Halo display of 11 Jan 1999 (Fig. 11-46 and Fig. 11-54), photographed by Marko Riikonen, was a magnificent complex halo display with arcs that traversed the entire sky. Fig. 11-54 is an all-sky, or fisheye view, where the zenith is at the center and the circumference represents the horizon. This is shown side-by-side with the simulation of the complex using the 6-layer model with up to 10 million beams (Fig. 11-55). Atmospheric conditions used in the model include surface pressure, p_{sfc} = 700 hPa, atmospheric turbidity = 1.05 with aerosols of radius, r_{AER} = 0.3 μm, and the ice crystal cloud at the surface with optical depth, τ_{CLD} =

0.05 and 10% junk crystals. The halo-producing ice crystals, their relative abundance and properties are listed in Table 11.5.

The simulation captures the major features of the display though it makes the halos too narrow and colorful and makes the parhelic circle too faint. These discrepancies can be reduced by increasing the maximum tilts of the crystals, and the percentage of oriented plate crystals. Furthermore, the simulated sky near the horizon remains spotty. That problem can be reduced by either increasing the number of beams or by an improved method of smoothing. The photo itself is also an imperfect copy of the real halos, largely because it suffers from the unavoidable overexposure of the Sun and of the brightest halos, which causes both bleaching of the colors and unrealistic broadening.

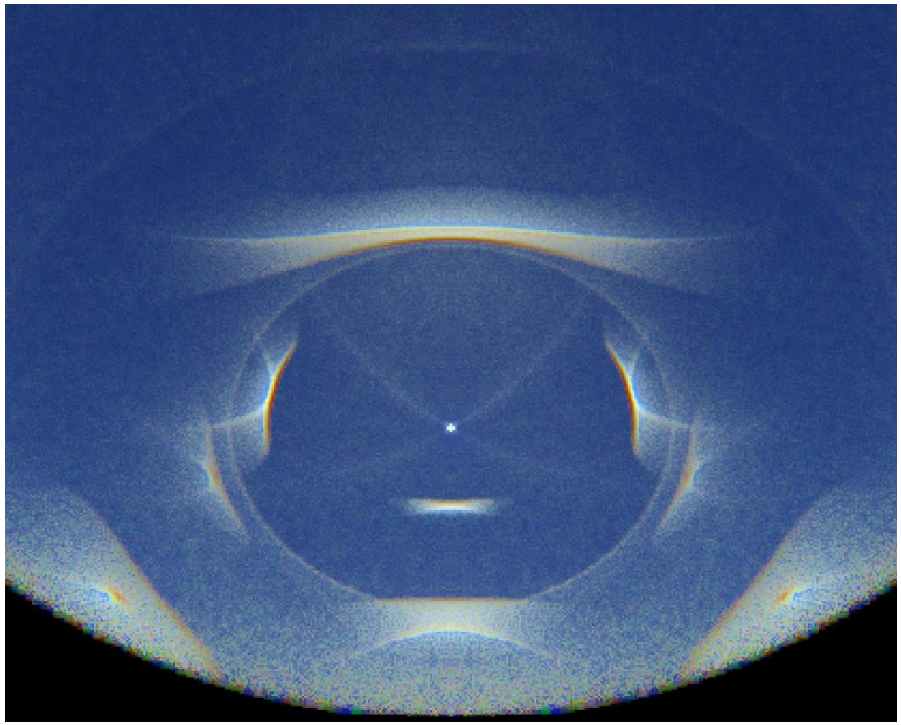

Fig. 11-56. Simulation of Walt Tape's Lunar halo display of 06 Jan 2004 produced by oriented stunted bipyramidal crystals. SDG.

Fig. 11-56 represents a simulation of the halo display over Fairbanks, AK at 4:19 AM on 06 Jan 2004 photographed by Walt Tape (Fig. 15.11, ***Atmospheric Halos and the Search for Angle x***) when the Moon's elevation $\boldsymbol{H}_{LUN}$ = 35°. The simulation used 80% stunted bipyramids with the c-axis tilted up to 15° and included for the purpose of reference 20% tumbling thick plates that were not in the actual display so as to include the 22° halo as a reference frame. Cloud optical thickness was set to τ_{CLD} = 0.05 in a molecular atmosphere. The simulated arcs match the shape and relative brightness of the real arcs reasonably well, and though the simulated arcs are far more distinct, narrow, and colorful, they do indicate what is possible for perfect crystals in a perfect atmosphere.

Less than a week before going to virtual press we came across another of those once-in-a-lifetime photographs of an odd radius halo display captured by Brian Mulligan. It occurred on 21 Oct 2019 over Ottawa, Ontario Canada (Fig. 11-57), is featured at Les Cowley's website,

https://atoptics.co.uk/blog/pyramidal-crystal-plate-arc-halo-display-ottawa/

and was simulated by Martin Viala using the model, HaloSim. The photo includes features at the horizon, making it possible to determine the Sun's height in the sky as $\boldsymbol{H}_{SUN}$ = 20.9°. Following Viala's lead, we modeled the halo assuming stunted bipyramidal crystals with tops truncated at 20% of full extent and bottoms truncated at 50%. Half of the crystals were assumed to tumble randomly and half were assumed to fall like swinging parachutes with a maximum tilt angle of 12°.

Viala's simulation includes a bright arc at the base of the bright 20° halo, which are absent in the photograph, where the cloud thickened toward the horizon. Our simulation (Fig. 11-58) includes multiple scattering in clear air and cloud. It provided a reasonable match to the photo with an aerosol content 20% of the optical depth of the clear air, 30% junk ice, the cloud at 9 km, and, τ_{CLD} = 0.2, which faded the bottom of the 20° halo and eliminated its tangent arc.

Fig. 11-57. Halo display over Ottawa, Ontario, Canada, 21 Oct 2019. © Brian Mulligan.

Our simulation includes the 18°, 20°, 22°, 23°, 24°, and 35° halos, (the latter, not visible in the photo) as well as their arcs, all of which correspond to the main features of the photo, albeit with significant differences, such as that the simulated halos are more distinct and colorful. Other differences arise from the pronounced variations of cloud thickness in the photograph that the model does not allow.

Even though perfection eludes us in these simulations, given how rare extraordinary halo displays are, simulating halos is a rewarding substitute while wishing and waiting for the real thing.

11.10 Halo Gallery

Oh, what fun!

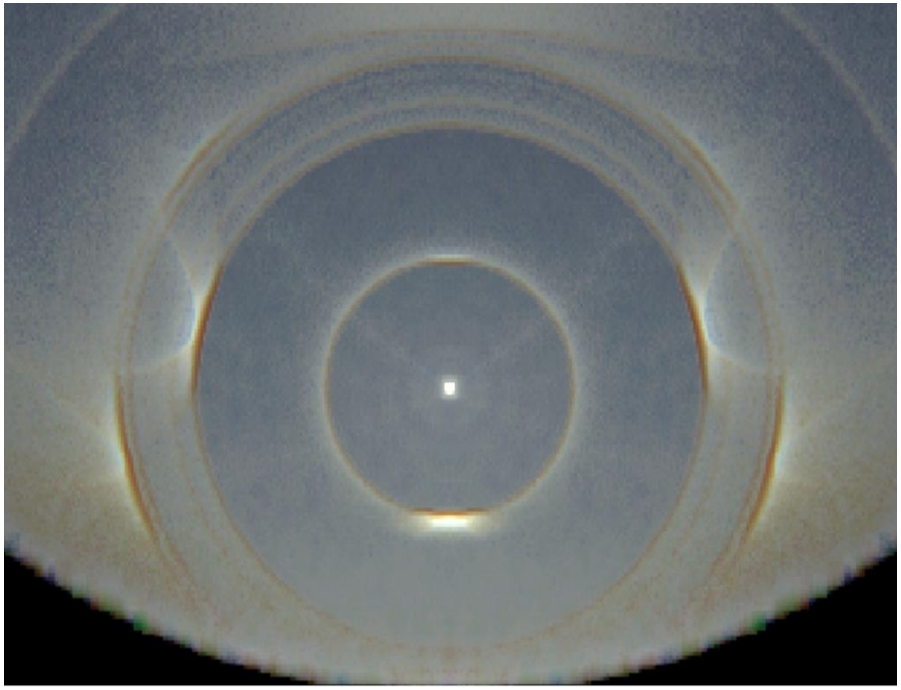

Fig. 11-58. Simulation of halo display of Fig. 11-57. SDG.

Fig. 11-59. Sun pillar facing NW at twilight forming below altocumulus at 8200 m and T = -26°C, San Mateo, CA, 28 Jun 2015. SDG.

Fig. 11-60. Diamond dust halo display in ice fog, Klinovec, Czech Republic, 13 Dec 2024, with faint sunvex Parry arc, tangent arcs, 22° halo, parhelia, parhelic circle, sun pillar, and subsun. © Claudia and Wolfgang Hinz.

Fig. 11-61. Diamond dust halo display with sunvex Parry arc above upper tangent arc and 22° halo minutes before Fig. 11-60. With the Sun slightly higher, the arcs are not quite as steep. The ice fog is natural, not produced by snow making. © Claudia and Wolfgang Hinz.

Fig. 11-62. Suncave Parry arc above upper tangent arc with H_{SUN} = 24° in cirrus clouds and contrails over Boynton Beach, FL, 3 Jan 2026. The arcs lasted less than two minutes. SDG.

Fig. 11-63. Ice crystal light pillars. When ice crystals tinkle all around without the Moon to produce halos, colored street lights substitute. Each light produces its own pillar at Toledo, OH, 17 January 2018. © Ross Night.

Fig. 11-65. Sudden sun pillar in stratocumulus at *T* = -10°C, Cheyenne, WY, 22 Nov 2025. JC.

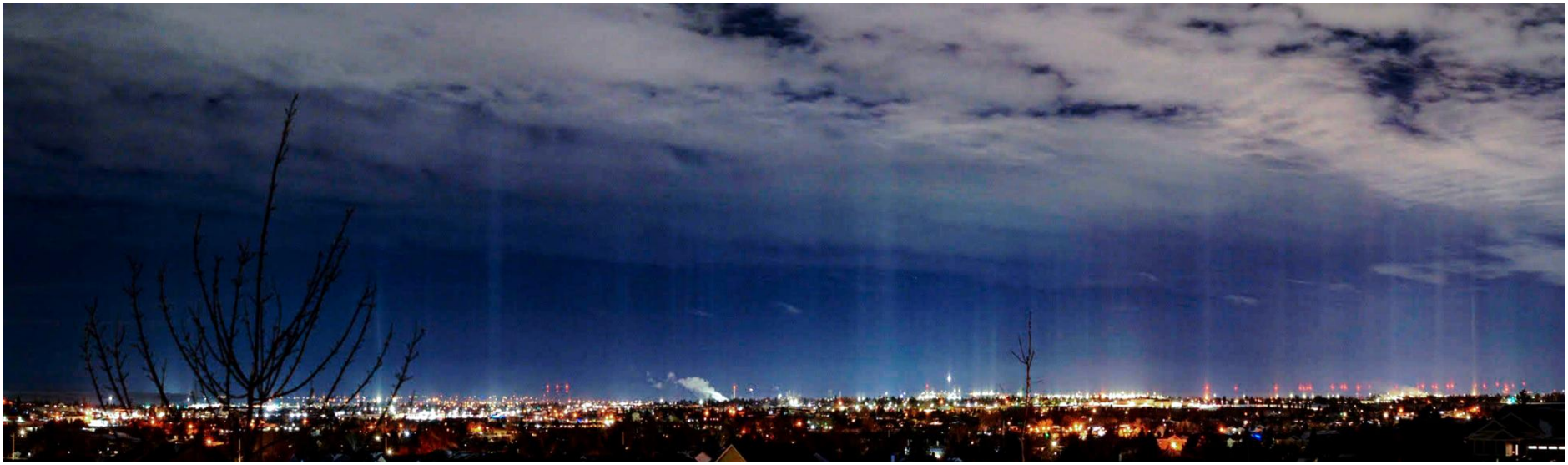

Fig. 11-64. Ice crystal light pillars over Cheyenne, WY, 18 Jan 2024. Ice crystals fell from stratocumulus clouds at *T* = -12°C. JC.

Fig. 11-66. One lucky cirrus streamer gets the parhelion over Okeelanta, FL, 17 Jan 2016. Faint iridescence can be seen at fringe of mixed ice-water cloud at lower left. The simultaneous presence of halos and iridescence is much rarer than might be expected (see §15.6). SDG.

Wonders of the Atmosphere
Chapter 12: Patterned Cloud Sheets

Fig. 12-1. Altocumulus stratiformis undulatus, Boynton Beach, FL, 07 Jan 2025. SDG.

Fig. 12-2. Cellular Altocumulus, 27 Oct 2017 (top). Fig. 12-3 Banded Altocumulus undulatus, 19 Nov 2018 (bottom). Both over Cheyenne, WY. JC.

Wonders of the Atmosphere
Chapter 12: Patterned Cloud Sheets

12.1 Properties of Patterned Cloud Sheets

Think back to a glorious sunrise or sunset when an intricately patterned cloud layer, riveted ruby red, gilded with gold fringes, and perfected with patches of purple, were all set in a spectral sky. Recall also gossamer cloud ripples that distilled the sunlight into brilliant glowing kaleidoscopic opalescence, with iridescent fringes or circular coronas, the subject of Chapter 14.

Can you remember the humble cloud genera that made these visual feasts possible?

They are almost invariably the patterned layer clouds, altocumulus and cirrocumulus in the troposphere and nacreous in the stratosphere. They are the clouds of honeycomb cells or rippled waves (Fig. 12-1), or orderly bands crisscrossing the sky in woven shredded-wheat patterns of ranks and rows (Fig. 12-2 and Fig. 12-3). Sometimes the patterned cloud sheet contains all these and more, as in Fig. 12-4, 1st place winner in the 2021 Weatherwise Magazine Photo Contest. Its extra feature is the field of oval lacunae (cavities) at upper right. Little wonder the ponderous official classification of this delicate cloud is *cirrocumulus translucidus undulatus radiatus lacunosus*!

One more species of patterned cloud sheets is lenticularis, the flying saucer or lens (lentil) shaped clouds that hover motionless around mountain peaks and ridges. It forms the subject of Chapter 13.

The patterns of the elements in thin cloud sheets are molded by the patterns of the airflow. Honeycomb cells are due to gentle, overturning cellular convective motions confined to a humid layer that is either heated at its base or cooled at its top. The honeycomb

Fig. 12-4. Cirrocumulus translucidus undulatus radiatus lacunosis, Cheyenne, WY, 31 Jan 2021. JC.

cells form when there is little or no vertical wind shear. As wind shear increases, the flow marshalls the cells into waves, ranks, and

rows. Obstacles to the flow such as mountain-topped islands create downwind wakes and vortices in the (mainly) stratocumulus patterned cloud fields, so large they are best seen from Space.

Patterned sheets of stratocumulus, altocumulus, cirrocumulus, and the rare nacreous and noctilucent clouds of twilight have such similar form they probably should constitute a single genus. However, they have been classified as distinct cloud genera, distinguished mainly by the heights of their bases. Stratocumulus bases are generally less than 2 km above the surface, altocumulus bases between about 2 and 6 km and cirrocumulus bases are usually above about 5 km. Nacreous or Mother of Pearl clouds (named for their astounding iridescence) reside in the Stratosphere, between about 15 and 25 km. Noctilucent clouds reside in the Mesosphere, between about 75 and 85 km.

Fig. 12-5. Thin Altocumulus band with sunlit side showing its small depth, and transverse shear waves over Cliffside Park, NJ. SDG.

Largely as a result of the height of the sheets, the three tropospheric cloud genera are also distinguished by the apparent size of the elements. A good rule of thumb is to use your thumb. Hold your outstretched hand above your head. Stratocumulus cells or ripples are wider than your thumb (span an angle > 5°), Cirrocumulus cells or ripples are narrower than your pinky nail (< 1°). Altocumulus elements are between (1° to 5° wide).

The patterned cloud sheets are often geometrically and optically thin, of order 100 m, as in the sidelit cloud line of Fig. 12-5. Optical thickness of the sheets generally decreases with height as temperature and vapor capacity of the air decrease. Stratocumulus, lowest and warmest, generally has the greatest optical thickness of the patterned cloud sheets. Cirrocumulus, highest and coldest, is usually the thinnest and most delicate of the structured cloud sheets. Quite often cirrocumulus cloud sheets have fine ripples and are gossamer thin, conditions ideal for coronas and iridescence.

Much of the differences in form of the three genera result from differences in their origin. Cellular stratocumulus clouds, especially over the subtropical oceans, form when the gently subsiding air near the surface of the great subtropical anticyclones is cooled by contact with the cold waters. Vertical wind shear is often too small to align the cells. Islands align cells by diverting the brisk winds.

Cirrocumulus and altocumulus often derive from droplets and ice crystals ejected from storm tops by outflowing winds, often with significant vertical wind shear. As they move out away from the storms that ejected them, they may evaporate. However, at some distance downwind, especially after a night or two of cooling, they may recondense as broken cloud sheets. These high cloud sheets often appear fully developed the moment the rising Sun illuminates them (recall Fig. 6-50. They often evaporate when the Sun heats the layers during the day, only to reappear yet again when the Sun sinks, just in time to embellish the evening fire-sky spectacle.

12.2 Fire Skies

> “The Sun was setting - Suddenly the sky became a bloody red…the flaming clouds … hung like blood and a sword over the blue-black fjord and city….I felt a loud, unending scream

piercing nature….I painted this picture, painted the clouds as real blood." Edvard Munch.

Fig. 12-6. Deep red stage: Altocumulus 50 minutes before dawn over Cheyenne, WY, 29 Oct 2018. JC.

Fig. 12-7. Red stage: Altocumulus 38 minutes before dawn, tinted orange near the horizon by the yellow sky over Cheyenne, WY, 05 Oct 2018. JC.

Awestruck and briefly paralyzed by a striking twilight sunset scene (produced by either tropospheric lenticular clouds or stratospheric mother of pearl clouds), Edvard Munch was inspired to paint his iconic work, ***The Scream*** (Fig. 15-22). Though few people feel such overwrought anxiety when viewing flaming twilight fire skies, we can't help being inspired and awestruck by the color and light show.

Fig. 12-8. Orange stage: Altocumulus about 10 minutes before sunrise at Vail, AZ, 24 Feb 2023. JC.

Fig. 12-9. Orange and yellow stage: Telephoto view of Altocumulus, Cheyenne, WY, 10 minutes before dawn, 24 Nov 2017. JC.

The colors and drama of clear sky twilights, beautiful as they are, can be greatly embellished by clouds. This we have already shown, mainly with cumulonimbus clouds and their appendages in §4.2, and it is true of all cloud genera that allow sunlight or skylight through at

Fig. 12-10. Panoramic view of multicolored, 'swirling' altocumulus 10 minutes before dawn, 24 Nov 2017, Cheyenne, WY. JC.

twilight. The multicolored cirrus sunset of 15 Nov 2022 with green sky highlights (Fig. 4-2) is one of many examples.

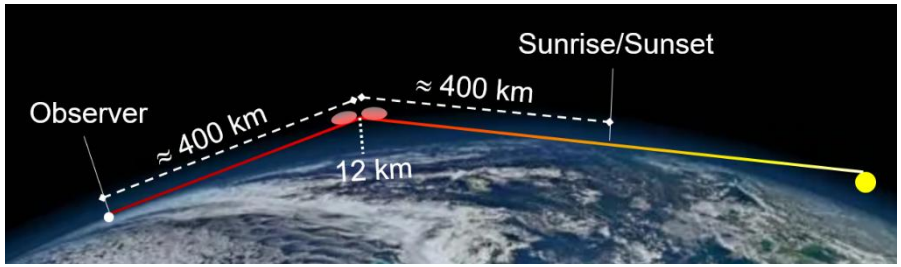

Fig. 12-11. Maximum distance into twilight sunlit clouds 12 km high can be seen. SDG.

Even so, many of the greatest twilight sky shows are reserved for the wavy or dappled sheets of altocumulus and cirrocumulus. Why not stratocumulus? Height matters for twilight colors on the spherical Earth. The higher the cloud, the further into twilight the cloud can still be sunlit and the deeper red it can be, while the deeper blue the twilight sky aloft can be. Let's look first and explain later.

Twilight skies form a color continuum but are prolonged enough to be divided into two stages: the red stage of deep twilight and the orange stage near sunrise and sunset. A full 50 minutes before sunrise on 29 Oct 2018 deep red clouds appeared in a deep blue sky toward the eastern horizon of Cheyenne, WY (Fig. 12-6). Three weeks before that, on 05 Oct 2018, only 38 minutes before sunrise,

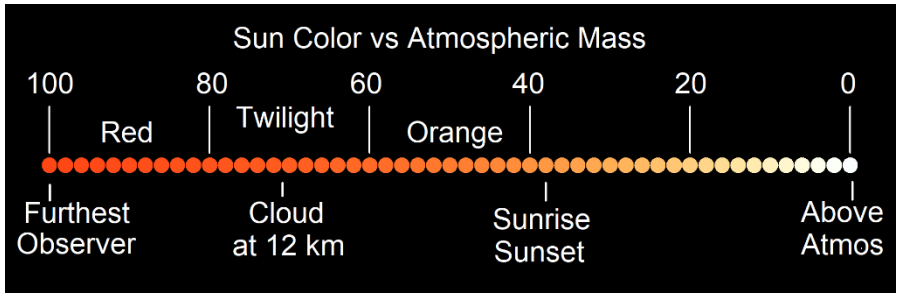

Fig. 12-12. Sun (or illuminated cloud) color vs atmospheric mass. SDG.

the altocumulus cloud sheet still gleamed red in the deep blue sky above, but orange-red near the horizon, where it was tinted by the bright yellow strip of sky just above the horizon line (Fig. 12-7).

These red twilight clouds with their deep blue skies aloft contrast with the orange twilight altocumulus and paler blue skies, sometimes tinged with a distinctive strip of green, that rule within about 10 minutes of sunrise or sunset, as in Fig. 12-8. Other colors emerge as skylight and sunlight combine to contribute to the light that clouds reflect or transmit. In Fig. 12-9 and the panoramic Fig. 12-10, both 10 minutes before sunrise on 24 Nov 2017, blazing yellow horizon skylight appears below the orange sunlit altocumulus. At the same time, the rose-speckled cloud on the right side of the photo gets its color from the mixture of blue skylight aloft plus orange sunlight.

Clouds can be sunlit deep into twilight because of the Earth's curvature. A cloud at 12 km and normal atmospheric refraction will remain sunlit until it is ≈ 400 km into twilight. An observer at sea level can be up to an additional ≈ 400 km for a total of ≈ 800 km or 7.2º deep into twilight (Fig. 12-11). At the equator, where the Sun goes straight down or up on the equinoxes, that translates to 29 minutes. In the mid or high latitudes, where the Sun goes down at a slant, clouds in the upper troposphere can be sunlit an hour or more before sunrise or after sunset.

Why are deep twilight clouds so red? Add it all up and the reflected or transmitted sunlight on the cloud that reaches the observer had to pass through up to the equivalent of 100 atmospheric masses. Recall (§2.4 and Fig. 2-13) that the greater the total atmospheric mass sunlight must pass through the smaller the fraction of short waves that penetrates. Orange clouds prevail a short distance into twilight while red clouds prevails deep into twilight (Fig. 12-12). Of course, the light is feeble because the deepest red light passing through 100 atmospheric masses is reduced by over 96%. Shorter waves are gone.

The sky aloft in the deep twilight photos of Fig. 12-7 and Fig 12-8 is deep blue because ozone absorbs much orange light when sunbeams pass obliquely through the stratosphere (recall §2.9 to 2.11). When the Sun is straight overhead and the atmospheric ozone content is near its mean depth of 300 Dobson Units (3 mm when compressed to sea level pressure), 5% of the orange light is absorbed (but less than 1% of the blue light). During twilight, sunbeams lighting the sky aloft have taken such an oblique path through the ozone laden stratosphere that almost all the orange light has been absorbed – hence the deep blue scattered skylight.

Because of their greater height, nacreous, and especially, noctilucent clouds can be seen even deeper into twilight. Noctilucent clouds

Fig. 12-13. Noctilucent clouds over southern Alberta, Canada, 27 Jun 2021. ©Alan Dyer.

often appear wavy because of shear produced in the enormous wind speeds of the Mesosphere up to 650 km/hr. They are rarely seen as far south as Cheyenne, WY, where they have been captured, but they are better in Canada (Fig. 12-13) and northern Eurasia, especially around 60º latitude and are summer clouds when the mesopause is coldest.

On the twilight side of sunrise and sunset the sunlit sides of towering cumulonimbus clouds exhibit a continuous color gradation much like that of Fig. 7-6 from near white at top to near red near the base as the effective atmospheric mass the sunlight must penetrate to reach the cloud increases. For cloud layers at discrete heights the color differences are discrete, as on 22 Oct 2022, where the altocumulus cells are pronounced pink and deep orange while the patch of higher cirrocumulus is a pale orange much closer to white (Fig. 12-14).

Fig. 12-14. Cloud color vs height over Vail, AZ, 22 Oct 2022. JC.

Fig. 12-15. Twilight cloud with underlit mamma, 38 minutes before sunrise, Cheyenne, WY, 23 Dec 2019. JC.

A distinctive aspect of twilight cloud sheets is that they are underlit because the Sun is below the horizon. Features of cloud bases that are shaded or even masked during the day suddenly light up during twilight and add drama. In Fig. 12-15 pouches of mamma hanging below the body of a sheet of altocumulus were lit a lurid, blood red by the sunlight of deep twilight. As we will see in Chapter 13, some of the most dramatic twilight underlighting, and certainly the weirdest, occurs with mountain wave clouds.

12.3 Honeycomb Cloud Cells

Cellular convection is one of the simple motions of patterned cloud sheets. It is mostly a gentle form of convection as opposed to the more vigorous and even violent penetrative convection of cumulus

Fig. 12-16. Closed Cell Altocumulus, Keene, NY. SDG.

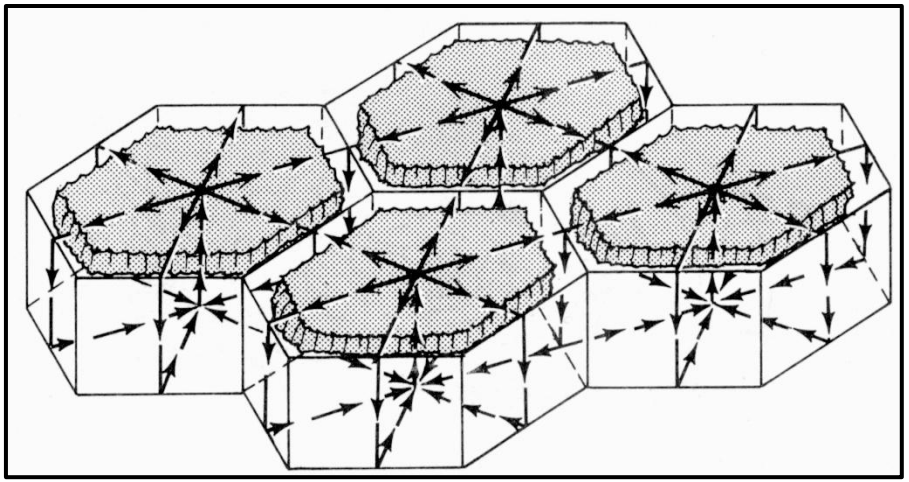

Fig. 12-17. Air motions for closed cellular clouds. SDG.

and cumulonimbus. When vertical wind shear is weak, cloud sheets often consist of tightly packed cells with a honeycomb appearance,

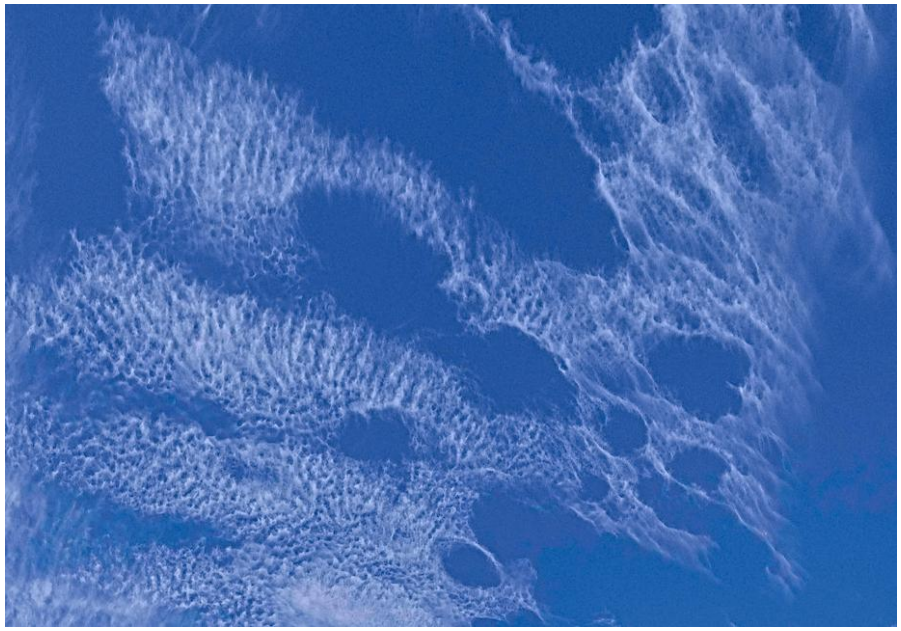

Fig. 12-18. Open Cell Cirrocumulus, 31 Jan 2021, Cheyenne, WY. JC.

ideally as hexagons. This is caused by gentle, cellular convective motions in which the layer becomes slightly unstable (due to heating from below or cooling at the top) and fractures into a series of distinct circulation cells.

There are two classes of cloud cells, closed cells (Fig. 12-16 and Fig. 12-17) and open cells (Fig. 12-18). Closed cells have rising, cloudy air in the center of each cell, and clear alleys of sinking air, illustrated in Fig. 12-17. Closed cells tend to form when the top of the layer cools. The sinking motion is more intense and narrower than the rising motion. (Note: Some closed cells are donut-shaped with larger donut-hole clearings at triple junctions.) If the entire humid layer is slowly rising, even the alleys will be cloud-filled, resulting in a mottled overcast, as in Fig. 12-19. Large areas of closed stratocumulus cells hover over the cold waters west of each continent in subtropical latitudes, as off the coast of California, Chile, or Namibia, as in the bottom frame of Fig. 12-20, centered at 23.8º South Latitude and 0.5º West Longitude on 04 Jan 2024.

Fig. 12-19. Closed Cell Altocumulus with banding and cloud-filled alleys, 08 Apr 2009, Coulterville, CA. SDG.

Open cells have narrow, cloud fringes of rapidly rising air, and broad clear centers with gently sinking air. They tend to form when a humid layer of air is heated from below. Open cells that form over warm ocean waters resemble diamond studded bracelets because they consist of interlaced rings of penetrative cumulus or cumulonimbus, as in the top frame of Fig. 12-20, centered at 57.8 South Latitude and 72.2 West Longitude (see also Fig. 5-14 and Fig. 5-30). Such open cells are so large they can only be recognized from space.

12.4 Shear Wave Clouds and Cloud Streets

Tiny (Rayleigh-Bénard) convection cells can form at the top of a cup of hot cocoa that is cooling. If you stir the cocoa gently the cells will stretch into bands. In the atmosphere, wind shear can align the honeycomb cells into long bands or cloud streets parallel to the wind or swirl them into vortices. Cloud streets often form when cold, dry polar air acquires heat and moisture as it pours over warmer ocean waters and act as wind vanes (recall §6.5). Since vertical wind shear

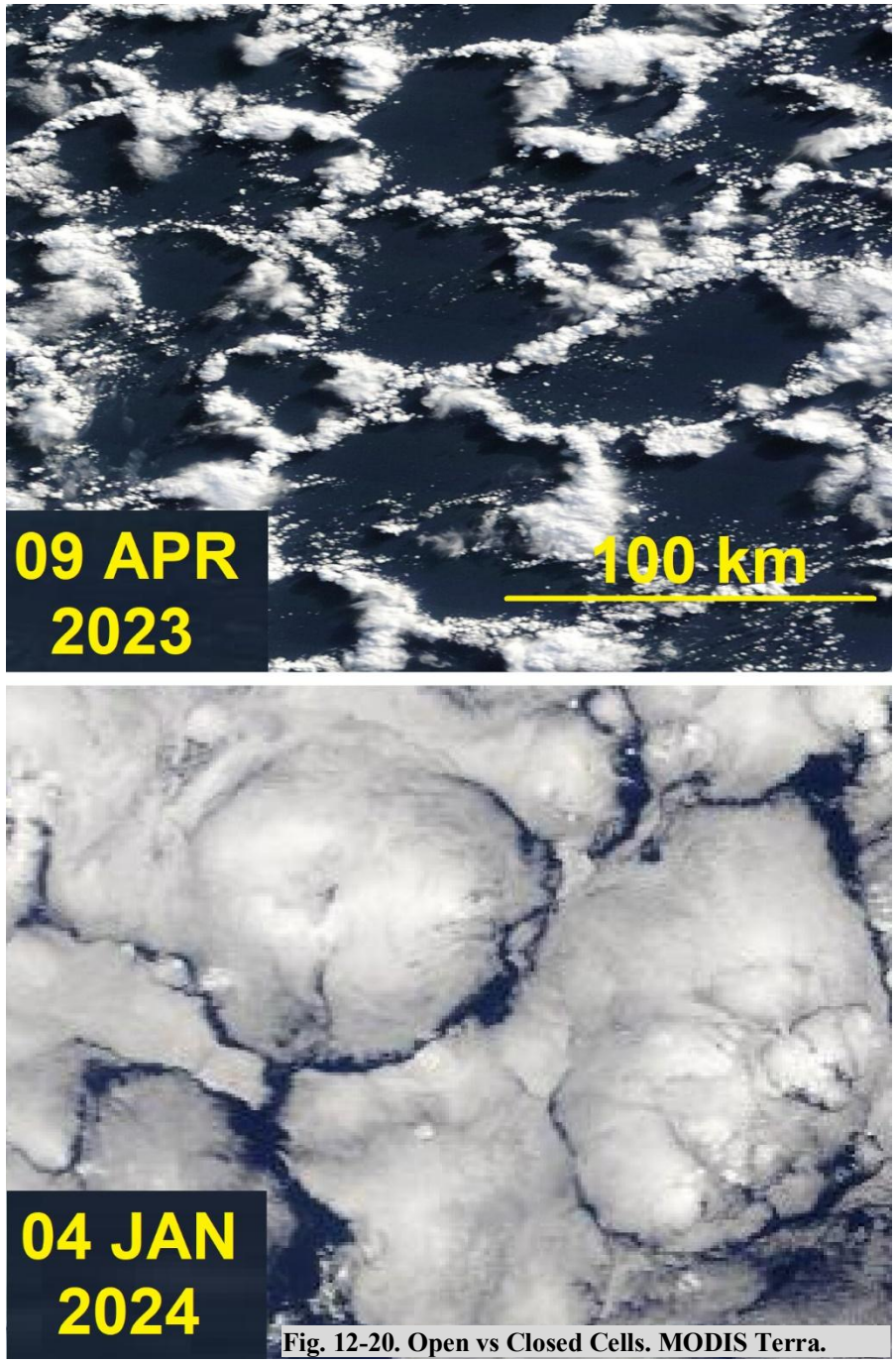

Fig. 12-20. Open vs Closed Cells. MODIS Terra.

Fig. 12-21. Train of a dozen Kelvin-Helmholtz wave clouds riding on an inversion, 30 minutes before Sunrise east of Cheyenne, WY 03 Jan 2020. JC.

can also marshall clouds in wave crests perpendicular to the wind, a cloud matrix can include any or all of these forms simultaneously. When two trains of wave clouds cross the cloud pattern is called a mackerel sky because it resembles fish scales.

Fig. 12-22. Kelvin-Helmholtz wave clouds over the Czech Republic. ©Lukas Gallo.

The vertical wind shear that bends cirrus streamers or whips up huge ocean waves produces waves in the air with crests perpendicular to the shear. In dry air the waves are invisible, but if an air layer has just the right humidity, cloud bands fill the crests where the air rises above its condensation level and clearings occupy the troughs, where air sinks below the condensation level.

Many waves develop as the result of an instability first diagnosed by Lord Kelvin and Hermann von Helmholtz. When wind blows over water that may appear glass smooth, any miniscule irregularity or disturbance will ripple the airflow. The wind accelerates where it is 'squeezed' to pass over a 'hump'. As it speeds, pressure is reduced by Bernoulli's principle. If the wind is fast enough, i. e., if its kinetic energy is larger than the potential energy needed to lift the denser water, then the lowered pressure will lift the 'lump' further. At the same time, the wind spreads and slows over any depression, deepening it as pressure increases. The result is amplifying waves.

Kelvin-Helmholtz (K-H) waves form in the atmosphere when wind speed changes abruptly at the interface of inversions in which a warm layer with faster winds overlays a cold layer. If the difference of wind speed between the two layers is large enough, Kelvin-Helmholtz waves will form, grow, and break in the air like plunging ocean waves break as they approach a beach, but in slow motion. And, if a line of cloud exists just below the inversion it will trace the motions of the growing K-H waves, illustrated in Fig. 6-38. Fig. 10-11, Fig. 12-21, and Fig. 12-22 are among the examples of K-H wave clouds seen in graceful development perhaps several times in a cloud watcher's lifetime. Why are they so rare when breaking waves are

Fig. 12-23. Cirrocumulus waves over Granada, Spain. SDG.

common on a beach? The conjunction of factors (without a beach) needed to produce K-H waves and make them visible as clouds plus their brief lifespan of several minutes all contribute to making them rare creatures, which adds a special note to their geometrical beauty.

Curling K-H waves (recall Fig. 6-39) also appear for a few brief moments when rogue thermals, usually in cumulus cloud streets, poke up above the parent cloud into large wind shear. The vorticity of the thermals adds to the ambient shear to produce the waves, which quickly break and disappear. These more common rogues tend to occur as one or two waves rather than as a laminar wave train. Far more often, vertical wind shear ripples patterned cloud sheets into trains of small-amplitude waves that do not grow and break. The same is true for ocean waves out at sea, which do not break unless strong winds rip their tops off. Examples of clouds that render simple wave trains in the air visible include Fig. 12-23, a delicate, evanescent case of rippling in cirrocumulus above the Alhambra in Granada, Spain (where the crest barely reach the condensation level, altocumulus rolls over San Mateo, CA (Fig. 12-24) and stratocumulus waves in the overcast at Boynton Beach, FL (Fig. 12-25).

Fig. 12-24. Altocumulus waves over San Mateo, CA, 17 May 2014. SDG.

Fig. 12-25. Stratocumulus waves, Boynton Beach, FL, 25 Dec 2022.SDG.

Fig. 12-26. Stratocumulus ripples extending for over 1000 km across Little Sandy Desert of west Australia, 10 Sep 2020. NASA Suomi.

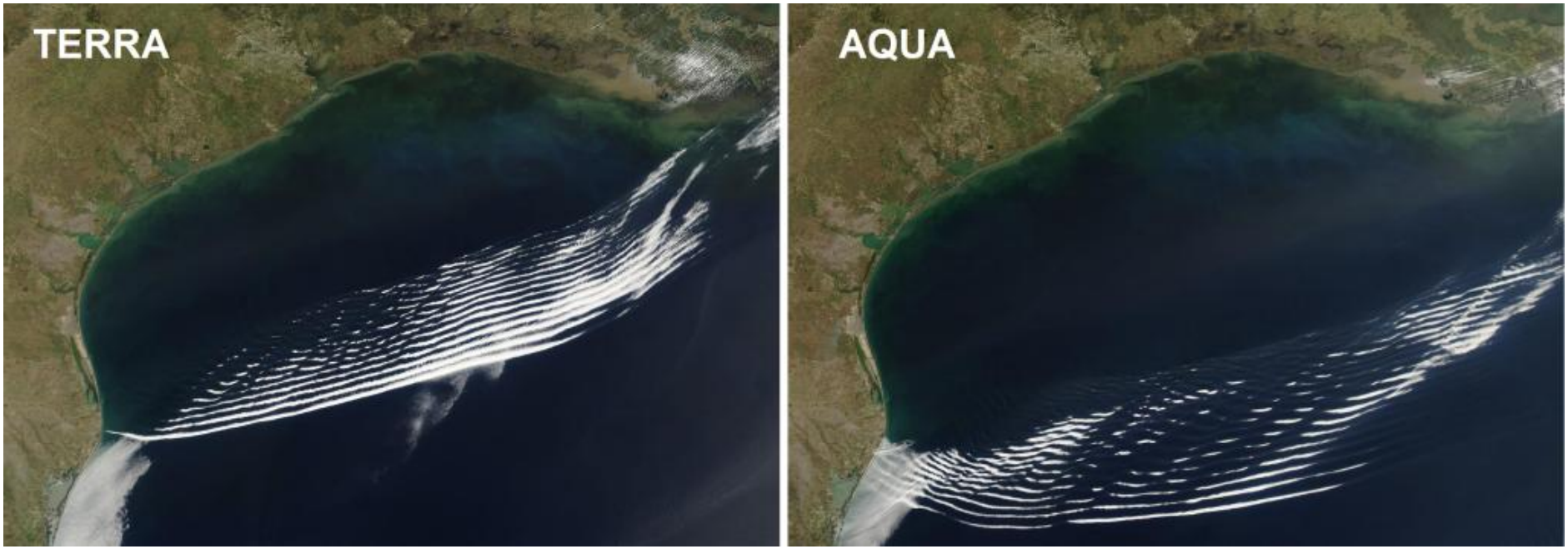

Fig. 12-27. Propagating gravity waves over the Gulf of Mexico on the Ides of March 2008. MODIS Terra and Aqua(4 hours later).

Fig. 12-28. Morning Glory Cloud, Burketown, Australia 11 Aug 2009. ©Mick Petroff.

From Space, cloud waves can be seen extending over hundreds of km. Dramatic examples include the 1000+ km long band of stratocumulus cloud waves over Western Australia's Little Sandy Desert, produced in a very thin humid layer with large vertical wind shear 1500 m above sea level that was capped by an inversion (Fig. 12-26).

Perhaps more striking was the sinusoidal train of gravity waves captured by the MODIS satellites in the act of crossing the Gulf of Mexico on 15 Mar 2008 (Fig. 12-27). The cause was a rapid increase of NW winds impinging on a humid veneer at 400 m above sea level capped by a pronounced inversion. The wave train that spread out resembles a train of water waves produced when a board is shoved forward. The clouds (and their motions) resemble arcus roll clouds advancing away from a thunderstorm downdraft

The most famous stratocumulus roll or rope cloud is the Morning Glory, which forms over the Gulf of Carpentaria, Australia in a similar manner, in association with the sea breeze. One of the classical photos was taken from a plane on 11 Aug 2009 by Mick Petroff (Fig. 12-28). Sailplane pilots converge on Burketown around October, when it is most likely to soar the updraft ahead of the advancing clouds.

Fig. 12-29. Longitudinal Stratocumulus bands 1500 m above Boynton Beach, FL, 28 Jan 2020. SDG.

Cloud streets or bands that may be confused with waves form parallel to the wind, as the result of helical motions illustrated in Fig. 6-27. Fig. 12-29 is an example of stratocumulus cloud streets with mostly smooth edges aligned parallel to the west wind.

12.5 Ranks and Rows

Most of the time patterned cloud sheets contain messy mixtures of cells, waves, streets, ranks, and rows. (The artist, J. M. W. Turner loved these complex cloud sheets.) For example, while the dominant wave pattern of cloud-filled crests and clear troughs that cross the shearing west wind at 6600 m in Fig. 12-1 is oriented N-S, bands that extend E-W are also visible. The pattern of crossing waves and bands is more pronounced in Fig. 12-3, where distinctive lacunae (cavities) form in some of the clear checkerboard troughs of sinking air. And Fig. 12-30, with cells, gaps, and ripples in long bands, is so complex it can be interpreted as Pac-Man seeking his heart.

Fig. 12-30. Pac-Man altocumulus seeking his heart. Killington, VT, 07 Mar 2010. SDG.

The simplicity of the motion of patterned cloud sheets stands in stark contrast to the complexity of their form. Yet, time lapse videos show that the fine-scale cells and ripples undergo very little dynamical change during the few minutes the sheets take to traverse the sky. Examples abound, including videos of the late afternoon cell-lined bands of altocumulus of 31 Dec 2023 over Cheyenne (Fig. 12-31).

https://www.flickr.com/photos/cloud_spirit/53433605237/in/album-72157673924732027/lightbox/

and the mackerel sky of 14 Mar 2016,

https://www.flickr.com/photos/cloud_spirit/25774629235/in/album-72157662969788496

where all the cloud elements remain almost frozen in form as the sheet traverses the sky.

Fig. 12-31. Altocumulus bands moving over Cheyenne, WY, 31 Dec 2023,. JC.

Visible changes of the clouds result more from larger scale fields of rising and sinking air, where blotches of patterned clouds appear or disappear in fixed form. It dramatizes the very slow speed of the small-scale churning motions of the cells and ripples.

Dynamic waves do appear in the time-lapse video of 12 March 2016, where two patterned cloud sheets at different heights move in opposite directions.

https://www.flickr.com/photos/cloud_spirit/25443517670/in/album-72157662969788496/

The higher sheet, a frozen field of cellular altocumulus moves away from the camera. The lower sheet is riddled with cloud fragments that move with the wind at that level toward the camera. The fragments grow as they catch up to the slower-moving wave crests marked by the cloud lines and shrink or even evaporate as they exit the cloud wave crests and pass through the wave troughs.

All in all, the cells, waves, ranks and rows of the patterned cloud sheets produce some of the most spectacularly beautiful skies, but lack the violence needed to win weather photography contests.

12.6 Cloud Wakes and Vortices

Obstacles in the flow can add a final twist to patterned cloud sheets. When moving patterned cloud sheets encounter mountainous islands the airflow and resulting cloud patterns are distorted in at least two distinct ways, best seen from space because the patterns tend to extend several hundred km downwind from the islands.

A: Kelvin Wake Wave Clouds

First are the Kelvin wake waves, whose classical cases form in the wake of moving boats and ducks, as in Fig. 12-32. Water piles up in front and a series of waves spreads out at a 17° angle on each side of the track of the vessel. (Ships are now designed with torpedo-shaped protrusions in their bows below water line to reduce the bow waves and their hydrodynamic drag.)

In the atmosphere, islands with isolated, often volcanic peaks serve in place of the moving boat or duck when fast winds pass by. An inversion capping the cloud top is the ideal scenario to produce waves with appreciable vertical motions in the airflow. The wake clouds show to greatest advantage when the cloud layer is thin enough so that it evaporates in the wave troughs and thickens noticeably in the crests.

Fig. 12-32. Kelvin wake waves made by a swimming duck. Note bow wave crest in front of the duck. ©Daderot.

Fig. 12-33. Kelvin wake waves of Zavodovski (Z) and Visokoi (V, with bow wave) Islands, 10 Feb 2017. NASA MODIS Terra.

The remote South Sandwich Islands, a chain of 11 major volcanic islands that runs N-S, serve as ideal barriers to the relentless, often gale speed, westerly winds of the 'Screaming 50's'. The meteorological setting is often optimal for Kelvin wake waves, with low-level clouds capped by stable layers or inversions somewhat above the height of the peaks. In some cases, each of the islands, like ships in an armada, produces its own wake.

On 10 Feb 2017, one of countless cases, a cloud layer less than 100 m thick at 1 km, the height of the peak on Visokoi Island, proved the perfect setting for a long train of Kelvin Wake Clouds (Fig. 12-33). The split pattern of wake clouds in both Fig. 12-32 and Fig. 12-33, separated by calm central wedges, occurs when the duck or wind is faster than the wave speed (Froude Number > 1). Zavodovski Island did not produce as marked a wake wave pattern because its highest peak is only 550 m. Fine scale ripples, whose cause is uncertain because there was little vertical wind shear, can be seen dappled across much of the disrupted cloud field.

B: Wake Vortex Clouds

The graceful cloud vortices that form in the flow downwind from peninsulas, capes, or islands are produced by primarily horizontal motions that occur with brisk but slower winds and lower Froude Numbers (typically ≈ 0.4) than for the Kelvin wake wave clouds, which are primarily the result of vertical motions. On rare occasion, an island can generate wake waves and vortices simultaneously, as with Robinson Crusoe Island on 02 Feb 2019 (Fig. 12-34).

Fig. 12-34. Kelvin wake waves and von Karman vortices downwind (N) of Robinson Crusoe Island, 02 Feb 2019. NASA MODIS Aqua.

Peninsulas or capes that jut into the flow produce single vortices in their wake. A pronounced mesoscale cyclonic vortex developed off the coast of Portugal on 16 Jul 2017 as the NNE winds rounded Cape Finisterre of Galicia, Spain. The vortex in turn distorted the stratocumulus cloud field. Fig. 12-35 shows two images of the large

Fig. 12-35. A cyclonic vortex swirls the stratocumulus cloud field in the wake of Cape Finisterre 17 May 2017 and wraps up during the four hours between NASA MODIS Terra and Aqua.

cloud vortex and how it wrapped up in the four hours between the morning Terra and afternoon Aqua images.

Islands immersed in a moving cloud field split the airflow. As the wind skirts around the island it is 'squeezed' laterally and accelerates. The resulting horizontal shear often generates a regular pattern of von Kármán vortices that spin in opposite directions and are shed alternately on opposite sides of the island. Each vortex wraps up as it moves downwind and its trajectory is affected by the velocity field of its neighbors.

Since the motions of the von Kármán vortices are largely horizontal, their main effect is to align clouds rather than to create or destroy them. The result might be considered a beautification of a patterned cloud sheet that is beautiful to begin with. Examples abound downwind of many islands (e. g., Guadalupe, the Canary Islands, the Juan Fernández Islands, and the South Sandwich Islands when wind speed abates), with one of the paradigm cases occurring downwind from Guadalupe Island off the western coast of Mexico on 24 May 2017 (Fig. 12-36). The von Kármán vortices aligned the cloud cells so perfectly that the distorted wind field can be traced easily even without the help of videos. Of course, videos always add vibrancy.

https://www.youtube.com/watch?v=SawKLWT1bDA

As the spirals wrap up, they may develop large clear 'eyes' mainly by encircling areas of clear air in the wake of the island. A paradigm case of clear vortex 'eyes' occurred in the wake of Heard Island

Fig. 12-36. Vortices in the stratocumulus cloud field trace von Kármán vortices downwind of Guadalupe Island, 24 May 2017. NASA Landsat.

(with its 2945 m peak) in the South Indian Ocean on 03 May 2016 (Fig. 12-37) with motions and scale shown in Fig. 12-38.

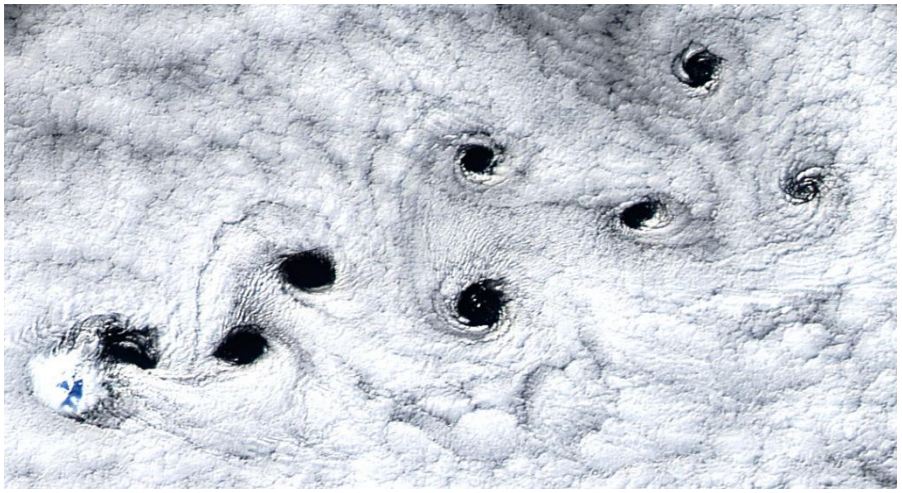

Fig. 12-37. Vortices with clear cores in lee of Heard Island, 03 May 2016. NASA MODIS Aqua.

Von Kármán vortices occur in many places, and not always on Earth. For example, they occur around the Great Red Spot and in other bands of Jupiter's atmosphere as well as in the atmospheres of all the gas giant planets.

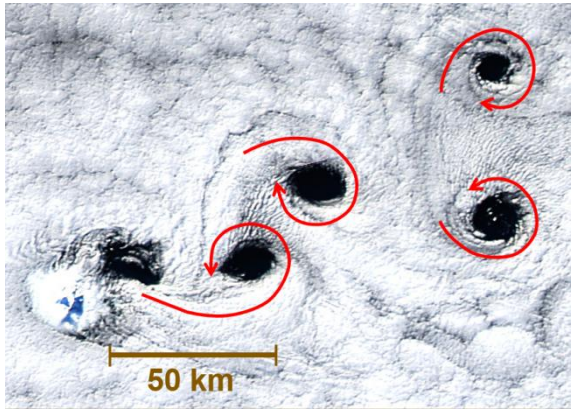

Fig. 12-38. Motions and scale for Fig. 12-37.

12.7 Patterned Cloud Sheet Gallery

Endless variations on a theme!

Fig. 12-39. Rippled altocumulus cells over Vail, AZ, 06 Dec 2022. JC.

Fig. 12-40. Stratocumulus undulatus from the air. SDG.

Fig. 12-41. Stratocumulus undulatus from the air. SDG.

Fig. 12-42. Stratocumulus undulatus over CCNY. SDG.

Fig. 12-43. Stratocumulus undulatus over CCNY. SDG.

Fig. 12-44. Altocumulus over San Mateo, CA, Jun 2015. SDG.

Fig. 12-45. Hole punch altocumulus, Fort Lauderdale, FL. SDG.

Fig. 12-46. Altocumulus over Mt. Lafayette, NH, Jul 1999. SDG.

Fig. 12-47. Altocumulus over Chicago, IL, 13 Jul 2009. SDG.

Fig. 12-48. Altocumulus Big Bend National Park, TX, 02 Mar 2012. SDG.

Fig. 12-49. Altocumulus vertebratus, Boynton Beach, FL, 12 Dec 2014. SDG.

Fig. 12-50. Altocumulus waves and cells Boynton Beach, FL, 06 Jan 2018. SDG.

Fig. 12-51. Altocumulus duplicatus Boynton Beach, FL, 12 Dec 2014. SDG.

Fig. 12-52. Altocumulus Bands at acute angles, Boynton Beach, FL, 01 Feb 2015. SDG.

Fig. 12-53. Cirrocumulus undulatus, Sapphire, NC, 20 Oct 2018. SDG.

Fig. 12-54. Cirrocumulus, San Mateo, CA, 09 Nov 2016. SDG.

Fig. 12-55. Cirrocumulus (9.5 km) above altocumulus (5.5 km), Boynton Beach, FL, 14 Jan 2010. SDG.

Fig. 12-56. Cirrocumulus grading to Altocumulus, Boynton Beach, FL 28 Nov 2023. SDG.

Wonders of the Atmosphere
Chapter 13: Mountain Wave and Banner Clouds

Fig. 13-1. Saucers over Cheyenne, WY, 09 Feb 2017. JC.

Fig. 13-2. Pile of plates lenticular clouds over Cheyenne, WY, 19 Jan 2019. JC.

Fig. 13-3. Mayan Volcano with cloudy ‘hat’, 05:53 23 April 2019. ©Patryk Reba.

Wonders of the Atmosphere
Chapter 13: Mountain Wave and Banner Clouds

13.1 Flying Saucers are Mountain Wave Clouds

Fig. 13-4. Altocumulus Lenticularis over the Grand Canyon, 31 Mar 2010. SDG.

Of all the patterned airflows that marshal clouds into waves, ranks, and rows, flying saucer altocumulus lenticularis (lentil or lens-shaped) mountain wave clouds (Fig. 13-1) stand out. Mountain wave clouds may form directly over peaks or ridges, downwind as series of lee (downwind) waves (Fig. 13-2), or even tilt upwind with height. They can be models of smoothness and symmetry, as the cap cloud that forms over Mayan Volcano, as on 23 Apr 2019 (Fig. 13-3), so that from the photo alone it is near impossible from the photo to tell the wind direction. They are unique in that, like a silent helicopter (Fig. 13-4), they hover in place as the wind blows through them, and they often have an *almost* unchanging form. Their smoothness (and uniform gradient of droplet sizes) often turns their fringes iridescent when seen near the Sun (Chapter 14).

Though artists have portrayed mountain wave clouds for centuries, and though they are seen so often in favored places that they have earned longstanding nicknames (e. g., the Tablecloth over Cape Town, South Africa, and the Taieri Pet SE of the long ridge of the Rock and Pillar Range in southeastern New Zealand) worldwide attention was riveted on them for the first time after a likely sighting on 24 June 1947. Experienced pilot, Kenneth Arnold labelled what he saw as 9 shiny Unidentified Flying Objects (UFO's) with saucer shapes apparently racing past Mount Rainier. Within two days newspaper reports suggested flying saucer space ships, and the UFO craze was on. We cannot be sure if Kenneth Arnold did, in fact, see mountain wave clouds as astronomer Donald Menzel argued, but there is no doubt that saucer-shaped mountain wave clouds often form above and around Mount Rainier, and many other peaks.

Lenticular clouds form when stable air with humid layers is forced to ascend steep mountain peaks or ridges by fast winds aloft. The smooth appearance of the clouds shows that the flow is laminar, not turbulent, and is the proof that the air is stably stratified and has been forced to rise over the peak or ridge. That forced ascent often sets in motion a train of lee waves.

Mountain wave clouds appear at the height that humid layers in the airstream arch above their condensation levels, for example, downwind of Mount Washington in New Hampshire (Fig. 13-5) as illustrated in Fig. 13-6. As the air rises above the condensation level, droplets or ice particles form. The droplets and ice particles move with the wind through the unmoving cloud, continuing to grow while the

air rises (Fig. 13-7). After passing the wave crest, the air sinks and warms adiabatically, causing the droplets and ice particles to shrink and eventually evaporate.

Fig. 13-5. Concave, saucer-shaped lenticular clouds over Mt. Washington, NH. ©Al Saucier.

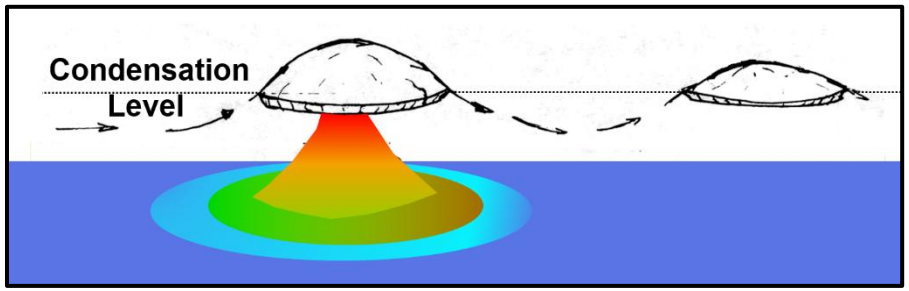

Fig. 13-6. Wave motions for saucer-shaped lenticular clouds over and downwind of isolated peaks. SDG.

Mountain wave clouds are, anchored to the wave pattern, which is anchored to the mountains but wave length and amplitude do vary with wind speed and static stability. They tend to occur when wind speed increases with height and static stability decreases with height.

What causes the wavy motion that produces trains of wave clouds on the lee side. After the wind has forced the stable air over a peak or ridge, the air's excess density forces it to descend the lee slope. But, like a swing that has been pushed too high, the downward momentum carries the air below its initial equilibrium level, where it is buoyant. This causes the air to rebound, an a series of diminishing waves results. Wave clouds fill each wave crest that extends above the condensation level, and clearings occupy the troughs.

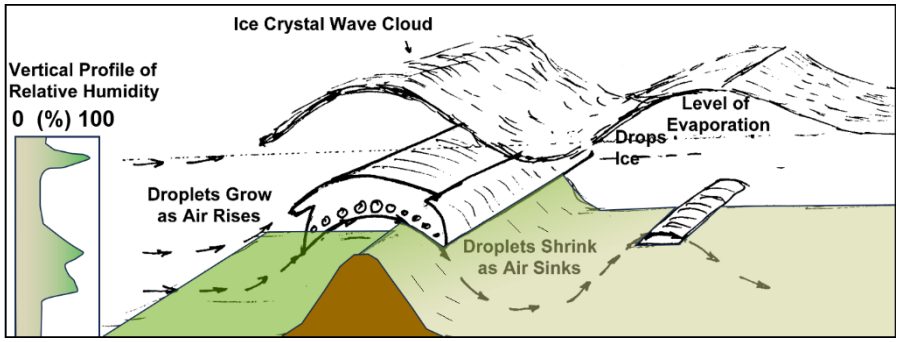

Fig. 13-7. Wave motions for cigar-shaped lenticular clouds over ridges. SDG.

Fig. 13-8. Train of long, wavy cigar-shaped lee wave clouds downwind from the long ridge of Schunemunk Mt., NY. SDG.

The shape of the wave cloud reflects the shape of the mountain and the humidity structure of the atmosphere. Trains of UFO shaped saucers form over isolated peaks (Fig. 13-5), while trains of long clouds form over long mountain ridges, as over modest, 500 m high Schunemunk Mt., NY (Fig. 13-8). The oft cigar-shaped Taieri Pet, seen from above in the LandSat image of Fig. 13-9 forms downwind of the modest, but straight, escarpment of the long straight-ridged Rock and Pillar Range in southern New Zealand.

Fig. 13-9. The Taieri Pet, 07 Sep 2024, Middlemarch, New Zealand. Earth Observatory image by Lauren Dauphin, using Landsat data from the U.S. Geological Survey.

The shapes of the tops and bases of lenticular clouds depend on the vertical profile of humidity in the ambient air. When a humid veneer is embedded in an otherwise dry atmosphere, the cloud arches upward in center like an eyebrow and the base is concave, with a hollow look, as in Fig. 13-5. When humidity decreases gradually below the level where it is maximum, cloud base is convex and the cloud is lentil- or flying saucer shaped, as in Fig. 13-10.

Surprisingly often, the atmospheric column has a complex profile of alternating layers of humid and dry air (Fig. 13-7). The humid layers remain invisible when not forced to rise. But when they are forced to

Fig. 13-10. Lenticular Ac with convex base over Cheyenne, WY, 18 Jan 2020. JC.

Fig. 13-11. Pile of Plates over Cheyenne, WY, 02 Nov 2019 with at least 12 alternating humid and dry layers. JC.

rise, cloud veneers can stack up like piles of plates, as in Fig. 13-2 and Fig. 13-11, which reveals at least 12 humid layers. The Renaissance artist, Piero della Francesca, who lived amidst the Appenine Mountains, was the first to paint a pile of plates over the sky in San Sepolcro, Italy in his ***Baptism of Christ*** (1450).

Fig. 13-12.Thin lenticular Cirrocumulus with pronounced transverse waves over Cheyenne, WY, 21 Dec 2021. JC.

Fig. 13-13. Altocumulus lenticularis undulatus over Cheyenne, WY, 27 Oct 2018. The waves are only visible at the fringes of the optically thick cloud but dominate the thin cloud at top. JC.

The winds that race through mostly smooth, standing lenticular clouds, carrying the cloud droplets and/or ice particles with them, are revealed by irregular features resulting from humidity variations, convection cells, thermals, or ripples due to transverse waves produced by wind shear, as in Fig. 13-12 and Fig. 13-13.

Fig. 13-14. Rippling becomes dominant as the mountain wave cloud over Cheyenne, WY, 24 Dec 2014 thins and dissipates. JC.

It is likely that shear waves often 'ride' atop even smooth lenticular clouds but remain invisible or inconspicuous so long as the cloud thickness and wave amplitude are dominant. In the top frame of Fig. 13-14 over Cheyenne, WY on 21 Dec 202, transverse waves are visible only at the fringes of the thick lenticular cloud, but visibly spread through the main cloud as it thins in the bottom frame, and ultimately dissipates. The dynamism is dramatized in the video,

https://www.flickr.com/photos/cloud_spirit/25791302405/in/album-72157682860359541

Still-life comes to life with time lapse videos. They show mountain wave clouds as if taking a stand, fighting to stay in place against the wind while the fine scale features and other cloud genera or species succumb to the wind, and whiz across the sky and through the main cloud. In such situations, the videos, of which there are many at,

https://www.flickr.com/photos/cloud_spirit/albums/72157682860359541/with/44240106612

bring out the striking contrast between the upright lenticular clouds and all other fleeting cloud species and genera.

Fig. 13-15. Horizontal striations spin cyclonically around the periphery of the cylindrical wave cloud over Cheyenne, WY, 16 Oct 2020. JC.

For example, the video, starting at daybreak on 11 Dec 2024,

https://www.flickr.com/photos/cloud_spirit/54199111035/in/album-72157682860359541/lightbox/

begins with ripples traversing the length of elongated wave clouds. A few hours later, convection cells 'jump' from one stationary wave cloud to a second, evaporating in the trough between them.

In the time-lapse video of 15 Nov 2021 over Cheyenne, WY, which compressed 30 minutes of real time into 10 seconds,

https://www.flickr.com/photos/cloud_spirit/51681764842/in/album-72157682860359541

horizontal striations and other irregular features rotate around the periphery of a cylindrical wave cloud, almost as if it were a tornado. A hint of the cyclonic rotation is seen in Fig. 13-15 by comparing the positions of the striations of two frames from the video.

The thin, horizontal gray striations, so prominent in Fig. 13-15 are seen quite often at the heights the lenticular clouds are widest. The relative darkness of the striations compared to the thicker main cloud occurs because most of the light entering any thin cloud veneer is scattered vertically.

The time lapse video of the pile of plates over Cheyenne, WY on 19 Jan 2019 (Fig. 13-2) shows endless bands of cirrus racing across the sky while the lenticular clouds stay more or less in the same place, pulsing, swelling, shrinking, appearing or disappearing according to the changes in ***RH*** over a range of heights and over a period of almost 3 hours. A satellite loop of the scene viewed from Space is shown at the end of the video,

https://www.flickr.com/photos/cloud_spirit/46807241071/in/album-72157682860359541

Underlighting of lenticular clouds at twilight reveals structures normally masked or invisible during the day. Fig. 13-16 illustrates the simple situation when two humid veneers, embedded in an otherwise dry atmosphere are forced over an isolated, conical peak at twilight. In

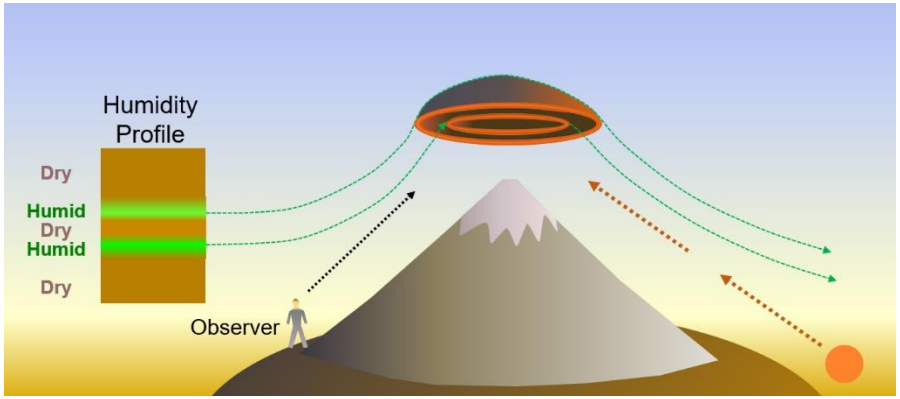

Fig. 13-16. Diagram of an underlit lenticular cloud over an isolated peak at twilight with two humid veneers in an otherwise dry atmosphere. SDG.

Fig. 13-17, the cloud base has red rings that encase shaded concavities. Slightly right of center is an inner red ring revealing a second humid veneer nestled below the main cloud.

Nature sometimes provides even greater complexity.

Fig. 13-18 shows the lurid level of phantasmagoria that the undersides of lenticular clouds can display at twilight if the humidity profile is complex and abrupt enough. This image, the Mother Ship of lenticular complexity (classified as asperitas because of its contorted base) was photographed by Witta Priester in the valley of Hanmer, NZ. The valley is enclosed by mountains on all sides with two narrow canyon openings of the Waiau Uwha River. The tortuous flow and cloud

Fig. 13-18. Under the Mother Ship of lenticular clouds at twilight at Hanmer Springs, NZ, 06 Mar, 2005. ©Witta Priester.

patterns follow from the complex topography of the Southern Alps, with ridges and valleys pointing in multiple directions, though with highest peaks to the NW. At the time, on 06 Mar 2005, fast NW winds crossed the Southern Alps. Three hours before sunset the entire troposphere was saturated. Around sunset time humidity began

Fig. 13-17. Lenticular Ac underlit at twilight with concavities in the base revealing a second (donut-shaped) humid veneer over Cheyenne, WY. JC.

decreasing. That increased the probability of the distinct alternating dry and humid laminae needed to produce the fantastic underlit wave clouds.

Fig. 13-19. Screaming blood-red lenticular cloud 13 minutes after sunset, Cheyenne, WY, 11 Dec 2024. JC.

At twilight, underlit mountain wave clouds can turn as blood red as Edvard Munch suggested when describing the inspiration for ***The Scream*** (see Fig. 15-22). On 11 Dec 2024, the underlit mountain wave clouds over Cheyenne, WY turned 'screaming' blood-red a mere 13 minutes after sunset (Fig. 13-19).

Mountain wave clouds develop tails (Fig. 13-20) on their downwind sides when the droplets that condense at the upwind side freeze inside the cloud. This is likely if the air near the crest of the wave cloud is cold enough, typically, $\boldsymbol{T} \leq -30°C$. Once ice forms, it grows rapidly at the expense of the supercooled droplets and has a lower saturation vapor pressure (recall §4.3). The result is that ice-filled tails do not evaporate until they descend below the initial condensation level, and they may even persist through the troughs, revealing the entire wave pattern (illustrated in Fig. 13-7).

Pilots flying or gliding near lee wave clouds must be on high alert. The worst case is to get caught in the *rotor*, a giant, often invisible vortex on the lee side of the mountain that can plunge unfortunate pilots into the ground like huge breaking waves can wipe out surfers. Why would anyone take such a risk? The answer: Fig. 13-21, shot from a motorized plane. See the video,

https://www.youtube.com/watch?v=0j2LHdP1Gg0

Fig. 13-20. Altocumulus lenticularis with ice particle tails over Colorado Front Range. ©Robert Gedzelman.

The entire pattern of mountain wave clouds may be so large it can only be seen from space. Imposing trains of lee wave clouds often extend 200 to 500 km or more downwind from the Blue Ridge Mountains when strong northwest winds prevail during outbreaks of cold air, as on Stan's 80th Birthday, 23 Nov 2024 (Fig. 13-22). Some subtlety is involved in the formation of the lee wave clouds because a foehn wall formed on the upwind side of the Blue Ridge and skies remained clear downwind over Virginia on 16 Nov, 2024 despite similar vertical profiles of temperature, humidity, and wind on the two dates. Most likely, wind speed at ridge top (≈ 1 km) was too small to excite lee waves on 16 Nov (8 knots vs 20 knots on 23 Nov).

Fig. 13-21. The Taieri Pet in all its glory from the Air over the Otago region, NZ, 1630 NZST 29 Aug 2020. ©Geoff Beckett.

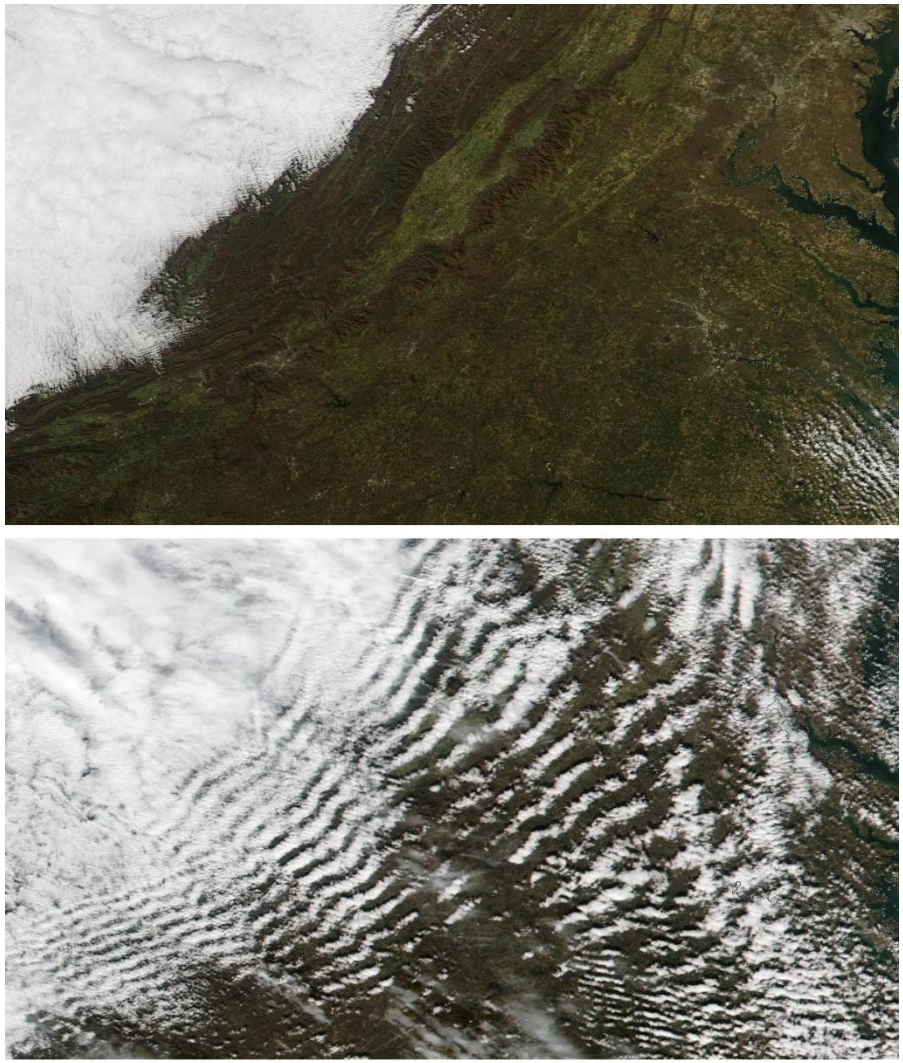

Fig. 13-22. Clear skies east of the crest of the Blue Ridge Mountains of Virginia and West Virginia on 16 Nov 2024 (top, NASA AQUA image) vs. Lee Wave Clouds on 23 Nov 2024 (bottom, SUOMI VIIRS/NPP image).

The Foehn Wall Cloud is a common sight on the lee side of long mountain ranges, such as the Andes over Argentina, the Sierra Nevada over Nevada, the Rockies over Colorado, the northern slopes of the Alps, and the Southern Alps of New Zealand to mention a few. Fig. 13-23 shows a Foehn Wall Cloud over the Presidential Range of the White Mountains in New Hampshire. No lee wave clouds formed in this case.

Fig. 13-23. Foehn Wall Cloud over the Presidential Range of the White Mountains, NH. No lee waves formed. SDG.

One reason Foehn Wall clouds may form without lee wave clouds is illustrated by the contrast between the two panels of Fig. 13-24. In the top panel, when a thin, elevated humid layer surmounts the crest, droplets or crystals remain so small they move with the wind. On the lee side, the air rebounds after sinking, and clouds re-form at the same height they formed atop the crest. In the bottom panel a thick humid layer with a low condensation level ascends the upslope side. Droplets or ice crystals grow large enough to fall, collide, coalesce, and produce precipitation. This dries the air so that when it sinks after surmounting the crest, the remaining droplets and crystals evaporate and disappear at a greater height than they formed. Lee waves will still be produced but will be cloudless. Thus the lee side will not only be a rain shadow, it will be a cloud shadow as well.

Mountain wave clouds are not merely things of beauty. Glider pilots maintain an ongoing love affair with them because of the reliable uplift the standing waves provide. By using mountain wave clouds to locate

updrafts, gliders have soared to heights of 15 km over the Rocky Mountains and over 8 km at Mount Washington in New Hampshire, in other words roughly 4 times higher than the peaks! Long distance flights of 3000 km have been made in the waves both of the Andes and the Rockies.

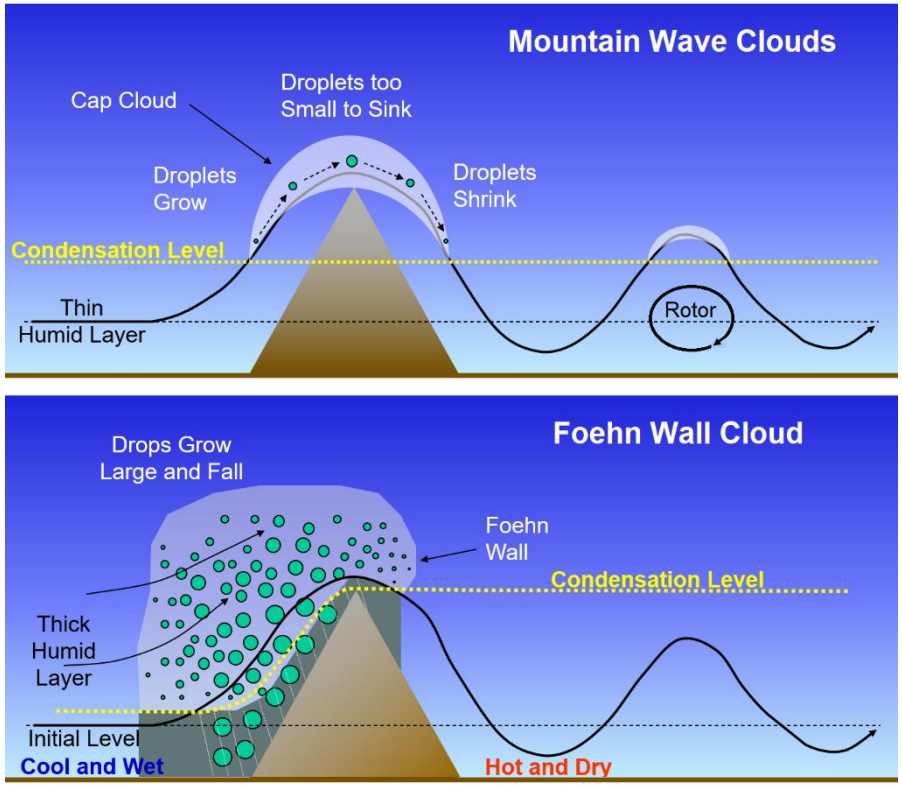

Fig. 13-24. Lee Wave Clouds (top) vs Foehn Wall Cloud (bottom), where precipitation dries the air so that lee wave crests remain below the elevated condensation level. A rotor may also occur with a Foehn Wall Cloud. SDG.

13.2 Pileus Plus: Mountain Wave Cousins

Pileus, the cap cloud, is essentially a mountain wave cloud produced by a rising penetrative cloud instead of a mountain. The pileus of 8 Oct 2007 at Granada, Spain (Fig. 13.25) appeared to be a pile of plates mountain wave cloud but the sounding (Fig. 13-26) showed that winds

Fig. 13-25. Pileus over cumulus Granada, Spain 08 Oct 2007. SDG.

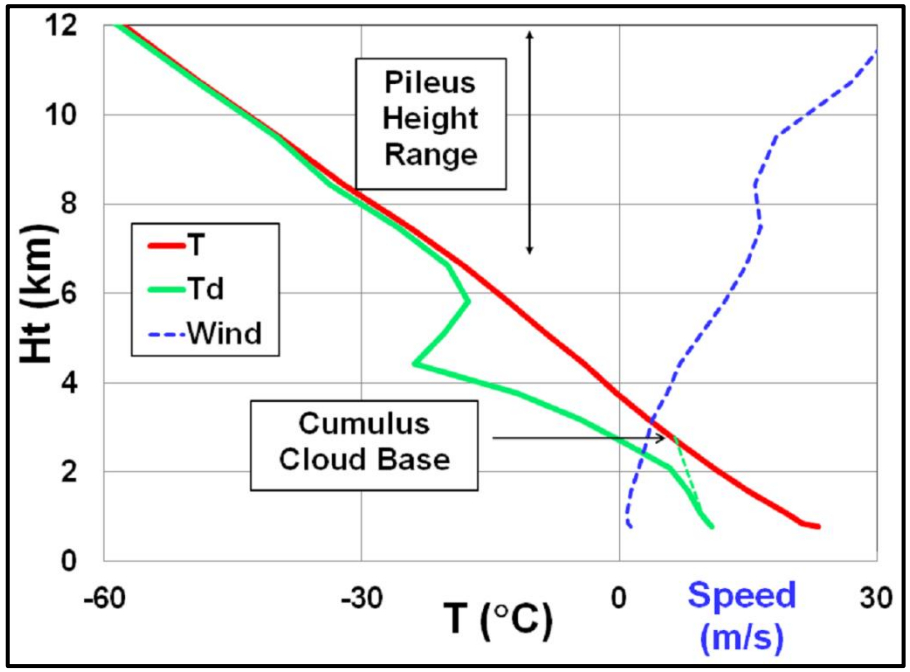

Fig. 13-26. Sounding at Granada, Spain 1500 UTC 08 Oct 2007. SDG.

were almost calm below 4 km, well above the nearby peaks. Winds increased atop the cumulus congestus in the almost saturated air above 6 km where the pile of plates pileus formed Thus, even though a rising cumulus is not as solid as a mountain it still acts as a solid barrier to the ambient air and a dynamic, rising one at that.

This dynamism has several consequences for pileus.

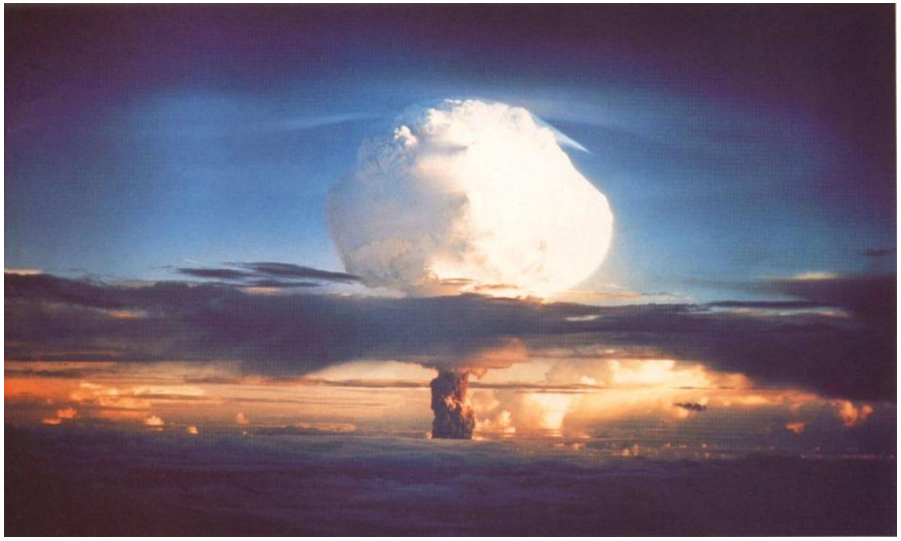

Fig. 13-27. Pileus above Ivy Mike's rising mushroom cloud, 01 Nov 1952. Charles Wyckoff, Public Domain.

1: The faster the updraft and the higher it rises, the more likely pileus will occur, and possibly at several levels. This connects pileus to some of the most awesome natural and anthropogenic phenomena in the atmosphere, thunderstorms, and the even more violent major volcanic eruptions and nuclear explosions.

The infamous mushroom cloud of Ivy Mike created a pileus on the way up (Fig. 13-27) and then wrapped its rising stem in several skirt clouds (velum) (recall Fig. 6-34) by Bernoulli's Principle, just as your finger gets pulled into a water jet shot from a nozzle.

Perhaps the most ironic and ephemeral cloud is the halo-shaped cloud, produced in lows of the explosive shock waves of the nuclear blasts. The Dakota device, detonated on 25 Jun 1956 produced the 'pile of halos' of Fig. 13-28. What irony that such an angelic looking cloud form was produced by such a diabolic device!

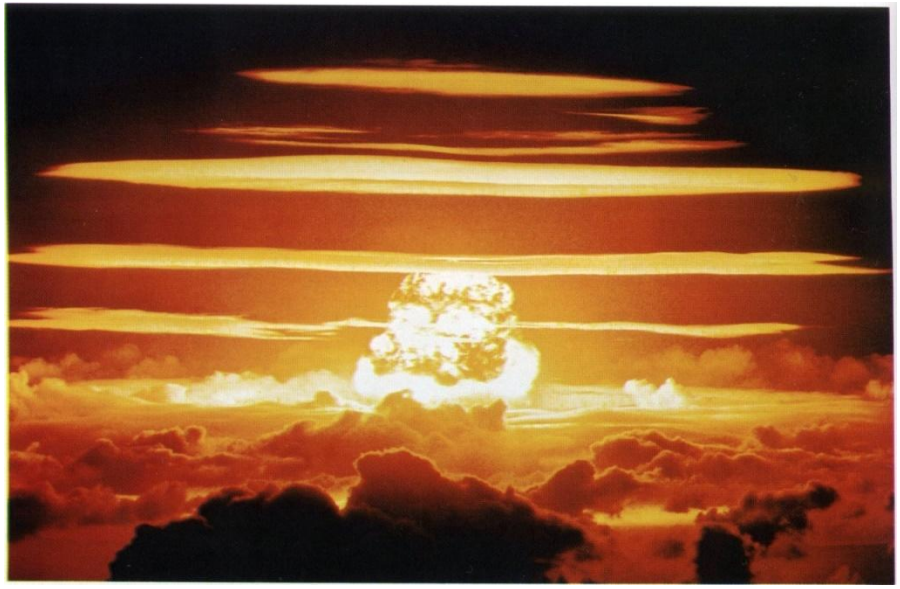

Fig. 13-28. Short-lived halo-like ring clouds produced by Dakota's blast, 25 Jun 1956. Public Domain.

Clouds of explosive volcanic eruptions vie with nuclear mushroom clouds, so it is no surprise they produce the same attendant clouds. A pileus (out of sight) and several skirt clouds dressed the rising shaft of Tonga's preliminary eruption cloud (Fig. 13-29) on 14 Dec 2022. Tonga's major explosive eruption the next day produced a ring cloud seen from space. A NASA satellite passed directly over Sarychek peak in Siberia just as the burgeoning volcanic cloud produced an arching pileus with a small spreading ring (Fig. 13-30). All these features of nuclear and volcanic clouds are illustrated in the video,

https://www.youtube.com/watch?v=BMc8Tdr7Hcw

Fig. 13-29. Skirt clouds Tonga Eruption, 14 Dec 2022. Tonga Geol Svcs,

Fig. 13-30. Pileus capping the ash cloud of Sarychev Peak 12 June 2009. A pyroclastic flow cascades down from the peak at bottom. NASA/JPL.

2: Pileus tends to be highly ephemeral, with a lifespan from mere seconds to a few minutes. It forms as the rising cap of penetrative cloud impinges on and lofts the humid layer and evaporates once the cap has passed above the humid layer and the downdraft surrounding

the cap causes the humid layer to sink. On occasion it survives and "change clothes" to a skirt cloud. which, as we have seen, forms when air is drawn into a rising plume.

3: Unlike mountain wave clouds, pileus can form with a calm ambient wind. All it requires is a layer of stable air near saturation just above the rising cloud. Then, a cumulus humilis (Fig. 13-31), or even an altocumulus, or a cirrus generating cell can produce pileus! Of course, penetrative clouds with strong updrafts do this much more often.

Fig. 13-31. Humble cumulus humilis generates pileus over Louisville, KY, 18 Aug 2009 with ambient winds with slight left to right vertical shear. SDG.

We cannot leave the subject of pileus without again stressing the contrast between the chaotically bubbling protuberances and violence of the parent mushroom clouds of nuclear explosions, explosive volcanic eruptions, and thunderstorms, and the fleeting delicacy of the pileus they produce. A paradigm example is the translucent, gossamer thin double layered pileus over a rising cumulus congestus at Cheyenne, WY on 23 Aug 2022 (Fig. 13-32).

Fig. 13-32. Translucent Lenticular Cloud over rising cumulus congestus, Oracle, AZ 23 Aug 2022. JC.

13.3 Banner Clouds

Fig. 13-33. Banner Cloud of Huayna Picchu, Peru. SDG.

Fig. 13-34. Banner Cloud of the Matterhorn, 27 Feb 2009. ©rac819 Flickr.

One more impressive cloud feature, the banner cloud, clings to the lee slope of steep, towering, pyramidal peaks such as Mount Everest, Huayna Picchu in Peru (Fig. 13-33), the Matterhorn (Fig. 13-34), and the Durrenhorn (Fig. 13-35). Like a huge flag, the banner cloud flaps in the wind and may extend several km downwind.

Fig. 13-35. Banner Cloud of the Durrenhorn, Jun 2004. SDG.

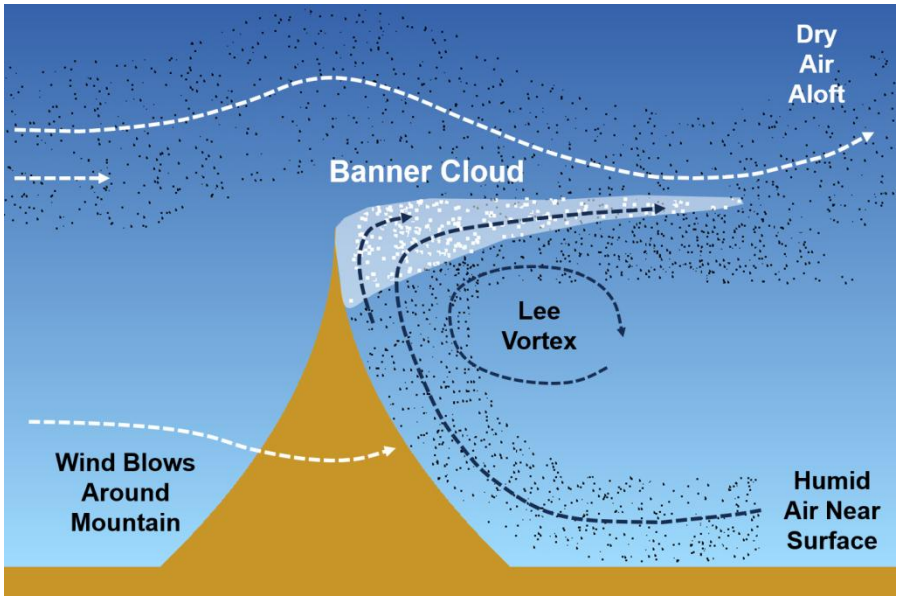

Fig. 13-36. Illustration of the typical situation leading to banner clouds. Fast winds aloft force a lee vortex with air rising up the lee slope. SDG.

As air flows over and around the peak, it creates low pressure on the lee side with a rotor-like vortex that forces air to rise up the lee face of the peak (Fig. 13-36). Typically, but not necessarily, the humidity is high near the surface and decreases to low values aloft. If the air rises enough and is humid enough the banner cloud forms in the updraft hugging the peak. As the wind sweeps the banner cloud downwind, it mixes with the drier surrounding air aloft, gets diluted, and evaporates in a short distance.

It is perhaps appropriate to conclude this section by pointing out another irony. Most of the mountains that produce banner clouds owe their steep, jagged, pyramidal banner-producing shape to erosion by mountain-tearing glaciers. (Huayna Picchu is a geologically active exception.) And the glaciers owe their existence to storm clouds. Thus, with few exceptions, only after clouds have torn away at a mountain, is the mountain able to fly its banner cloud.

13.4 Gallery

Fig. 13-37. Pileus soaring to freedom, Boynton Beach, 18 Dec 2021. SDG.

Fig. 13-38. Colorado Front Range Lenticular clouds seen from Cheyenne, WY, 10 Jan 2025. JC.

Fig. 13-39. Lee waves over Fairfield Lake, NC 22 May 2025. SDG.

Fig. 13-40. Symmetric lenticular cap cloud over Mount Shasta, CA. Mount Shasta rises 3 km above the surroundings. © Dean Lobovits.

Fig. 13-41. Pile of plates at twilight, La Seu d'Urgell , Catalunia, Spain, 27 January 2011. © Jordi Solé Javal.

Fig. 13-42. Pile of plates lenticular cloud over Mount Shasta. © Kevin Lahey.

Wonders of the Atmosphere
Chapter 14: Coronas, Iridescence, and Glories

Fig. 14-1. 3-ring corona morphing toward iridescence with crepuscular rays in cirrocumulus lenticularis over Cheyenne, WY 10 Mar 2025. JC.

Wonders of the Atmosphere
Chapter 14: Coronas, Iridescence, and Glories

14.1 Coronas, Glories, Iridescence, and Icarus

Coronas, Glories, and Iridescence, three ***Crowning Glories*** of the atmosphere's wonders, were conspicuous by their absence in Chapters 12 and 13 even though they often adorn patterned cloud sheets and lenticular clouds. Now, we give them their due.

Fig. 14-2. A corona in cellular altocumulus, over Cheyenne, WY 29 Aug 2016. JC.

First, a correction of a classical Greek myth with words of caution that may save your eyes. One crucial detail is wrong in the myth of Icarus. Daedalus and his son, Icarus were imprisoned in the labyrinth (likely the foundational ruins of the Palace at Knossos) that Daedalus, symbol of the scientific and inventive mind, had designed. To escape the labyrinth Daedalus designed wings. The next point is where the myth is wrong. Daedalus never would have warned Icarus not to fly too close to the Sun because he knew the Sun is too far away. The warning he gave Icarus was to avoid *looking* too close to the Sun, which would blind him.

On the day of their escape, Daedalus saw lenticular mountain wave clouds in the sky. He knew this meant there were coronas, iridescence, glories, and updrafts, the last which meant excellent soaring weather. You would barely have to flap your wings.

They took off and soon were high above the labyrinth. Icarus looked up at the nearest lenticular cloud to locate the updraft and saw it gleaming iridescent. Looking too close to the Sun, a corona blinded him. Disoriented, Icarus got caught in the turbulent rotor, which shredded his wings. Meanwhile, Daedalus soared above the lenticular clouds, looked down and saw a glory around his shadow on the cloud below and watched bereft as his son plunged into the sea.

At their best, coronas, iridescence, and glories are among the most colorful atmospheric optical phenomena, as in both frames of Fig. 14-1. All are produced when tiny droplets, ice, and other particles, though usually droplets scatter sunlight or moonlight. In general, the largest particles produce the smallest coronas and glories. Iridescence, which spreads the furthest, is produced by the tiniest droplets, usually at cloud fringes. Particle shape when not spherical, as with pollen grains, affects the shape of coronas.

Coronas are small, concentric, and for the most part, more or less circular rings of light around the Sun or Moon that follow a more or less standard color sequence. The aureole is the innermost and

brightest part of the corona and the part seen most often, as in Fig. 14-2. It consists of a blindingly bright bluish-white core surrounded by a yellow ring that grades outward to red. For cloud droplets with $r_{DROP} >\approx 5$ μm, the outer red part of the aureole only extends < 5° from the Sun. Therefore, coronas must be viewed with great caution, blocking the Sun with some object or with your extended hand, and viewing them through dark sun glasses. Even with the Sun blocked by the seat of a Ferris wheel in Fig. 14-3, the corona's inner aureole was blindingly bright.

Fig. 14-3. Corona aureole with iridescence in streaks parallel to cloud bands from bottom left to top right, San Mateo, CA, 16 Jun 2016. SDG.

There are other tricks to viewing coronas safely. They can be seen more easily around the Sun's reflection on smooth water or on a car's windshield because the albedo of water is only ≈ 3% and of glass is only ≈ 7%. Coronas around the Moon are safe to look at and their colors are easier to see than solar coronas because sunlight is so bright it oversaturates the eye and (often) the camera.

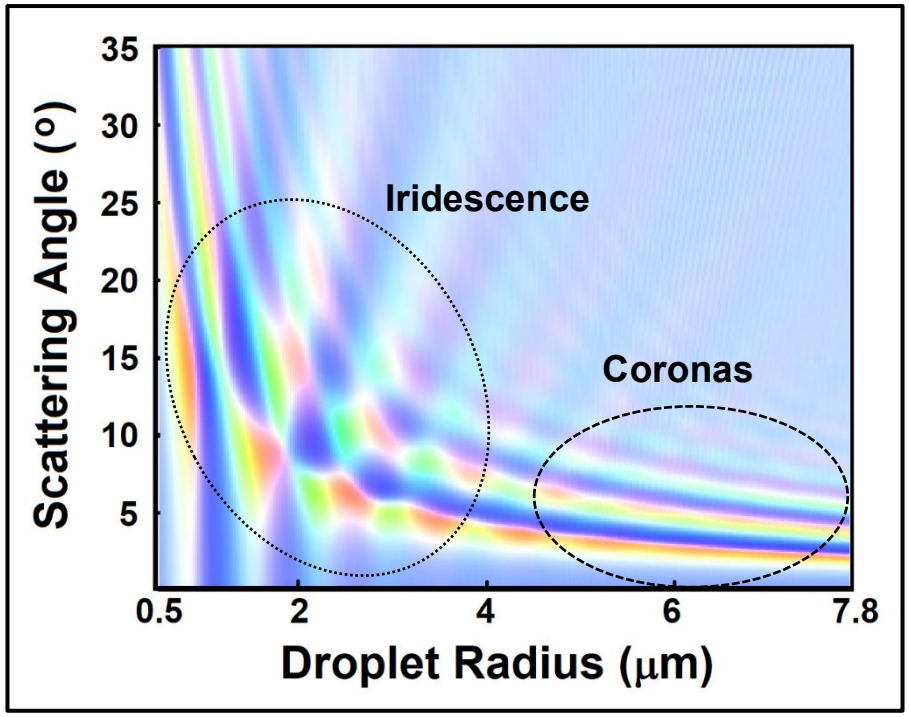

Fig. 14-4. Colors of perfect, single scattering Lee Diagram showing where coronas and iridescence dominate. SDG.

Iridescence is produced by the same scattering process as coronas but differs in shape, tending to follow the fringes of the cloud elements, as in Fig. 14-3 (taken at the San Mateo Fair) where iridescent streaks extend from bottom left to top right parallel to cloud bands outside the aureole of the corona in the central cloud mass. Because droplets are smaller at the cloud fringes, iridescence tends to span a wider angular range of the sky than coronas, sometimes stretching more than 30° from the Sun, where it can be viewed safely. The play of colors is also more irregular, and while often pastel may be more vivid, particularly in some polar stratospheric (nacreous) clouds.

Glories tend to be circular rings around the antisolar point (i. e., the viewer's or camera's shadow). There is no trouble looking at glories. They can be beautifully colored but are never blinding.

14.2 Coronas vs Iridescence: Lee Diagram

Fig. 14-5. Corona with 4 rings in cirrostratus translucidus over Cheyenne, WY, 21 Nov 2024. JC.

Coronas are often explained in terms of diffraction of light around spherical droplets, but this only works well for $r_{DROP} > 4$ μm. Mie scattering is needed to explain coronas and iridescence produced by droplets with $r_{DROP} < 4$ μm, as Jim Lock and Leiming Yang first showed in 1991. Twelve years later, Phil Laven and independently, Stan and Jim Lock simulated coronas and glories photorealistically. Constructing a Lee diagram, much like Fig. 14-4, Laven went on to show the distinction between coronas and iridescence.

Let's decipher the Lee diagram of Fig. 14-4. It is a 'perfect', single Mie scattering model, an ideal few coronas approach. It shows the color of sunlight scattered by a droplet of any size up to $r_{DROP} = 7.8$ μm and at any angle up to 35° from the Sun. For example, sunlight scattered by an angle of 15° by a droplet with $r_{DROP} = 2$ μm is purplish red.

Fig. 14-4 does not show irradiance, though the Mie solution includes it. The relative irradiance of the scattered light is highly oscillatory for any wavelength and radius, and decreases rapidly as scattering angle increases. One example of the Mie solution for relative irradiance as a function of scattering angle is shown for droplets with $r_{DROP} = 8$ μm as the green curve in Fig. 1-16.

Fig. 14-6. Elliptical corona with three rings and an indentation, Cheyenne, WY 22 Nov 2023. JC.

The Lee diagram can be divided into two distinct regimes – the corona regime for $r_{DROP} > 4$ μm at small scattering angles (the lower right quadrant), where diffraction is an excellent approximation to Mie scattering, and the iridescence regime for $r_{DROP} < 4$ μm over a wider range of scattering angles. A momentary glance shows that diffraction fails to explain the color pattern of the iridescence regime.

Fig. 14-7. Corona in cirrocumulus translucidus undulatus over Cheyenne, WY, 31 Mar 2020. JC.

In the corona regime diffraction is an excellent approximation to Mie scattering. Coronas are 'well behaved', with an angular width that varies inversely with droplet radius. The aureole for r_{DROP} = 4 μm extends 4° from the Sun; the aureole for r_{DROP} = 8 μm extends only 2° from the Sun. In this way, coronas provide casual observers a way to estimate the size of droplets or ice particles in the cloud above.

The corona regime's color pattern is almost constant and is easily extended to droplets larger than r_{DROP} = 7.8 μm. Four or five distinct but progressively fainter cycles of color sequences (blue – yellow – red) occur, although 4-ring coronas, such as the one produced in a translucent sheet of mountain wave cirrostratus over Cheyenne, WY on 21 Nov 2024 (Fig. 14-5), are very rare. Even 3-ring coronas are exceptional, such as the corona seen in lee wave-induced cirrostratus through an almost leafless cottonwood tree in Cheyenne, WY on 22 Nov 2023 (Fig. 14-6). But color purity can be as great for a 2-ring corona, as on 31 March 2020, which formed in a gossamer thin rippled cirrocumulus translucidas undulatus (Fig. 14-7), also a lee wave cloud.

Fig. 14-8. Near circular corona produced in altocumulus by a full Moon over Cheyenne, WY, 25 Feb 2021. The corona is blotted out where the cloud is optically thick at lower right. JC.

Coronas are circular only if the droplet size spectrum is constant across a wide enough area of the cloud sheet, as in Fig. 14-2 and in the corona around the full Moon over Cheyenne, NM on 25 Feb 2021 (Fig.14-8). If the cloud has a gradual horizontal gradient of mean droplet size, elliptical coronas result, as in Fig. 14-6. The indentation of that corona extending to the upper left indicates larger droplet sizes, likely where air rose in the crest of a wave in the cloud.

Fig. 14-9. Distorted corona with iridescence in altocumulus lenticularis translucidus over Cheyenne, WY, 18 Dec 2019. JC.

Greater distortions in the shapes of coronas occur when droplet sizes vary irregularly over a cloud sheet. Not only is the corona in the right panel of Fig. 14-1 oblong, it also has a large indentation along the crepuscular ray, whose shadow somehow resulted in illumination by larger droplets than elsewhere. Fig. 14-9 contains a highly distorted corona because it traverses several waves in the parent lenticular cloud. Similar fluctuations of distorted coronas appear near the edges of standing lenticular clouds on 10 March 2025, where they are animated in the time lapse video,

https://www.flickr.com/photos/cloud_spirit/54381993431/in/photostream/lightbox/

Fig. 14-10. Iridescence circling lenticular cloud, Cheyenne, WY, 13 Feb 2024. At upper left, corona fragments in cumulus ring the Sun. JC.

Fig. 14-11. Iridescence tracing contours of droplet sizes in an altocumulus lenticularis over Cheyenne, WY, 30 Dec 2019. JC.

If the gradient of droplet radii in a cloud is large enough it will dominate the resulting pattern of color and light so that it will circle the cloud, tracing the contours of droplet sizes, as in Fig. 14-10. The iridescence regime has a distorted checkerboard pattern of vibrant colors, like one that would be painted by an abstract artist. It is in this regime of tiny droplets or ice particles that the fringes of lenticular clouds (Fig. 14-10 and Fig. 14-11), pileus atop thunderstorms (Fig. 14-12), and the nacreous polar stratospheric clouds (Fig. 14-14 and Fig. 14-15) display fantastical, peacock colors.

The rich colors of the pileus atop the cumulonimbus cloud at the left of the image of Fig. 14-12 in Delray Beach, FL on 31 July 2012 were enhanced because the pileus with its radial gradient of droplet (or ice particle) sizes ringed the Sun almost exactly as a corona would. Comparing the RGB colorimetric analyses (Fig. 14-13) running the half width of the pileus at left of Fig 14-12 to that (Fig. 9-6) of the vivid rainbow at bottom of Fig. 9-5 reveals that under optimal conditions, the color purity of iridescence can equal or exceed that of the brightest primary rainbows!

Fig. 14-12. Iridescent pileus over a thunderstorm at Delray Beach, FL, 31 Jul 2012. ©National News and Pictures, Ken Rotberg.

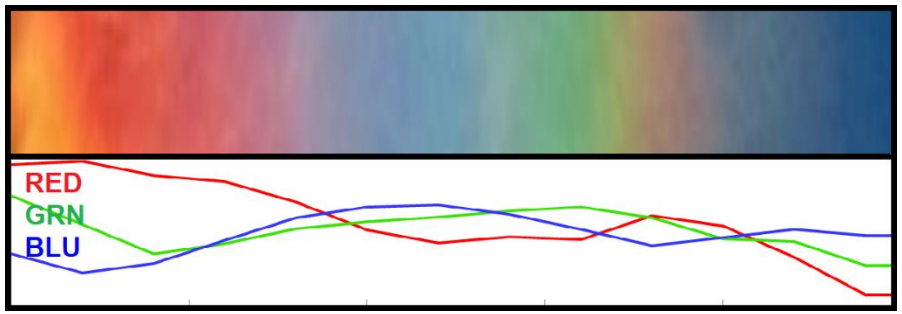

Fig. 14-13. RGB colorimetric analysis of the iridescent pileus at left of Fig. 14-12. SDG.

The iridescent displays of the optically tenuous polar stratospheric clouds only light up in twilight when the troposphere lies darkened in the Earth's shadow and when the near horizontal path through the clouds increases the effective optical thickness. They are produced in

Fig. 14-14. Nacreous cloud over Norway. Video at https://www.reddit.com/r/Damnthatsinteresting/comments/19dss5e/norway_mother_of_pearl_clouds_also_known_as/

wave clouds at $T < -85°C$ that consist of near-spherical ice particles with $r_{ICE} \approx 5$ μm and smaller at cloud fringes, which puts their displays mostly in the iridescence regime of the Lee diagram. Ice

particles, sometimes frozen cloud droplets, also dominate in the iridescent clouds in the upper troposphere, where typically $T < -50°C$. The brilliance of all these displays, like that of opals, varies from pale to fiery, and depends on the distribution of particle sizes.

Fig. 14-15. Nacreous cloud over Fairbanks, AK, late 1990's. JC.

14.3 Limiting Factors for Coronas

The photographs of coronas and iridescence presented in the last section are not by any means typical. Very few coronas and iridescence approach the color purity of these photos or certainly of the perfect scattering Lee diagram. This is due to three main factors. 1: The particles: As light passes through clouds it encounters droplets or ice particles with a range of sizes. Because scattering angles vary with wavelength and with droplet size, interference almost invariably washes out the colors. It is largely for this reason that most coronas consist only of the aureole. 2: Optically thin clouds ($\tau_{CLD} <\approx 0.005$) have too few droplets to scatter enough light while multiple scattering washes out coronas in optically thick clouds ($\tau_{CLD} > 2$). Much as with halos, coronas and iridescence have maximum lighting contrast and color purity for clouds of optical thickness, $\tau_{CLD} =$ O(0.1), As τ_{CLD} increases, so do the corona-impairing effects of multiple scattering and the range of droplet sizes. 3: Skylight adds a blue tint, but mainly for iridescence at large scattering angles.

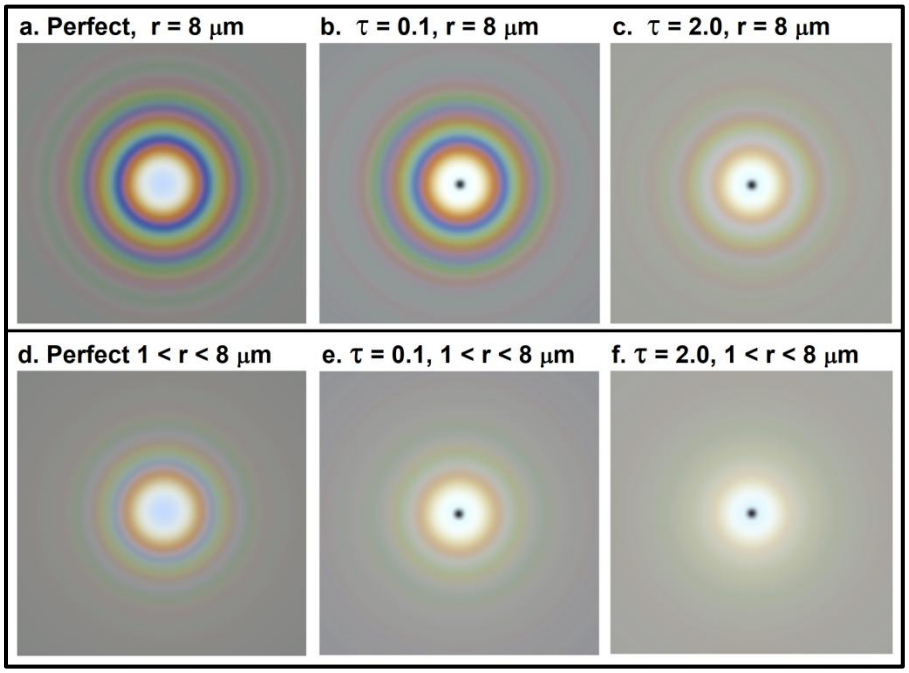

Fig. 14-16. Simulated coronas for perfect single scattering and cloud optical thicknesses, $\tau = 0.1$ and $\tau = 2.0$ for droplets with $r = 8$ μm (top row) and a wide, constant distribution from $1 < r < 8$ μm. SDG.

Coronas approach the theoretical limit when all droplets are the same size and the cloud is optically thin. The corona simulations in Fig 14-16 (using Mie scattering) show how severely the color purity of coronas is washed out by broadening the droplet size spectrum and by increasing the cloud's optical thickness. For a wide spread of droplet sizes all that remains is the aureole. Increasing optical thickness to $\tau = 2$ reduces color purity and brightness markedly, even when all droplets are the same size. Increasing cloud optical thickness to $\tau = 4$ (not shown) leaves but a faded aureole. Doing the same to an opal would diminish its value from $100,000 to $100.

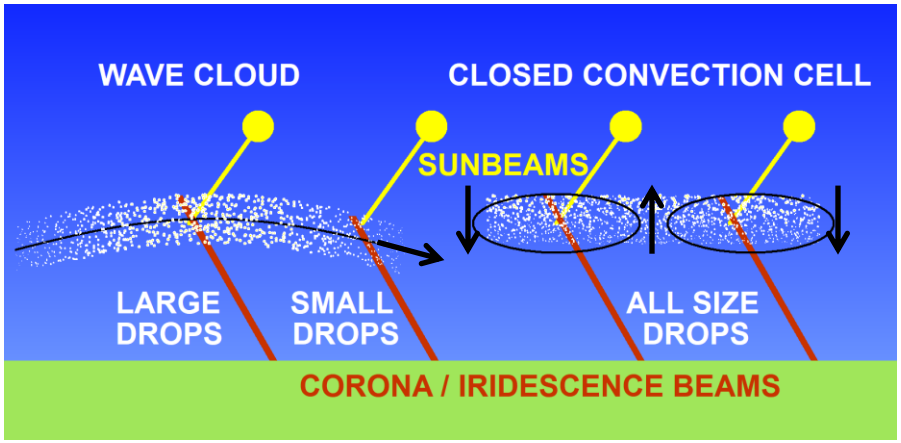

Fig. 14-17. Narrower drop size distributions along beam give wave clouds more colorful coronas and iridescence than convective clouds. SDG.

As the photographs in this section suggest, and observations confirm, lenticular wave clouds produce some of the most vivid coronas and especially iridescence. Similarly, altocumulus and cirrocumulus consisting of fine ripples (undulatus) produce more vivid coronas and iridescence than those composed of polygonal convection cells. The main reason for this, illustrated in Fig. 14-17, is that the corona / iridescent beams (**red** lines) encounter a much smaller range of droplet (or ice particle) sizes from top to bottom through wave clouds than through convective clouds. In convection cells, air rises almost vertically so droplet sizes range from zero at cloud base to a maximum at cloud top. The result is that corona / iridescent beams passing through convection cells encounter a full range of droplet sizes. In wave clouds, droplet size, and usually optical thickness as well, increase horizontally from tiny values at cloud fringe to maxima at the wave crest. This horizontal segregation of droplet sizes in wave clouds means that corona / iridescent beams passing through the fringes encounter tiny droplets of almost constant size, while corona / iridescent beams passing through the crests encounter larger droplets of reasonably uniform size provided the cloud is optically thin. If the cloud is optically thick in center it will be white or gray from multiple scattering.

Uniform fields of optically thin cellular altocumulus cloud sheets are more likely than wave clouds to produce circular coronas, but seldom with vivid colors and multiple rings unless wave activity is involved, particularly when wind shear orients the cells in ranks and rows.

14.4 Pollen Coronas

It's spring. You are feeling poorly. Your nose is running and your eyes are watery. The sky seems to be clear but you are pretty sure you see a small, odd-shaped corona around the Sun. You are right. The pollen that disturbs you disturbs sunlight too.

Fig. 14-18. Pollen coronas from alder trees (left and center) and birch (right). ©Jari Piikki.

In the spring of 1989, Finnish observers of the Ursa Astronomical Association noticed odd-shaped coronas in clear, cloudless skies (Fig. 14-18). But the clear sky was tainted with tiny pollen grains from the surrounding forests.

Pollen grains can produce bright, vibrant coronas because the grains of particular species of tree are all close in size and shape and therefore diffract light coherently. But pollen coronas are not circular because pollen grains are not spheres. Alder pollen is ridged and

oblate (flattened) (20μm high and 25 μm wide). Birch pollen is slightly elliptical, with 3 small lobes (30–35 μm), while pine and spruce pollen (50–>75 μm), has a round body and two bladders that resemble Mickey Mouse ears (Fig. 14-19). Since non-spherical pollen grains fall so that the widest side is almost horizontal, alder and birch pollen produce elliptical coronas that are higher than wide and pine pollen produces coronas with polygonal lobes.

Fig. 14-19. Ponderosa pine pollen. Rocky Mountain National Park.

Fig. 14-20. Glory and fog bow from the Golden Gate Bridge, 13 Jul 2007. ©Mila Zinkova.

14.5 Viewing Glories

The first time that members of the scientific expedition to Peru saw the Sun rise on the summit of Pambamarca (now Ecuador) perhaps in 1737, they noted with "boundless astonishment" three concentric rainbow-like rings around the shadow of their heads surrounded by a much larger whitish ring, all on the thin mist no more than 20 steps away. Antonio Ulloa and Pierre Bouguer, much less conceited and more scientific than Benvenuto Cellini, found that as they moved from side to side the apparition moved with each of them, but what was most impressive was they noted that each of the six or seven other people saw the apparition only around their own shadows.

What they saw, illustrated, and measured was the multi-ringed, colored glory and the near white cloud bow. They found the inner ring and the cloud bow extended about 2.75° and 33.5° respectively from their shadows.

Fig. 14-21. Multi-ringed glory with rainbow colors inside a white fog bow atop the Zugspitze, 15 Nov 2014. ©Claudia Hinz.

Glories resemble coronas, but appear almost directly *opposite* the Sun. Glories are rings of light colored like small rainbows that surround an observer's shadow on a cloud deck or fog bank. Before the age of powered flight, glories were seldom seen but were (as just

noted) described in almost ecstatic terms by mountaineers and balloonists. Now that planes fly above clouds, glories have almost become mundane. The next time you fly, look down at the shadow of the plane on the clouds below and you will probably see a glory surrounding it. Yet the glories seen from high-flying jets far above the cloud decks below rarely are bright and colorful enough to evoke much excitement. In many cases they are surrounded by cloudbows so faint, broad, and colorless that they are only detected by a trained eye.

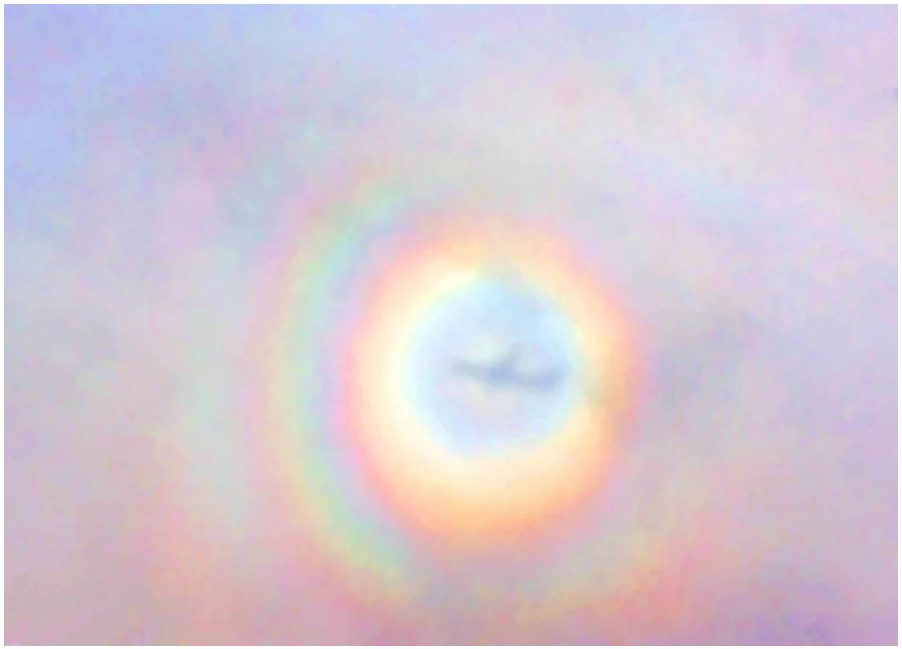

Fig. 14-22. Glory around the shadow of a jet. ©Stephen James O'Meara.

All the best sightings and photos of glories occur when the observer is very near the cloud or mist. Knowing this, Mila Zinkova perched herself on the walkway of the Golden Gate Bridge, where a long tongue of fog often pours through the Gate. She came on many late afternoons when the western Sun was low enough in the sky for a photo op should the top of the fog pass under the walkway so that she could see the Sun shine on it. And that is how she was able to take the photo in Fig. 14-20. Note that whitecaps can be seen below.

Fig. 14-23. 3-ring Glory near sunset. Stan does not fly First Class. SDG.

Claudia Hinz (whom we have already met in Chapter 11 through her mountaintop photos of halos) also positioned herself perfectly to capture glories and fogbows atop several peaks including the Zugspitze, Germany (Fig. 14-21), which, because of its greater height, produced the best and most frequent glories.

From the air, the best views of glories occur when the plane is only a short distance above the cloud deck. For the majority of long-distance flights, glories are seldom dramatic because they tend to appear in cloud decks far below flight level of 11 or 12 km. That is why on short flights that barely rise above cloud top Alexander Haussmann always reserves a window seat opposite the Sun. Glory seekers including Phil Laven and Stephen James O'Meara (Fig. 14-22), know when to reserve seats facing away from the Sun (but never over the wing) and know to be ready the moment the jet rises above a cloud layer (Fig 14-23) or is about to descend into one.

A standing joke, based on the fact that the glory is centered around the photographer's shadow and almost all glory photos are centered in the middle or back of the planes, is that glory aficionados seldom fly first class.

Fig. 14-24. Striped glory SW of Guadalupe Island and von Karman vortices aligning cloud cells in the island's wake, 20 May 2008. NASA MODIS Terra.

Glories are even seen from space, though they are seldom dramatic, even after intervening skylight has been removed by processing, as in NASA MODIS images (Fig. 14-24). These images occasionally capture glories when the Sun is near the zenith above the decks of stratocumulus over the subtropical oceans. The best 'MODIS' glories occur when the deck consists of fine, almost translucent cells. The 'MODIS' glories always appear as two parallel multicolored stripes because the satellite sensors sweep back and forth, east and west as they circle the globe, capturing narrow bands that are stitched together to form coherent images. Note that the glory stripes in Fig. 14-24 are brightest and most colorful where the cloud cells are very thin and disappear where they are optically thick and bright white.

14.6 Modeling Glories: Lee Diagram

A simple physical explanation for the glory remains elusive. The closest we have come to solving the mystery of the glory is that it appears to be due in good part to light that strikes cloud droplets and skirts around their surfaces before scattering almost directly back from the direction it came. The angular size of the glory's rings varies almost, but not exactly, inversely with the size of the drops, so, as with coronas, 1: the largest glories are produced by the smallest droplets and, 2: the best glories are produced when the droplets are almost all the same size to minimize destructive interference.

Even though glories do not seem to be governed by a simple physical principle, they are still modeled accurately using Mie scattering. The Lee diagram of Fig. 14-25 of the perfect single Mie scattering model shows two distinct but overlapping regimes. The glory regime prevails close to the antisolar point for larger droplets and at all angles for small droplets or particles, including and extending somewhat beyond the lower left half of the diagram. These idealized glories include the aureole plus five distinct bands, each successively less saturated and distinct. The bands are large for small droplets and decrease in size as droplet size increases.

The regime of fog / cloud bows also reveals up to five distinct bands, but in contrast with the glory, 1: fog / cloud bows increase in size as droplet size increases and, 2: the most distinct fog / cloud bows occur furthest from the antisolar point. As a result, the overlapping region of glories and fog/cloud bows always appears indistinct, even in the

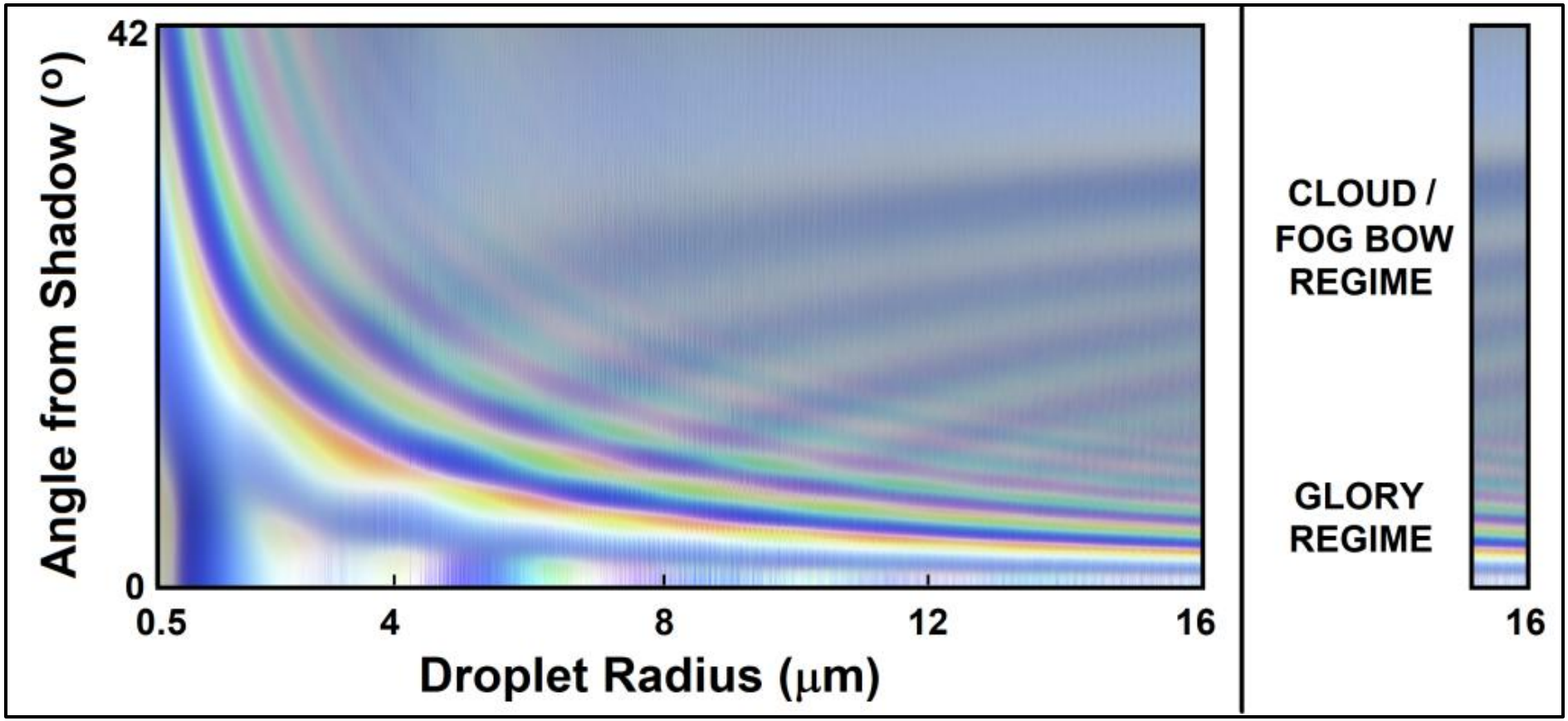

Fig. 14-25. Lee diagram of perfect single Mie scattering for regimes of glories (bands tilting down to the right) and of cloud / fog bows (bands tilting up to the right) as a function of droplet size and scattering angle from the shadow (antisolar point). Extract at right shows the change of regimes for $r_{DROP} \approx 16$ μm. SDG.

most superlative sightings and photos, for example atop the Zugspitze on 13 Jan 2013 (Fig. 14-26).

Glories always fall far short of the theoretical maxima of brightness and color purity given by perfect, single Mie scattering theory for a single particle. Glories suffer the same limitations of brightness and color purity as do rainbows, halos, and coronas. First is the inherent inefficiency of radiative transfer in clouds of particles because many sunbeams pass through optically thin clouds without being scattered, and multiple scattering vitiates all optical phenomena in optically thick clouds. The result is that the maximum possible scattering efficiency equals $e^{-1} \approx 36.8\%$, which occurs when optical thickness, $\tau_{CLD} = 1$, but only in a cloud with all particles the exact same size and shape. Interference further reduces peaks of color purity and brightness, and may obliterate the outer rings whenever there is a broad drop size distribution, as is the case in most clouds. Under such conditions, the glory is reduced to a bright, inner pale yellow ring and a single red ring. The inner blue ring of glories is seldom distinctly visible even if outer red rings can be seen. The blue ring is easily washed out by interference caused by a drop size distribution because it occurs in a brightness minimum.

Fig. 14-26. Multi-ringed glory and fog / cloud bow atop the Zugspitze on 13 Jan 2013. ©Claudia Hinz.

Skylight of the foreground and background, and reflected light from the ground further vitiate the visual contrast of glories. Foreground skylight between observers flying at jet stream levels and the top of a stratocumulus cloud deck over the subtropical oceans is several times brighter than the glory beam. No wonder, glories stand out best when the observer is located near the cloud and when the background is dark and nearby.

The color purity and distinctness of the glory rings are also impaired by the Sun's finite angular width, particularly for droplets larger than $r_{DROP} > 20$ μm because the rings are only a few times wider than the Sun. We have seen that this is also the case with rainbows, halos, and coronas.

The simulated glories in Fig. 14-27 (which do not include scattering in the clear atmosphere) illustrate the impact of multiple scattering, cloud optical thickness, and droplet size variation. The left panel shows the perfect single Mie scattering solution for droplets with radius, $r_{DROP} = 4$ μm. In this perfect case, the glory's multiple rings are colorful and extend out to the regime of the cloud bow about 40° from the Sun. The next panel illustrates how much multiple scattering in a cloud of near optical thickness ($\tau_{CLD} = 0.5$) fades the

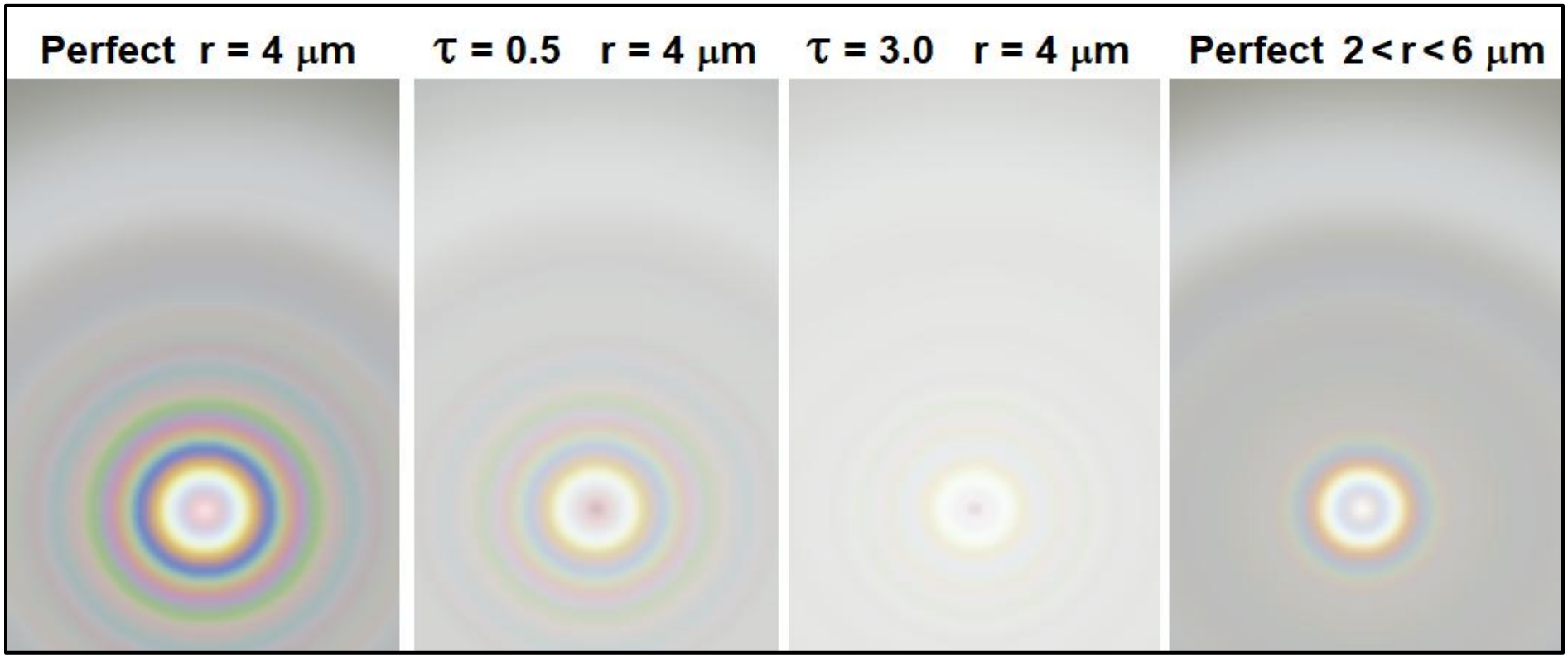

Fig. 14-27. Simulated glories up to 60° from the antisolar point (vertically). From left to right Perfect single Mie scattering: multiple scattering model with τ_{CLD} = 0.5 and 3.0 in a cloud of droplets with r_{CLD} = 4 μm, and: Perfect single Mie scattering model with a spread of droplet sizes given in text. SDG.

glory's color purity and brilliance and renders the fog bow faint. When cloud optical thickness is increased to τ_{CLD} = 3, the background cloud light overwhelms all but the aureole. Finally, the far-right frame shows how greatly a spread of droplet sizes with radii that range in size from, 2 μm ≤ r_{DROP} ≤ 6 μm, impair the color purity and brilliance of the glory, leaving only one distinct ring, even for perfect single scattering.

The fact that on occasion glories (and coronas and iridescence) are so bright and colorful despite these potentially crippling limitations makes them all the more marvelous to behold.

14.7 Iridescent Contrails

The vast majority of contrails that crisscross the sky during the day appear white, in part because they are seen from a great distance and in part because the long-lasting contrails form in the turbulent flow of the moisture-charged jet exhaust (§10.1). Right behind the jet, the shorter-lived contrails of uniformly tiny droplets or ice particles that form in the laminar flow over the wing offer a chance of being iridescent if they appear near the Sun.

The best chances to see iridescent contrails without a telescope are therefore for an observer flying just below another jet, as in Fig. 14-28 or for a ground-based observer standing below a jet that is either

taking off or landing, as in Fig. 14-29, or, best of all, for an observer with a window seat above or behind the wing where a thin cloud forms just above the wing.

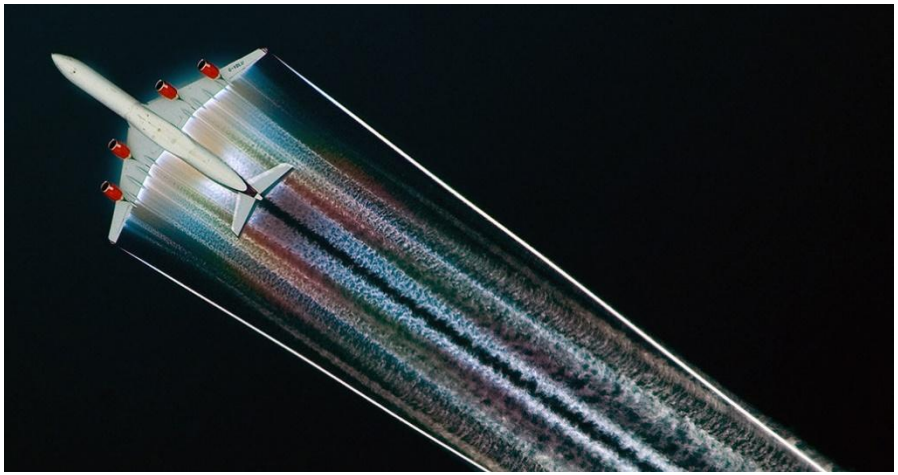

Fig. 14-28. Iridescent contrail made by ice crystals 24 Jul 2006 Jet at 9600 m over China, seen from another high-flying jet. ©Jeffwell.

Fig. 14-29. Iridescent contrail made by jet coming in to land at Vienna Airport. © Franz Kerschbaum.

14.8 Gallery

Fig. 14-30. Iridescence tracing outline of altocumulus band, Boynton Beach, FL, 29 Dec 2023. SDG.

Fig. 14-31. Corona in altocumulus stratiformis seen through trees, over Sapphire, NC, 22 Jun 2024. SDG.

Fig. 14-32. Corona in supercooled altocumulus with hole punch clouds present, Boynton Beach, FL, 6 Dec 2023. SDG.

Fig. 14-33. Elliptical corona in cirrocumulus stratiformis undulatus over Cheyenne, WY, 26 December 2025. Droplet size increases toward bottom of photo. JC.

Fig. 14-34. Pollen corona, Socorro County, NM, 17 March 2010. © Colleen Gino.

Wonders of the Atmosphere
Chapter 15: Diverse and Artistic Skies

Fig. 15-1. A momentary burst of white ground fog lifted by a wind gust under a layer of altostratus Cheyenne, WY, 22 Dec 2018. JC.

Fig. 15-2. Cirrocumulus and Cirrus on opposite sides of a cloud band over Boynton Beach, FL, 08 Jan 2010. SDG.

Fig. 15-3. Altocumulus lenticularis and Cirrocumulus, with Earth's shadow, Belt of Venus and Anticrepuscular ray, Cheyenne, WY, 29 Nov 2021. JC.

Wonders of the Atmosphere
Chapter 15: Diverse and Artistic Skies

15.1 Matching Painted and Photographed Skies

Fig. 15-4. Cumulus and altocumulus over Boynton Beach, FL, 1330 EST 26 Dec 2011. SDG.

The time has come to celebrate celestial diversity. Until now, largely in the name of simplicity, we have almost exclusively shown photos of skies with only a single cloud genus or optical phenomenon. The sky knows no such limitation. It often houses several cloud genera at the same time, as in Fig. 15-1 to Fig. 15-4, and on occasion, more than one optical phenomenon.

First, we display painted skies. Long before the camera was invented artists provided the only visual records of the sky, painting skies of great beauty with fidelity and insight. This section and the next

Fig. 15-5. Claude Monet, *The Basin at Argenteuil*, 1872, Musée d'Orsay, Paris.

contain a few highlights of sky paintings treated at length in ***The Soul of All Scenery: A History of the Sky in Art***.

"Every sky chaser's dream is to capture the perfect rainbow, aurora, tornado, though since there is no such thing as perfection the search remains lifelong. My dream includes capturing skies that match the skies of great paintings. One of the times I struck paydirt was at Boynton Beach, FL at 1330 EST on 26 Dec 2011." Stan.

A few cumulus mediocris had sprung up within the previous half hour and reached a layer of altocumulus at the base of a capping

inversion (Fig. 15-4). It was a pretty sky, though not extraordinary by any standard, except that both the form and lighting of the clouds matched those in Claude Monet's painting, ***The Basin at Argenteuil*** (Fig. 15-5), which contains similar cumulus mediocris below a sheet of altocumulus at top left.

The Basin at Argenteuil was designed as a topographical painting, with its view facing ENE along the Seine River. The trees on the left cast long shadows toward the right, showing the Sun was not high in the sky and north of west (to the left and just behind the artist). This set the time and day near 4:30 PM around the summer solstice. In the photograph of Fig. 15-4 the view faces due east and the Sun is in the WSW (to the right and behind the viewer.)

The lighting of the clouds in the ***Basin*** also matches that of the photo and of nature in general. The sunlit sides of the optically thick cumulus clouds are brighter than the altocumulus, which is illuminated by transmitted light. The shaded bases of the optically thick cumulus are the darkest. Thin sheets of altocumulus can be blinding bright when seen near the Sun, but tend to be much less bright more than 90° from the Sun, as in the painting and the photo.The close match of both cloud forms and lighting between painting and photo strongly suggests that Monet created his painting not only as a document of a specific place and time, but also of the very sky he saw that afternoon in 1872.

It is not always possible to tell if the sky in a painting, even a topographic work, was a studio production or was drawn from direct observation. For example, after seeing cumulus a few times, it can be painted convincingly with endless variations without ever looking at another cumulus. But there are some phenomena so specific, such as a rainbow, or so distinct and unusual, such as an arcus cloud beneath a thunderstorm, that the artist must have seen and remembered it. Of course, artists often make astute observations and then manipulate scenes according to their tastes.

One example may be Frederic Church's ***Rainy Season in the Tropics*** (Fig. 15-6), Church was one of the great sky painters. He considered himself the painter that Alexander von Humboldt had always wanted to document his findings during his world travels for his multivolume ***Kosmos***. Church's intent was to capture in realistic detail the varied aspects of nature. As a result, his repertoire included a number of cloud forms, atmospheric optical phenomena, and even the aurora, all done with an incisive eye for 'truth'.

That makes ***Rainy Season in the Tropics*** something of a mystery. A double rainbow arches over the scene. The colors are in the proper order for both bows and the primary is brighter than the secondary. The sky is brightest inside the primary and darkest in Alexander's dark band. Bright and dark spots on the primary bow are accompanied by segments of anticrepuscular rays that cross the bow at right angles. Recognizing and depicting all those subtle details accurately is the mark of a great observer and artist.

The mystery is why Church made the spacing between the bows exactly half what it should be. It was no accident. In a study for the work, Church gave the two bows the proper spacing. One likely solution to this mystery was suggested by George Siscoe. He pointed out that George Inness, praised by art critics for his fidelity to nature was a known practical joker, and, to humble the critics, deliberately reversed the color sequence of the primary bow and the order of sky brightness making Alexander;s dark band a bright band and the sky darkest inside the primary bow in ***A Passing Shower*** (1860). We'll never know for sure, but perhaps Church, who also celebrated for the fidelity to nature in his paintings (Mark Twain was one of his admirers) and also known as a practical joker, used Inness's joke as a model for his closely spaced bows in ***Rainy Season***.

Jean-François Millet didn't joke about the weather of ***The Coming Storm*** (Fig. 15-7), which he certainly based on direct observation – note the close match with Fig. 15-8). An arcus with a turbulent top is plowing its way across the field. Rain fall streaks inside the arcus are tilted outward by the downburst's outflow. The sky is darkest under the arcus and much lighter where the rain is falling. The arcus is only a last-minute warning. It is led by the thunderstorm's overhanging anvil, with clear or at least brighter skies in the distant horizon.

Fig. 15-6. Frederic Church, *Rainy Season in the Tropics*, 1866, Fine Arts Museums, San Francisco, CA. Was the close spacing of the bows a deliberate joke?

Fig. 15-7. Jean-François Millet, *The Coming Storm*, 1868, MFA, Boston, MA.

One meteorological difference between drawing and photo is the drawing's much richer earth tone color. That too may be real, given that the dark ground of the drawing suggests a distant source of illumination, which scattering would have reddened. Touches that Millet may or may not have observed at the time include the farmer freeing his stupid, domesticated cattle from the plow and struggling to pull the stubborn animals out of harms way while the wild birds at top right need no encouragement to flee the coming storm.

15.2 A Capsule Survey of Artistic Skies

The paintings shown above are just three of many that portray the sky in a convincing manner, often with a documentary quality that served when there were no photographs, and can be matched to photographs. They are a testament to the fact that the great artists, many of whom were also scientists, engineers, leaders, and

Fig. 15-8. Arc cloud with outflowing rain shaft under a severe thunderstorm east of Keyes, OK, 31 May 2007. ©Jimmy Deguara.

diplomats, were astute observers of all aspects of nature, who devoted attention, care, and knowledge to the sky. These artists instinctively recognized John Ruskin's directive to paint from nature because,

> There is more beauty about [cloud] forms than can be arrived at by any random felicity of invention, however brilliant. ***Modern Painters***, Vol. 3, Ch. 2.

As a result, in many cases their painted skies are inspired by

1. Specific skies or weather events.
2. The climate that enveloped them.
3. The character of the times.

For example, ***The Basin at Argenteuil*** is one of the many placid Impressionist scenes painted directly from Nature that also reflects the climate of France, with summer skies frequented by cumulus, and winter skies dominated by nimbostratus. Impressionist paintings also

quietly advertise late 19th century triumphs of science and technology. Few violent storms disrupted their paintings, And who would think from the glistening water in ***The Basin*** that the Seine at Argenteuil was choked by endless effluent flowing out of the sewers of Paris.

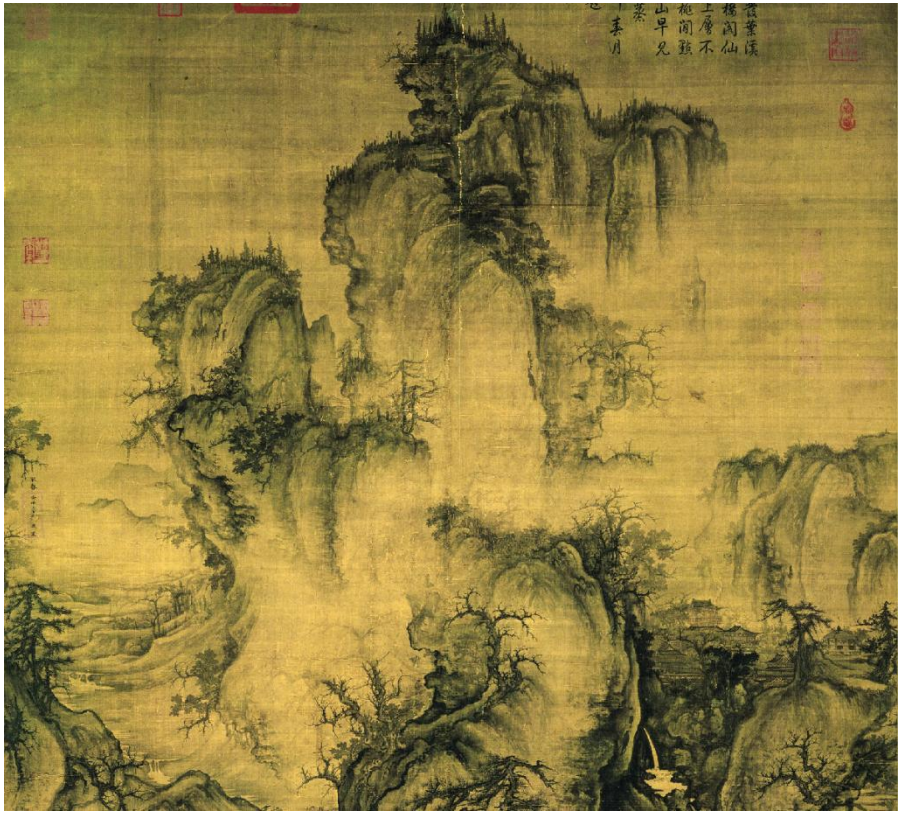

Fig. 15-9. Guo Xi, *Early Spring*, 1072, National Palace Museum, Taipei.

We start our brief survey of sky paintings about 1000 years ago, when Chinese landscape painters began their enduring love affair with a meteorological setting exemplified by Guo Xi's ***Early Spring*** (Fig. 15-9). Precipitous pinnacles topped by trees emerge from fog-filled valleys into an empty sky. A narrow ribbon waterfall is almost always included in the foreground while progressively obscured peaks recede into the distance. The setting, in defiance of or relief from an already densely populated China, is remote, with a few almost inconspicuous villas and travellers.

Fig. 15-10. Fog at dawn, Zhangjiajie National Park, China, 19 Oct 2017. ©Albert Wirtz.

Inspiration for these works comes from precipitous karst limestone peaks in several regions of China, for example in the Zhangjiajie National Park (Fig. 15-10), and from China's climate, where valley fog is common on clear mornings, especially in Autumn.

In 1819, some 750 years after ***Early Spring***, a similar setting inspired Caspar David Friedrich to paint ***Wanderer Above the Sea of Mist*** (Fig. 15-11). The solitary figure stands atop a peak overlooking the tree-topped pinnacles of the Bastei in the Elbe Sandstone Mountains, which emerge from the fog that fills the Elbe River valley. The viewer faces SE to the Zierkelstein, a sandstone butte, and the triangular Kipphorn, both of which are rendered less distinct by mist.

Though the ***Wanderer*** closely resembles the Chinese paintings, there are two meteorological differences. While the Chinese painted fog is

amorphous, Friedrich's fog is shredded at top by the wind. And while the Chinese fog painters left the sky vacant, Friedrich filled the sky of the ***Wanderer*** with altocumulus castellatus in the foreground and altocumulus stratiformis toward the horizon, though the cloud cover often acts like a blanket that reduces the cooling of the ground and reduces the chance of nocturnal ground and valley fog.

Fig. 15-11. Caspar David Friedrich, *Wanderer Above the Sea of Fog*, 1818, Kunsthalle, Hamburg.

Friedrich used a new source of information and inspiration for his clouds. He completed the ***Wanderer*** in 1819, six years after Thomas Forster's ***Researches About Atmospheric Phenomena*** broadcast to the world Luke Howard's 'discovery' that clouds have distinct, identifiable forms. Friedrich, as well as John Constable and J. M. W. Turner in England were leaders of the early 19th century Romantic sky painters who benefitted from and were inspired by that new knowledge. Constable's cloud studies were inspired by Luke Howard's work.

Fig. 15-12. J. M. W. Turner, *Entrance of the Meuse*, 1819, Tate, London.

Turner had been painting landscapes and seascapes with dramatic skies including rainbows for at least 20 years before he learned of Luke Howard's work. The ***Entrance of the Meuse*** (1819) (Fig. 15-12) reveals familiarity with Howard's classification scheme because it is the first of his shipwreck paintings to include a sheet of cellular altocumulus, and one of very few Turner paintings with almost text-book cloud forms.

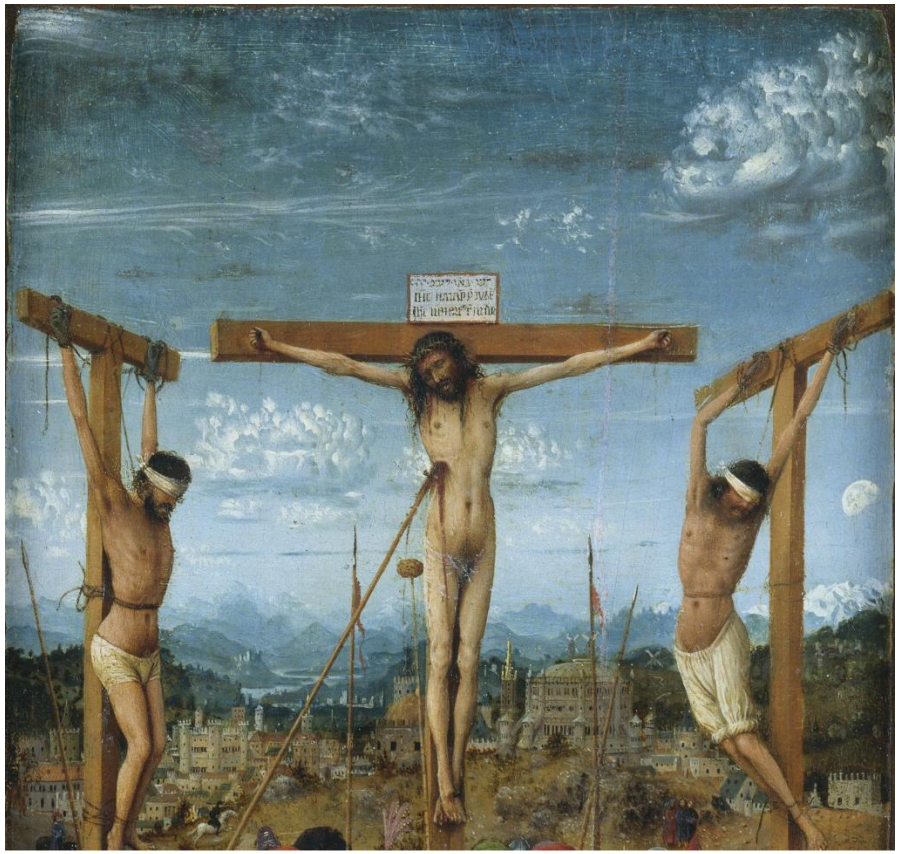

Fig. 15-13. Jan van Eyck, *The Crucifixion*, ca 1435, Metropolitan Museum of Art, New York.

Luke Howard's classification and naming of clouds certainly gave sky painters a boost, but artists had for centuries been painting the various cloud forms. ***The Crucifixion*** of Jan van Eyck (Fig. 15-13) painted around 1435 at the dawn of the Renaissance, is a remarkable meteorological document. In all the history of painting it is the closest to a cloud atlas, with almost textbook examples of four of the cloud genera, cumulus mediocris, cirrus fibratus, altocumulus lenticularis, and cirrocumulus lacunosus, 370 years before Luke Howard and Lamarck. The painting also contains an evolving weather situation based on both the meteorological and biblical setting.

The ***Crucifixion*** shows the moment a Roman soldier lanced Christ's side. This sets the date within month after the vernal equinox, at 3:00 PM on Good Friday, when Christ expired after three hours of darkness. The mid afternoon spring Sun is located in the WSW, behind and to the left of the viewer. Even though (as David Lynch pointed out) the Moon should already have set in the southwestern sky, it has been resurrected as a symbolic compass to point to the Sun and establish that the scene faces north. That suggests an Italian setting just south of the Alps, though it has never been identified.

The rendition of aerial perspective is flawless. No vegetation covers the brown foreground, for it is a place of death. Beyond the city, green forest grades to blue and ultimately to almost white in the furthest distance, even where the mountains are not covered by snow. The sky grades from deep blue above to white near the horizon.

The clouds have textbook form. The boxlike cumulus have flat bases and corrugated sides and tops. They are still growing, but are not large or threatening. The cirrus fibratus in the ***Crucifixion*** is the paradigm of painted cirrus. It consist of distinct streamers that converge and slope down toward the left at a gentle, 2.5º angle. This indicates the wind aloft is from the left, or west, the jet stream's prevailing direction over the Low Countries in spring. A small patch of cirrocumulus lacunosus appears just above the cirrus at top center. The miniature cloud group at extreme upper left consists of a stack of about 7 smooth veneers that arch upward in the center like eyebrows. This is a pile of plates altocumulus lenticularis produced by the west wind crossing over the mountains.

The Crucifixion was meticulously designed to tell a meteorological tale consistent with the mandated guidelines of Scripture and the observed behavior of north Europe's weather. Though there are no dark or stormy clouds there is compelling evidence it had been dark and stormy a short time before and that a slowly moving cold front had just passed through.

Slowly moving cold fronts are often associated with unbroken cloud shields that last for several hours around frontal passage and then clear abruptly. The high visibility and deep blue sky of ***The Crucifixion*** are associated with a cold, dry air mass that follows a cold front. The arrested vertical development of the cumulus shows that the cold air mass is shallow and implies that the front is not far and has passed quite recently. Cirrus and mountain wave clouds in crystalline skies indicate thin humid layers aloft in an otherwise dry atmosphere, typical of skies in the hours following the passage of slowly moving cold fronts. The north surface wind direction, determined from the three windmills just beyond the Temple of Jerusalem, is also consistent with dramatic clearing following the passage of a slowly moving cold front.

Van Eyck's imposed sense of meteorological order focus on perfectly formed individual specimens of all of God's creations. Skies of high visibility, and serene weather were dominant characteristics of the early Renaissance simplistic, optimistic, and pious outlook.

All that began to change shortly after 1500. Complexity replaced simplicity in art. Painted forests replaced stands of individual trees and cloud fields were added to individual clouds. Hazy or smoky skies and stormy weather, sometimes with optical phenomena, increasingly replaced skies with infinite visibility and placid weather.

Leonardo da Vinci was among the leaders. He added haze (sfumato) to give a sense of grandeur, as in the ***Mona Lisa***, and cataclysmic storms, as in his ***Deluge*** drawings. Done in the last decade of his life, the ***Deluge*** drawings have been interpreted as the pessimistic views of an aging man obsessed with death and destruction. But they are masterpieces of fluid dynamics, showing double vortex downbursts descending from storm clouds and vortex outflow of flood water along the ground (Fig. 15-14), which is identical to the outflow vortex of thunderstorm downbursts. That flow was rediscovered in two steps over 450 years later, first by meteorologists Tetsuro Fujita and then by Fernando Caracena in 1982. A compelling case of the downburst and its outflow vortex was captured in the video,

https://www.youtube.com/watch?v=a_G2KRzha7o

Fig. 15-14. Leonardo da Vinci, *Deluge*, ca 1517, Royal Collection Trust.

Albrecht Altdorfer, artist/engineer/mayor, was one of the leaders in painting forests and complex skies of cloud fields. Altdorfer gave the ***Battle of Issus*** (Fig. 15-15) a viewpoint so elevated Earth's curvature is pronounced. It was painted in 1529, seven years after the remnants of Magellan's fleet completed the first (known) circumnavigation of the globe on 6 Sep 1522. Its south facing view of the eastern Mediterranean shows the Nile River with imaginary meanders that open into a delta, bounded by fanciful mountains. The sky is shown just before sunset, near the end of the battle. At right, just above the western horizon, crepuscular rays penetrate a gap in a towering cumulus whose top appears to spread out into a truncated anvil. A field of small, bright cloud cells appears under and to the left of the anvil. It is uncertain if the cells are mamma on the anvil's underside or if they are cirrocumulus. At upper left a ringed corona around the waxing crescent moon (that should be turned 90° counterclockwise) illuminates an opening in a field of altocumulus.

Fig. 15-15. Albrecht Altdorfer, *Battle of Issus*, 1529, Alte Pinakothek, Munich.

Fig. 15-16. El Greco, *View of Toledo*, ca 1599, Metropolitan Museum of Art.

El Greco's ***View of Toledo***, (Fig. 15-16) also has a curved horizon, not to show that the Earth is a sphere but to exaggerate the city's elevation and aggrandize the stark scene. Even so, it is largely topographic. It faces north, showing the city from the south rim of the Tagus River Valley. The shadow on the Alcázar shows that it is mid morning with the Sun in the ESE.

In this painting, El Greco used his customary vertically stretched scale for the field of cumulus mediocris that covers most of the deep

Fig. 15-17. Jacob van Ruisdael, *View of Haarlem with Bleaching Fields*, Ca 1670-75, Kunsthaus, Zürich.

blue sky. Lighting contrasts of the clouds are also exaggerated to the extreme. The shaded cloud centers are almost jet black, especially just above the city, while the illuminated cloud fringes graded to blinding white. Such extreme lighting contrasts do occur when optically thick cumulus form in pristine air (recall Fig. 6-54).

The contrast between the living, light green spring ground cover and the dead gray buildings and cathedral of this capital of the Inquisition

only add to the picture's austere mood. As a final note, stick-figure people are shown fishing or sporting in the water or on the walkway leading to or from the bridge into the city, but not a living soul can be seen inside the city gates.

The expansive sky and its grand clouds became symbols of life and liberty in 17th century Dutch sky paintings. Taken together, they show almost every aspect of Holland's weather and climate, from the Little Ice Age's joyous ice skating scenes to its brutal winter storms and relentless cold, to thundery or even placid, warm summer days. Faithful to nature, soft-edged stratiform clouds dominated the winter scenes while burgeoning convective clouds dominated summer scenes, as the Impressionists would depict later in nearby France.

Jacob van Ruidsael's ***View of Haarlem with Bleaching Fields*** (Fig. 15-17) was one of hundreds of thousands of convincing sky paintings that adorned Dutch homes. The city with the great Church of St. Bavo is seen from the NW. The right face of the Church is sunlit but the north face is shaded, making it early or mid afternoon. All the windmills face the SE (Fig. 15-18 left), indicating a SE wind.

Fig. 15-18. (Left) Detail of Fig. 15-16 with windmills facing SE wind. (Right) Explosive turret of towering cumulus over Jacob Lake, AZ. SDG.

Although the ***View of Haarlem*** appears photographic two aspects of the meteorology are problematic. First, the sky is filled with three parallel cumulus cloud streets that stretch from SW to NE. Cloud streets are seen often over Haarlem especially when a westerly wind blows inland from the North Sea. But the cloud streets in the ***View of Haarlem*** cross the SE wind at almost 90° instead of lining up parallel to it. Second, the cumulus turret at the center diverges explosively upward from a focal point. This certainly is possible (Fig. 15-18 right) because of the mushroom shape of thermals (recall §6.4), but most cumulus rise from a flat base, which the 17th century Dutch sky painters either denied or disguised at all costs.

Fig. 15-19. Peter Paul Rubens, *Landscape with Bird Catcher*, Ca 1635-1640, Louvre.

Just south in Belgium, Peter Paul Rubens tended to be more accurate in the meteorology of his landscape paintings. One outstanding but lesser known work is his ***Landscape with Bird Catcher*** (Fig. 15-19). It is just after dawn around mid-October, based on the foliage, so it faces ESE. The sails of the windmill face north to greet the brisk north wind following a cold front passage some hours before. The north wind sweeps the frigid post-dawn polar air across the warm waters of the stream, lifting shreds of steam fog that tilt up to the south before evaporating (recall Fig. 4-32). Any scene with such detailed and accurate meteorology could not possibly be an a priori

Fig. 15-20. Frederic Church, *Twilight in the Wilderness*, 1860, Cleveland Museum of Art.

creation of the mind; it had to be drawn from direct observation of a specific event. This was a painting not made for sale, but from Rubens' love of Nature during his well-deserved retirement.

Love of Nature and its spacious skies was a propelling motive for the Romantic painters of the early 19th century and even more so for the American painters of the Hudson River School. The American

painters had a mission to save the vanishing sublime wilderness. Jasper Cropsey couldn't have said it better.

> The axe of our civilization is busy with our old forests….Yankee enterprise has little sympathy with the picturesque, and it behooves our artists to rescue from its grasp the little that is left efore it is eer too late.

Frederic Church, a disciple of Thomas Cole, was an examplar of that attitude. His ***Twilight in the Wilderness*** (Fig. 15-20) is an imaginative composite of topographic scenes around Mount Desert Island and Mount Katahdin, ME. It was a studio work but based on intimate knowledge of the sky and a photographic memory. The setting is just after sunset and the air is pristine. At this time, the sky is orange up to an elevation angle of 1.5°, which the mountains in the background block, leaving only a blazing yellow strip of sky up to the far edge of the altocumulus cloud deck. The underlit cloud bands blaze orange near the horizon and deep red above. The reflected light from the cloud base tints the lake red. Higher up, clear openings in the cloud deck expose dark blue sky

One year later, in 1861 as the Civil War began, Church painted a variant of ***Twilight in the Wilderness*** that he named ***Our Banner in the Sky***. It added stars in the clearings and transformed the altocumulus bands to stripes to mimic the flag, while a bare, tilted tree trunk stood as the flag pole.

By about 1880 fickle fashion and arthritis turned the public from the once renowned Frederic Church and his detailed realism to new styles of painting. About that time the arts began to undergo an unprecedented sea change. Nature still served as a model for artists but now to express their often troubled and tortured emotions.

Vincent van Gogh could not paint his landscapes without a view of nature and the sky before him but his renditions became increasingly tortuous, as in ***Cypresses*** (Fig. 15-21). It was during a Mistral, a burst of the north wind, when the trees and the clouds were set in motion. To the left of waving cypresses are wavy, possibly lenticular clouds crossing the Alpilles. On the right below a crescent Moon, a mushroom-capped thermal bulges with protuberances. Most European and American painters attempted to capture solid cloud form; Van Gogh and da Vinci followed the tradition of Chinese painters by rendering clouds as living, vibrant, fluid entities.

Fig. 15-21. Vincent van Gogh *Cypresses*, 1888, Metropolitan Museum of Art.

Edvard Munch portrayed a wavering world in his iconic masterpiece, ***The Scream*** (Fig. 15-22). Despite the distortions, the scene is identifiable and based on a singular meteorological observation that Munch wrote about, unfortunately without dating it. It is a view of Oslo (then Christiana) facing west to its church and port and the hills beyond, set just after sunset. In Munch's oft quoted words,

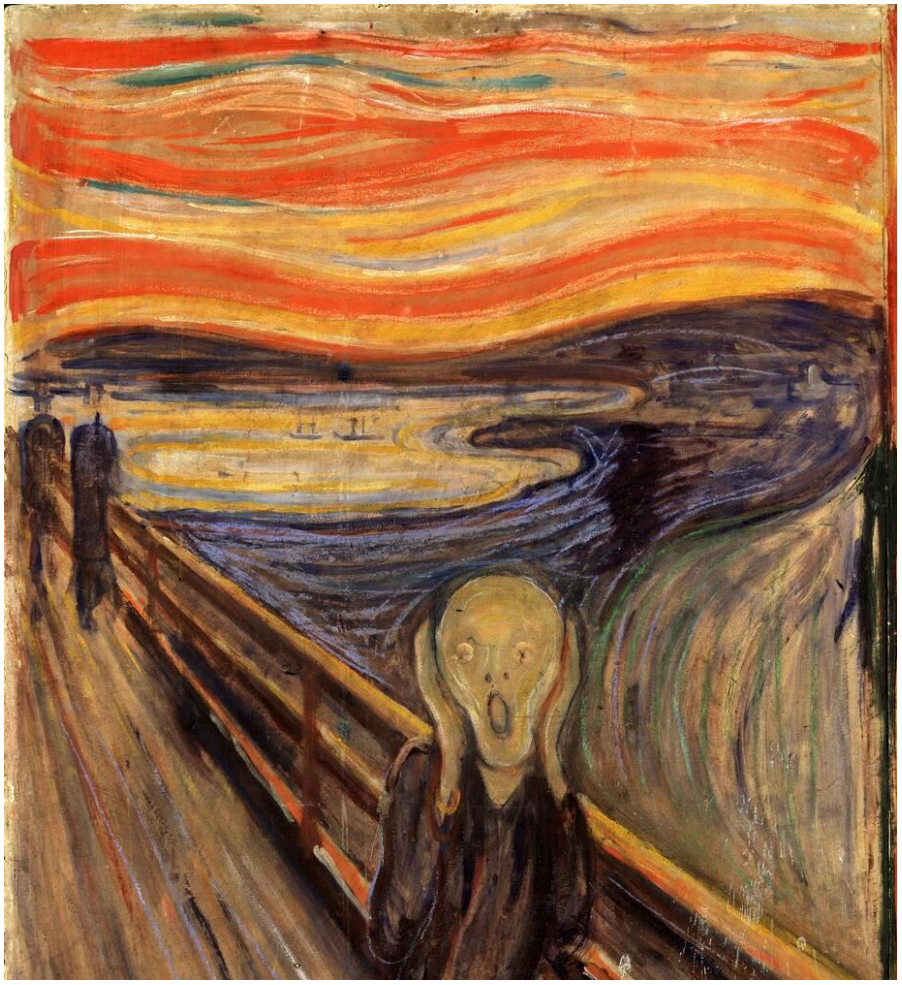

Fig. 15-22. Edvard Munch, *The Scream* , 1893, National Museum, Oslo.

> I was walking along the road with two friends – the Sun was setting – I felt a wave of sadness – the Sky suddenly turned blood-red. I stopped, leaned against the fence tired to death – looked out over the flaming clouds like blood and swords – The blue-black fjord and city – My friends walked on – I stood there quaking with angst– and I felt as though a vast, endless scream passed through nature. [Added later] It seemed to me that I could hear the scream. I painted this picture, painted the clouds as real blood. Diary entry 22 Jan 1892, weeks after the event.

Taking out the emotions, the description matches that of lenticular wave clouds. There are two possibilities. One is iridescent polar stratospheric, mother of pearl clouds. This is problematic because Munch left Oslo before any of the recorded cases in late 1891. The other is underlit tropospheric wave clouds, somewhat like Church's ***Twilight in the Wilderness***.

European artists went on to further abstractions, either relegating nature to a subservient role or ignoring it completely as they descended into the night of senseless and horrific World Wars.

Artists of America's Heartland had less time and tolerance for terrors of the psyche and self-immolation. Celebration of America's spacious skies and survival in the face of raw nature were their themes. A group of Midwestern artists known as the Regionalists documented life out on the Great Plains in a time of tornadoes and Dust Bowl storms. John Steuart Curry was perhaps foremost among these meteorological artists. In ***The Line Storm*** (1934), Curry created the first known painting of a green thunderstorm with lightning bolts behind an advancing arcus.

Five years earlier, just before the Depression and the Dust Bowl, and a decade before ***The Wizard of Oz***, Curry painted ***Tornado over Kansas*** (Fig. 15-23) depicting a family retreating to their storm cellar as a tornado that stirred up a dust ring threatened. Curry also painted the once controversial unfinished mural that now proudly graces a wall in the Kansas State Capitol, controversial because it correctly pointed out that the ravages of the Dust Bowl were enhanced by poor farming methods.

Fig. 15-23. John Steuart Curry, *Tornado over Kansas*, 1929, Muskegon Art Museum.

Throughout America's history, even in the midst of the Dust Bowl, celebration of its spacious skies has been an abiding theme for artists. Certainly, there is no better place in the world for viewing the monarch of clouds, the cumulonimbus, with all its attendant features. Wilson Hurley was one of its premier apostles. Sensitive to color and nature from infancy, he dreamed of painting the beautiful sights of our planet from his time as a pilot during World War II. One day, after two decades of misery as a lawyer, Wilson decided to live his dream and walked out of his office into New Mexico's open skies. Largely self trained, he began painting those skies and more. His ***Thunderstorm Building in the Sandias*** (Fig. 15-24) is one of his glorious renditions of the towering cumulonimbus so often seen in full profile in the Western states.

Georgia O'Keefe also drew her inspiration directly from nature, and moved to New Mexico in good part because of its open skies. But, she used her great sensitivity to color and form in her paintings to transform what she saw. On her first flight at age 75, she was so taken with the "Both Sides Now" view of clouds that she painted four increasingly cartoonish, yet convincing, versions of a pancake flat deck of cellular stratocumulus including the panoramic ***Sky Above Clouds IV*** (Fig. 15-25).

Fig. 15-24. Wilson Hurley. *Thunderstorm Building in the Sandias*. 1998. Private Collection.

Limitations imposed by space require concluding this brief section with a few mere words on the countless professional and amateur sky painters around the world, who increasingly, use fractals or Artificial Intelligence (AI) techniques by computer. Examples of the increased attention to and knowledge of the sky abound on the Web.

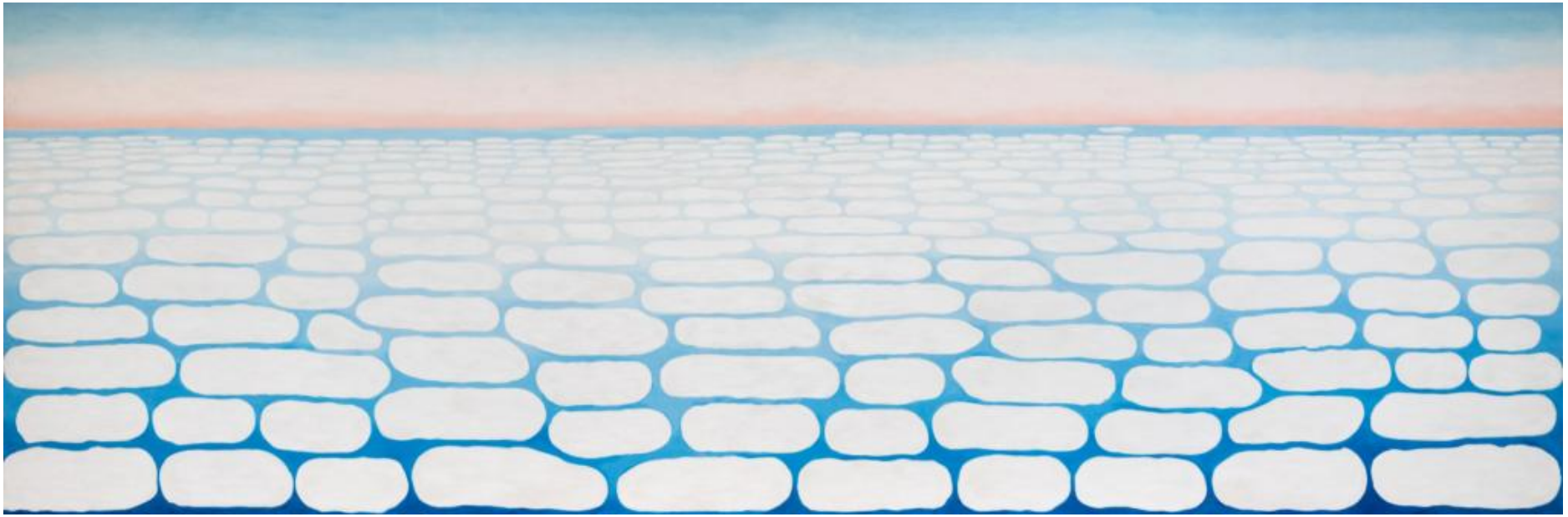

Fig. 15-25. Georgia O'Keefe, *Sky Above Clouds IV*, 1965, Chicago Art Institute.

Artists and photographers (with the computer's help) face fewer limitations than nature imposes. They can alter according to their whims. They can exceed the modest maximum values of the color purity of real rainbows, ice crystal halos, and sky color. They can program the computer to produce perfect parallel ranks and rows of altocumulus or cirrocumulus or circular wave trains, remove unaesthetic obstructions or irregularities, and eliminate haze, as in Fig. 15-26. They can program in small irregularities to make it difficult to distinguish image from reality, as with the wrinkles in the AI generated arcus cloud of Fig. 15-27. They can generate garish images, or create monstrosities or impossibilities such as upside down cumulus. The cirrus and cumulus in the band on the left side of Fig 15-26 would match nature better upside down. But there is no denying the beauty and impressive photorealism of the images already created using AI, as in the twilight towering cumulus of Fig. 15-28. And the AI-generated images are rapidly improving.

Fig. 15-26. AI generated scene with a sky of cirrus and cumulus that would be closer to nature up-side down. ©Ryan Allen.

Fig. 15-27. AI generated scene with arcus below a thunderstorm. In reality, the cloud brightens inside the arcus and may turn green. ©Ryan Allen.

15.3 Complex Clouded Skies: Animation

We also, in much of ***Wonders of the Atmosphere***, restricted the photos and treatment to one cloud species or optical phenomenon at a time. Now, at last, we acknowledge and celebrate the atmosphere's complexity, displaying scenes where several cloud forms or optical phenomena, often at different heights, occur simultaneously.

We did treat a few aspects of limited complexity. Hole punch clouds, as in Fig. 4-17 and Fig. 10-14, with their simultaneous presence of liquid droplets and ice crystals in a single layer, exemplified growth processes of hydrometeors. Halos in the cirrus fall streaks (Fig. 11-15) constitute proof that they consist of ice crystals. Coronas or iridescence constitute strong evidence that the surrounding altocumulus clouds consist of supercooled droplets. Unfortunately, we have yet to capture a hole punch cloud with both a halo in the cirrus and a corona in the altocumulus. One lucky day we may.

Fig. 15-28. AI generated scene of cumulus congestus at sunset. ©Freepik.

Another case of limited complexity is the pile of plates lenticular wave cloud, which reveals multiple alternating layers of dry and humid air, though with a single cloud genus, as in Fig. 13-2, Fig. 13-11, and other figures in Chapter 13. Pileus (§13.2) is similar to lenticular clouds though it is classified as an attendant cloud because it is produced by another cloud instead of by a mountain.

Multilevel clouds bespeak multiple sources for air at different levels. Soundings, satellite loops, time-lapse videos, and direct observations reveal that winds at different heights often blow at different speeds and sometimes even different directions, proving multiple sources.

In §5.7, we pointed out the strange change of wind with height, called the *thermal wind*, which blows with cold air to its left (right) in the Northern (Southern) Hemisphere. It helps determine the pattern of clouds in tropical and extratropical cyclones. In tropical cyclones, which have warm cores or centers, the thermal wind is anticyclonic, opposing the furious inflowing cyclonic winds near the surface, which ultimately become anticyclonic and outflowing in the upper troposphere. The result for clouds in the outer regions of tropical cyclones is that cumulus and cumulonimbus sprout upwards

from near the surface and spiral inward while cirrostratus and cirrus, sometimes as parallel streamers, spiral outward in the upper troposphere, as with Hurricane Isabel (Fig. 15-29). As these cirrus bands and spokes move out from the storm they mix with the drier environment, sink, warm adiabatically, and evaporate.

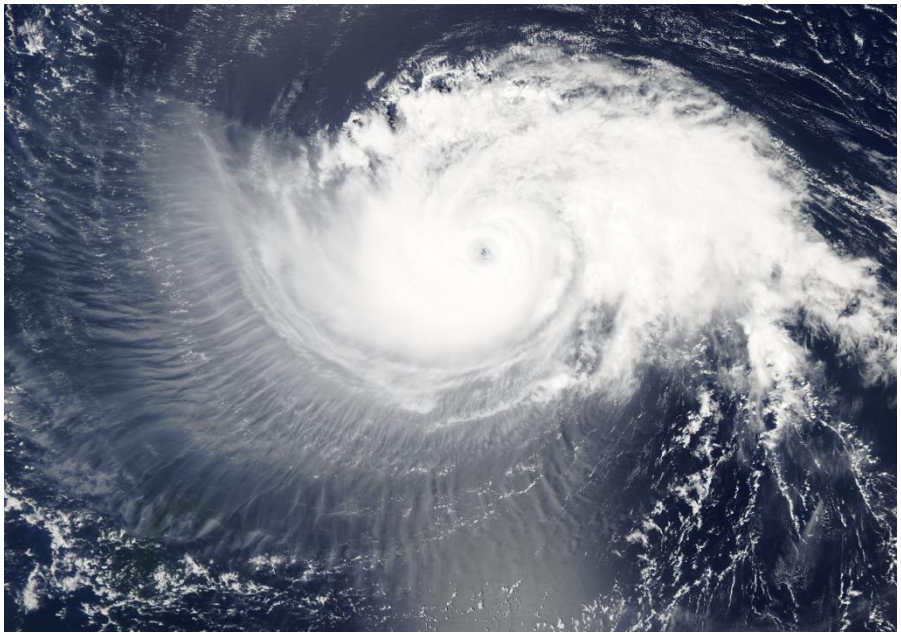

Fig. 15-29. Hurricane Isabel with spiral bands swirling inward cyclonically and parallel curved cirrus streamers spiraling outward in the upper troposphere, 10 Sep 2003. NASA AQUA.

In extratropical cyclones, which form at and (early in their lives) intensify the boundary between cold polar and warm tropical air, the west wind increases with height to form the jet stream in the upper troposphere. At the outer, upper edge of the warm, moist conveyer belt, broad cloud bands are expelled and turn eastward as they join the jet stream. These upper cloud bands also tend to evaporate in the sinking air departing the storm.

Cumulus cloud streets often form in the polar air below the cold frontal surface while cirrus, cirrocumulus, or altocumulus clouds

Fig. 15-30. Cirrus, altocumulus and cumulus streets at Loxahatchee Park, FL, 14 Dec 2013, two days after a cold front passage. The scene faces north and the cloud streets and cirrus are aligned with the west wind. SDG.

above the frontal surface race across the sky from the west, as in Fig. 15-30, two days after a cold front passage at Loxahatchee Groves Park, FL. Just behind the cold front at Fairfield Lake, NC on 8 Oct 2025 (Fig. 15-31), cumulus mediocris formed in slightly unstable air while a line of cirrus vertebratus (identifiable from satellite) 150 hundred km long stretched from west to east across the sky.

Elevated vantage points offer better views of the relative heights of cumulus and cirrus clouds. From the top of Old Bald Rock Mountain, NC it is obvious that the cumulus clouds, are much lower than the cirrus streaks (Fig. 15-32). Flying 3 km high over Spring Valley, NY a day after a summer cold front, left no doubt about the different heights occupied by cumulus and cirrus (Fig. 15-33). The tops of cumulus humilis that formed in the hazy surface boundary layer below flight level barely poked up into the clear, dry air while a band of cirrus uncinus with distinct comma-shaped trails traversed the deep blue sky above flight level.

Fig. 15-31. Cirrus over cumulus at Fairfield Lake, NC, 8 Oct 2025. SDG.

Fig. 15-32. Cumulus and cirrus seen looking west from the summit of Old Bald Rock Mountain, NC, 26 Jun 2024. SDG.

From the ground, and especially from an elevated vantage point such as a mountain top or from a jet, both the forms and relative heights of cumulus, altocumulus, and cirrus are often easy to distinguish. However, in complex, chaotic skies it can be difficult from ground level to disentangle different cloud species and heights, and it is especially difficult in satellite images, where gossamer cirrus clouds that overlay cumulus cloud streets are often almost invisible.

Fig. 15-33. Cirrus uncinus above with cumulus humilis emerging from the surface haze layer over Spring Valley, NY the day after a cold front. SDG.

In all cases, animation is a magic key that not only adds drama and dynamism, but also provides a sense of depth that makes it easy to distinguish different cloud forms and their different heights. This is especially true when the speed and direction of the wind change with height, carrying the clouds along.

This was the case for the sky over Cheyenne, WY, late on the afternoon of 05 July, 2023 (Fig. 15-34). A glance at the photo might well give the impression that there is only one cloud species with varied lighting. But the video from which the photo was extracted,

https://www.flickr.com/photos/cloud_spirit/53025445108/in/album-72157665379832755/

shows that there are two species moving in two different directions. The bright, optically thin sunlit clouds, which move from left to right

and toward the camera (from the SW) are altocumulus. The dark cloud is a broken line of shaded cumulus that moves from right to

Fig. 15-34. The moment of a cold front passage at Cheyenne, WY, 05 Jul 2023. Altocumulus and cumulus are easy to distinguish in a video. JC.

left (from the north) and marks the leading edge of a cold front.

It would also be almost impossible without the video,

https://vimeo.com/173004483

to unravel the baffling complexity of the chaotic sky over Cheyenne, WY on 30 June 2016 (photo not shown here). The video makes it easy to identify the constantly changing cloud species and genera which appear at three or more heights. Not only that, but it reveals that the highest clouds move from the NW, the mid-level clouds from the S, and the low-level clouds from the east. And it would be almost impossible to recognize two clashing outflow boundaries amid the general cloudiness (photo not shown) without the video,

https://www.flickr.com/photos/cloud_spirit/24606595334/in/album-72157665379832755/

Recall that many of the 1000+ time-lapse videos that show clouds at different levels moving at different speeds and directions, at

https://www.flickr.com/photos/cloud_spirit/albums/72157664743046092/with/25094176990

15.4 Complex Thunderstorm Clouds

Fig. 15-35. Spreading anvils from distant thunderstorms fraying into altocumulus and cirrocumulus over Cheyenne, WY, 06 Jun 2019. JC.

A thunderstorm may sport several cloud genera, especially as the anvil, its exhaust plume, extends out of the parent cumulonimbus. The anvil often fractures into cirrus, cirrocumulus, or altocumulus before evaporating. The expelled clouds may disappear but the expelled water vapor does not and this outflow is a major source of interspersed humid layers in the mid and upper troposphere.

Often, the outer edge of the spreading anvil simply thins and evaporates but at times it frays into individual streamers of cirrus, as in Fig. 7-1 or fractures into altocumulus or cirrocumulus, (Fig. 15-35). Many thunderstorms vanish from the bottom up, with the anvil the last remnant to fragment and disappear, as in Fig. 15-36. Sometimes, cloud bands are thrust out of the anvil like pulsed waves, as in Fig. 15-37.

Fig. 15-36. Anvil remnants fraying into altocumulus with a cumulonimbus behind, over Cheyenne, WY, 22 Jun 2023. JC.

Skies are more complex when several nearby thunderstorms form. Updrafts at the leading edge of the outflow boundary that move away from mature thunderstorms often kindle new thunderstorms, which are likely to rise into the anvil of the old storms, as in Fig. 15-38. The spreading anvils of nearby thunderstorms may overlap, and get woven into a cover of high clouds that new thunderstorms rise into, as in Fig. 15-39, where two thunderstorms are rising into the edge of a cirrocumulus sheet that formed from the merger of several anvils.

15.5 Skies of Multi-level Clouds

The water vapor expelled from the tops of storms can move invisibly for hundreds or even thousands of kilometers before condensing once again into visible clouds. Independently, other clouds may form at lower levels to add variety to the sky.

Fig. 15-37. A banded anvil, Cheyenne, WY, 14 Aug 2021. JC.

Fig. 15-38. A thunderstorm rising into cirrus at anvil edge of an older thunderstorm. Cheyenne, WY, 04 Aug 2023. JC.

Fig. 15-39. Two thunderstorms poking up into a sheet of cirrocumulus from older thunderstorms. Cheyenne, WY, 12 Aug 2017. JC.

Two cooling processes make clouds reappear in the mid and upper troposphere – adiabatic cooling in ascending air and radiational cooling. Radiation can either cool or heat humid layers. Water vapor emits and absorbs infrared radiation with much higher efficiency than dry air does. On average, infrared radiation cools the mid and upper troposphere at ~ 1°C per 24 hours, but on clear nights when the ground is cold, humid layers emit infrared radiation much more rapidly than they absorb from the ground and can cool faster than 1°C per hour. As a result, much cirrus and many mid and high-level patterned cloud sheets (as well as fog and stratus near the ground) form overnight, and are seen most frequently early in the morning. Conversely, when the Sun is high in the sky and the ground is hot, humid layers absorb radiation more rapidly from the ground (and to a lesser extent directly from the Sun) than they emit it. This heating occurs without any uplift in stable layers. As a result, mid and upper-level clouds tend to evaporate during the heat of the day and reform by late afternoon or overnight as the ground cools.

Atmosphere humidity was high enough between 7 and 12 km over much of the Southeast United States on the morning of 23 Oct 2023, so that the sky was laced with cirrus and a web of contrails. The contrails that formed over Fairfield Lake, NC (Fig. 15-40) spread

into altocumulus bands consisting of supercooled droplets near the bottom of this layer where $T > -20°C$ and cirrus streamers consisting of falling ice crystals higher in the humid layer where $T < -40°C$.

Fig. 15-40. Cirrus and altocumulus spread from contrails over Fairfield Lake, NC, 23 Oct 2023. SDG.

At intervals of several days, middle and high clouds grace the rainless summer skies on the eastern side of the subtropical highs. They occur when disturbances with large areas of ascending, humid air propagate through the highs. The resulting cirrus or patterned cloud sheets stand out visually because the air below the clouds down to the surface boundary layer is dry and almost always pure (except during forest fires) and the ascending air tends to produce distinct cloud forms. Along the coast, fog or fractostratus produced adds variety and, near sunrise or sunset, color as well to the scene.

Such was the case at San Mateo, CA on 02 Sep 2013 shortly before sunset. Altocumulus at 7 km formed above altostratus at 5 km at the same time fog poured from the cold ocean over the Coast Range and shredded into fractostratus over the warmer land (Fig. 15-41). The fractus and lower sheet of altocumulus have begun to assume orange

Fig. 15-41. Altocumulus above altostratus with fog and fractostratus below at San Mateo, CA, 02 Sep 2013. SDG.

Fig. 15-42. Altocumulus above stratus, Tromsø, Norway, 03 Jul 2008. SDG.

and gold sunset colors. Half an hour later (not shown here), the altostratus fragmented into altocumulus and turned blazing orange while the higher altocumulus remained white.

Broken sheets of stratus or stratocumulus often occupy the surface boundary layer at high latitudes and over cold polar waters, and persist at all hours of the day or night. Mid and high-level clouds help beautify such subdued skies. On the afternoon of 03 July 2008 altocumulus stratiformis passed over Tromsø, Norway while a broken deck of stratus occupied the boundary layer (Fig. 15-42).

Inland from cold waters and over land not covered by snow, early morning fog and low stratus burn off and are replaced in spring and summer by growing cumulus clouds, which take their turn sharing the sky with evaporating remnants of mid and upper clouds.

Fig. 15-43. Cirrocumulus and cumulus over Cheyenne, WY, 31 Mar 2020. JC.

During the cold time of year over much of the mid latitudes, when thunderstorms take a break from their summer dominance of the sky, and jet stream winds often zoom overhead, middle and high clouds are much more likely to dominate the sky and reveal themselves in all their glory. This is particularly true in the dry and clean atmosphere over the western United States (when there are no wildfires), which provides an excellent setting to showcase all cloud forms, and helps highlight differences when distinct cloud species share the sky.

On 31 Mar 2020 it was easy to distinguish both form and height of the cumulus humilis and cirrocumulus over Cheyenne, WY (Fig. 15-43). On 1 Nov 2018, it was more difficult to discern the smaller difference in height between the cirrocumulus that dominated the sky over Cheyenne and the altocumulus on the right, but the difference in form was unmistakable (Fig. 15-44).

Fig. 15-44. Cirrocumulus and altocumulus over Cheyenne, WY, 1 Nov 2018. JC.

Fig. 15-45. Cirrocumulus stratiformis undulatus and altocumulus stratiformis undulatus over Cheyenne, WY, 5 Jan 2019. JC.

Fig. 15-46. Altocumulus lacunosus above stratocumulus lenticularis with fractocumulus on left over Cheyenne, WY, 11 Feb 2019. JC.

This was also the case on 5 Jan 2019 (Fig. 15-45), where the cirrocumulus contained ripples oriented in several directions, much as the ocean contains complex wave trains from various directions.

The cloud complex of 11 Feb 2019 over Cheyenne, WY (Fig. 15-46) formed under high wind conditions. Shear waves crossed by cirrus-type streamers in the partly glaciated altocumulus helped produce the

Fig. 15-47. Twin anvils tower behind stratocumulus cloud streets at Jaraíz de la Vera, Spain, 15 June 2008. SDG.

lacunar appearance of the altocumulus. Closer to the ground the line of stratocumulus with smooth tops at the left of the line) resulted from an intertwining of surface heating and laminar lee wave flow.

Similar intertwining of laminar and convective flow occurred on the morning of 15 June 2008 over Jaraíz de la Vera, Spain and led to the unusual cloudscape of Fig. 15-47. At the time, strong west winds crossed the ridge line of the Sierra del Grados. The mostly smooth tops indicated laminar lee wave flow capped by a stable layer except in the few places where thermals had enough buoyancy to burst through the stable layer into tops that resembled anvils.

When conditions are just right (e. g., $\boldsymbol{T} \approx -32^{\circ}C$) nature, with no help from jet planes, can produce supercooled altocumulus next to cirrus, as over Suffern, NY on 02 Dec 2011 in a 300 km long cloud line parallel to the jet stream marked by transverse bands (Fig. 15-48).

Fig. 15-48. Neighboring bands of opaque altocumulus and cirrus streamers over Suffern, NY, 02 Dec 2011. Alas, sans optical phenomena. SDG.

Multiple cloud layers often exhibit intriguing contrasts of shade and color. An unusual case of spotted shading occurred in the sky over Vail, AZ on 7 Mar 2019. Distinct spots of fractocumulus resembling gray chicken pox were darkened by an overlying cover of altostratus (Fig. 15-49). Climate worlds away, over Cliffside Park, NJ (Fig. 15-50), cirrus streamers returned the favor by casting their shadows on a sheet of altostratus. The optically thin altostratus, reddened by the setting watery Sun in turn shaded an opaque fractostratus (at top left) in the lower troposphere, turning it almost black.

Overcast, gray skies can be alluring when cloud bases are distorted into forms such as arcus or asperitas, or when multiple cloud layers are distinct. At Cheyenne, WY, on 18 Mar 2018 strong vertical wind shear produced altocumulus undulatus in a humid layer beneath a cover of altostratus (Fig. 15-51). Color was added to the scene by the setting Sun which broke through either beyond the edge of the altostratus sheet or where thinned.

Fig. 15-49. Altostratus with shaded and darkened fractocumulus at Vail, AZ, 07 Mar 2019. JC.

Fig. 15-50. Altostratus with cumulus below and shadows of Ci above at Cliffside Park, NJ, SDG.

Fig. 15-51. Altocumulus undulatus shaded by higher altostratus Cheyenne, WY, 18 Mar 2018. JC.

Fig. 15-52. Twilight tints a phoenix-like cirrus and shades a translucent sheet of altocumulus over Boynton Beach, FL, 2 Jan 2024. SDG.

Twilight, sunrise, and sunset enrich the play of colors on multilevel clouds, as we have already seen (Fig. 4-40, Fig. 12-14). Twilight helped create a cloud color puzzle over Boynton Beach, FL on 2 Jan 2024. The cirrus gives the impression it is below the altocumulus by seemingly blocking it, but the slight purple-gray color and relative darkness of the translucent altocumulus implies it is in the Earth's shadow and hence lower than the cirrus.

Clouds sometimes do not wait for twilight and exhibit unusual colors in the middle of the day. Optically thick cumulus clouds have gray bases almost everywhere except in places like the plains of La Mancha, Spain (the country of Don Quixote). There, scattered, optically thick cumulus clouds typically have reddish bases because a significant fraction of sunlight reaches the red earth below and is reflected up to redden the dark cloud base (Fig. 15-53). This is also the case in other dry regions with largely bare red iron oxide rocks or soil, such as Australia's Great and Little Sandy Deserts. Les Cowley (personal communication) mentioned that cumulus bases over extensive fields of yellow-blooming soybeans are tinted yellow.

Fig. 15-53. Red-base cumulus Alcázar de San Juan, Spain, 16 Jun 2008. SDG.

On rare occasion, overcast skies grade from gray above to blue near the horizon. A blue horizon cloud base appeared to the SW down the Sognafjord from Skjolden, Norway late on the afternoon of 6 July 2008 (Fig. 15-54). Why? A few hours earlier skies had been clear. The most likely source of this unusual blue color was blue skylight reflected off the nearby glaciers from clear skies ≈ 50 km to the NW.

15.6 Final Search: Multiple Optical Phenomena

If several different cloud species or genera can occupy the sky at the same time, so can several different optical phenomena. We have already seen anticrepuscular rays crossing rainbows at 90° (e. g., Fig. 9-54), and cloud bows appearing with glories (e. g., Fig. 14-26), though Mie Scattering suggests that they are different manifestations

Fig. 15-54. Blue overcast horizon over Sognefjord, Skjolden, Norway, 6 Jul 2008. SDG.

of the same phenomenon. And we have had one tantalizing glimpse of a parhelion appearing with iridescence in Fig. 11-62 and will end the book on the hunt for the surprisingly elusive combination of halos with a corona or iridescence.

Thunderstorms sport multiple cloud features, so it is no surprise they host multiple optical phenomena as well. Start with lightning and rainbows. Sebastian Hobbs captured lightning bolts with a double rainbow (the secondary bow is present but faint), in Fig. 15-55. The bows are red as the result of some photographic artifice since red bows only occur when the Sun or Moon is at the horizon and not at an elevation angle of 18°. The rainbow's colors appear better in Chris Leboe's photo with lightning (Fig. 15-56).

Fig. 15-55. Lightning with a double rainbow, Mont Alto, PA, 18 Aug 2019. © Sebastian Hobbs.

Fig. 15-56. Lightning with a rainbow, Prince George, BC, Canada, 2 August 2, 2015. © Chris Leboe.

It is no surprise that lightning occurs in green thunderstorms, as in Fig. 15-57, where the bolt struck a bit too close to Sebastian Hobbs. And in an almost cosmic shot (Fig. 15-58), Brandon Montgomery captured a blue-green thunderstorm with a symmetric, flying saucer-

Fig. 15-57. Green thunderstorm with lightning a bit too close for comfort near Kadoka, SD, 8 Jun 2018. © Sebastian Hobbs.

shaped arcus and lightning. Note that a blue-green sliver appears in the gap above the arcus and just below the main cloud. An additional feature is that by shading the nearby sky, the storm reddened the pre-sunset horizon sky in the clearing to the left of the arcus (recall §2.5).

Perhaps the most unusual combination of phenomena – an aurora with a moonlit spray bow from the waterfall, Skógafoss – was captured by Par Stéphane Vetter (Fig. 15-59). The reason that the aurora does not appear vivid is that the full Moon needed to produce the bow brightens the nighttime the sky too much, just as bright city lights make it difficult, if not impossible to see the stars.

Each of these cases represents something incredibly rare or difficult to capture even for expert photographers who know where to go and

Fig. 15-58. Lightning in a blue-green thunderstorm with reddened horizon sky shortly before sunset at Laverne, OK, 9 Sep 2025. © Brandon Montogomery.

Fig. 15-59. Aurora with moonlit spray bow, Skógafoss, Iceland. A moonlit sky, needed for the bow, is no friend to the aurora. © Par Stéphane Vetter.

what to look for. Even so, they only succeed by a combination of

incredible patience and incredible luck. Fortune may favor the well prepared but there are no guarantees.

It is fitting to conclude the book with a search for two distinct optical phenomena that might seem simple but has proven to be quite elusive. It is not too unusual to see a sky with both water droplet and ice crystal clouds such as altocumulus and cirrus or cirrostratus at the same time. That makes it reasonable to expect that coronas or iridescence should appear at the same time as ice crystal halos. But that combination turns out to be quite rare.

Why?

Fig. 15-60. Cirrus and cirrocumulus over Vail, AZ, 5 Dec 2018. JC.

We have already seen the necessary conditions for brilliant coronas (§14.3) and halos (Chapter 11). For both, clouds must be optically thin, i. e., translucent. Multiple scattering, which is almost invariably incoherent, kills any optical phenomenon that must pass through opaque clouds. For coronas, droplet size along a sunbeam must also be almost constant because the scattering angle is highly size dependent. Wave clouds fit this requirement best; droplet sizes in convective clouds range from near zero at cloud base to near maximum at cloud top. This always holds for penetrative convection and generally for gentle cellular convection.

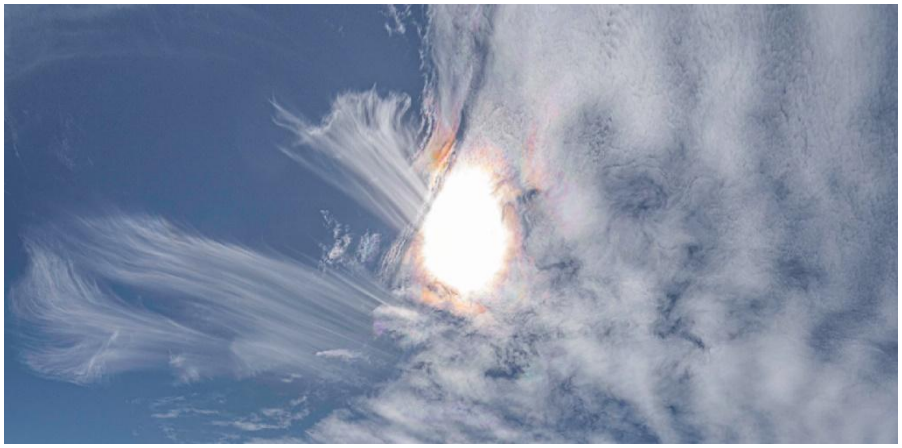

Fig. 15-61. Cirrocumulus with corona but cirrus without halo phenomena, Vail, AZ, 20 Feb 2020. JC.

To produce brilliant halos, crystals must be pristine and large. So-called junk crystals that consist of rimed particles, etc., produce incoherent scattering. Crystals' effective diameter must be larger than about 100 μm so that diffraction does not seriously vitiate geometric optics.

It is not unusual to see a sky with both cirrus and either altocumulus or cirrocumulus, but each of these produce optical phenomena only a small fraction of the cases, and for brief times, perhaps just moments. On 02 Dec 2011, parallel bands of opaque cirrus streamers lined up side-by-side with opaque bands of altocumulus to cover much of the sky over Suffern, NY (Fig. 15-48) but with nary a hint of either optical phenomenon. On 5 Dec 2018, more delicate cirrocumulus and cirrus shared the sky over Vail, AZ (Fig. 15-60), with only faint iridescence in the wavy segments of the cirrocumulus to the left of the tall palm tree but with no halos, in part because the cirrus was not at the proper place – e. g., at the height of the Sun and ≈ 22º to its left. A short time later, after the iridescence disappeared, faint halos did appear in the cirrus. And on 20 Feb 2020 a corona appeared in

wavy cirrocumulus over Vail, AZ but with no halo in the cirrus, because it was too close to the Sun (Fig. 15-61).

Most cases of beautiful coronas or iridescence occur in optically thin clouds or cloud edges that have ripples or waves, and/or resemble translucent veils. One afternoon, a sheet of altocumulus stratiformis consisting mainly of closed cells but with one small optically thin veil-like patch passed over the skyscrapers of midtown Manhattan. For about ten minutes there was no iridescence but since the veil was drifting slowly toward the Sun, the hope of seeing iridescence was well worth the wait, all while every other Manhattanite raced about his or her business never glancing up and therefore, oblivious when the blazing opal fired up in the sky for one brief minute (Fig. 15-62).

Fig. 15-62. Iridescence only in fibrous veil of altocumulus over NYC. SDG.

Hole punch clouds offer tantalizing prospects of producing simultaneous coronas and halos since they are in effect combinations of altocumulus and cirrus, but as mentioned in §11.2, are almost always disappointing. Of course, the cirrus-filled holes must be in the proper place with respect to the Sun. Thus, the parhelion in Fig. 11-14 did not appear until the hole moved to the same height in the sky

Fig. 15-63. A corona appeared in the altocumulus around a cloud canal with top and bottom of the 22° halo or its tangent arcs in the canal over Boynton Beach, FL, 17 Jan 2014. SDG.

as the Sun and 22° to its right. When the hole moved away the parhelion vanished. And there was no corona or iridescence.

A feeble corona did appear in the altocumulus just around the Sun with both the top and bottom of either the 22° halo or its tangent arcs in a cloud canal (Fig. 15-63). Unfortunately, almost all holes form in altocumulus with closely packed opaque convection cells, a lethal combination for coronas. Of over 60 cases of hole punch clouds in our collections, many in the part of the sky near the Sun, this was only one of two in which the altocumulus cells were either iridescent or sported a corona.

Fig. 15-64. Iridescent cirrocumulus at left, and parhelion at right in cirrus in jet stream, Boynton Beach, FL, 8 Jan 2010. SDG.

Another promising weather situation for dual optical phenomena in Boynton Beach FL, occurs during days following cold fronts, when long bands of jet stream clouds, often mixtures of cirrus and gossamer waves of cirrocumulus, sometimes with hole punch clouds in them, are injected into crystal clear skies. When the cirrocumulus is wavy and translucent, a corona or iridescence appears. If there are cirrus streamers at the same time, halos may also appear.

For a few brief moments on 8 Jan 2010 iridescence flared in a patch of a cirrocumulus near the Sun the same time a faint parhelion formed in cirrus streamers a little more than 22° to its right (Fig. 15-64).

Fig. 15-65. Elliptical halo and iridescence, Mount Fichtelberg, 22 Apr 2016. © Claudia Hinz.

This was a rare find, but it fell short of the extraordinary needed to end ***Wonders of the Atmosphere***.

The ever-alert Claudia Hinz captured a double rarity – an elliptical halo plus iridescence (Fig. 15-58). Elliptical halos are colorless, showing that they are produced solely by reflection. The crystals involved are either plates or star-shaped dendrites that fall in a gyroscopic mode with a near constant tilt of the c-axis (in this case about 1° from vertical). The halo flashed on and off several times, lasting but seconds each time, and was produced by an ice cloud so optically thin it was invisible. (That is sometimes the case with sun pillars seen in the clear air below altocumulus clouds.) This is just one of many cases of extraordinary halo phenomena at,

https://www.haloblog.net/

And now for the finale. Nature photographer, Brent Mckean, recognized the extraordinary on a frigid night (most likely) 12 February 2020 near the time of the full Moon (9 Feb).

> That night was extremely cold and it was roughly 4:30 in the morning, I was on my way to Winnipeg. I usually carry my

camera and tripod with me…just in case. I had to get out of the car and capture this right away because when you see something rare like that, it could come and go…. A few minutes later…the halo and arcs had disappeared."

Fig. 15-66. Halo complex around a multi-ringed corona over Manitoba, 12 Feb 2020. ©Brent Mckean.

What Brent saw and photographed (Fig. 15-66) on that moonlit night was a brilliant halo complex with a colorful, multi-ringed corona. The halo complex included the 22° halo, much brighter upper and lower tangent arcs (implying horizontal pencil crystals), as well as the paraselenae (moon dogs) and the parselenic circle (implying horizontal plates) just outside the halo. Matching the angular size of the corona with the Lee Diagram (Fig. 14-25) indicated droplets or near spherical ice particles with radius 10 μm.

A few days after the full Moon, on the early morning of 12 Feb, the temperature, $T \approx -26.5°C$, was perfect for a mix of ice and supercooled water radiation fog. No distinct cloud or fog was visible, in the blue moonlit sky so its optical thickness had to be very small, and indeed, stars and/or diamond dust ice crystals could be seen.

And just as fast as the thin fog congealed it dissipated. Beauty is too often too fleeting. Yes, but by capturing the fleeting beauty…

Thus, though we cannot make our Sun
Stand still, yet we will make him run.
Andrew Marvell, ***To His Coy Mistress***

With this extraordinary photo we come to the end of ***Wonders of the Atmosphere***. While we (and many others) continue the endless search it remains for us to point out that.

When the sky is the limit there is no limit.

Wonders of the Atmosphere
Appendix: Sky Photography

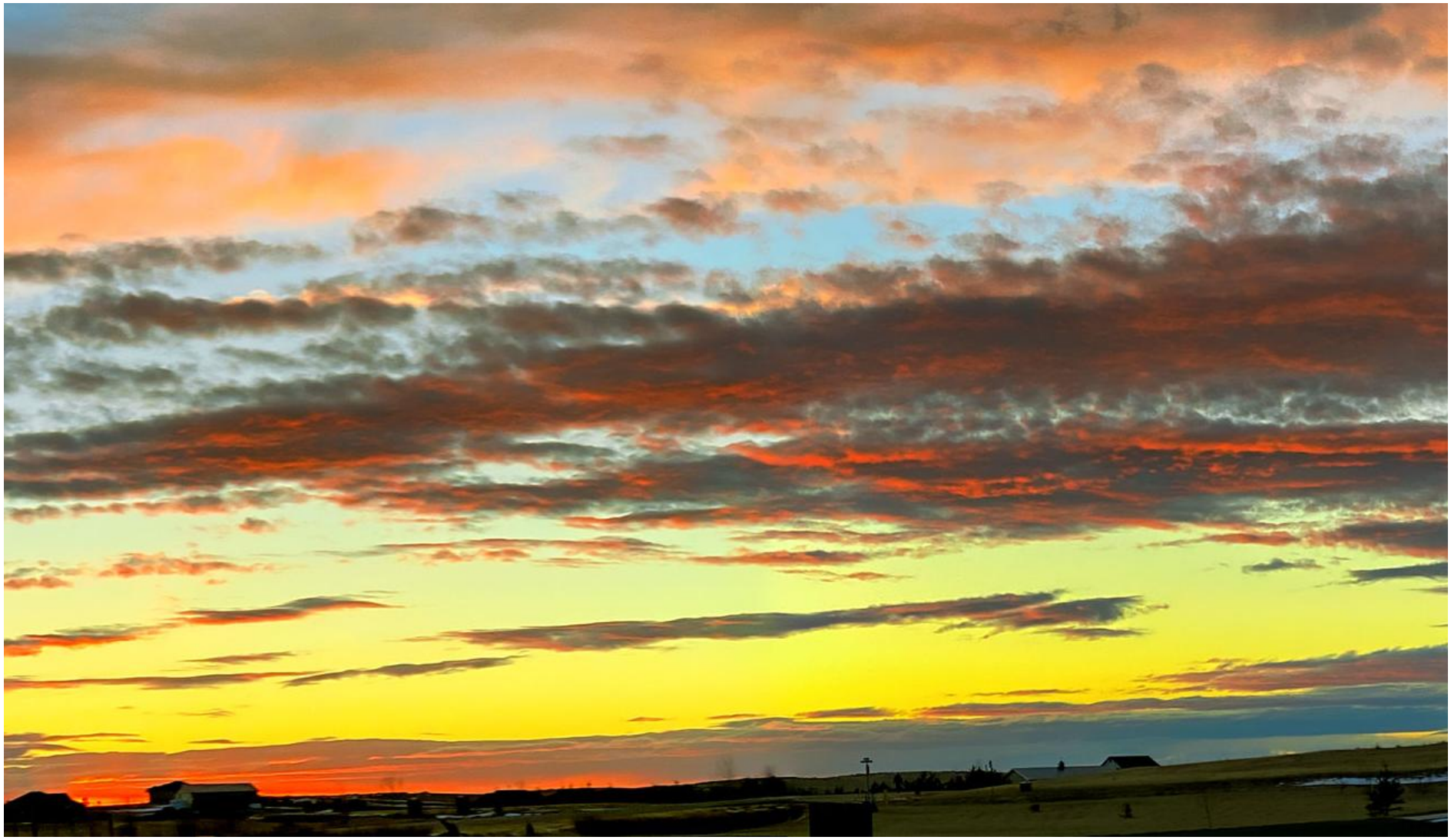

Fig. A-1. Altocumulus multicolored twilight sky six minutes after sunset over Cheyenne, WY, 7 Jul 2021. JC.

Fig. A-2. Cirrus with mamma over Cheyenne, WY at dawn 26 Oct 2025. JC.

Fig. A-3. Morning fog over Fairfield Lake, NC, 3 Oct 2025. SDG.

Wonders of the Atmosphere
Appendix: Sky Photography

The Digital World

Photography has come a long way since film. With the usual limit of 36 exposures per roll of film, each time the shutter was released, one had to ensure that the camera was framed perfectly and all its settings (exposure, focus, depth of field, etc.) were spot on. In addition, the time and expense to get prints or slides back did not guarantee quality.

Enter the digital age of photography with post-processing software. We now have the freedom to take and manipulate as many images and time lapse videos as we want without the concern of cost (other than the initial expense for camera, computer and software). Smart phones reduce costs further, and the quality of the captured moments only improves with each new model. Table 1 compares film and dSLR.

One doesn't need to be a meteorologist or an Ansel Adams to start photographing thunderstorms, lightning, fiery sunsets, halos, or even the northern / southern lights (aurora). What is needed is to take lots and lots of images when you look up and see something that captures your imagination and tells a story. Because the sky is continuously changing, there is a high probability that one image will be a 'keeper'.

Several techniques will improve photos but experience and patience are perhaps the two most important things to remember. Just like the farmer who senses what the weather will be after years living at the

Category	35mm Film SLR	Full-Frame dSLR (2005–2020 era)	Winner / Comments
Image quality (resolution)	12–20 MP equivalent depending on film + lens	12–45 MP (5D = 12 MP → D850 45 MP)	**dSLR** now wins easily
Dynamic range	Outstanding with negative film (especially Portra 400)	Very good, but negative film still slightly ahead	**Film** slight edge
High-ISO / low light	ISO 800–3200 very grainy, expensive (Portra 800, Delta 3200)	Clean up to ISO 6400–25600 on newer bodies	**dSLR** massive win
Color rendition	Unique, loved "film look"; each stock different	Excellent, but more clinical; can mimic with presets	Tie – taste dependent
Immediate feedback	None – wait for development	Instant review on LCD	**dSLR**
Cost per shot	$0.50–$1.50 per frame (film + lab)	Essentially zero after purchase	**dSLR** huge win
Up-front cost (2025 used market)	Body $150–600 Lenses $100–2000	Body $300–1200 Same lenses work (Canon EF, Nikon F)	Roughly equal now
Lens selection	Same legendary lenses as dSLR (often cheaper)	Same lenses + modern AF designs	Tie
Autofocus speed/accuracy	Good-to-excellent on late models (EOS-1V, F100)	Faster, more points, face/eye detect on newer ones	**dSLR**
Battery life	30–80 rolls per set of batteries/CR123	800–3000 shots per charge	**Film** wins
Weather sealing	Pro film bodies (EOS-1V, F5, F100) are tanks	Most pro dSLRs also tanks	Tie
Size & weight	Usually a little lighter	Slightly heavier (sensor + LCD)	**Film** slight edge
Long-term archiving	Negatives/scans can last 100+ years if stored well	Hard drives die; need active backup	**Film** if you store properly
Editing flexibility	Scan once → limited by scan quality	Full raw files, re-edit forever	**dSLR**
Fun / tactile joy	Winding, changing rolls, mailers, surprise factor	Point, shoot, chimp	**Film** for many people
Reliability in 2025	Mechanical – will keep working for decades	Electronic shutter/mirror eventually fail; capacitors die	**Film** long-term
Repairability	Still many repair techs for classic SLRs	Fewer and fewer people fixing 15–20-year-old dSLRs	**Film**

Table A-1. Comparison of film and dSLR photography. JC.

Category	Full-Frame (FX) dSLR	APS-C (DX) dSLR	Clear Winner 2025
Sensor size	36 × 24 mm	≈24 × 16 mm (1.5× crop Nikon/Sony, 1.6× Canon)	—
Resolution (typical range)	24–45 MP (5D IV 30 MP, D850 45 MP, D780 24 MP)	20–32 MP (D500 20 MP, D7500 20 MP, 90D 32 MP)	FX
Real-world detail/sharpness	Noticeably higher, especially in prints >24"	Very good, but FX pulls ahead on close inspection	FX
Dynamic range	13.5–15 EV (best-in-class on D850, 5D IV, Z6-based)	13–14 EV (½ to 1 stop behind)	FX
High-ISO / low-light performance	Typically 1–1.5 stops cleaner (ISO 12,800 looks like DX 6400)	Still excellent (D500 and 90D are legends)	FX
Shallow depth of field	Easy with f/1.4–f/2.8 lenses → creamy bokeh	Possible but harder (50 mm f/1.4 acts like 75 mm f/2.1)	FX
Wide-angle performance	True 14–24 mm is actually ultra-wide	10–12 mm needed → more expensive, more distortion	FX
Telephoto reach	300 mm is 300 mm	300 mm acts like 450–480 mm → free reach!	DX
Autofocus performance	Excellent (D850, 5D IV, D6)	Frequently *better* (D500 & 7D II still beat most FX)	DX (slight edge)
Frame rate	5–9 fps (D850 7–9, 5D IV 7 fps)	8–12 fps (D500 10 fps, 7D II 10 fps, 90D 11 fps)	DX
Viewfinder size/brightness	Big, bright, 100% coverage	Smaller image in viewfinder because of crop	FX
Battery life	800–2500 shots	1000–4000+ shots (DX bodies are battery champs)	DX
Body size & weight	Larger & heavier (D850 1005 g, 5D IV 890 g)	Usually lighter (D500 860 g, 90D 701 g)	DX
Weather sealing (pro bodies)	Tanks	Also tanks (D500, 7D II, K-3 III are legendary)	Tie
Lens cost & size	Full-frame lenses are bigger & pricier	Same lenses work, plus cheaper DX options	DX
Used price 2025 (body only)	$800–1800 (D850 ~$1600, 5D IV ~$1200, D780 ~$1300)	$350–900 (D500 ~$650–800, 7D II ~$500, 90D ~$700)	DX
Best wildlife/sports value	Needs long, expensive glass	70–200 becomes 105–300 → huge savings	DX
Best portrait/landscape value	Shallower DOF + better wide angles	Good but not the same “look”	FX

Table A-2. Comparison of FX and DX dSLR photography. JC.

same location (sticking his moistened finger in the air), you will be more able to forecast what specific clouds look like and how they change over time. The adage, “Red skies in morning, sailor’s warning, Red skies at night, sailor’s delight”, is a good example of weather forecasting through repeated observation.

Of course, pictures are greatly improved by a setting that is unique or awe-inspiring. For example, visualize a scene overlooking the Grand Canyon when in the distance there is a huge thunderstorm with lightning striking at the canyon’s rim. Perhaps experiencing a sunset over the Canyon when suddenly the clouds turn shade of fire while the canyon’s walls reflect the last of the setting sun’s rays and dark shadows envelop the valley floor. The possibilities are endless and there are always surprises around the next instant the camera is used

What about equipment beyond cell phones? If you are new to photography, camera technology and terminology can be overwhelming. Beginners should get a basic digital camera and go out and experiment. Take a snap shot and see if it accurately captures what you are seeing. Take lots of images and pick the best few. Ask yourself if they were under or over-exposed, or whether the focus was off.

Most experienced photographers use full frame (FX) dSLR cameras that usually cost at least twice as much of crop (DX) dSLR cameras. Table A-2 compares FX and DX dSLR cameras. An important advantage of a cropped DX camera is that the telephoto reach is about 1.5x that of the full frame FX dSLR (consider this a free upgrade). DX cameras are also considerably lighter to carry and their batteries last at least a third longer. dSLR cameras work for nearly everything. GoPro works for wide field time lapse. iPhones work for on-the-go panoramas and the northern lights Security camcorders work for remote monitoring of sky conditions and time lapse videos.

Preferred lenses for dSLR cameras depend on what you are photographing. Ultra-wide field (8mm) lenses are needed for nearby thunderstorms and complex halo displays. Wide field (16 to 24mm)

lenses are good for cloudscapes, fire sky sunrises & sunsets and most halos, rainbows, and auroras. Normal field (35mm to 50mm) for sun pillars, rain shafts, lightning. Telephoto (>100mm) for distant storms, the green flash, and coronas.

Although digital images with automatic settings produce an approximation to what the eye sees, they lack the spatial resolution, depth of field and color and light sensitivity we perceive. If you take pictures "'as is" in auto mode and use it for casual viewing on social media and for archiving memories, that's great but manual settings and raw image format (used in post-processing) gives more control over the final image. For example, if you are attempting to capture the sky that is very bright and very dark at the same time, in photography vernacular this is referred to as dynamic range and is an important factor to consider especially with approaching thunderstorms and during sunrises (dawn) and sunsets (dusk) when rapidly changing lighting becomes challenging. Whether you want to keep the exposures so that the event is fully visible under all lighting conditions (auto settings) or whether you want to create the event as closely as possible to what the eye sees (manual setting), this factor will determine whether auto or manual settings is your preference. In photography, there are no right or wrong ways of taking a picture or processing it.

In bright daylight use at 1/3 to 2/3 f-stop reduction from the camera's default setting. An ISO between 100 and 400 depending on the amount of clouds present. An aperture setting (f-stop) of f/5.6 to f/8 in daylight and F/2.8 to f/4 at night. Short exposures of faster than 1/500 second in daylight and up to 30 seconds in very dark skies though less in moonlight.

Also, to be creative and produce something more refined or artistic requires a level of sophistication and experience that is acquired over time with the use of very popular post-processing software such as Photoshop, Lightroom and Final Cut Pro

Editing software such as PhotoShop and Lightroom enables one to better match what is seen. Image noise can be reduced or completely eliminated. Contrast between the shadows and highlights can enhance depth of field. Tonality can warm or cool an image depending on how you want to convey a mood. The list of possibilities is nearly infinite. Or you can also abandon post-processing edits and let artificial intelligence (AI) take your direct camera image and do its own thing to it. However, if you are taking photos of nature, it is more important to tweak the initial camera capture in an attempt to render it as closely as you saw it.

Some Specific Ideas

Here are some ideas to help improve your cloudscapes and skyscapes with ratings on the degree of difficulty:

Using panoramas. The sky stretches 180 degrees in elevation from east to west and north to south and 360 degrees in azimuth around the compass. Although images will be smaller in size when taking these vast expanses, you are more likely in capturing what you aim for without missing anything
(https://www.flickr.com/photos/cloud_spirit/28218645144
You can always crop an image to focus on what you like to emphasize. There are several apps available to help speed the editing along, some already on your smart phone.
Difficulty: Low.

Using time-lapse. Smart phones and action cams can take one image at a predefined interval and when finished will combine the images automatically. Using a tripod is essential to keep a stable scene without distracting shake. Whether watching the clouds race across the sky or seeing the sun sets as a fire skies changes color, time-lapse clips are fun to take
https://www.flickr.com/photos/cloud_spirit/53934739821
Difficulty: Low.

Time-lapse with dSLR (35mm cameras). By taking higher resolution frames at a set interval (in raw format), you then have the option to post-process each image based on global settings such as exposure,

contrast, color saturation, highlight, shadows, whites and blacks, texture, sharpness, etc. There are tons of YouTube clips on how to do this. The advantage is to develop the highest quality time-lapse possible. However, be aware that these files are quite large and takes a lot of computer run-time to complete.
Difficulty: Medium.

Using slow motion. Movies are generally recorded at 24 to 30 fps for normal speed. However, newer cameras usually can bump up the frame rate to 240 fps or 8 to 10 time faster. When these clips are played back at normal frame rate, it takes longer to play and thus is viewed as slower motion. See example with my dog Hunter,
https://www.flickr.com/photos/cloud_spirit/34253072894
The effects are even more startling with lightning:
https://www.flickr.com/photos/cloud_spirit/52256821316
Difficulty: Low.

Using High Dynamic Range. Images are automatically processed in-camera by taking in quick session as under, normal and over-exposed images. The reason for using this option is in cases where the dynamic range of lighting is high. The camera's programming balances areas where there is under or over exposure and compares it to the normal exposure. This HDR method helps to capture details that would normally be invisible because of areas that deviate considerably from the normal exposure. Although the use of this technique has faded over time, there are still good reasons to use it. Difficulty: Low.

Using Long-Time Exposures. At night, light entering a camera's lens is 1000's of times less than during day. As a result, longer exposures are required to record images. The amount of time is determined by the f-stop used (f/2.8 vs. f/8), the iso (100 vs. 1000), the focal length (16mm vs. 85mm), and the moon's phase. The longer the exposure, the more noise is generated, the greater chance for blur due to motion and the greater chance for over-exposure. When the moon is full, exposures can be decreased significantly. Most night sky images should have the lens near the lowest f-stop, don't set the iso above 1250 (noise in introduced) and keep exposures below 15 seconds. Also factor in that wide angle lenses tend to gather less light than telephoto lenses because objects are smaller.
https://www.flickr.com/photos/cloud_spirit/51607715876
Difficulty: Low to moderate.

Usually, lightning activity is best captured before and after the rainfall although just because the storm isn't overhead doesn't mean that you aren't at risk for getting struck by a bolt
https://www.flickr.com/photos/cloud_spirit/51417257579
https://www.flickr.com/photos/cloud_spirit/42235605330
Visibility improvement and saving your equipment from getting water damage are two good reasons for not taking your shots during the peak intensity of the storm.
Difficulty: Low to Medium.

When taking a long-time exposure of night lightning, depending on how active the storm is and its distance, exposures can range from 1 to 30 seconds, usually at a f-stop of f/5.8 to f/11 with an iso rating between 400 to 800. What determines these settings is based in part on the lens' focal length (wide field 8mm to 35mm) or long lens (greater than 85mm) (telephoto). Wide field lenses make everything smaller and thus fainter, so it takes lower f-stops such as f/2.8 to record lightning. Quite a bit of practice is needed at mastering the best camera settings.
Difficulty: Medium to High.

Taking lightning photos during daylight is difficult because of the lack of contrast and one's inability to take long exposures. While there are lightning triggers available that will tell the camera when to take a shot, they only work with dark backgrounds for the lightning to be visible
https://www.flickr.com/photos/cloud_spirit/35471308281

A work around this problem is to record a lightning storm in movie or slow-motion modes. After the storm, screen save the movie frames that contain the best strikes.
Difficulty: Medium to High.

Stacking night lightning is a bit challenging and requires some knowledge with Photoshop. Take identical positioned frames containing lightning (preferably cloud to ground strikes) and then stack and lighten the frames. Use the best frame as your background and for each other frame, mask any cloud artifacts (they will be obvious). Your final image should look something like this,

https://www.flickr.com/photos/cloud_spirit/53280552796/

Try to avoid using too much lightning because the clutter and over-exposure become chaotic and washed-out.
Difficulty: Medium.

Fire Skies: Best captured +/- 10 minutes of actual sunrise and sunset. Best clouds for colors are altocumulus, cumulonimbus and sometimes altostratus. The chances for success depend on whether the rising or setting sun has a cloud free horizon. If there are layers of clouds, don't be fooled into thinking that the fiery sky event is over when it may all repeat again as other cloud layers are hit by the sun's last rays

https://www.flickr.com/photos/cloud_spirit/24198091479
https://www.flickr.com/photos/cloud_spirit/25906345101

When using time- lapse, keeping camera settings on automatic is best. However, if your settings are fixed on manual, the skies will darken at sunset or lighten at sunrise, creating an interesting short-term effect.
Difficulty: Low.

Halos and iridescence around the moon can be taken in auto mode. After seeing the result, adjust exposure, f-stop and iso to your desired effects. Halos and iridescence around the sun can be taken with auto settings but you need to limit your exposure directly on your camera to avoid damaging its sensors. Best to find something to block the sun directly

https://www.flickr.com/photos/cloud_spirit/53460325657
https://www.flickr.com/photos/cloud_spirit/53694927113

Some smartphone and action cams can be aimed directly at the sun without problems. Warning, never look at the sun through the view finder! If your camera uses a live view screen on the back of the camera, you can look at the sun only this way. When in doubt, just avoid looking at the sun with a camera.
Difficulty: Low.

Auroras come in many different shapes, colors and brightness. Since they occur at night, long exposures are necessary. Generally, exposure of 10 seconds, iso 800, f/2.8, and 24mm focal length is a good starting point. Longer exposures will blur if the aurora is moving quickly. Using GoPro in time lapse mode with iso 800, exposure 10 to 20 seconds worked well during the Severe Aurora storm of 10-11 May 2024

https://www.flickr.com/photos/cloud_spirit/53714784399

Crepuscular rays are best captured if under-exposed and if post-processed, under most lighting environments, by keeping the contrast setting low. While this seems counter intuitive, it actually enhances the contrast of the rays

https://www.flickr.com/photos/cloud_spirit/50016455537

By increasing contrast, the landscape appears unrealistic, and the entire image appears very harsh. These rays when viewed are soft (heavenly-like), not like a spotlight seen on stage.

Always remember to look in the opposition direction from the sun to see if there are anti-crepuscular rays converging to the horizon

https://www.flickr.com/photos/cloud_spirit/34627015072

Rainbows are a common atmospheric optical phenomenon that are very popular to photograph. However, they encompass a large portion of the sky and thus are generally small in photos. There is a tendency to saturate their colors to make them more noticeable at the expense of realism. A way to capture their physical attributes is to use a telephoto lens

https://www.flickr.com/photos/cloud_spirit/49825267533
https://www.flickr.com/photos/cloud_spirit/53206890335

Alternatively, a wide field lens (28mm or less) will capture a complete rainbow or double rainbow. If possible, have it framed over something of interest
https://www.flickr.com/photos/cloud_spirit/52239070413

Finally, whether photography is your profession, hobby or means to share experiences, it is very tempting to exaggerate your image through camera settings or software manipulations. As an art form, photography offers a multitude of creative possibilities. However, when documenting nature, as in sky photography, you should strive for a result that is both realistic and awe-inspiring. Above all, experiment and have fun.

Wonders of the Atmosphere is a scientific and aesthetic tour de force that illustrates, describes, and explains the atmosphere's awe-inspiring phenomena. Its authors, Stanley David Gedzelman and Jan Curtis, are meteorologists who have dedicated their lives to revealing the atmosphere's beauty and majesty.